

**UNCLASSIFIED**

**AD NUMBER**

**AD481383**

**LIMITATION CHANGES**

**TO:**

**Approved for public release; distribution is unlimited.**

**FROM:**

**Distribution authorized to U.S. Gov't. agencies only; Administrative/Operational Use; JUN 1965. Other requests shall be referred to Army Engineer Research and Development Labs., Fort Belvoir, VA.**

**AUTHORITY**

**USAMERDC ltr 25 Jan 1972**

**THIS PAGE IS UNCLASSIFIED**

✓  
481383

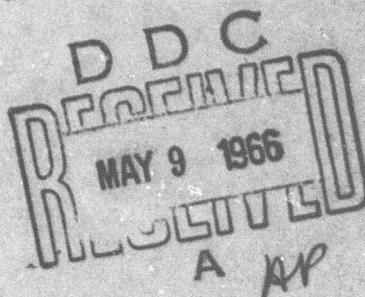
O  
AJ

CAE REPORT NO. 976

DESIGN REPORT  
CONTINENTAL TS120 TURBOSHAFT ENGINE

JUNE 1965

DA-44-009-AMC-760(T)



U.S. ARMY ENGINEER RESEARCH AND DEVELOPMENT LABORATORIES  
FORT BELVOIR, VIRGINIA

CONTINENTAL AVIATION AND ENGINEERING CORPORATION  
12700 KERCHEVAL AVENUE • DETROIT, MICHIGAN 48215

ACCESSION NO.	WHITE SECTION	<input type="checkbox"/>
CFSTI	F SECTION	<input checked="" type="checkbox"/>
DDC		<input type="checkbox"/>
U.S. DDCR		
17-16-101		
DISTRIBUTION/AVAILABILITY CODES		
DIST.	AVAIL. AND OR SPECIAL	
3		

"U. S. Government Agencies may obtain copies of this report directly from Defense Documentation Center (DDC). Other qualified DDC users should request through Commander, USAERDL, Fort Belvoir, Virginia."

(14) CAE-976

CAE REPORT NO. 976

(9) DESIGN REPORT.,

(6) CONTINENTAL TS120 TURBOSHAFT ENGINE.

(11) JUN 1965, (12) 496 p.

(15) DA-44-009-AMC-760(T) <sup>New</sup>

(10) R. Smith.

1.1.1. (1324)

U.S. ARMY ENGINEER RESEARCH AND DEVELOPMENT LABORATORIES  
FORT BELVOIR, VIRGINIA

CONTINENTAL AVIATION AND ENGINEERING CORPORATION  
12700 KERCHEVAL AVENUE • DETROIT, MICHIGAN 48215

eef

CONTINENTAL AVIATION AND ENGINEERING CORPORATION  
DETROIT, MICHIGAN

DESIGN REPORT

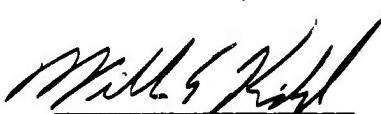
CONTINENTAL TS120 TURBOSHAFT ENGINE

Contract DA-44-009-AMC-760(T) - <sup>New</sup>

By

R. Smith

Submitted By

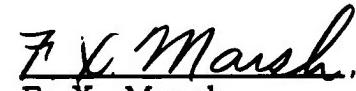
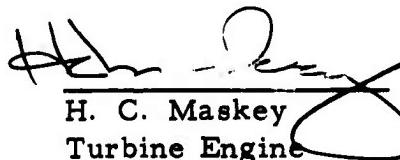


William E. Kidd  
Project Engineer

CAE Report No. 976

June 1965

Approved By

  
J. V. Shields  
Chief Design Engineer  
F. X. Marsh  
Industrial & Vehicle  
Turbines Chief Engineer  
H. C. Maskey  
Turbine Engine  
Development Manager

## TABLE OF CONTENTS

SECTION I	- SUMMARY
SECTION II	- INTRODUCTION
SECTION III	- AERODYNAMIC FLOW PATH
SECTION IV	- ROTOR SYSTEM
SECTION V	- STATIC STRUCTURE
SECTION VI	- ACCESSORY DRIVES
SECTION VII	- ENGINE LUBRICATION
SECTION VIII	- ENGINE WEIGHT
SECTION IX	- GEARED ENGINES
SECTION X	- ENGINE PERFORMANCE AND AEROTHERMO-DYNAMIC DESIGN
SECTION XI	- POWER CONTROL SYSTEM
SECTION XII	- MAINTENANCE
SECTION XIII	- MANUFACTURING
SECTION XIV	- NOISE CONTROL
SECTION XV	- HUMAN FACTORS
SECTION XVI	- REGENERATIVE ENGINES
APPENDIX XVI-A	
APPENDIX XVI-B	

## FOREWORD

This report, prepared by Continental Aviation and Engineering Corporation, presents the mechanical and aerothermodynamic design of a family of small turboshaft engines derived from a single basic design. The design discussed herein represents the family of engines at the end of the initial design phase.

This design report is submitted in fulfillment of Phase I of ERDL Contract DA-44-009-AMC-760(T).

## ABSTRACT

This report presents the design of a basic single-spool turboshaft engine and the variations possible with this basic design. These variations cover engines with outputs of 60, 90, and 120 horsepower, recuperated and nonrecuperated versions, along with direct drive and geared output speeds. The engine accessories include a starter, battery charging alternator, fuel control and integral lubrication system. The engines feature rapid replacement of static hot parts and turbine inspection.

The report includes a complete analytical design analysis of the aerothermodynamic components, performance, rotating elements, static structure, accessory drives, reduction gearing and miscellaneous parts of the engine.

SECTION I

SUMMARY

## SECTION I - SUMMARY

This report presents the design of a basic turboshaft engine and variations designed under ERDL Contract DA-44-009-AMC-760(T).

The basic engine design is a single spool, direct drive, 120 horsepower simple cycle engine. The design variations of the 120 horsepower engine covers engines of 60 and 90 horsepower, recuperated versions, and geared output speeds. The design of the direct drive, simple cycle 120 horsepower engine is presented in detail along with the modifications necessary for the alternate versions.

Engine designations have been assigned as follows:

TS120 - Simple Cycle Direct Drive, 120 HP

TS90 - Simple Cycle Direct Drive, 90 HP

TS60 - Simple Cycle, Direct Drive, 60 HP

TS120-G6 - Simple Cycle, 6000 RPM, Geared Drive, 120 HP

TS120-G12 - Simple Cycle, 12,000 RPM Geared Drive, 120 HP

TS120 R - Regenerative Engine, Direct Drive, 120 HP

TS90 R - Regenerative Engine, Direct Drive, 90 HP

TS60 R - Regenerative Engine, Direct Drive, 60 HP

Figure I-1 shows the basic arrangement of the simple cycle Model TS120 engine. It incorporates a rotatable side entry air inlet, an axial exhaust, and the power take-off at the front of the engine. The engine accessories include a starter, a battery charging alternator, an oil pump, a combination fuel pump and governor and an automatic sequence control.

## Section I

The performance targets are summarized below with radial exhaust adapter:

<u>Condition</u>	<u>HP</u>	<u>SFC</u>
Sea Level, Standard Day	120	0.694
8000 Feet, 90°F	120	0.660

The aerothermodynamic design of the TS120 engine is based on an airflow of 1.67 pounds per second, which will produce 120 horsepower on a standard sea level day with a turbine inlet temperature of 1385°F. The engine maintains 120 horsepower to 8000 feet altitude on a 90°F day with a turbine inlet temperature of 1765°F.

The engine, with accessories mounted, shown in Figure I-2, is 26.50 inches long, 25.00 inches wide, and 19.68 inches high.

The engine accessories are located at the front of the engine immediately behind the power take-off flange, and are mounted at a right angle to the engine axis. A single side entry air inlet is located behind the accessories and can be rotated 90°F to either side of the vertical centerline. A single can combustor is located behind the air inlet and approximately tangent to the engine and can be rotated to alternate positions. The engine exhaust is discharged axially on the engine centerline. An alternate radial exhaust adapter can be attached to the existing axial exhaust.

The main power take-off is a 66,800 r.p.m. drive located at the front and on the engine centerline. The engine incorporates three mounting points; two are located on the accessory case and one on the combustor housing. The design will accommodate operational attitudes of 36 degrees from the horizontal in any direction, operation from sea level to 8000 feet, and ambient temperatures between minus 65° and plus 160°F with a maximum of 125°F air delivered to the compressor air intake.

## Section I

The engine fuel control is a scheduling system with an integral fuel pump and fuel cut-off valve. Isochronous governing can be provided with a minimum modification when desired.

Even though the engine is flat rated at 120 horsepower, it was designed mechanically for full temperature cold day power output with margin for growth potential.

Section I

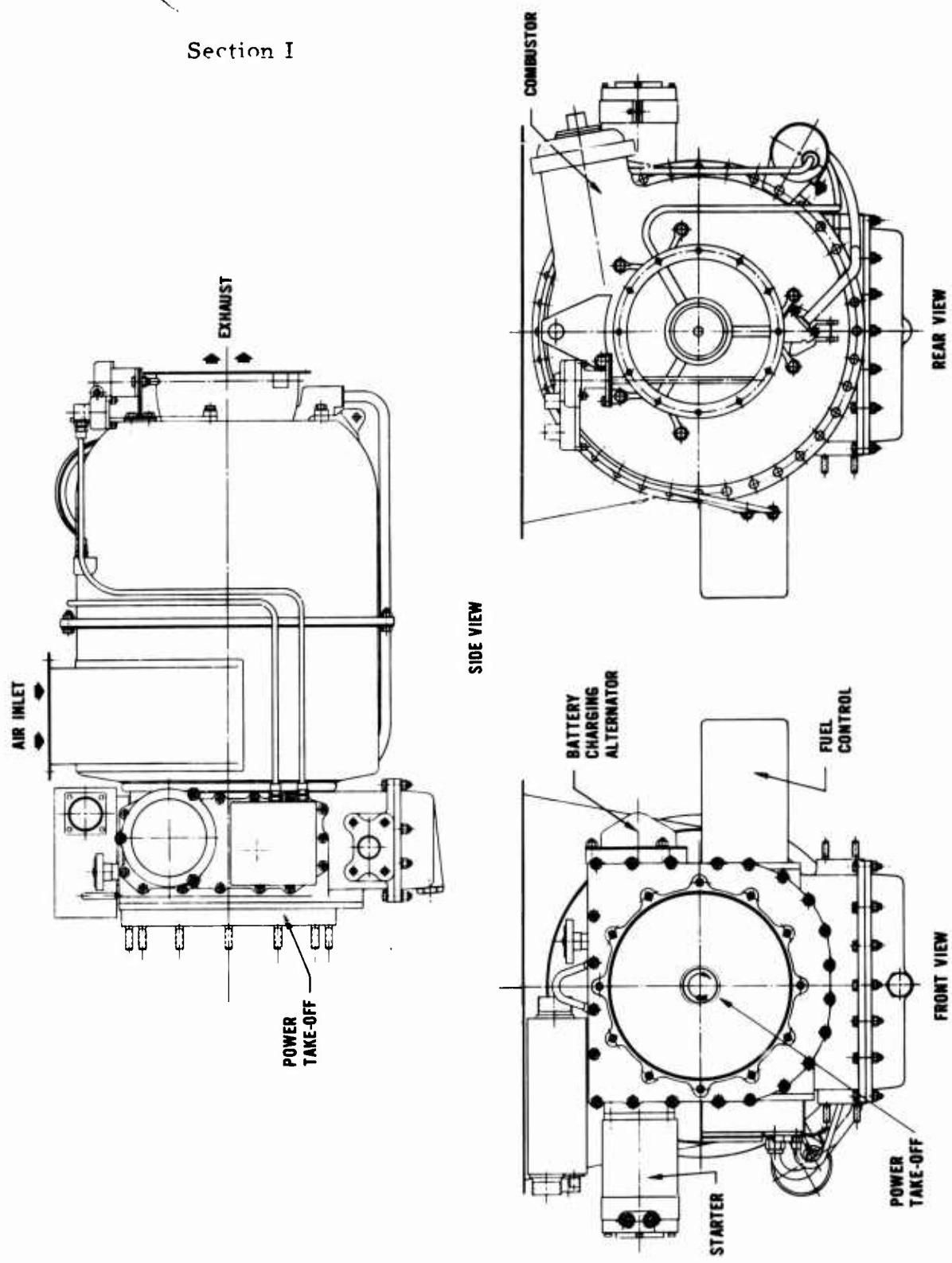
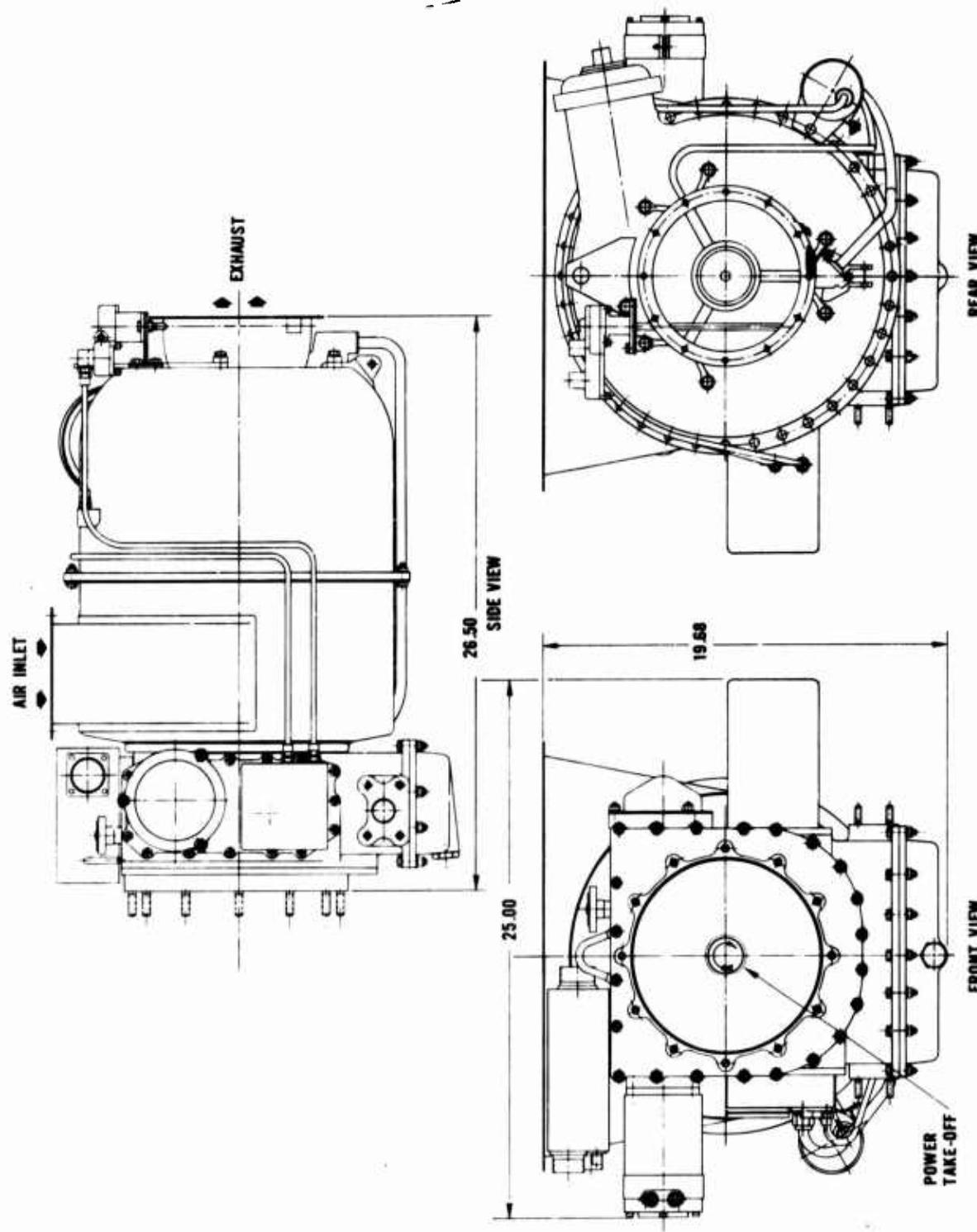


Figure I-1. Continental Model TS120 Turboshaft Engine Basic Arrangements,  
Simple Cycle, Direct Drive.

**Section I**



**Figure I-2. Continental Model TS120 Turboshaft Engine Basic Installation Drawing.**

SECTION II

INTRODUCTION

## SECTION II - INTRODUCTION

The TS-120 engine, Figure II-1, is a single spool turboshaft engine flat rated at 120 shaft horsepower to 8000 feet on a 90 degree day.

The engine employs a single side entry air intake. Air from the intake enters an annular plenum, then passes successively through a single-stage transonic axial compressor, a two-stage stator, a single-stage centrifugal compressor, a three-stage radial diffuser, a single can combustor, a volute, a turbine inlet nozzle, a radial turbine and an axial exhaust that discharges along the engine axis.

The engine is direct drive with the power output on the engine centerline at 66,800 r.p.m. The accessory drives originate with a helical gear mesh, a bevel gear set and then a helical gear train. A starter, battery charging alternator, fuel control and oil pump are driven at right angles to the engine axis. Helical gears are used in the accessory train in the interest of noise reduction. An over-running clutch is provided in the starter drive to permit smooth re-engagement of the starter.

The power control system used on the TS-120 engine is a scheduling system, consisting of a fuel pump, relief valve, acceleration scheduling system, automatic fuel density compensation, exhaust gas temperature limiter, governor and a fuel cut-off valve. Compensation of the governor set speed for engine optimization as a function of inlet air temperature is provided, along with an electrically operated override for the turbine temperature limiter and a remotely resettable governor speed setting. The system is planned for maximum versatility with a minimum of modification. It includes provisions for adaptation to isochronous governing with load sharing and paralleling features required in the geared drive system. Provisions will be made for incorporating recuperator temperature compensation and a bypass system for overspeed protection in the recuperated engine design.

The engine lubricating system is the wet sump type, designed to operate 36 degrees from the horizontal in any direction with MIL-L-2104, MIL-L-7808, and MIL-L-10295 lubricating oil.

**Section II**

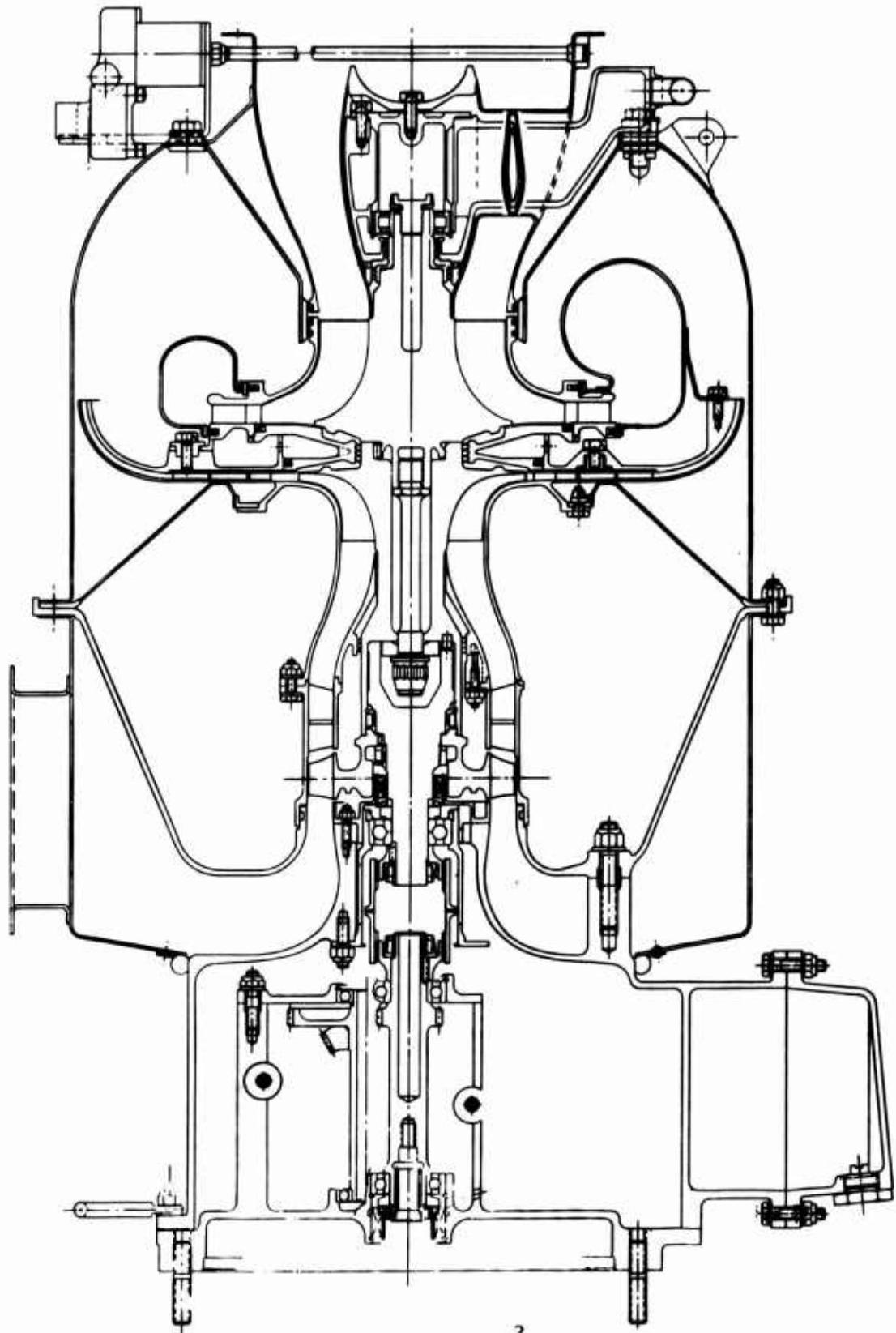


Fig. II-1. Continental Model TS120 Turboshaft Engine.

SECTION III

**AERODYNAMIC FLOW PATH**

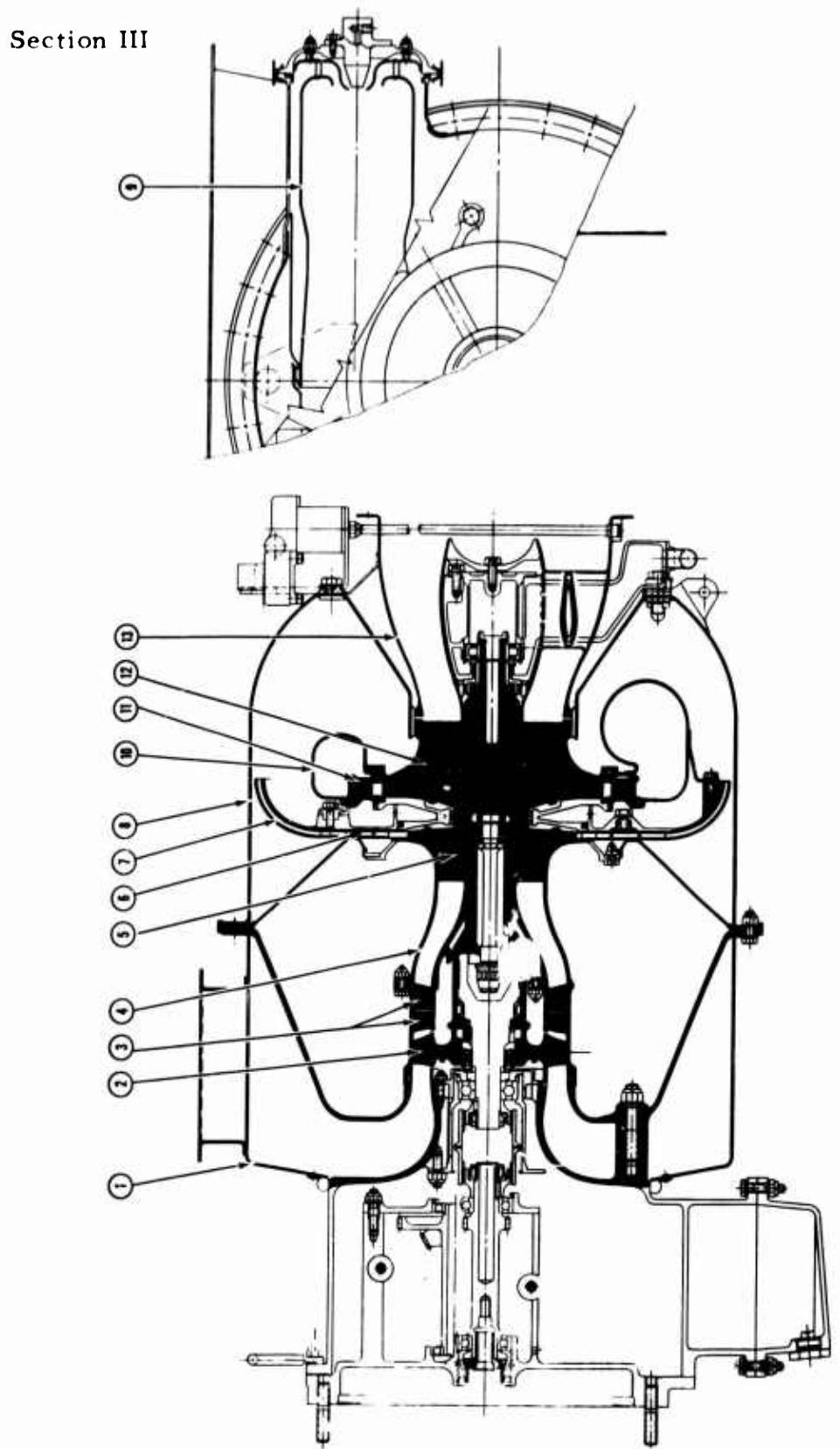
### SECTION III - AERODYNAMIC FLOW PATH

The TS-120 engine aerodynamic flow path is shown in Figure III-1. The flow path incorporates a minimum number of parts and aerodynamic turning, consistent with a side entry, can combustor and radial turbine, to ensure a minimum cost and maximum performance. Air enters the engine through a single side entry fabricated sheet aluminum plenum (No. 1, Figure III-1). From the inlet plenum the air passes through a cast steel 1.6 pressure ratio transonic axial compressor rotor (2). The air from the axial compressor rotor is diffused through a two-stage cast aluminum stator (3). An interstage duct (4) directs the air into a machined steel centrifugal compressor (5). From the centrifugal compressor the air passes through a three-stage fabricated steel radial diffuser (6) then through a guided diffusing turn (7) into the combustor housing (8). From the combustor housing the air flows into a single can combustor (9) where fuel is added and combustion takes place.

From the combustor the hot gases flow through a fabricated volute (10) into a precision cast nozzle (11) and through a machined single-stage radial turbine (12). The gas from the turbine passes through a fabricated exhaust diffuser (13), completing the basic engine flow path.

The basic 120 horsepower engine flow path requires only two physical modifications for the 60 and 90 horsepower versions. Referring to Figure III-2 these modifications are the additional fixed inlet guide vanes (14) and a reduced area turbine inlet nozzle (15).

Fig. III-1. TSI20 Aerodynamic Flow Path.



**Section III**

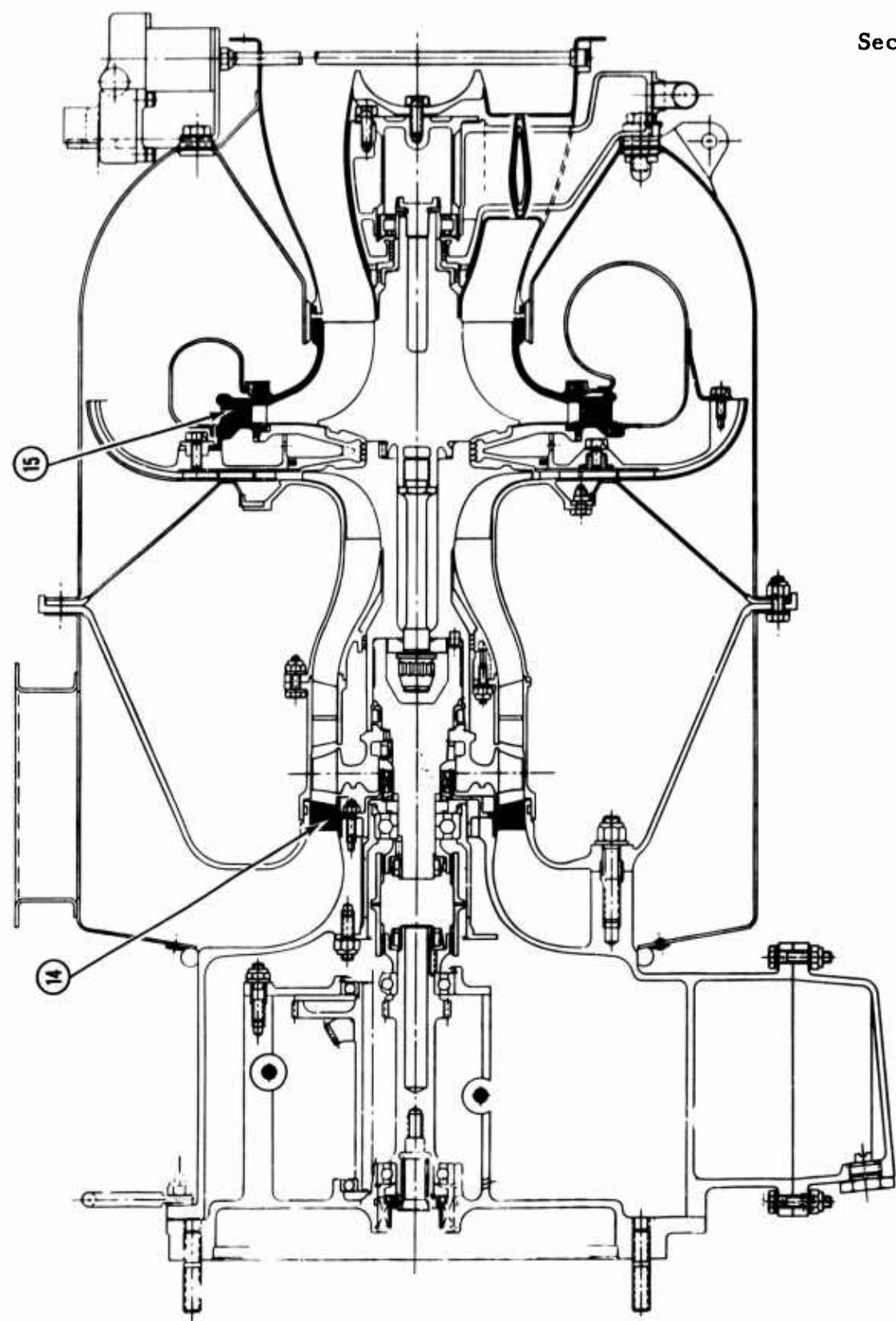


Fig. III-2. Modification to TS120 Aerodynamic Flow Path For  
TS60 and TS90 Horspower Engine.

SECTION IV

**ROTOR SYSTEM**

## SECTION IV - ROTOR SYSTEM

The Model TS120 rotor system, Figure IV-1, comprises three aerodynamic components bolted together and supported by two bearings mounted in flexible supports. The selection of three aerodynamic components was made on the basis of providing a moderate pressure ratio engine with a simple rotor system. The axial compressor (1), is a steel casting; the radial compressor (2), and the turbine (3), are fully-machined from wrought alloys. The front shaft (4), is machined from alloy steel. The radial turbine (3), is clamped to the compressor (2) by a bolt (5). A disc spring (6) is used under the head of the nut (7), to increase the elasticity of the clamping section. The turbine is piloted to the compressor through a thin conical leaf designed to maintain a tight fit over the complete operating range of the engine. The turbine torque is transmitted through two round pins (8). The front shaft (4), is piloted into an integral extension of the radial compressor rotor, driven through two pins (9), and clamped in place with a nut (10). The axial compressor (1), is piloted into the rotor system, driven through two flat keys (11), and clamped in place with a nut (12). The aerodynamic rotating components are designed as individual pieces, bolted together, to facilitate replacement of individual parts.

### MAIN BEARINGS

The main shaft assembly . supported by a ball bearing at the front end and a roller bearing at the turbine end. The front bearing, which absorbs the rotor thrust, is an angular contact, split inner race type with ball complement, contact angle, race curvatures and retainer construction designed to accommodate the load and high speed involved.

The calculated  $B_{10}$  life of the thrust bearing is over 2200 hours at full speed and maximum load. This life is based on a combined thrust-radial load application of 160 and 50 pounds respectively. Testing experience of various bearing manufacturers has indicated that a life extension factor, between three and five to one, can be expected from the combination of material and processing characteristics specified for this bearing.

## Section IV

The races and balls will be manufactured from consumable electrode vacuum-melt M-50 tool steel heat-treated to Rockwell C-61 minimum hardness. It has been Continental's practice to assign a life factor of five to one for C. E. V. M. 52100 steel, and ten to one for C. E. V. M. M-50 steel even previous to the announcements by certain bearing companies that a life factor of three to one could be applied to the catalog ratings of their bearings manufactured from vacuum degassed 52100 steel. The consumable electrode vacuum remelting process results in a cleaner grade of steel than that obtainable through vacuum degassing, and it is felt that this superior degree of cleanliness is responsible for the higher reliability of C. E. V. M. bearings. The further two to one improvement of M-50 over 52100 is attributable to its higher stabilized hardness of RC-61, and its ability to retain this hardness in the ball raceways where instantaneous load-induced hot spots would reduce the local hardness of standard bearing materials, causing a resultant reduction in over-all life.

The cage will be machined from hardened steel bar stock, silver-plated to increase corrosion resistance and improve frictional properties. Balls and cage will be retained in the outer race to facilitate assembly and disassembly procedures. The cage is outer-ring guided to enhance lubrication of the guide surfaces at the high speed involved.

The DN value of the bearing is in the range of  $1.3 \times 10^6$  at maximum turbine speed. This parameter is well within the range of successful Continental experience. The internal geometry of the bearing is based on configurations which have allowed bearing companies to successfully test this size bearing at a speed of 120,000 rpm, about 80 percent higher than our maximum rated speed.

The outer race of the bearing is positively retained by a nut and snap ring in its flexible housing. The inner race is pressed on the shaft with an interference fit and held through a spline coupling member by a nut and lockwasher.

## Section IV

The rear bearing is a double-lipped outer-race roller bearing with a wider than standard inner-race to accommodate the differential thermal expansion between the housings and the rotor shaft. The roller complement and retainer construction are set up primarily to favor high-speed capability rather than radial load capacity, because most of the unbalance will be absorbed in the flexible bearing mount. By allowing the shaft to rotate about its mass center of gravity, rather than its geometric center, the maximum radial force seen by the bearing will be less than 50 pounds and the resulting  $B_{10}$  life will be in excess of 20,000 hours.

Rollers and races on this bearing will be manufactured from C. E. V. M. M-50 tool steel. The material will be stabilized to retain hardness and dimensional stability at  $600^{\circ}\text{F}$ , although it is not expected that operating temperature will exceed  $400^{\circ}\text{F}$  with the scheduled oil supply.

The cage for this bearing will be a one-piece outer land riding, high-strength, hardened steel machining, silver-plated to improve frictional characteristics. Silicon iron bronze cages, used in similar applications, have sometimes tended to lose their roller retaining tangs, thus raising the possibility of foreign particle damage at this or some other location in the engine. These problems were solved through the use of steel cages.

The bearing will be press-fitted on the shaft and held by a nut and cup lock. The outer-race will be retained by a snap ring against a solid shoulder in the flexible support. This practice was used successfully in previous Continental gas turbine engines.

### ROTOR SUSPENSION SYSTEM

The principal source of mechanical vibration in the gas turbine engine is unbalance in the rotor system. This unbalance may excite critical speeds of the rotor itself, and/or induce resonance in any combination of structural elements that may be tuned to the running frequency of the rotor. The TS120 engine was designed to

## Section IV

minimize the effect of rotor unbalance and critical speeds through the proper combination of rotor and supporting structure compliances.

The rotor-suspension system of this engine is based on the concept of a relatively rigid rotor shaft assembly mounted on flexible, hydrodynamically, damped bearing supports. Critical speeds are controlled by regulating the spring rates and damping constants of the bearing retainers. The flexible mounting also serves to isolate rotor unbalance from the bearings and outer structure.

Design values of bearing support flexibility are determined from a series of curves covering the complete spectrum of possible critical speeds over the engine operating range, Figure IV-2. The curves are developed by a digital computer programmed to determine the flexural resonant frequencies of a variable cross section shaft rotating on elastic supports. Gyroscopic stiffening effects of large disc inertias are included in the calculations.

Spring rates are selected to place the first two critical speeds below the normal engine operating range. The first and second modes will occur at 8500 and 18,000 rpm for front and rear bearing spring rates of 20,000 pounds per inch. Shaft deflection in these two modes is almost completely described by the bearing displacements, Figure IV-3. The third mode, which involves considerable shaft bending as well as bearing displacement, occurs at 98,000 rpm.

Required bearing support compliance is provided by a flexible retainer consisting of a cylindrical member containing a number of longitudinal slots. The slot dimensions determine the radial spring rate of the bearing cage, with maximum deflection controlled by an oil-fed snubber surface. The deflection snubber limits the maximum stringer bending stresses at resonance to 40,000 psi.

The effect of structural compliance on the over-all system is negligible compared to the relatively low spring rates of the cage, and critical speeds can be accurately established. Figure IV-4 illustrates the application of this design feature in the bearing cage.

## Section IV

Operation in the region above resonance causes the shaft to seek a rotational centerline about its mass center of gravity. The effect of unbalance is merely to displace this center of gravity slightly from the geometric centerline. The only force experienced by the bearings and support system is then equal to the product of the displacement and the spring rate of the bearing cage. For an eccentricity of 0.001-inch and a spring rate of 20,000 pounds per inch, this rotating force would be equal to 20 pounds.

Loss of one inch from the tip of the turbine would cause an unbalanced load of only 50 pounds, although the centrifugal weight of this blade section at full engine speed would be 4900 pounds. The capability of this system to accommodate large unbalances was experimentally verified on similarly suspended gas turbine engines by deliberately introducing massive unbalances into the rotors and running at full speed with very little increase in external vibration levels.

The stiff construction of the TS120 main rotor shaft minimizes the tendency to go out of balance at high speeds. If sufficient flexibility exists in a rotor system, locked-in bending moments caused by the uneven distribution of unbalance along the length of the rotor will cause the shaft to deflect at high speeds, destroying the balance that was obtained at a much lower balancing speed. In some cases, it is necessary to balance such flexible rotors at high speeds and in three or more planes to attain satisfactory running balance. This will not be necessary with the TS120 engine.

Bearing support deflection is limited at resonance by two concentric, oil-fed snubbing surfaces that also prevent excessive pounding due to the gyroscopically induced moment of the rotor under vehicular driving conditions. The clearance, width, and diameter of these surfaces are parameters of a viscous damping system in which the hydrodynamic force-vector generated by the rotating oil film squeeze action varies in both magnitude and direction with speed and unbalance. There is a certain optimum combination of values for which the damper is adequate to provide low frequency vibration absorption without increasing transmissibility at high speeds to such an extent that the bearing support spring no longer functions as an effec-

## Section IV

tive mass isolator. The design parameters used in this system were derived through analytical methods, verified by full-scale laboratory tests, and proven by over one million hours of service in Continental engines.

### ROTOR STRUCTURAL ANALYSIS

The contractual requirements are for a rotating system that is structurally sound at the design speed of 66,800 rpm and at ten percent overspeed for ten percent of the time. The stresses in the rotating elements are presented at design speed and at the overspeed condition. The nature of a flat rated engine is to run at a higher turbine inlet temperature at altitude than at sea level and for this reason the stresses in the parts affected by temperature are presented at the sea level and altitude conditions.

The bursting of a rotating disc with reasonable ductility is considered to be a function of the average tangential stress. A burst margin based on average tangential stress and material properties is presented for each rotor. The burst margin is defined as:

$$BM = \frac{K \times UTS (\text{Min})}{\sigma t_{\text{avg}}}$$

where:

- UTS (Min) is the minimum ultimate tensile strength,
- $\sigma$  t avg is the average tangential stress,
- K is a constant equal to 0.75.

### AXIAL COMPRESSOR

The axial compressor, Figure IV-5, is an integrally bladed rotor, machined from an AMS 5355 precision steel casting. The basic disc "A" is supported through a cylindrical extension "B". The minimum material properties are:

## Section IV

Ultimate Tensile Strength	140,000 psi
Yield Strength at 0.2 Percent Offset	125,000 psi
Elongation	8 percent

The disc and blade stress summary and burst margins are shown in Figure IV-6, and the blade interference diagram in Figure IV-7. The blade gas bending stress is considered negligible. Referring to Figure IV-5, the maximum stresses in the cylinder "B" connecting to the disc "A" are 53,400 psi hoop stress and 98,130 psi bending. Based on past experience the margins shown are adequate.

The compressor blade is a scale of an existing blade. Calculated vibratory frequencies have shown reasonable correlation with measured frequencies on similar blading. Past Continental experience on this type blading indicates that the vibratory margins shown in Figure IV-7 are sufficient.

### RADIAL COMPRESSOR

The radial compressor, Figure IV-8 is an integrally bladed rotor, machined from a Continental MS718 (Inco. 718) forging. An integral extension of the radial compressor forms part of the rotor shafting. The minimum material properties are:

	<u>Room Temperature</u>	<u>1200°F</u>
Ultimate Tensile Strength	170,000 psi	140,000 psi
Yield Strength 0.2% Offset	140,000 psi	125,000 psi
Elongation	10 percent	10 percent

Due to the close proximity of the radial compressor to the hot turbine, the effects of temperature were considered in the radial compressor analysis. The radial compressor estimated temperature distribution at sea level is shown in Figure IV-9, and at altitude in Figure IV-10. The definition of front-face, back-face, blade root and blade tip is shown in Figure IV-8.

## Section IV

A stress summary is presented in Table IV-I. Figures IV-11 through IV-22 describe the disc and blade stresses for various conditions.

TABLE IV-I  
RADIAL COMPRESSOR STRESS SUMMARY

<u>Item</u>	Sea Level			Altitude		
	<u>Design Speed</u>	<u>10 Percent Overspeed</u>	<u>Design Speed</u>	<u>10 Percent Overspeed</u>	<u>Design Speed</u>	<u>10 Percent Overspeed</u>
Average Tangential Stress - psi	45,790	55,410	45,790	55,410		
Burst Margin	1.62	1.47	1.60	1.45		
Average Disc Temp. - °F	430	430	580	580		
Max. Tangential Stress - psi at 1.90R Back Face	48,300	59,000	43,000	53,720		
Max. Tangential Stress - psi at Bore	99,500	118,200	89,272	108,780		
Max. Blade Stress - psi at 2.1R Blade Tip	41,500	48,000	42,600	50,800		

The turbine pilots into the radial compressor through a press-fitted pilot on a conical extension from the turbine wheel. The pilot is interrupted at four places on the circumference to provide further flexibility in the pilot extension. The effect of a pilot load of 10,000 pounds on the radial compressor stresses is shown in Figure IV-23.

The radial compressor deflection summary is shown in Tables IV-II and IV-III.

Section IV

TABLE IV-II

TS120 RADIAL COMPRESSOR, RADIAL DEFLECTIONS

<u>Radius</u>	<u>Condition</u>	<u>Stress Deflection</u>	<u>Temperature Deflection</u>	<u>Total Deflection</u>
.75 Back Face	SL Nom	1270 (10) <sup>-6</sup>	2223 (10) <sup>-6</sup>	3493 (10) <sup>-6</sup>
	SL 1.10	1566 (10) <sup>-6</sup>	2223 (10) <sup>-6</sup>	3789 (10) <sup>-6</sup>
	Alt Nom	1227 (10) <sup>-6</sup>	2884 (10) <sup>-6</sup>	4111 (10) <sup>-6</sup>
	Alt 1.10	1523 (10) <sup>-6</sup>	2884 (10) <sup>-6</sup>	4407 (10) <sup>-6</sup>
	Cold Nom	1411 (10) <sup>-6</sup>	0	1411 (10) <sup>-6</sup>
	Cold 1.10	1707 (10) <sup>-6</sup>	0	1707 (10) <sup>-6</sup>
Tip	SL Nom	2963 (10) <sup>-6</sup>	4598 (10) <sup>-6</sup>	7561 (10) <sup>-6</sup>
	SL 1.10	3408 (10) <sup>-6</sup>	4598 (10) <sup>-6</sup>	8006 (10) <sup>-6</sup>
	Alt Nom	4226 (10) <sup>-6</sup>	4788 (10) <sup>-6</sup>	9014 (10) <sup>-6</sup>
	Alt 1.10	4689 (10) <sup>-6</sup>	4788 (10) <sup>-6</sup>	9477 (10) <sup>-6</sup>
	Cold Nom	2205 (10) <sup>-6</sup>	0	2205 (10) <sup>-6</sup>
	Cold 1.10	2669 (10) <sup>-6</sup>	0	2669 (10) <sup>-6</sup>

TABLE IV-III

RADIAL COMPRESSOR AXIAL DEFLECTION TIP

Sea Level, Nominal	.0098 In.
Sea Level, 1.10	.0107 In.
Altitude, Nominal	.0095 In.
Altitude, 1.10	.0103 In.
Cold, Nominal	.0031 In.
Cold, 1.10	.0038 In.

## Section IV

### RADIAL TURBINE

The radial turbine, Figure IV-24, is an integrally bladed rotor, machined from a Continental MS-700 (Udiment 700) forging. An integral extension of the radial turbine forms the rear bearing support for the rotor shafting. The minimum material properties are:

	<u>Room Temperature</u>	<u>1400°F</u>
Ultimate Tensile Strength - psi	170,000	135,000 psi
Yield Strength, psi, (0.2 Percent Offset)	125,000	110,000 psi
Elongation, Percent in 4D	10	15
Reduction in Area, Per- cent	12	15

The radial turbine estimated temperature distribution at sea level is shown in Figure IV-25, and at altitude in Figure IV-26. The definition of front-face, back-face, blade root and blade tip is shown in Figure IV-24. A stress summary for the radial turbine is presented in Table IV-IV.

Figures IV-27 through IV-44 describe the disc and blade stresses for various conditions. The effect of an applied radial load of 10,000 pounds due to the pilot is shown in Figure IV-45 and IV-46. The disc radial growth is shown in Figures IV-47 and IV-48, and the axial deflection in Figure IV-49. A comparison of the summary stresses shown in Table IV-IV, with the minimum material properties, indicates an adequate margin for the turbine rotor.

### TEMPERATURE DISTRIBUTION ANALYSIS

The temperature distribution in the radial flow turbine and compressor wheels was calculated for steady-state operating conditions. The knowledge of the metal temperatures was essential in calculating the rotor stresses and defining the material properties required for continuous operation of the turbine wheel.

## Section IV

TABLE IV-IV  
**RADIAL TURBINE STRESS SUMMARY**

<u>Item</u>	<u>Sea Level</u>		<u>Altitude</u>	
	<u>Design Speed</u>	<u>10 Percent Overspeed</u>	<u>Design Speed</u>	<u>10 Percent Overspeed</u>
Average Tangential Stress - psi	47,793	57,829	47,793	57,829
Burst Margin	1.56	1.42	1.53	1.40
Average Disc Temperature - °F	627	627	810	810
Maximum Radial Stress - psi (Back Face)	82,000 @ .625R	99,051 @ .270R	90,682 @ .608R	105,935 @ .608R
Maximum Tangential Stress - psi (Back Face)				
Blade - Max. Stress - psi	70,800	73,256	66,779	78,907
Radius - In.	1.55	1.41	1.217	1.217R
Temp. - °F	772	757	980	980

Metal temperatures for the final design configuration, as shown in Figure IV-50, were calculated for sea level (Turbine Inlet Temperature, T.I.T. = 1834°R) and altitude (T.I.T. = 2210°R) operation. To estimate the boundary conditions for the two wheels, heat transfer coefficients and gas temperatures had to be calculated, using gas properties and flow conditions as specified by the aero-thermodynamic design. The results of the temperature calculations are summarized in Tables IV-V and IV-VI. Figures IV-51 through

Section IV

TABLE IV-V

TURBINE WHEEL - SUMMARY OF METAL TEMPERATURES

<u>Location</u>		<u>Sea Level</u> (TIT = 1834°R)	<u>Altitude</u> (TIT = 2210°R)
Blade Tip at	r = 3.38 In.	1572°R	1891°R
at	r = 2.14 In.	1480°R	1624°R
Disc Rim at	r = 2.5 In.	1459°R	1728°R
Disc Bore at	r = 0	Front Face 1039°R	1348°R
at	r = 0	Rear Face 1049°R	1373°R

TABLE IV-VI

COMPRESSOR WHEEL - SUMMARY OF METAL TEMPERATURES

<u>Location</u>		<u>Sea Level</u> (TIT = 1834°R)	<u>Altitude</u> (TIT = 2210°R)
Blade Tip at	r = 2.5 In.	774°R	793°R
at	r = 1.6 In.	649°R	709°R
Disc Rim at	r = 2.5 In.	773°R	783°R
Disc Bore at	r = .43 In.		
	Front Face	745°R	801°R
at	r = .43 In.		
	Rear Face	898°R	1095°R

IV-54 show the temperature fields in the two wheels represented by isotherms, lines of uniform temperature.

## Section IV

The maximum metal temperatures inside the wheels are encountered when operating at altitude condition:

Turbine Wheel	$t = 1268^{\circ}\text{F}$
Compressor Wheel	$t = 750^{\circ}\text{F}$

The temperature gradient existing between the back faces of the two wheels represented a serious problem for the joint design. With successive redesigns of the joint area, the temperature gradient has been reduced to approximately  $184^{\circ}\text{F}$  representing a radial growth differential at 0.00105 inch.

### METHOD OF ANALYSIS

The temperature distribution in a turbine wheel operating in steady-state depends on the heat conduction within the wheel, the environment, and the heat transfer conditions across its boundaries. Because of the difficulties encountered in trying to determine the exact environmental and boundary conditions, certain simplifying assumptions were introduced in order to establish a practical procedure for the calculations. For example, the geometry of the system had to be confined to reasonable limits by separating the shaft from the wheel. However, the heat conduction process between the shaft and the wheel was accounted for in the heat transfer calculation.

The calculation procedure chosen to estimate the temperatures is based on the so-called energy integral method, generally used to conduct transient heat transfer analysis. Detailed descriptions of the method are given in References 1, 2 and 3. The actual calculation process as applied here is a simplified version of the original method adopted for steady-state heat flow condition, utilizing digital computer techniques. According to the procedure the disc is divided into 50 small, but finite thickness concentric hollow cylindrical elements. A mean energy balance is obtained for each element by expressing temperature variation between elements in terms of finite differences. A temperature profile is assumed for the axial direction.

## Section IV

Solving a system of simultaneous equations for the energy balances and the boundary conditions yields the temperature distribution in the rotor.

In specifying the boundary conditions for the cylindrical elements the temperature and heat transfer coefficient for the front and back face of the disc must be known. The temperature values are defined as adiabatic wall temperatures using the free stream velocity of the surrounding gas relative to the disc. The rate of heat transfer through the face of the disc is defined by calculating the Biot Numbers. The Biot number for a disc is expressed as a ratio of the heat transfer coefficient through the boundary layer to the heat conduction coefficient of the disc material multiplied by the disc outer radius. (See References 4 and 5). The boundary layer heat transfer coefficient is obtained from the Nusselt number. Several authors published experimentally established formulas from which the Nusselt number can be calculated for a disc rotating at high speed surrounded by a fluid (e.g., References 4 and 6). To calculate the adiabatic wall temperatures and the heat transfer coefficients, the gas flow velocities and temperatures must be known and the gas properties are to be evaluated at the proper temperature levels.

It has been shown that the heat flow into and out of the disc through the front and back faces is estimated by using experimental formulas to calculate the heat transfer coefficient for a rotating disc. However, there are a number of blades located on the front face of the disc. These blades, acting like ribs, increase the heat flow between the gas and the disc. Therefore, the coefficient of heat transfer calculated for a flat disc cannot be properly used. To include the effect of the blades, a calculating method was worked out, whereupon a corrected coefficient of heat transfer for the front face was introduced, combining the heat flows through the disc and the blades as well. To calculate corrected heat transfer coefficients, the blades were treated as thin flat plates exposed on two sides to a high velocity turbulent gas flow. (Reference 6).

## Section IV

The solid connection between the shaft and the disc front face and the metal-to-metal contact at the back face has represented a considerable difficulty to properly assess the boundary conditions. At the front face where the disc extends into the shaft the Biot number was determined to express conduction heat transfer from the surface of the disc to a known temperature at a known distance on the shaft; the temperature was then used as the boundary temperature for the same area. This approach can also be described as maintaining a constant temperature heat sink in the shaft at a given distance.

To calculate the Biot number for the back face contact area of the two wheels a similar approach was used. However, the boundary temperature, (always represented by the metal temperature in the other wheel) had to be determined by an iterative process.

Design studies conducted for the back face joint of the two wheels revealed that the size of the contact area has a large effect on the temperature gradient existing between the two wheels. It was found that having maximum possible contact between the two wheels that the temperature gradient across the pilot surface could be reduced from 300°F to approximately 80°F.

Section IV

REFERENCES

1. The Design and Performance Analysis of Radial Inflow Turbines; Northern Research and Engineering Co.; Cambridge, Mass. 1964.
2. Reynolds, W. C., Dolan T. A.; Use of Integral Methods in Transient Heat Transfer Analysis; ASME Paper No. 58-A-248.
3. Goodman, T. F.; The Heat Balance Integral - Further Considerations and Refinements; TRANS ASME, Vol. 83, Series C No. 3; August 1959.
4. Kreith, F.; Principles of Heat Transfer: International Textbook Co.; 1964.
5. Grober, Erk, Grigull; Fundamentals of Heat Transfer; McGraw-Hill, 1961.
6. Schlichting; Boundary Layer Theory; McGraw-Hill, 1962.

**Section IV**

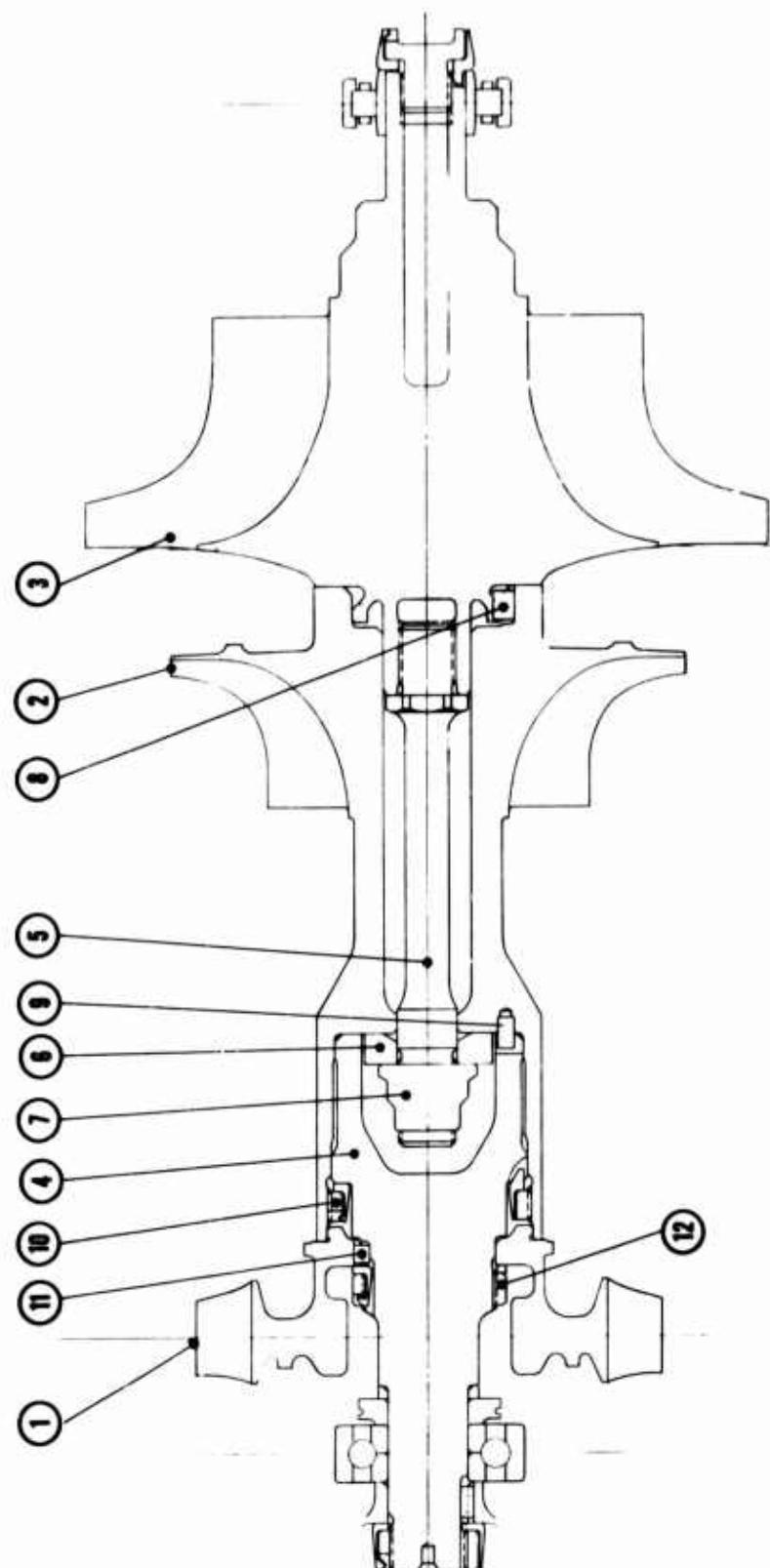


Figure IV-1. TSi20 Rotor Assembly.

## Section IV

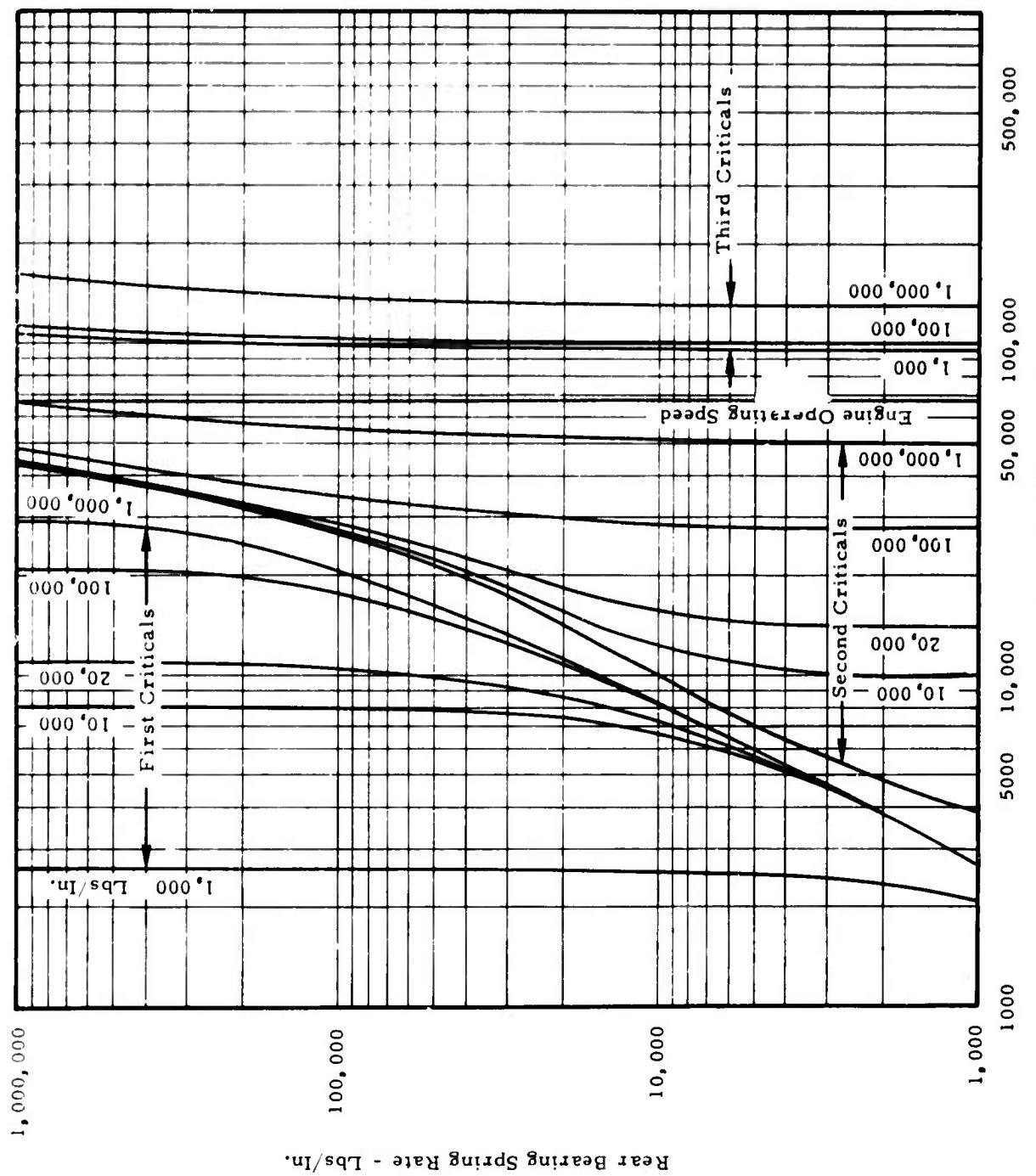


Figure IV-2. TS120 Critical Speed Versus Spring Rate of Rear Bearing Support for Various Values of Front Bearing Support Spring Rate.

Section IV

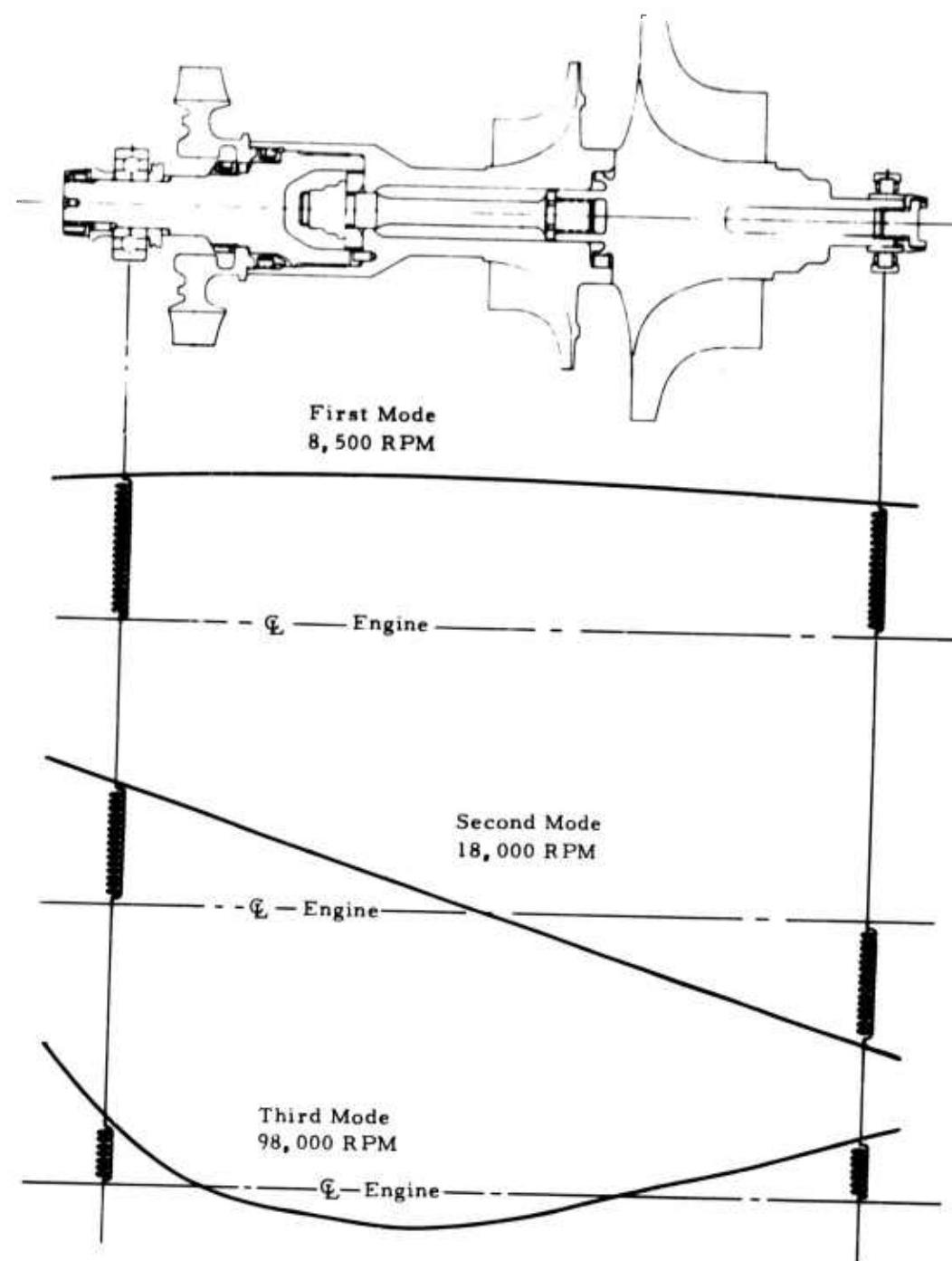


Figure IV-3. TS120 Shaft Deflection Diagram.

Section IV

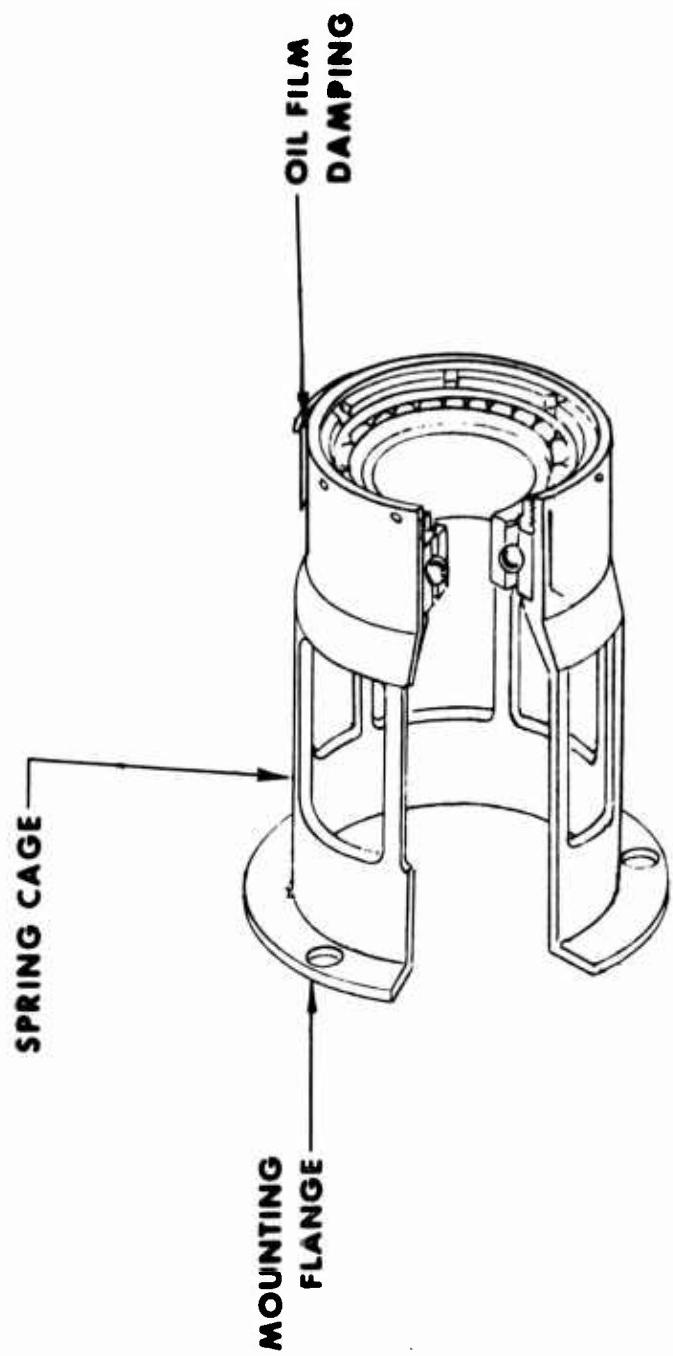
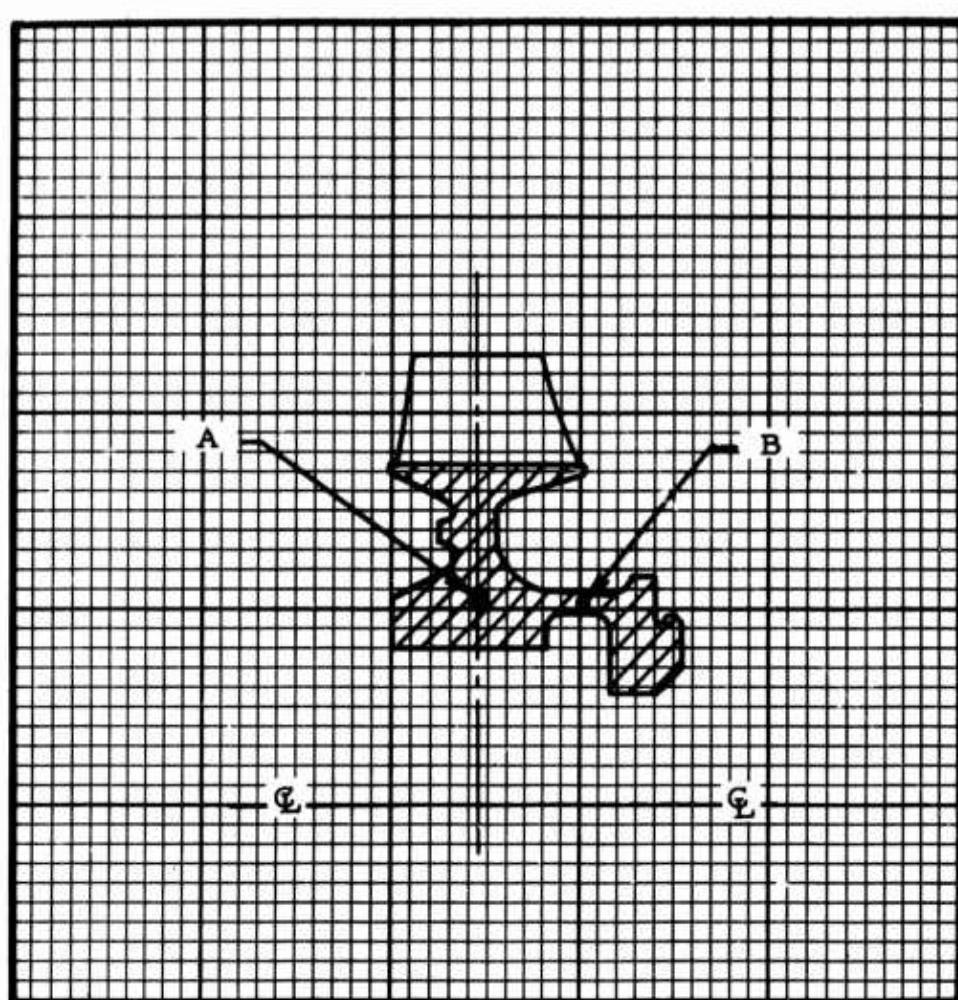


Figure IV-4. TS120 Flexible Front Bearing Support.

**Section IV**



**Figure IV-5. TS120 Axial Compressor.**

## Section IV

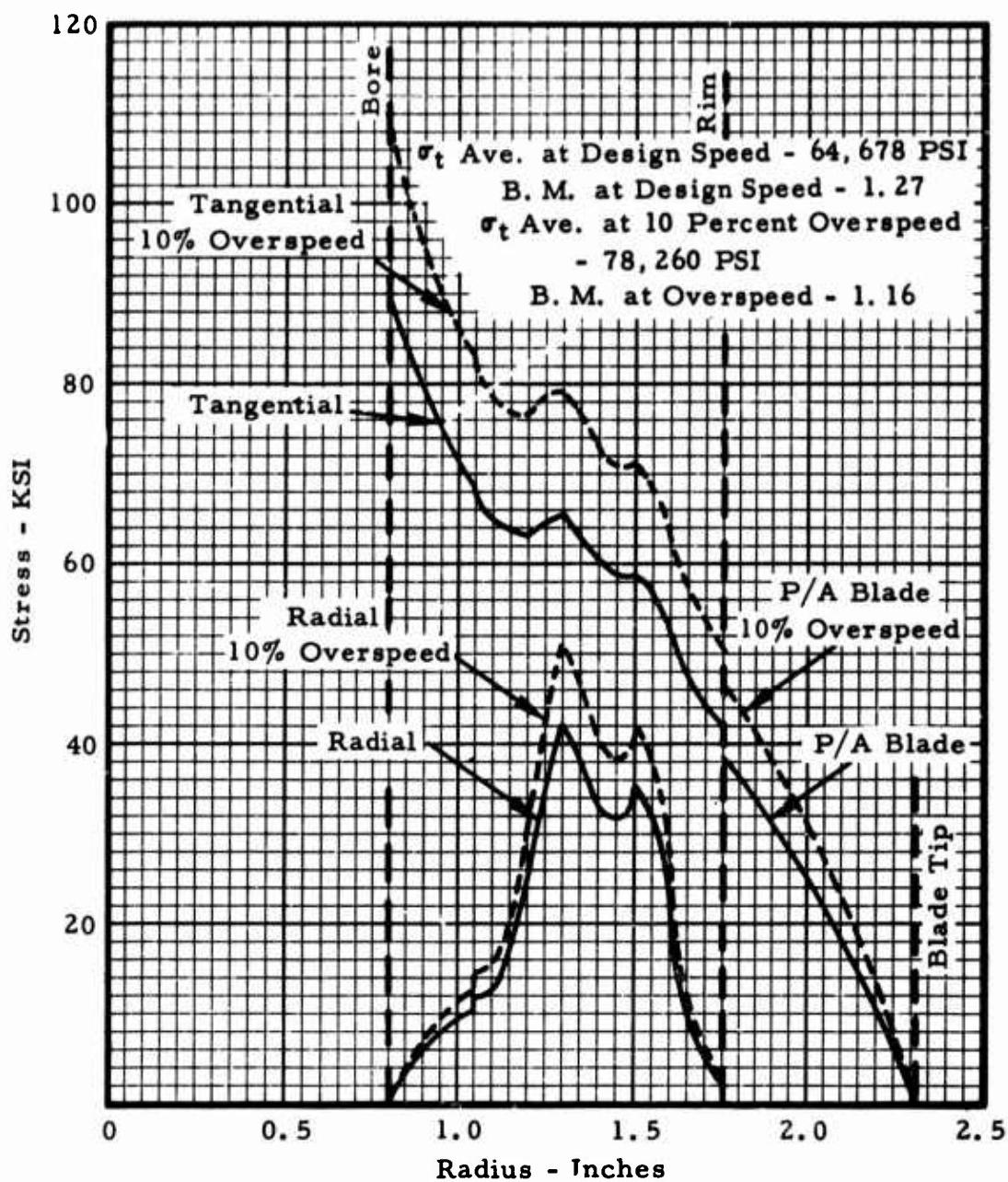


Figure IV-6. TS120 Axial Compressor Stresses at Design Speed and Ten Percent Overspeed.

## **Section IV**

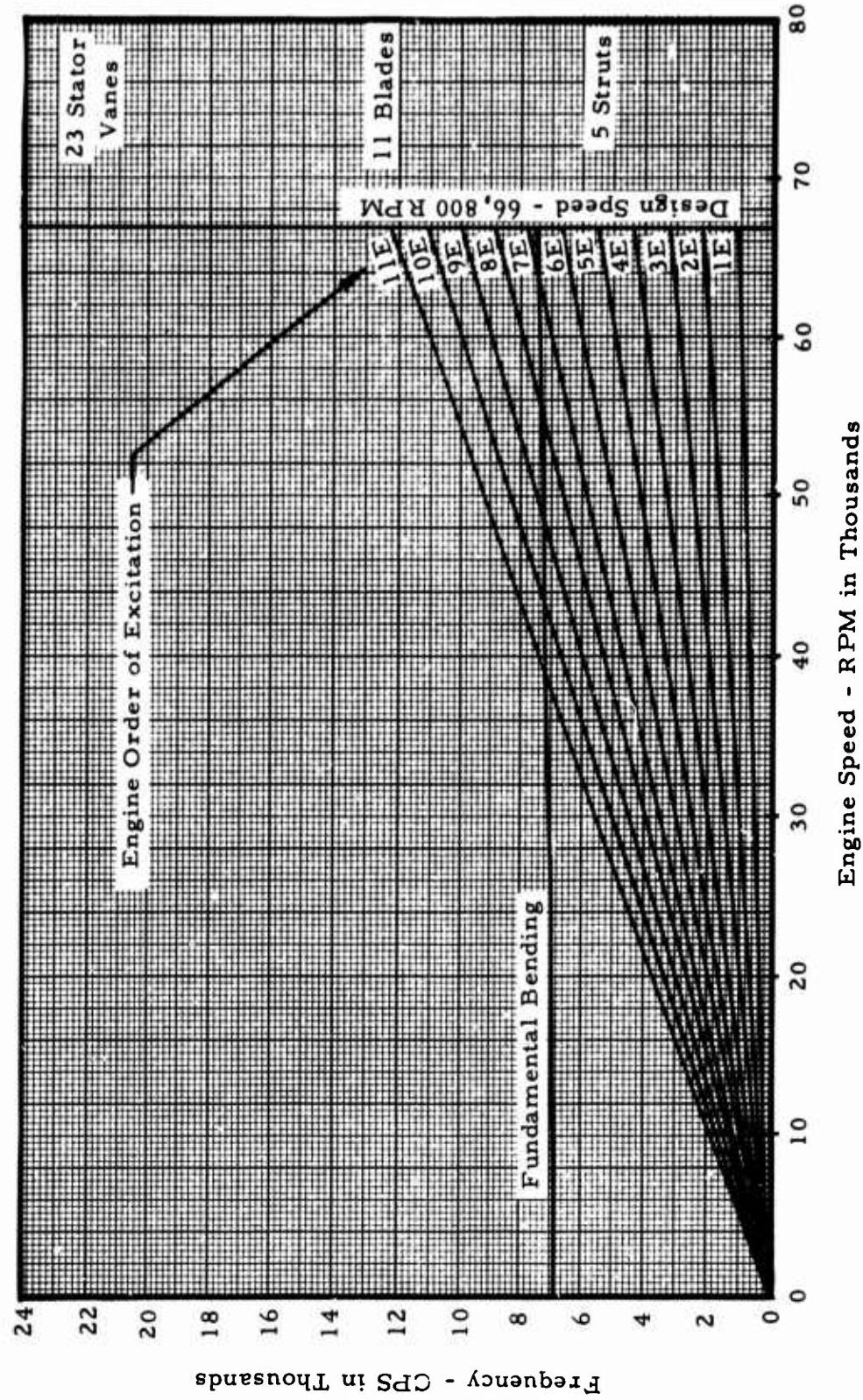


Figure IV-7. TS120 Axial Compressor Blade Interference Diagram.

Section IV

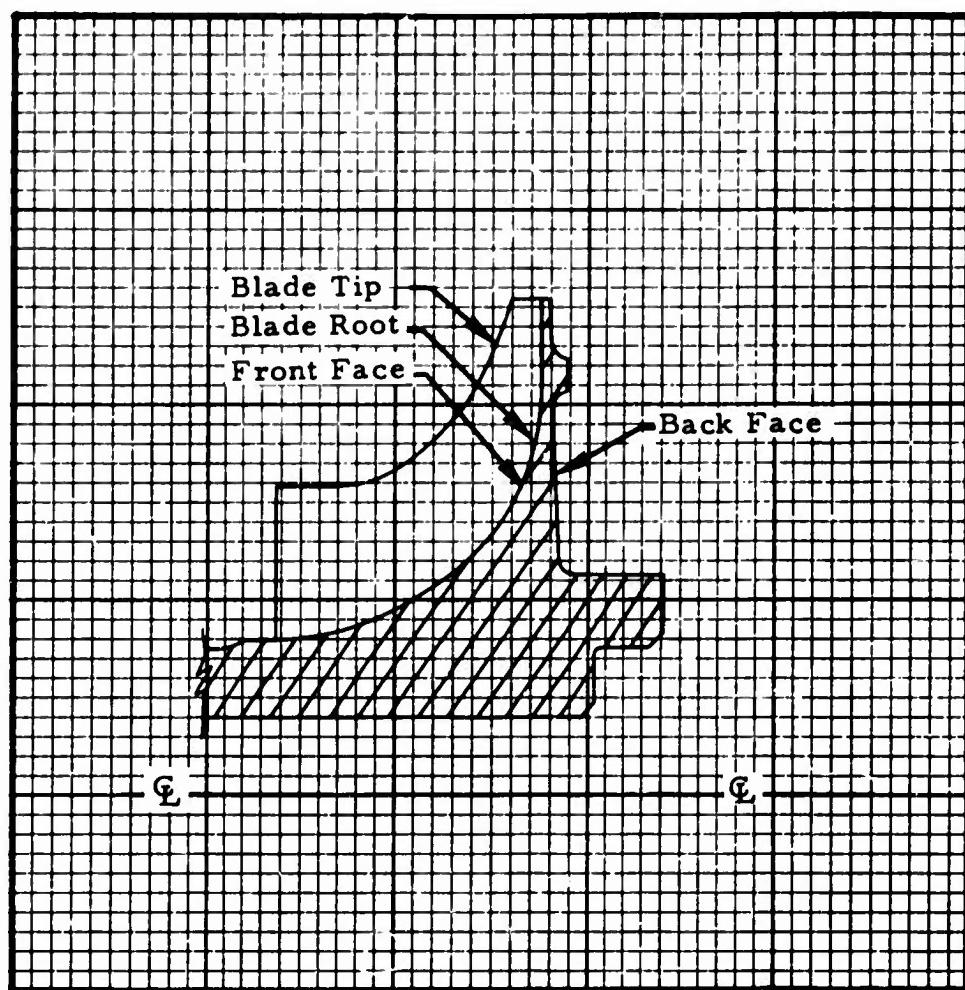
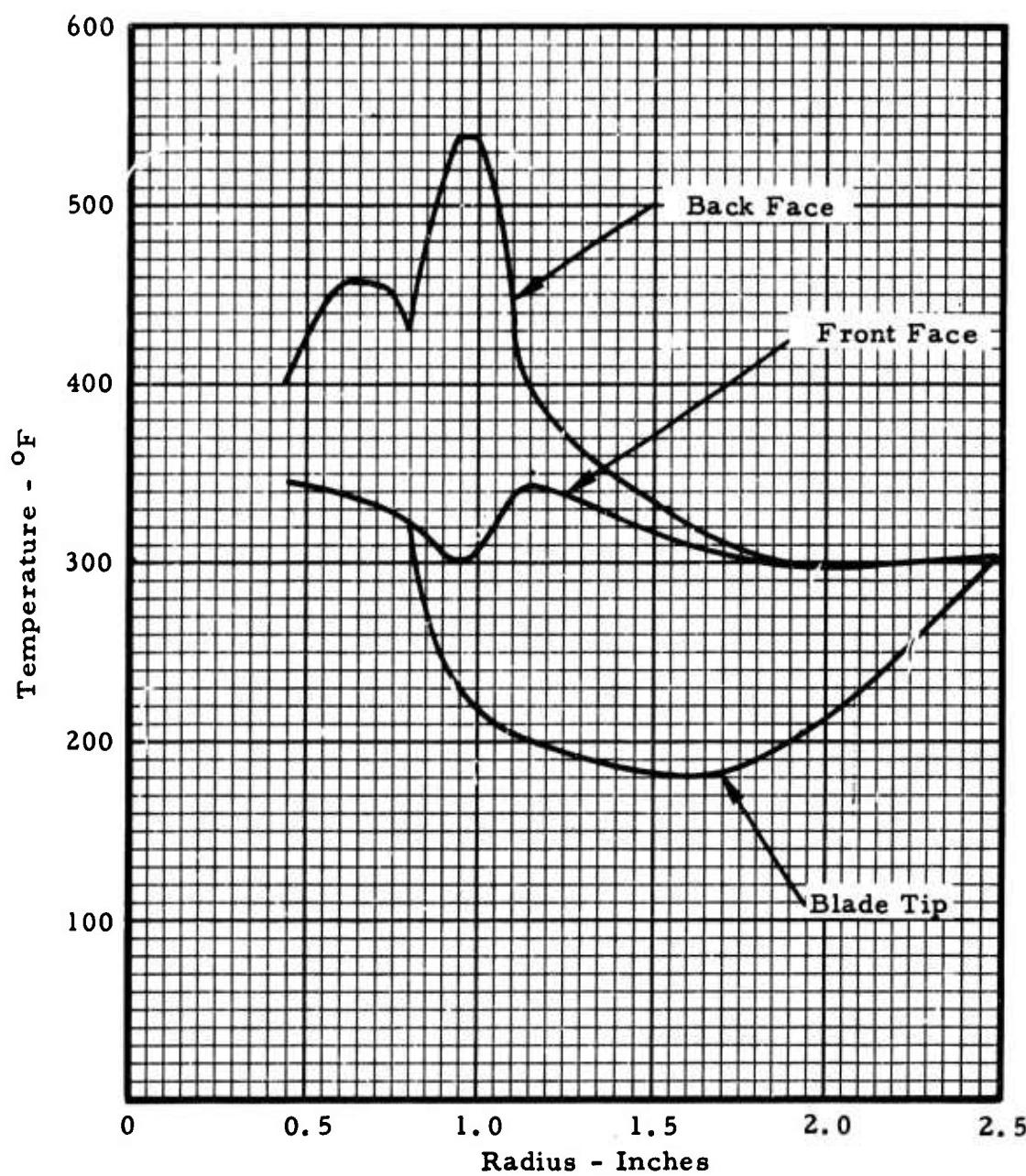


Figure IV-8. TS120 Radial Compressor.

**Section IV**



**Figure IV-9. TS120 Radial Compressor Estimated Temperature Distribution at Sea Level.**

**Section IV**

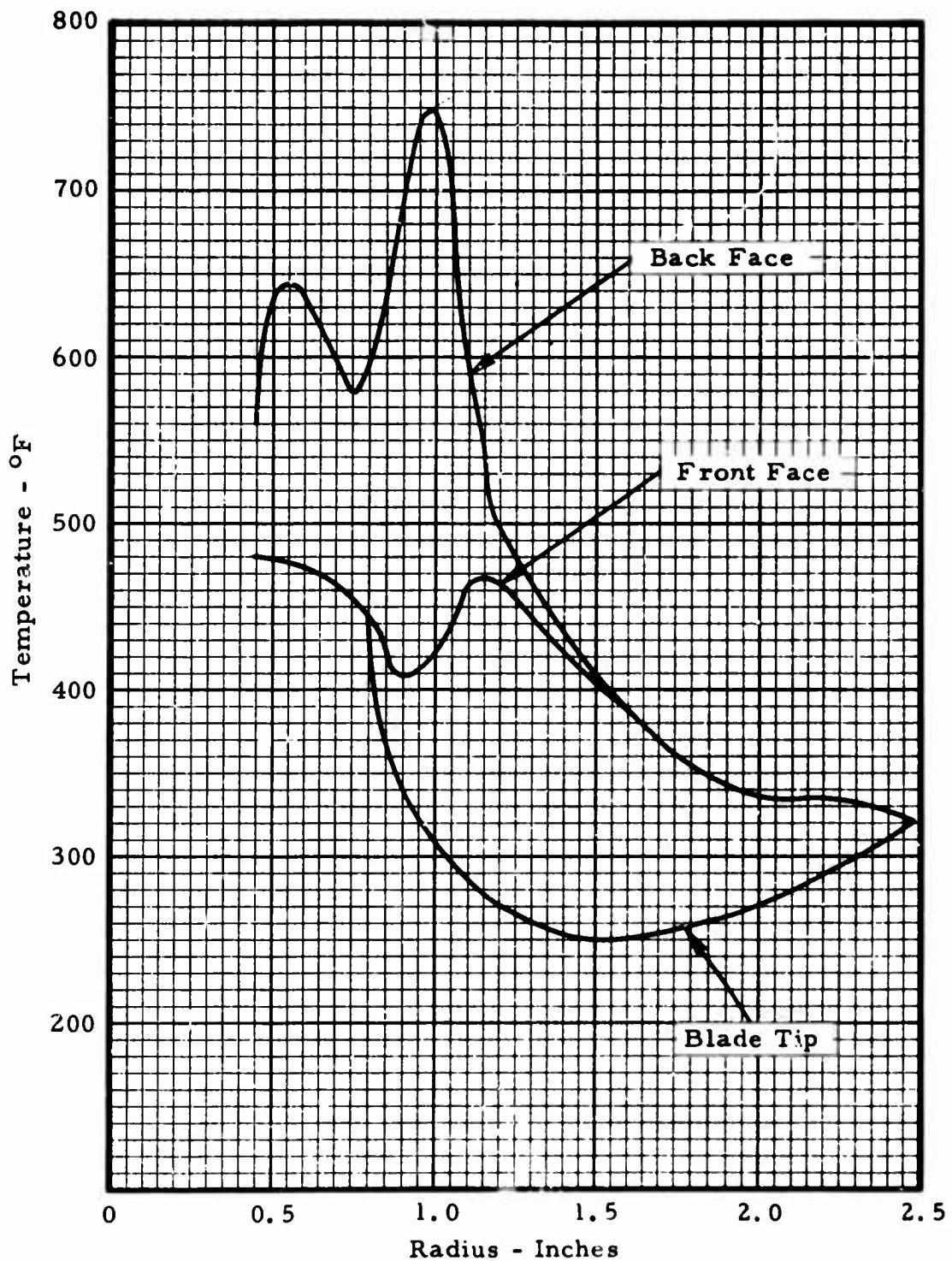


**Figure IV-10.** TS120 Radial Compressor Estimated Temperature Distribution at Altitude.

**Section IV**

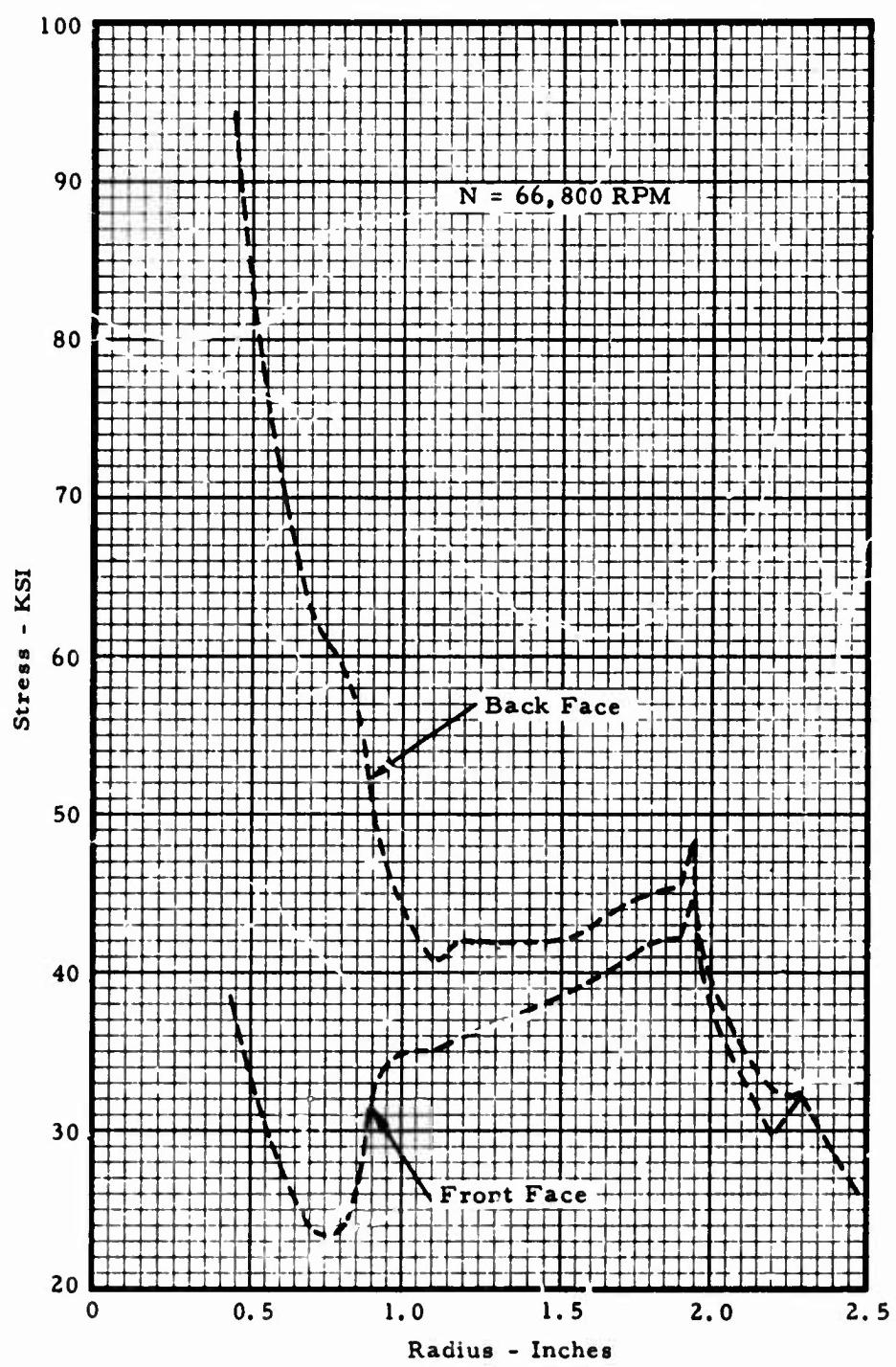
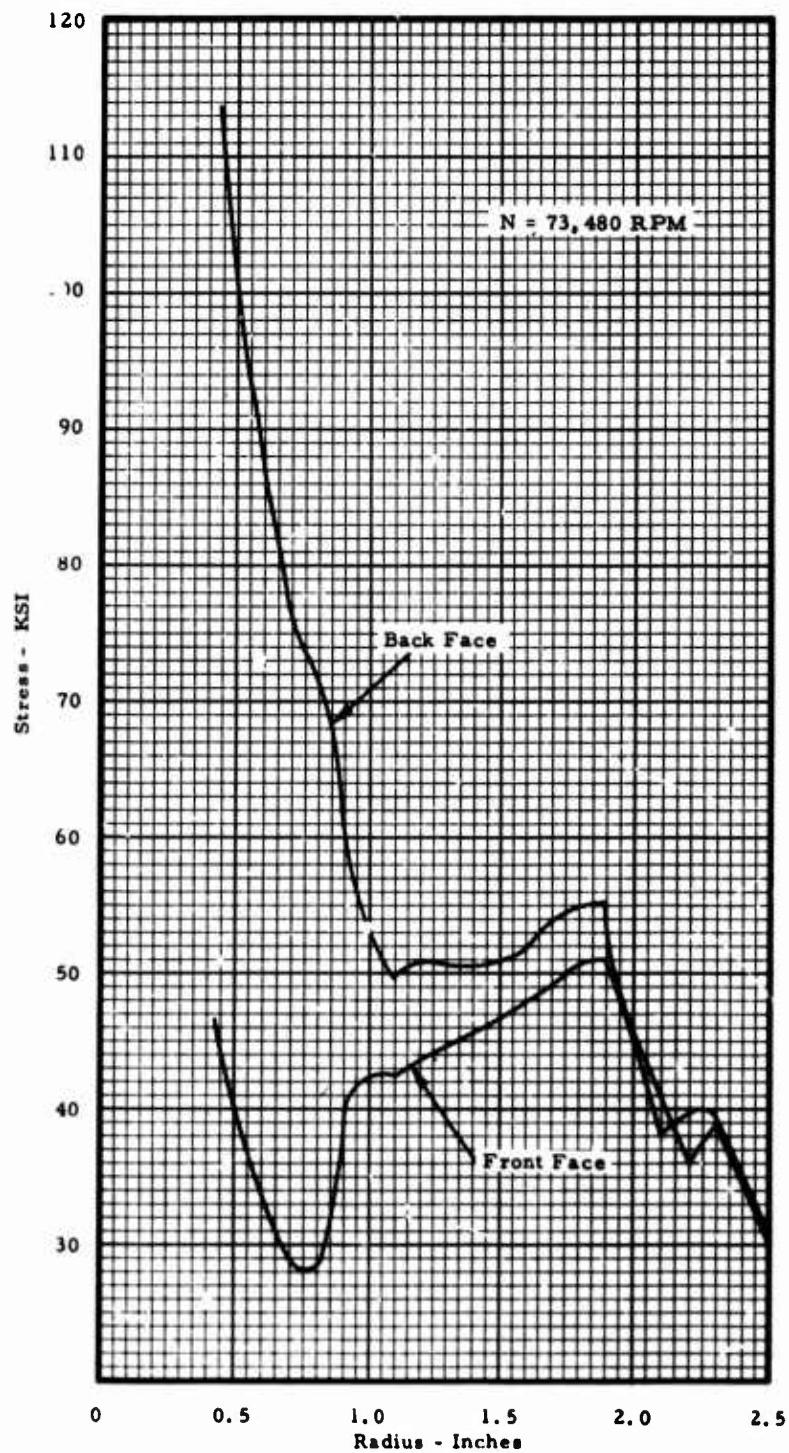


Figure IV-11. TS120 Radial Compressor Design Speed Tangential Stress (Cold).

**Section IV**



**Figure IV-12. TS120 Radial Compressor Tangential Stress (Cold).**

**Section IV**

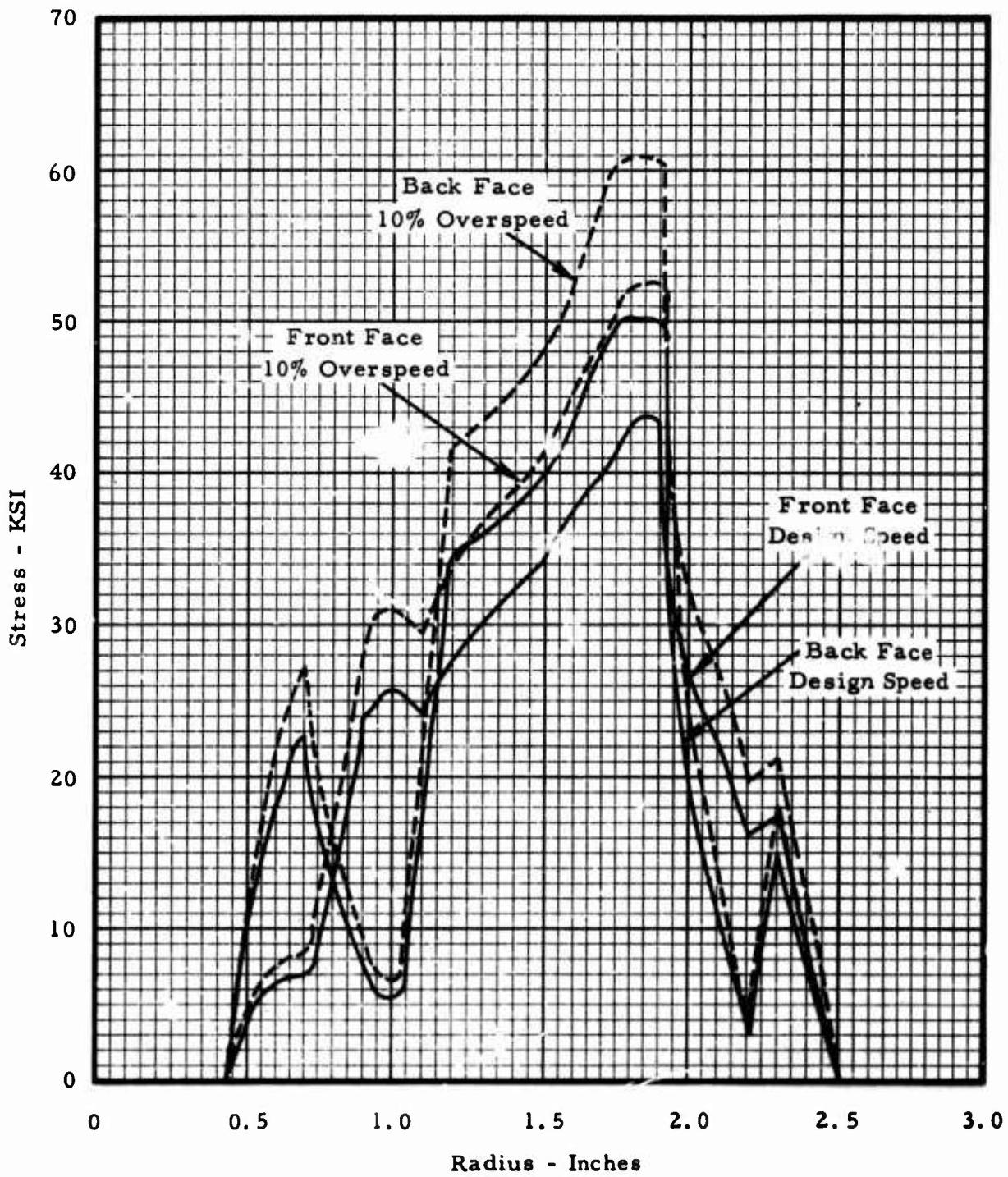


Figure IV-13. TS120 Radial Compressor Radial Stress (Cold).

Section IV

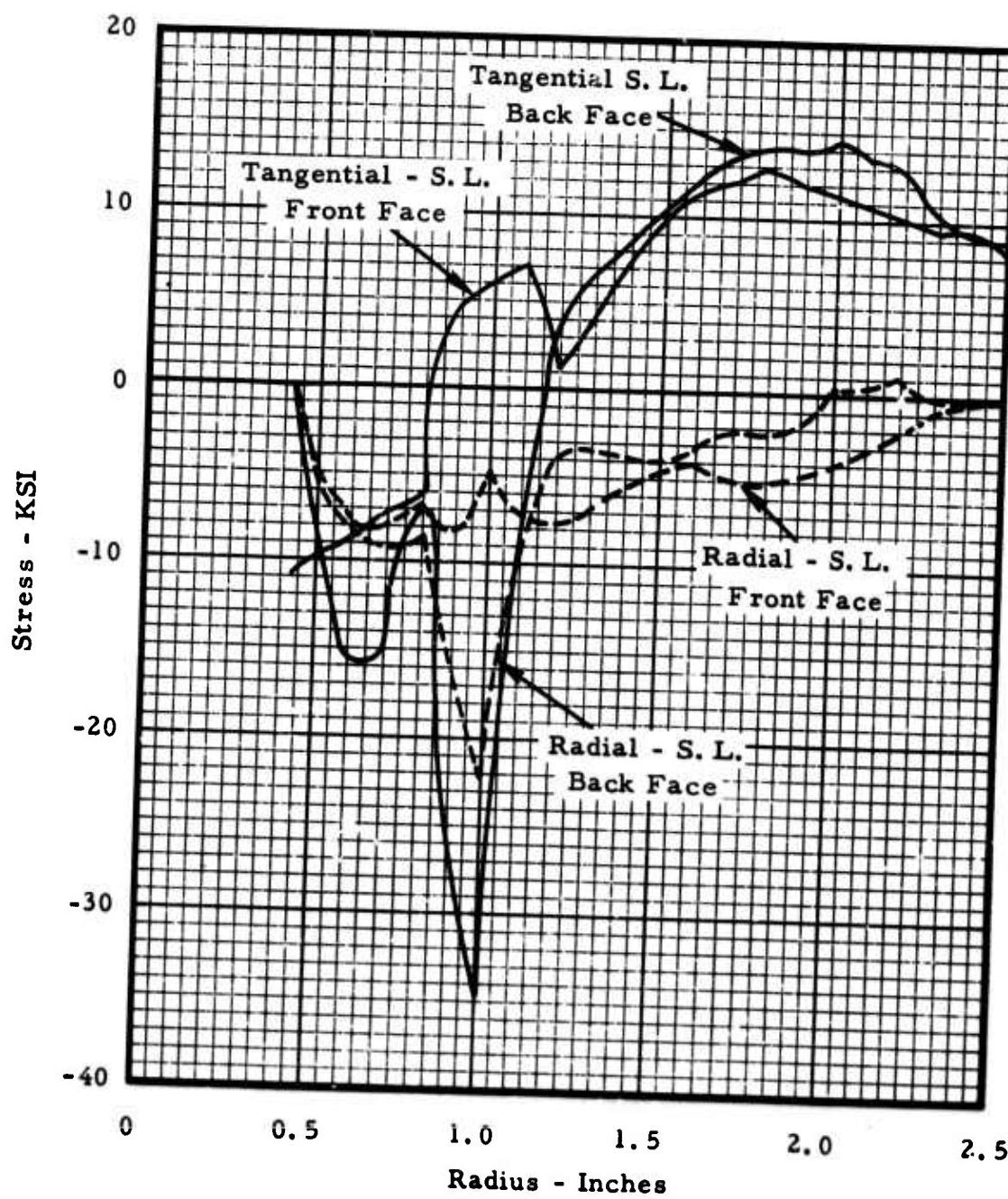
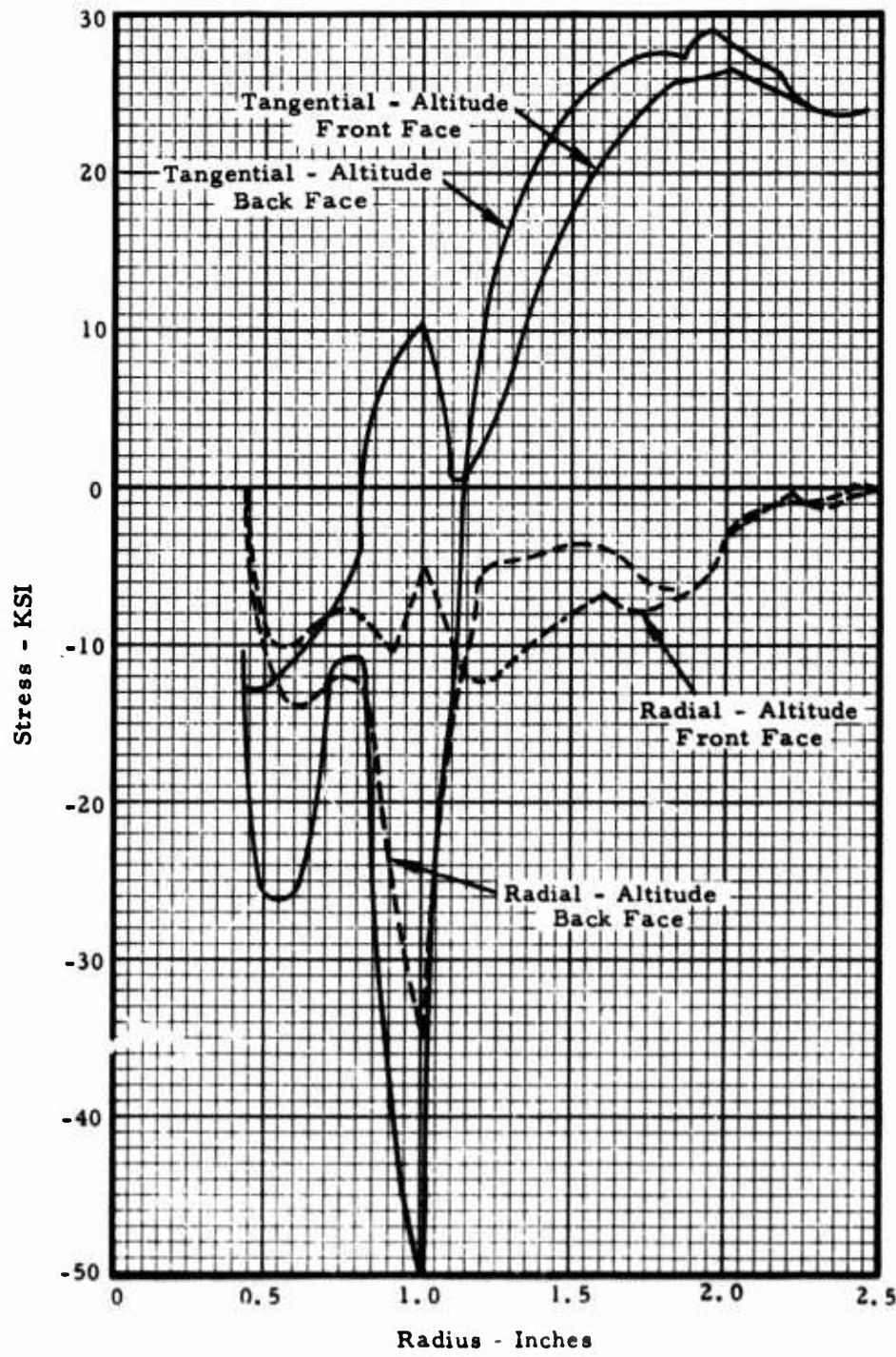


Figure IV-14. TSI20 Radial Compressor Thermal Stress, Sea Level.

**Section IV**



**Figure IV-15. TS120 Radial Compressor Thermal Stress, Altitude.**

## Section IV

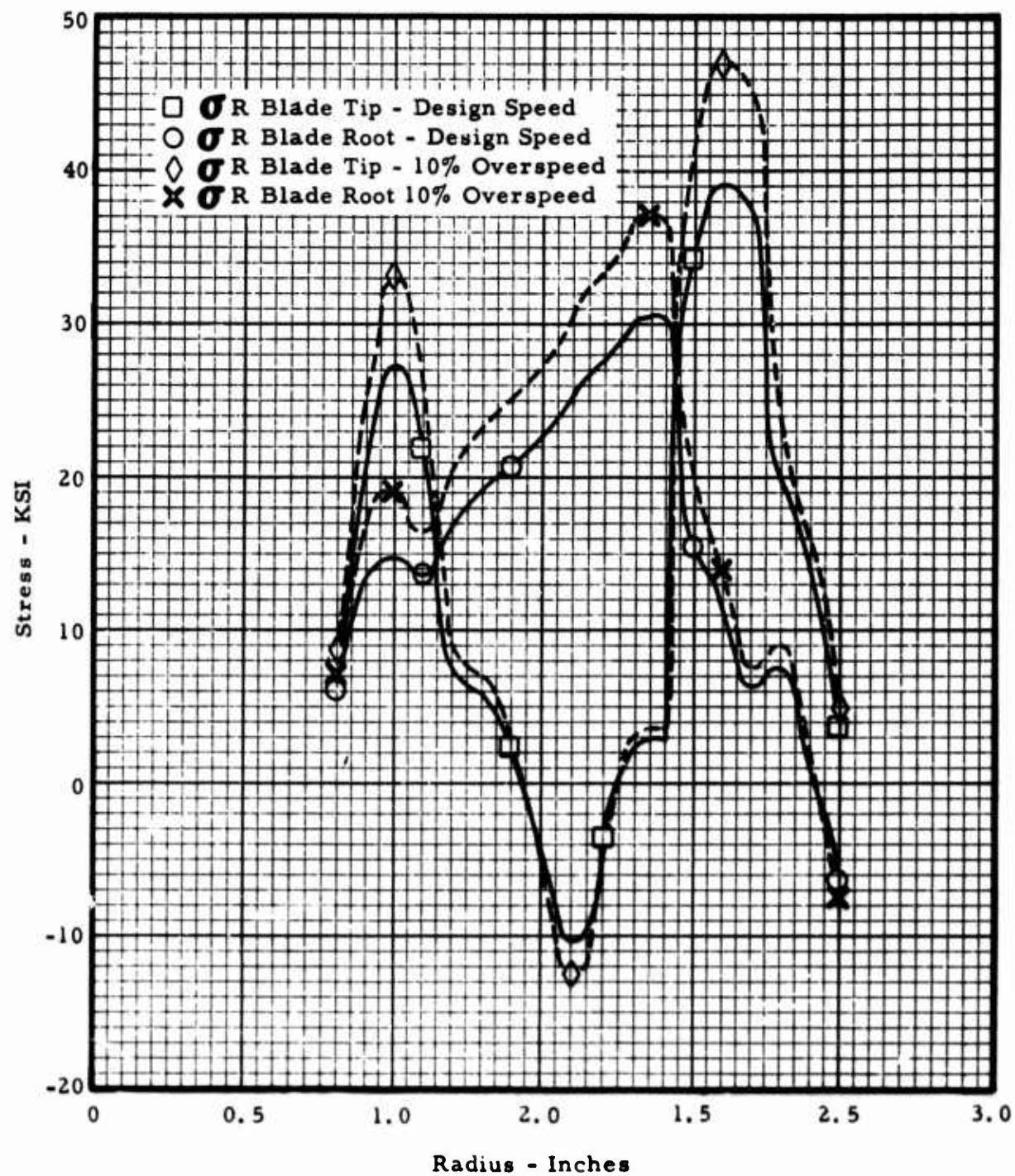


Figure IV-16. TS120 Radial Compressor Blade Radial Stress (Cold).

Section IV

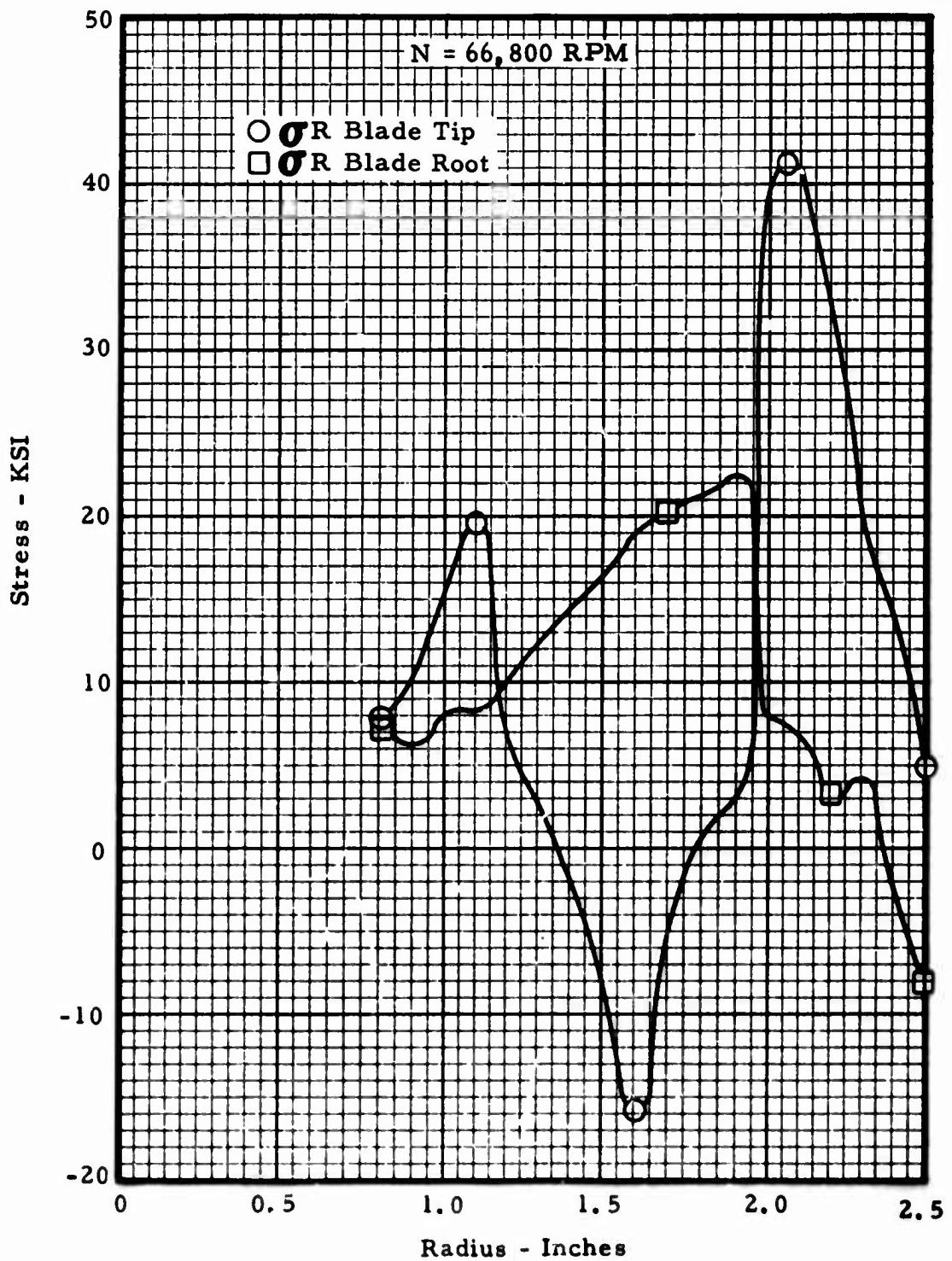


Figure IV-17. TS120 Radial Compressor Blade Radial Stresses,  
Design Speed (Sea Level).

Section IV

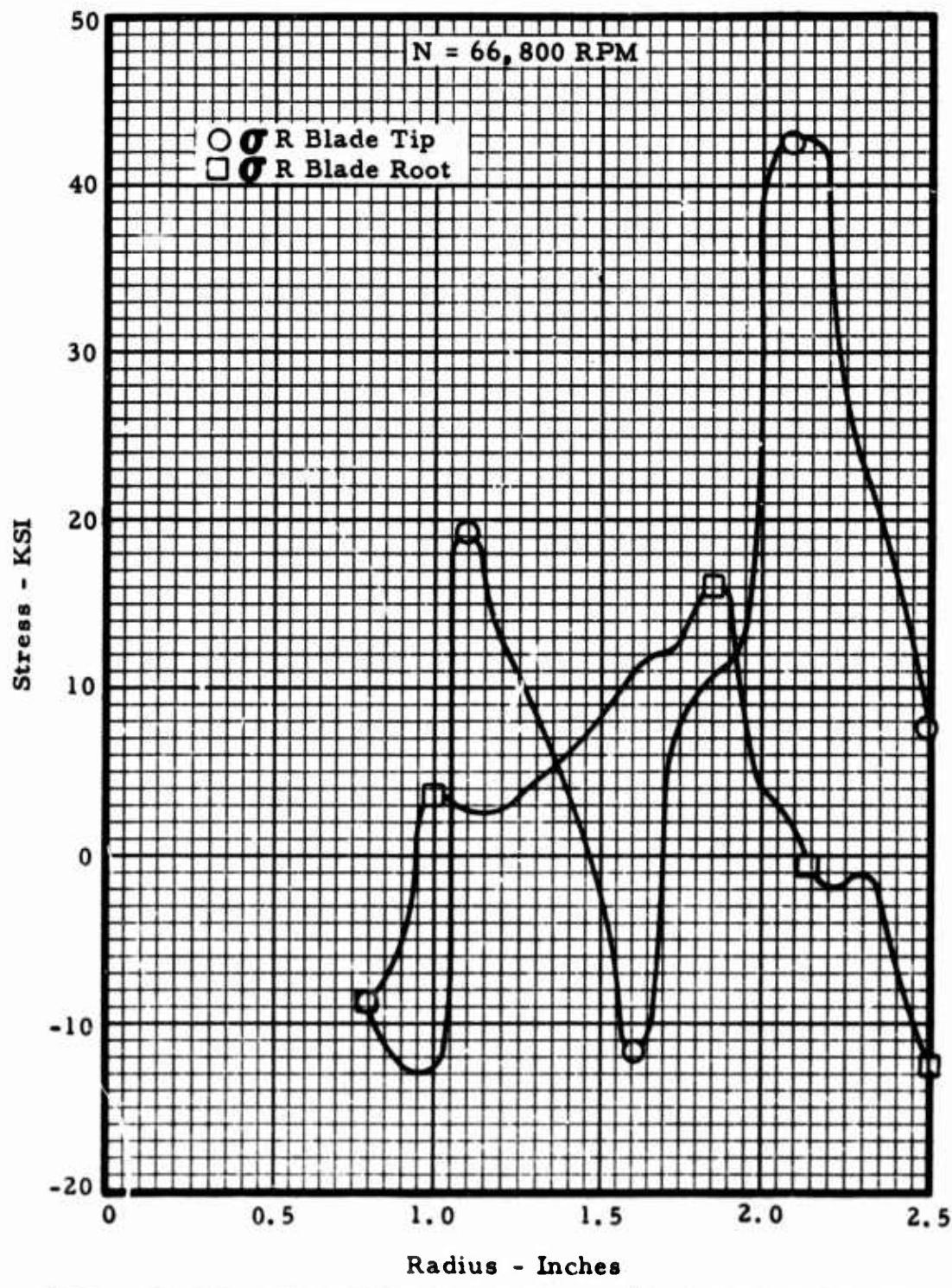


Figure IV-18. TS120 Radial Compressor Blade Radial Stresses,  
Design Speed (Altitude).

Section IV

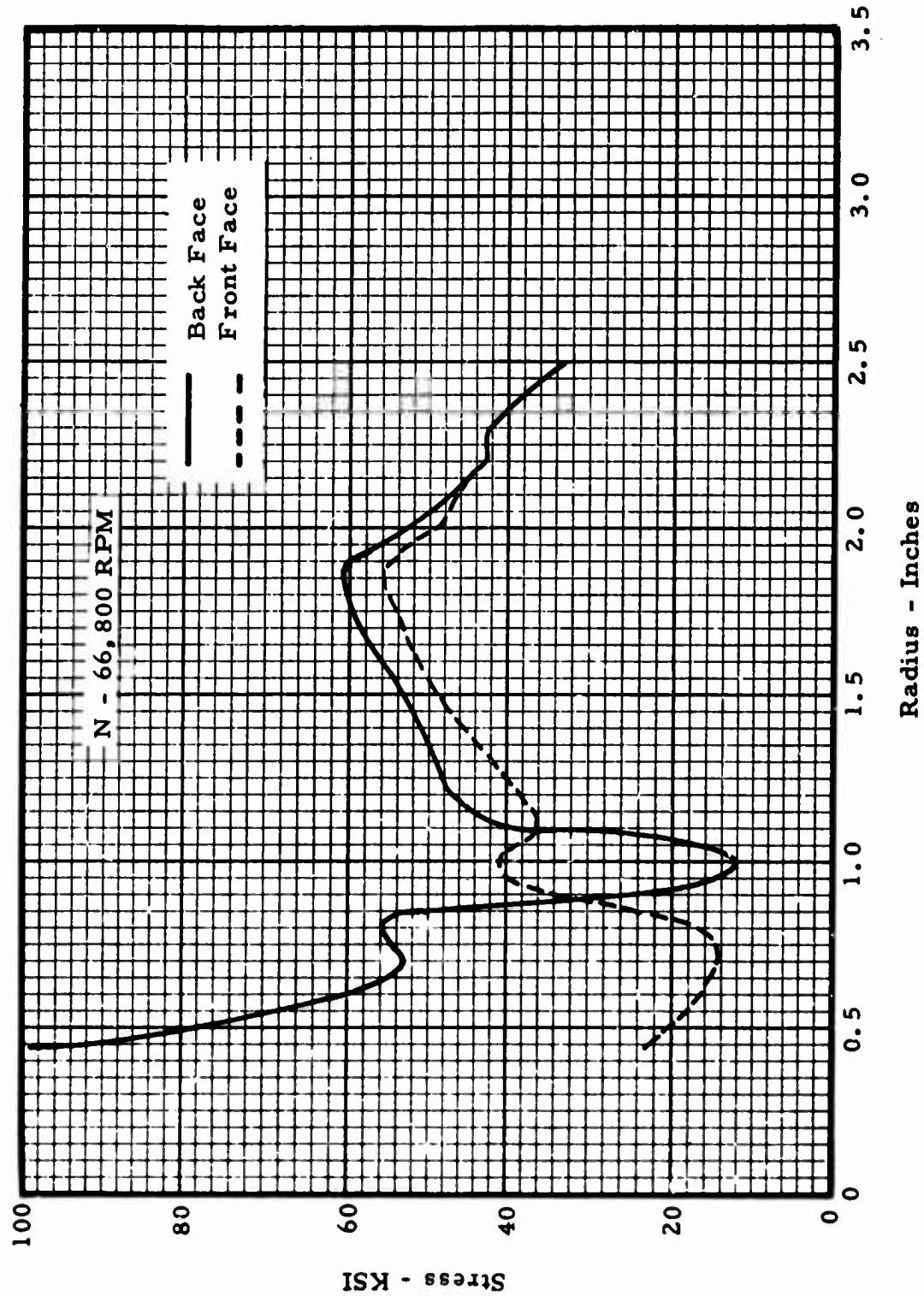


Figure IV-15. TS120 Radial Compressor Disc Tangential Stress Design Speed (Sea Level).

Section IV

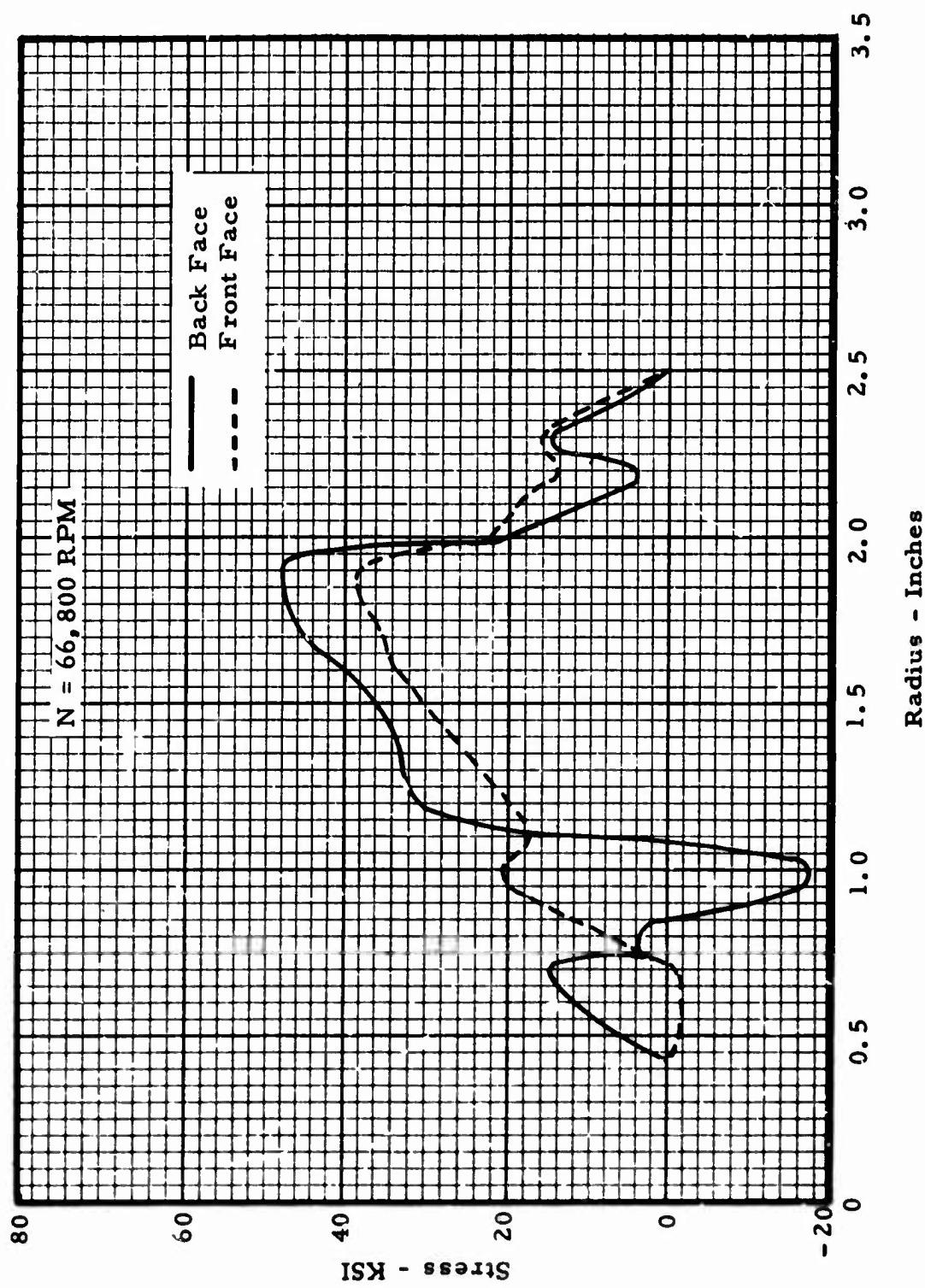
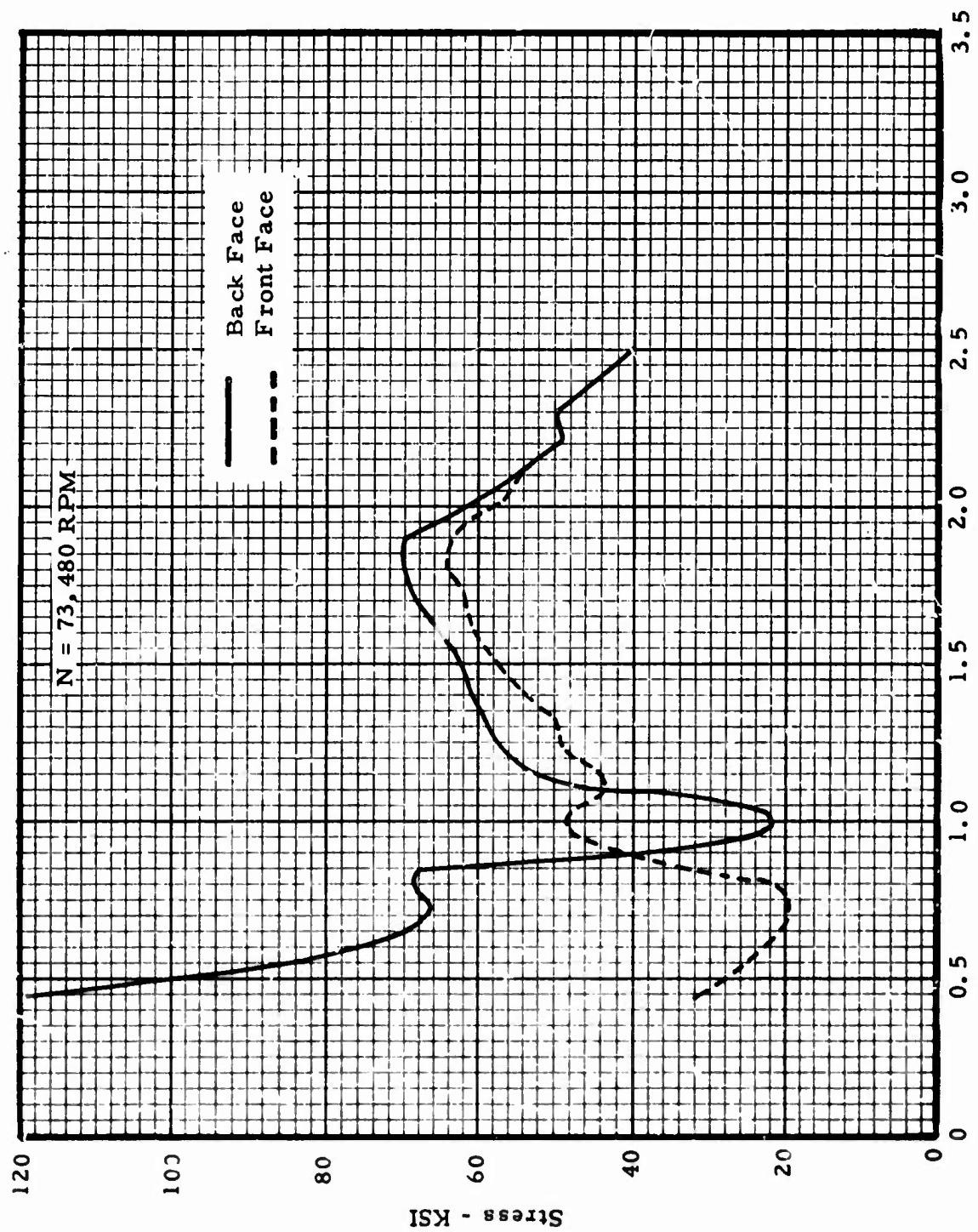


Figure IV-20. TS120 Radial Compressor Disc Radial Stress Design Speed  
(Sea Level).

**Section IV**



**Figure IV-21. TS120 Radial Compressor Disc Tangential Stress Ten Percent Overspeed (Sea Level).**

## Section IV

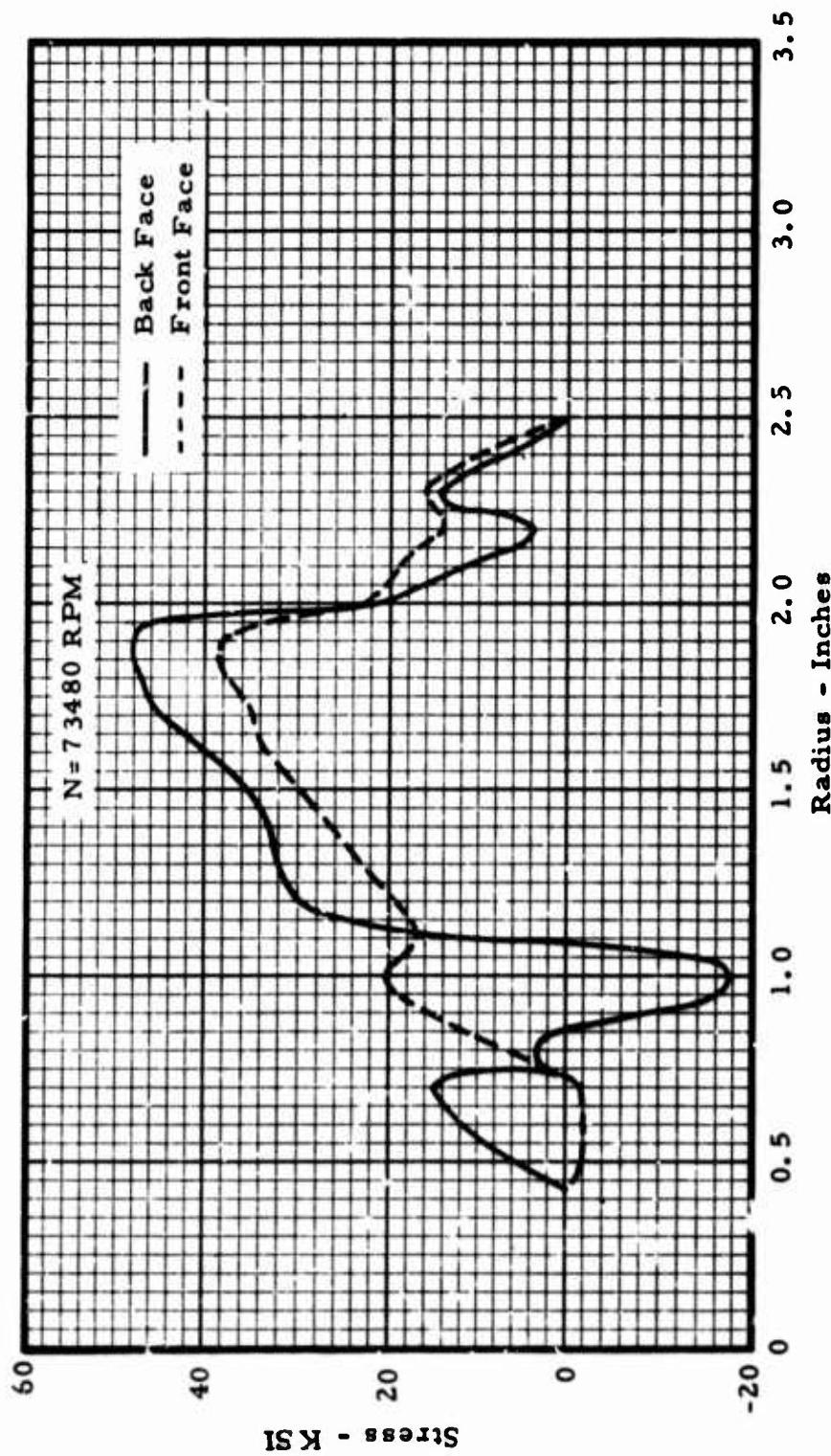


Figure IV-22. TSI20 Radial Compressor Disc Radial Stress Ten Percent Overspeed (Sea Level).

## Section IV

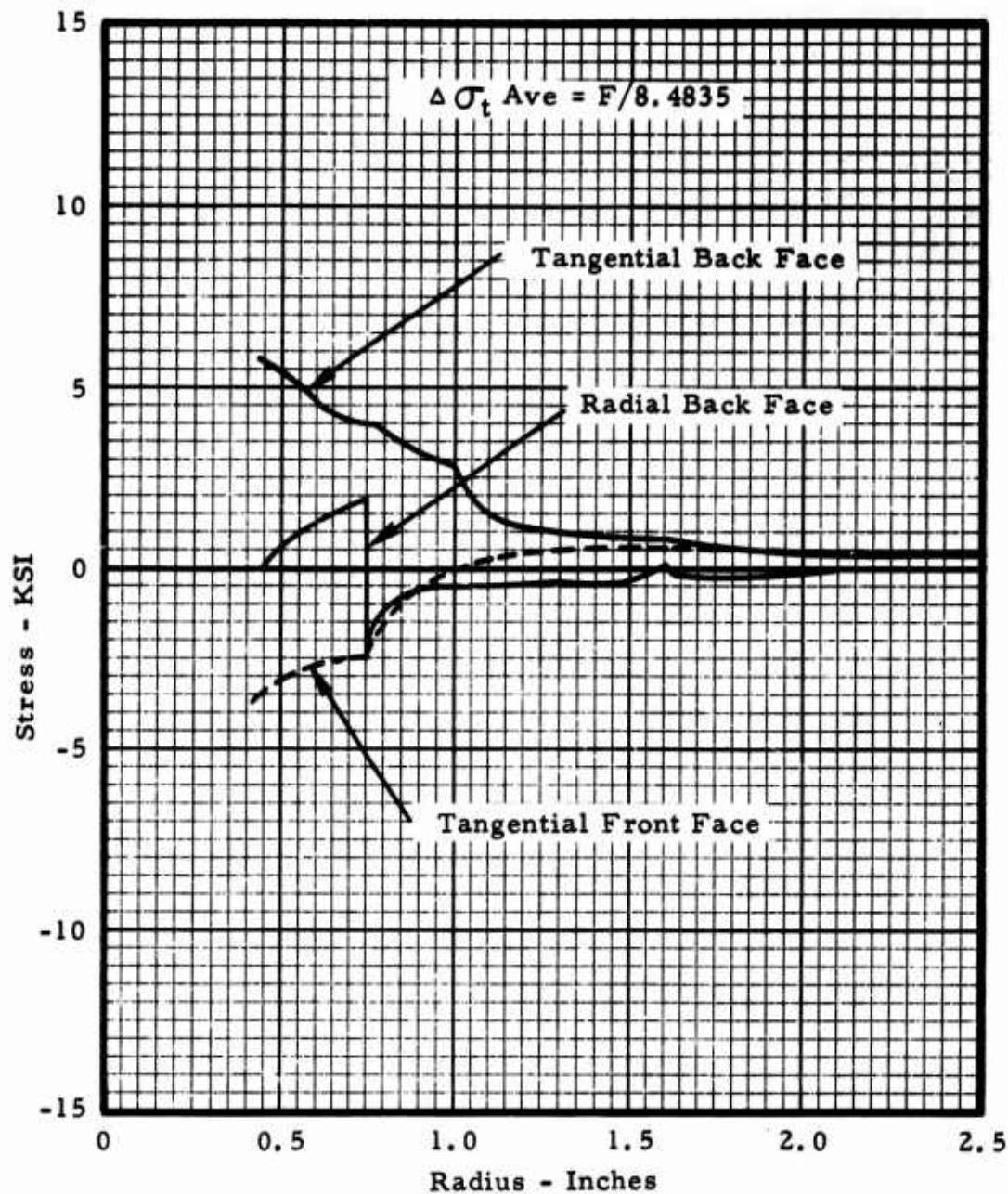
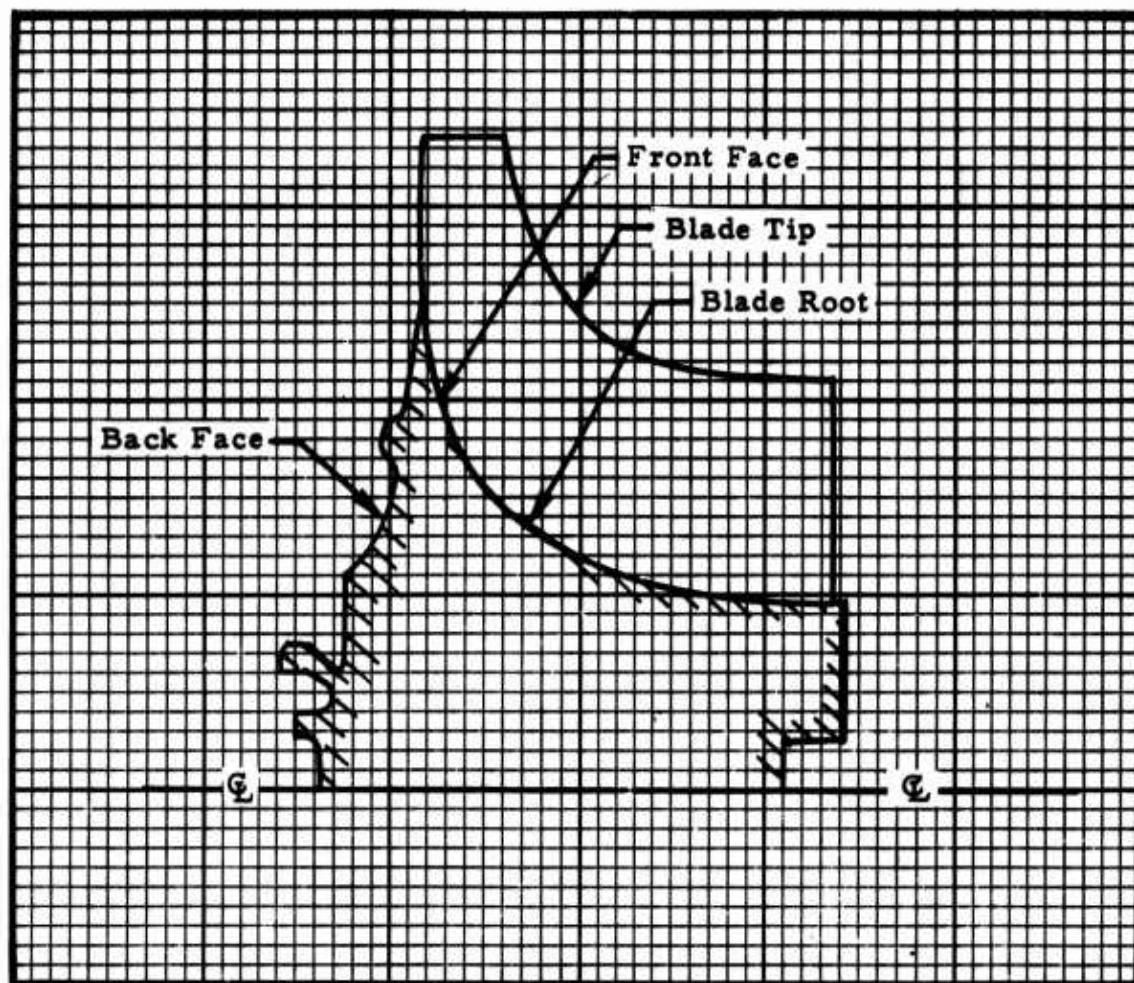


Figure IV-23. TS120 Tadial Compressor Radial and Tangential Stress for a 10,000 Pound Load at 0.750 Radius on Back Face.

**Section IV**



**Figure IV-24. TS120 Radial Turbine.**

**Section IV**

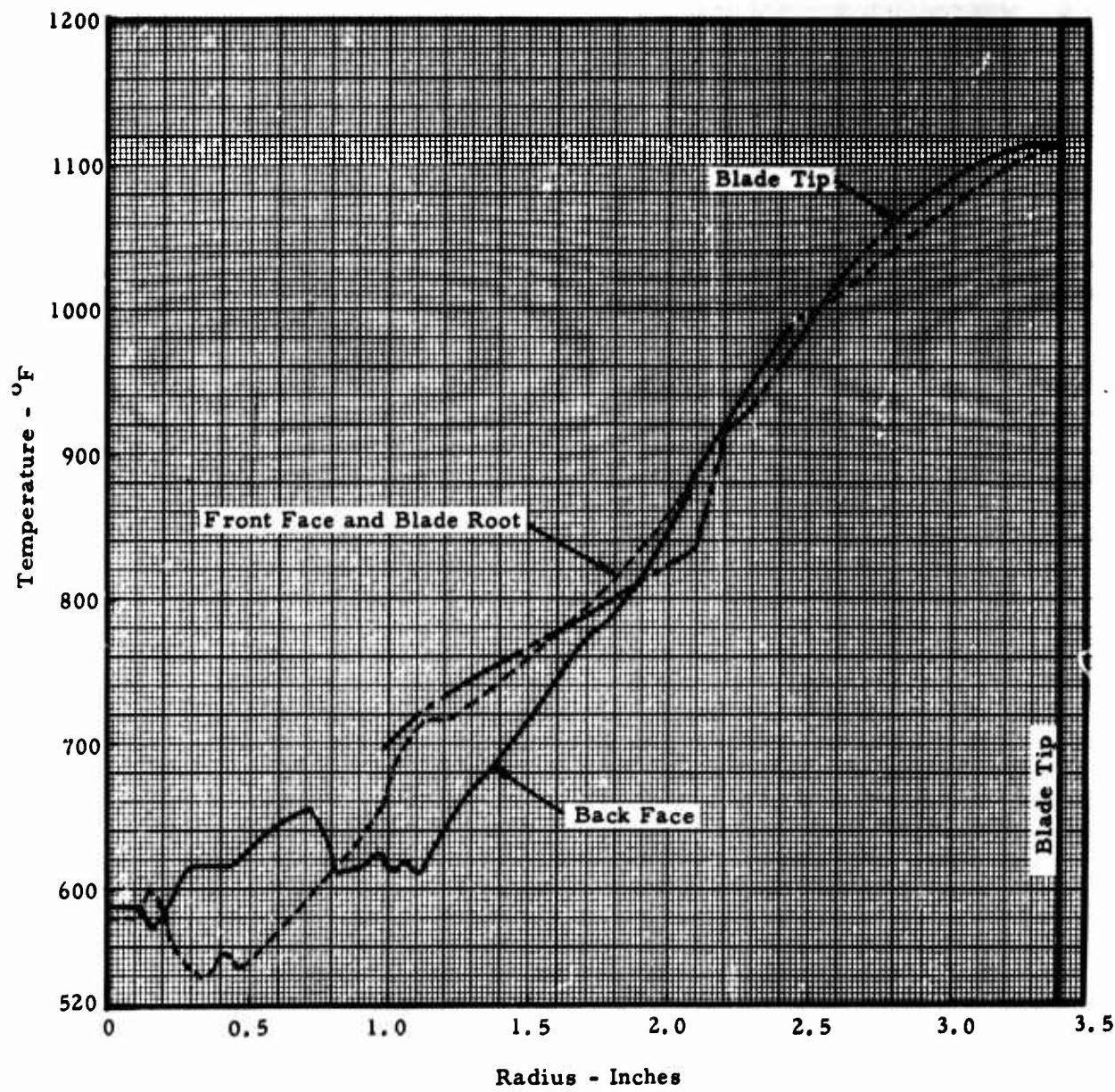


**Figure IV-25. TS120 Radial Turbine Estimated Temperature Distribution at Sea Level.**

## Section IV

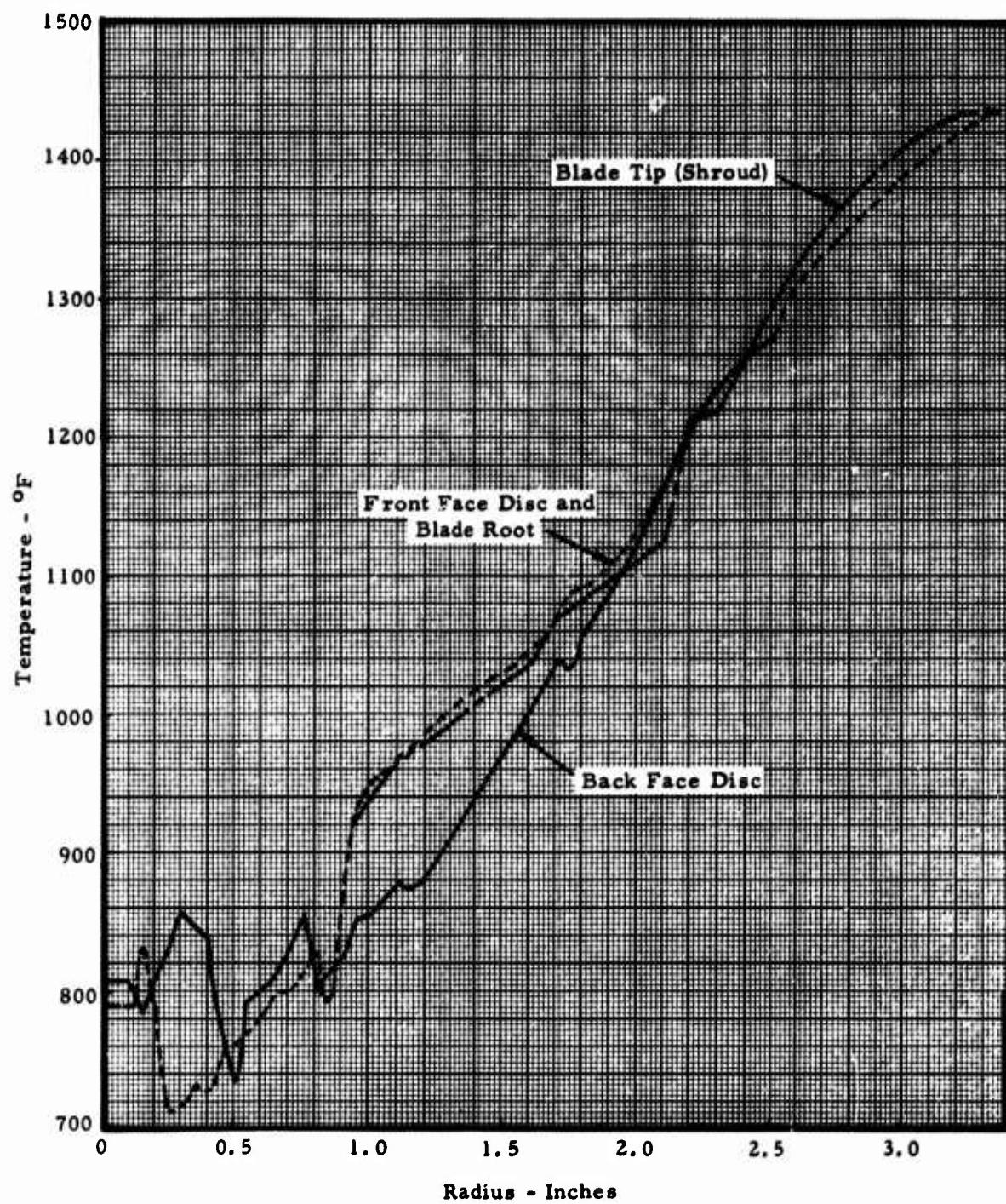


Figure IV-26. TS120 Radial Turbine Estimated Temperature Distribution at Altitude.

**Section IV**

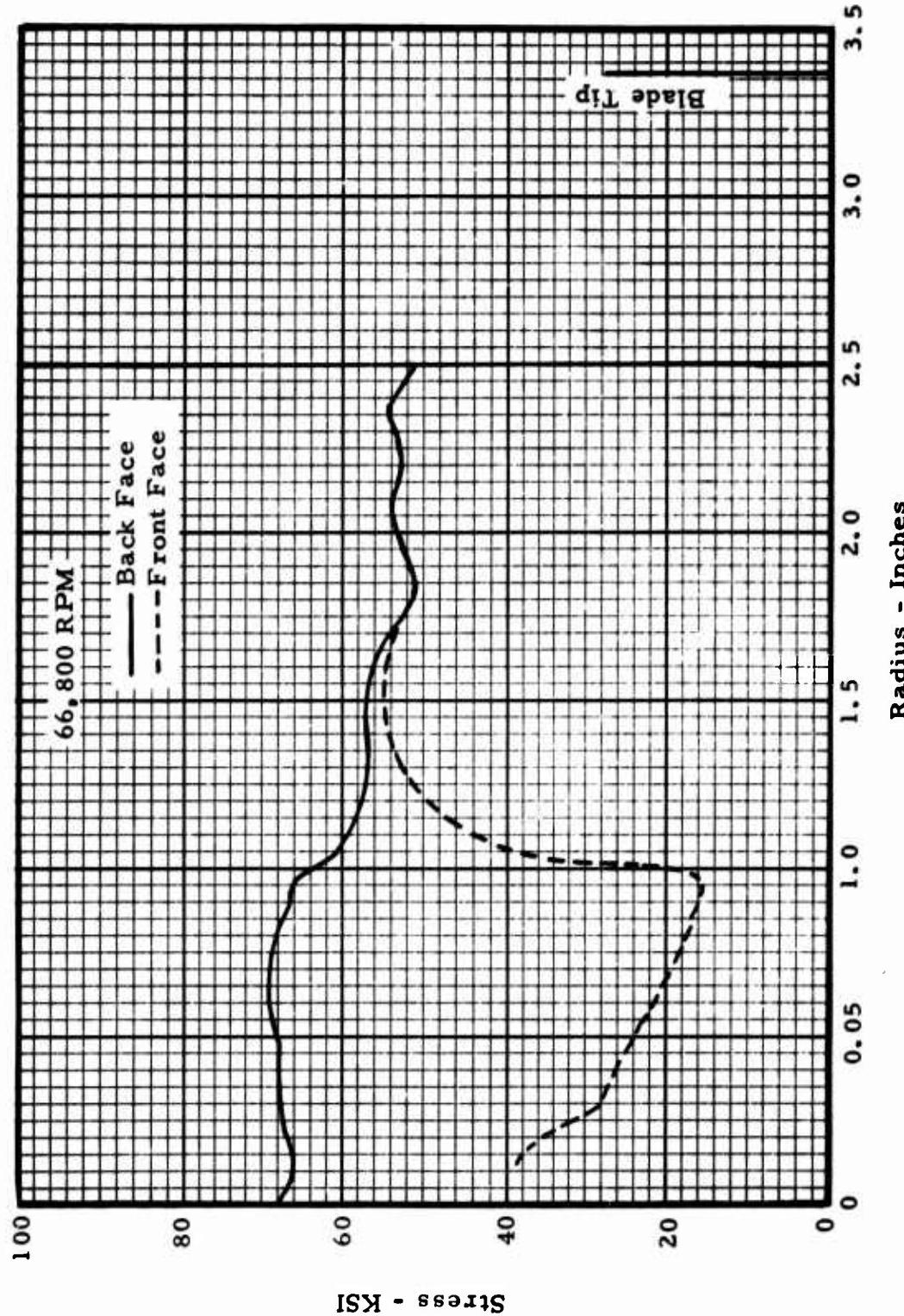


Figure IV-27. TSI20 Radial Turbine Disc Tangential Stresses Design Speed (Cold).

**Section IV**

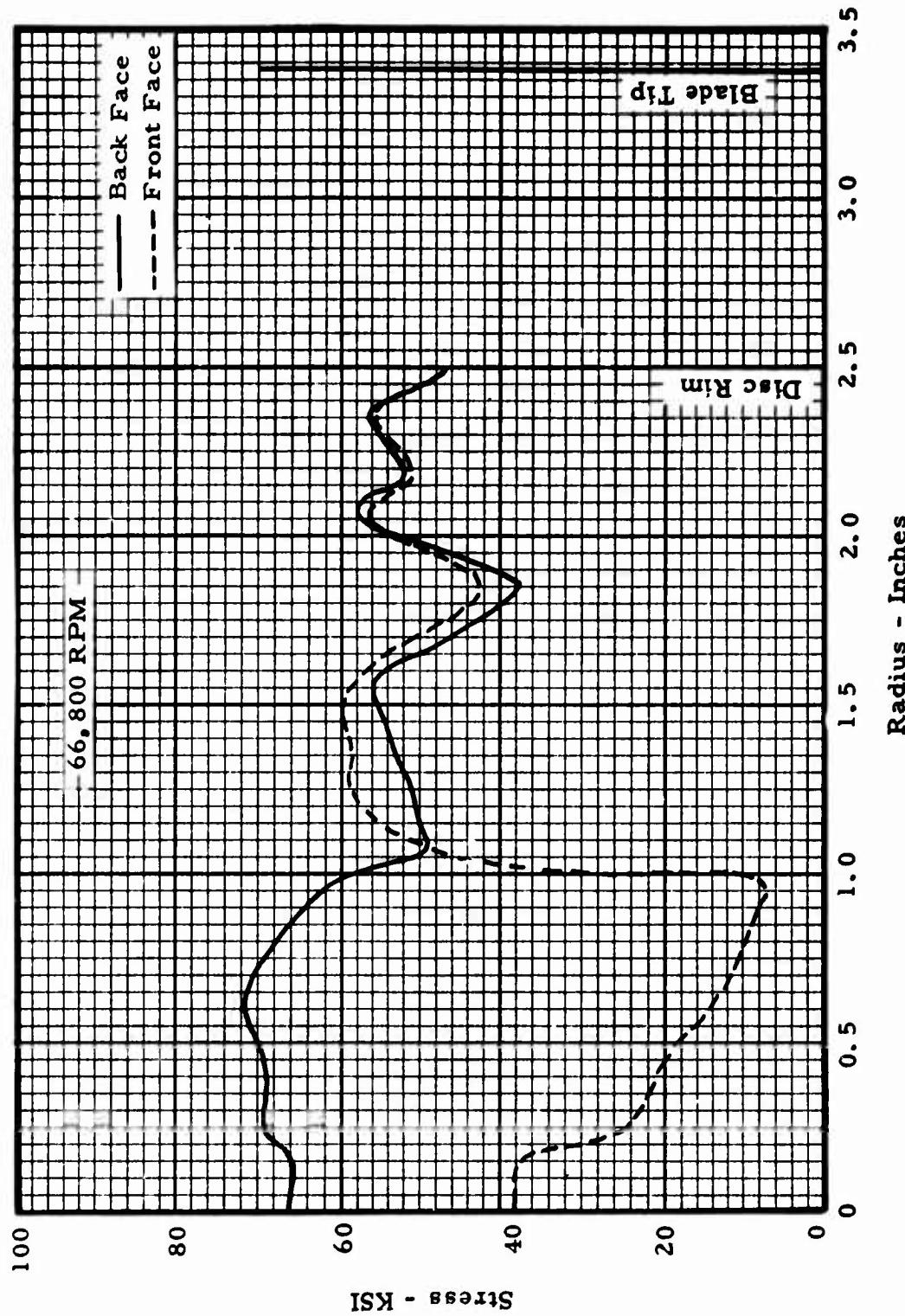


Figure IV-28. TS120 Radial Turbine Disc Radial Stresses Design Speed (Cold).

**Section IV**

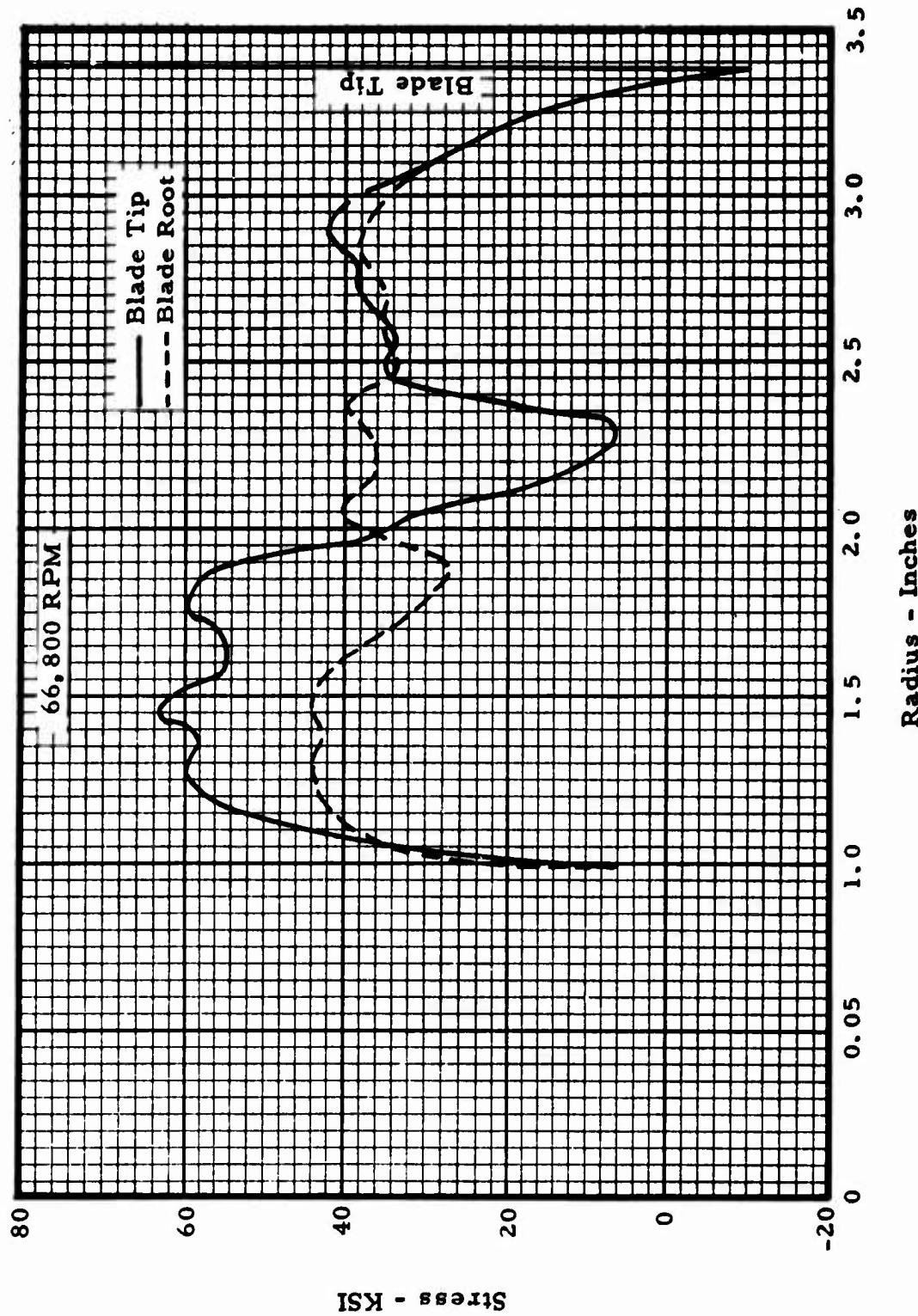


Figure IV-29. TSI20 Radial Turbine Blade Radial Stresses Design Speed (Cold).

## Section IV

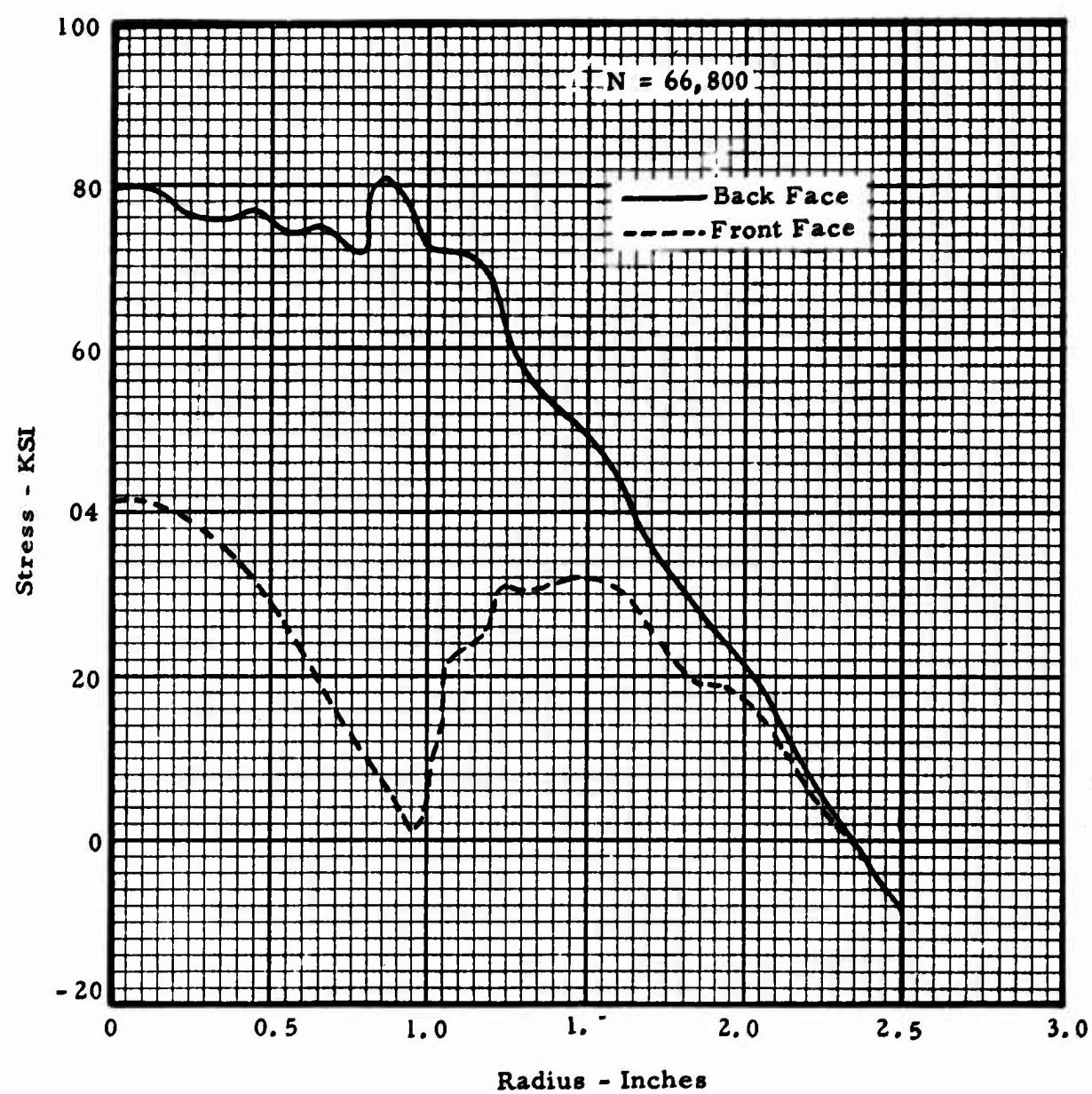


Figure IV-30. TS120 Radial Turbine Disc Tangential Stresses  
Design Speed (Sea Level).

Section IV

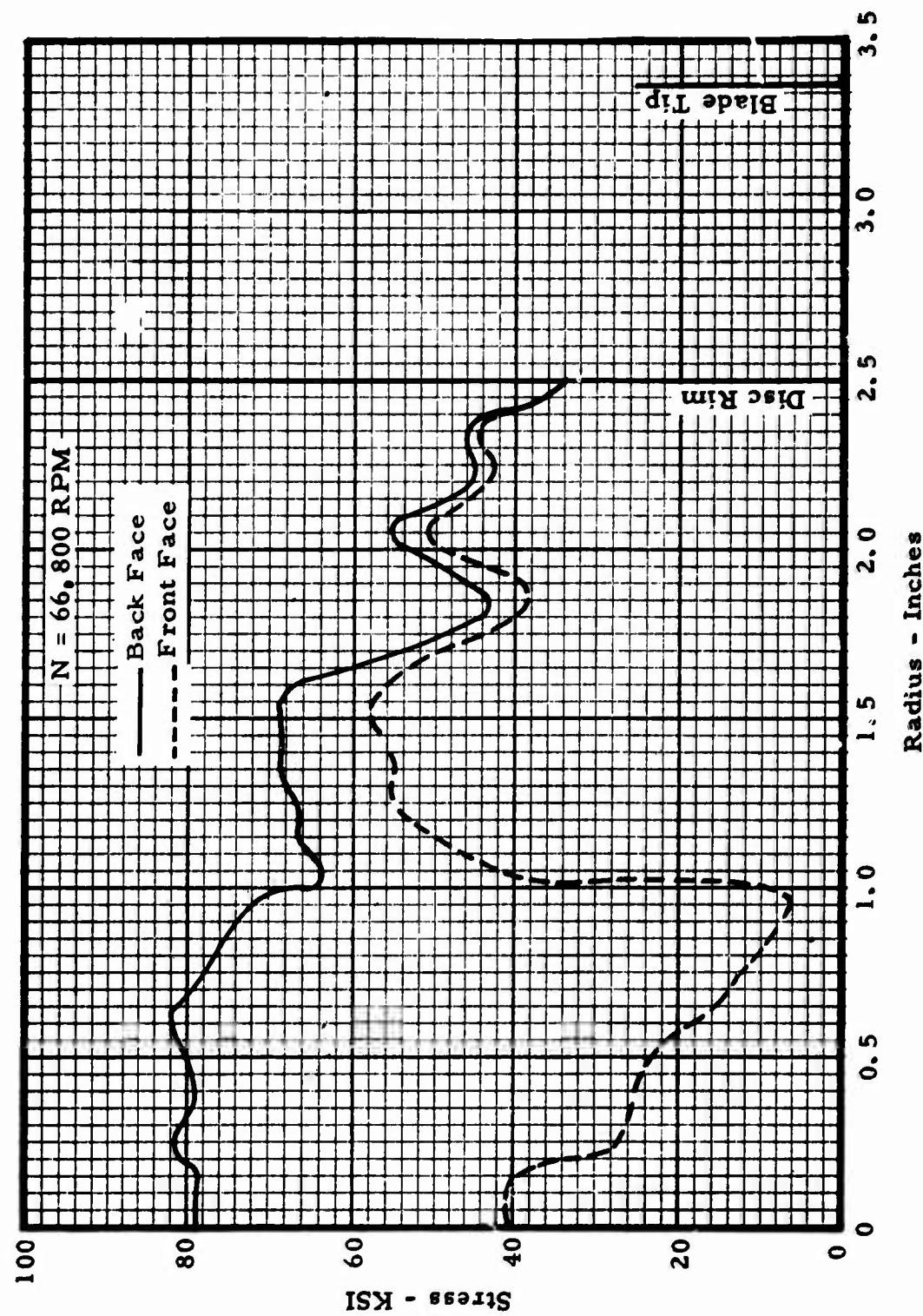


Figure IV-31. TS120 Radial Turbine Disc Radial Stresses Design Speed (Sea Level).

**Section IV**

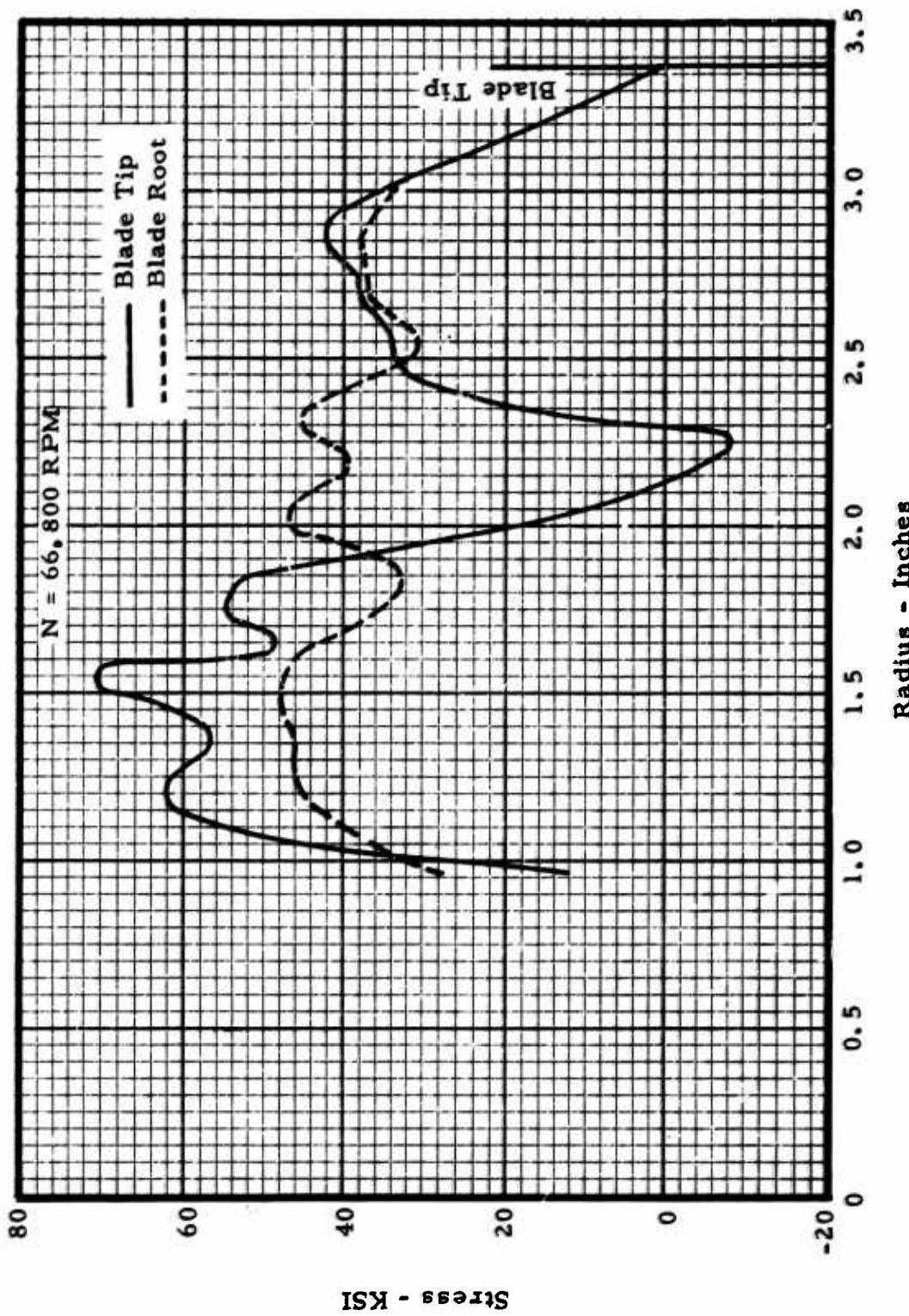


Figure IV-32. TS120 Radial Turbine Blade Radial Stresses Design Speed (Sea Level).

## Section IV

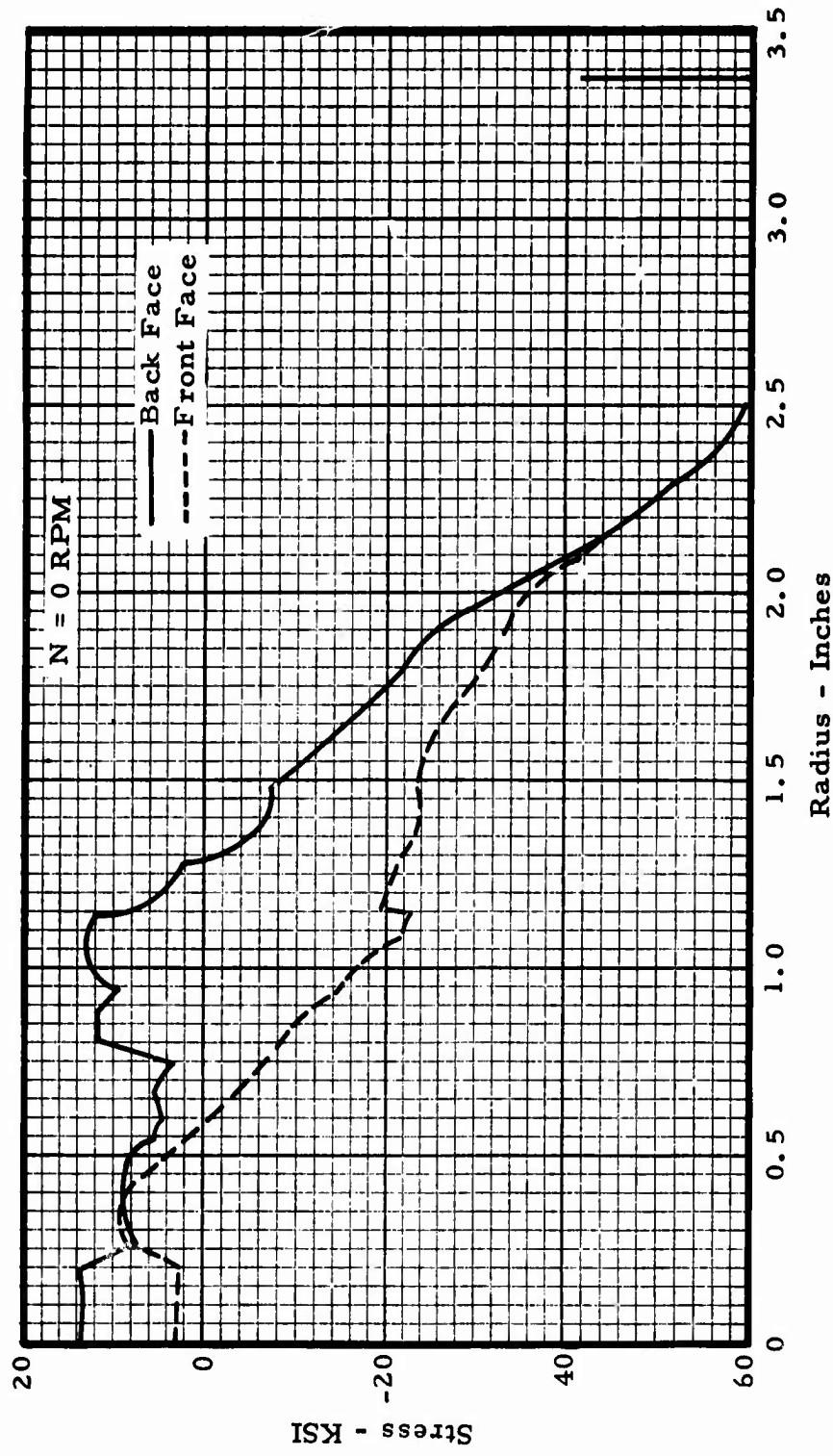
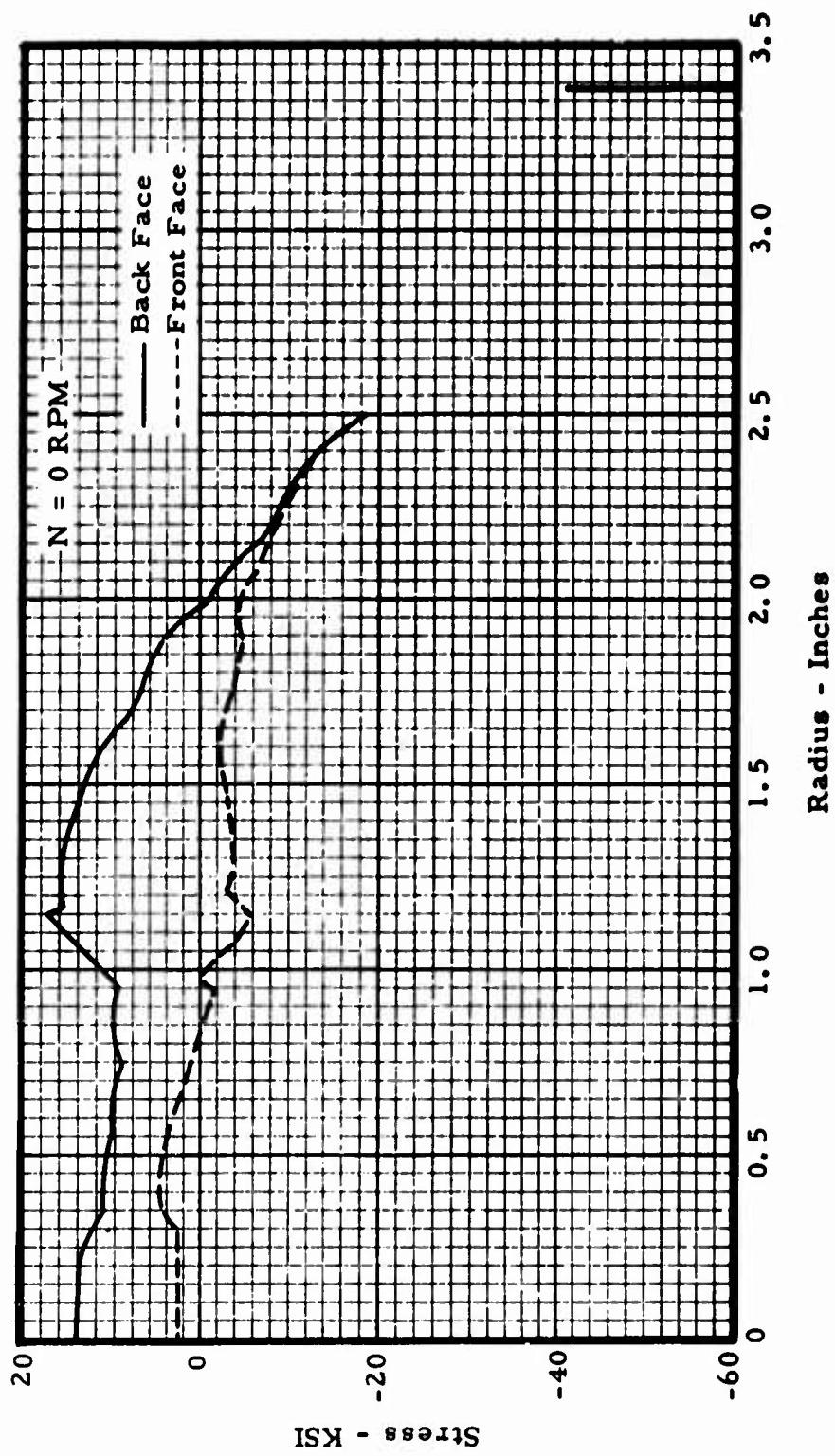


Figure IV-33. TS120 Radial Turbine Disc Tangential Thermal Stresses (Sea Level).

**Section IV**



**Figure IV-34.** TSI20 Radial Turbine Disc Radial Thermal Stresses (Sea Level).

**Section IV**

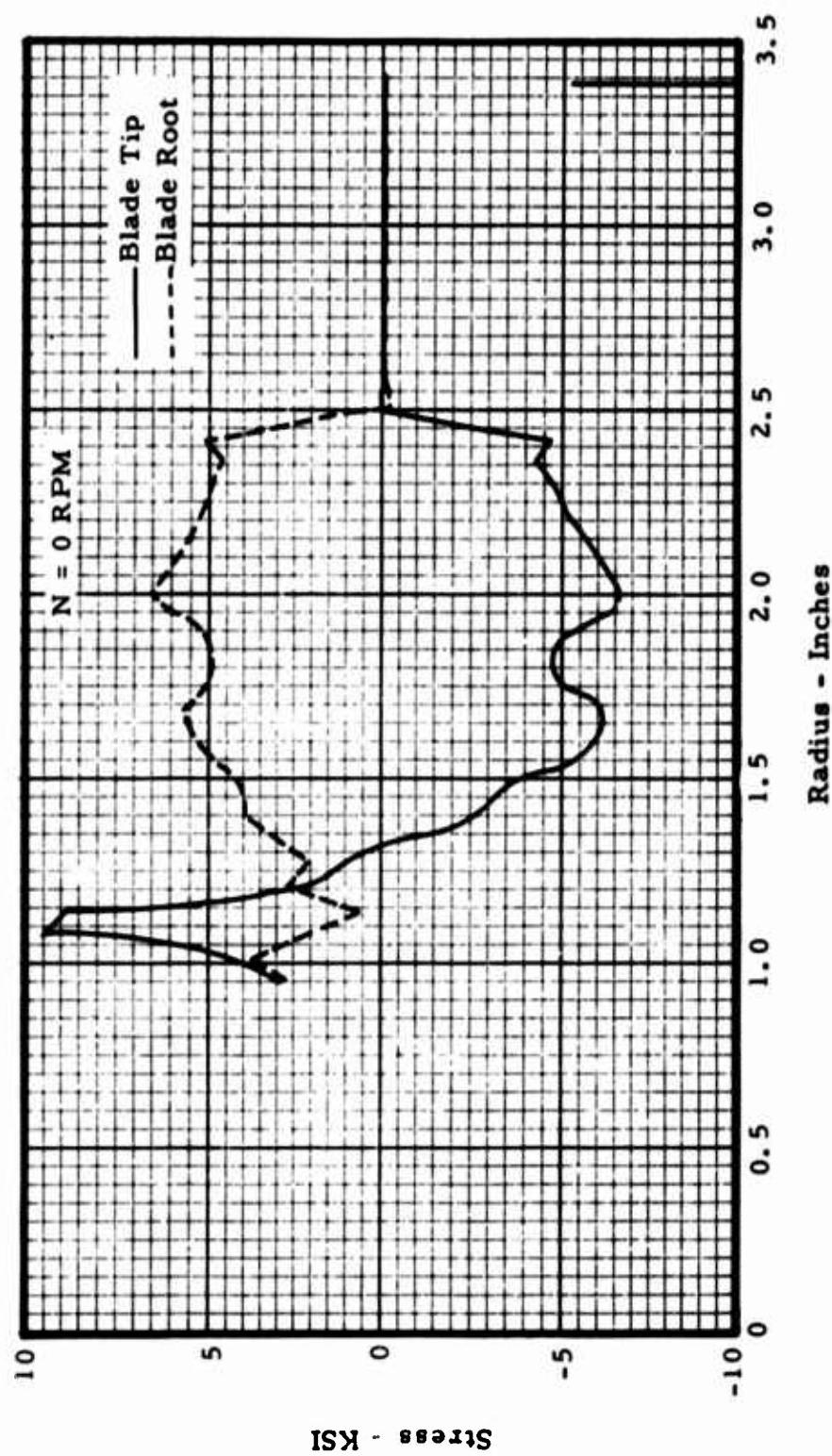
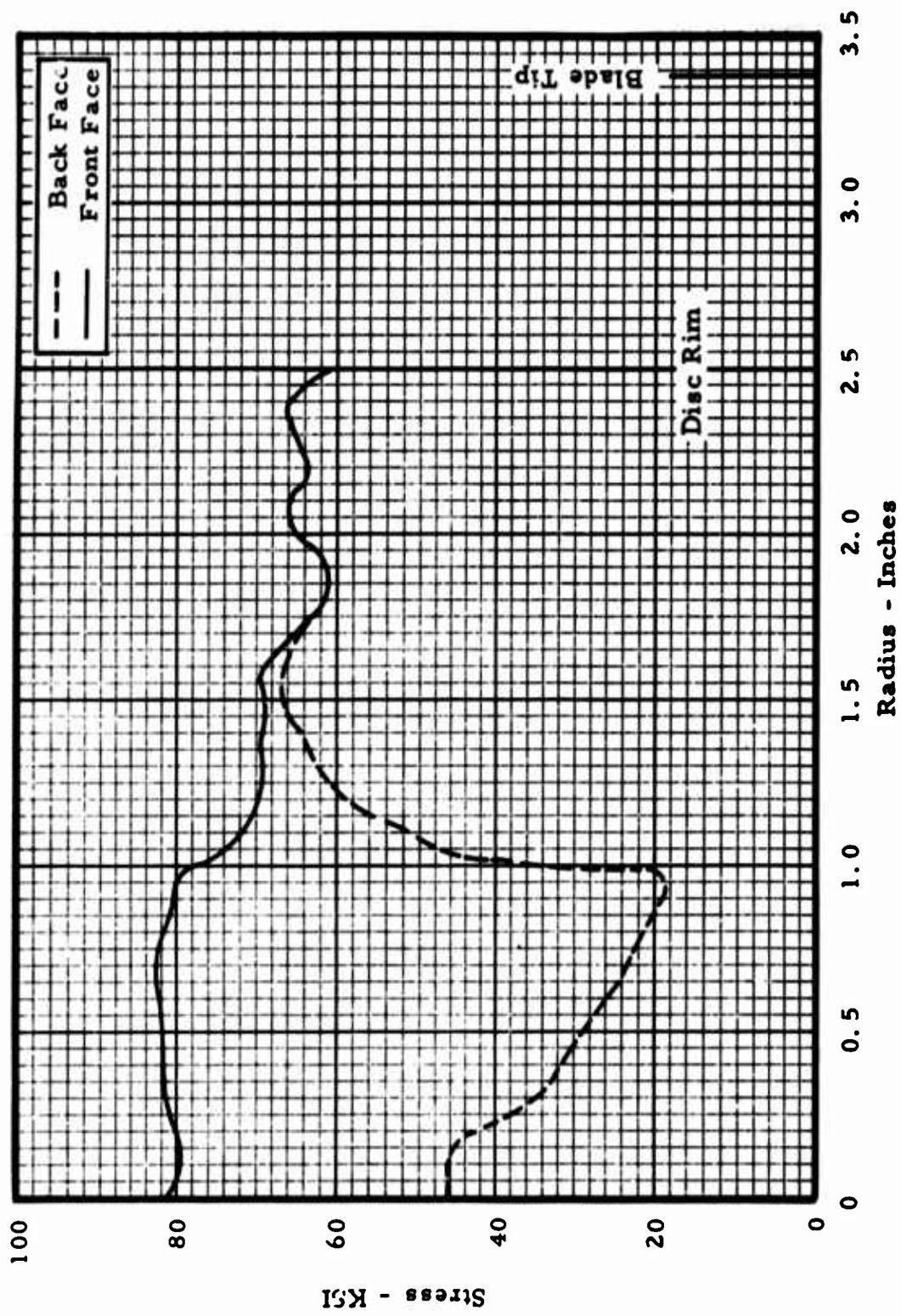


Figure IV-35. TS120 Radial Turbine Blade Radial Thermal Stresses (Sea Level).

**Section IV**



**Figure IV-36.** TS120 Radial Turbine Ten Percent Overspeed (Cold) (73,480 RPM).

**Section IV**

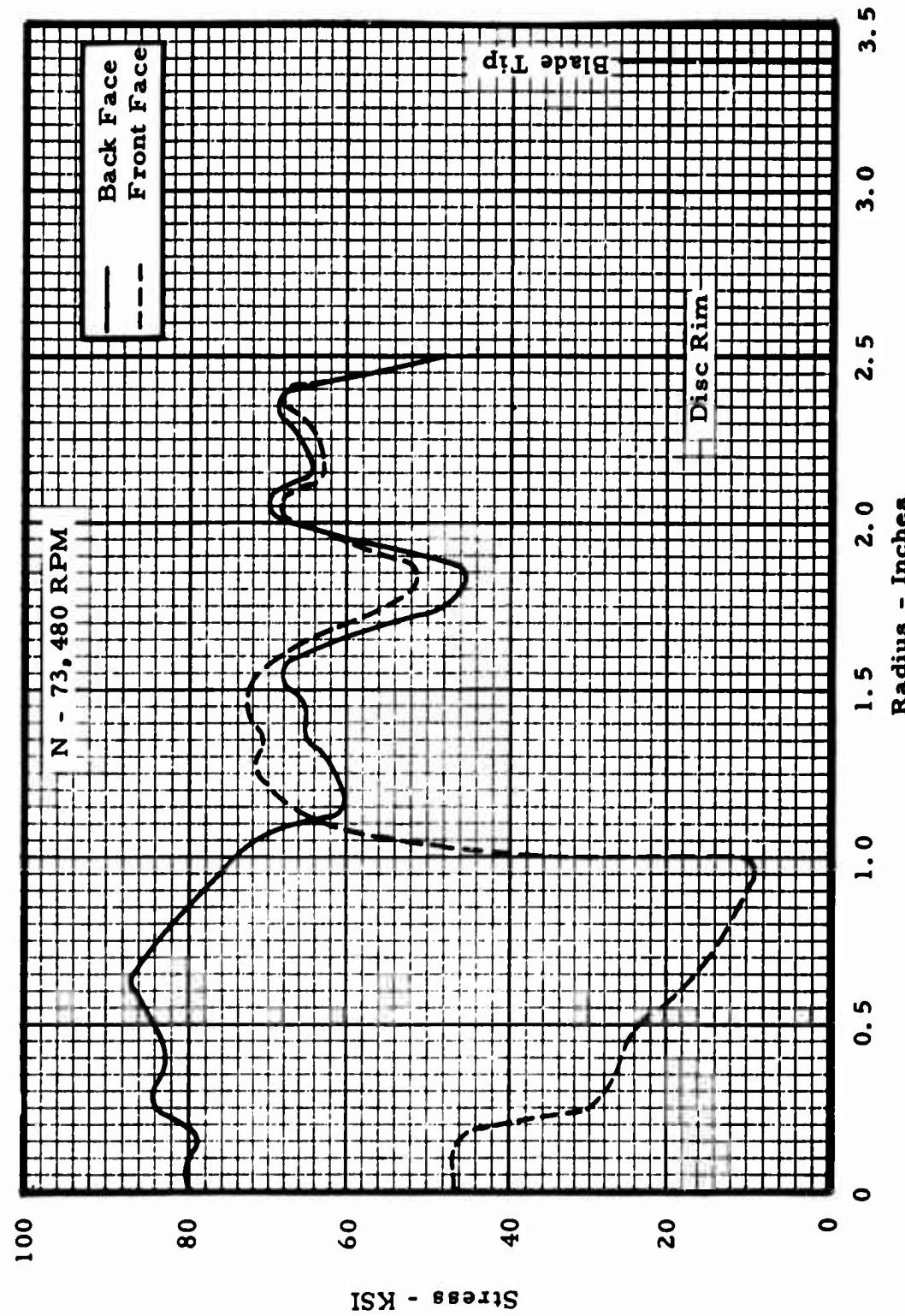


**Figure IV-37.** TS120 Radial Turbine Disc Radial Stresses Ten Percent Overspeed (Cold).

Section IV

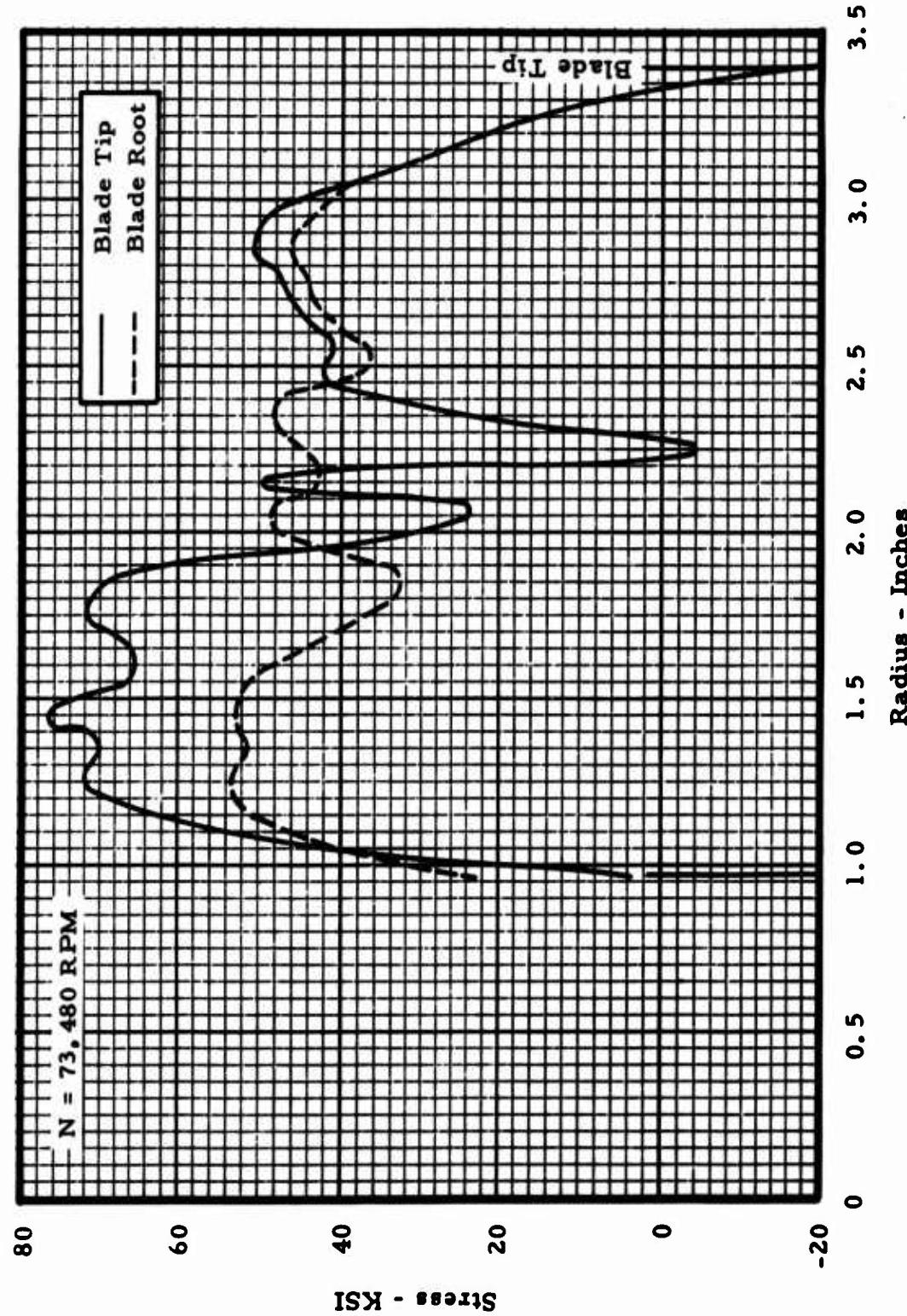
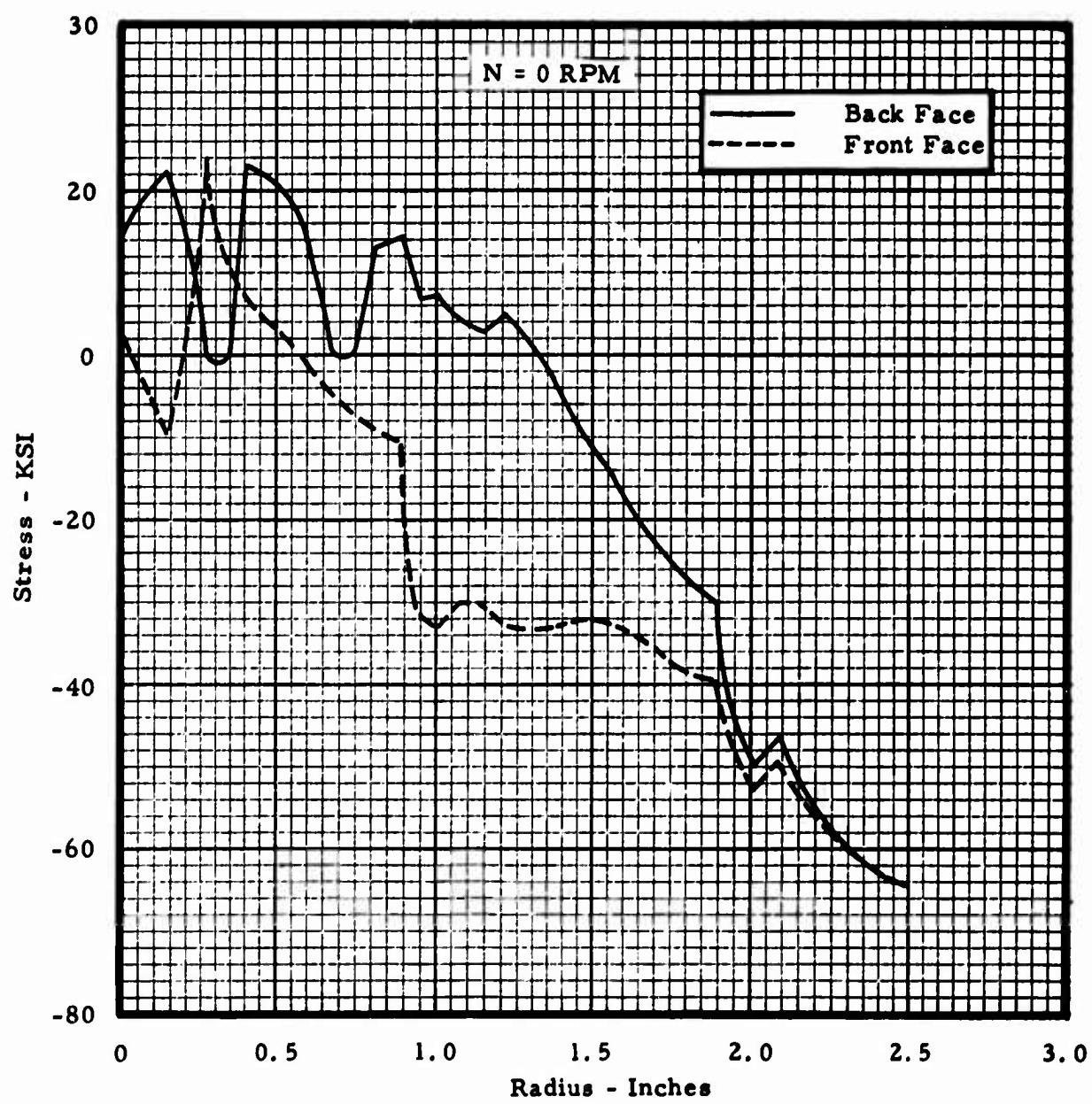


Figure IV-38. TS120 Radial Turbine Blade Radial Stresses Ten Percent Overspeed (Cold).

**Section IV**



**Figure IV-39. TS120 Radial Turbine Disc Tangential Thermal Stresses (Altitude).**

**Section IV**

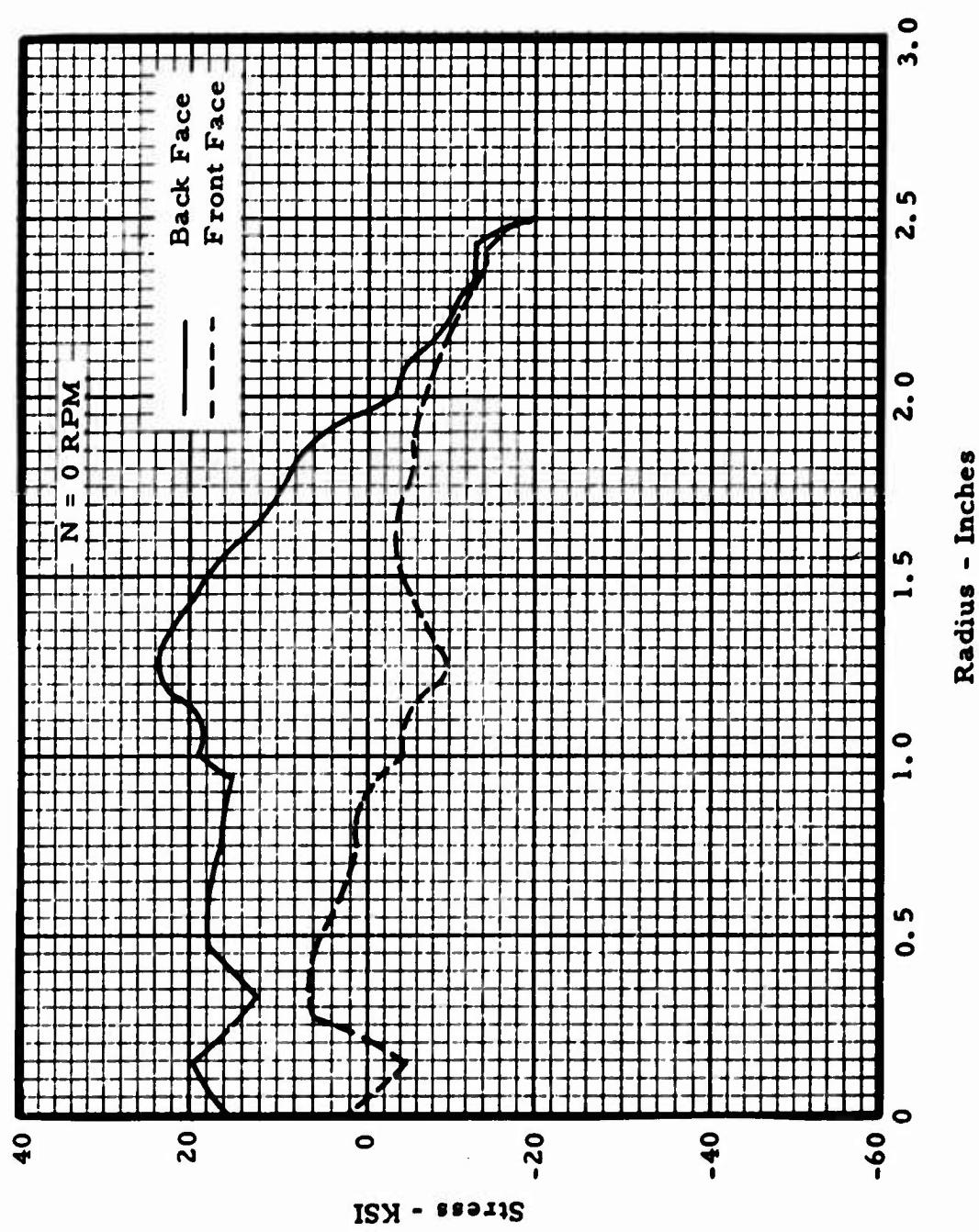


**Figure IV-40.** TS120 Radial Turbine Disc Radial Thermal Stresses (Altitude).

**Section IV**

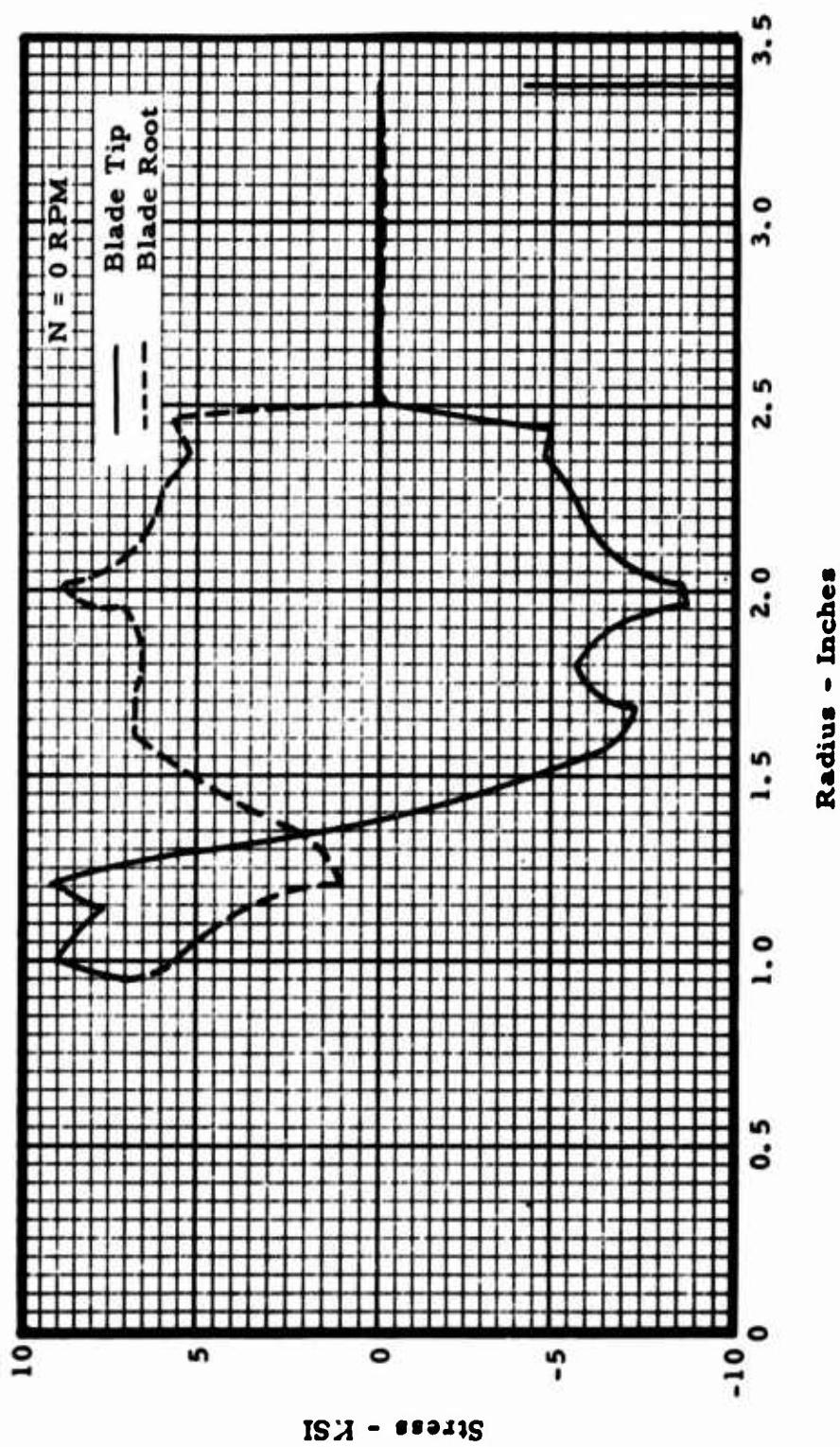
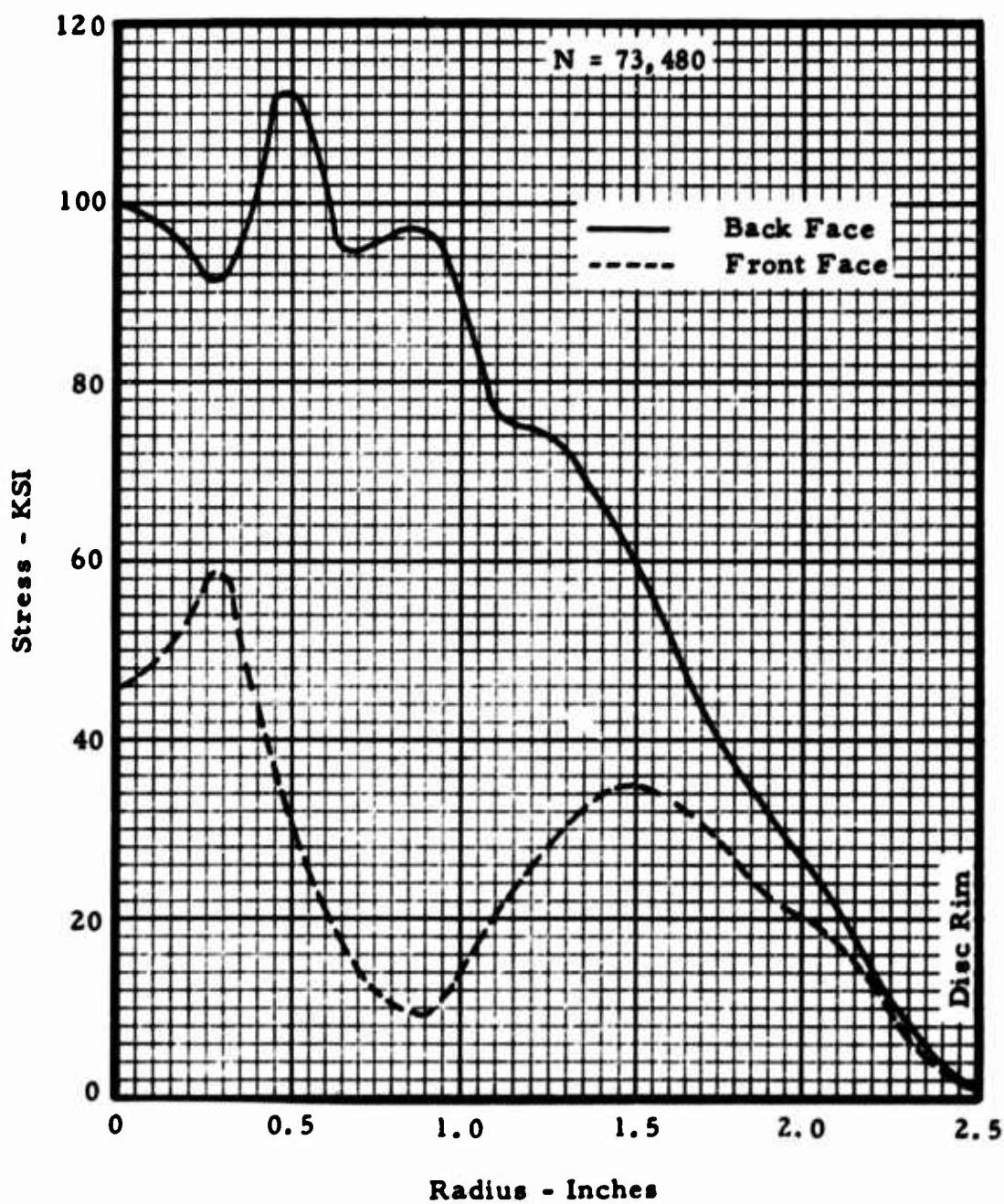


Figure IV-41. TSi20 Radial Turbine Blade Radial Thermal Stresses (Altitude).

**Section IV**



**Figure IV-42. TS120 Radial Turbine Disc Tangential Stresses  
Ten Percent Overspeed (Altitude).**

**Section IV**

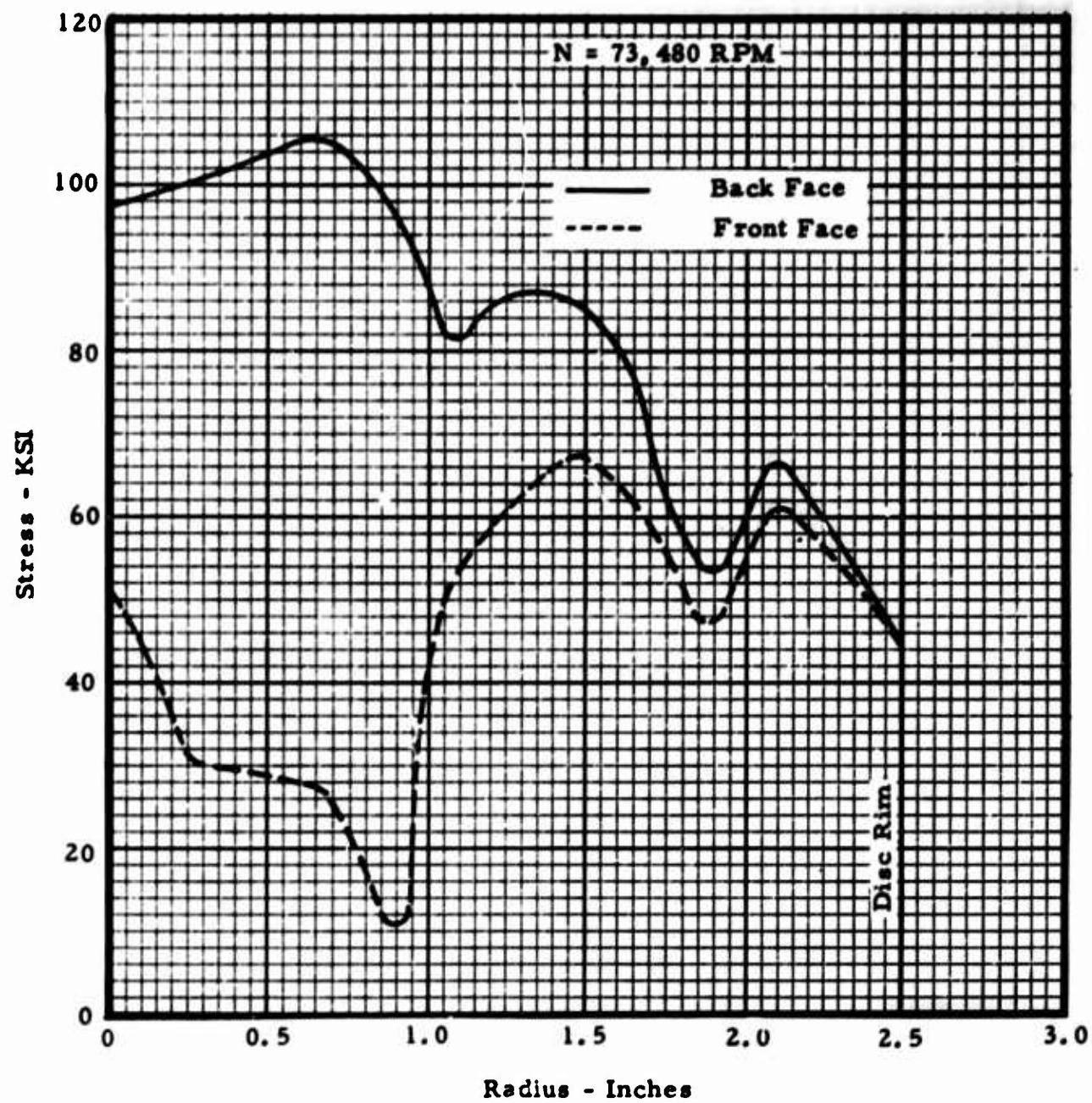


**Figure IV-43.** TS120 Radial Turbine Disc Radial Stresses Ten Percent Overspeed (Altitude).

**Section IV**

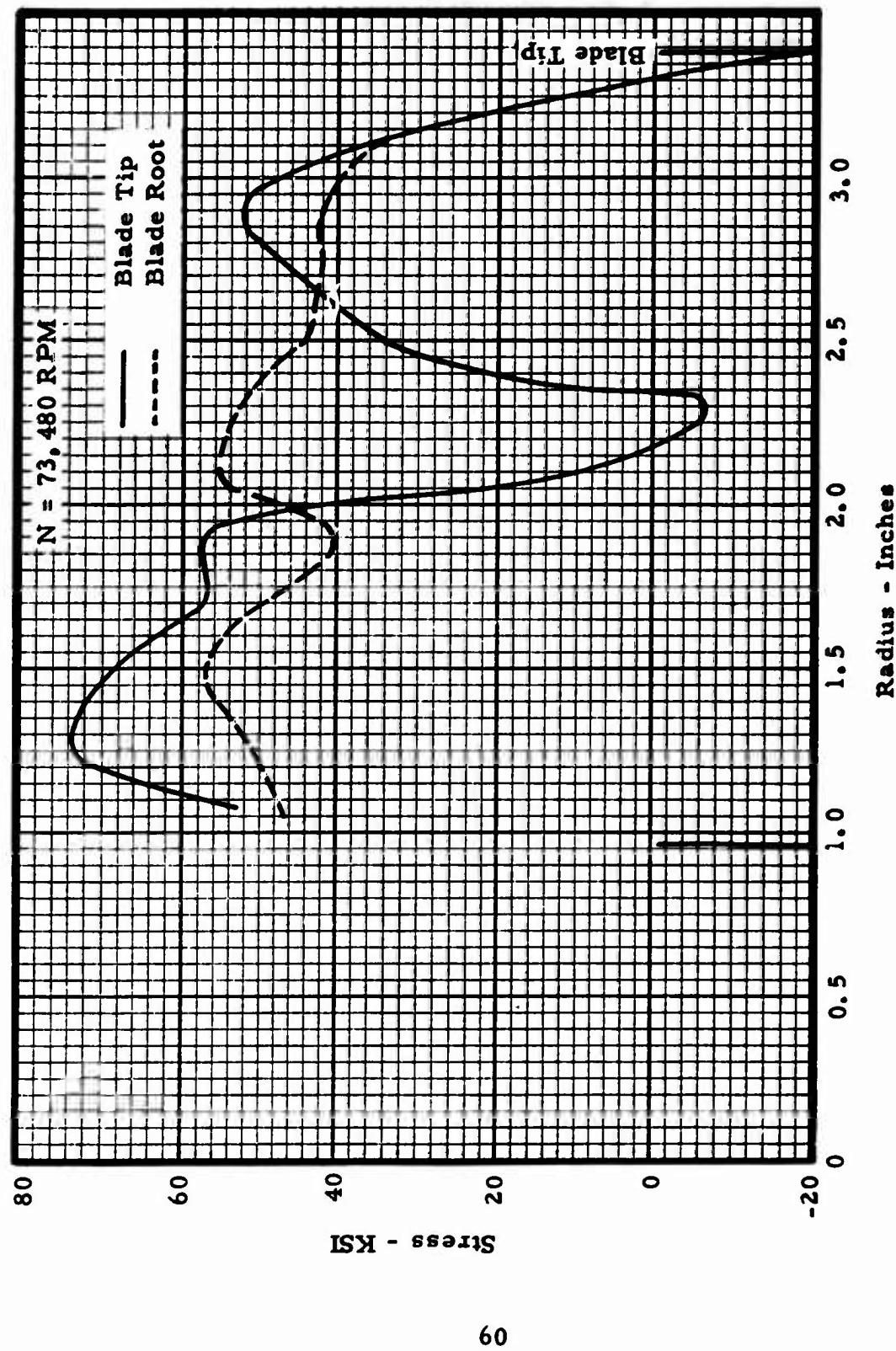


Figure IV-44. TS120 Radial Turbine Blade Radial Stresses Ten Percent Overspeed  
(Altitude).

Section IV

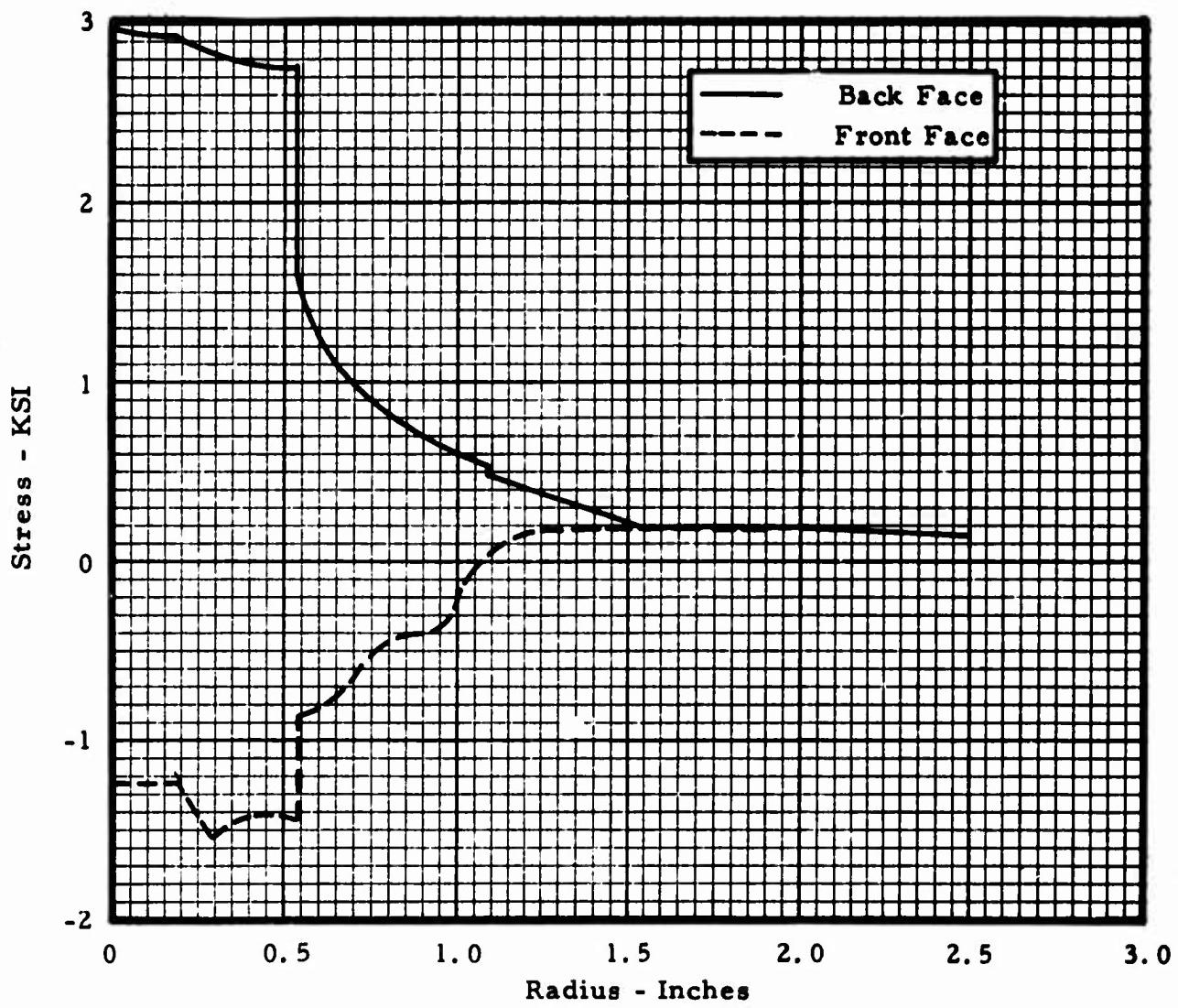
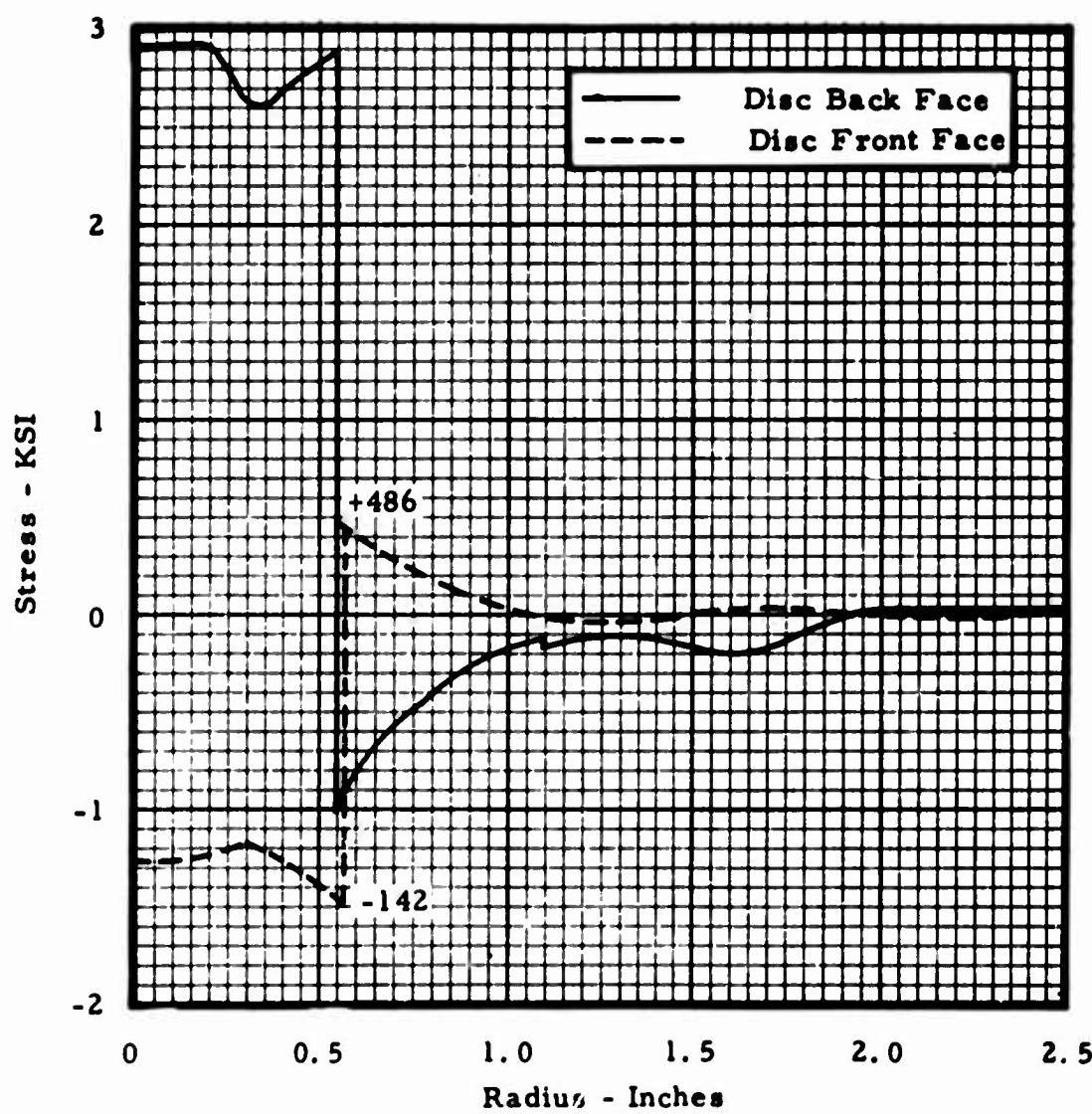


Figure IV-45. TS120 Radial Turbine Disc Tangential Stress Due to Applied Load of 10,000 Pounds at  $R = 0.55$  Inch.

**Section IV**



**Figure IV-46.** TS120 Radial Turbine Disc Radial Stress Due to Applied Load of 10,000 Pounds at  $R = 0.55$  Inch.

**Section IV**

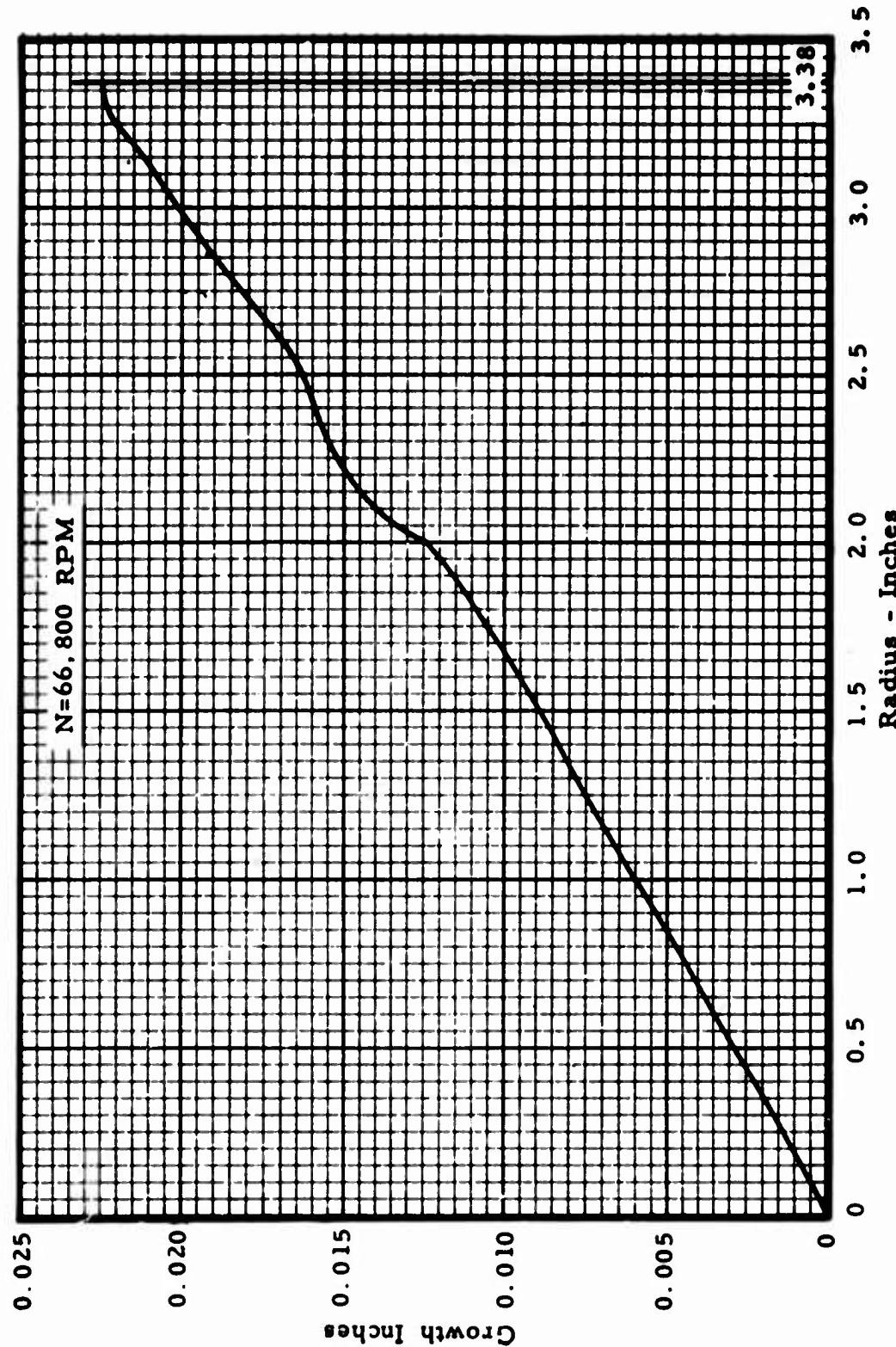


Figure IV-47. TS120 Radial Turbine Back Face Radial Growth Design Speed (Sea Level).

## Section IV

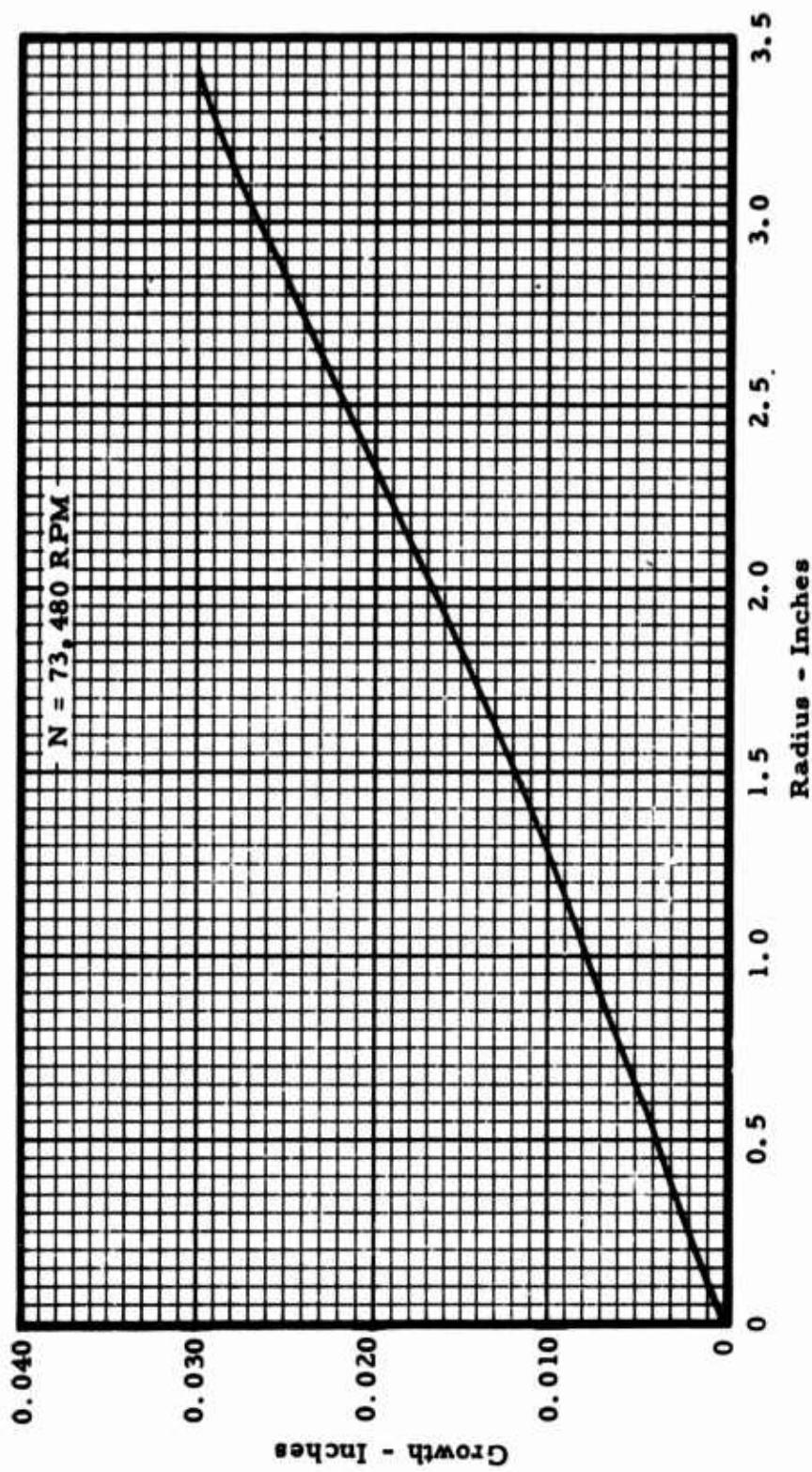


Figure IV-48. TS120 Radial Turbine Back Face Radial Growth Ten Percent Overspeed (Altitude).

## Section IV

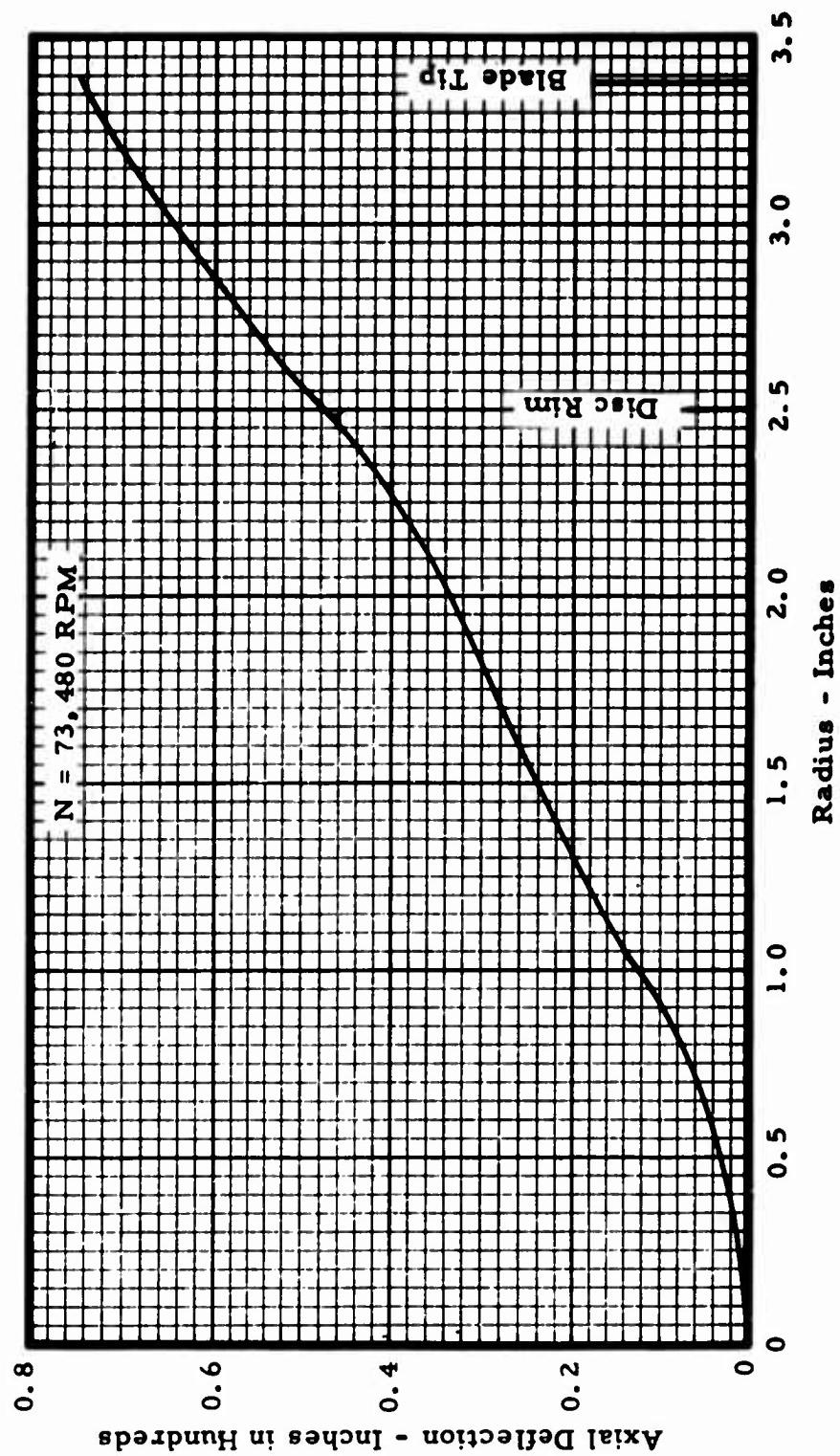
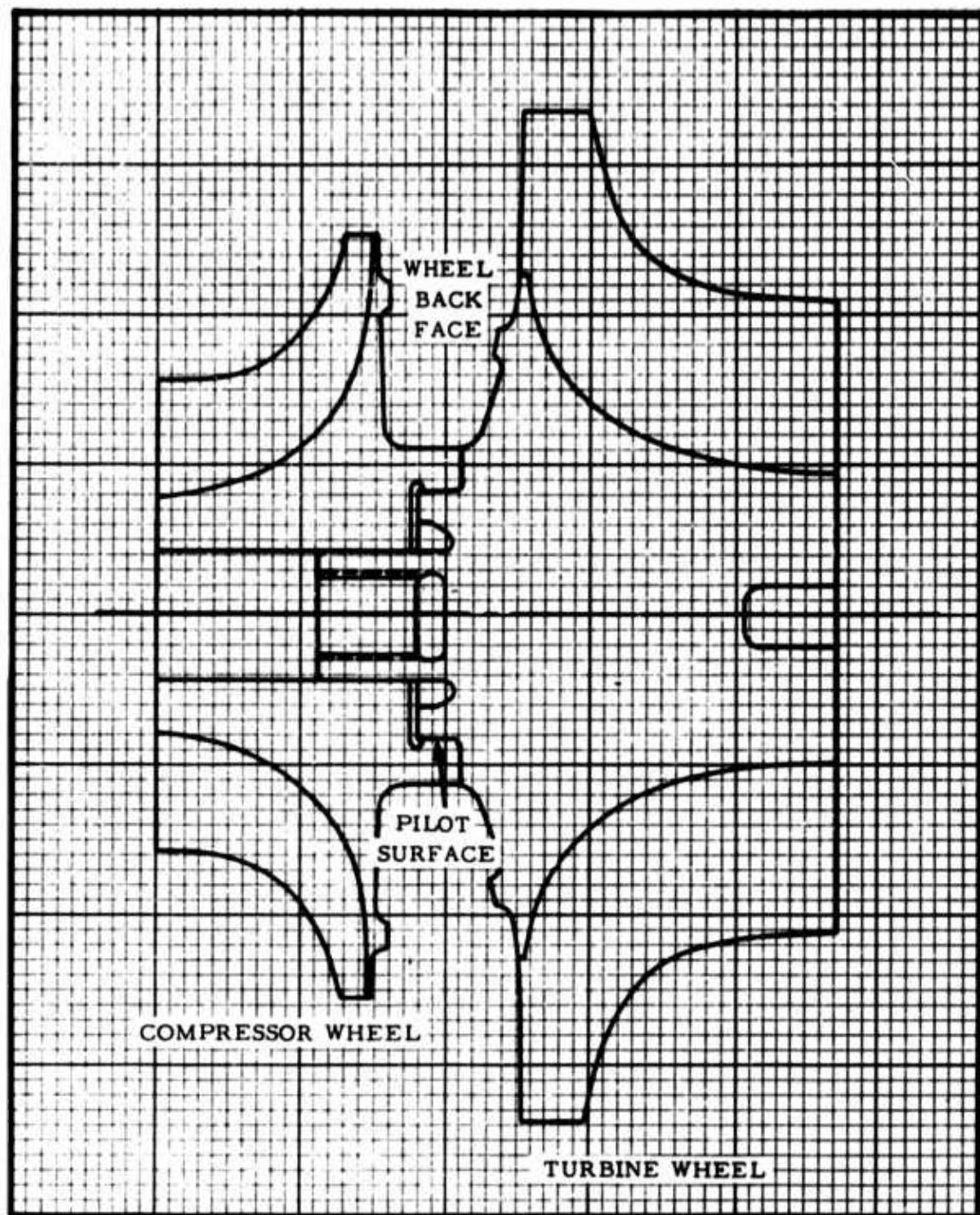


Figure IV-49. TS120 Radial Turbine Disc Axial Deflection Ten Percent Overspeed (Altitude).

**Section IV**



**Figure IV-50. Radial Compressor and Turbine Rotor Assembly.**

## **Section IV**

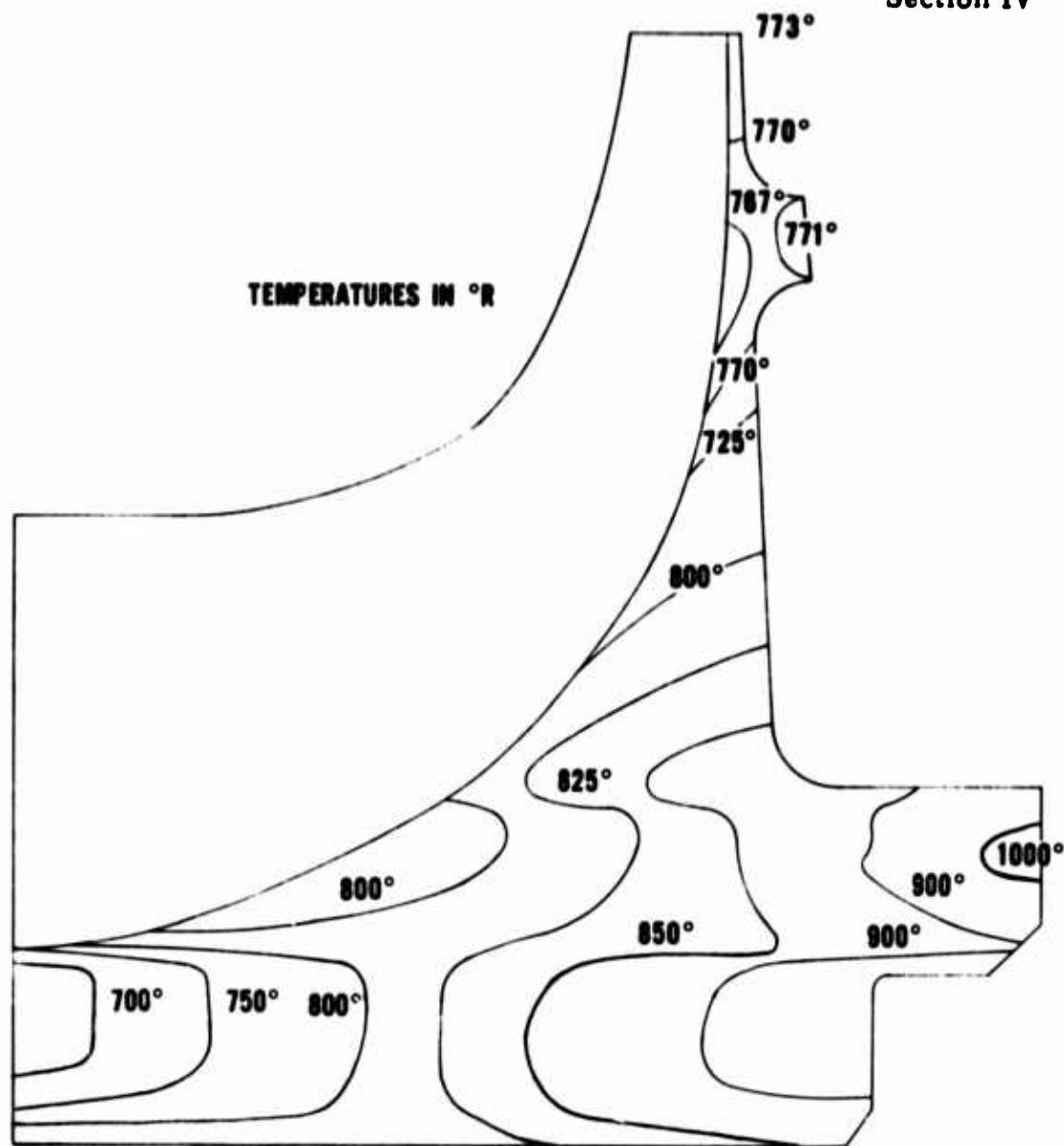


**Figure IV-51. Radial Compressor Temperature Distribution Profile, Sea Level Condition.**

## Section IV

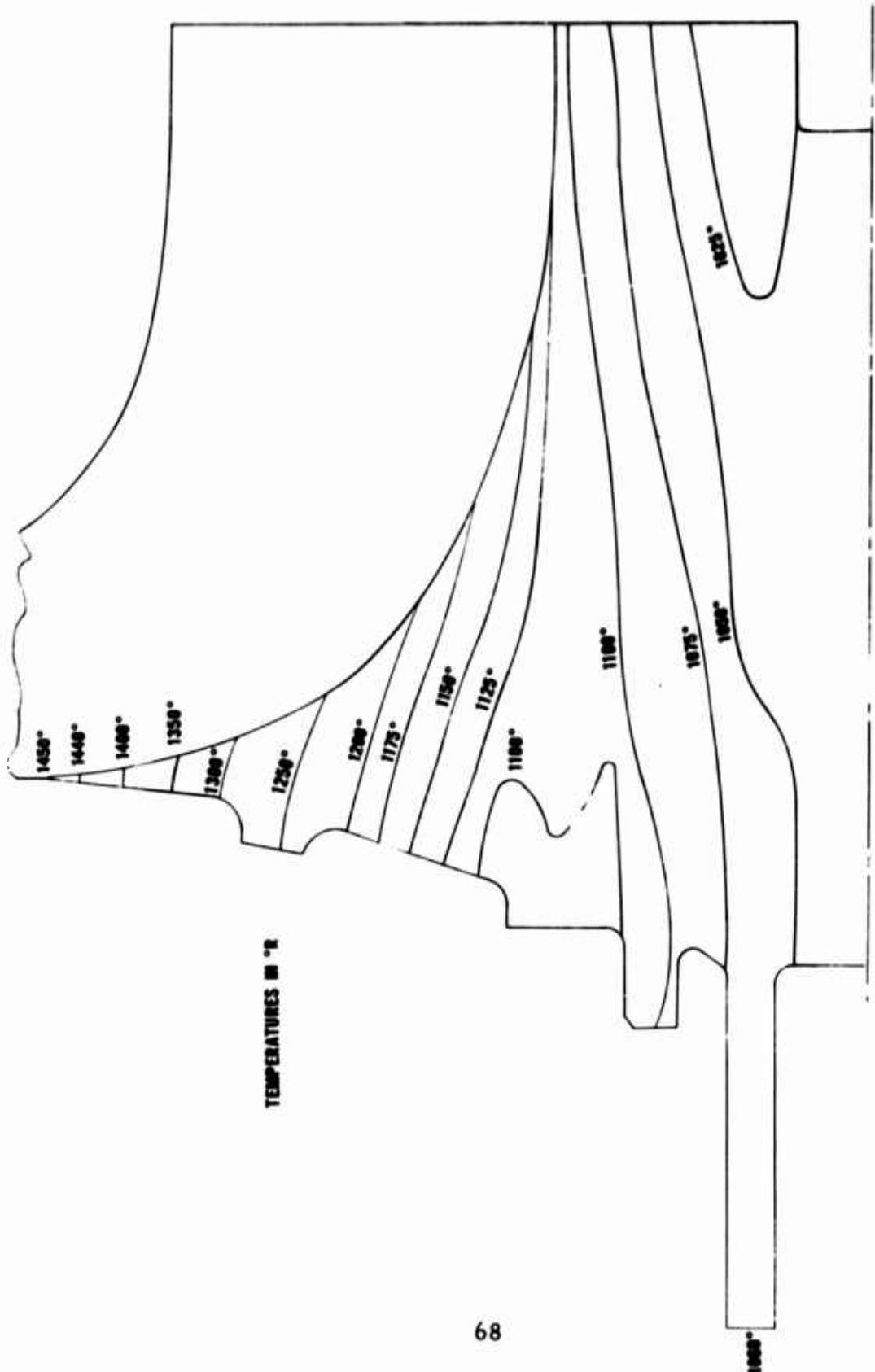
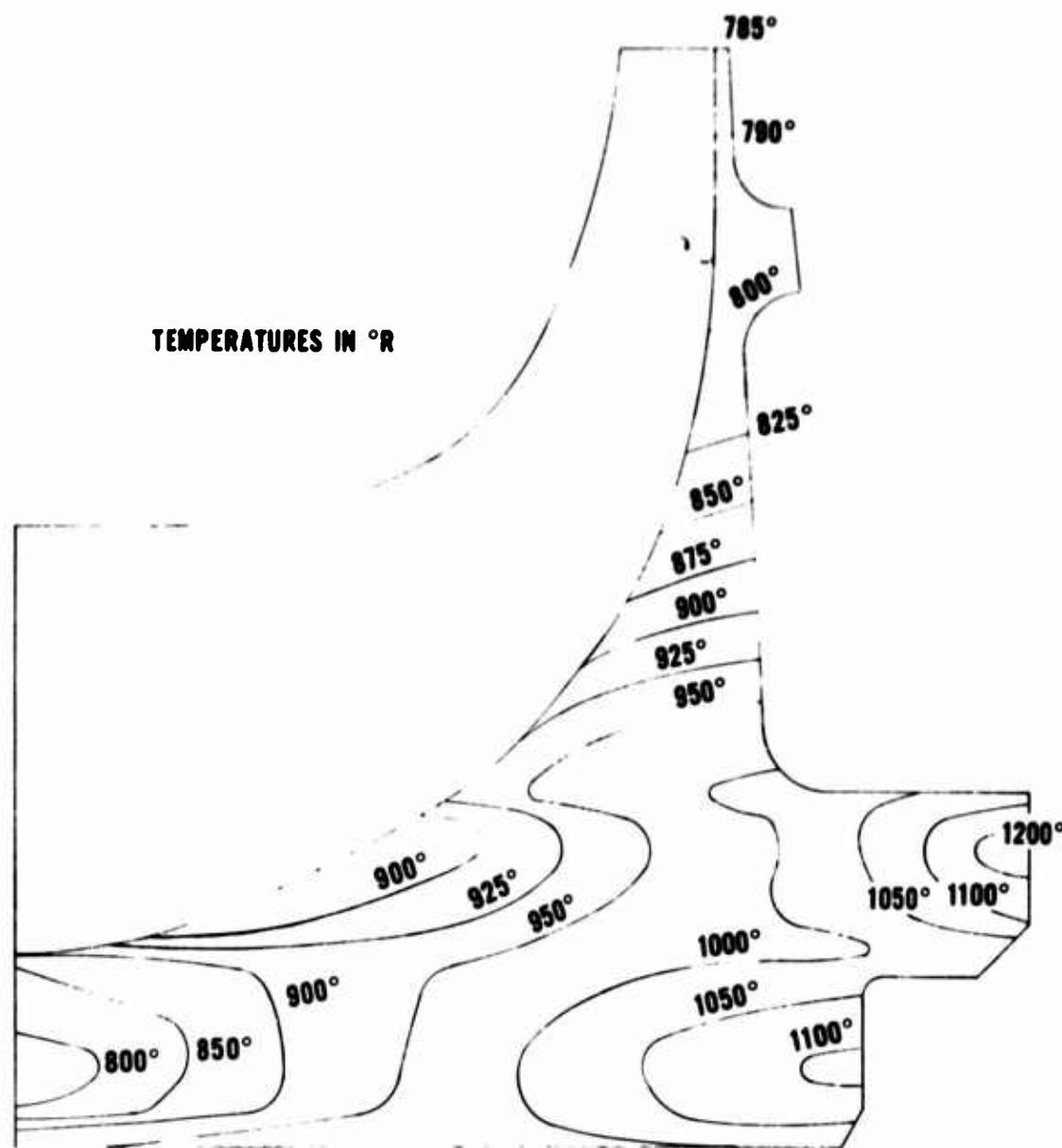


Figure IV-52. Radial Turbine Temperature Distribution Profile, Sea Level Condition.

**Section IV**



**Figure IV-53. Radial Compressor Temperature Distribution Profile, Altitude Condition.**

**Section IV**

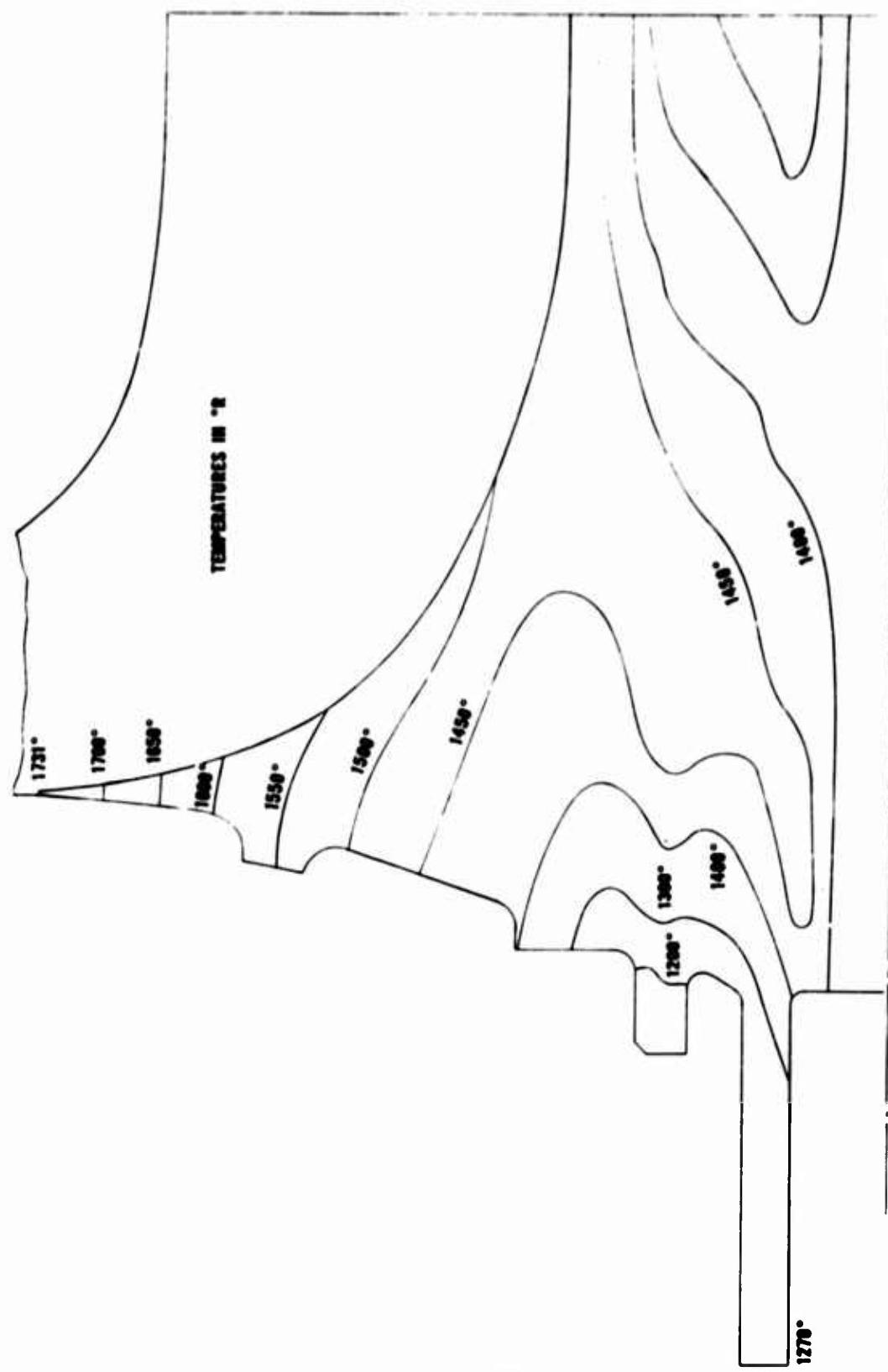


**Figure IV-54.** Radial Turbine Temperature Distribution Profile Altitude Condition.

**SECTION V**

**STATIC STRUCTURE**

## SECTION V - STATIC STRUCTURE

Careful attention was given to the static structure throughout the TS120 engine, Figure V-1. Particular emphasis was placed on maintaining maximum section modulus. The use of flat areas in the pressure vessel section of the engine was avoided. Maximum usage of conical, cylindrical, and curved surfaces was employed to provide maximum stiffness with minimum weight, and the resulting stress levels are such that material thickness is generally decided on the basis of producibility rather than stress.

The power take-off flange (No. 1, Figure V-1), is a magnesium casting bolted to a cast magnesium accessory case (2). The front rotor bearing is supported from an integral cylindrical extension from the accessory case. The accessory case is bolted to a cast magnesium conical diaphragm (3), through five struts in the air inlet passage. The combustor housing (4) is a steel weldment. The rear bearing housing (5) is supported through three struts bolted to the combustor housing. The radial diffuser (6) is a steel fabrication, supported from the outside diameter of the engine through a conical diaphragm. The interstage compressor duct (7) is semi-machined from a steel casting and supported from the radial diffuser. The two-stage stator (8) is precision cast from aluminum and supported from the interstage compressor duct. An "O" ring snubber (9) is provided at the front of the axial stators. A split aluminum fairing (10) is supported from the axial stators.

A steel cover (11) is bolted to the back side of the radial diffuser. The turbine inlet nozzle (12) is a steel casting attached to the compressor cover through a sliding joint. The interstage seal diaphragm (13) is a split steel casting centered from the compressor cover (11) and trapped between the radial diffuser and turbine inlet nozzle. The exhaust diffuser (14) is a weldment welded around the rear bearing housing (5), and supported by a partial flange from the combustor housing (4). The volute (15) is a weldment attached to the compressor cover (11) through flexible leaf sections. The combustor (16) is attached to a cap (17) and supported in the volute by a spring joint (18). The cap (17) and the combustor is attached by a vee band clamp (19).

## Section V

The adaptation of a radial exhaust to the basic engine is shown in Figure V-2. The exhaust weighs 7.7 pounds and adds 5.4 inches to the engine length.

### ENGINE MOUNTS

Engine specifications require that the complete engine assembly (including the generator and generator attachment to the engine) be capable of withstanding a 5g load in the sidewise and end directions and a 10g load in the drop direction.

The weight of the engine, less generator, is 195 pounds and the weight of the high speed generator is 110 pounds. In addition, the design must also be capable of accommodating an alternate configuration consisting of a 135 pound generator cantilevered on the outboard side of a reduction gear case which also adds an additional 21 pounds to the engine.

The whole assembly is supported forward by trunions at the lower side of the accessory gear case and, at the rear, by a flange engaging a pinned strut permitting differential growth between the engine structure and the supporting base.

The 10g drop requirement will impose a 5500 pound-inch moment and a 1100 pound shear load on the power take-off flange in the case of the high speed generator; a 10,100 pound-inch moment and a 1350 pound shear load on the gear box cover flange in the case of the 6000 r.p.m. generator configuration. It will also impose a 12,800 pound-inch moment capability and a 1560 pound shear capability on the flange joining the reduction gear case to the engine. Analysis based upon an average clamping load, developed in the flange fastenings, indicates that the current design has many times the required moment capabilities as well as several times the required shear capabilities.

In the case of the design of the engine mounts, adequate provisions are made to accommodate the total assembly weight under the specified g forces.

## Section V

### COMBUSTOR HOUSING CONICAL DIAPHRAGM

It is necessary to thoroughly investigate the combustor housing conical diaphragm because it forms part of the main pressure vessel of the engine and supports most of the interstage static structure between the radial compressor and the turbine. It is subjected to a pressure differential of approximately 61 psi and moderately severe thermal conditions. The Continental Aviation shell computer program enables the stress analyst to consider combinations of several rings, cylinders, and cones linked together in series and subjected to pressure gradients, temperature gradients, and boundary loading conditions.

The following tabulation exhibits the resulting stresses in the combustor housing conical diaphragm under the assumed environmental conditions:

	<u>Outer Radius</u>	<u>Inner Radius</u>
Longitudinal Bending Stress (psi)	28,800	22,500
Longitudinal Membrane Stress (psi)	-4,300	- 700
Tangential Bending Stress (psi)	8,200	6,300
Tangential Membrane Stress (psi)	-36,700	- 200
Shear Stress (psi)	1,300	700

These values are well within the range of acceptable stresses for the material specified.

The axial deflection of the inner radius, and therefore, the intermediate stage static structure, is 0.016-inch.

### COMBUSTOR HOUSING AND REAR BEARING SUPPORT

The combustor housing has two critical stress areas: (1) at the juncture of the combustor can, and (2) at the juncture of the bearing support arms. Otherwise, the tangential and axial stresses in the cylindrical portion are less than 10,000 psi.

## Section V

A substantial reinforcing ring is indicated because the combustor can intersects the combustor housing in a tangential attitude and its diameter is an appreciable percentage of the diameter of the combustor housing. A ring was designed for this location of cross sectional area so that each segment of the ring will elongate under the influence of the stress field resulting from the combined effects of the pressure in the combustor housing and the combustor can. The amount of elongation is the growth of the corresponding line of juncture of the intact cylinder under the influence of the combustor housing pressure, on the theory that the combustor housing cylinder has no stresses or strains in this area greater than the intact cylinder. A plot of the ring cross sections area versus angular location on the cylinder is shown in Figure V-3. Thermal compatibility is assured by making the ring of the same material as the housing.

The other critical area of the combustor housing is at the juncture with the rear bearing support arms because there is a thermal gradient between these two members. If these two members were rigidly attached, excessive local stresses might result at both the juncture of the radial arms with the combustor housing, as well as at the juncture of the radial arms with the rear bearing support housing. In order to control the reactions at these points, a leaf spring with a known flexibility is located at the juncture of the radial arms and the combustor housing.

### CONTAINMENT

The specifications require that provisions be made in the engine design for some means of containing the destructive effects of a bursting turbine rotor initiated at 10 percent over rated speed. The most generally accepted method of rotor containment of mobile turbines, in use at the present time, is a heavy ring in the plane of the rotating disc. The basic analytical approach to determine the size of the ring is to compare the total kinetic energy of the rotating turbine disc and blades to the potential energy available in the ring in stretching to its ultimate strength. This approach is both conservative and optimistic, and it becomes apparent after careful evaluation that at the present state-of-the-art, an exact sizing is not possible by

## Section V

analytical means.

On the one hand, the ratio of translational energy to rotational energy of the disc fragments after rupture is a function of the number of fragments which, of course, cannot be forecast. Therefore, we assume that the disc breaks into a large number of masses which causes the ring to absorb most of the kinetic energy in translational form.

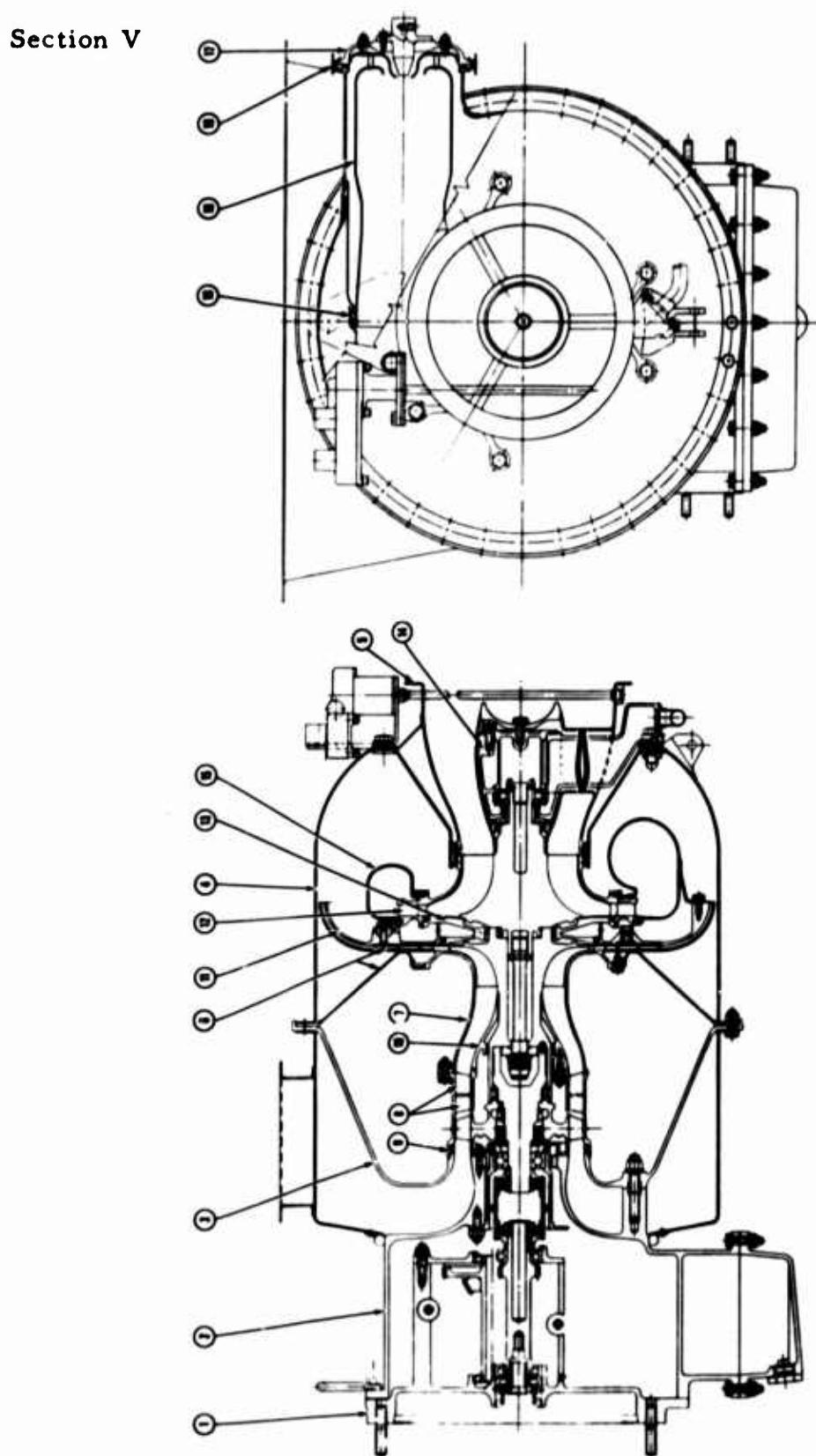
On the other hand, the analytical approach does not include the effects of sharp edges which would tend to shear through the ring rather than elongate it through its elastic and plastic regions.

Another consideration is the anchoring of the ring because any unbalanced release would tend to cause the fragments to transfer some of their momentum to the ring with possible devastating results.

Reference to Figure V-4 indicates that the some of the static structure in the plane of the turbine, shown by area "A," are substantially strengthened. These members are the first retaining structure that the rotor fragments will encounter upon bursting. It is recognized that these structures will probably be insufficient to contain the burst rotor and that additional structure will be required. It is planned to commence the containment development work by increasing the containment capability to a factor of two times the kinetic energy by adding material in the area designated by "B."

If additional containment capability is required, additional material may be added at areas designated by "C" and "D."

Figure V-1. Model TS120 Static Structure.



**Section V**

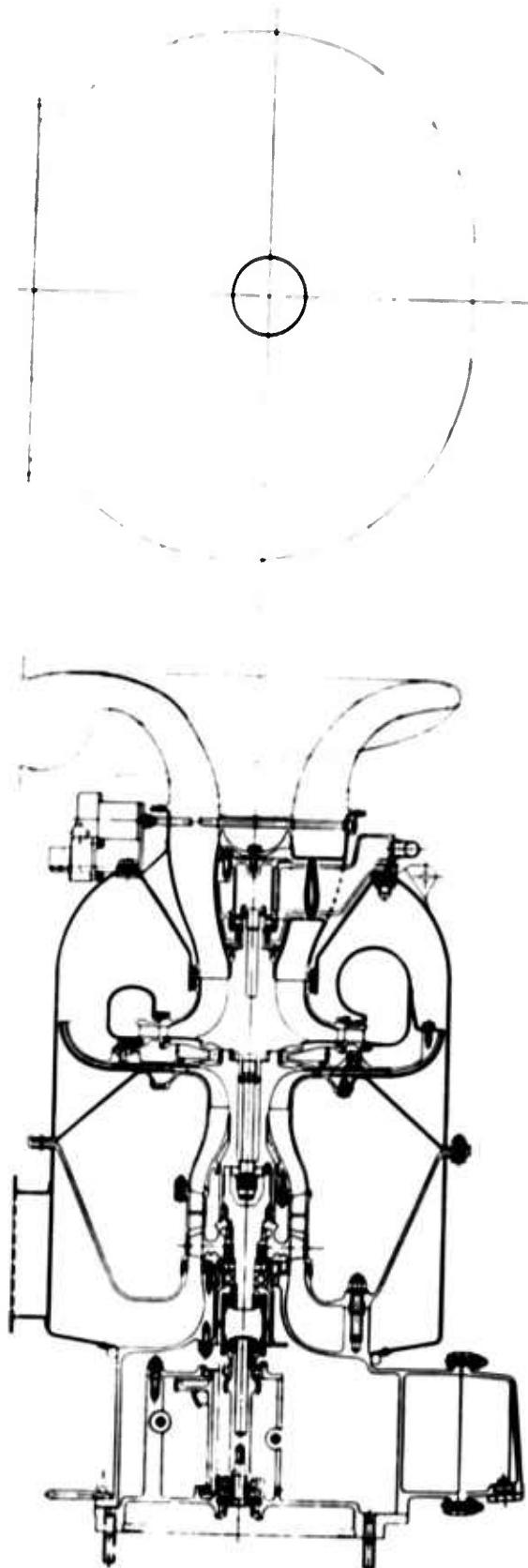


**Figure V-2. Model TSL120 Turboshaft Engine With Radial Exhaust.**

## Section V

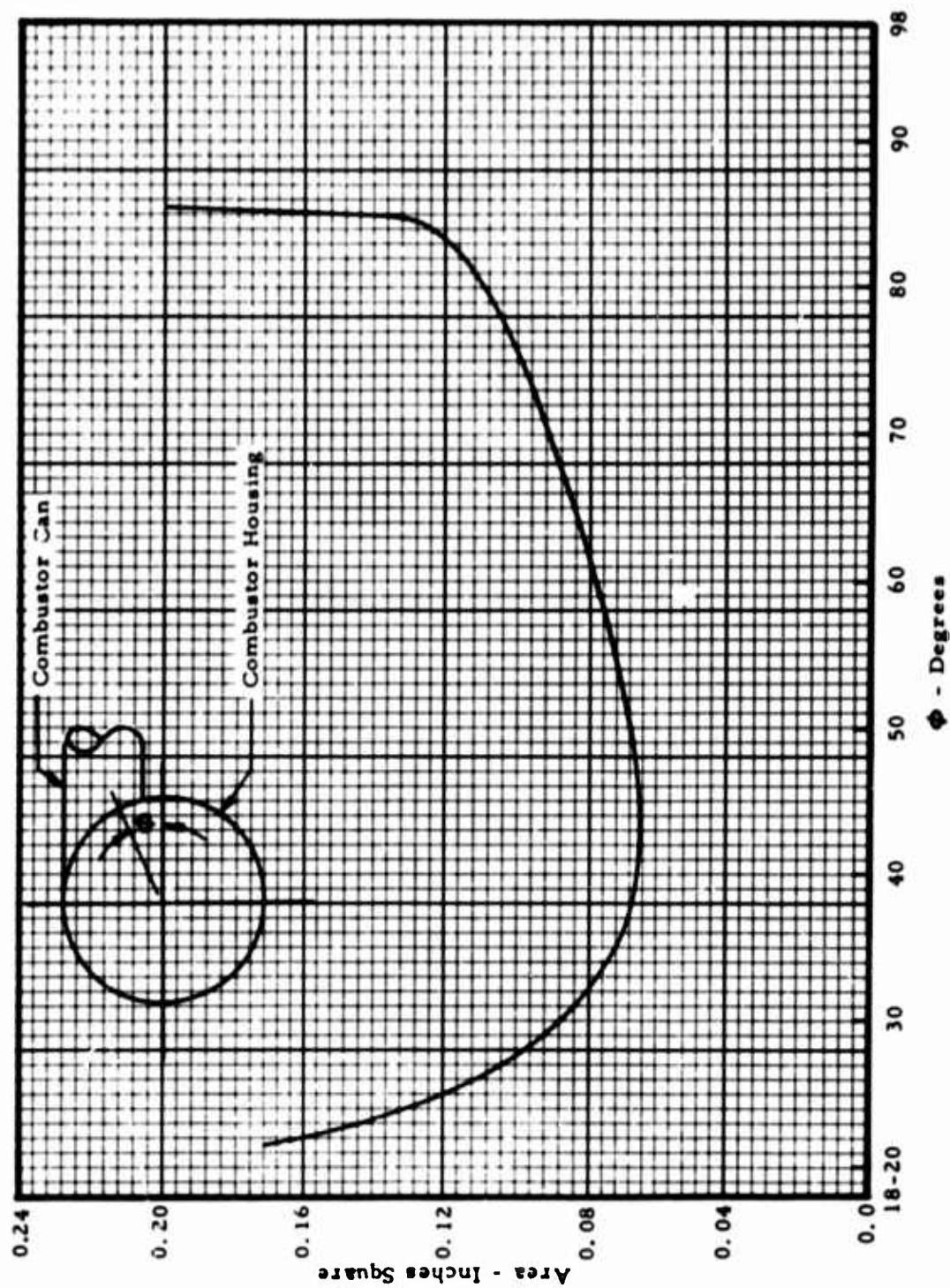
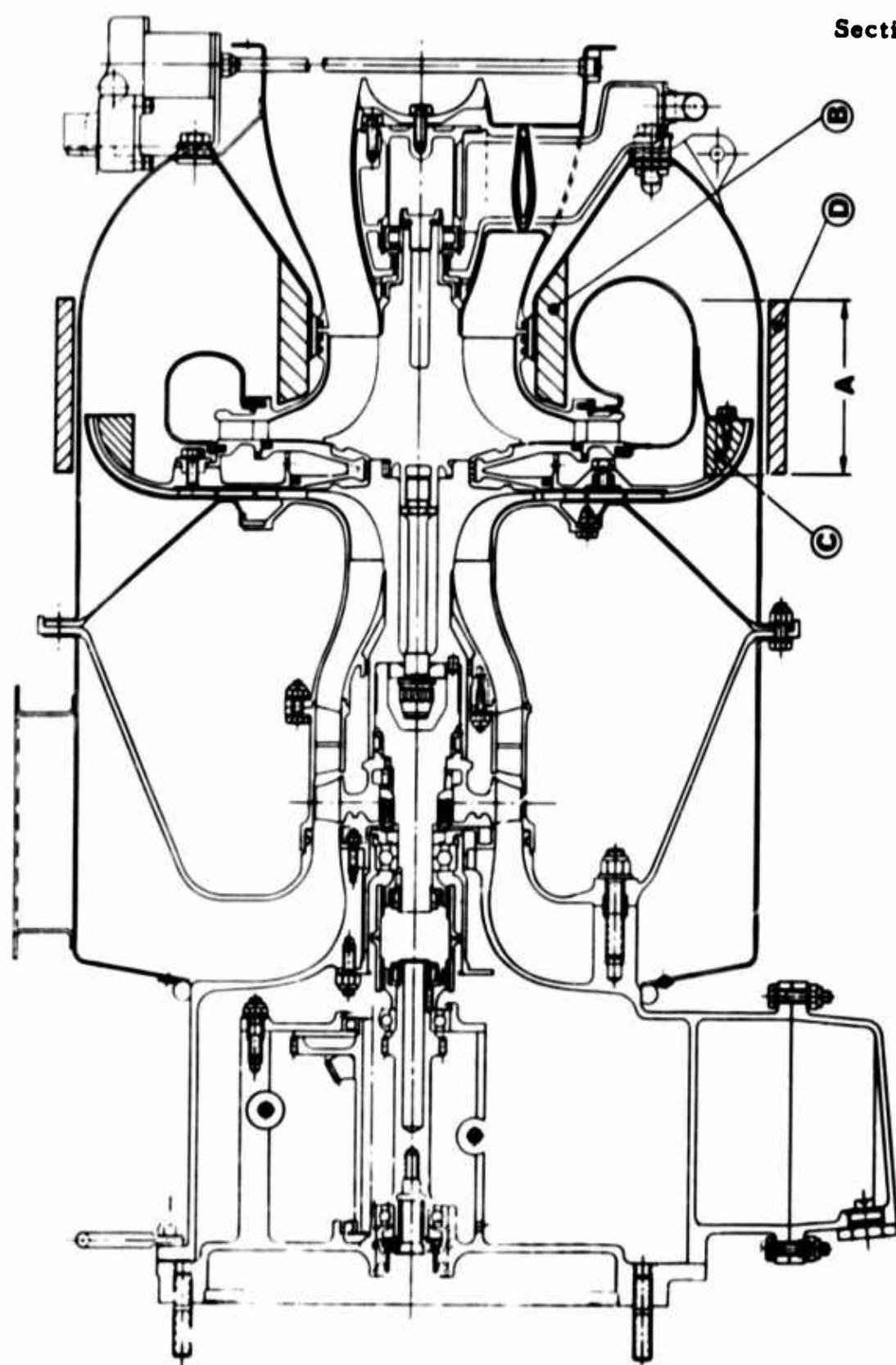


Figure V-3. Model TS120 Cross Sectional Area of Reinforcing Ring at Juncture of Combustor Housing and Combustor Can Versus Angular Location.

**Section V**



**Figure V-4. Model TS120 Turbine Rotor Containment.**

SECTION VI

**ACCESSORY DRIVES**

## SECTION VI - ACCESSORY DRIVES

The accessory drive, Figure VI-1, consists of six helical gears and a set of spiral bevel gears that provide the five drives tabulated below:

<u>Drive</u>	<u>Design Power or Torque</u>
Starter	165 Lb-In. Torque
Alternator	1.0 HP
Oil Pump	1.0 HP
Power Control Drive	1.0 HP
Free Pad	<u>0.5 HP</u>
Total Power      3.5 HP	

The accessories are mounted perpendicular to both sides of the accessory case, permitting free access to all the pads, with unlimited removal length.

Referring to Figure VI-2, a high-speed helical pinion (1) which is replaced by a main power reduction gear in the geared engine originates at the centerline of the turbine and drives a compound gear-shaft(2) which contains the pinion (3) of a spiral bevel gearset. The driven bevel gear(4) is in turn compounded with two helical gears (5) and (6), one of which engages a high-speed pinion (7), while the other one meshes with a low-speed gear (8).

The high-speed driven pinion shaft is directly coupled to the battery charging alternator armature at one end and is connected at the interior end via a splined quill shaft (9) to the outer race of an over-running clutch (10). The inner race of the clutch (11) carries an internal spline for engagement with the starter drive shaft. The clutch is of the centrifugally disengaging type; consequently, when the starter reaches a cut-out speed of approximately 16,000 r.p.m., the sprags will disengage the inner race and remain with the outer race without slippage at the inner surface. If the outer race speeds falls below 16,000 r.p.m. (approximately 40 percent engine speed) a garter spring will overcome centrifugal force on the sprags and contact will again be made with the inner race permitting a restart attempt without requiring engine speed to drop to zero.

## Section VI

The low-speed helical gear (8) provides a spline drive for the combination fuel pump, fuel control and governor at one end and is connected to the oil pump drive quill shaft (12) at the interior end. The oil pump main drive shaft (13) is double ended, receiving its drive from the oil pump drive quill shaft and in turn providing a free splined pad at its exterior end.

The choice of helical and spiral bevel gears over spurs and straight bevels was dictated by noise reduction requirements rather than for speed or load capacity. In all meshes except the primary gear set, contact ratios in excess of three to one have been achieved. It was not possible to obtain a three to one contact ratio in the primary mesh because the main drive pinion is determined by consideration for a reduction gear version of the engine. A high helix angle would have resulted in excessive bearing loads in the reduction gear. The primary mesh has a 16-degree helix angle, which results in a contact ratio over two to one, however, all other accessory drive helical gears have 45-degree helix angles. The bevel gear set has a spiral angle of 35 degrees.

Where necessary in the high-speed train, Belleville washers are utilized to provide thrust loads for preventing ball bearing skidding problems. In addition, the Belleville springs determine the spiral gear cone centers against the thrust generated by the accessory loads. Under starting loads the spiral gear pinion thrust will reverse, causing it to maintain the cone center established by the Belleville springs.

Since the accessory mounting distances have essentially determined gear center distances and pitch diameters, and high contact ratios have set the face widths for the helix angles involved, the gear stresses are extremely low for the project accessory power draw. The gears have no predictable endurance limit and should provide the ultimate in reliable accessory drive performance.

The bearing loads due to accessory power absorption are very low, and bearing lives are limited only by the thrust loads imposed by the Belleville springs. In all locations the calculated minimum bearing lives are in excess of 20,000 hours, which would provide two and a

## Section VI

half years of continuous operation before replacement would have to be considered.

### ELECTRICAL SYSTEM

A starting and automatic sequencing system has been designed for the TS120 turboshaft engine to meet the contract requirements. Basic to the final design is the use of economical components with ruggedness, reliability and light weight as requirements of prime importance. Basic to the design study was the premise that the total TS120 system would be field operated under combat and extreme environmental conditions. Simplicity in the mode of operation, as well as replacement or repair of the sequencing components, was made a prime objective.

A total of three automatic sequencing systems were evaluated and they are illustrated in the electrical schematics shown in Figures VI-3 and VI-4.

Figure VI-3 is the electrical schematic which describes the selected system I. This system is a compromise in components of systems II and III except for an electronic speed switch performing some of the sequencing functions.

Figure VI-4 is the electrical schematic for systems II and III. The first of these follows an automotive approach, using a heavy starter and alternator and a wide-tolerance speed switch. The second is an aircraft-type approach, using lightweight components and a more precise speed switch.

Tables VI-I, VI-II, and VI-III correspond to the three systems concerned and list the various components with vendor's name, part number and unit weight.

The control system has been designed to operate with a nominal 24 volt DC battery power supply. During low temperature operation and upon starter impact, the battery voltage is seldom above 10 to 12

## Section VI

volts; therefore, components such as the starter relay, fuel solenoid coil, and relays have been designed to function over a voltage range of 10 to 30 volts. All other electrical components are designed to operate over a voltage range of 18 to 30 volts.

The operation of the start, sequencing and protective systems, Figures VI-3 and VI-4, is as follows.

A customer-supplied 24 volt DC battery is the external power source that must be attached to the starter relay ( $K_1$ ) at the contact terminals ( $E_1$ ). From the positive terminals of  $E_1$ , 24 volt DC power is fed through the sequence box to a customer-provided start switch, (it is understood that a 15 ampere circuit breaker will be provided by the customer to prevent current overloads).

The automatic starting sequence will begin by closing the start switch. This will energize the starter relay,  $K_1$ , through the normally closed protective relay contacts  $E_2$  and the normally closed load contacts  $E_6$ . The energization of  $K_1$  will close the  $E_1$  contacts in the starter circuit and the engine will begin to rotate. As the engine begins to rotate, the oil pump will build up oil pressure, closing the pressure switch,  $S_3$ , which will energize relay  $K_7$ .

The activation of relay  $K_7$  will close the normally open contacts  $E_7$  in the fuel solenoid and ignition coil circuit, allowing combustion to take place.

The engine will now accelerate and as the r.p.m. is increased beyond 40 percent of maximum engine speed, the normally open speed switch,  $N_1$ , will close. This will energize relay  $K_6$  which in turn will close contacts  $E_6$  in the hourmeter and start counter circuit, allowing a start to be recorded and will begin timing the engine running. The starter and igniter will be de-energized by the opening of the  $E_6$  contacts at this time and the engine will accelerate to maximum speed. The normally open contacts  $E_6$  in the low oil pressure circuit will now also close; however, if switch  $S_5$  has not opened (15 psig needed) the engine start sequence will be terminated. In addition the low oil pressure failure light will come on and stay on due to contact  $E_3$  being now closed.

## Section VI

At this point it must be emphasized that should the low oil pressure arm - disarm switch be switched to the disarm position, the engine will recommence its starting cycle. The proper sequence in the event of a system shut-down is to restore the start switch to the "off" position before attempting further starts or investigation of the failure.

The overtemperature and the overspeed safety circuits are similar in operation to the low oil pressure system. If, during any period of the starting sequence, the engine exceeds the preset exhaust temperature limit of 1150°F, the main fuel solenoid igniter, and starter will be shut off through the overtemperature relay K<sub>4</sub> and the protective relay K<sub>2</sub>, which are actuated by the contacts in the overtemperature switch S<sub>2</sub>. Electrical power will be provided to the customer control panel for an overtemperature light. This light will remain "on" to indicate the cause for engine shut-down and the engine cannot be restarted until corrective action is taken or until the start switch is turned "off" and then "on" again. An emergency override switch is provided in the overtemperature circuit which is mounted on the customer control panel. By opening the override switch, the overtemperature relay K<sub>4</sub> is eliminated from the protective circuitry and the engine will not shut down if engine overtemperature occurs.

Overspeed protection is provided at 112 percent of normal rated engine speed. At the alternator frequency representing the overspeed condition, the K<sub>5</sub> relay will be activated. The same shutdown sequencing conditions mentioned for the overtemperature will take place; however, this circuit does not have override and it cannot be disarmed.

A suggested addition to the circuit is a connection between the positive side of relay K<sub>4</sub> and the decrease line of the governor positioning cam. This addition will serve as an automatic temperature safeguard. When an overtemperature condition exists, temperature switch S<sub>2</sub> will close, relay K<sub>4</sub> will energize, the engine will be shutdown and the governor positioning cam will rotate to the full decrease position. The overtemperature failure light will come on and stay on.

## Section VI

TABLE VI-I  
STARTING AND SEQUENCING SYSTEM I

<u>Component</u>	<u>Vendor</u>	<u>Vendor Part No.</u>	<u>Weight - Lbs.</u>
Starter	Bendix Corp.	6B49-2	8.75
Alternator	Phelon Co.	X-20-2	2.50
Rectifier	Phelon Co.	X-20-15	1.00
Voltage Regulator	Phelon Co.	X-20-15	
Thermocouple and Harness	Fenwall	77143-0	0.19
Overtemperature Switch	Control Products	X2	0.11
Oil Pressure Switch S <sub>3</sub> and S <sub>5</sub>	Hobbs	MI 1545	0.20*
Hourmeter	Hobbs	MI-980-24	0.45
Start Counter	Durant Mfg. Co.	6-Y-11312	1.00
Coil (Ignition) Including Lead	Benton	18300	0.75
Fuel Solenoid	Valcor	V-500	0.45
Speed Switch	Consolidated Controls Corp.	R23SJ02	0.80
Relay K <sub>1</sub>	Cutler-Hammer	AN3370-1	1.25
Relay K <sub>2</sub> K <sub>6</sub>	Potter-Brumfield	MB-4279	0.60*
Relay K <sub>3</sub> K <sub>4</sub> K <sub>5</sub>	Potter-Brumfield	KHS-17D11	0.42*
Relay K <sub>7</sub>	Potter-Brumfield	KA-14AG	0.12
Connectors	Bendix Corp.	See List	1.25
Capacitors C <sub>1</sub> and C <sub>2</sub>	Sprague	CP53B1EF105K	0.31*
* Combined Weight			Total <u>20.15</u>

**Section VI**

**TABLE VI-II**  
**STARTING AND SEQUENCING SYSTEM II**

<u>Component</u>	<u>Vendor</u>	<u>Vendor Part No.</u>	<u>Weight - Lbs.</u>
Starter	Delco-Remy		28.0
Alternator	Delco-Remy	X-3838	9.0
Rectifier	Delco-Remy		
Voltage Regulator	Delco-Remy	90005	1.3
Thermocouple and Harness	Bendix Corp.	77820, 10-347453-1	0.18
Overtemperature Switch	Control Products Inc.	X2	0.11
Oil Pressure Switch S <sub>3</sub> and S <sub>5</sub>	Hobbs	MI-1545	0.20*
Hourmeter	Hobbs	MI-980-24	0.45
Start Counter	Durant Mfg.	6-Y-11312	1.0
Coil (Ignition)	Bendix	10-369550-1	1.0
Fuel Solenoid	Valcor	V-500	0.45
Speed Switch	AC	"Speed AC"	0.94
Relay K <sub>1</sub>	Cutler-Hammer	AN3370-1	1.25
Relay K <sub>2</sub> K <sub>6</sub>	Potter-Brumfield	MB4279	0.60*
Relay K <sub>3</sub> K <sub>4</sub> K <sub>5</sub>	Potter-Brumfield	KHS17D11	0.42*
Relay K <sub>7</sub>	Potter-Brumfield	KA-19AG	0.12
Packaging, Wiring Connectors			1.25
Capacitors C <sub>1</sub> and C <sub>2</sub>	Sprague	CP53B1EF105K	0.31*
* Combined Weight			46.58

## Section VI

TABLE VI-III  
STARTING AND SEQUENCING SYSTEM III

<u>Component</u>	<u>Vendor</u>	<u>Vendor Part No.</u>	<u>Weight - Lbs.</u>
Starter	Bendix Corp.	6B49-2	8.75
Alternator	Phelon Co.	X-20-2	2.5
Rectifier	Phelon Co.	X-20-15	1.0
Voltage Regulator	Phelon Co.		
Thermocouple and Harness	Bendix Corp.	77820/ 10-347453-1	0.18
Overtemperature Switch	Control Products Inc.	X2	0.11
Oil Pressure Switch S <sub>3</sub> and S <sub>5</sub>	Gorn	GP8000	1.06*
Hourmeter	A. W. Haden Co.	C4222	0.38
Start Counter	A. W. Haden Co.	E7817	0.50
Coil (Ignition) Including Lead	Bendix Corp.	10-369550-1	1.0
Fuel Solenoid	Valcor	V-500	0.45
Speed Switch	A. C.	640-4150	1.0
Relay K <sub>1</sub>			1.25
Relay K <sub>2</sub> K <sub>6</sub>			0.60*
Relay K <sub>3</sub> K <sub>4</sub> K <sub>5</sub>			0.42*
Relay K <sub>7</sub>			0.12
Packaging, Wiring, Connectors, etc.			1.25
Capacitors C <sub>1</sub> and C <sub>2</sub>	Sprague	CP53B1EF105K	0.31
<hr/>			<hr/>
* Combined Weight		Total	21.30

## Section VI

### TS120 BATTERY CHARGING ALTERNATOR

The battery charging alternator, being designed into the TS120 engine, is manufactured by the R. E. Phelon Company of East Longmeadow, Massachusetts.

It is an inductor-type alternator of Phelon's exclusive design and is shown in Figure VI-5. The rotor is mounted on a shaft provided in the accessory case with no mechanical connection between the rotor and the stator. The stator consists of generator windings disposed on the stator teeth and a single field coil to generate flux, which flows through the teeth of the stator into the rotor teeth, thence in a magnetic circuit through the wheel itself and back to the center of the stator. No brushes, slip rings, commutators, or the like are required.

All windings, both generating and exciting, are mounted on the stator and are therefore stationary. There are no windings whatever in the rotor. The generator itself is three-phase, which is accomplished by maintaining a ratio of stator teeth to rotor teeth of three to two, respectively. In this way the flux level in the wheel remains substantially constant, even though the flux level in the rotor and stator teeth varies widely. For this reason it is possible to make the rotor wheel out of a high-strength forging rather than having to make a laminated build-up. The only laminations required are in the stator and the rotor teeth. Since all windings are stationary it is possible to impregnate the stator windings into a single unit for protection.

This generator is impervious to water, sand, dust, and oils, and so forth, with no particular provision required for sealing. Elimination of all rubbing contacts, such as brushes and slip rings, plus utilization of a solid-state regulator, makes elaborate shielding and radio noise suppression unnecessary. This type of construction means that the generator will have an indeterminate life since there are no parts to wear out.

It has no speed limitations except for the centrifugal stress limitations of the wheel itself, and the entire unit can be furnished at relatively low cost as compared to competitive designs that will withstand the same environment and service. Design modifications to facilitate

## Section VI

integration into the engine are currently under discussion.

The alternator frequency is 4000 cps at an alternator speed of 40,000 rpm. At this speed it will produce approximately 18 amperes at 40 volts DC. The higher voltage capability has been designed into the machine because of a possible need of 22 volts DC into the frequency controlled speed switch. The Phelon alternator voltage/current performance is presented in Figure VI-6.

During the design phase of the TS120 engine, a total of five alternator sources were investigated. The Phelon design was chosen because existing hardware in this speed and electrical output range was already available. The Phelon alternator also provides a marked economic advantage to the total engine package over the other four alternator sources.

The General Electric designed alternator for the TS120 engine is shown in Figure VI-7. It, like the Phelon alternator is a 40,000 rpm machine that weighs approximately three pounds. In addition, General Electric had designed a 68,000 rpm alternator for the TS120 engine. This unit was to have been incorporated into the accessory gearbox and was to become a part of the turbine shaft or turbine output quill shaft.

In addition to Phelon and General Electric, the Bendix Corporation, TKM, and Lear Siegler had all proposed alternators for use with the TS120 engine.

### ELECTRONIC SPEED SWITCH

In the sequencing System I presented for use with the TS120 engine, two parameters are controlled as a function of engine speed. Both functions - starter drop-out and engine overspeed - are triggered by an alternator frequency signal that is fed into an electronic speed switch.

## Section VI

Three versions of these electronic speed switches were evaluated during the design phase of the TS120 engine. The system devised by the Consolidated Controls Corporation, which has been qualified for use with the F-111 aircraft, was the one chosen for the TS120 engine. Principle of operation of the Consolidated Controls electronic speed switch is as follows. Output amplitude of the 15 ampere alternator is only approximately proportional to speed. While frequency is an exact function, varying AC out of the alternator is used to trigger a monostable multivibrator whose output pulse is regulated in amplitude and time duration independent of the incoming pulse frequency. As a result, and as shown in Figure VI-8, the average DC level of the output signal is proportional to the frequency at which the constant area pulses are generated. This DC signal is filtered and fed into the input circuit of one or more bistables, which give the required switching point with a high degree of accuracy. Each bistable is temperature compensated with the multivibrator so that all variations with temperature are taken into account.

A second frequency triggered speed switch was designed by Continental's Electronics Laboratory. One such system was built in bread-board form and was evaluated both at room temperature and at -65°F. The block diagram of the Continental electronic speed switch is shown in Figure VI-9.

The third frequency triggered circuit that was designed for the TS120 engine was proposed by the Bendix Corporation, Redbank Division. No effort beyond the circuit design was expended on this system because preliminary cost estimates made the system prohibitive for use with this engine.

The Continental electronic speed switch consists of individual units to trigger at the required speed points. Principle of operation of one of these units is as follows. The sine wave output of the 15 ampere alternator is fed to a series resonant circuit. This high Q circuit is sharply peaked at the desired frequency. It is followed by a buffer stage that performs the function of a temperature compensating and impedance matching stage. Output of the buffer stage triggers a silicon-controlled rectifier, which in turn energizes a relay.

## Section VI

### TS120 ENGINE STARTING

Two starters (General Electric and Bendix) have been designed to meet the torque requirements of the TS120 engine. The starters have been sized based upon the following:

1. Known polar moment of inertia of the engine.
2. Estimated polar moment of inertia of the ERDL alternator.
3. Estimated engine drag torque, presented in Figure VI-10.
4. Additional 30 percent starter torque required to overcome the drag imposed by the customer-furnished alternator.

The two starter designs and their respective torque outputs are shown in Figures VI-11 and VI-12.

The torque requirements of the TS120 engine and ERDL coupled generator are presented in Figure VI-12. The drag imposed by the ERDL alternator, however, is not reflected in the drag curve because it has not been defined to date. As can be seen from Figure VI-10, the maximum torque demanded by the engine/generator combination occurs at engine light-off, which is at approximately six percent engine speed. The Bendix starter output torque (curve 1, Figure VI-10) is approximately 100 percent greater at 60°F temperature: and 30 percent greater at -65°F than required and it is felt this additional torque will be sufficient to overcome the imposed alternator drag.

Two alternate starters, with higher torque characteristics, are available; one unit weighs 17 pounds and the other 12.5 pounds.

**Section VI**

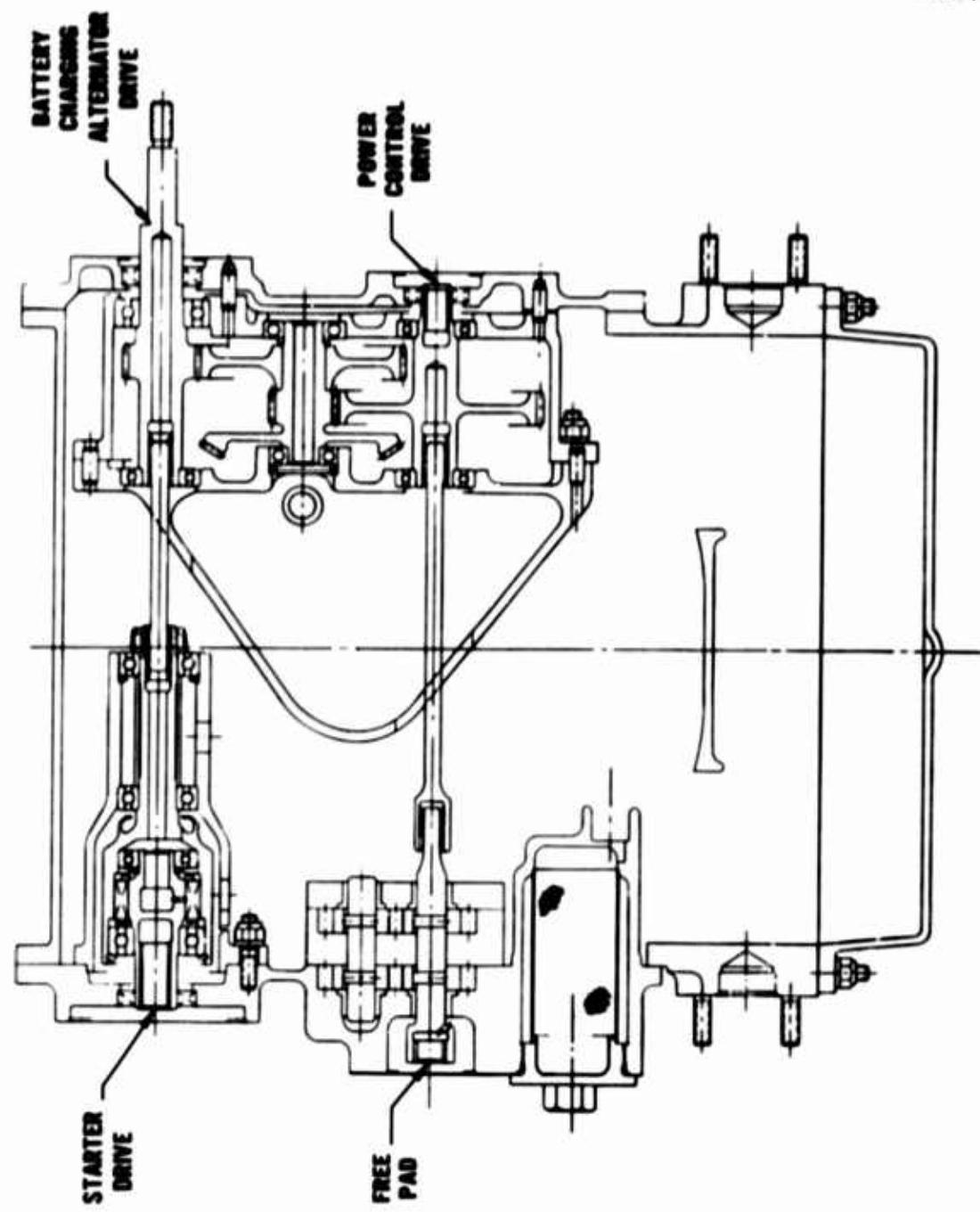
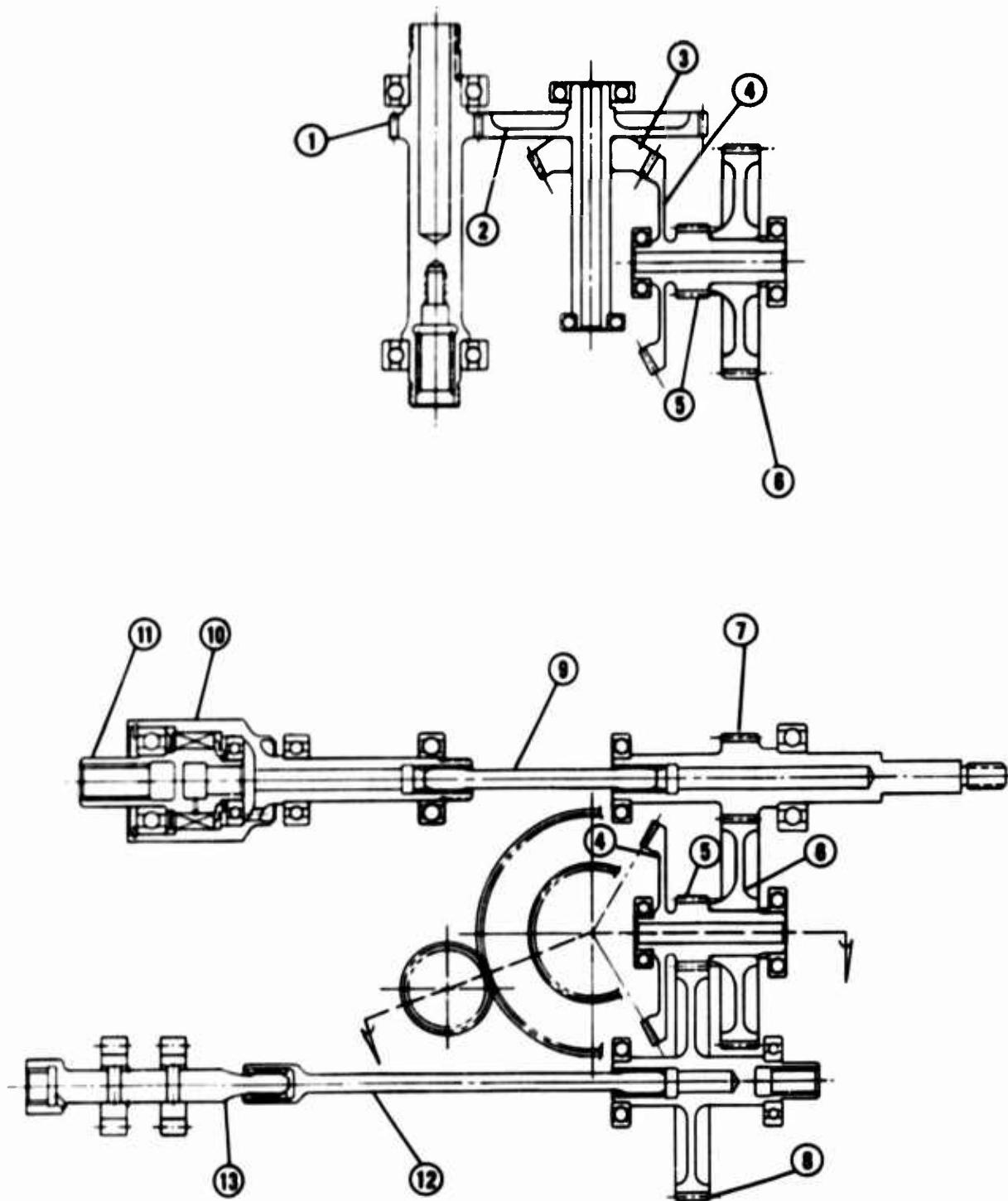


Figure VI-1. TS120 Accessory Drive (Front View Through Accessory Gears).

**Section VI**



**Figure VI-2. TS120 Accessory Drive Train.**

## **Section VI**

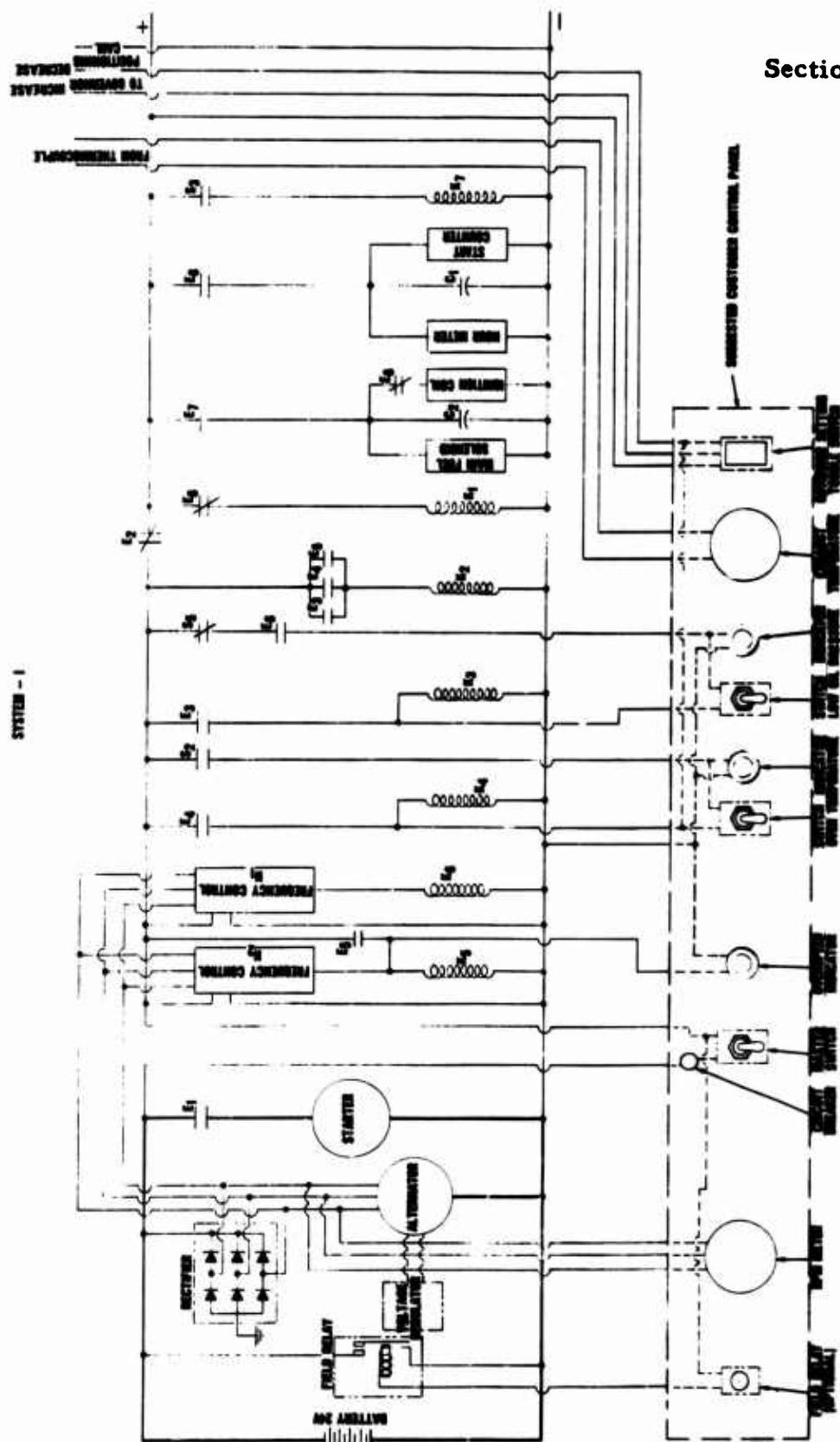


**Figure VI-3.** TS120 Electrical Schematic -System I.

**Section VI**

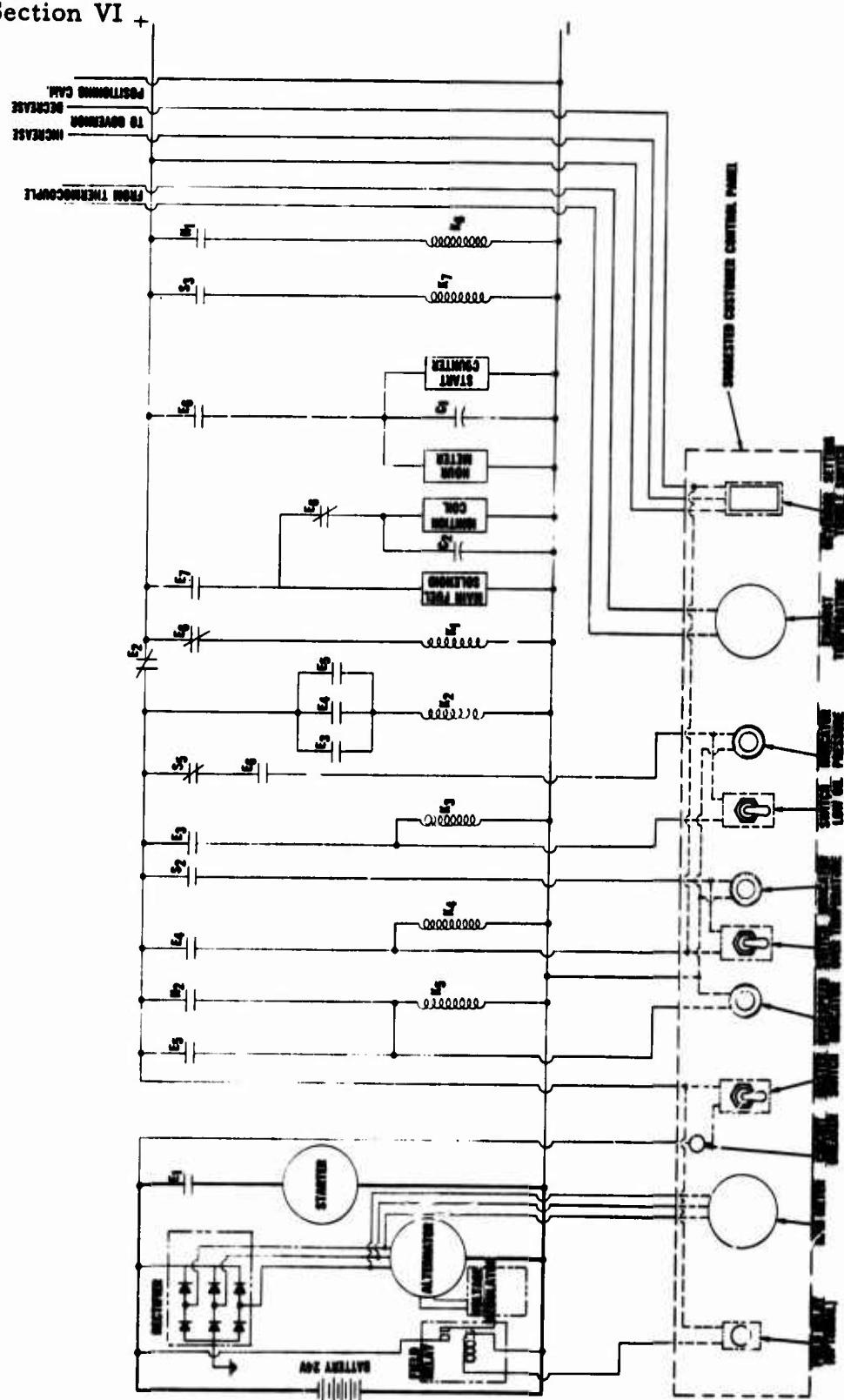
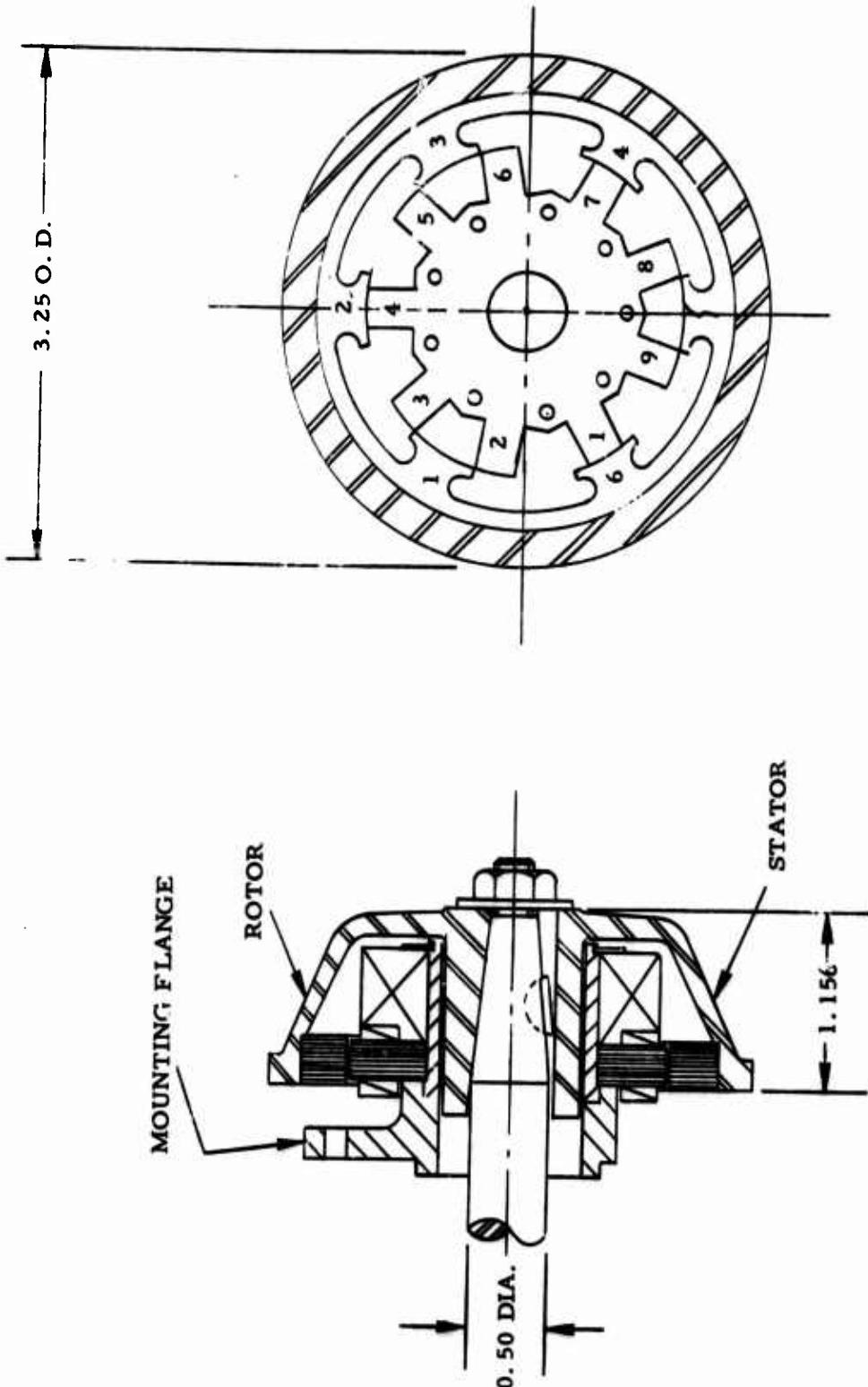


Figure VI-4. TS120 Electrical Schematic - Systems II and III.

**Section VI**



**OUTPUT - 15 AMP - 40,000 RPM**

**Figure VI-5. R. E. Phelon Company Battery Charging Alternator.**

Section VI

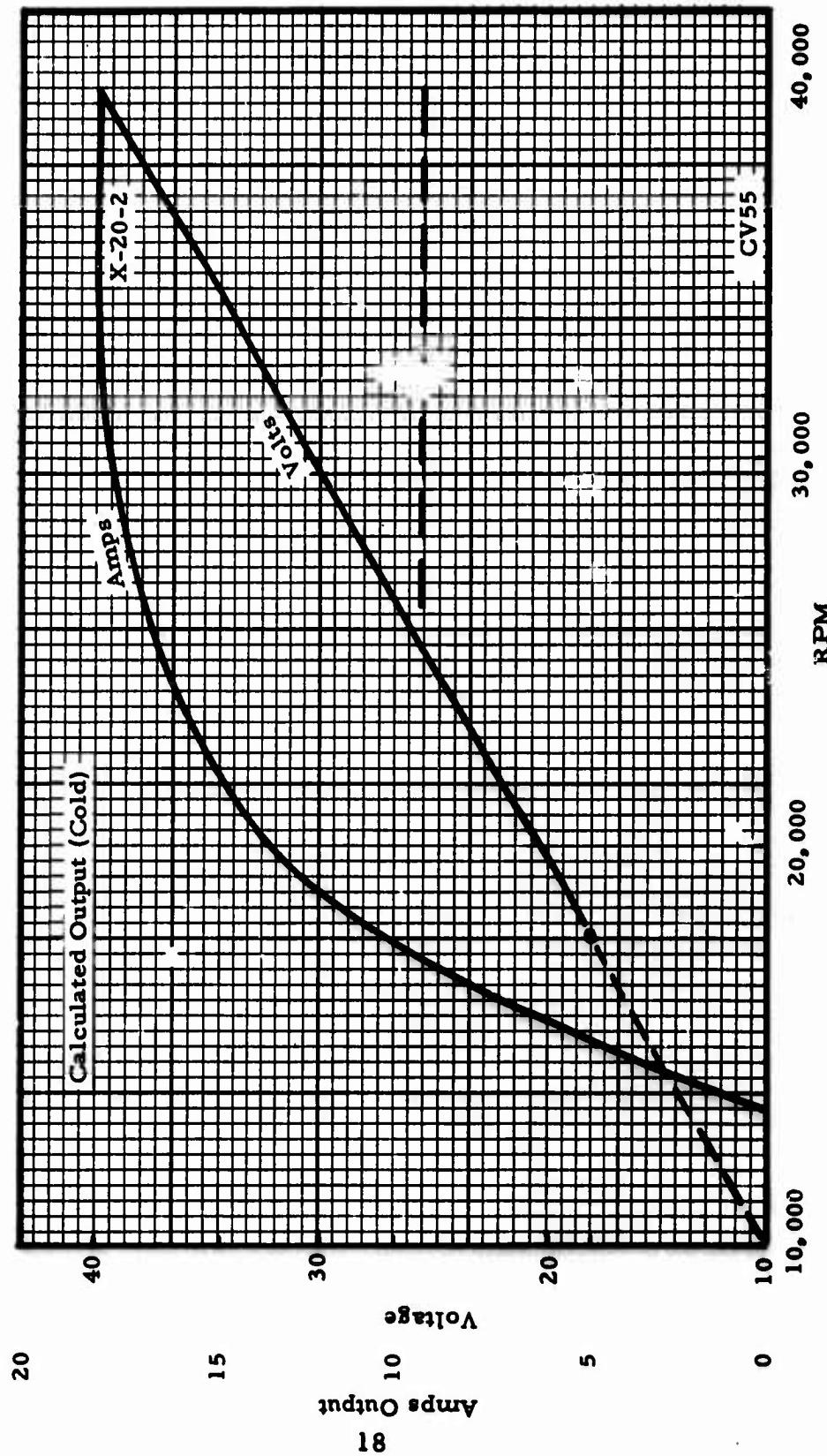
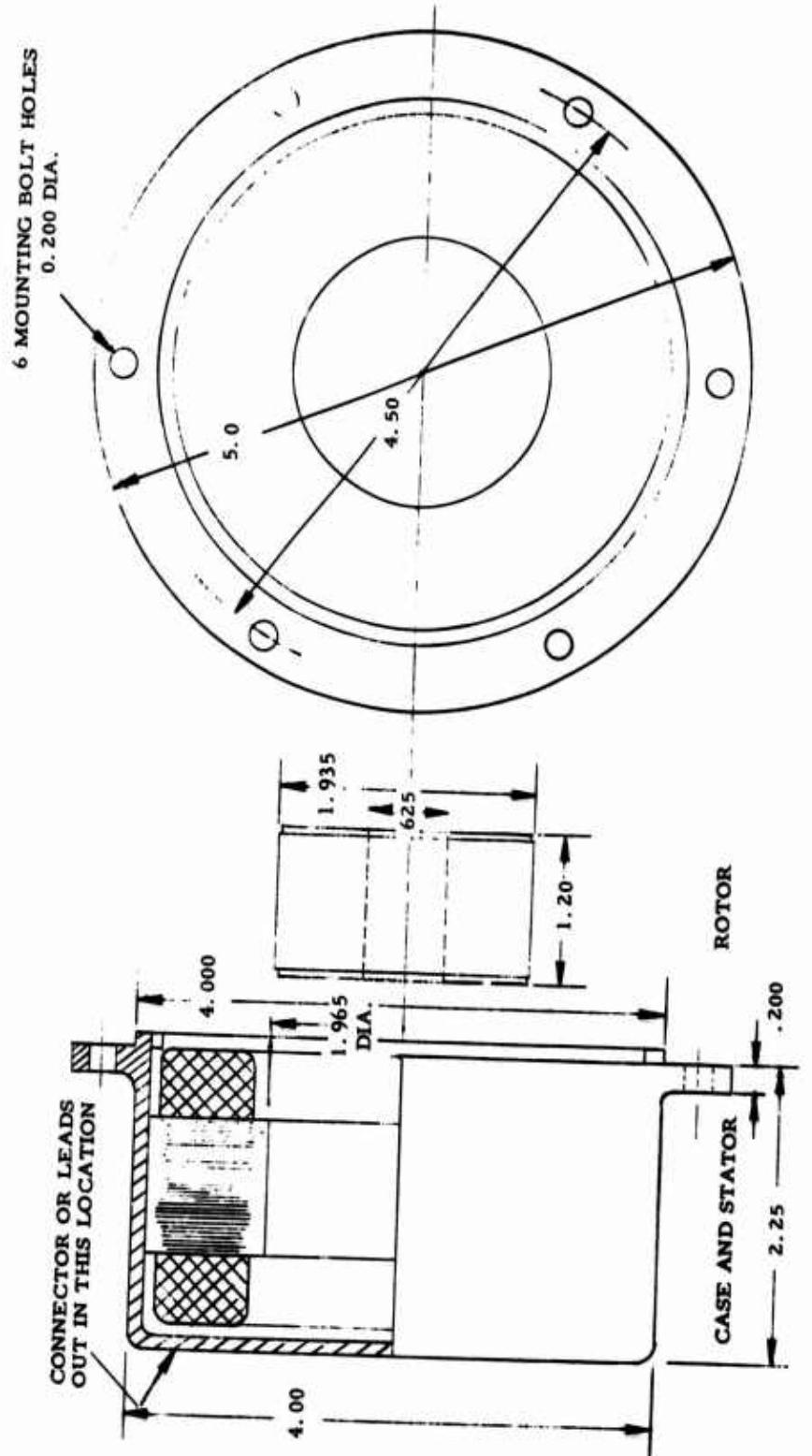


Figure VI-6. Phelon Company Alternator Voltage Current Performance.

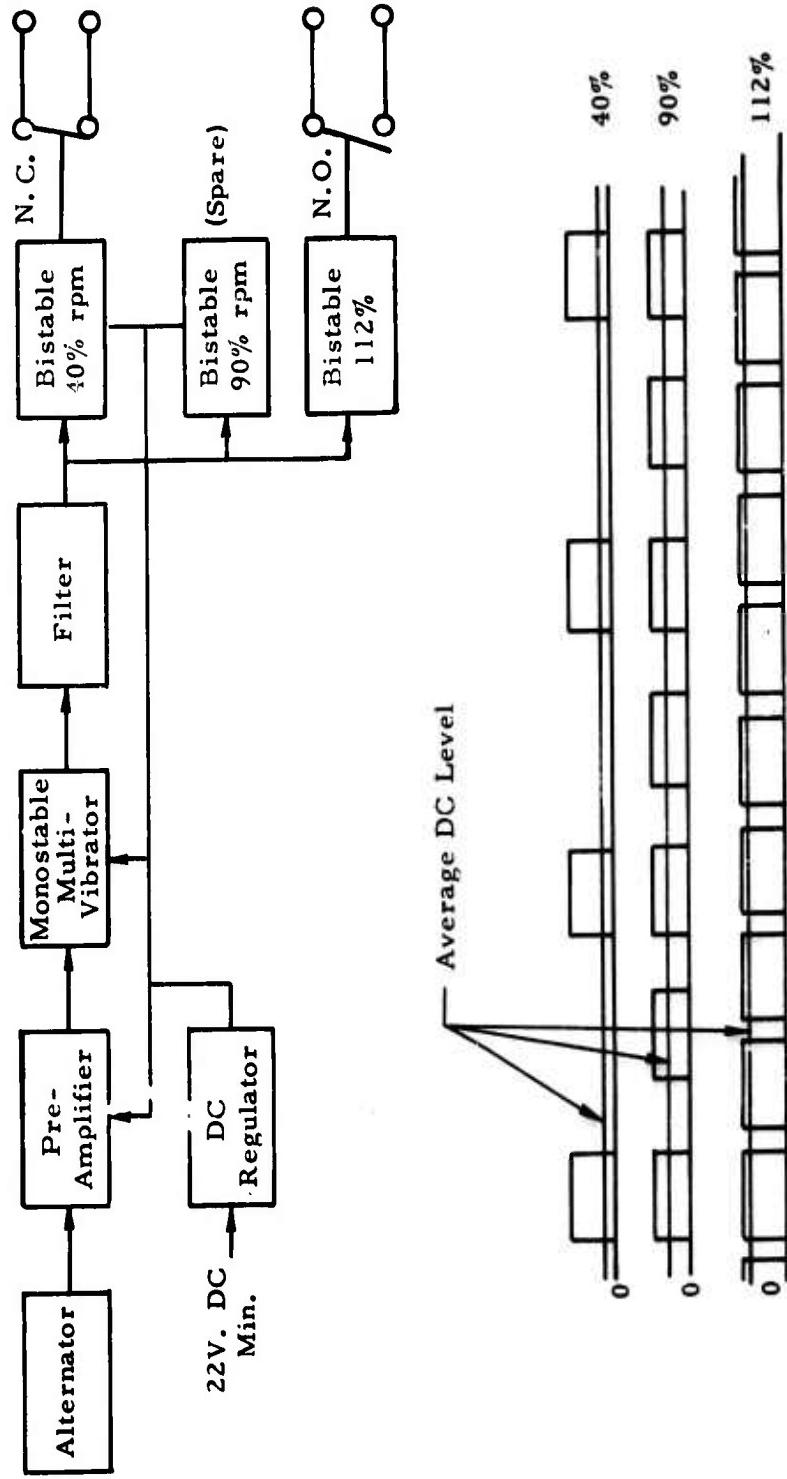
**Section VI**



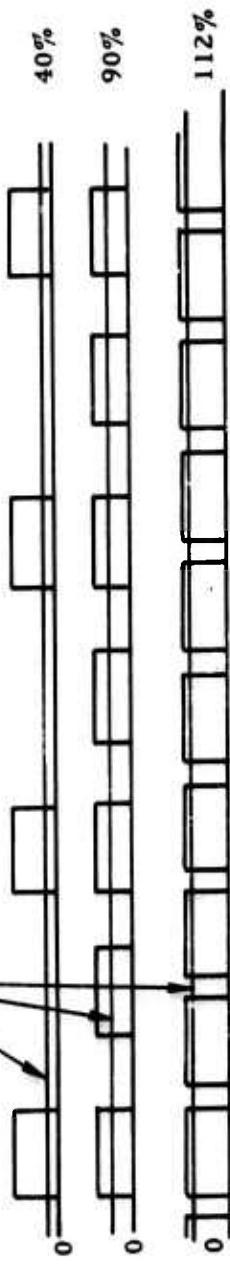
**Figure VI-7. General Electric Designed Alternator.**

## Section VI

BLOCK DIAGRAM OF TRIPLE  
SETTING SPEED SWITCH BY  
CONSOLIDATED CONTROLS



Average DC Level



CONSTANT AREA PULSES VERSUS TIME AT TWO DIFFERENT ENGINE SPEEDS.

Figure VI-8. Consolidated Controls Corporation Electronic Speed Switch Schematic.

**Section VI**

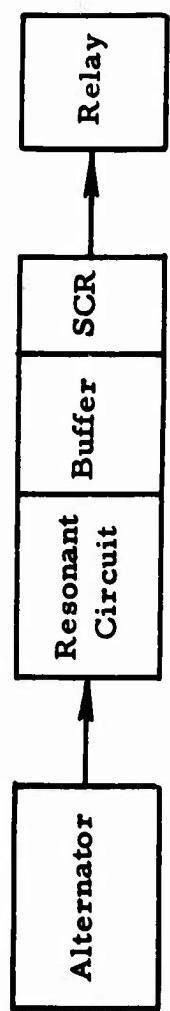


**Figure VI-9.** Continental Electronic Speed Switch Block Diagram.

**Section VI**

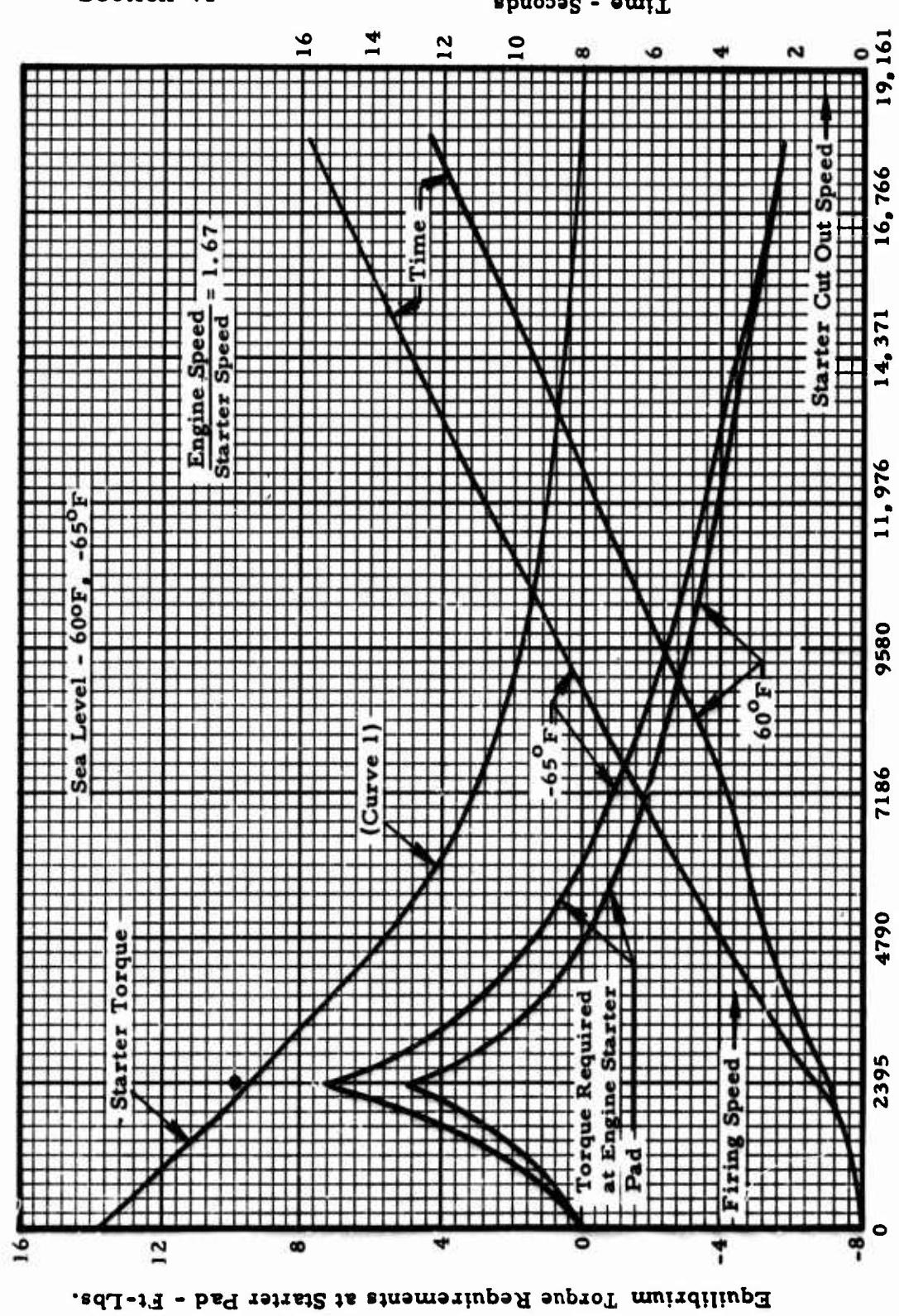


Figure VI-10. TS120 Estimated Starter Cycle.

## Section VI

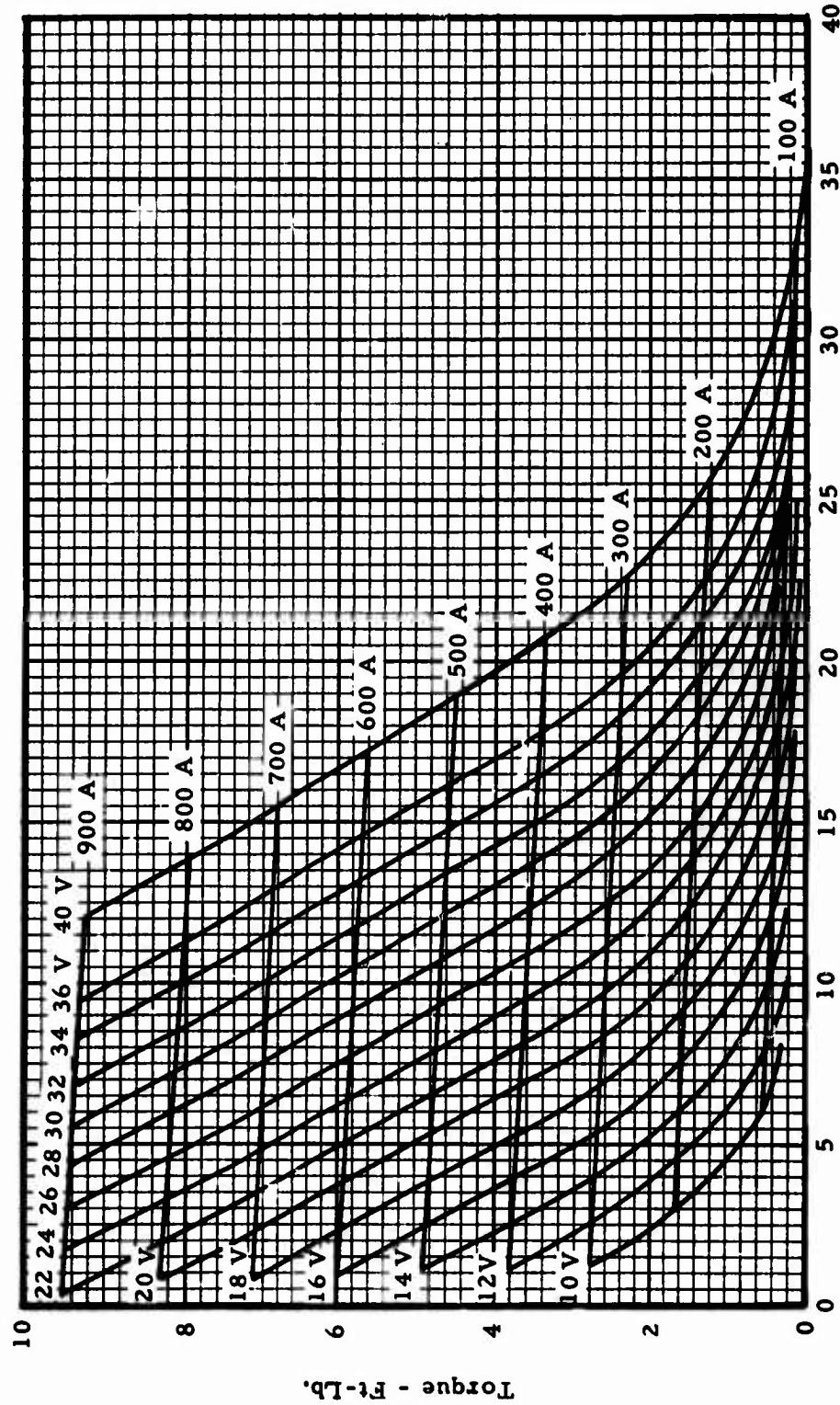


Figure VI-11. Starter Torque Characteristics - General Electric.

## Section VI

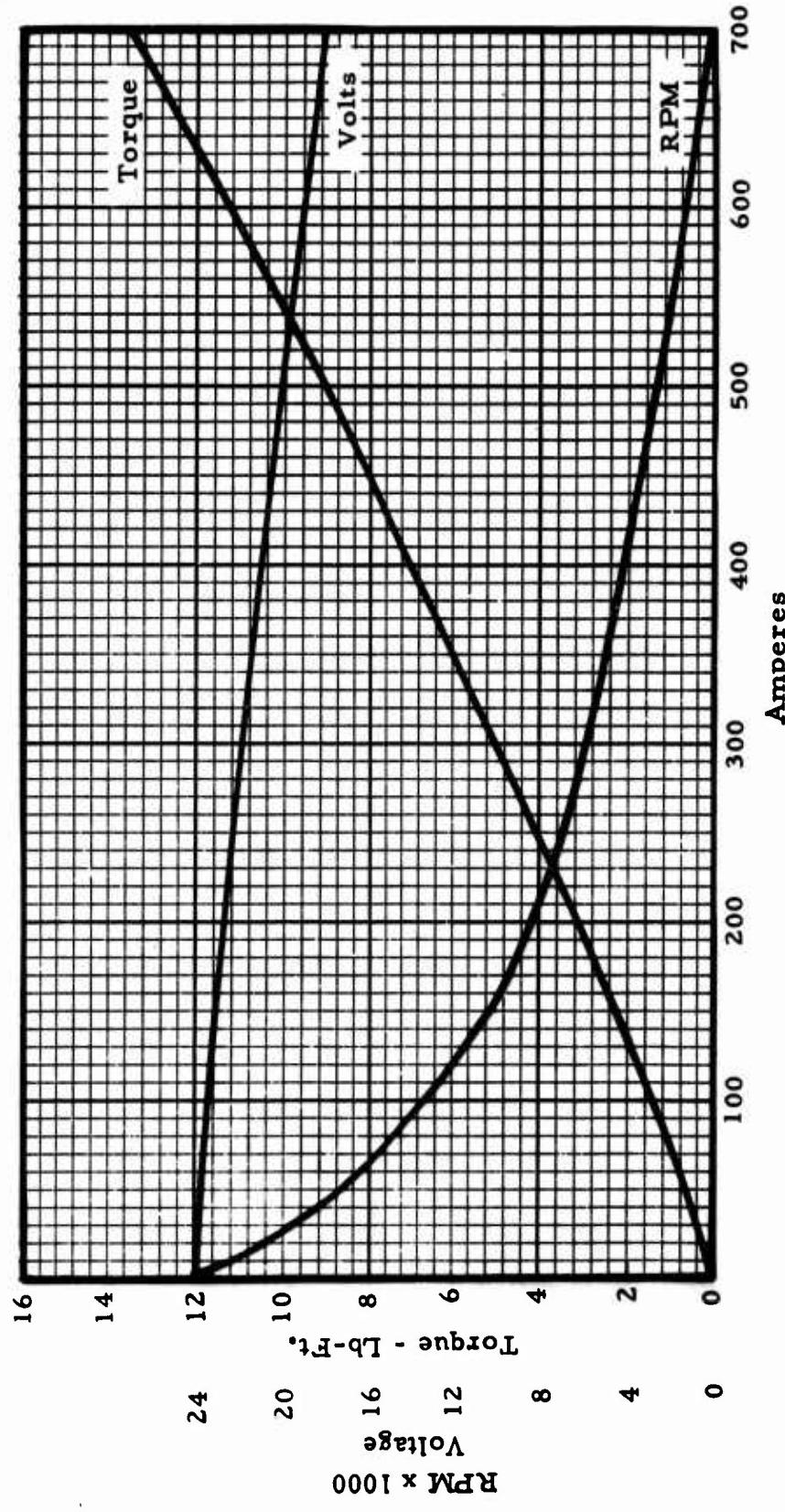


Figure VI-12. Starter Torque Characteristics - Bendix.

SECTION VII

**ENGINE LUBRICATION**

## SECTION VII - ENGINE LUBRICATION

The lubrication system is predicated on the requirements for the reduction gear version of the basic engine with the same basic lubrication system being applicable to the direct drive engine.

The engine lubrication system schematic is shown in Figure VII-1. Two positive displacement gear pumps of 5.75 gpm capacity each are used, one to provide engine oil pressure, the other to scavenge the rear bearing cavity. The system lube pressure of 30 psi is regulated by a valve that senses pump pressure after the filter, thereby making delivery pressure regulation insensitive to oil filter pressure drop. A ball and spring valve is mounted in parallel with the full-flow, replaceable element filter to protect the engine in case of filter plugging.

The integral, wet sump oil reservoir is located in the accessory case; its static capacity of approximately 3.5 quarts provides an adequate reserve for 50 hours of operation without oil addition. The engine running reservoir oil volume is estimated at three quarts. The oil flow of 4.3 gpm for the reduction gear engine will provide a dwell time of 10.5 seconds and the direct drive engine with a flow rate of 2.65 gpm will have a dwell time of 17 seconds.

All bearings and gears considered to be rotating at a relatively high speed, or heavily loaded, are jet lubricated. The remaining bearings and gears, all in the accessory drive train, are lubricated by the oil mist abundantly provided by the rotating gears. The oil flow at each lubrication point is controlled by a properly sized orifice and by the system pressure. Except in the case of the reduction gear meshes at the turbine shaft rear bearing, the oil flow to all other points is dictated by the choice of a minimum orifice diameter of 0.04 to reduce the probability of oil jet plugging. At a pressure of 30 psi, a 0.04 jet will flow 0.17 gpm, a reasonably low flow, yet sufficient to remove the friction heat.

The reduction gear engine has 19 lubrication points as shown in Figure VII-2. The oil jet sizes, flow rate and heat rejection summary is presented in Table VII-1.

Section VII

TABLE VII-I

TS120-G6 REDUCTION GEAR ENGINE  
LUBRICATION SUMMARY

Line Pressure 30 psi

Jet No.	Location	Jet Dia.	Flow (GPM)	Estimated Heat Rejection (Btu/Min.)
Seal - Turbine Shaft Thrust				
1	Bearing	.04	.17	2.0
	Bearing - Turbine Shaft			
2	Thrust	.04	.17	6.5
3	Coupling - Drive	.04	.17	2.0
	Bearing - Roller, Pinion			
4	Aft	.04	.17	2.3
	Bearing - Roller, Pinion			
5	Front	.04	.17	2.3
	Bearing - Ball, Pinion			
6	Thrust	.04	.17	1.2
	Gear Mesh - Pinion to Red.			
7	Gear Idler	.062	.4	60.0
	Gear Mesh - Red. Gear			
8	Idler to Power Output Gear	.062	.4	60.0
	Bearing - Ball, Red. Gear			
9	Idler Rear	.04	.17	1.80
	Bearing - Roller, Red.			
10	Gear Idler Front	.04	.17	4.15
	Bearing - Roller, Power			
11	Output Gear Rear	.04	.17	1.75
	Bearing - Ball, Power			
12	Output Gear Front	.04	.17	1.20
13	Gear Mesh - Bevel	.04	.17	1.0
	Overrunning Clutch			
14	Starter	.04	.17	1.0
	Bearing, Ball - Starter			
15	Driven Shaft Rear	.04	.17	1.0

**Section VII**

**TABLE VII-I (Cont'd.)**

**TS120-G6 REDUCTION GEAR ENGINE  
LUBRICATION SUMMARY**

**Line Pressure: 30 psi**

<b>Jet No.</b>	<b>Location</b>	<b>Jet Dia.</b>	<b>Flow (GPM)</b>	<b>Estimated Heat Rejection (Btu/Min.)</b>
16	Bearing, Ball - Alternator Drive Rear	.04	.17	1.0
17	Bearing, Ball - Alternator Drive Front	.04	.17	1.0
18	Bearings, Plain - Oil Pump (4 Bearings)		.15	1.0
19	Bearing, Roller - Turbine Shaft Rear	.087	.80	150.0
<b>TOTAL ENGINE OIL FLOW</b>			<b>4.30</b>	
<b>TOTAL ENGINE HEAT REJECTION</b>				<b>301.2</b>

The direct drive engine has 12 lubrication points as shown in Figure VII-3. The oil jet sizes, flow rate and heat rejection summary is presented in Table VII-II.

The oil flow at the front of the engine is returned to the wet sump by gravity. Only the oil from the rear bearing is returned by a scavenge pump. The shaft rear bearing oil is scavenged by a pump whose 5.75 gpm delivery compares with the 0.8 gpm rear bearing lube to provide a 7:1 scavenge ratio to accomodate entrained air. Based on measured data from other Continental

Section VII

TABLE VII-II

TS120 DIRECT DRIVE ENGINE  
LUBRICATION SUMMARY

Line Pressure: 30 psi

<u>Jet No.</u>	<u>Location</u>	<u>Jet Dia.</u>	<u>Flow (GPM)</u>	<u>Estimated Heat Rejection (Btu/Min.)</u>
	<b>Seal - Turbine Shaft Thrust</b>			
1	Bearing	.04	.17	2.0
	<b>Bearing - Turbine Shaft Thrust</b>			
2	Thrust	.04	.17	6.5
	<b>Coupling - Drive</b>			
3		.04	.17	2.0
	<b>Bearing - Ball, Power Output Shaft, Rear</b>			
4		.04	.17	1.0
	<b>Bearing - Ball, Power Output Shaft, Front</b>			
5		.04	.17	1.0
	<b>Gear Mesh - Bevel</b>			
6		.04	.17	1.0
	<b>OVERRUNNING CLUTCH - STARTER</b>			
7		.04	.17	1.0
	<b>Bearing, Ball - Starter Driven Shaft Rear</b>			
8		.04	.17	1.0
	<b>Bearing, Ball - Alternator Drive Rear</b>			
9		.04	.17	1.0
	<b>Bearing, Ball - Alternator Drive Front</b>			
10		.04	.17	1.0

## Section VII

TABLE VII-II (Cont'd.)

**TS120 DIRECT DRIVE ENGINE  
LUBRICATION SUMMARY**

Line Pressure: 30 psi

<u>Jet No.</u>	<u>Location</u>	<u>Jet Dia.</u>	<u>Flow (GPM)</u>	<u>Estimated Heat Rejection (Btu/Min.)</u>
11	Bearings, Plain - Oil Pump (4 Bearings)		.15	1.0
12	Bearing, Roller - Turbine Shaft Rear	.087	.80	150.0
<b>TOTAL ENGINE OIL FLOW GPM</b>				<b>2.65</b>
<b>TOTAL ENGINE HEAT REJECTION</b>				<b>168.5</b>

engines, the oil entering the cooler from the rear bearing sump is estimated to reach 300°F; in the cooler it is expected to drop 125°F with a resultant heat rejection to the 125°F (maximum) cooler air of 300 Btu/Min. This heat rejection equals the entire estimated engine lube heat gain. Leaving the cooler at 175°F, the oil returns to the sump where it mixes with the reservoir oil to reduce the over-all sump temperature, maintaining it below the guaranteed maximum of 250°F. The use of an adequately sized cooler assures engine lube oil temperature control without the need to rely upon the cooling effect through radiation, provided by the excellent heat transfer properties of the magnesium gear case and sump.

The oil cooler system is applicable to both the reduction gear engine and the direct drive configuration. However, the latter engine, with a heat rejection approximately one-half that of the former, may be capable of operating without an oil cooler or with a substantially reduced cooling unit, or perhaps, with a fuel-

## Section VII

to-oil cooler; the choice of these cooler systems alternatives must necessarily await data accrued through actual engine operation.

### MODEL TS120 OIL COOLER FAN DRIVE

The oil cooler fan is mounted on top of the alternator and driven by the alternator shaft at 39,749 rpm, Figure VII-4. To preclude oil cooler clogging and fan blade erosion, the inlet air is piped from the screened engine air inlet housing; the discharge air collects in an annulus surrounding the fan and is led to the cooler housing through flexible ducting. The fan design is of the radial type, delivering 400 cfm at a pressure head of 12 inches of water. The low blade tip speed of 500 feet per second should provide a relatively low level of noise. The oil cooler mounting arrangement and air ducting is shown in Figure VII-5.

Section VII

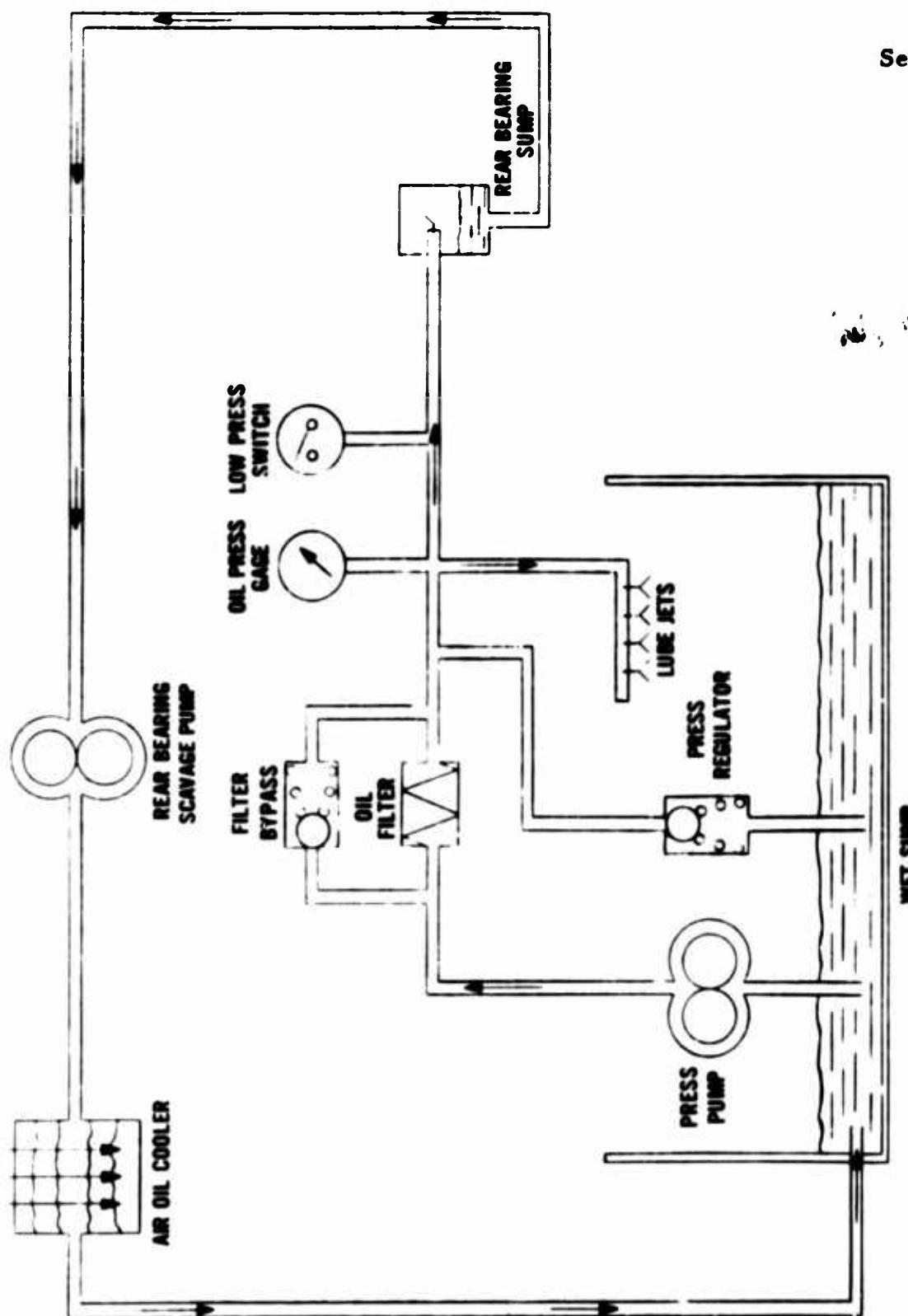
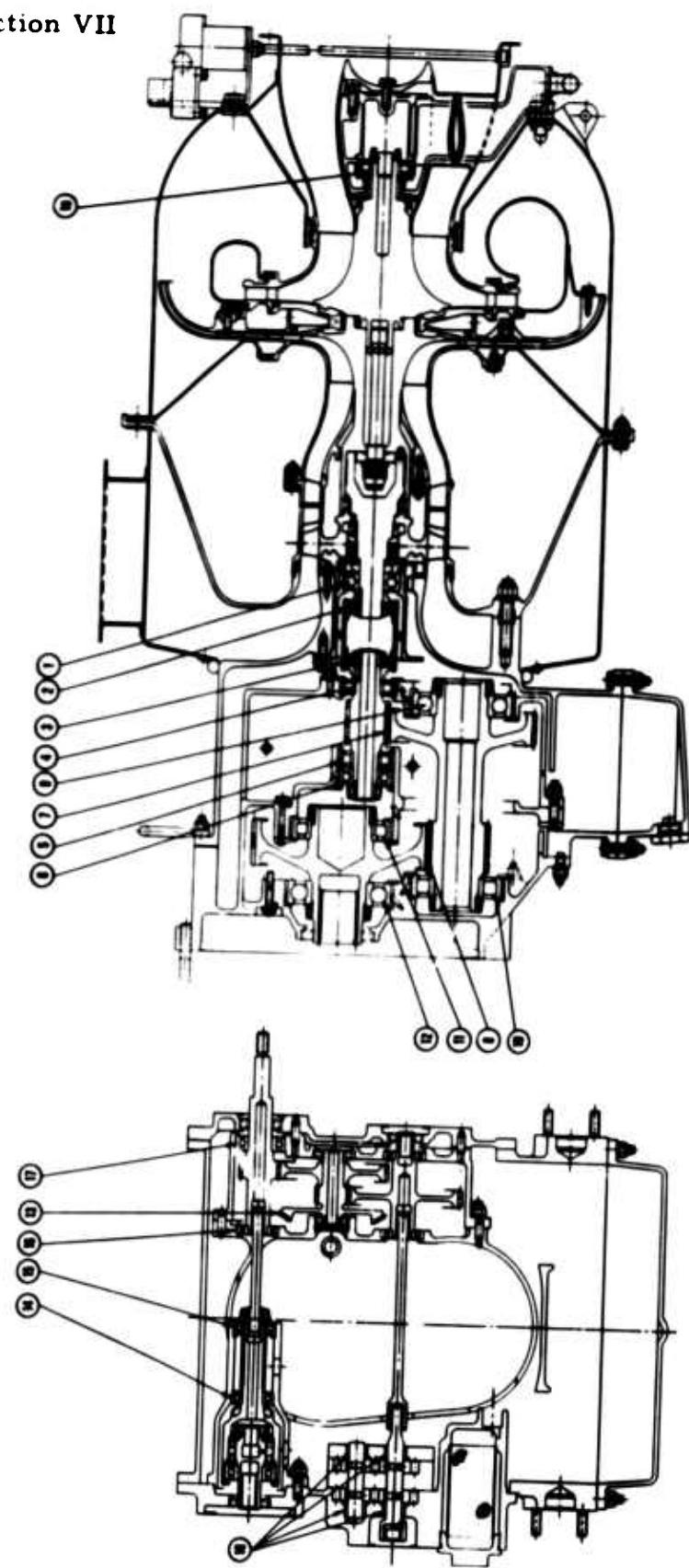


Figure VII-1. TSI 20 Lubrication System Schematic.

**Section VII**



**Figure VII-2. TS120-G6 Engine Lubrication Points.**

**Section VII**

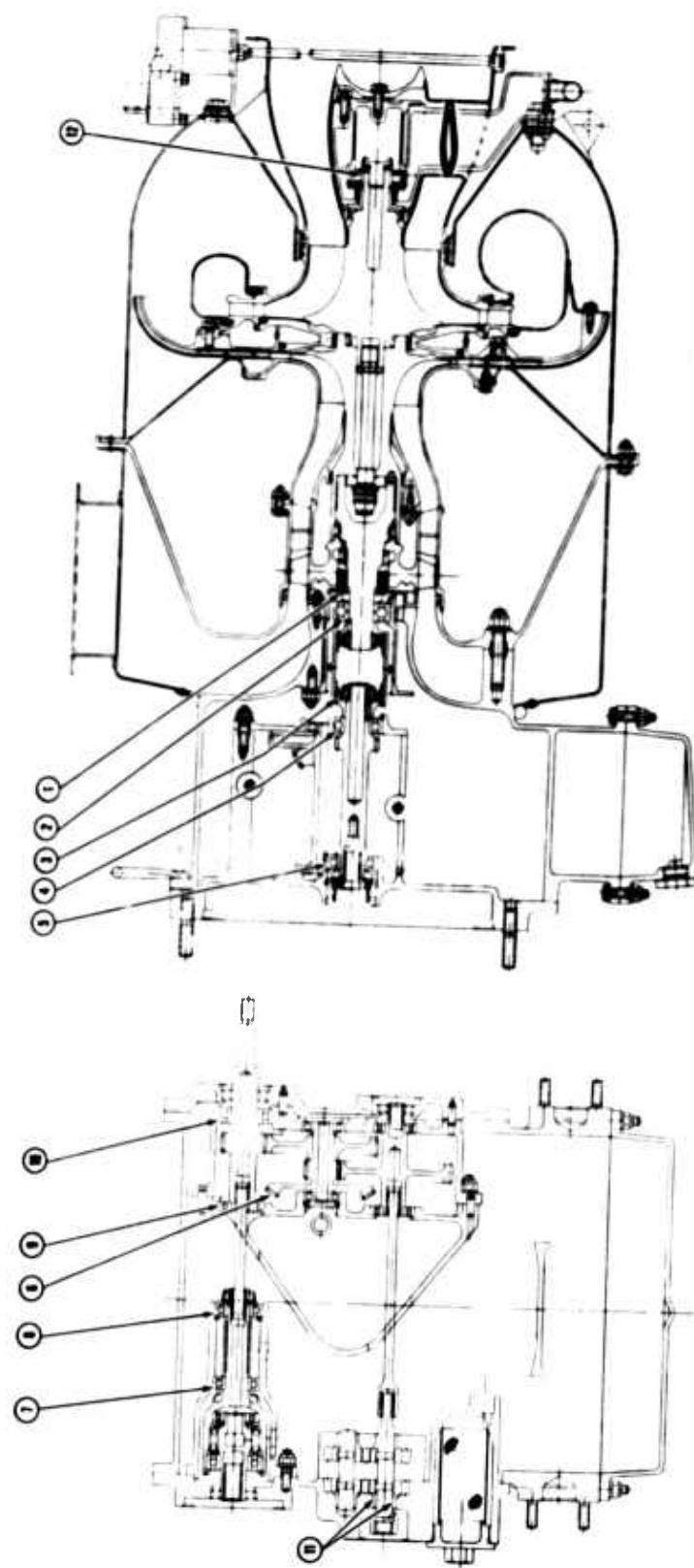


Figure VII-3. TS120 Engine Lubrication Points - Direct Drive.

**Section VII**

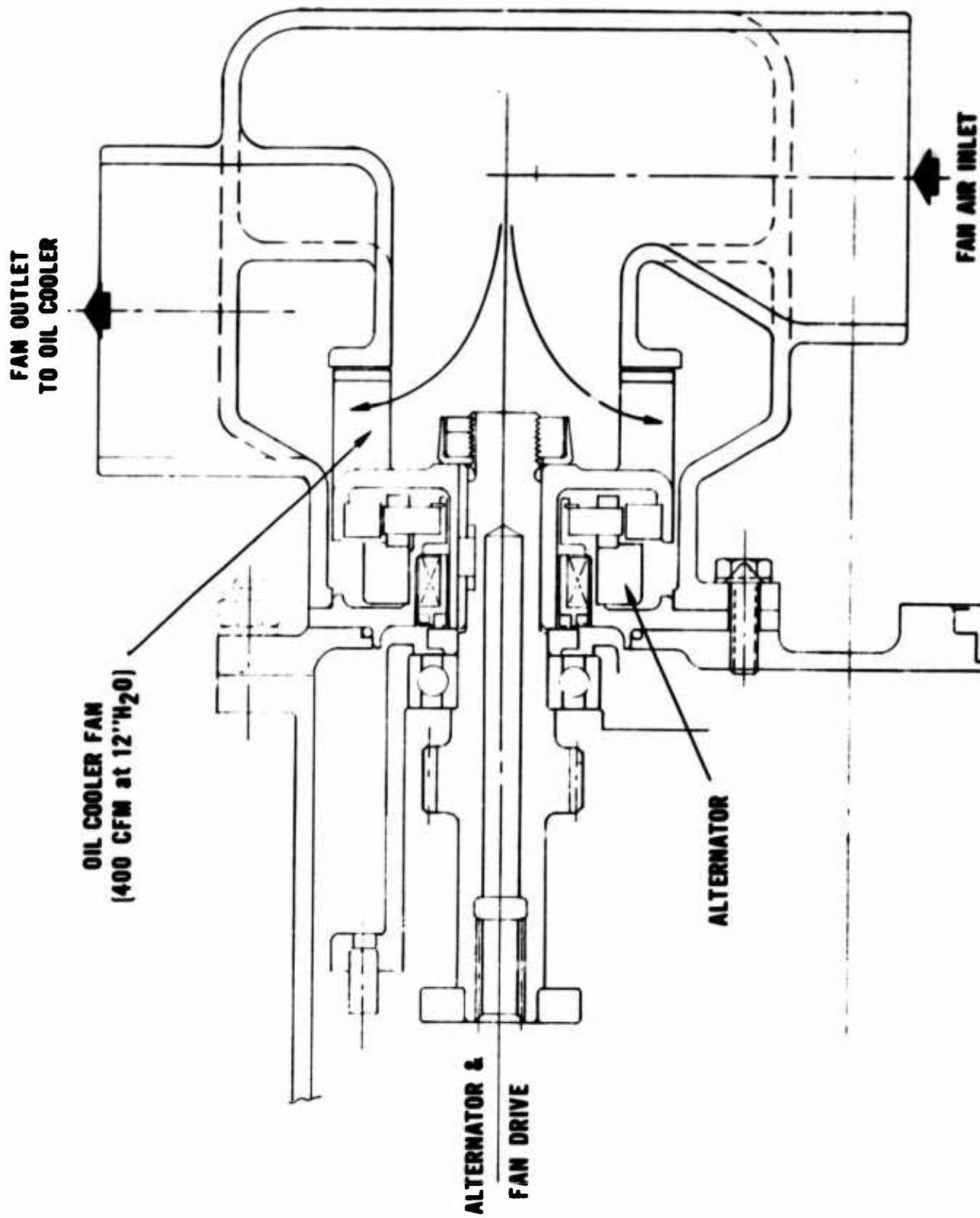
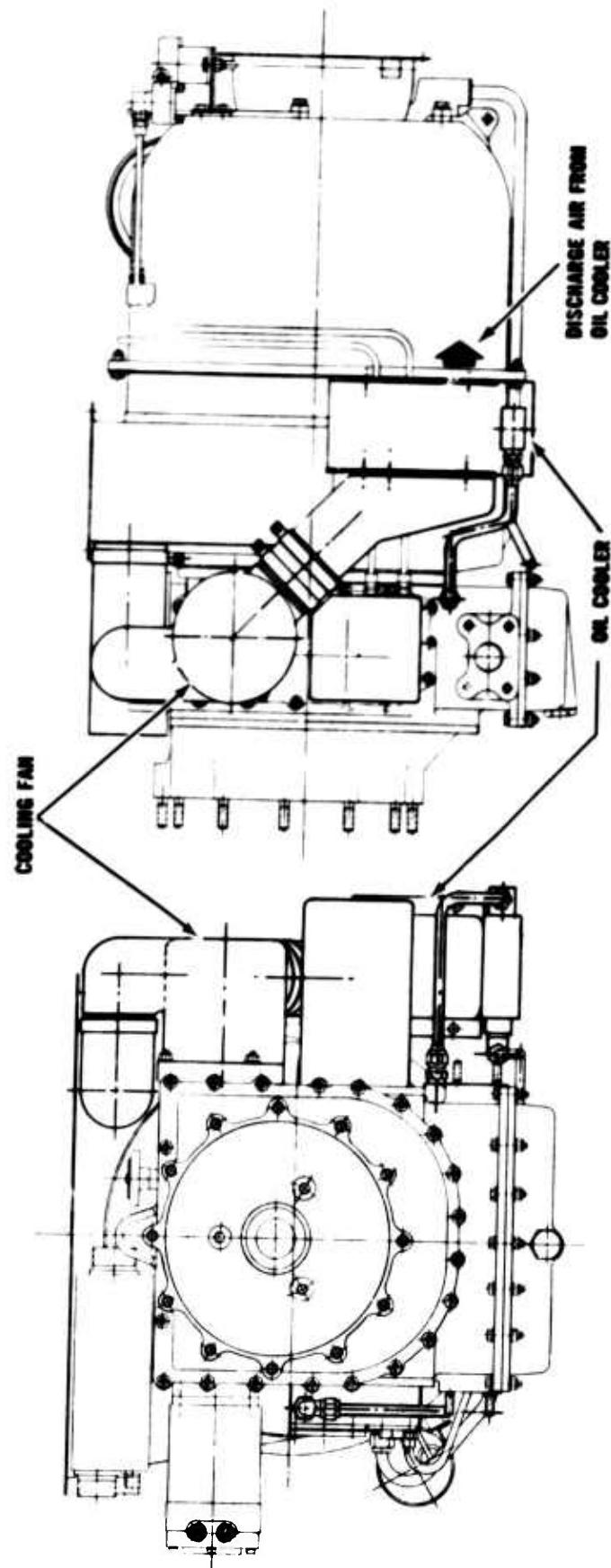


Figure VII-4. TS120 Oil Cooler Fan Drive.

**Section VII**



**Figure VII-5. TS120 Oil Cooler Mounting and Air Ducting Arrangement.**

**SECTION VIII**

**ENGINE WEIGHT**

## SECTION VIII - ENGINE WEIGHT

The TS120 estimated engine weight is presented in Figure VIII-1. The estimated additional weight for turbine rotor containment, discussed in a previous section, is shown as a separate item. The weight of the magnesium parts is based on sand castings. A reduction in weight of 5.4 pounds can be realized by the use of die castings. The identification of strategic national defense materials is shown in Figure VIII-2.

Part Name	Weight	Part Name	Weight
<b>ROTOR ASSEMBLY</b>			
Rotor-Radial Compressor	-	Case-Accessory	9.15
Rotor-Turbine	-	Power Take-Off Cover	3.20
Shaft, Front-Turbine	-	Power Take-Off Shaft	.84
Rotor-Axial Compressor	-	Cover-Accessory Gears	3.50
Miscellaneous	-	Clutch Assembly-Starter Overrunning	2.10
Total	16.90	Cover Assembly-Oil Pump	3.50
		Oil Pump	3.50
<b>COMPRESSOR ASSEMBLY</b>			
Stator-Axial Compressor	.80	Sump-Oil	2.00
Housing-Compressor	4.86	Alternator	2.00
Diffuser-Radial Compressor	4.00	Power Control	11.00
Housing-Air Intake	2.45	Starter Assembly	8.75
Duct-Air Intake	1.70	Filler-Oil	.50
Miscellaneous	1.00	Gears and Shafts	4.30
Total	14.81	Bearing	.62
		Miscellaneous	4.00
		Total	58.96
<b>COMBUSTOR ASSEMBLY</b>			
Interstage Diaphragm	2.12	Indicator-Exhaust Gas Temperature	2.00
Nozzle-Turbine Inlet	5.50	Switch-Oil Pressure	.32
Volute-Combustor	11.70	Control Assembly-Sequence	4.00
Cover-Radial Diffuser	6.20	Thermocouple	.20
Housing-Combustor	13.60	Cooler Assembly-Oil	4.50
Cover-Combustor	2.40	Fan-Cooling	3.50
Combustor	2.10	Miscellaneous	2.00
Miscellaneous	1.57	Total	16.52
Total	45.19		
<b>EXHAUST DUCT AND REAR BEARING SUPPORT</b>			
Duct-Exhaust	10.25	Lines/Fitting/Ignition	
Miscellaneous	4.50	Total	8.05
Total	14.75		
		<b>BASIC ENGINE WEIGHT</b>	
			<u>175.18</u>
		<b>Turbine Rotor Containment Ring</b>	
			<u>20.00</u>
		<b>TOTAL ENGINE WEIGHT</b>	
			<u>195.18</u>

Fig. VIII-1. Model TS120 Turboshaft Engine Weight Summary.

## Section VIII

Piece	Weight	Material	%	Wt	%	Wt	%	Wt	%	Wt	%	Wt	%
Rotor-Radial Compressor	4.00	AMS 5662	1.0	.04	52.5	2.10	19.0	.76	4.8	.19	3.0	.12	
Rotor-Turbine	6.90	Udimet 700	17.0	1.17	55.0	3.80	15.0	1.04	5.0	5.0	.34		
Rotor-Axial Compressor	1.60	AMS 5398			3.0	.05	15.5	.25	.45	.01			
Inter-stage Diaphragm	2.10	AMS 5391	1.0	.02	70.0	1.47	12.0	.25	1.8	.04	3.8	.08	
Nozzle-Turbine Inlet	5.50	AMS 5391	1.0	.06	70.0	3.85	12.0	.66	1.8	.10	3.8	.21	
Volute-Combustor	11.70	AMS 5532	19.0	2.22	20.0	2.34	21.0	2.46	.8	.09	3.0	.35	
Housing-Combustor	13.60	AMS 5512			10.0	1.36	18.0	2.45	1.1	.15	.5	.07	
Cover-Combustor	2.40	AMS 5512			10.0	.24	18.0	.45	1.1	.03	.5	.01	
Combustor	2.10	AMS 5532	19.0	.40	20.0	.42	21.0	.44	.8	.02	3.0	.06	
Duct-Exhaust	10.25	AMS 5512			10.0	1.03	18.0	1.85	1.1	.11	.5	.05	
WEIGHT TOTAL				<u>3.91</u>	<u>16.66</u>	<u>10.59</u>		<u>.74</u>	<u>1.29</u>	<u>.34</u>			

Fig. VIII-2. Model TS120 Turboshaft Engine Strategic National Defense Materials.

SECTION IX

**GEARED ENGINES**

## SECTION IX - GEARED ENGINES

Geared versions of the Model TS120 direct drive turboshaft engine feature a minimum impact on the over-all size of the direct drive engine. The geared engine (TS120-G6), shown in Figure IX-1 is 29.00 inches long, 25.00 inches wide and 19.68 inches high. The only exterior dimensional change was an increase in length of 2.50 inches and relocating the power output shaft 0.68-inch above the engine centerline.

Geared versions are accomplished with a compact two-mesh reduction gear. A 6000 rpm output engine, Figure IX-2, illustrates the basic type of reduction gear. A two-plane, two-mesh reduction gear was chosen to minimize the over-all impact of the reduction gear on engine weight and size. The reduction gear is composed of four relatively small diameter gears. These gears utilize the axial engine length required for the accessory drives in the direct drive engine to the maximum extent possible. The geared engine requires only the removal of the power take-off flange and the output shaft from the direct drive engine and the replacement of these parts with the reduction gear and its support diaphragms.

Referring to Figure IX-2, the reduction gear is composed of a high speed pinion (1) driving a compound idler (2), and the final drive gear (3). The reduction gear is supported by a cast magnesium power take-off flange (4), a cast magnesium diaphragm (5), and a cover adaptor (6). The reduction gear bearings are all press fitted on the inner race and clamped in place with a nut and lock combination. With the exception of the high speed pinion thrust bearing and radial bearing, the reduction gear bearings have clamped outer races. The high speed pinion thrust bearings are held in place axially with a snap ring (7), with the support relieved at the OD of the thrust bearing.

This type of mounting was used successfully on previous Continental engines and assures that the thrust bearing outer race will center from the inner race with a uniform contact angle, and will carry a pure thrust. These features are provided to minimize the effect of bearing race creep and the attendant fretting possibilities. The high speed reduction gear pinion replaces the originating

## Section IX

high speed accessory drive pinion discussed in the direct drive accessory gearing.

The 12,000 rpm output is obtained by simply changing the low speed mesh of the 6,000 rpm engine. This change requires only a different compound idler (No. 2, Figure IX-2), and final drive gear (3). Other output speeds may be obtained by the same procedure.

### GEAR REDUCTION UNIT

The basic configuration of the main power gear reduction unit, Figure IX-3, consists of a helical input pinion (1), driving a compound idler shaft (2), which in turn drives a helical output gear (3) at 6000 rpm in configuration (a) and at 12,000 rpm in configuration (b). The two configurations differ only in the size of the gears in the second-stage mesh. Therefore, either output speed may be obtained by simply changing two parts, the compound idler (2), and power take-off (3), gearshafts. The centers of the complete train are in a vertical plane with the center of the power take-off slightly above that of the turbine shaft.

The input gear is supported radially on roller bearings (8), which are incapable of resisting axial loads. Pinion thrust is absorbed through a split inner race ball bearing (9), which is mounted with sufficient housing clearance to avoid any radial load.

Both gear meshes have contact ratios greater than three by virtue of the overlapping action of the helical teeth. The resulting smooth flow of power is beneficial in reducing dynamic tooth engagement loads which in turn reduces gear noise to a low level, and also in lowering turbine and compressor blade excitation forces that might cause fatigue failures. The effects of any misalignment that might exist between the turbine shaft and the high speed pinion is reduced to negligible levels by the use of a full-floating splined coupling.

## Section IX

The gear teeth have been analyzed and designed against the three general types of gear failure; pitting, bending or tooth breakage, and scoring. The first two types are essentially fatigue in character and are functions of the total number of stress cycles as well as the magnitude of the dynamic load. Scoring is almost always caused by local friction welding and is independent of length of operation of the gears. If scoring does not occur on the first service application of maximum speed and torque, it is not likely to occur at all.

The design criteria used to evaluate the gears against each of the characteristic types of failure are: Hertz stress for pitting, root beam stress for bending, and the PVT factor for scoring.

The load used in computing Hertz and beam stress is composed of the total transmitted load plus a dynamic increment load. This dynamic increment results from the inertia forces developed in the gear train by instantaneous accelerations caused by inaccuracies in spacing, thickness, lead, tooth deflection and tooth profiles. A perfect involute will transmit uniform angular velocity, but any deviation from this form will cause a change in velocity which, over a very short time interval, represents a high acceleration of the gear mass and all other rigidly attached inertias in the train. These forces are minimized by keeping the gear blanks as light as possible.

The method used in calculating the dynamic increment load is based upon Buckingham's works. Although various sources have indicated that the dynamic overload as calculated by Buckingham's equations is larger than the actual dynamic load encountered, most authorities agree that it is the best method for comparing different designs. By applying this method to a number of different gear sets in the same field of application (such as aircraft gearing), it is possible to build up a background of experience based on these gears and define satisfactory limits of dynamic tooth stress. Continental's experience indicates that aircraft quality, hardened and ground helical gears will operate up to 230,000 psi wear (Hertz) stress with little or no development. Generally, higher wear stresses can be used only for limited life, or after a development

## Section IX

program with special consideration to mounting, lubrication, and tooth modifications. The first- and second-stage (6000 rpm output) meshes have wear stresses of 174,000 and 172,000 psi respectively, under full engine speed and power. These stresses are considerably below our established criterion and result from designing each gear to have a minimum of 1500-hour duty spectrum life with a theoretical failure rate of less than one-tenth of one percent (99.99% reliability). The design static contact (Hertz) stress levels were obtained from S-N curves for air-melted, carburized and hardened gears.

Tooth bending stresses are calculated by applying the dynamic tooth load to the Lewis beam stress equation. This formula determines the equivalent stress that would exist on a constant strength parabola inscribed within the tooth, tangent at the base and with its apex just intersecting the line of action of the applied tooth load.

Certain other criteria such as the AGMA fundamental stress formula are also checked but most of Continental's experience factors are correlated with the Lewis formula. The stress limit that Continental has successfully permitted on previous designs is 100,000 psi. Dynamic beam stresses under full power at the worst load point are 46,000 and 50,000 psi (6000 rpm output) for the first- and second-stages, respectively.

Scoring tendency of the gears is calculated using the PVT method, which is based on a study of aircraft engine gear failure reported by numerous manufacturers (including Continental). The tooth addenda are modified to obtain equal PVT factors between the drive and driven gear in each mesh if the PVT factor exceeds a given limit for either gear in the set. If the equalized PVT factors still exceed the design limit, further modifications in the gears must be made.

The PVT factor combines the (Hertz) contact pressure and the sliding velocity at the tip of the tooth with the length of the line of action from the pitch point to the tooth tip. Considering the product of tooth pressure and sliding velocity to be a measure of the

## Section IX

instantaneous rate of heat generation, the PVT curve from the pitch point to the outside diameter of the gear represents the total heat generated in this cycle and is an indication of the tendency of the gears to score.

The safe limit of the scoring factor for very accurate case-hardened gears lubricated with a medium weight petroleum oil is 1,500,000 (dimensionless). Tooth profile modifications to prevent scoring are not necessary if this limit is not exceeded. Continental's experience with mineral and synthetic turbine engine oil indicates that no decrease in the permissible scoring limit is necessary. The PVT factors for the high speed mesh have been equalized at 870,000 while no equalization was found to be necessary for the low speed mesh by virtue of its low PVT factor of 500,000. PVT factors for both meshes were obtained under full speed and power conditions.

Since PVT equalization generally requires increasing the addendum of the pinion and decreasing the gear on equal amount, the bending stress in the pinion will increase. The pinion tooth is then thickened to compensate for this correction and the inherently stronger mating gear is correspondingly decreased in thickness. In addition all the backlash in the mesh is taken on the larger gear to further equalize the bending stresses. These corrections are made in this design without requiring the use of nonstandard cutters. This is accomplished by changing the center distance between the work and the cutter until the correct thickness is obtained.

The pressure angle of  $20^{\circ}$  was selected as the best compromise between the higher bearing loads and lower contact ratios obtained with higher pressure angles, and the higher (Hertz) stress and scoring factors resulting from lower pressure angles. The resulting contact ratios are 3.2 for the first- and second-stage.

The normal diametral pitches of the two meshes were determined from beam stress and scoring factor calculations. In general, the finest pitch compatible with adequate tooth bending strength will provide the most satisfactory results for high speed gearing due to the higher contact ratios and lower scoring factors

## Section IX

obtained. A summary of pertinent gear tooth design data is given in Table IX-I.

As a result of choosing as the basic design criterion long life with a high degree of reliability, the gears evolved are relatively lightly loaded as compared to Continental's recent experience in aircraft reduction gearing. With heavily loaded gears, it may be found necessary to extensively modify the involute profiles. Negative involute correction of the tooth tip is sometimes required in the case where the deflection of the teeth in contact allows the driving gear to advance slightly on the driven gear. The incoming unloaded tooth is carried into mesh too soon, causing an impact on the tip of the tooth. It appears that this type of tooth correction is not necessary in these gears although a slight amount of crowning to prevent concentrated end-loading will be specified.

Gear blank deflections due to helical tooth thrust loads and nonsymmetrical disc centrifugal forces must be controlled if the tooth stress calculations are to be valid. These deflections can be minimized for a given blank size by proper selection of hub cone angle, taper, rim thickness, and rim-hub attachment location. Tooth profiles can also be modified to compensate for deflections, but due to the independence of strains (because of centrifugal body forces and external applied thrust load), such modifications can give optimum results for only one combination of speed and power. Gear blank configurations are based on both analytical calculations and previous experimental results obtained from static load tests of gear blanks of similar design.

All bearings in the main power reduction gear train are manufactured from vacuum degassed SAE 52100 steel. Each bearing has a minimum calculated B-10 life in excess of 50,000 hours based on the following duty spectrum derived from the endurance test schedule, Table IX-II.

## Section IX

TABLE IX-I

	First-Stage		Second-Stage		P.T.O.
	Pinion	Gear	Pinion	Gear	
No. of Teeth	22	79	29	89	.45
Pitch Diameter, Inches	1.3463	4.8343	1.8530	5.6868	2.9763
Normal Diametral Pitch	17	17	16	16	16
Normal Pressure Angle	20°	20°	20°	20°	20°
Helix Angle	16° R. H.	16° L. H.	12° L. H.	12° R. H.	19° 6' R. H.
Effective Face Width, Inches	1.05	1.05	1.45	1.45	1.45
Horsepower	120	120	120	120	120
Speed, rpm	66,800	18,603	18,603	6,061	18,603
Pitch Line Velocity, fpm	23,500	23,500	9,020	9,020	14,500
Wear Stress, psi	174,000	--	172,000	--	143,000
Static Hertz Stress, psi	68,000	--	83,000	--	70,000
Dynamic Beam Stress, psi	46,000	--	50,000	--	45,000
PVT Factor	870,000	840,000	280,000	500,000	340,000
Contact Ratio	3.2	3.2	3.2	3.2	3.2

## Section IX

TABLE IX-II  
BEARING ENDURANCE TEST SCHEDULE

% Rated Horsepower	Horsepower	% Duty Spectrum	Hours
100	120	63.73	956
50	60	18.13	272
10	12	18.13	272

This yields a reliability greater than 99.99% for each bearing to complete a 1500-hour endurance test duty spectrum as described above. Bearing load summaries of the 6000 and 12,000 rpm power take-off reduction gear versions appear in Figures IX-4 and IX-5 respectively and are based on 100 percent rated horsepower.

ENGINE WEIGHT

The TS120-G6 estimated engine weight is shown in Table IX-III. The identification of strategic national defense materials is the same as shown for the basic TS120 direct drive engine.

**Section IX**

**MODEL TS120-G6 TURBOSHAFT ENGINE WEIGHT SUMMARY**

Part Name	Weight	Part Name	Weight
<b><u>ROTOR ASSEMBLY</u></b>			
Rotor-Radial Compressor	-	Cover - Accessory Gears	3.50
Rotor-Turbine	-	Case - Accessory	9.15
Shaft, Front-Turbine	-	Clutch Assembly - Starter Overrunning	2.10
Rotor-Axial Compressor	-	Cover Assembly - Oil Pump	3.50
Miscellaneous	-	Oil Pump	3.50
Total	<u>16.90</u>	Sump - Oil	2.00
<b><u>COMPRESSOR ASSEMBLY</u></b>			
Stator-Axial Compressor	.80	Power Control	11.00
Housing-Compressor	4.86	Starter Assembly	8.75
Diffuser-Radial Compressor	4.00	Filler - Oil	.50
Housing-Air Intake	2.45	Gears and Shafts	4.30
Duct-Air Intake	1.70	Bearing	.62
Miscellaneous	1.00	Miscellaneous	3.00
Total	<u>14.81</u>	Total	<u>53.92</u>
<b><u>ATTACHING PARTS</u></b>			
Indicator - Exhaust Gas Temperature	2.00		
Switch - Oil Pressure	.32		
Control Assembly - Sequence	4.00		
Thermocouple	11.70		
Cooler Assembly - Oil	6.20		
Fan - Cooling	13.60		
Miscellaneous	2.40		
Total	<u>16.52</u>		
<b><u>COMBUSTOR ASSEMBLY</u></b>			
Interstage Diaphragm	2.12		
Nozzle-Turbine Inlet	5.50		
Volute-Combustor	11.70		
Cover-Radial Diffuser	6.20		
Housing-Combustor	13.60		
Cover-Combustor	2.10		
Combustor	1.57		
Miscellaneous	1.57		
Total	<u>45.19</u>	Line/Fitting/Ignition	<u>8.05</u>
<b><u>EXHAUST DUCT AND REAR BEARING SUPPORT</u></b>			
Duct-Exhaust	10.25		
Miscellaneous	4.50	Support - Reduction Drive Gear	3.90
Total	<u>14.75</u>	Cover - Reduction Drive	4.20
<b><u>REDUCTION DRIVE ASSEMBLY</u></b>			
Gears & Shafts & Coupling	9.41		
Bearing	3.13		
Miscellaneous	5.20		
Total	<u>25.84</u>		
<b><u>BASIC ENGINE WEIGHT</u></b>			
Turbine Rotor Containment Ring	<u>195.98</u>		
<b><u>TOTAL ENGINE WEIGHT</u></b>	<u>20.00</u>		
	<u>215.98</u>		

## Section IX

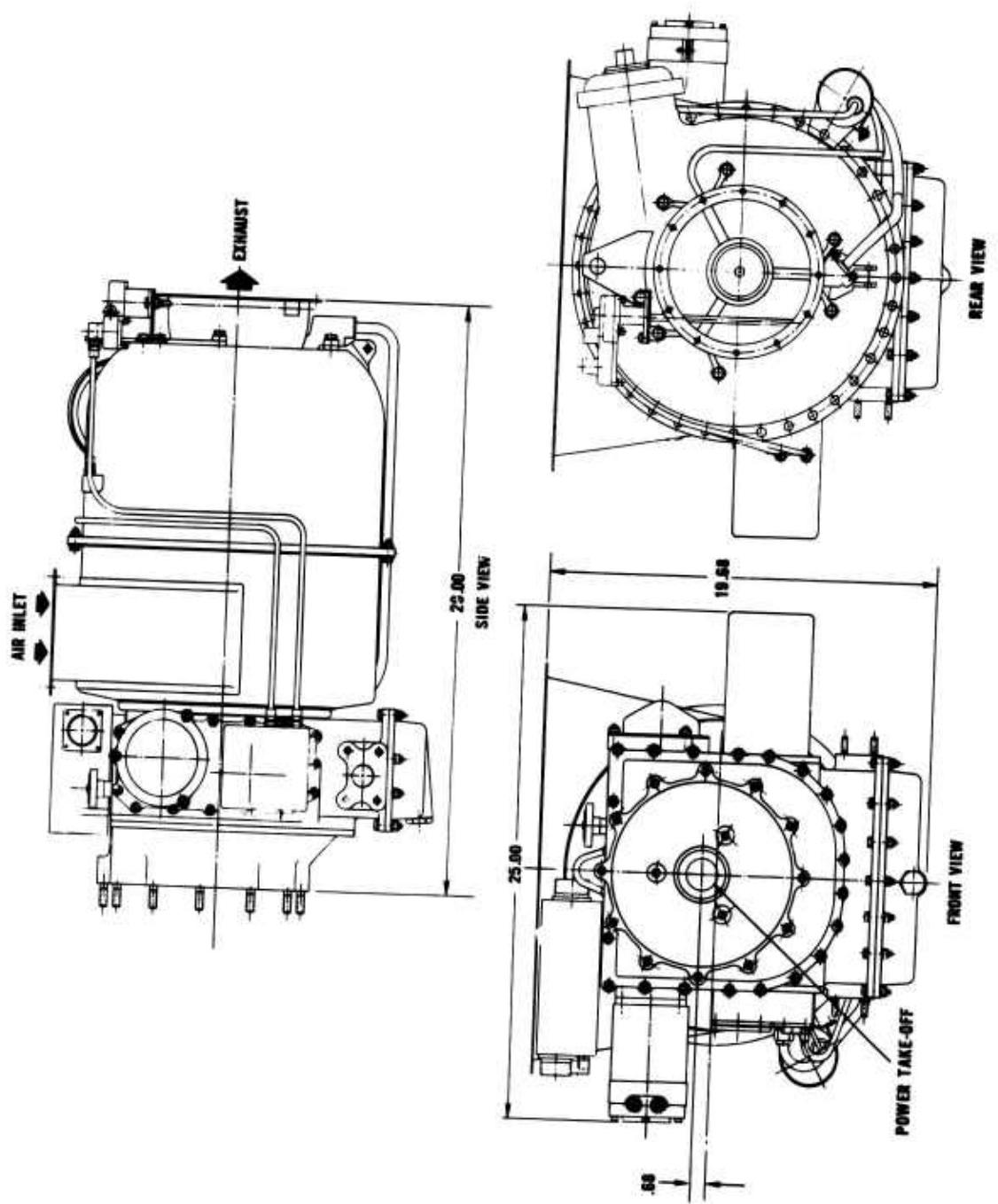


Figure IX-1. TS120-G6 Turboshaft Engine Installation Drawing.

**Section IX**

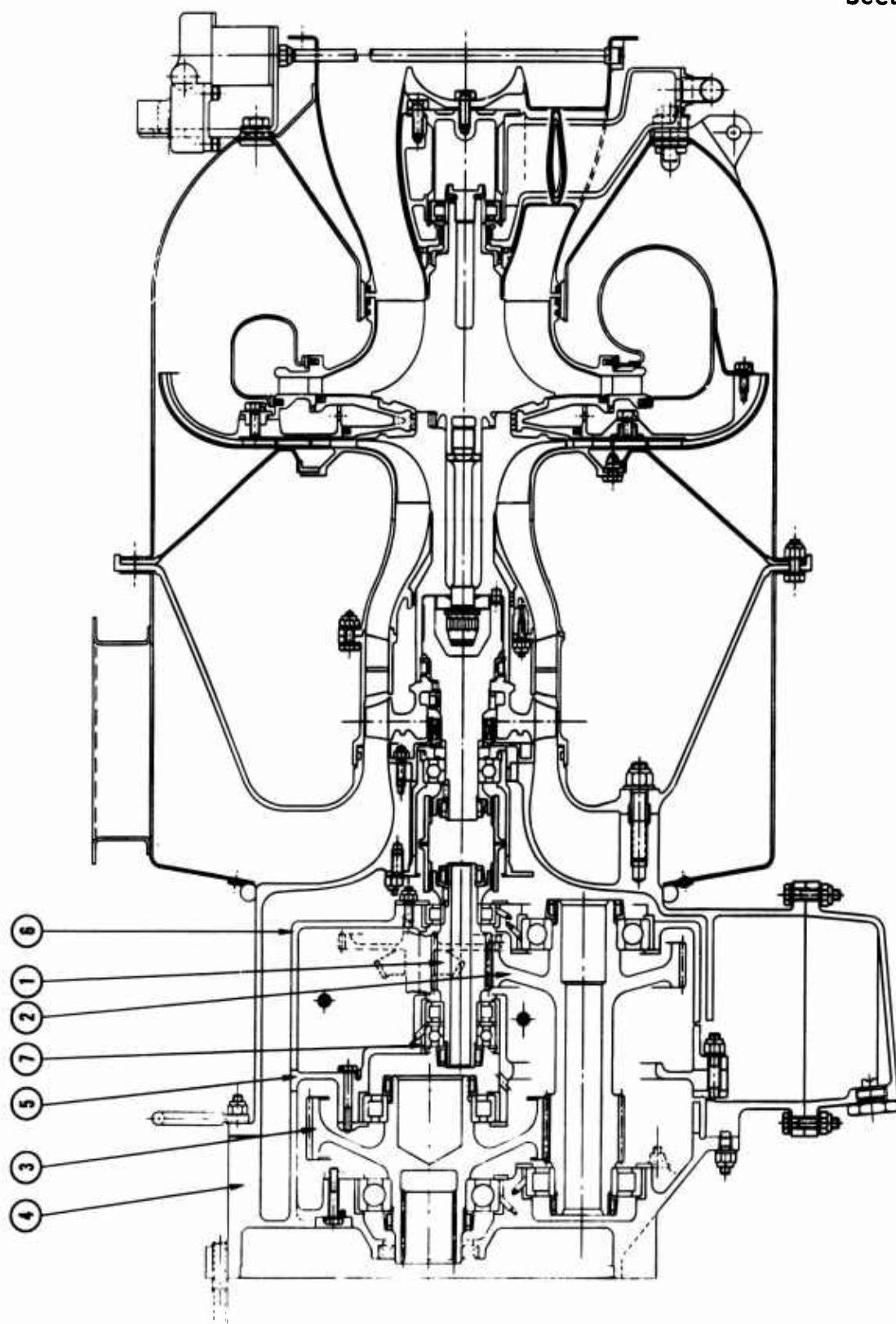


Figure IX-2. TS120-G6 Turboshaft Engine - 6000 RPM Power Take-off.

**Section IX**

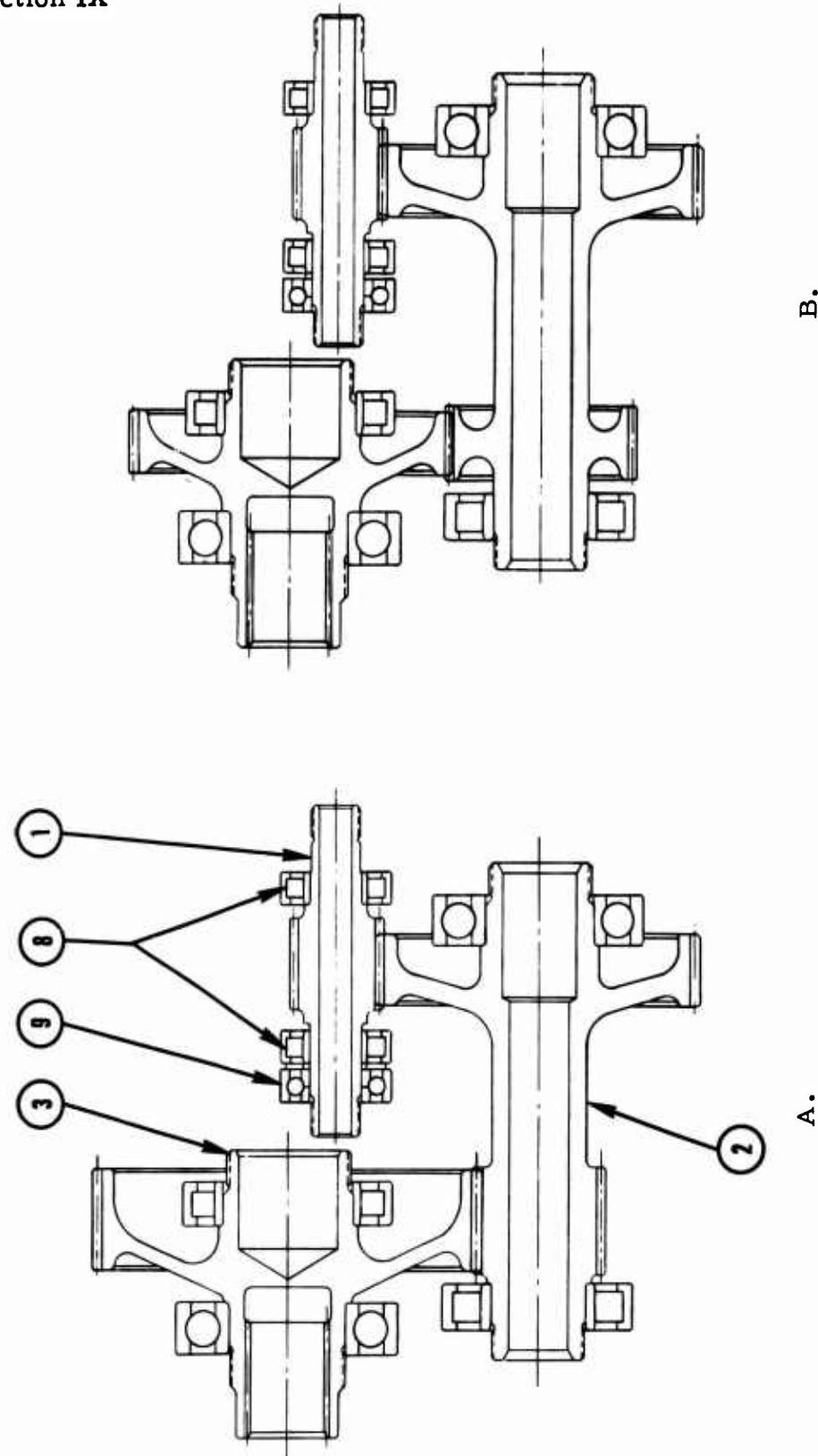
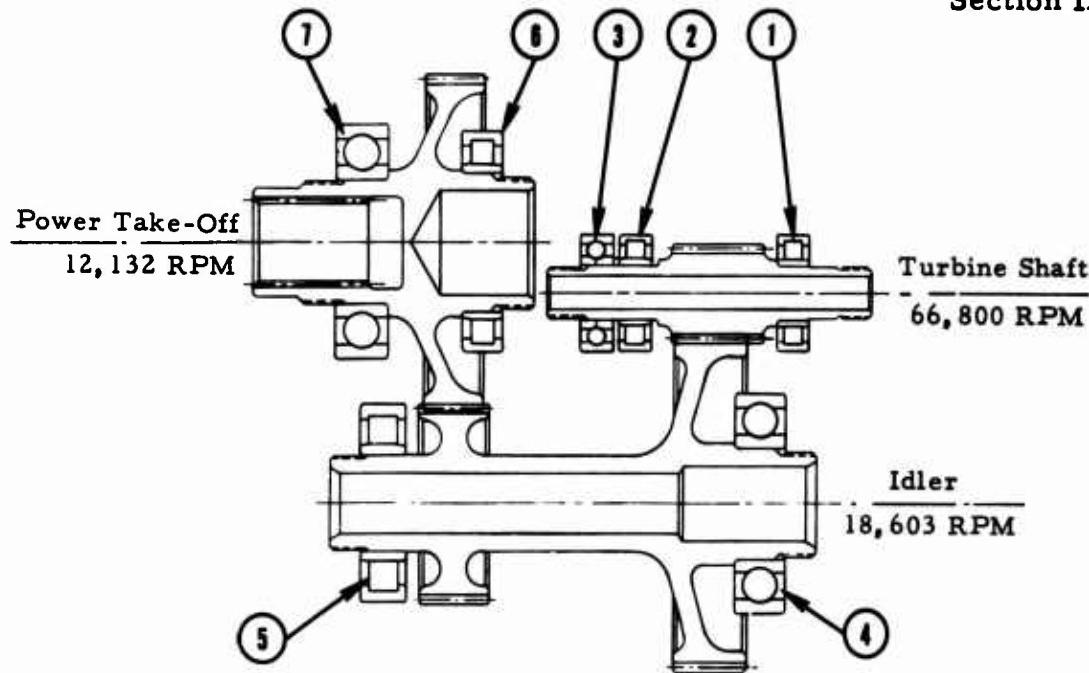


Figure IX-3. Reduction Gear - A - 6000 RPM; B - 12,000 RPM.

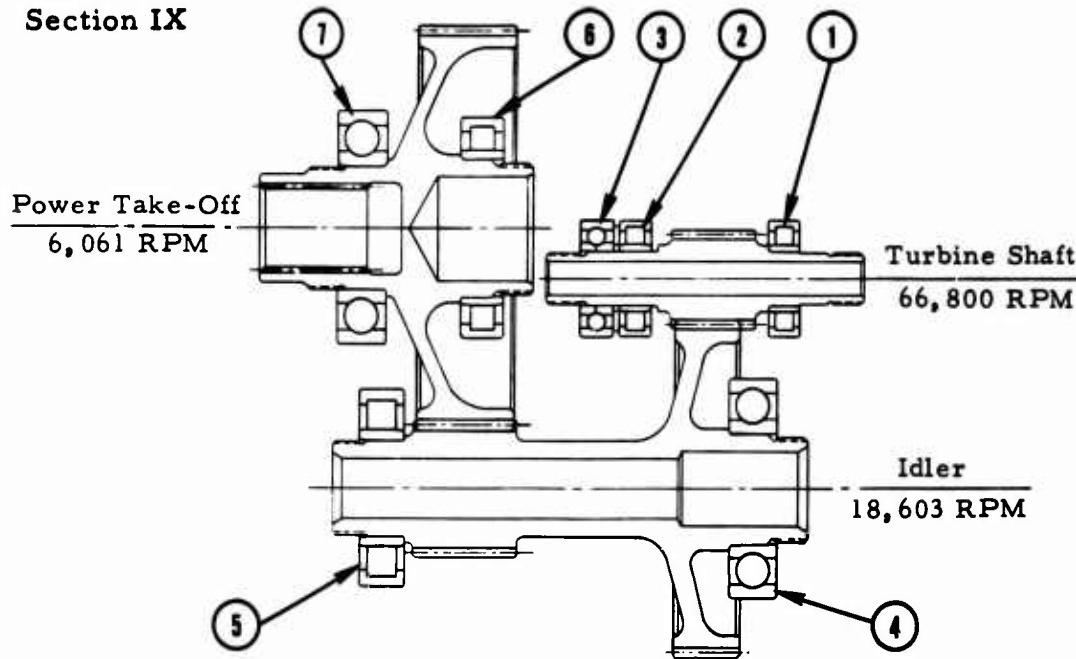
**Section IX**



No.	CAE P/N	Function or Drive	Speed RPM	Radial Load Pound	Thrust Load Pound
1	306669	1st. Stage Reduction Pinion, Rear	66,800	94	-
2	306669	1st. Stage Reduction Pinion, Front	66,800	90	-
3	306670	1st. Stage Reduction Pinion, Thrust	66,800	-	49
4	306681	Compound Idler, Rear	18,603	129	47
5	306682	Compound Idler, Front	18,603	228	-
6	306680	Power Take-Off, Rear	12,132	180	-
7	306679	Power Take-Off, Front	12,132	178	96

**Figure IX-4. Power Take-off Reduction Gear Bearing Summary - 12,000 RPM.**

**Section IX**



No.	CAE P/N	Function or Drive	Speed RPM	Radial Load Pound	Thrust Load Pound
1	306669	1st. Stage Reduction Pinion, Rear	66,800	94	-
2	306669	1st. Stage Reduction Pinion, Front	66,800	90	-
3	306670	1st. Stage Reduction Pinion, Thrust	66,800	-	49
4	306681	Compound Idler, Rear	18,603	101	46
5	306682	Compound Idler, Front	18,603	356	-
6	306680	Power Take-Off, Rear	6,061	344	-
7	306679	Power Take-Off, Front	6,061	197	94

**Figure IX-5. Power Take-off Reduction Gear Bearing Summary - 6,000 RPM.**

## SECTION X

### ENGINE PERFORMANCE AND AEROTHERMODYNAMIC DESIGN

	<u>Page</u>
AERODYNAMIC CYCLE . . . . .	1
COMPRESSOR DESIGN . . . . .	59
COMBUSTOR DESIGN . . . . .	93
APPENDIX X-A . . . . .	121
TURBINE AND EXHAUST SYSTEM DESIGN . . . . .	125
APPENDIX X-B . . . . .	163

## SECTION X - ENGINE PERFORMANCE AND AEROTHERMODYNAMIC DESIGN

### AERODYNAMIC CYCLE

Primary engine objectives affecting the aerodynamic cycle are:

1. Low fuel consumption.
2. Adaptability to regeneration.
3. Interchangeability of components between various engine versions.

The engine is the "coupled" type to assure achievement of the precise speed control required for geared-drive and precise power generation sets. It features a variable speed operation over a ten percent speed range for the direct drive ultra high frequency generator sets for improved fuel economy.

### 120 HORSEPOWER SIMPLE CYCLE ENGINE

In order to optimize the major parameters of cycle pressure ratio and turbine inlet temperature, a range of performance was calculated at both sea level 60°F and 8000 feet, 90°F, Figures X-1 and X-2. All component efficiencies and loss assumptions in these cycle calculations are those for the 120 horsepower simple cycle engine. They are shown in Figure X-3.

Two structural factors were also considered in making the final cycle choice. These were:

1. The turbine inlet temperature was limited to a value compatible with the use of currently available materials and coating technology - that is, 1800°F.
2. The engine rotor tip speed was limited to a value compatible with allowable stress levels.

## Section X

Based on the above-mentioned criteria, a pressure ratio in the range of 5.5 to 6.0 was selected as the best to meet the customer requirements. One of the main features of this pressure ratio selection is that a minimum number of turbomachinery components are required. For this particular engine it includes a single-stage axial compressor, centrifugal compressor, and a radial turbine.

### Components

Component performance characteristics are based on existing proven Continental hardware. The component performance sources are listed below.

1. Inlet Losses. Are based on test data from 650 horsepower Continental T72 engine and research inlet tests.
2. Axial Compressor. The axial stage is scaled from the second axial stage of the XT67; its performance map is shown in Figure X-4.
3. Centrifugal Compressor. The centrifugal compressor map is shown in Figure X-5. As explained in the Compressor Section, a redesign of the centrifugal impeller is expected to increase over-all performance by two to four percent.
4. Burner Can. These characteristics are based on generalized curves substantiated by test data. (See Burner Section.)
5. Radial Turbine. Turbine performance maps were derived from tests on a Continental research radial inflow turbine. The map shown on Figure X-6 was run specifically for this program to validate efficiency choices. It represents an approximate aerodynamic scale of the geometry to be used on the 120 horsepower engine.

## Section X

6. **Exhaust Duct.** The duct losses for the axial configuration are based on test data from the Continental T72 with a 1.4 percent loss added for the radial exhaust configuration.

### Compressor Matching

There are several criteria which must be met for optimum axial, centrifugal compressor match. These are:

1. Maximum efficiency at sea level 60°F at normal rated speed.
2. Sufficient surge margin at all operating points.
3. Sufficient aerodynamic overspeed efficiency to operate with reasonable fuel consumption at an ambient temperature of -65°F.
4. Good low speed surge margin for easy starting.

The compressor map, Figure X-7, has been optimized to match the peak efficiency of the axial to the peak efficiency of the centrifugal in the region of the sea level operating point for best over-all performance of all engine combinations.

### Engine Matching

A parametric approach was used to match the engine in order to ensure an optimum design point. Several criteria were used in obtaining the best match. These were:

1. 120 horsepower and BSFC = 0.70 at sea level and an ambient temperature of 60°F.
2. 120 horsepower at an altitude of 8000 feet for an ambient temperature of 90°F.
3. Minimize the altitude turbine inlet temperature.

## Section X

4. Minimize cycle pressure ratio in order to keep the turbine work requirement as low as possible.

Fifty-four engines were examined, each with a different operating point. Figure X-8 shows a summary of the matching study. Each of the engines indicated would have to be scaled on airflow to produce exactly 120 horsepower.

After examining each engine in the light of the four criteria previously mentioned, engine "B" was selected as the final design choice. Figures X-9 and X-10 show the variation of BSFC with horsepower for several engine speeds at sea level, 60°F and 8000 feet, 90°F respectively, and form the basis for selecting 66,800 rpm as the normal rated speed.\*

The engine rating points, established by the matching study for sea level 60°F and 8000 feet 90°F, are shown in Figure X-3 for both the axial and radial exhaust configurations. The performance of various components and the losses in the flow path are also indicated. Figures X-11 through X-19 show the no-load, part-load, and full-load performance characteristics for ambient temperatures of +60°, +90°, and -65°F at altitudes of 0, 4000, and 8000 feet respectively. Figure X-20 shows the sea level and altitude operating points located on the estimated combined compressor map as well as the no-load and surge margin lines. Figure X-21 indicates the operating points on the turbine map at sea level and altitude conditions.

### Effects of Flow Path Losses and Bleed

Effects of losses and bleed were obtained by operating the engine on the computer for given increases of losses and adding bleed. The radial exhaust configuration was used as the basis of these calculations. Figures X-22 and X-23 show the effects of compressor bleed air at sea level 60°F and 8000 feet, 90°F respectively. Figures X-24 and X-25 show inlet and exhaust loss correction factors plotted versus engine speed.

\* Normal Rated speed is defined as the speed which produces 120 horsepower at 8000 feet, 90°F and meets the sea level 60°F, horsepower, and BSFC specification requirement.

## Section X

Figure X-3 shows a tabulation of the performance in the axial and radial configuration. At sea level 60°F, the radial exhaust adds 1.42 percent total pressure loss causing the engine to rematch 10° hotter on turbine inlet temperature; BSFC increases to 0.694 from 0.686 of the axial configuration. At altitude the engine is also forced to operate hotter with a corresponding decrease in BSFC.

In addition to the effects of losses and bleed, the effect of other parameters (influence coefficients) on over-all performance were obtained. These values were calculated on the design point program and show the effect caused by a one-percent variation of the particular parameter involved, while all other parameters remain constant. These data are presented on Figures X-26 and X-27.

### Speed Modulation

An analysis was made of speed modulation for the direct drive engine in order to obtain the maximum fuel economy possible. Figures X-28 through X-30 show the effect of speed modulation on BSFC for several power levels at sea level and 4000 feet, 60°F and 8000 feet, 90°F respectively. Figure X-31 indicates that small change in r.p.m. is required with changing altitude to operate at best BSFC. It was therefore decided to bias the speed modulation control on ambient temperature only. An examination of Figures X-28 through X-30 show that for minimum BSFC:

1. Above 90°F an rpm of 66,800 is required.
2. At 100 percent power, the BSFC at 63,500 is equal to that of 66,800 r.p.m.
3. The lowest rpm possible at part power should be utilized.

Based on these considerations, Figure X-32 shows the speed modulation control bias limits furnished for power control system studies. Curve "B" is permissible, but Curve "A" is desired. It is anticipated that the final design will approach Curve "A."

## Section X

### GROWTH POTENTIAL

The growth potential capability of the 120 horsepower simple cycle engine was considered within the existing flow path only. Three significant methods of growth are available. These are increases in the following:

1. Turbine inlet temperature.
2. Engine speed.
3. Engine airflow.

Figure X-33 shows that increasing turbine inlet temperature to a value of 1800°F will increase shaft horsepower to approximately 190 horsepower at sea level and to 138 horsepower at 8000 feet, 90°F. It is also evident that increasing turbine inlet temperature decreases BSFC.

Figure X-34 shows that increasing engine speed to 68,000 r.p.m. from 66,800 increases the output by six horsepower at both sea level and altitude.

An investigation was made into the possibility of increasing engine airflow within the same flow path. Figure X-35 shows the variation of compressor inlet angle with increasing airflow. The efficiency decrease is also shown. An 8° opening was assumed with a two percent efficiency decrease. A turbine modification was assumed which would meet the same nominal performance. As shown in Figure X-34, approximately 17 more horsepower are available at the rating points by increasing airflow. It is also shown that a combination of increasing airflow, turbine inlet temperature and r.p.m. to their current allowable maximum values, will produce approximately 233 and 149 horsepower at sea level 60°F and 8000 feet, 90°F respectively.

## Section X

### 90 and 60 Horsepower Simple Cycle Engines

90 Horsepower Engine Optimization. - The main criteria in selecting the 90 horsepower engine configuration were:

1. Specification performance.
2. Maximum commonality of parts to 120 horsepower engine.

In order to obtain the optimum configuration, several types of 90 horsepower engines were examined. They are all modifications of the 120 horsepower simple cycle engine and are listed below.

1. Derating (i. e., lower turbine inlet temperature).
  - a. Nominal turbine nozzle.
  - b. Turbine nozzles closed 0.5 degree.
  - c. Turbine nozzles closed 1.0 degree.
2. Fixed Inlet Guide Vanes
  - a. With different combinations of inlet guide vanes and turbine nozzle settings.
3. Flow Path Area Reduction (Shaving).
4. Removing the Axial Compressor.
5. Substituting a Low Flow Axial Compressor and a Closed Centrifugal Impeller.
6. Derate and Use a Broad Range Centrifugal Compressor.

Each of the above engines were optimized for best performance. Tabulated in Table X-I is a summary of the study.

## Section X

TABLE X-I

90 HP SIMPLE CYCLE ENGINE OPTIMIZATION  
BSFC, NORMAL RATED SPEED, ALTITUDE SURGE MARGIN

	Sea Level 60°F BSFC Lb/HP-Hr.	Normal Rated Speed-RPM	Altitude Surge Margin
1. Derating			
a. Nominal turbine nozzles	0.756	64,000	5%
b. Turbine nozzles closed 0.5°	0.737	64,000	5%
c. Turbine nozzle closed 1°	0.726	65,000	5%
2. Fixed IGV and Turbine Nozzle Closed 1°	0.730	66,250	5%
3. Flow Path Shave			
a. 11.5% Shave	0.730	65,100	5%
b. 20.5% Shave	0.715	65,100	5%
c. 30% Shave	0.705	68,000	5%
4. Removed Axial Compressor	0.755	67,000	5%
5. Low Flow Axial Compressor and Closed Inducer			
a. 7% Flow Reduction	0.730	64,800	5%
b. 20% Flow Reduction	0.702	65,300	5%
c. 30% Flow Reduction	0.695	68,000	5%
6. Derated with Broad Range Centrifugal Compressor	0.743	65,000	5%

The above table indicates that the following configurations all make the 90 horsepower BSFC specification value:

1. 120 horsepower with fixed inlet guide vanes and closed turbine inlet nozzle.
2. 120 horsepower with flow path shaved 11.5 percent.
3. 120 horsepower with low flow axial.

## Section X

Flow path reductions above 10 to 12 percent were considered major redesign and discarded. On the basis of a minimum change, the engine finally selected was the 120 horsepower unit with IGV and the turbine nozzle closed 1°. Furthermore, the development problems anticipated for this engine, relative to other possible choices, would be minimized.

The selection of the 90 horsepower engine can best be made after test data are obtained from the 120 horsepower engine. For example, should the actual surge line be to the left of the estimated surge line, a derated 120 horsepower with turbine nozzles closed 1° would fulfill the 90 horsepower requirement without inlet guide vanes.

Figure X-36 shows test data for various IGV inlet angles for Continental T-72 compressor. These data were used as the basis for optimizing the IGV of the 90 horsepower engine.

Figures X-37 and X-38 show that the IGV's, the 90 horsepower minimum sea level BSFC, occurs at approximately 65,000 r.p.m. and meets altitude power at 1800°F. Increasing the engine speed to 66,250 r.p.m. satisfies the sea level BSFC target and develops altitude power at the significantly lower temperature of 1717°F.

The engine rating points, established by a matching study for sea level 60°F and 8000 feet, 90°F, are shown on Figure X-39 for both the axial and radial exhaust configurations. The performance of various components and losses in the flow path are also indicated. Figures X-40 through X-42 show the no-load, part-load, and full-load performance characteristics for an ambient temperature of 60°F and -65°F at sea level and 90°F at 8000 feet respectively. Figure X-43 shows the sea level and altitude operating points on the T72 size compressor map. Appropriate scale factors are indicated.

60 Horsepower Engine Optimization. - The main criteria in selecting the 60 horsepower configuration were identical to the 90 horsepower engine. These are:

1. Specification performance.

## Section X

### 2. Commonality of parts to 120 and 90 horsepower engines.

In order to obtain the optimum configuration, several types of 60 horsepower engines were examined. Each of the engines is a modification of the 120 horsepower or 90 horsepower simple cycle engine and are listed below:

1. 120 horsepower centrifugal compressor with turbine nozzles opened 0.5 degree - axial compressor removed.
2. Centrifugal compressor with various levels of shaving and turbine nozzles opened 0.5 degree.
3. Redesigned centrifugal impeller closed 9.3 degrees with turbine nozzle closed one degree and turbine rotor shaved 10 percent.
4. Various levels of shaved flow path of 120 horsepower engine.
5. Various levels of shaved flow path of 90 horsepower engine.
6. 90 horsepower engine with a low flow axial and closed inducer.
7. Derated 90 horsepower engine to 60 horsepower engine.

Each of the above engines were optimized for best performance. Tabulated in Table X-II is a summary of the study.

## Section X

TABLE X-II

60 HP SIMPLE CYCLE ENGINE OPTIMIZATION  
BSFC NORMAL RATED SPEED, ALTITUDE SURGE MARGIN

	Sea Level 60°F BSFC Lb/HP-Hr.	Normal Rated Speed-RPM	Altitude Surge Margin
1. Centrifugal Only	0.89	65,500	5%
2. Shaved Centrifugal			
a. 10% Shave	0.84	65,500	5%
b. 15% Shave	0.835	64,000	5%
3. Redesigned Closed Impeller	0.80	66,000	5%
4. Shaved Axial + Centrifugal			
a. 10% Shave	0.84	63,300	5%
b. 20% Shave	0.816	65,000	5%
c. 30% Shave	0.80	68,000	5%
5. 90 HP Shaved 11.5%	0.852	68,000	5%
6. 90 HP with Low Flow Axial and Closed Inducer	0.835	65,000	5%
7. Derated 90 HP	0.84	64,000	5%

Flow paths reduction above 10 to 12 percent were considered major redesigns and discarded from further consideration. Derating the 90 horsepower to 60 horsepower requires no change to the engine or development risk with minimal performance deterioration.

## Section X

A major redesign of the rotating machinery (configurations) will improve the BSFC by only 0.4-pound per horsepower-hour. The decision on any final hardware configuration can best be made after test data is obtained on the 120 horsepower simple cycle engine.

Figures X-37 and X-44 indicate that for the 60 horsepower engine the optimum sea level BSFC is obtained in the range of from 60,000 to 64,000 r.p.m. The engine develops 60 horsepower at altitude between 62,150 r.p.m. and 64,000 r.p.m. with turbine inlet temperatures varying from 1500°F to 1416°F. In the interest of maintaining lower altitude, turbine inlet temperature, 64,000 r.p.m. has been selected as the normal rated speed.

The engine rating points established by a matching study, for sea level 60°F and 8000 feet, 90°F are shown on Figure X-45 for both the axial and radial exhaust configurations. The performance of various components and losses in the flow path are also indicated. Since the engine is a derated 90 horsepower engine, the no-load, part-load, and full-load performance characteristics are similar and were shown on Figures X-40 through X-42. Figure X-43 shows the sea level and altitude operating points on the T72 compressor map. Appropriate scale factors are indicated.

**Section X**

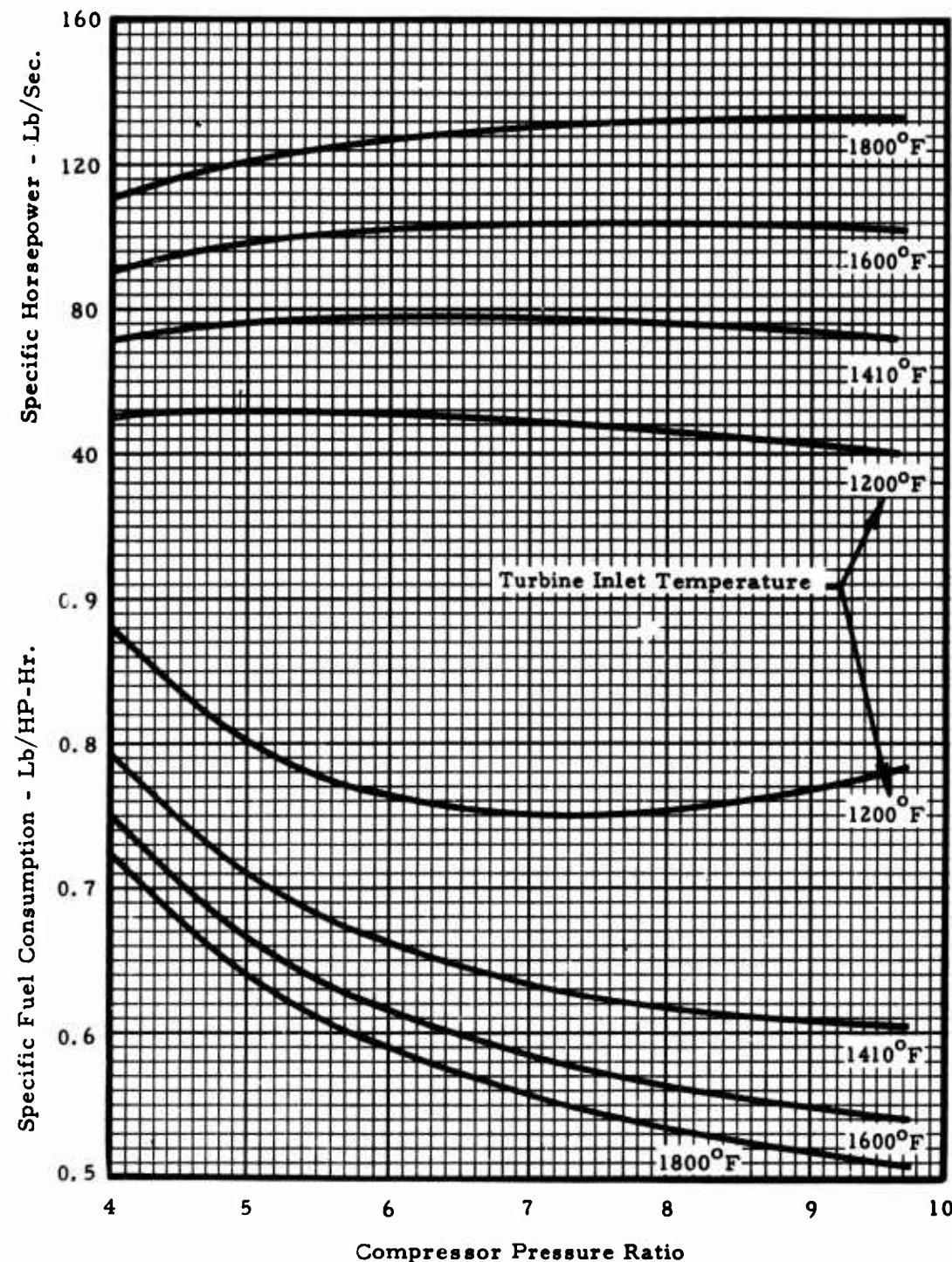


**Figure X-1.** TS120 - Design Point Study Sea Level, 60°F.

**Section X**

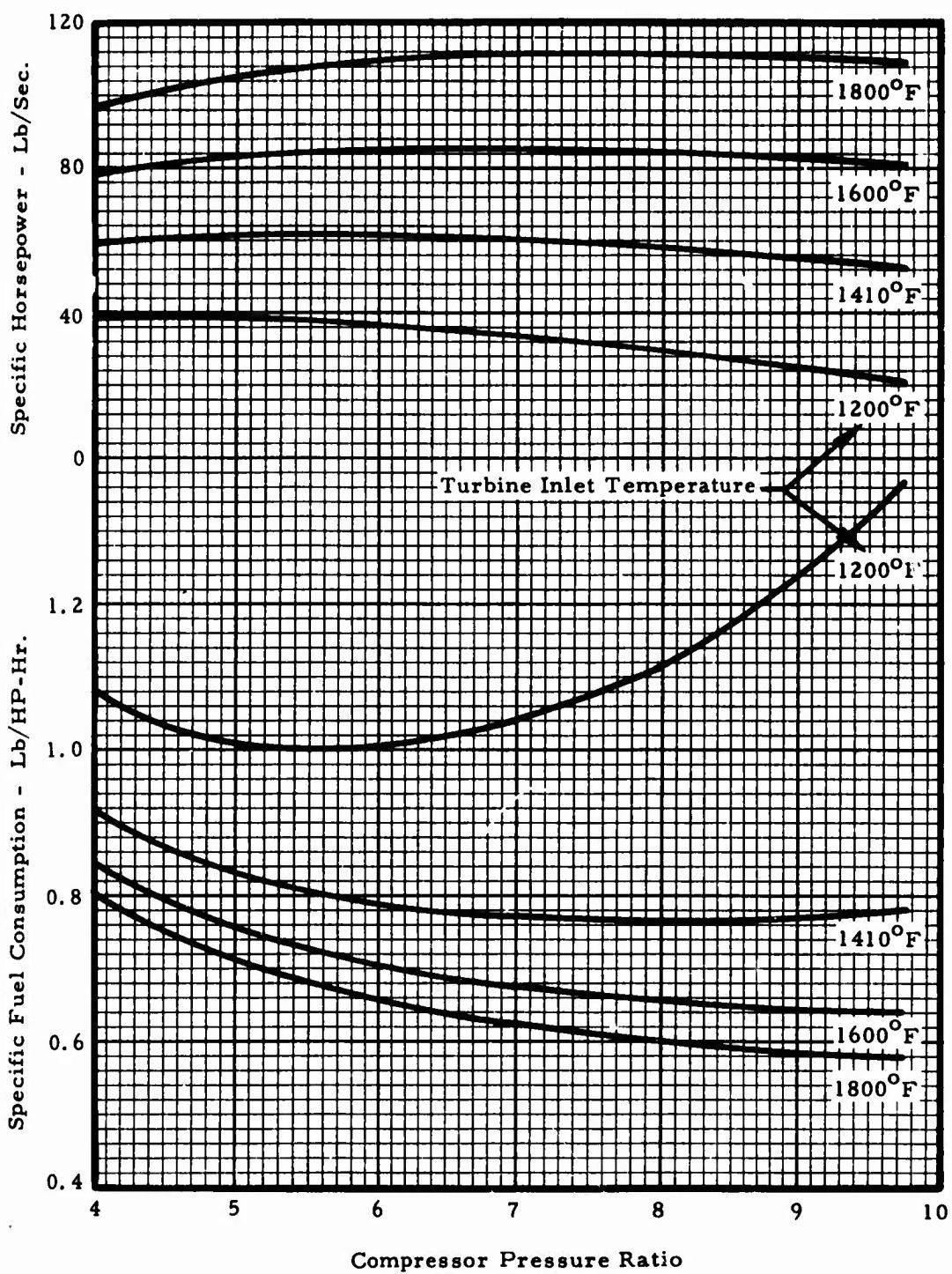


**Figure X-2. TS120 - Design Point Study 8000 Feet, 90°F.**

## Section X

	Sea Level - 60°F		8000 Ft., 90°F	
	Radial Exhaust	Axial Exhaust	Radial Exhaust	Axial Exhaust
Shaft Output Power	120.0	120.0	120.0	120.0
BSFC - Lb/HP-Hr.	0.694	.686	.66	.651
Engine Speed - RPM	66,800	66,800	66,800	66,800
Airflow - Lb/Sec.	1.67	1.67	1.11	1.11
Corrected Airflow - Lb/Sec.	1.68	1.68	1.55	1.55
Comp. Press. Ratio	5.73	5.72	5.50	5.50
Comp. Efficiency - %	81.7	81.6	82.7	82.7
Comp. Discharge Temp. - °F	465.1	464.9	499.7	499.3
Combustor Efficiency - %	.985	.985	.985	.985
Fuel LHV - Btu/Lb.	18,400	18,400	18,400	18,400
Turb. Inlet Temp. - °F	1385.3	1375.3	1765.3	1750.3
Turb. Exit Temp. - °F	832.6	821.8	1142.0	1125.9
Turb. Efficiency				
Inlet Total Press. Loss - %	.5	.5	.5	.5
Comp. Exit Coll. Tot. Press. Loss-%	1.92	1.92	1.92	1.92
Comb. Total Press. Loss - %	1.30	1.30	1.00	1.00
Turb. Inlet Scr. Tot. Press. Loss-%	.81	.81	.81	.81
Exh. Diff. (Axial) Tot. Press.Loss-%	2.79	2.81	2.81	2.81
Exh. Diff. (Rad.)Tot. Press. Loss-%			1.44	
Exh. Flange Total Press. Loss - %	1.50	1.50	1.50	1.50

NOTE: All efficiencies are total to total values.

Figure X-3. Rating Data - TS120 Simple Cycle Engine, Sea Level, 60°F and 8000 Feet, 90°F, Axial and Radial Exhaust.

## Section X

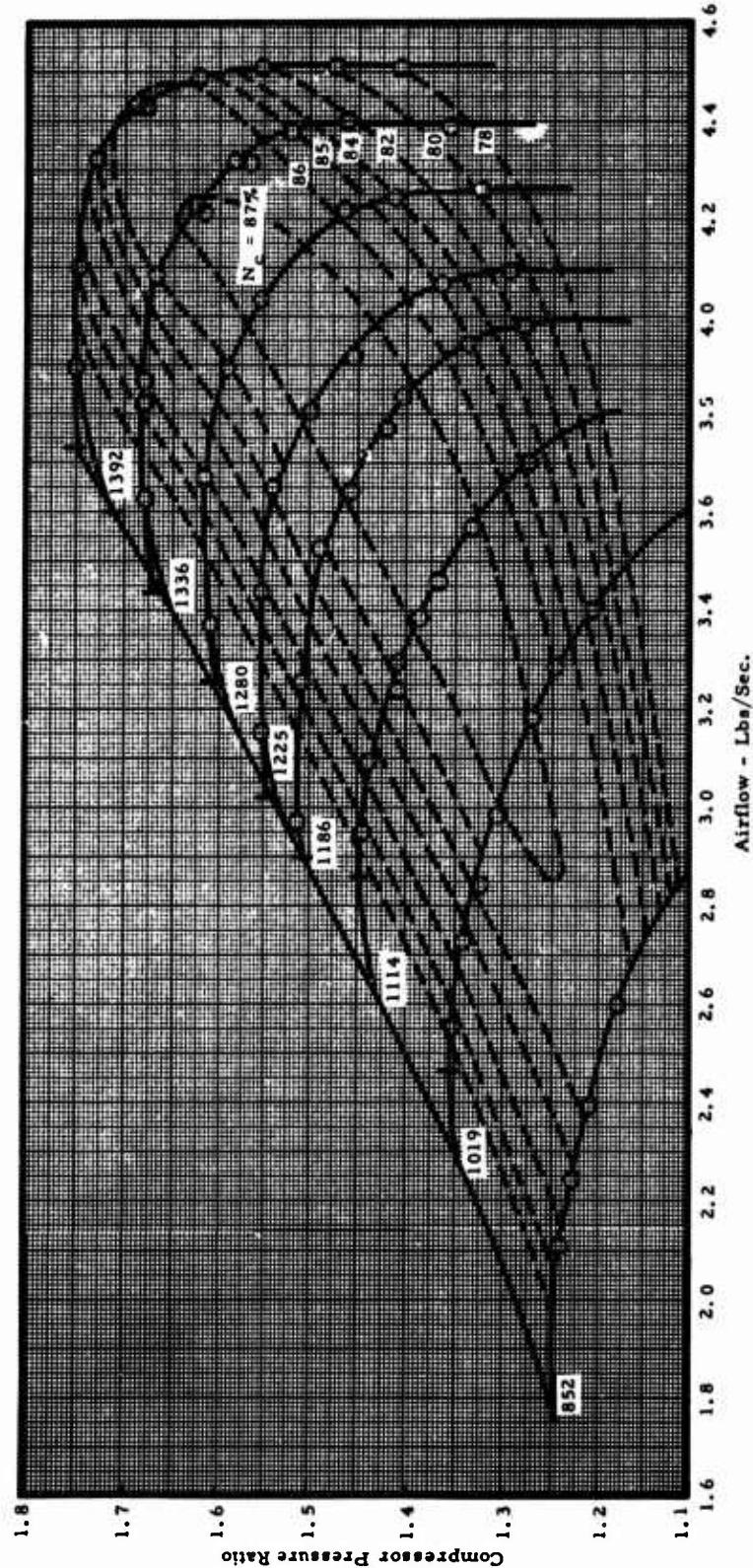


Figure X-4. TS120 Engine, Test Characteristics of Axial Compressor  
from XT67 Second Axial Stage.

## Section X

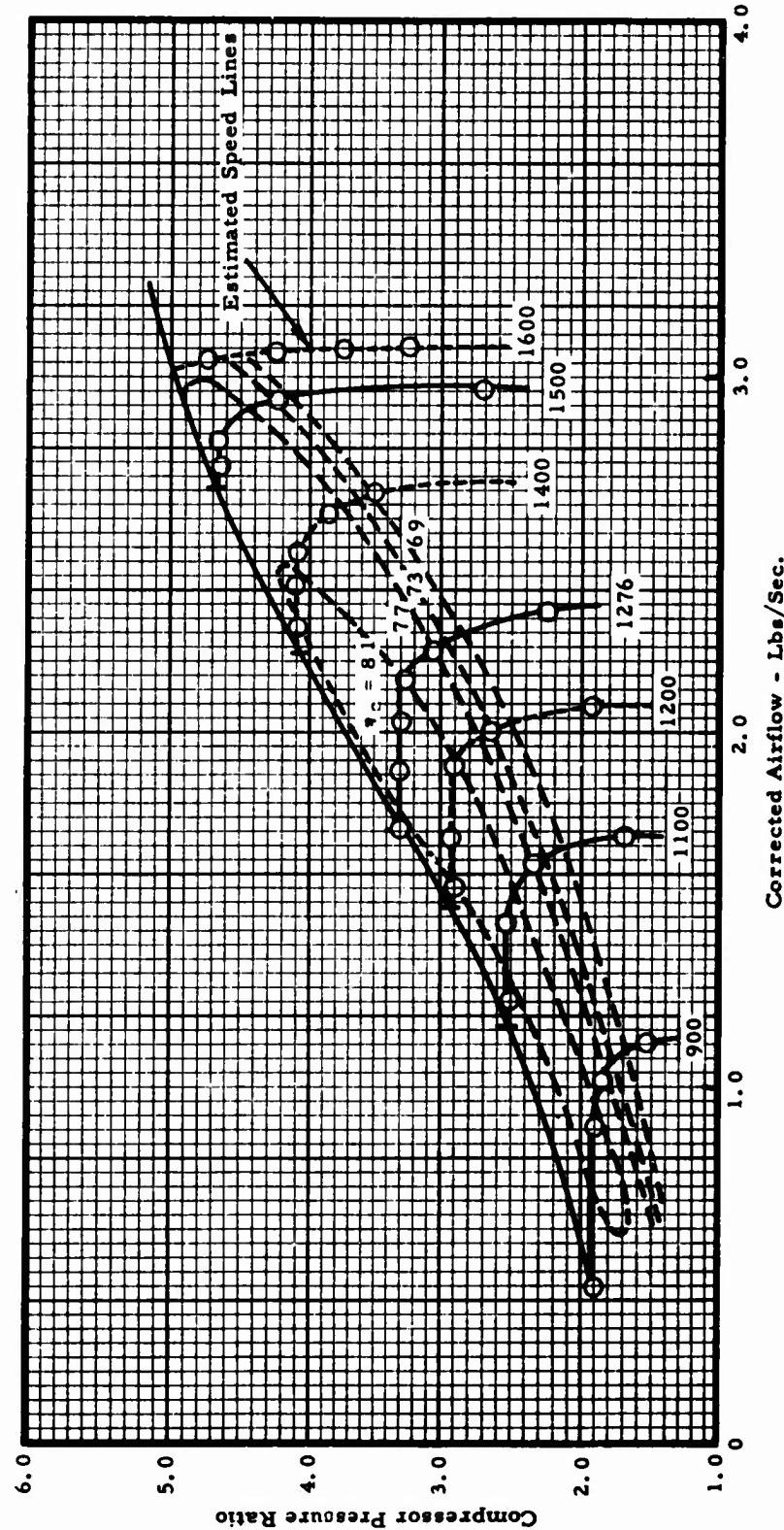


Figure X-5. TS120 Engine, Test Characteristics Research Centrifugal Compressor Model 217-10.

## Section X

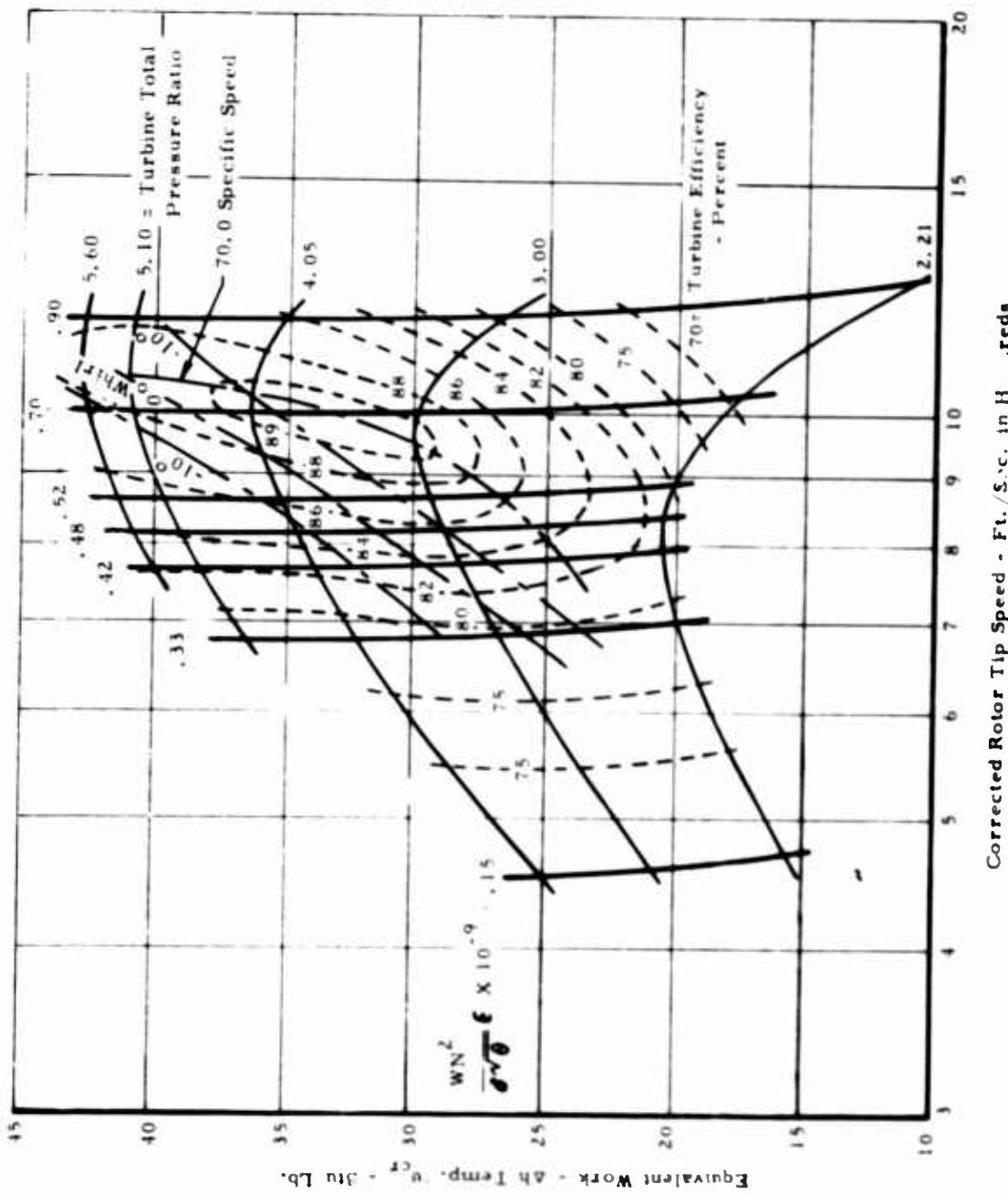


Figure X-6. Test Characteristics - Research 90° Radial Inflow Turbine.

**Section X**

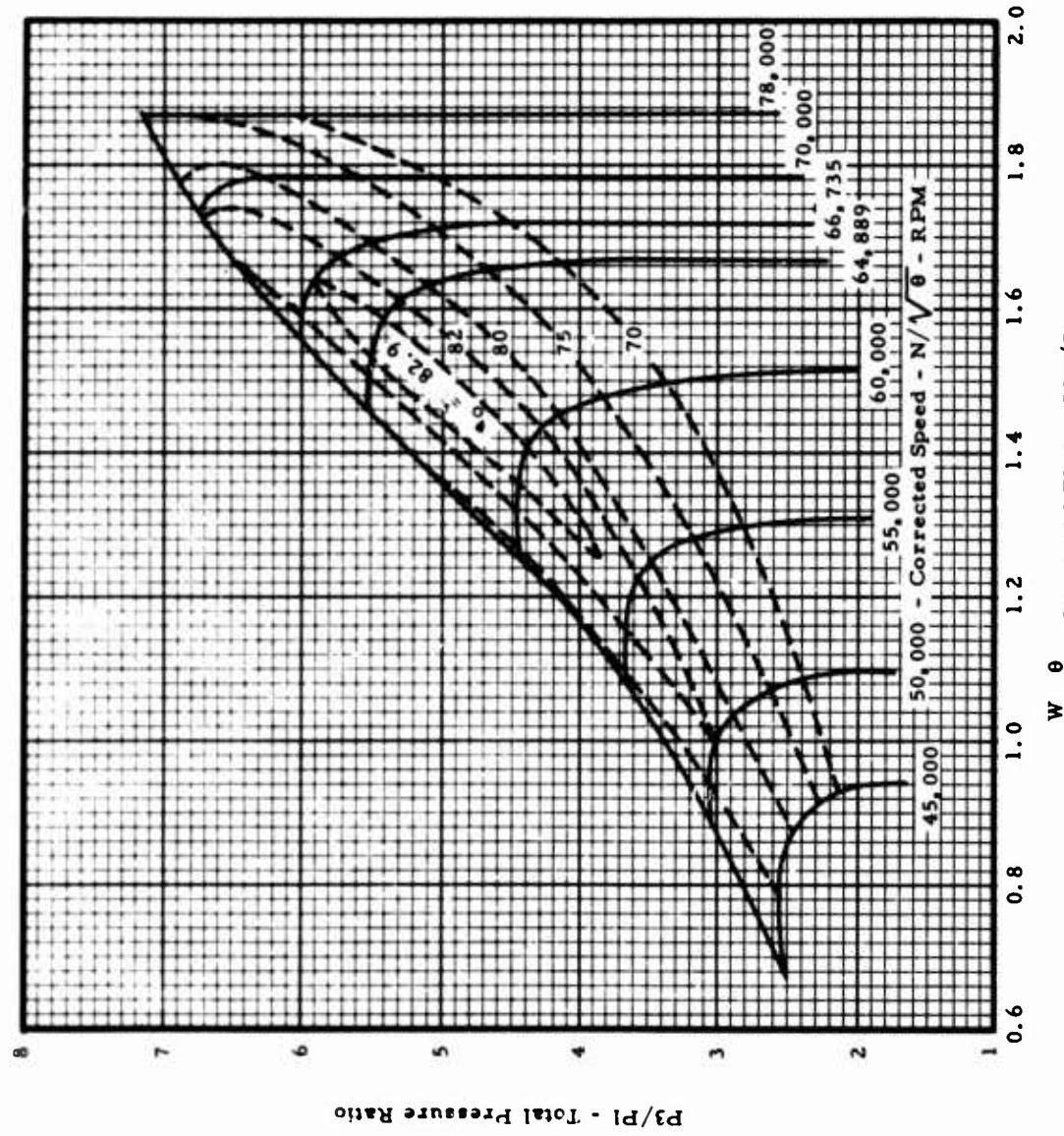


Figure X-7. Estimated Combined Axial, Centrifugal Compressor Characteristics.

ERDL 120 HP SIMPLE CYCLE ENGINE  
Section X  
MATCHING STUDY  
AXIAL EXHAUST CONFIGURATION

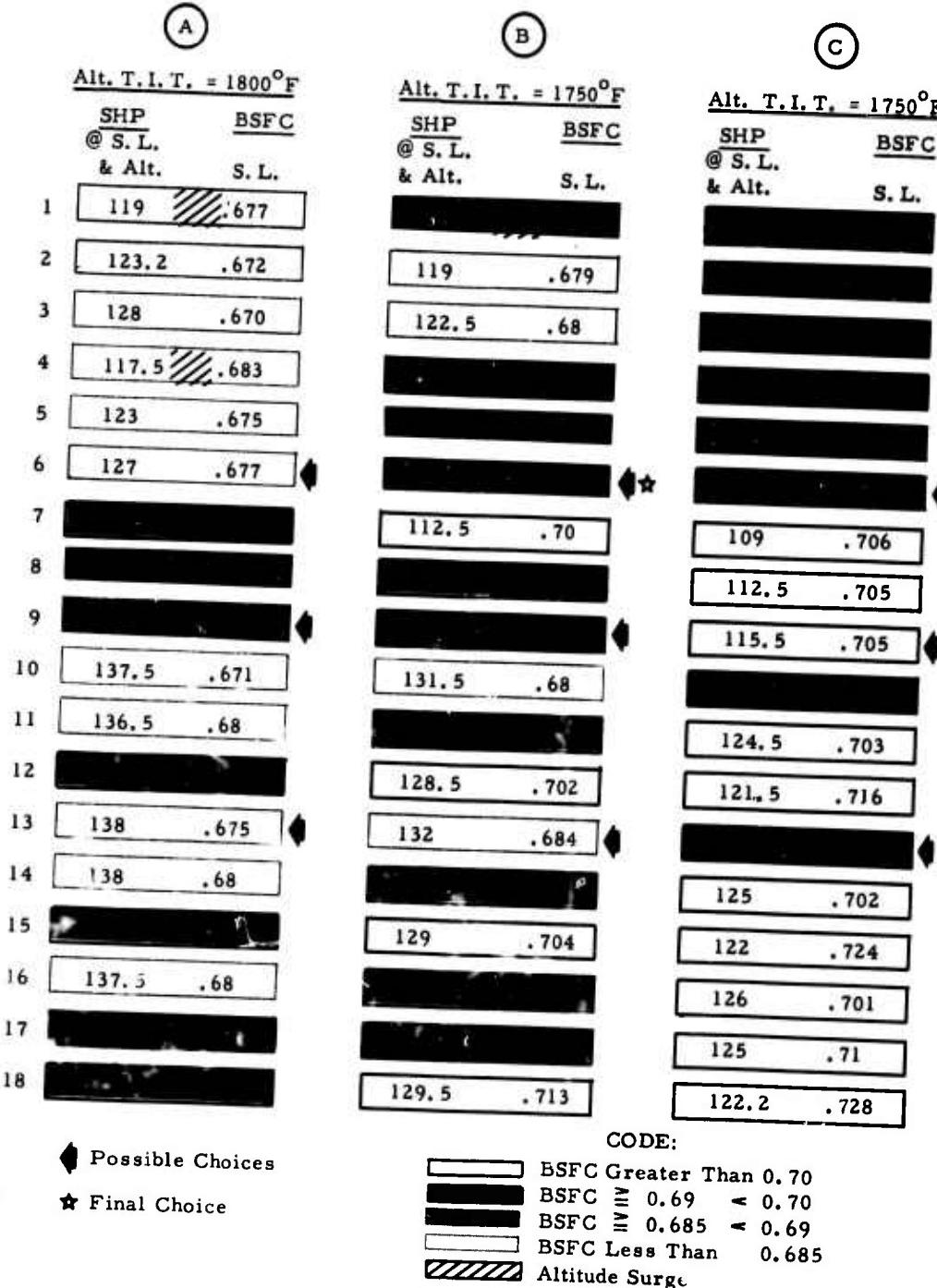


Figure X-8. TS120 Simple Cycle Engine, Matching Study Axial Exhaust Configuration.

## Section X

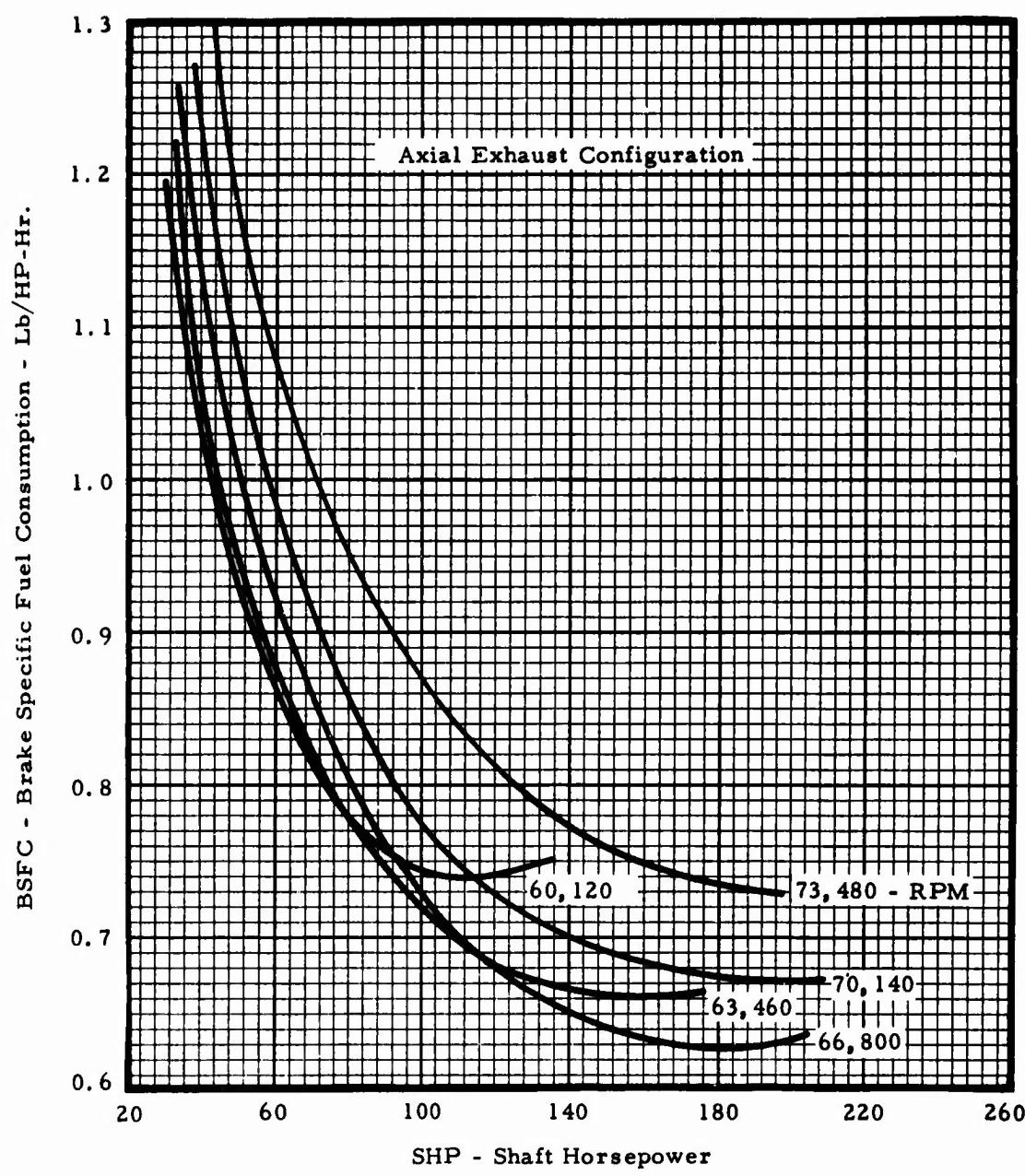
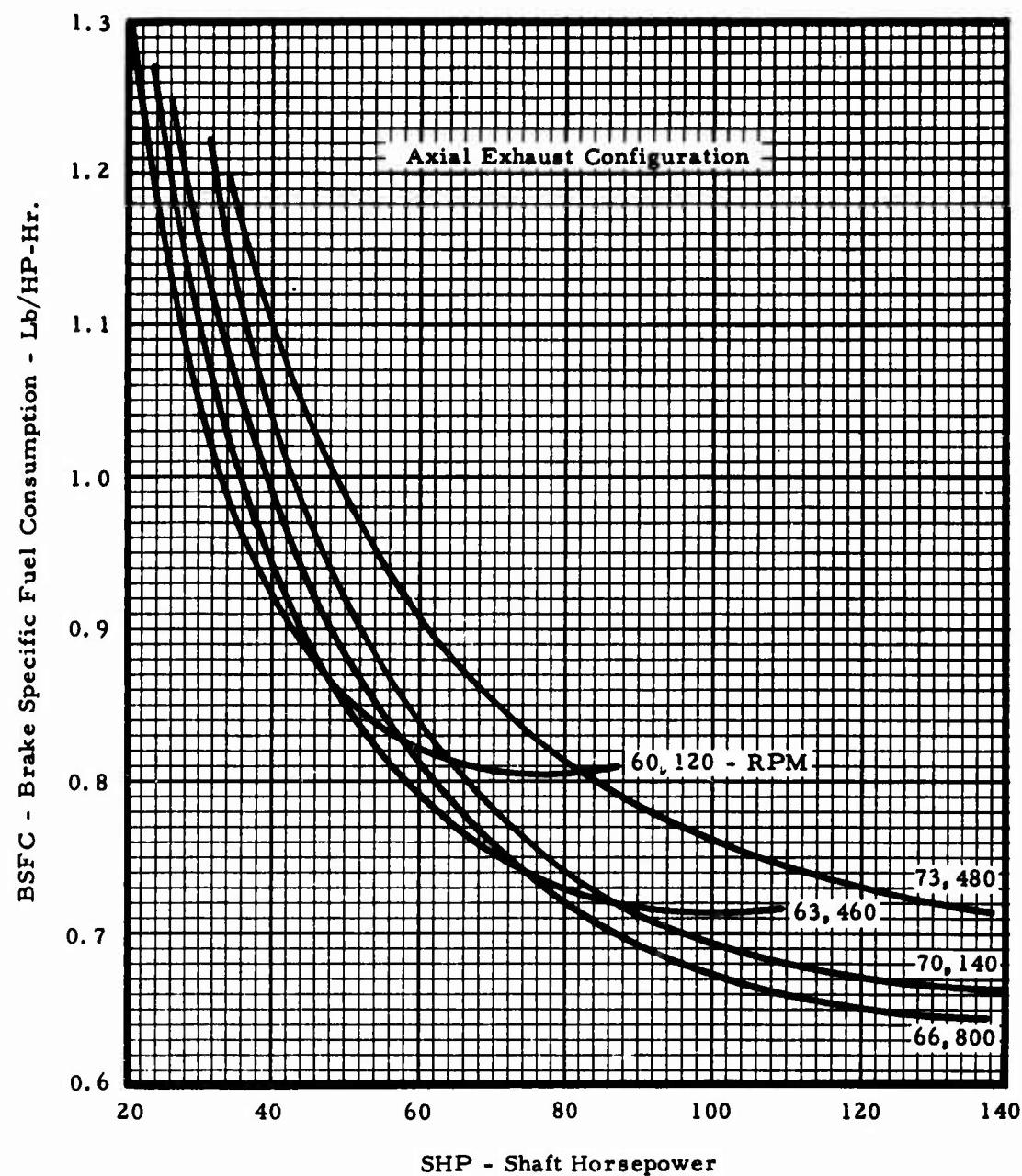


Figure X-9. TS120 Simple Cycle Engine, Horsepower Characteristics  
Sea Level, 60°F.

**Section X**



**Figure X-10. TS120 Simple Cycle Engine, Horsepower Characteristics 8000 Feet, 90°F.**

## Section X

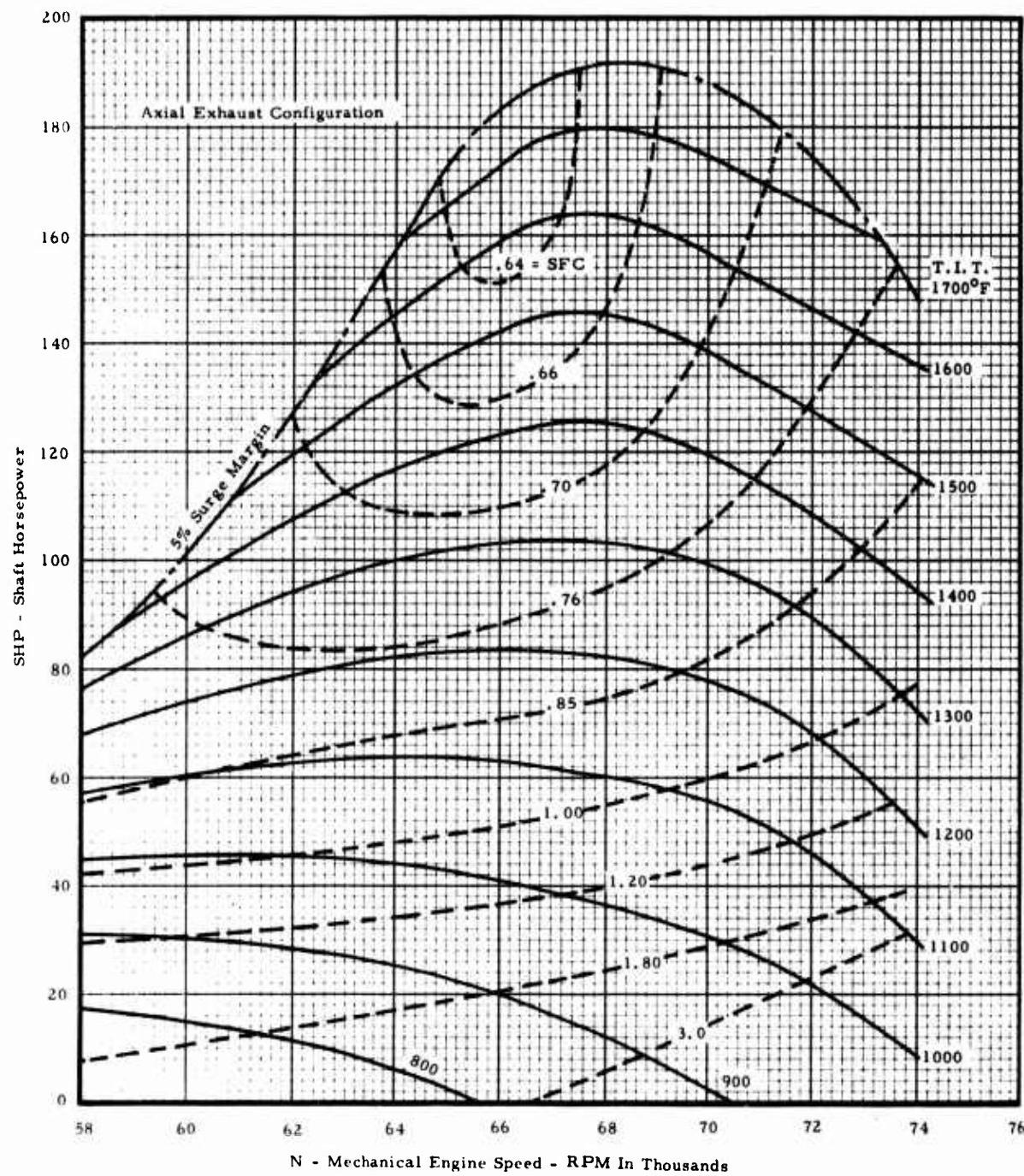


**Figure X-11. TS120 Simple Cycle Engine, Estimated Performance Characteristics Sea Level, 60°F.**

## Section X

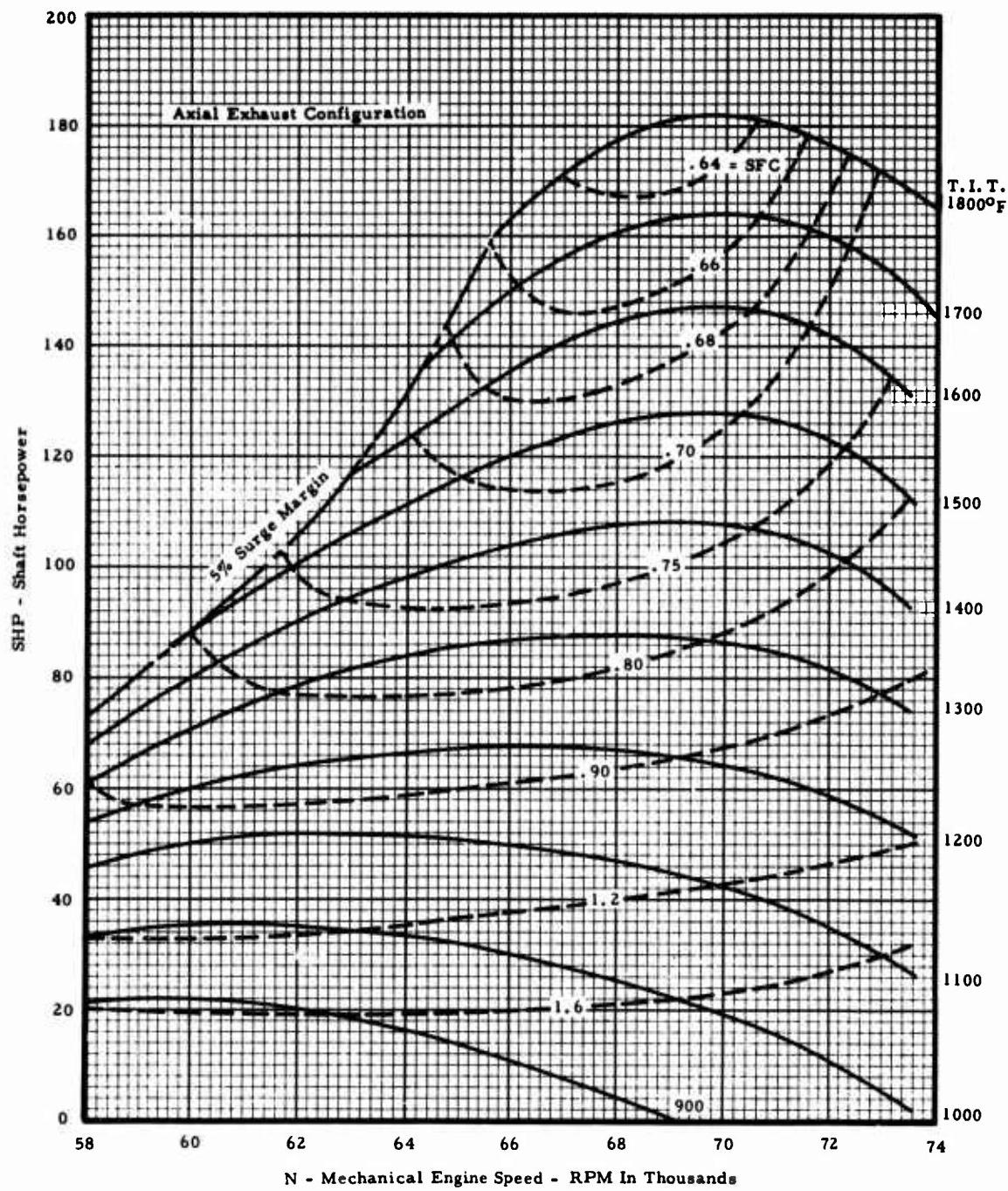


Figure X-12. TS120 Simple Cycle Engine, Estimated Performance Characteristics Sea Level, 90°F.

## Section X

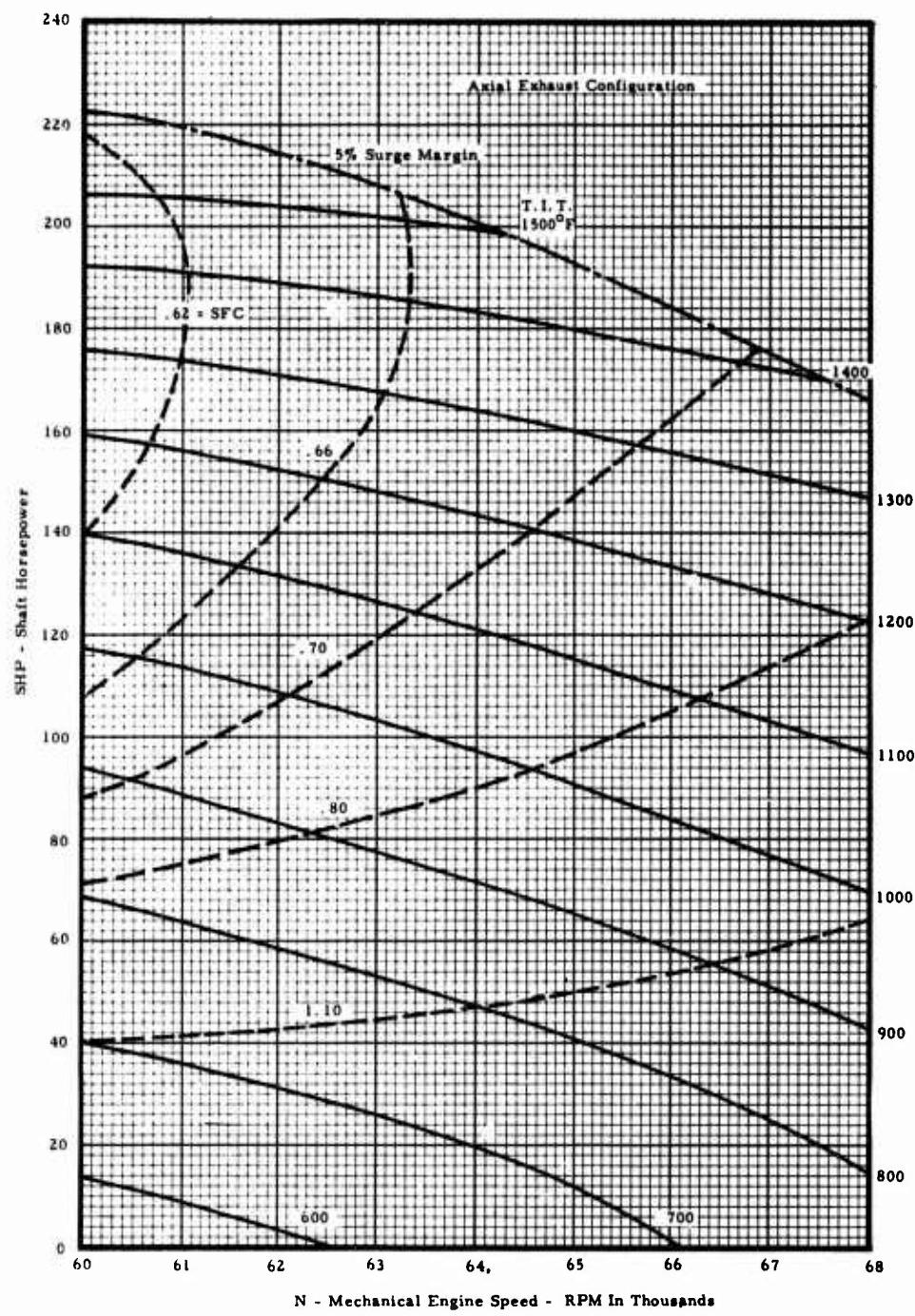


Figure X-13. TS120 Simple Cycle Engine, Estimated Performance Characteristics Sea Level, -65°F.

## Section X

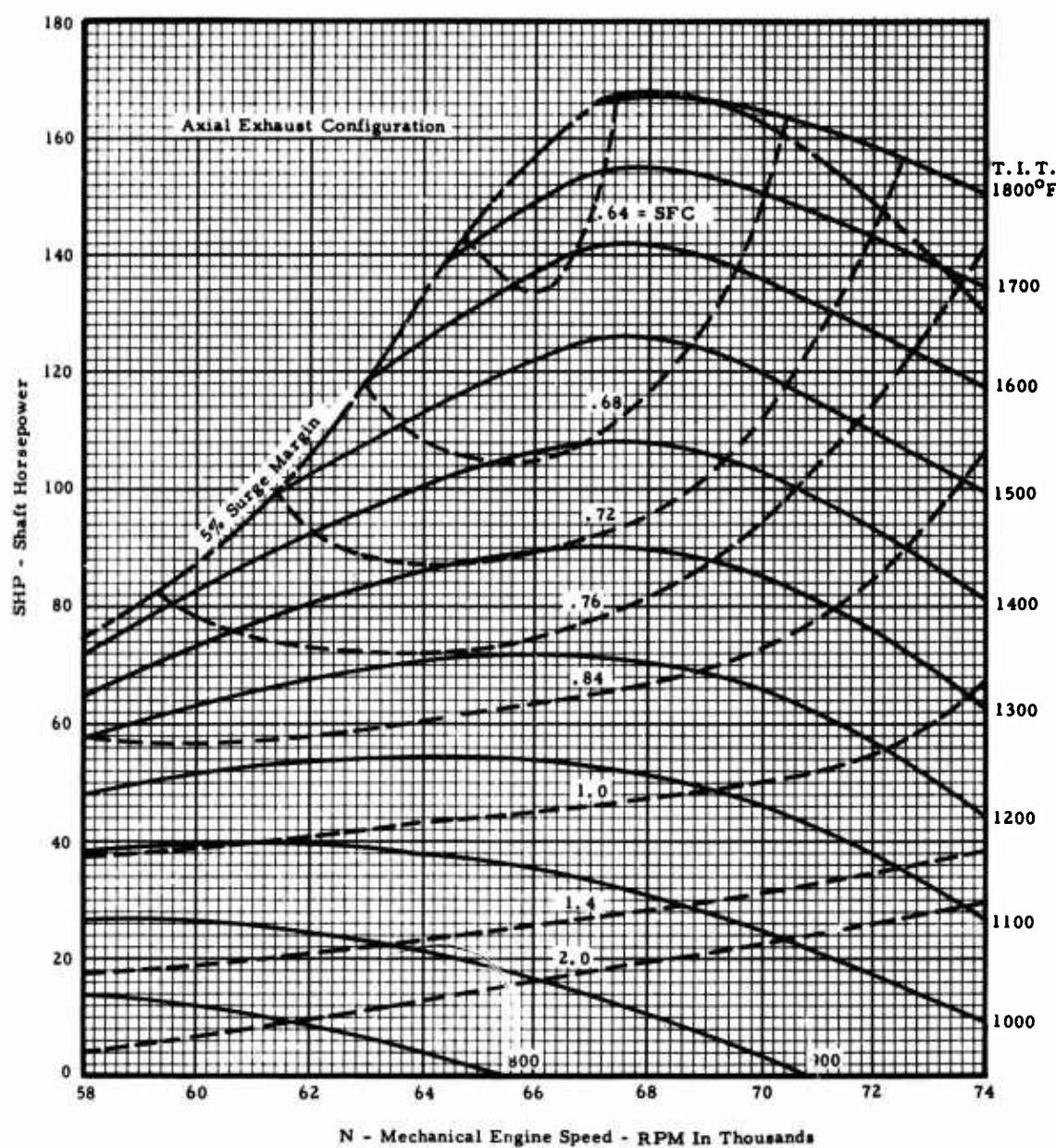


Figure X-14. TS120 Simple Cycle Engine, Estimated Performance Characteristics 4000 Feet, 60°F.

## Section X

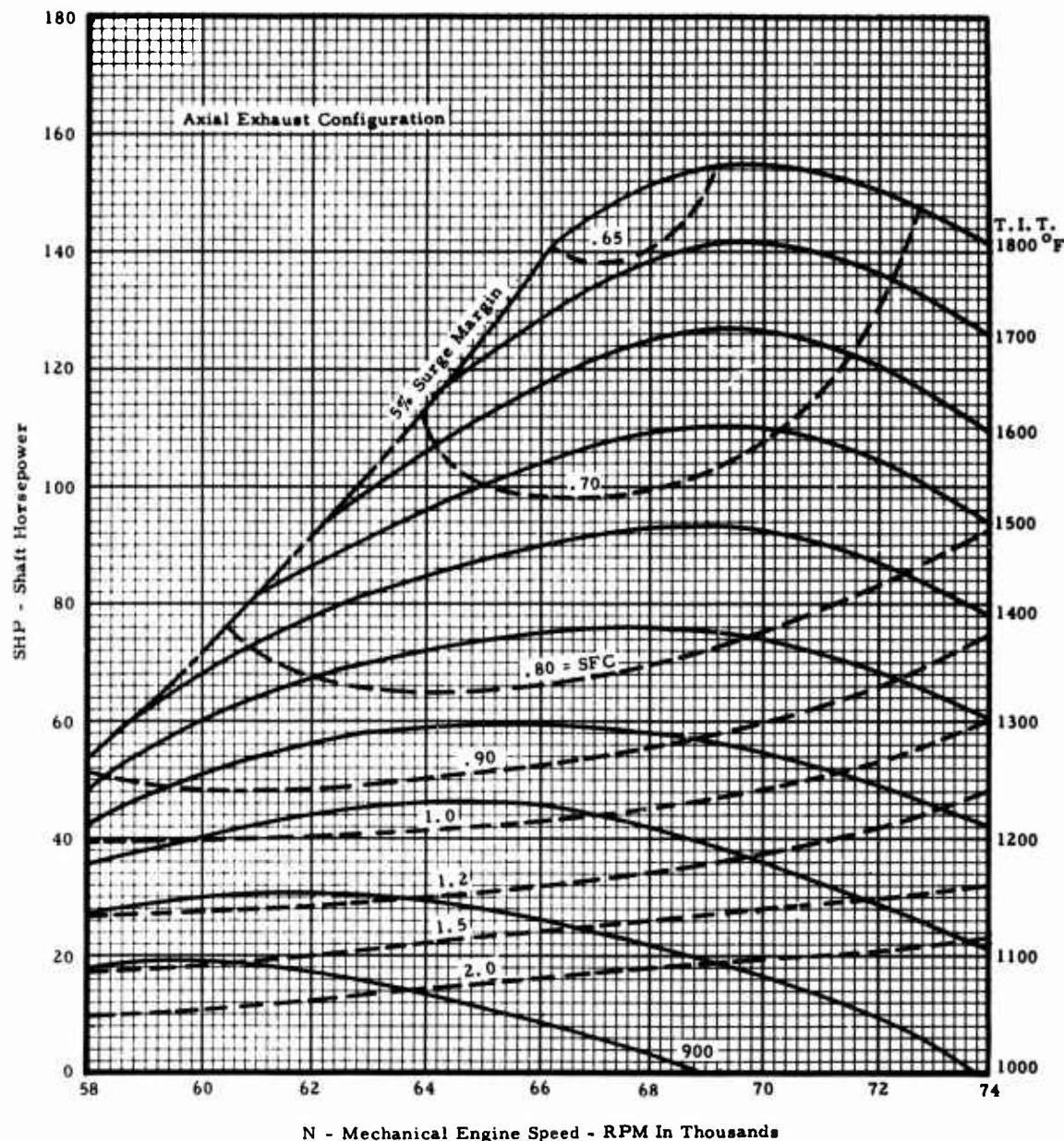
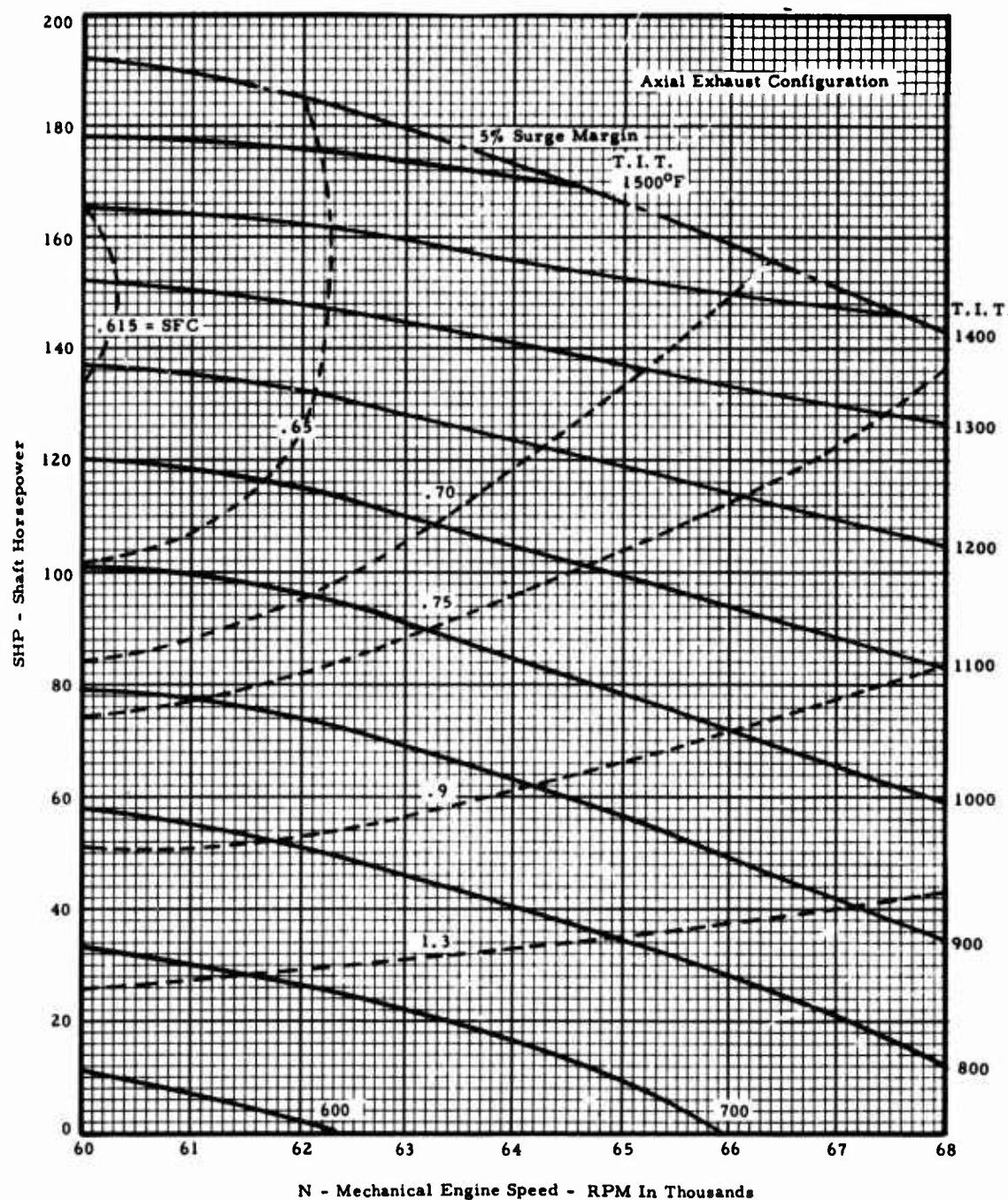


Figure X-15. TS120 Simple Cycle Engine, Estimated Performance Characteristics 4000 Feet, 90°F.

## Section X



**Figure X-16. TS120 Simple Cycle Engine, Estimated Performance Characteristics 4000 Feet, -65°F.**

## Section X

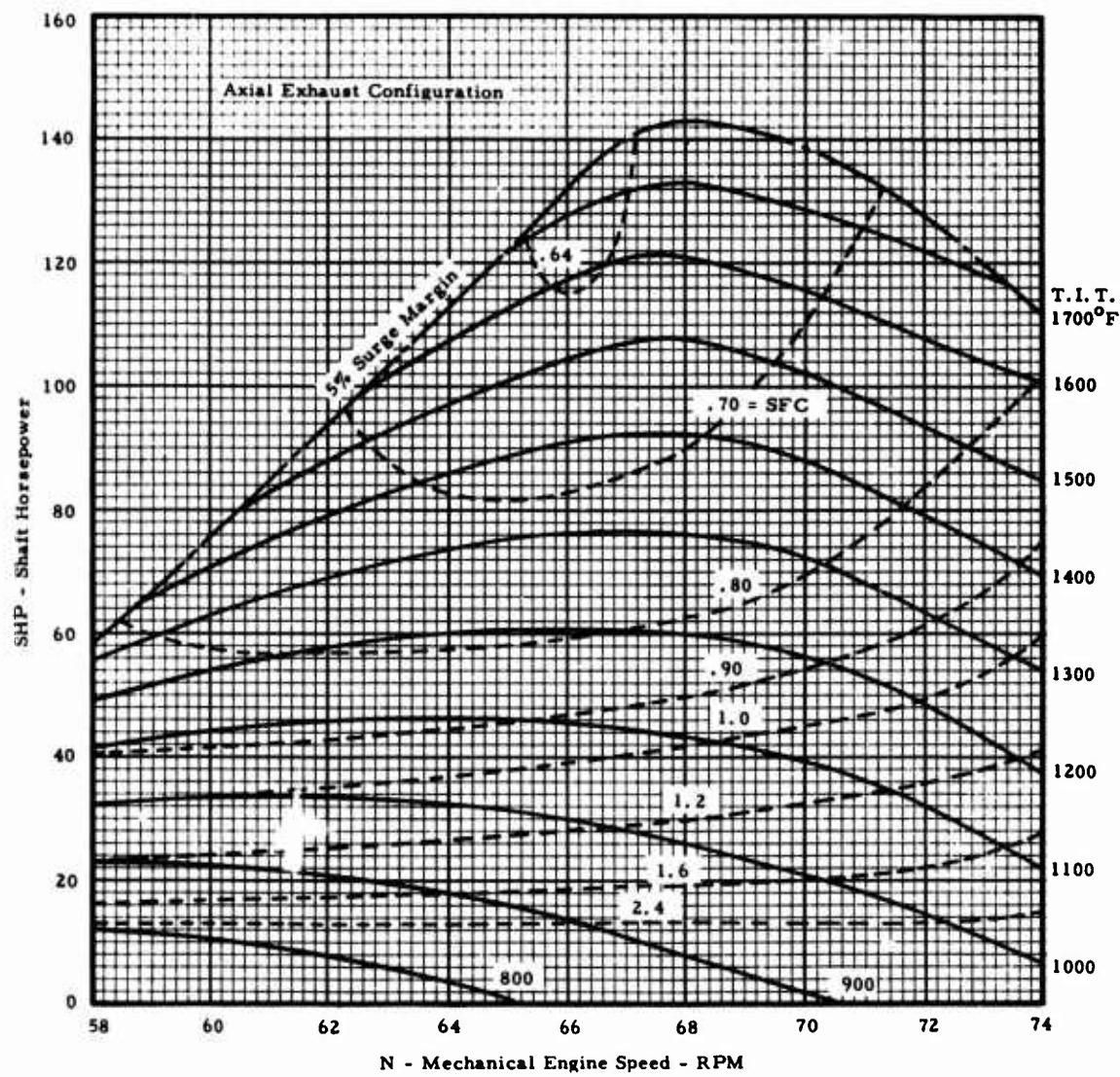
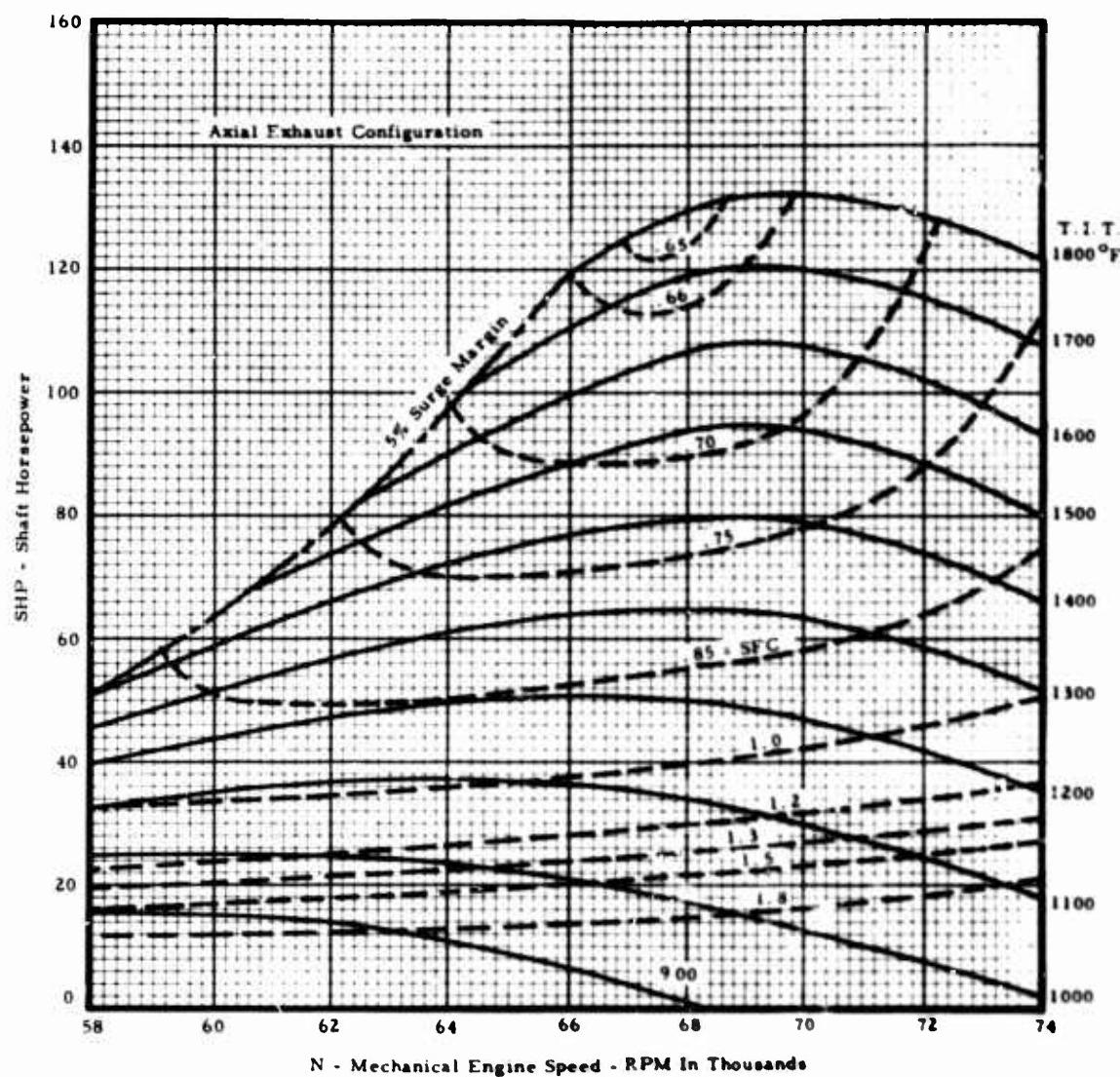


Figure X-17. TSI20 Simple Cycle Engine, Estimated Performance Characteristics 8000 Feet, 60°F.

## Section X



**Figure X-18. T8120 Simple Cycle Engine, Estimated Characteristics  
8000 Feet, 90°F.**

## Section X

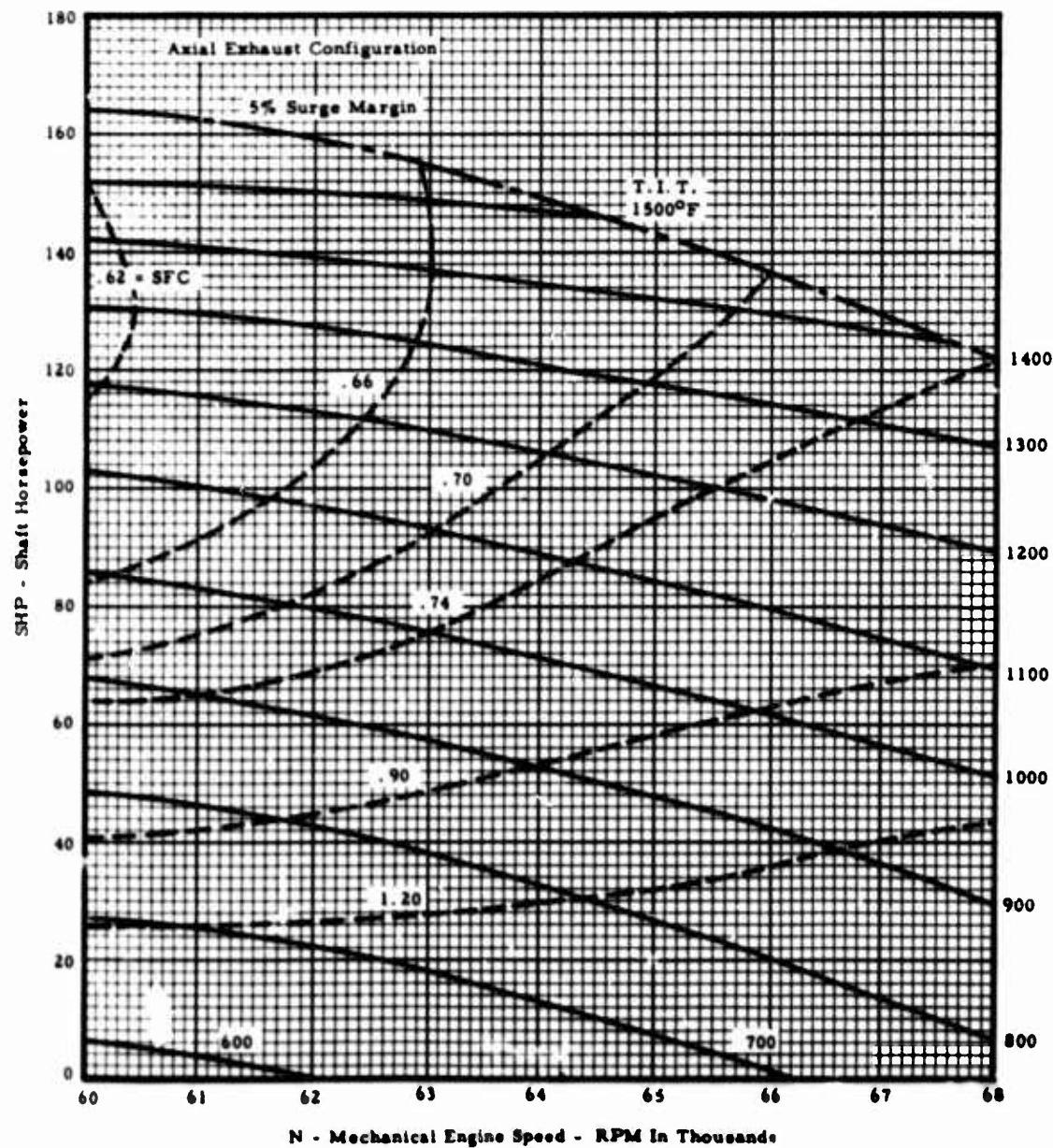
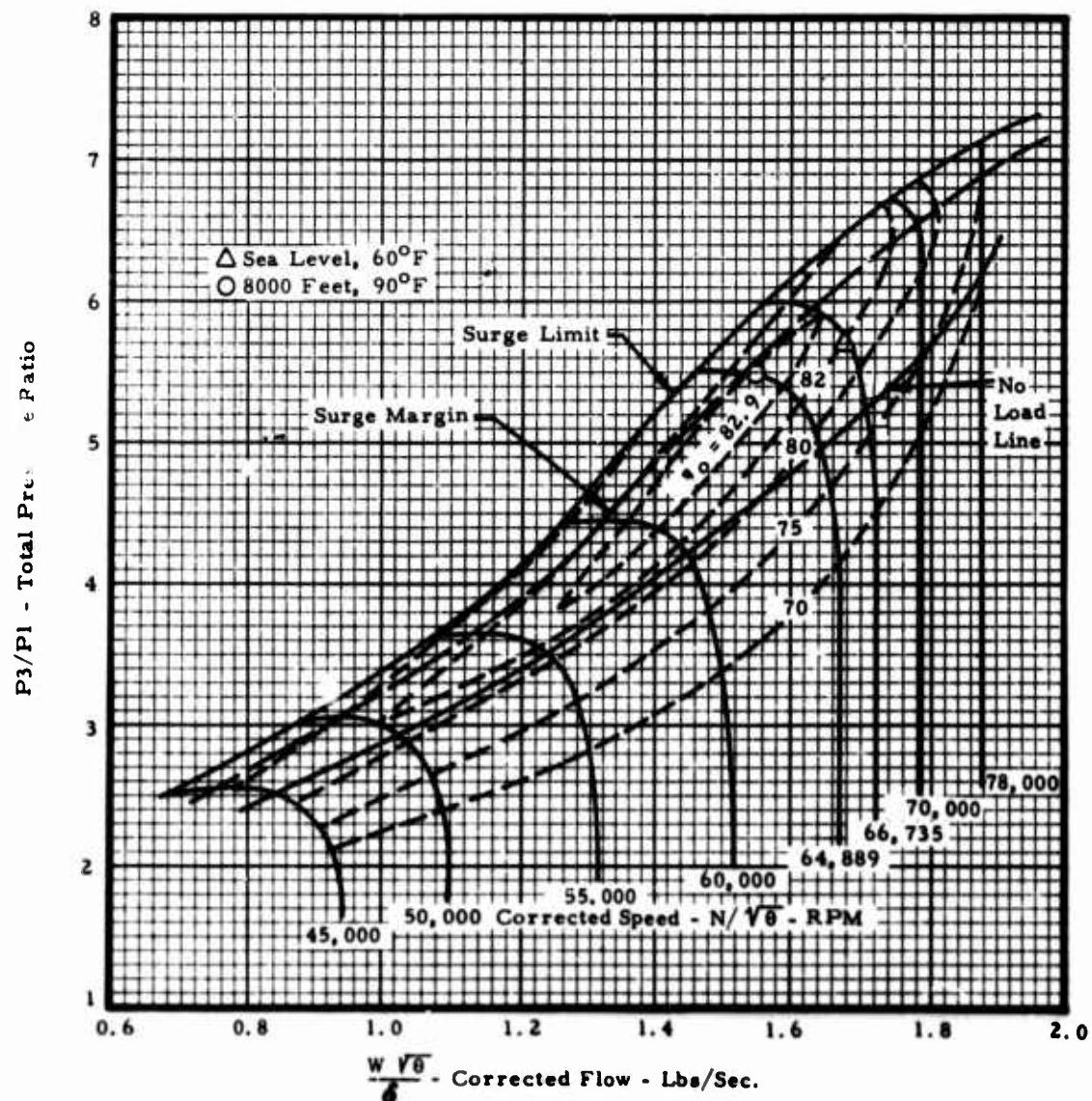


Figure X-19. TS120 Simple Cycle Engine, Estimated Performance Characteristics 8000 Feet, -65°F.

**Section X**



**Figure X-20. TS120 Simple Cycle Engine, Estimated Combined Axial, Centrifugal Compressor Characteristics.**

## Section X

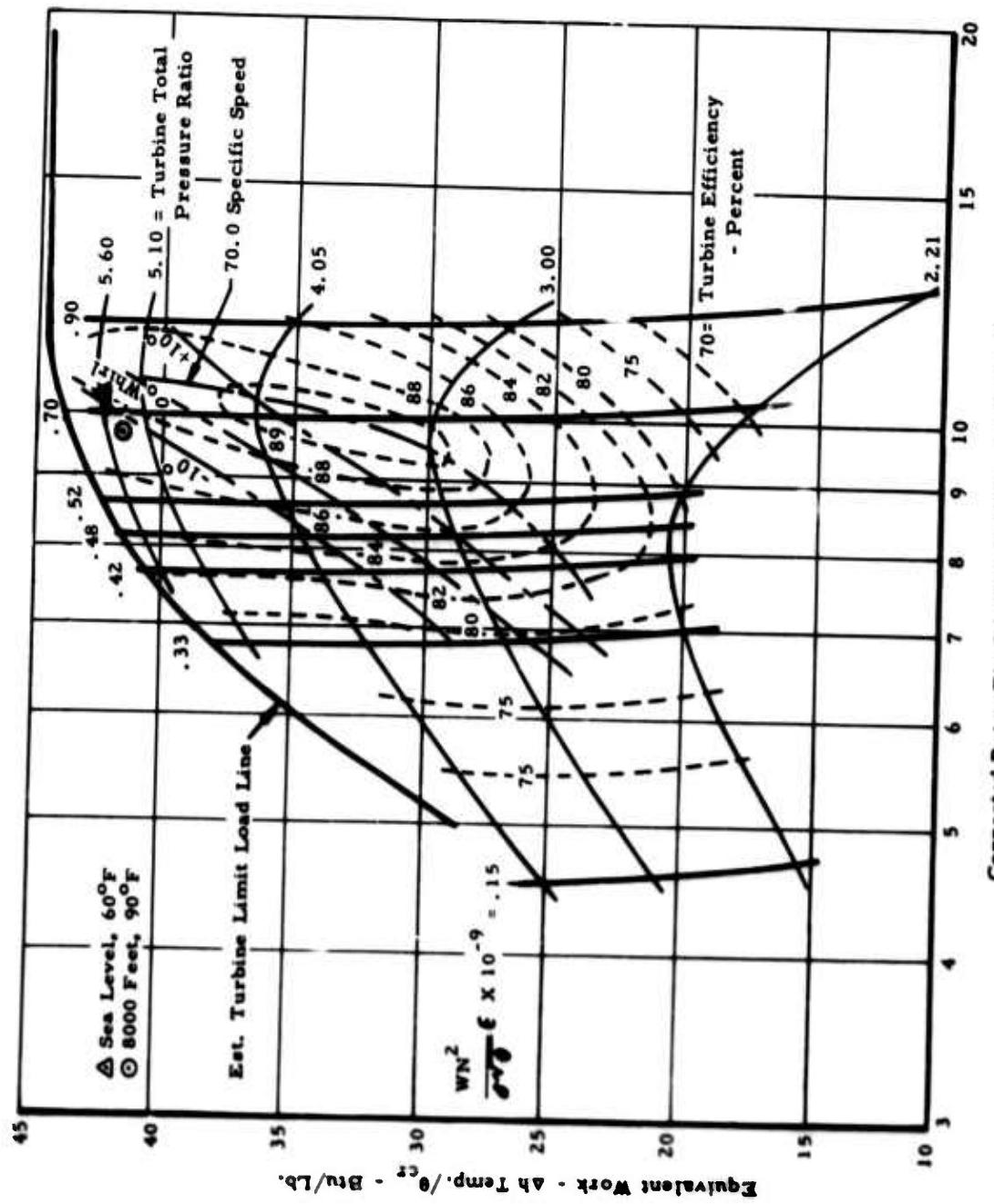


Figure X-21. Test Characteristics, 90° Radial Inflow Turbine.

## Section X

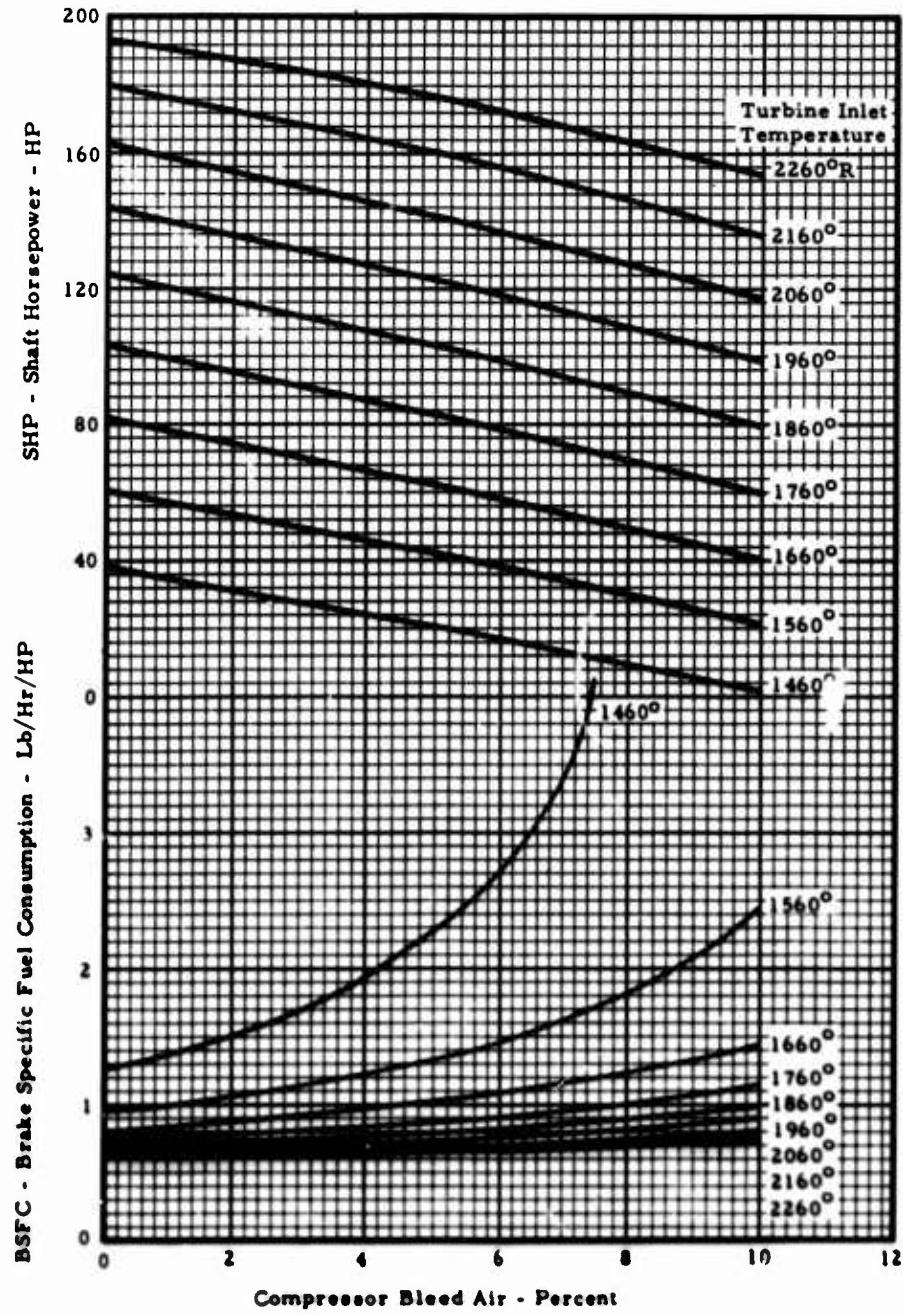
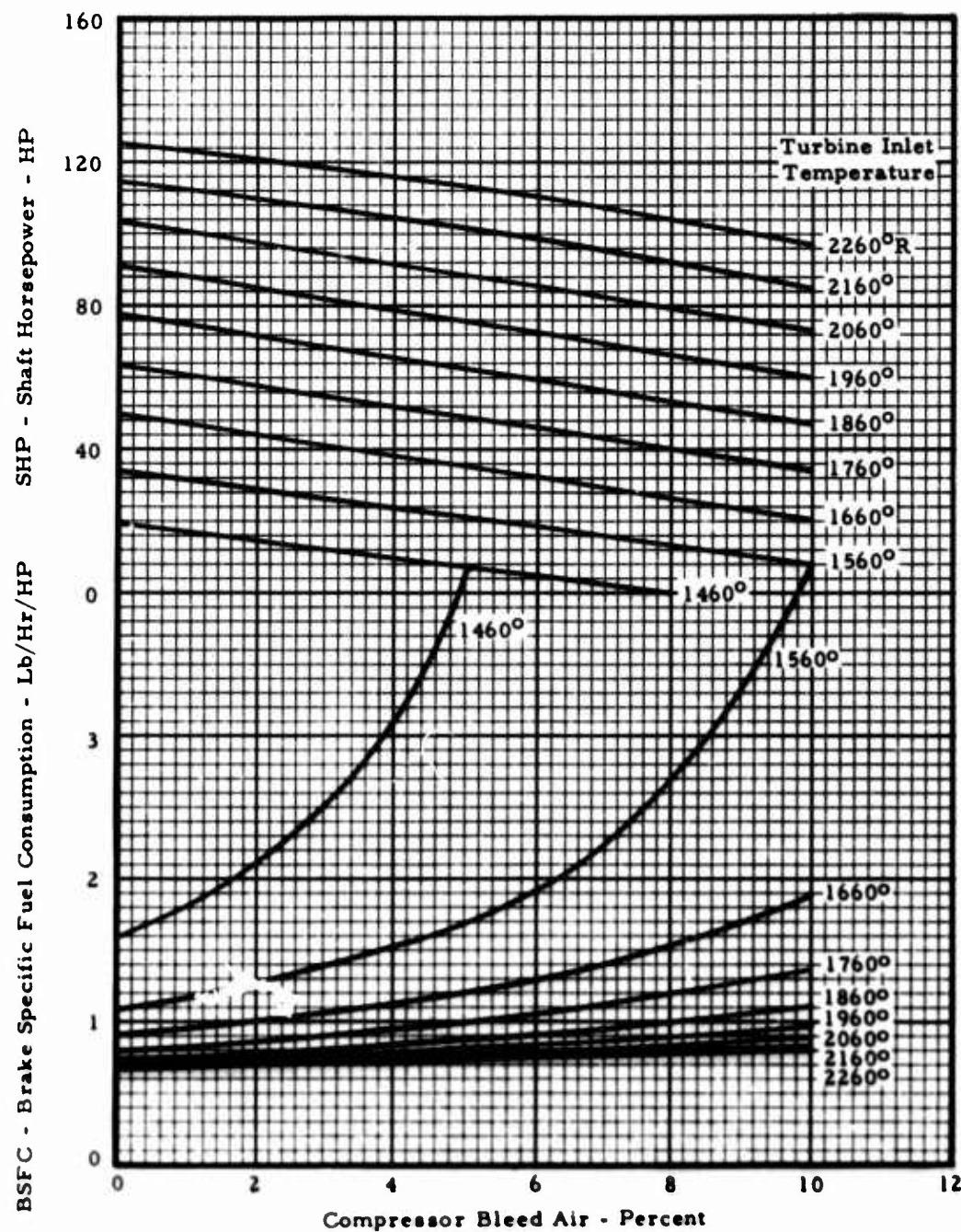


Figure X-22. TS120 Simple Cycle Engine, Effect of Compressor Bleed Air Sea Level, 60°F.

**Section X**



**Figure X-23. TS120 Simple Cycle Engine, Effect of Compressor Bleed Air - 8000 Feet, 90°F.**

## Section X

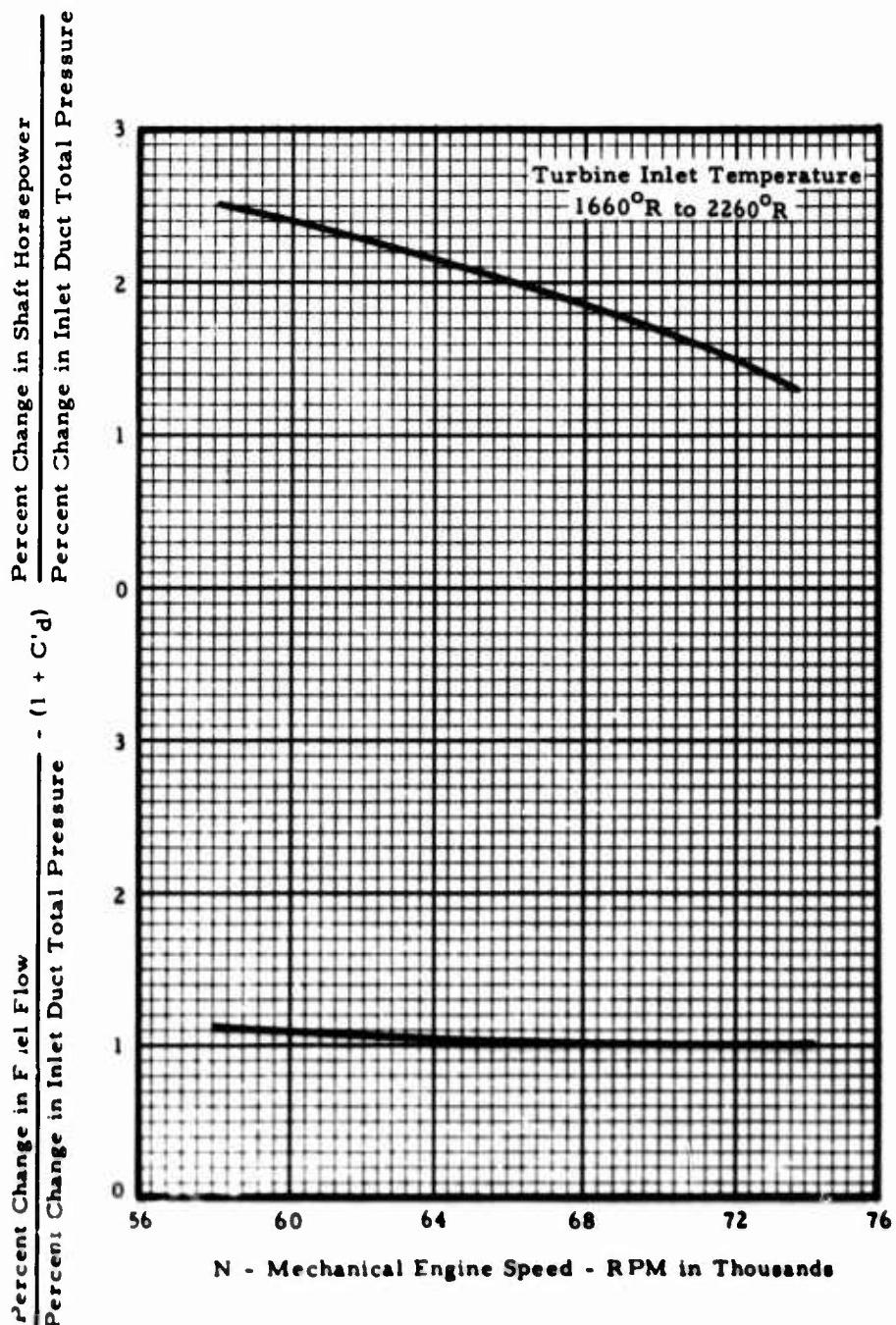


Figure X-24. TS120 Simple Cycle Engine, Inlet Duct Total Pressure Loss Correction Factors.

Section X

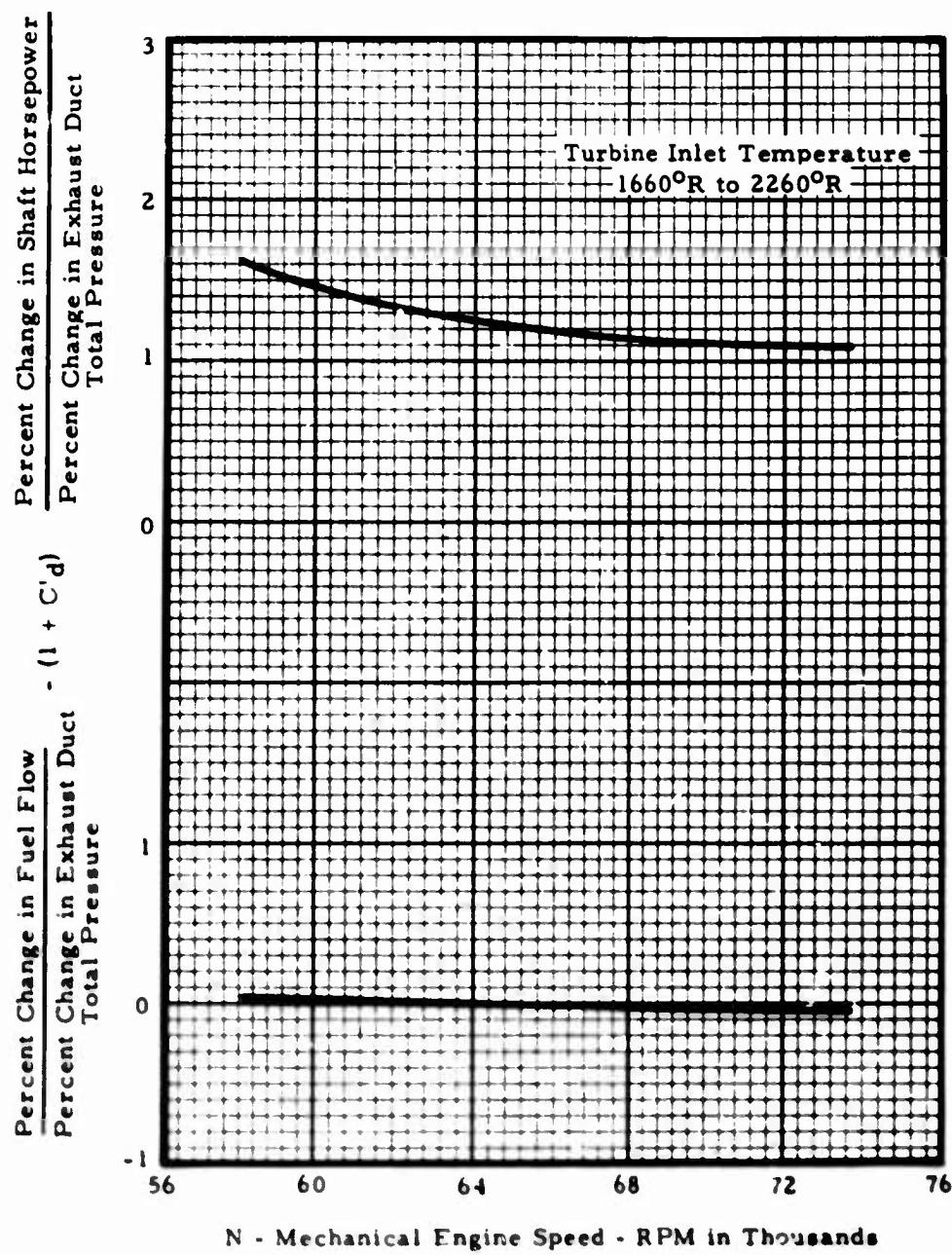


Figure X-25. TS120 Simple Cycle Engine, Exhaust Duct Total Pressure Loss Correction Factors.

**Section X**

<u>PARAMETER</u>	<u>PARAMETER CHANGE</u>	<u>% CHANGE IN SHP</u>	<u>% CHANGE IN BSFC</u>
Compressor Efficiency	1% -1%	2.42 -2.40	-1.70 2.00
Turbine Efficiency	1% -1%	3.4 -3.30	-3.30 3.40
Burner Total Pressure Loss (Comp. to Turb. Inlet)	1% -1%	-1.4 1.6	1.6 -1.5
Airflow	1% -1%	1.03 1.03	-.03% .03%
Compressor Pressure Ratio	.25 PR -.25 PR	0 -.166	-1.31% 1.46%
Turbine Inlet Temperature	50° -50°	9.0 -8.0	-2.4 3.0
Horsepower Extracted	1.0% -1.0%	-.8 .8	.8 -.8

**Figure X-26. TS120 Simple Cycle Engine, Influence Coefficients - Sea Level, 60°F.**

## Section X

<u>PARAMETER</u>	<u>PARAMETER CHANGE</u>	<u>% CHANGE IN SHP</u>	<u>% CHANGE IN BSFC</u>
Compressor Efficiency	1% -1%	1.65 -1.55	-1.2 1.25
Turbine Efficiency	1% -1%	2.55 -2.65	-2.5 2.8
Burner Total Pressure Loss	1% -1%	-1.3 1.2	1.3 -1.2
Airflow	1% -1%	1.03 1.03	-.03 .03
Compressor Pressure Ratio	.25 PR -.25 PR	0.80 -0.80	-1.85 2.15
Turbine Inlet Temperature	50° -50°	5.7 -5.5	-1.1 1.2
Horsepower Extracted	1% -1%	-0.8 0.8	0.81 -0.82

Figure X-27. TSI20 Simple Cycle Engine, Influence Coefficients -  
8000 Feet, 90°F.

## Section X

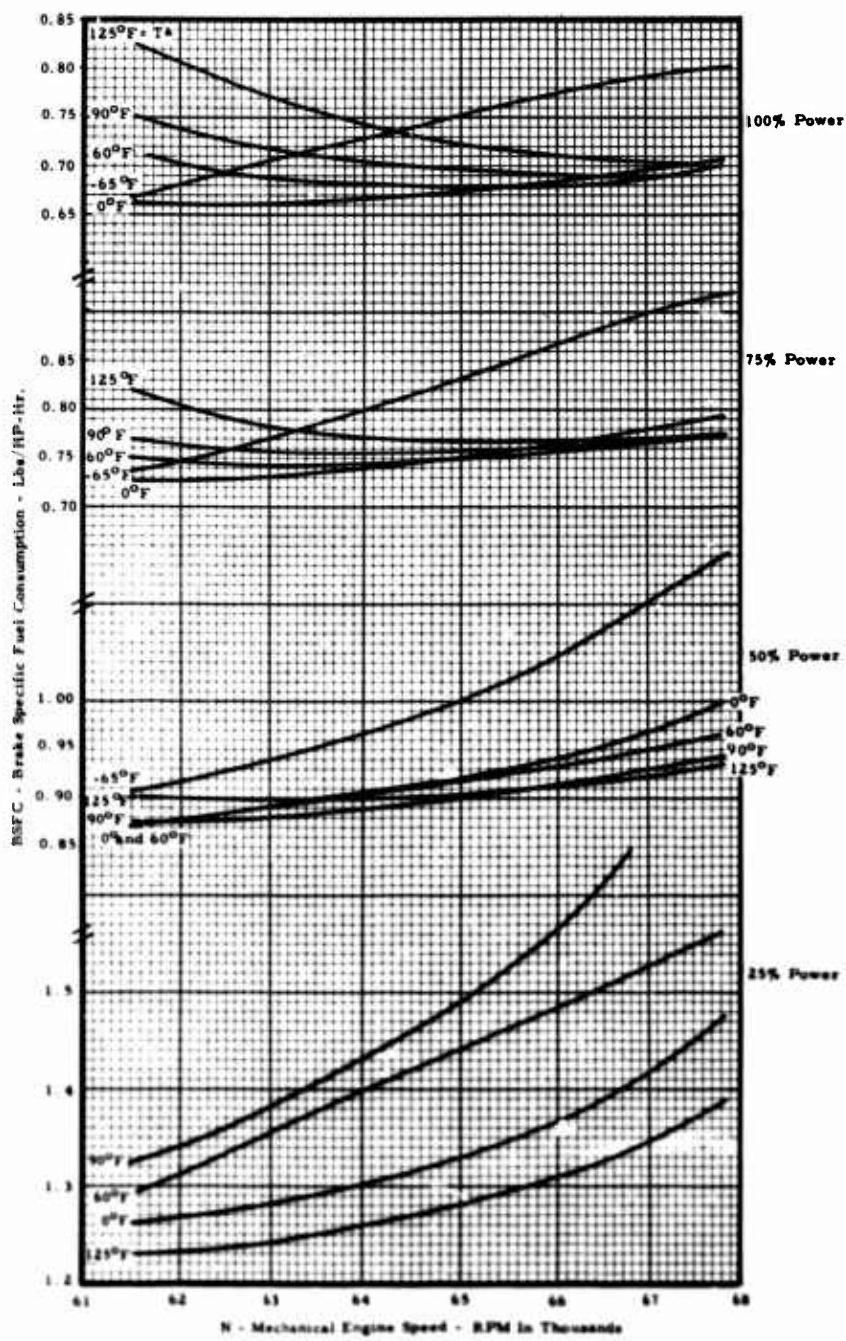


Figure X-28. BSFC - Speed Characteristics at Selected Power and Ambient Temperature Levels - Sea Level.

## Section X

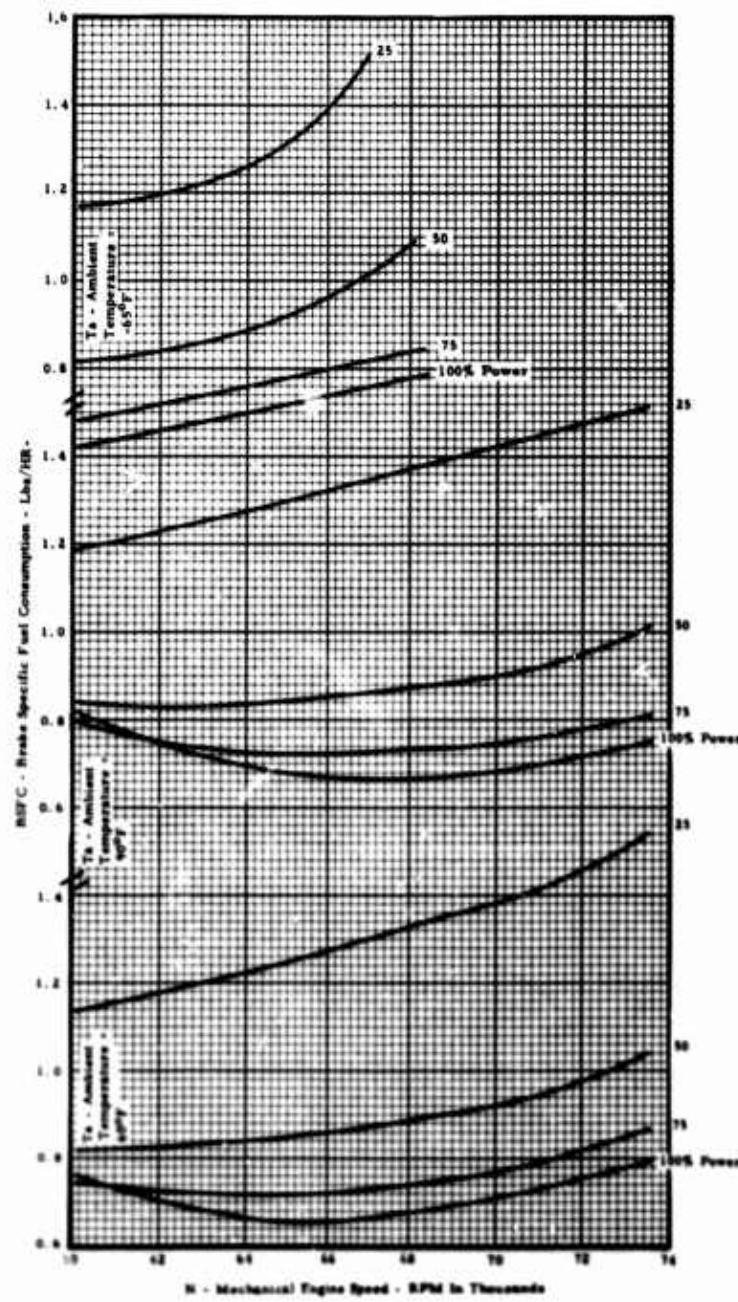


Figure X-29. TS120 Simple Cycle Engine, BSFC - Speed Characteristics at Selected Power and Ambient Temperature Levels - 4000 Feet.

## Section X

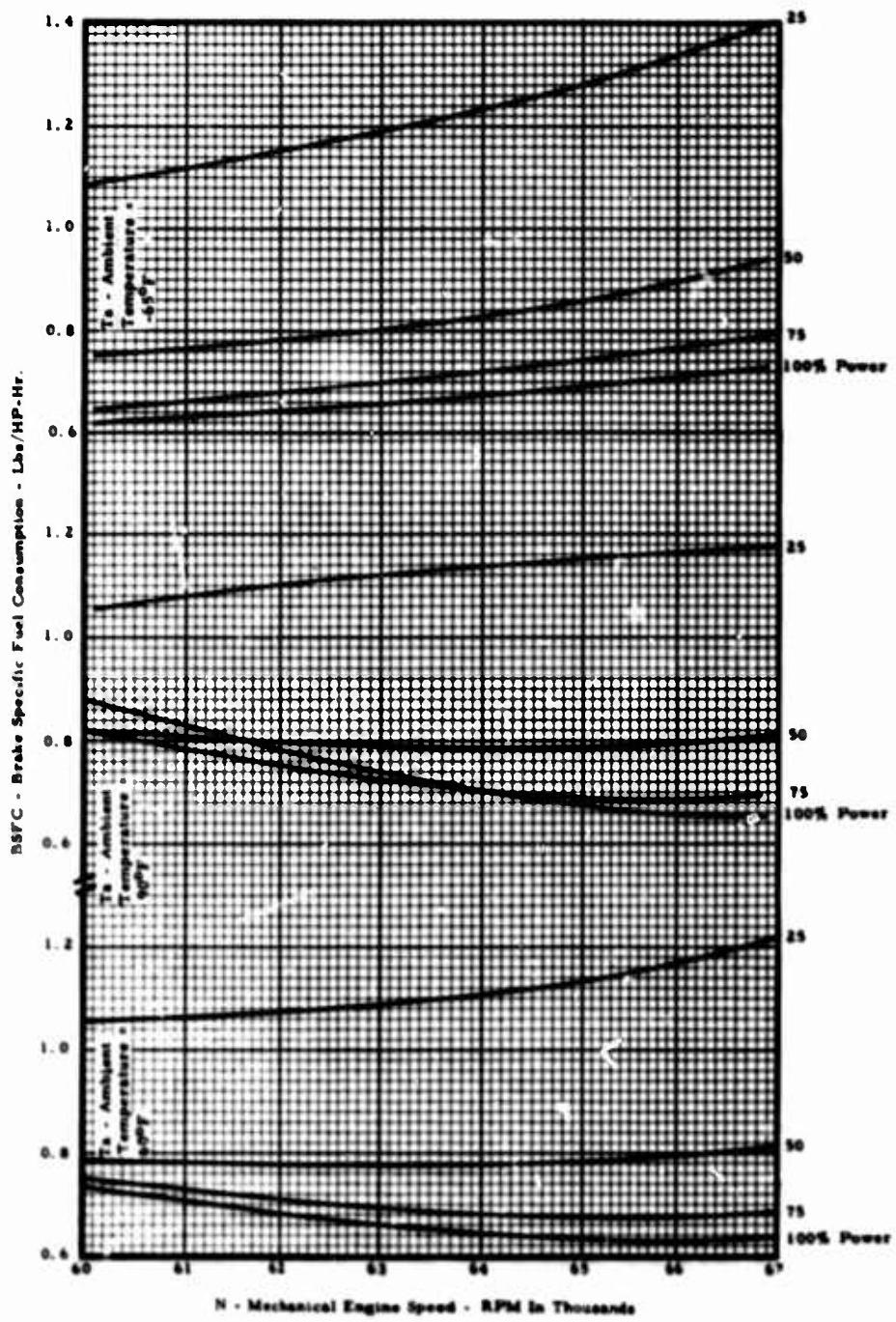
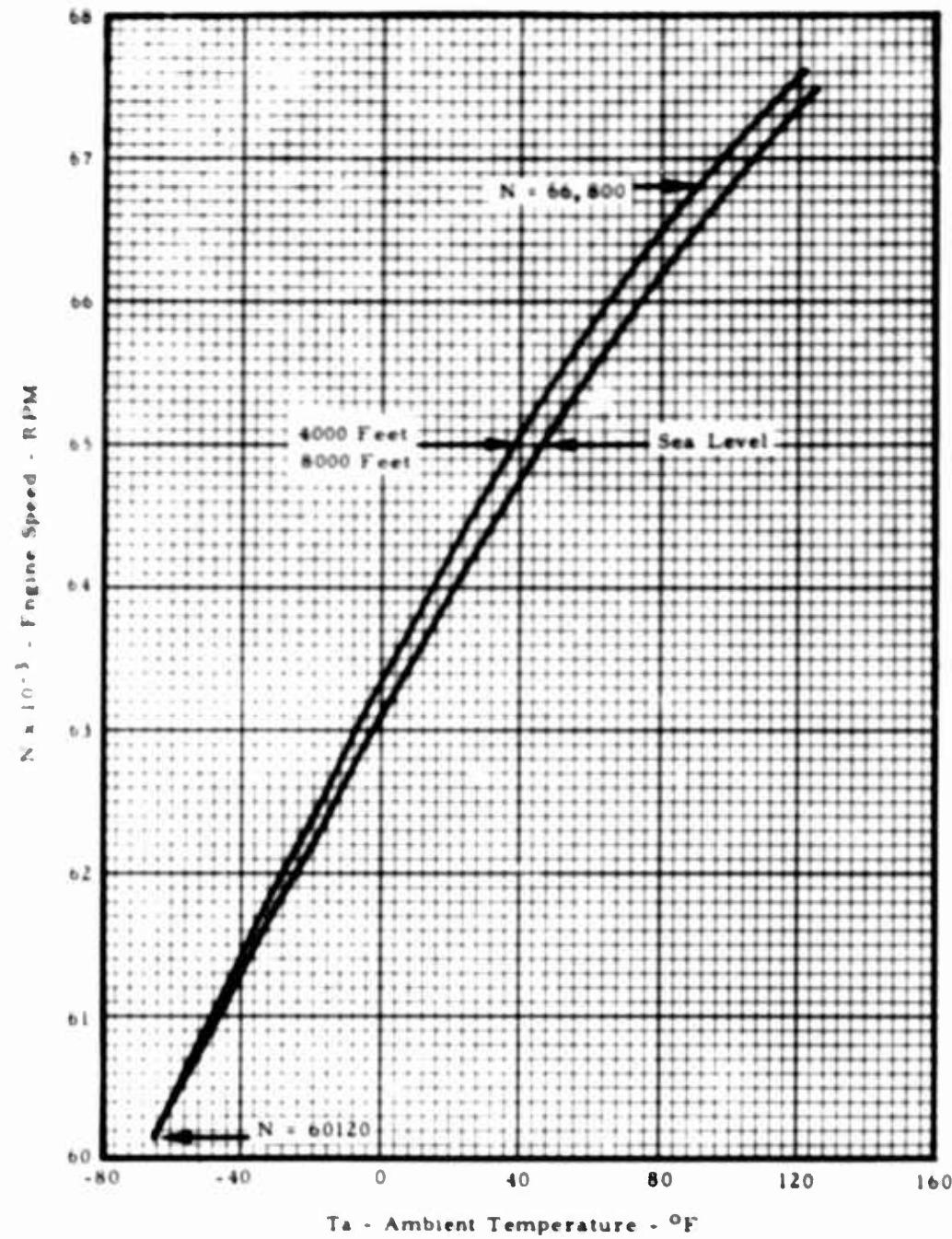


Figure X-30. TS120 Simple Cycle Engine, BSFC - Speed Characteristics at Selected Power and Ambient Temperature Levels - 8000 Feet.

**Section X**



**Figure X-31. TS120 Simple Cycle Engine, Speed Modulation for Optimum BSFC at 120 Horsepower.**

**Section X**

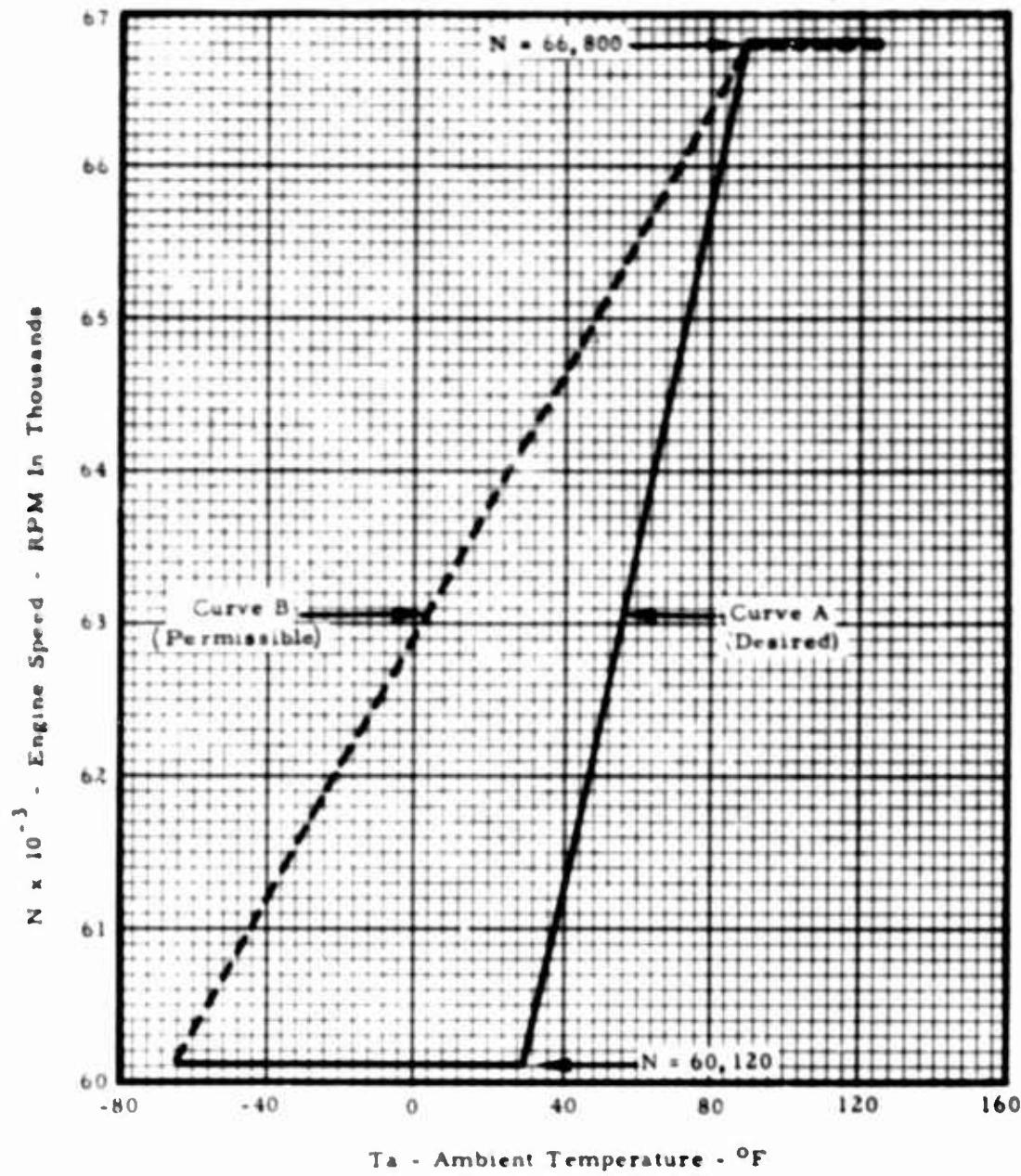


**Figure X-32. TS120 Simple Cycle Engine, Speed Modulation Requirement.**

**Section X**

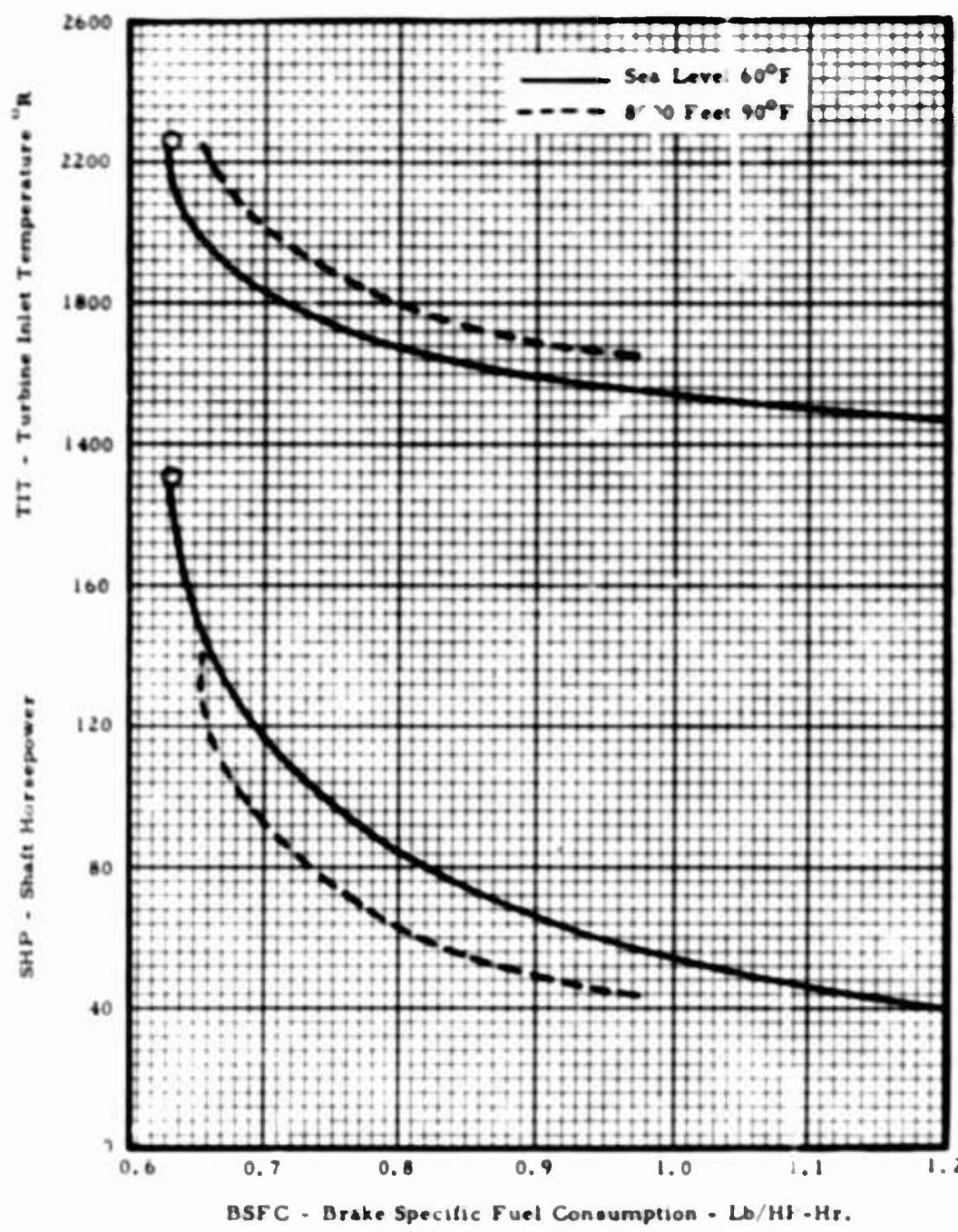


**Figure X-33. TS120 Simple Cycle Engine, Performance Characteristics, Normal Rated Speed = 66,800 R.P.M. - Radial Exhaust.**

## Section X

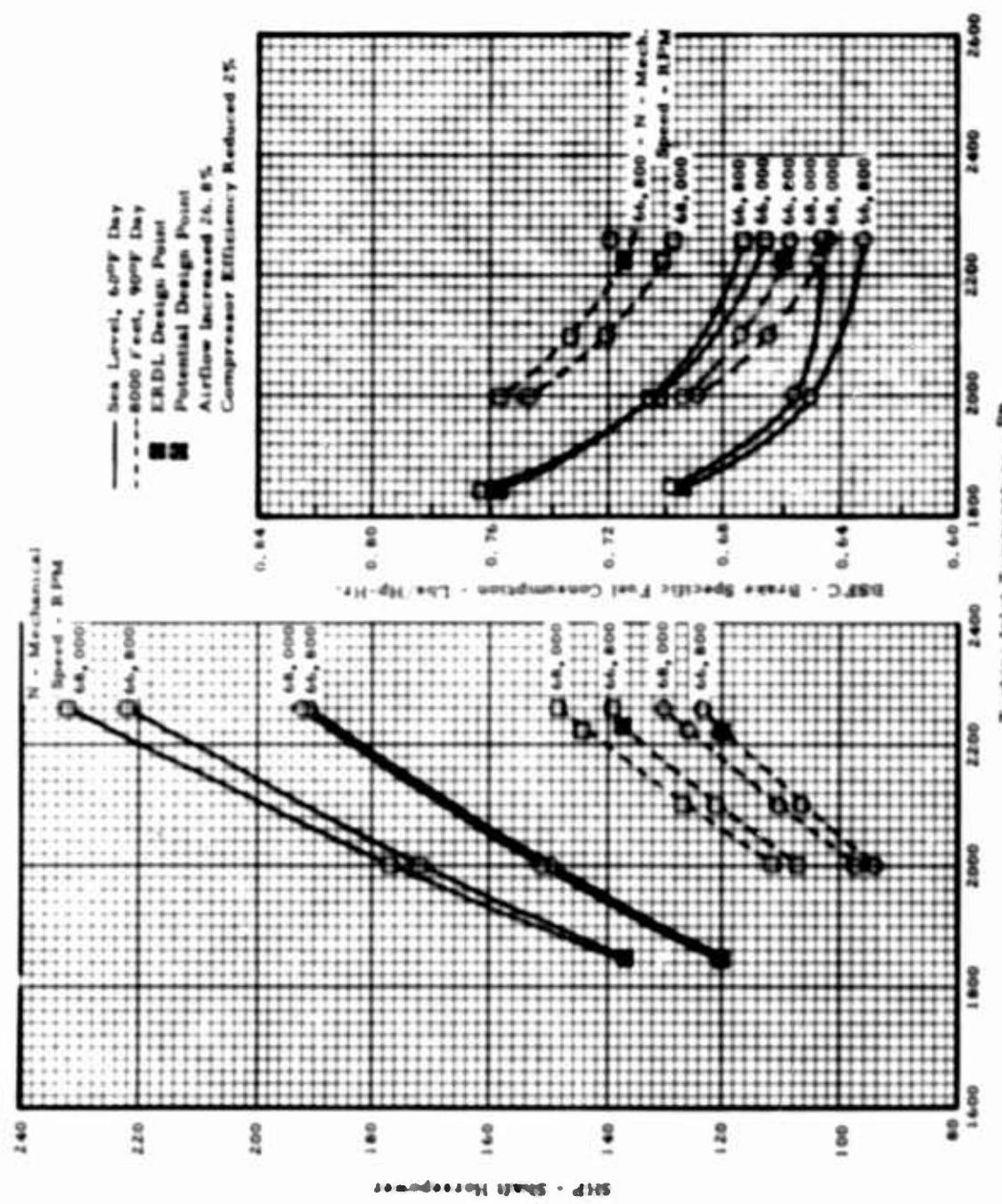


Figure X-34. TS120 Simple Cycle Engine, Growth Potential Study - Performance Characteristics.

Section X

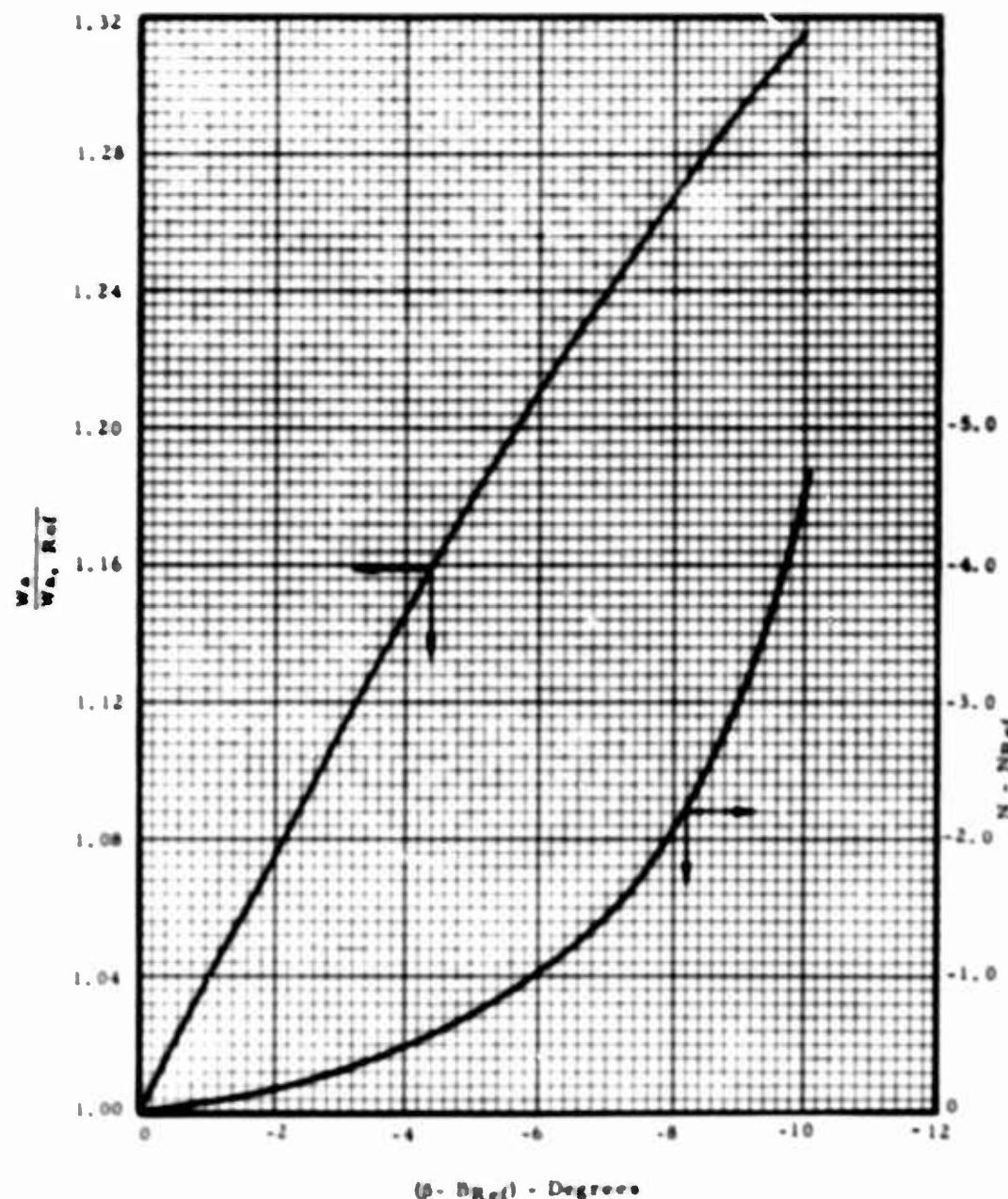


Figure X-35. Estimated Effect of Axial Stage Stagger Angle on Overall Compressor Efficiency and Airflow.

Section X

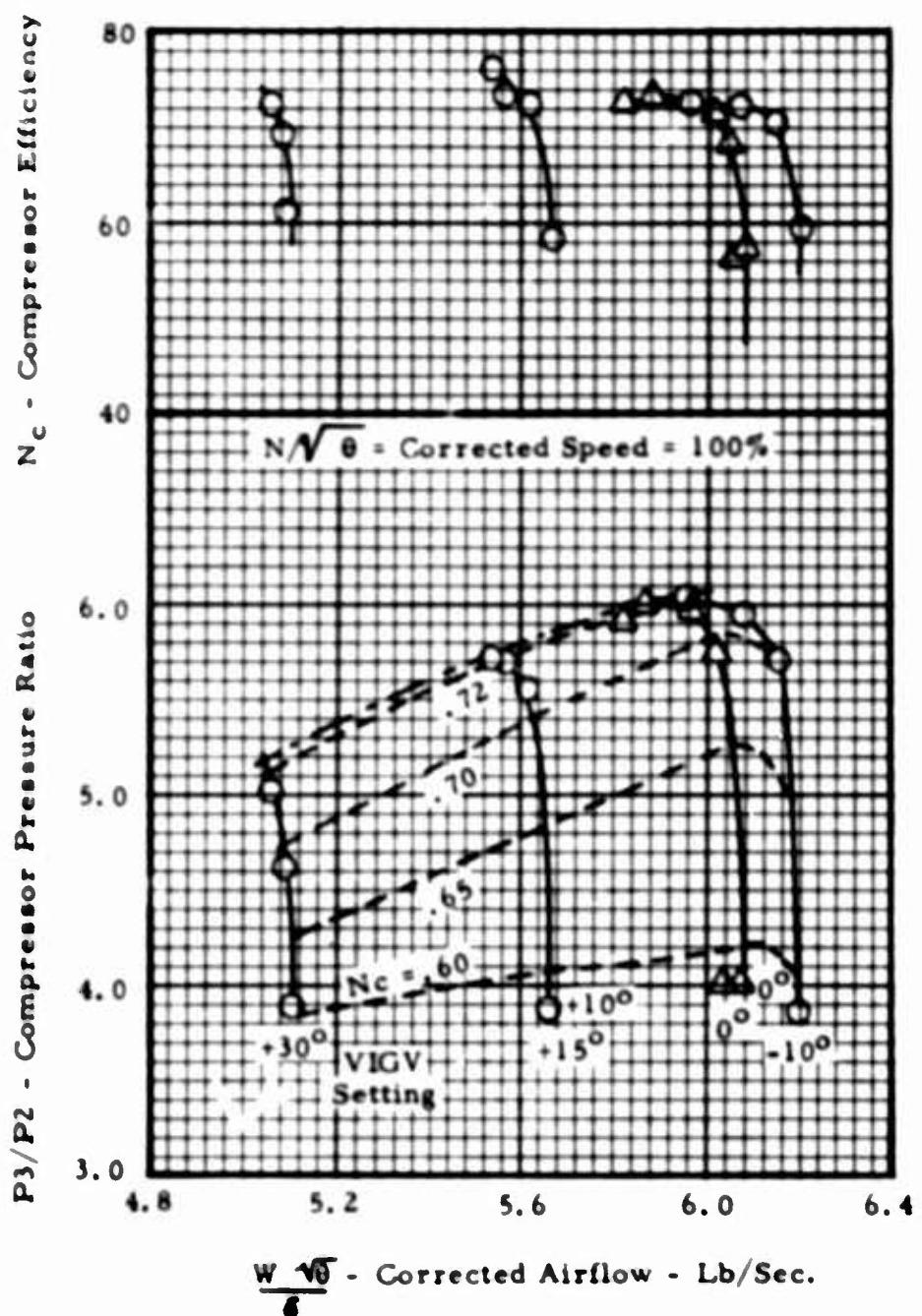
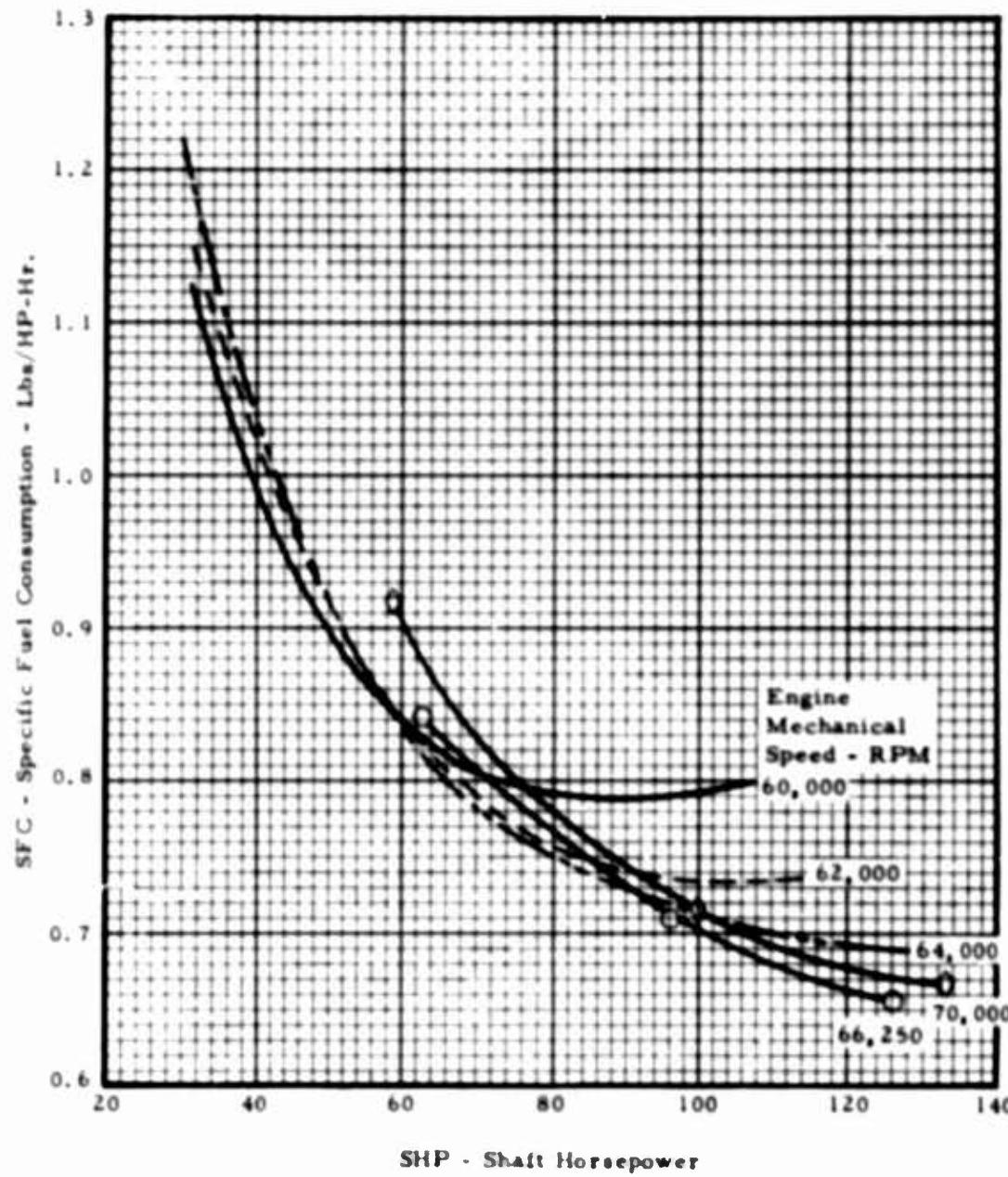


Figure X-36. T72 Axial-Centrifugal With Variable Inlet Guide Vane Engine Test Data.

**Section X**



**Figure X-37. TS90 Simple Cycle Engine, Estimated Performance Characteristics, Sea Level, 60°F Day.**

**Section X**

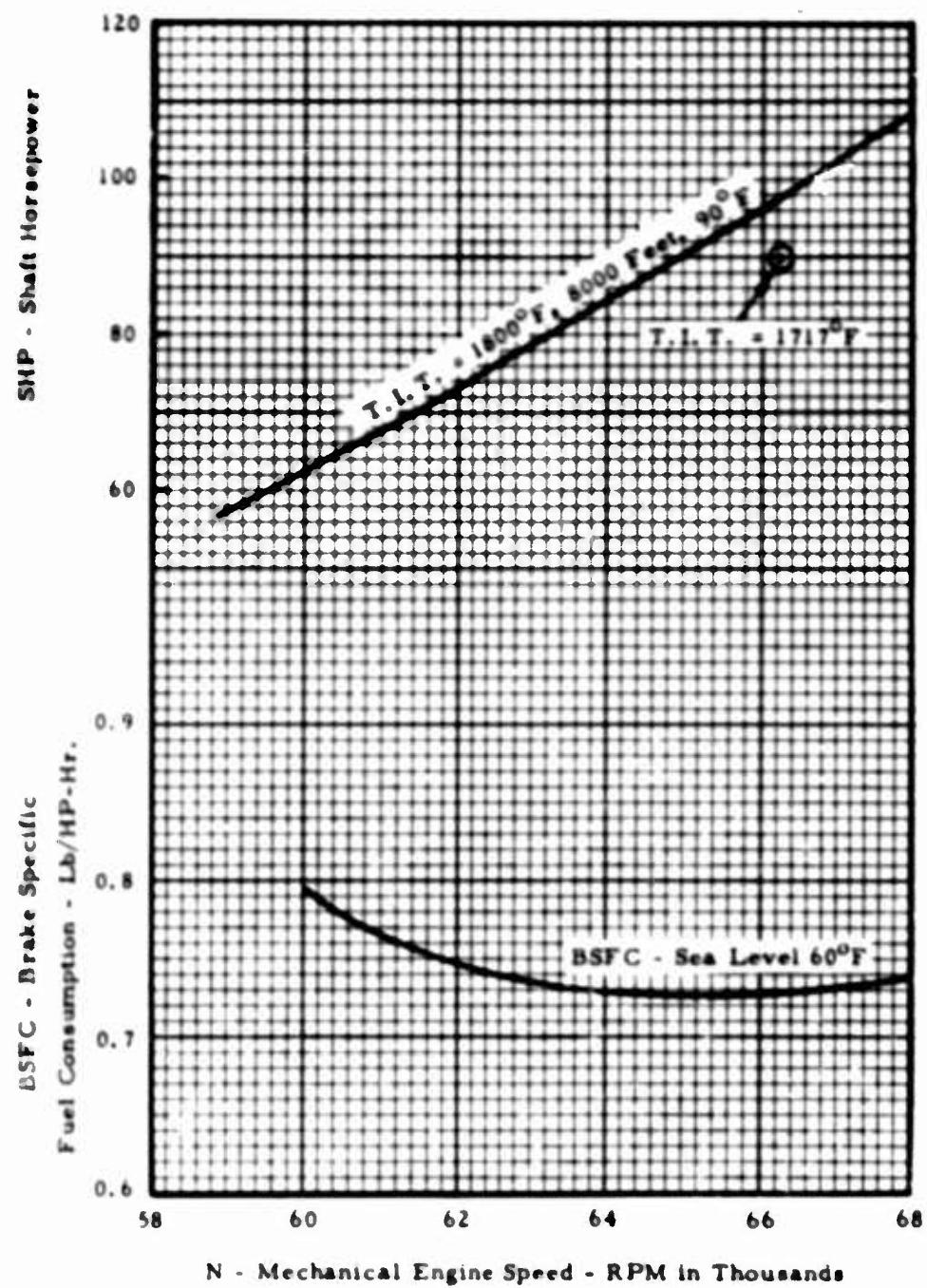


**Figure X-38. TS90 Simple Cycle Engine, Sea Level BSFC and 8000 Feet Horsepower Characteristics.**

## Section X

	Sea Level - 60°F		8000 Ft., 90°F	
	Radial Exhaust	Axial Exhaust	Radial Exhaust	Axial Exhaust
Shaft Output Power	90.0	90.0	90.0	90.0
BSFC - Lb/HP-hr.	0.730	0.723	0.701	0.693
Engine Speed - RPM	66,250	66,250	66,250	66,250
Airflow - Lb/Sec.	1.41	1.41	0.91	0.91
Corrected Airflow - Lb/Sec.	1.43	1.43	1.28	1.28
Comp. Press. Ratio	5.30	5.30	4.97	4.97
Comp. Efficiency - %	81.5	81.5	81.3	81.3
Comp. Discharge Temp. - °F	443.7	443.5	476.5	475.8
Combustor Efficiency - %	0.985	0.985	0.985	0.985
Fuel LHV - Btu/Lb.	18,400	18,400	18,400	18,400
Turb. Inlet Temp. - °F	1313.3	1302.3	1717.5	1697.3
Turb. Exit Temp. - °F	794.9	784.2	1132.4	1112.9
Turb. Efficiency - %	88.4	88.4	87.3	87.4
Inlet Total Press. Loss - %	1.5	1.5	1.5	1.5
Comb. Section Total Press. Loss - %	3.33	3.33	3.06	3.06
Exh. Diff. (Axial) Tot. Press. Loss - %	1.79	1.79	1.72	1.72
Exh. Diff. (Rad.) Tot. Press. Loss - %	1.0		1.0	
Exh. Flange Total Press. Loss - %	1.50	1.50	1.50	1.50

NOTE: All efficiencies are total to total values.

**Figure X-39. Rating Data - TS90 Horsepower Simple Cycle Engine,  
Sea Level, 60°F and 8000 Feet, 90°F, Axial and  
Radial Exhaust.**

**Section X**

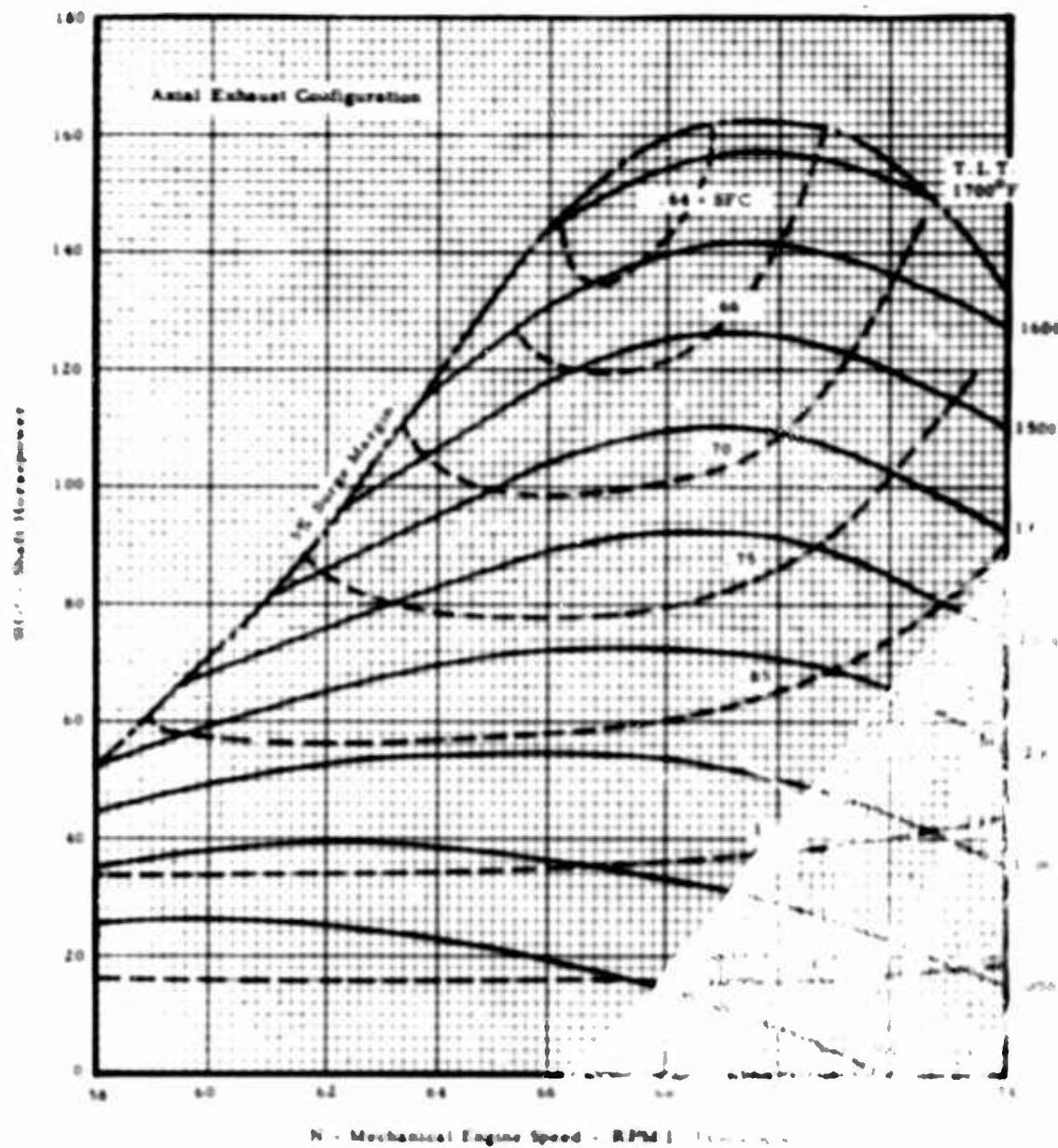


**Figure 40. TS90 and 60 Simple Cycle Engines. Estimated Performance Characteristics Sea Level, 60°F.**

## Section X

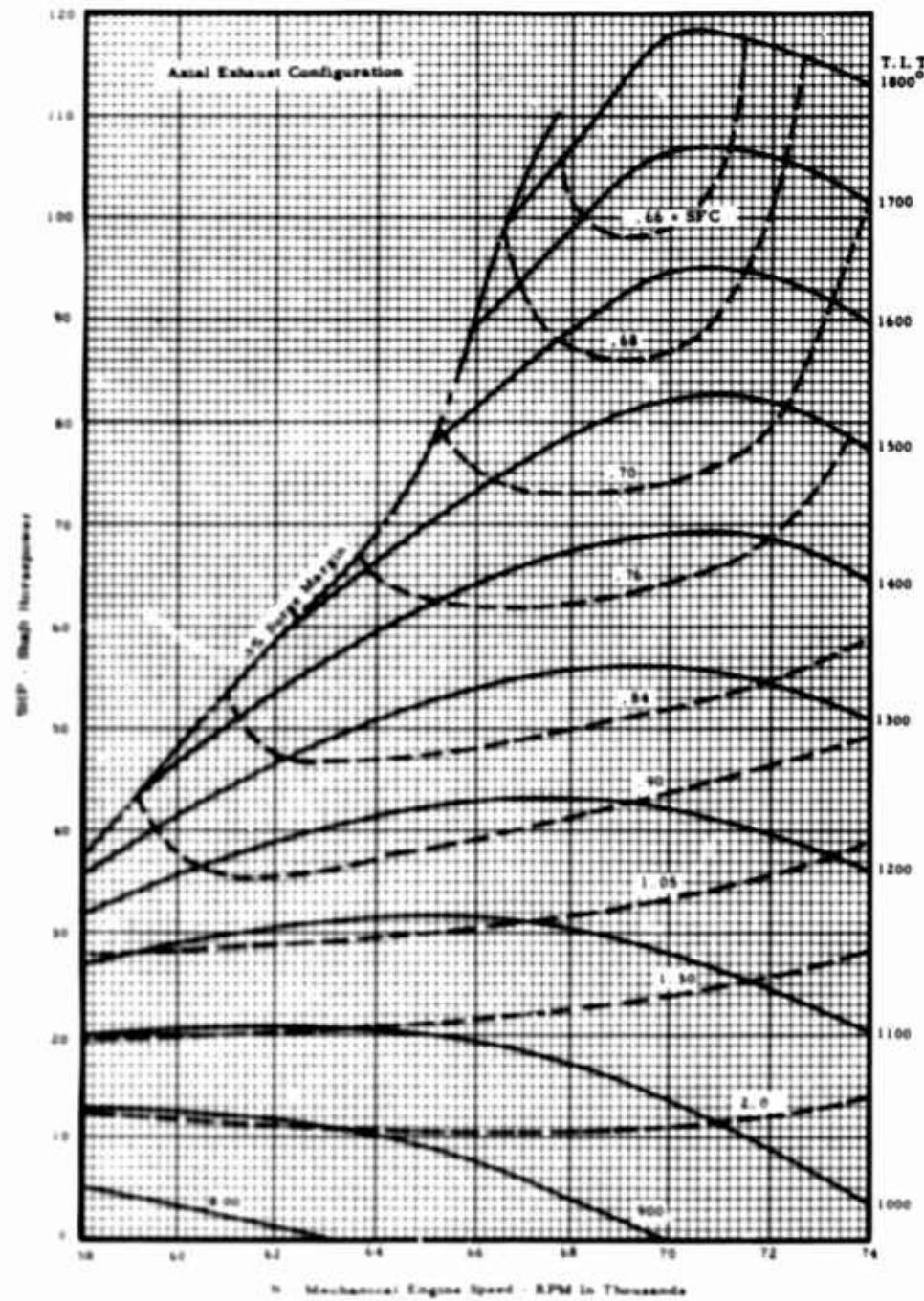
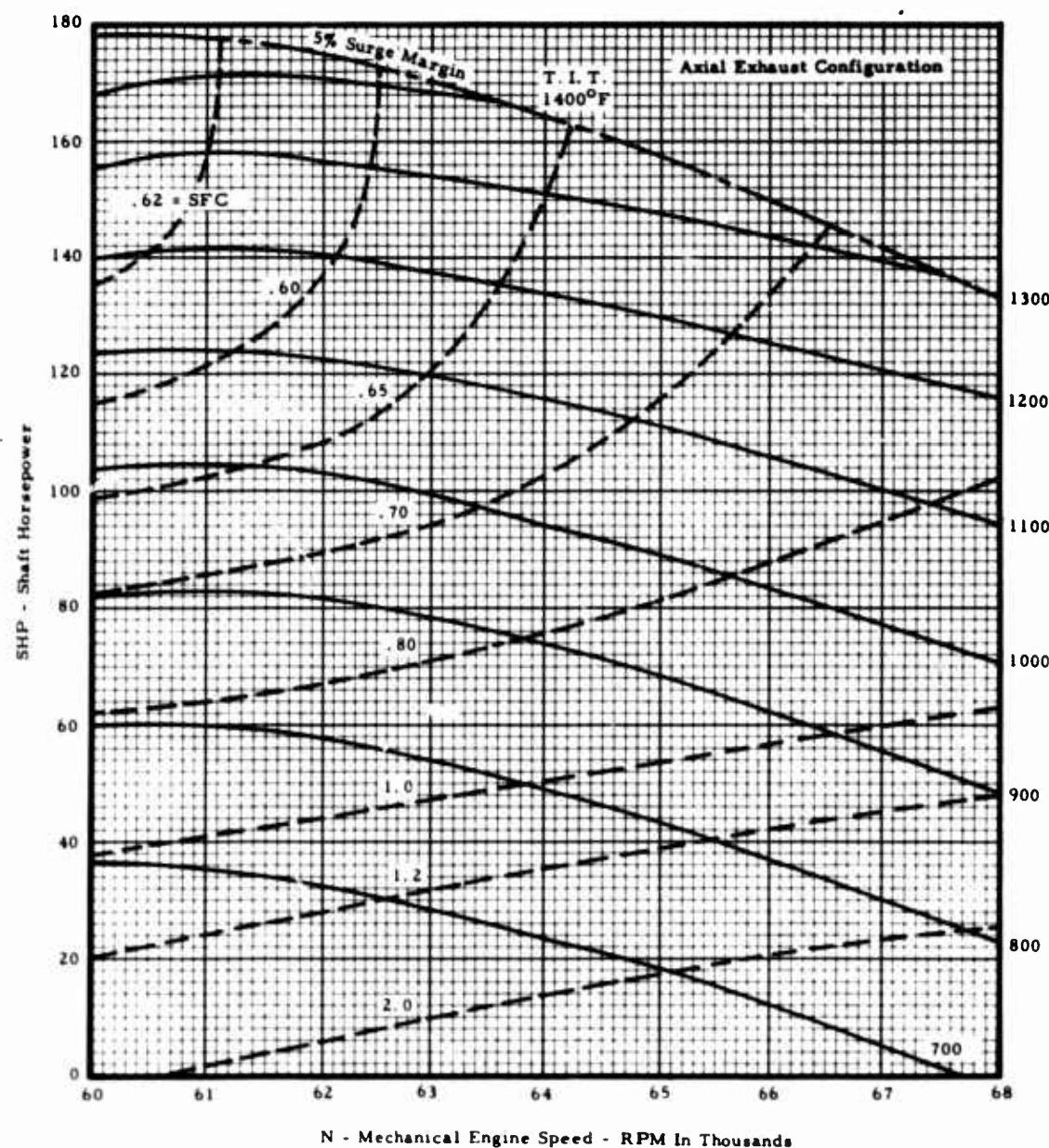


Figure 41. TS90 and 60 Simple Cycle Engines, Estimated Performance Characteristics, 8000 Feet, 90°F.

## Section X



**Figure X-42. TS90 and 60 Simple Cycle Engine, Estimated Performance Characteristics Sea Level, -65°F.**

## Section X

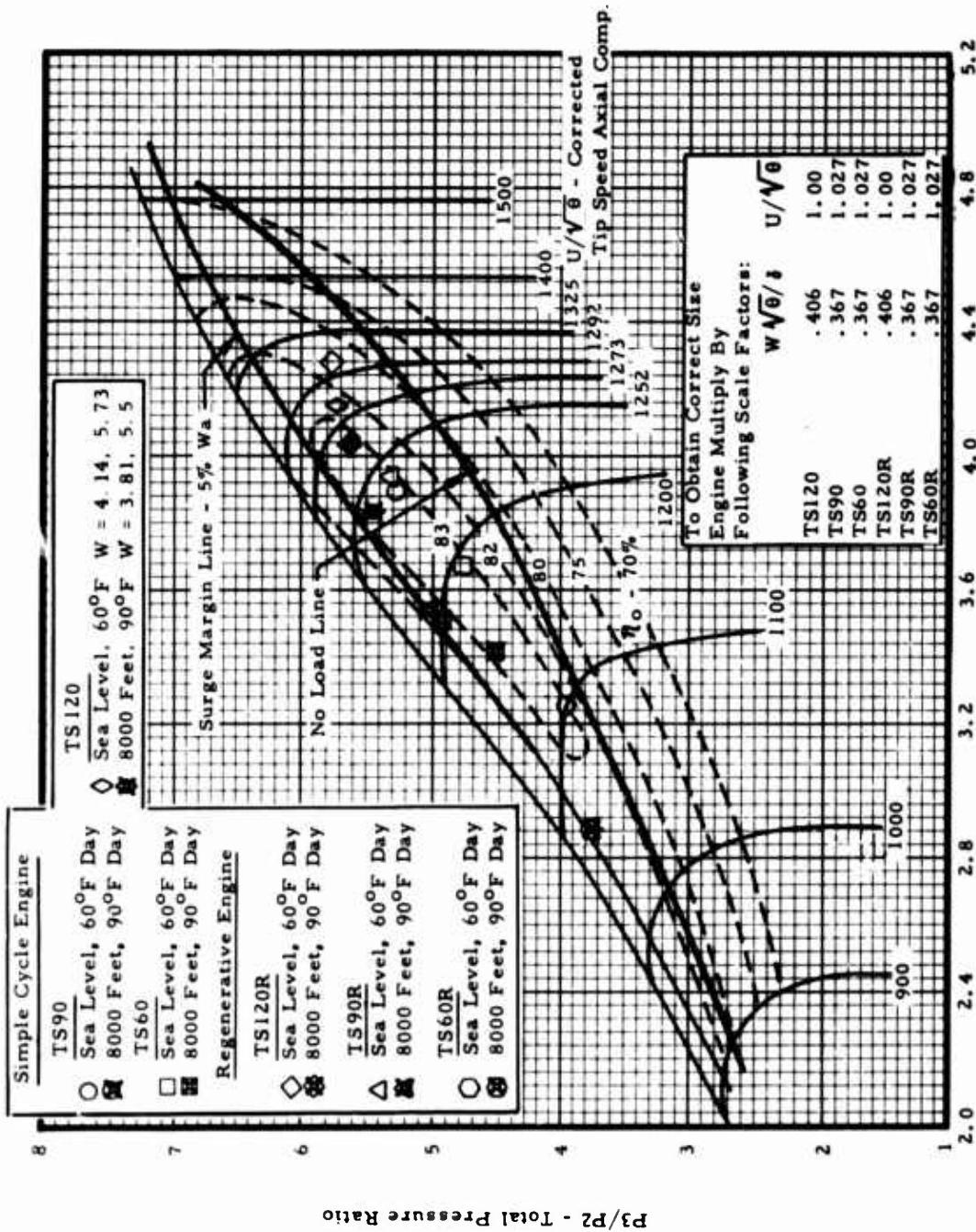
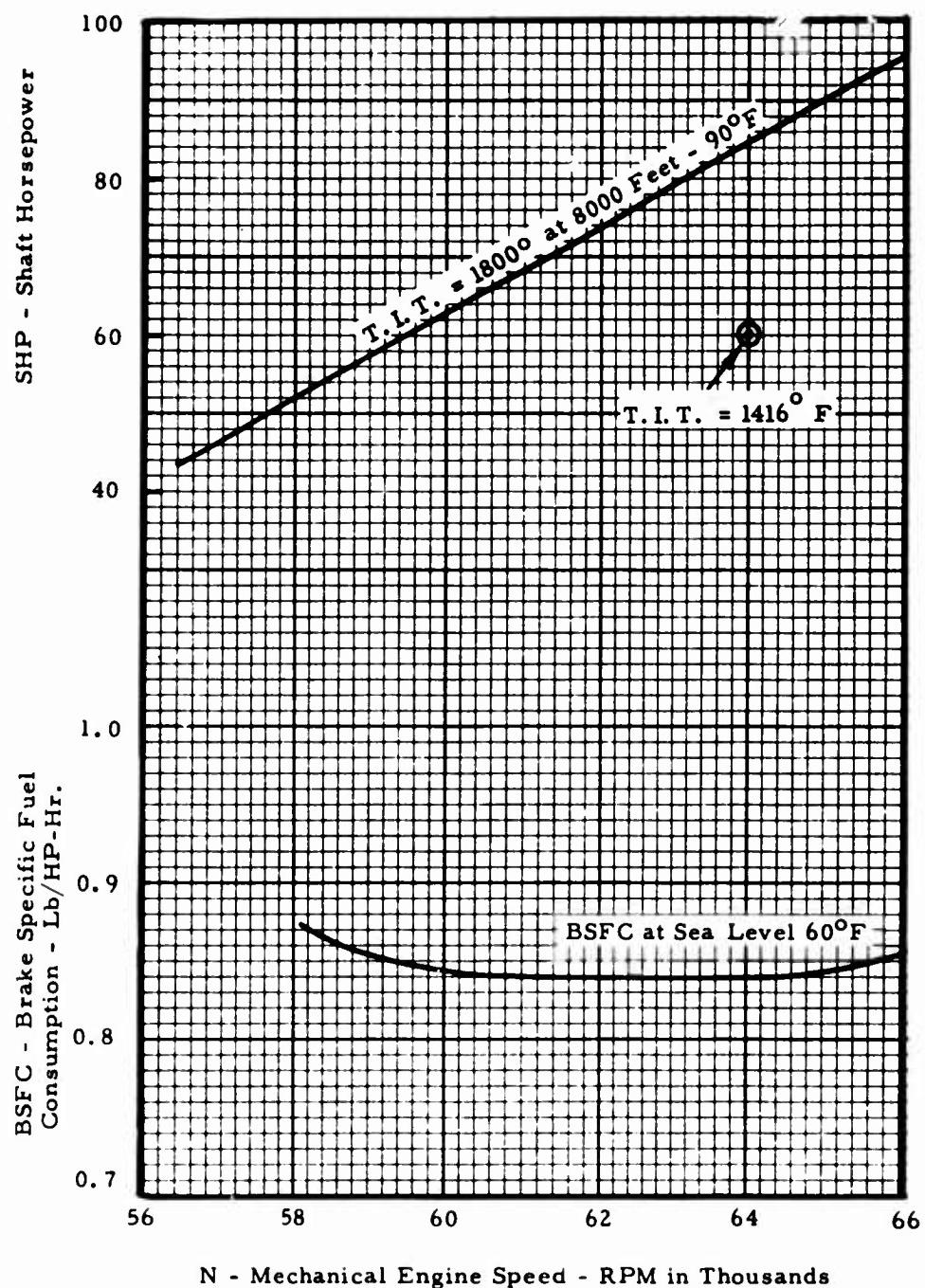


Figure X-43. TS120 Unscaled Compressor Characteristics - Selected Engine Operating Points.

**Section X**



**Figure X-44. TS60 Simple Cycle Engine, Sea Level BSFC and 8000 Feet Maximum Horsepower Characteristics.**

## Section X

	Sea Level - 60° F		8000 Ft., 90° F	
	Radial Exhaust	Axial Exhaust	Radial Exhaust	Axial Exhaust
Shaft Output Power	60.0	60.0	60.0	60.0
BSFC - Lb/HP-Hr.	0.845	0.839	0.780	0.773
Engine Speed - RPM	64,000	64,000	64,000	64,000
Airflow - Lb/Sec.	1.33	1.33	0.89	0.89
Corrected Airflow - Lb/Sec.	1.35	1.35	1.25	1.25
Comp. Press. Ratio	4.80	4.80	4.55	4.55
Comp. Efficiency - %	81.9	81.9	82.2	82.3
Comp. Discharge Temp. - °F	414.4	414.4	446.8	446.6
Combustor Efficiency - %	0.985	0.985	0.985	0.985
Fuel LHV - Btu/Lb.	18,400	18,400	18,400	18,400
Turb. Inlet Temp. - °F	1140.3	1133.3	1416.0	1408.3
Turb. Exit Temp. - °F	688.2	681.1	917.3	909.0
Turb. Efficiency - %	88.5	88.5	88.2	88.2
Inlet Total Press. Loss - %	1.5	1.5	1.5	1.5
Comb. Section Tot. Press. Loss - %	3.45	3.46	3.27	3.28
Exh. Diff. (Axial) Tot. Press. Loss - %	1.44	1.44	1.44	1.44
Exh. Diff. (Radi.) Tot. Press. Loss - %	0.75		0.75	
Exh. Flange Total Press. Loss - %	1.50	1.50	1.50	1.50

NOTE: All efficiencies are total to total values.

Figure X-45. Rating Data - TS60 Simple Cycle Engine, Sea Level, 60° F and 8000 Feet, 90° F Axial and Radial Exhaust.

## Section X

### COMPRESSOR DESIGN

The compressor consists of an axial stage producing a design pressure ratio of 1.598 and a radial stage producing a pressure ratio of 3.582. Two-stage pressure ratio will be 5.72 at an efficiency of 81.6 percent at the inlet of the third radial diffuser blade row. The compressor design point performance is specified in Table X-III.

The compressor flow path is defined in Figure X-46. Streamline location and velocity distributions were computed and used in defining the aerodynamic surfaces for the inlet duct, the transition duct, the radial rotor, and the vaneless diffuser.

### AXIAL COMPRESSOR INLET DUCT

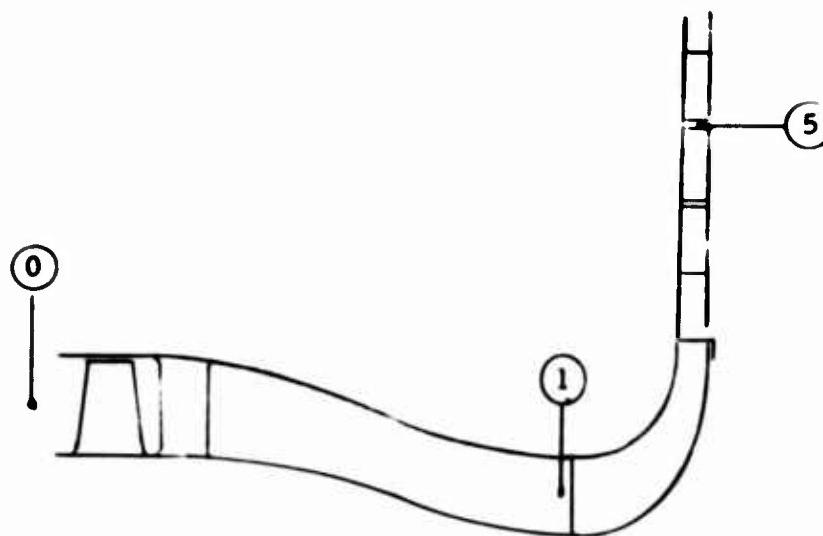
The choice of a passage shape with the purpose of delivering air to the axial compressor inlet was governed by the following criteria:

1.  $\Delta P/T$  not to exceed 0.005.
2. Smooth, steadily accelerating flow, through the passage.
3. Minimum distortion in the radial and circumferential velocity distributions at the axial compressor inlet.

A number of configurations were considered. The two shown in Figure X-46 were chosen for test evaluation. Configuration 2 is one inch shorter, axially, than Configuration 1. The variations in meridional velocity along the hub and shroud contours are presented in Figure X-47. Radial distributions in meridional velocity at the axial rotor leading edge are illustrated in Figure X-48.

Section X

TABLE X-III  
TS120 COMPRESSOR PERFORMANCE



		Sea Level - <u>60°F</u>	8000 Feet - <u>90°F</u>
$P_{05}/P_{00}$		5.72	5.50
$W\sqrt{\theta_0/\delta_0}$	Lb/Sec.	1.68	1.55
$\eta_{5-0}$	%	81.6	82.7
$N/\sqrt{\theta_0}$	RPM	66,733.9	64,885.5
$P_{01}/P_{00}$		1.598	1.646
$\eta_{1-0}$	%	86.47	86.13
$U/\sqrt{\theta_0}$	f. p. s.	1348.0	1323.3
$P_{05}/P_{01}$		3.582	3.336
$W\sqrt{\theta_1/\delta_1}$	Lb/Sec.	1.140	1.0242
$\eta_{5-1}$		83.0	84.1
$U/\sqrt{\theta_1}$	f. p. s.	1364.9	1320.4

## Section X

### AXIAL STAGE

The axial stage chosen for the TS120 engine is a scaled version of one presently running at Continental. The measured performance of this stage is shown in Figure X-49, where it may be seen that the machine has broad operating range and good efficiency. The match point, which is the basis for scaling the stage, is indicated on Figure X-49, showing the required equivalent tip speed as 1348 feet per second. With the corrected rotational speed fixed at 66,734, the required tip radius is 2.315 inches. This results in a scale factor of 0.648, which was applied to the shroud and blade dimensions. In order to satisfy the engine flow requirement, it was necessary to remove five percent of the blade span at the hub. The resulting flow path is shown in Figure X-46.

### INTERSTAGE TRANSITION DUCT

In selecting the transition duct hub and shroud contours, attention was directed toward minimizing the peaks and dips in the meridional velocity distributions, Figure X-50.

The final duct flow path (Figure X-46) incorporates an eight-degree ramp at the inducer hub inlet. A comparison of the boundary layer growth along a duct with a purely axial inlet, and one with a ramp inlet, showed that the use of a ramp improved the structure of the boundary layer on both walls, see Figure X-51. It also helps to improve rotor performance.

The high radial gradient in the meridional velocity at the inducer inlet is primarily the result of the restricted axial space provided for the transition duct and of the consequent tight radii of curvature.

## Section X

### RADIAL COMPRESSOR ROTOR

The impeller rotor design features are tabulated below. Locations of the stations in the radial compressor stage are defined in Figure X-46. The inlet and exit velocity triangles are defined in Figure X-52.

$P_{02}/P_{01}$	- 3.980
$\eta_{2-1}$	- 0.913
$P_{05}/P_{01}$	- 3.582
$\eta_{5-1}$	- 0.830
$M_{IT}$	- 0.893
$W_{IT}/W_2$	- 1.70
$P_{01}$	- 14.7 psia
$T_{01}$	- 519°R
$W \sqrt{\theta_1} / \delta_1$	- 1.140 lb/sec.
$\mu$	- 0.896
$U_2 / \sqrt{\theta_1}$	- 1364.9 f.p.s.
$D_2$	- 5.056 In.

A parametric study of the inducer tip flow properties, as a function of the inducer geometry, is presented in Figures X-52 and X-54. Shaft critical speed requirements fixed the inlet hub diameter at 1.60 inches. The resulting tip diameter, selected from the curves of Figure X-53, is 3.20 inches.

## Section X

The number of impeller vanes was fixed at 19. Splitter vanes were considered and were rejected on the strength of the following information:

1. Analytical estimates of rotor efficiency variation with impeller blade number, shown in Figure X-55, indicate little improvement in rotor efficiency as the blade number is increased beyond 20. Furthermore, existing Continental test data proves that as blade number is increased, higher blade wake mixing losses in the radial diffuser result in a lower stage efficiency.
2. Continental test data also show a large decrease in rotor flow range attributed to the use of splitters. Examination of a typical impeller loading diagram will show that this is due to an uneven flow entering adjacent passages, with the passage bounded by the pressure surface of the full blades receiving less flow than its two neighbors. The reduction in flow range would thus be caused by the premature breakdown of the flow in each of these alternate rotor passages.
3. A review of the literature showed that several analytical and experimental parametric studies agreed that the optimum blade number was in the range of 16 to 20.

The impeller slip factor was determined by Stanitz' relation which has shown good agreement with experiment:

$$\begin{aligned}\sigma &= 1 - 0.63 \frac{\pi}{Z} \\ &= 0.896\end{aligned}$$

In addition, the radius ( $R_X$ ), at which the blades cease to perfectly guide the flow is given by Stanitz as:

## Section X

$$\log_e R_X/R_2 = - \frac{2.23}{\pi} \left( \frac{2\pi}{z} \right)$$

$$R_X/R_2 = 0.791$$

The impeller flow path, Figures X-46 and X-56 was chosen after analyzing several meridional shapes combined with a large number of inducer blade angle variations. All rotor elements are radial.

The inviscid blade loading diagram is presented in Figure X-57. Hub and shroud contours and blade shapes were chosen so as to avoid flow separation. Use of a slight ramp at the rotor inlet permits rapid closing of the hub area without recourse to high gradients in meridional velocity. As a result, the deceleration in the hub relative velocity is gradual and separation is avoided.

The variation in static pressure along the hub and shroud surfaces is presented in Figure X-58.

An analysis of the boundary layer development along the blade pressure surface is given in Figure X-59. The initial shape factor at the blade leading edge is 1.0. Employing as a criterion,  $H_{separation} = 1.8$ , the estimated locus of separation points is illustrated in Figure X-56.

An estimate of the effect of clearance on rotor performance is presented in Figure X-60. Design static clearance in the present instance is 0.004 at the inducer tip and 0.008 at the impeller front face.

### RADIAL VANELESS SPACE

Close attention has been given to the design of the vaneless space because of its influence on both the rotor and on the vaned diffuser.

## Section X

1. Too high a rate of deceleration in the radial velocity component can result in a separation in the radial component of the boundary layer in the vaneless space with a consequent feedback of flow into the rotor causing premature surge. This has been avoided by choosing a constant area variation which has proven successful in previous applications at Continental.
2. The conditions in the vaneless space determine the location of the first vaned diffuser for optimum pressure recovery. The flow properties are determined from experimental variations in friction factor, Figure X-61, and tangential velocity, Figures X-62 and X-63, both obtained from Continental test results.

The friction factor is found from the measured drop in total pressure and includes effects of blade wake mixing losses:

$$f = \frac{g h R T_s}{V^3} \frac{1}{P_T} \frac{d P_T}{d R}$$

where  $h$  is the passage width.

The effects of frictional losses and of blade wake mixing losses on tangential velocity are illustrated in Figures X-62 and X-63. Tangential velocity variation in the present case was determined by the relation

$$V_0 = \frac{1}{(R/R_2)^{1.24}} \mu U_2$$

The resulting variation in flow properties in the vaneless space are defined in Figure X-64.

## Section X

### VANED DIFFUSER ROWS

A study of various diffuser configurations indicated that efficient diffusion of the high dynamic head would require three blade rows in order to keep the blade loading within limits established by Continental experience.

In locating the position of the first diffuser row it is necessary to determine the sum of vaneless space losses and first vane row losses as a function of radial position. Thus in Figure X-65 the location of the first row leading edge resulting in maximum pressure recovery was found to be  $1.25 R_2$ .

Figure X-66 and Table X-IV define the flow properties for all three blade rows. As a blade loading criterion, use was made of the conventional diffusion factor:

$$D = 1 - V_{\text{Exit}}/V_{\text{In}} + \Delta V_\theta/2\sigma V_{\text{In}}$$

It was found advantageous to leave some whirl in the flow at the third row exit. In this case  $20^\circ$  of whirl remains. One important advantage is a substantial reduction in blade loading with only a slight increase in leaving the dynamic head. The residue whirl will also benefit the performance of the vaneless diffuser and aid in moving the flow through the plenum and into the combustor.

A sketch of the diffuser is present in Figure X-67. One important feature of the design is the use of 26 vanes in all three rows. The vanes are so located that the operation of the second vane row is augmented by the flow from the first. The operation of the third row is in turn aided by the flow from the second.

Section X

TABLE X-IV  
TS120 RADIAL DIFFUSER - FINAL DESIGN

	<u>Rotor Exit</u>	<u>Row 1 Inlet</u>	<u>Row 2 Inlet</u>	<u>Row 3 Inlet</u>	<u>Row 3' Exit</u>
Station	2	3	4	5	6
$R/R_2$	1.00	1.25	1.44	1.77	2.08
R In.	2.528	3.160	3.64	4.475	5.258
M	1.0896	0.8074	0.510	0.318	0.216
$V_e$ f. p. s.	560.4	478.5	420	333	282.9
$\alpha$ Deg.	24.52	27.15	37.63	49.37	70.37
$\eta$	0.913	0.8617	0.8372	0.830	0.8271
Pressure Ratio	3.98	3.730	3.615	3.582	3.568
$\Delta P_t/P_t$ In.		0.03095	0.0091	0.00391	
Loss Coeff. $\zeta$		0.1042	0.05967	0.050	
Diffusion Factor D		0.509	0.543	0.583	
Chord - Inch		0.743	1.072	0.875	
Blade Number		26	26	26	
Solidity $\sigma$		0.905	1.092	0.745	

VANELESS DIFFUSER

In order to stay within the high performance requirements for the compressor stage, it is necessary to employ a vaneless diffuser to efficiently reduce the dynamic head ( $q/P_T = 0.032$ ) leaving the vaned diffuser.

## Section X

The diffuser also serves to turn the flow to the axial direction, (Figure X-46). The optimum expansion angle is found from a study of diffuser losses combined with dump losses assuming complete loss of the exit dynamic head. The results, for a three-inch diffuser, are illustrated in Figure X-68, and indicate an optimum equivalent cone angle of 15°. The diffuser configuration, (Figure X-46) incorporates a conical area variation between inlet and exit.

Total losses in transferring the flow from the compressor to the combustor are summarized below:

	$\Delta P_T/P_T$
Third Vane Row	0.00391
Vaneless Diffuser	0.00501
Rapid Expansion Loss	0.01031
Total	0.01923

As a result the flow delivered to the combustor will be at a pressure ratio of  $3.513 \times 1.598 = 5.614$ .

**Section X**

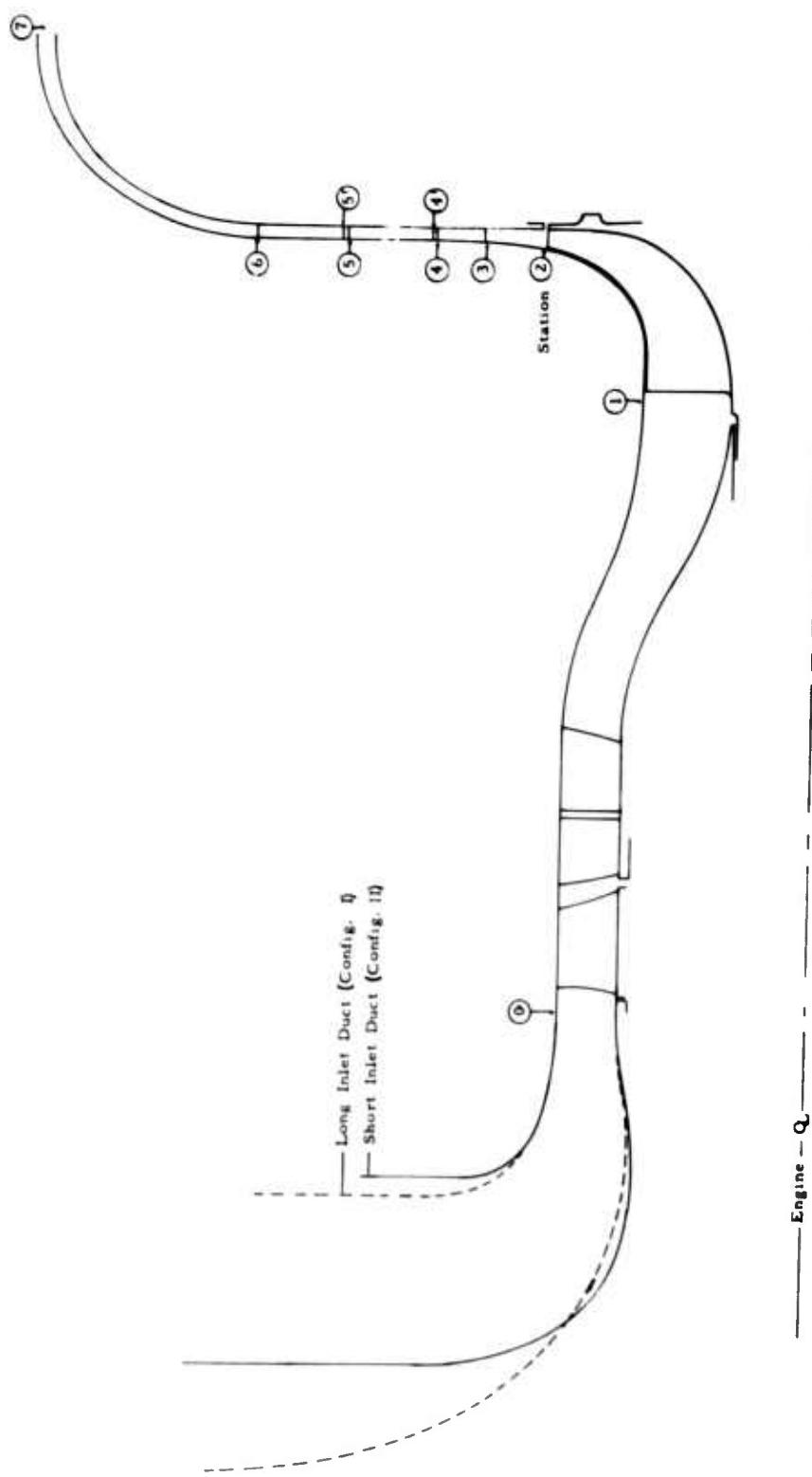


**Figure X-46.** TSI20 Two-Stage Compressor Flow Path.

**Section X**

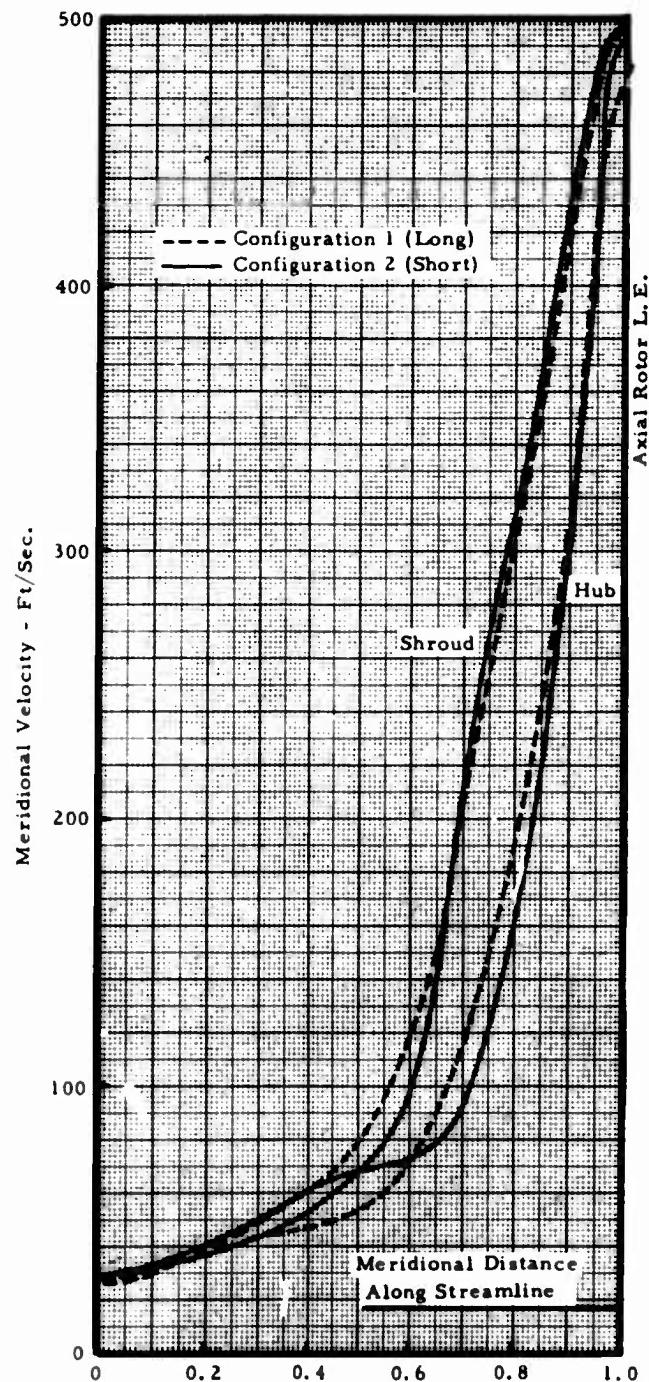


**Figure X-47. TS120 Inlet Duct Meridional Velocities.**

## Section X

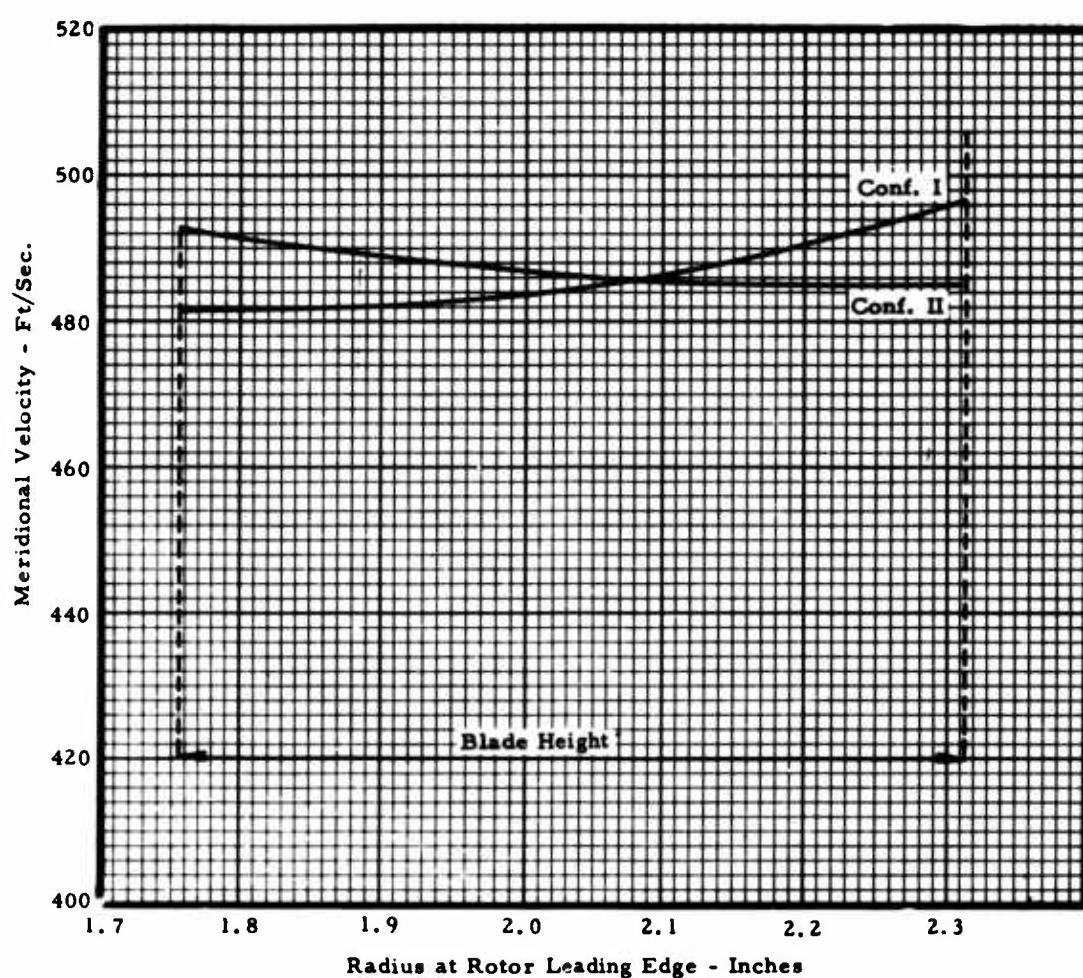


Figure X-48. TS120 Inlet Duct Meridional Velocities Along Rotor Blade Leading Edge.

**Section X**

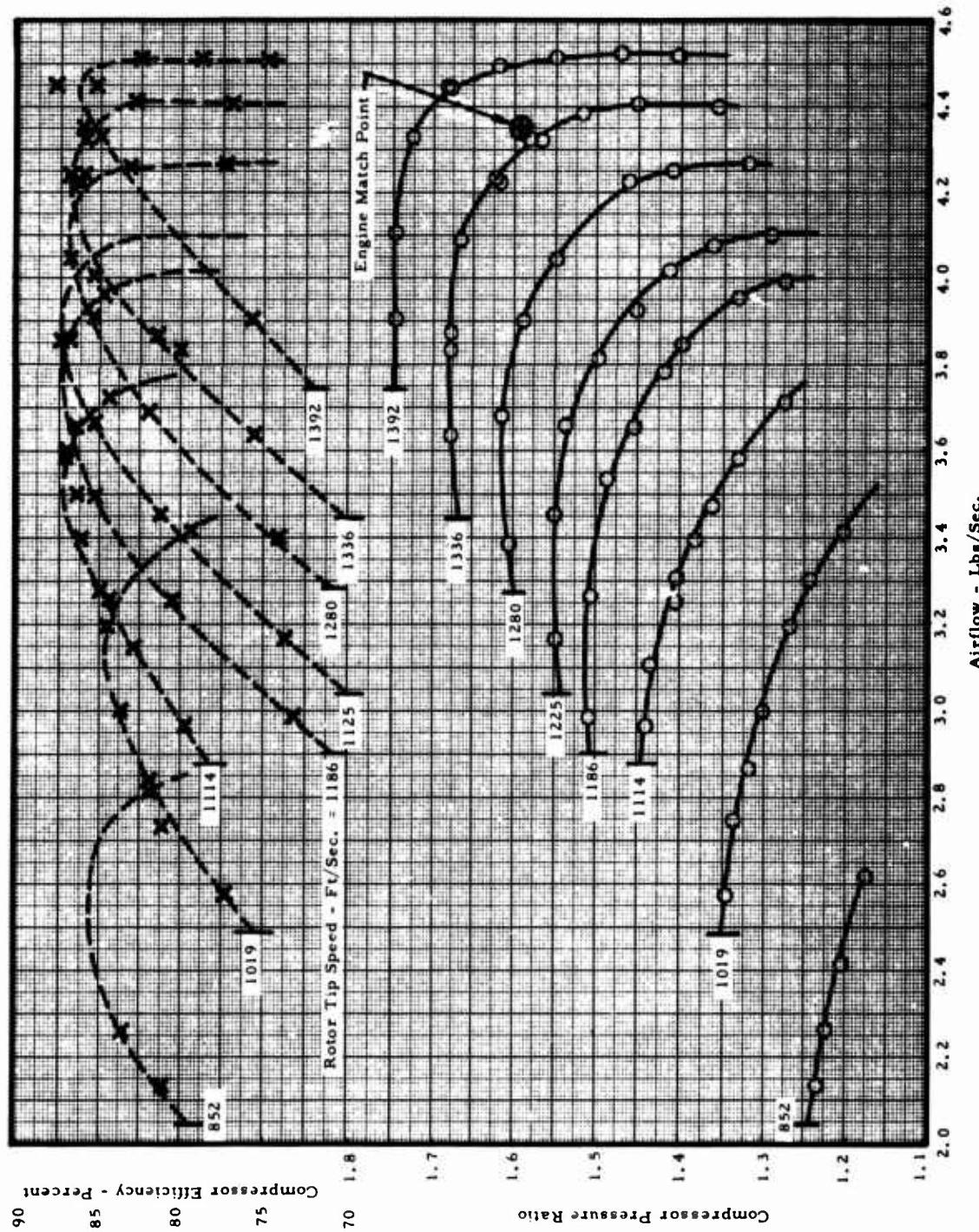


Figure X-49. TS120 Axial Compressor Stage Performance.

Section X

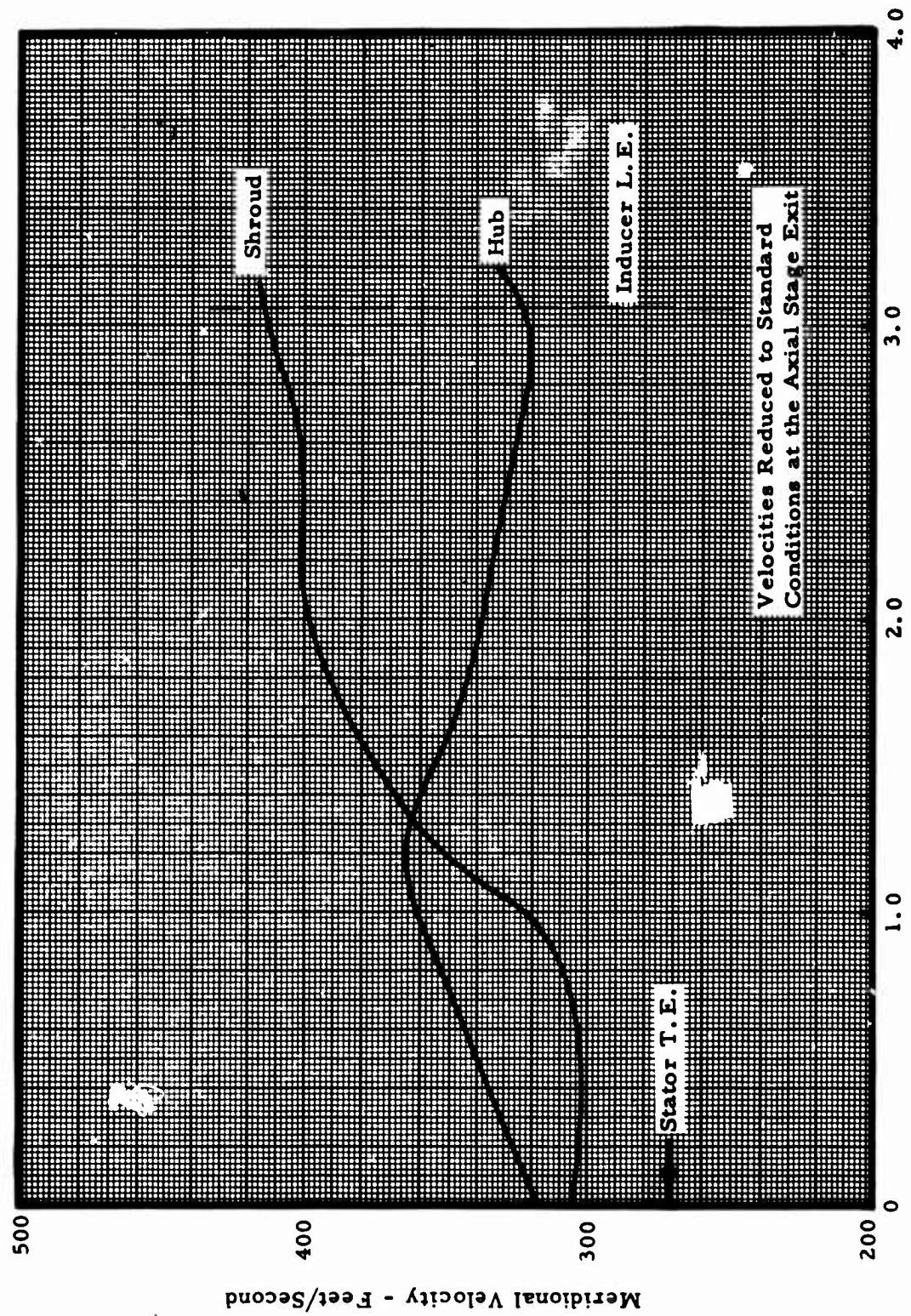
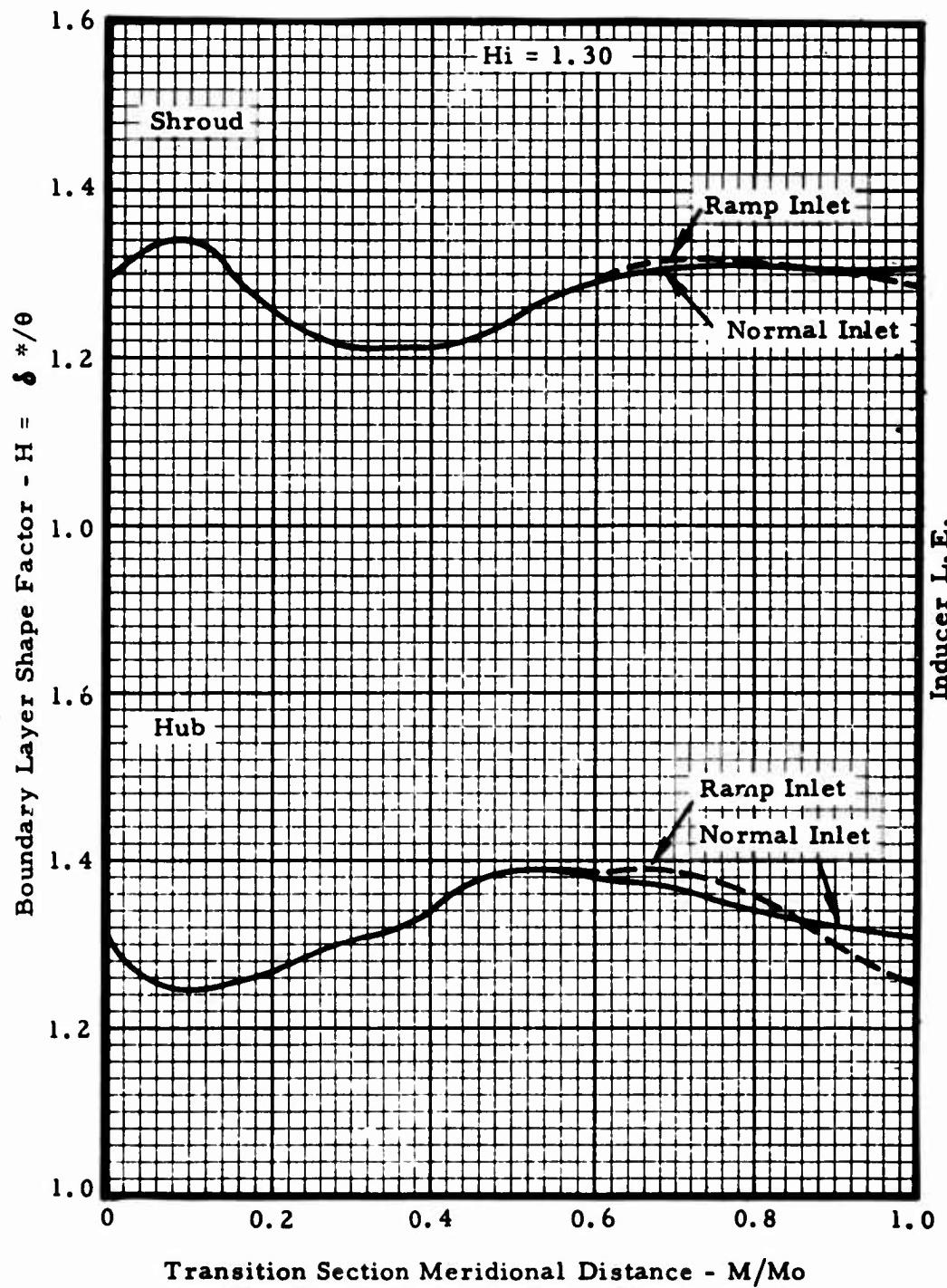


Figure X-50. TSJ20 Transition Section Velocities Ramp Compressor Inlet.

**Section X**



**Figure X-51. TS120 Transition Section Shape Factor Variation.**

**Section X**

**Velocities Reduced to Standard  
Conditions at Inducer Inlet**

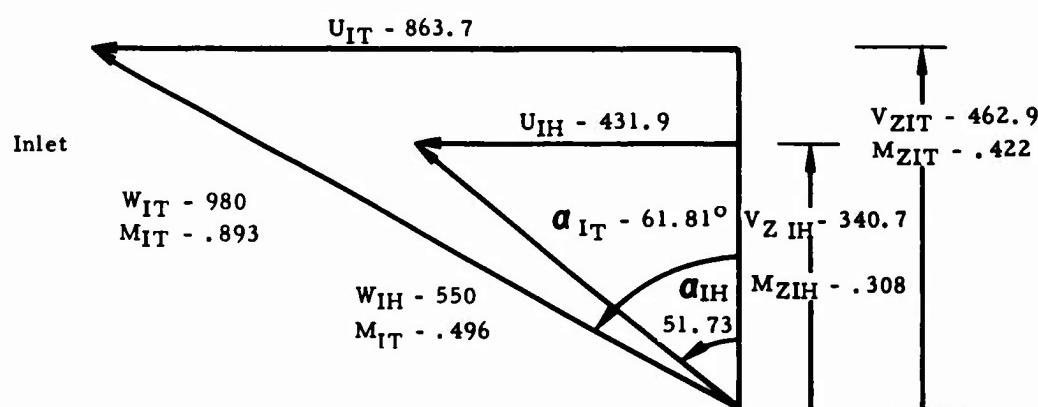
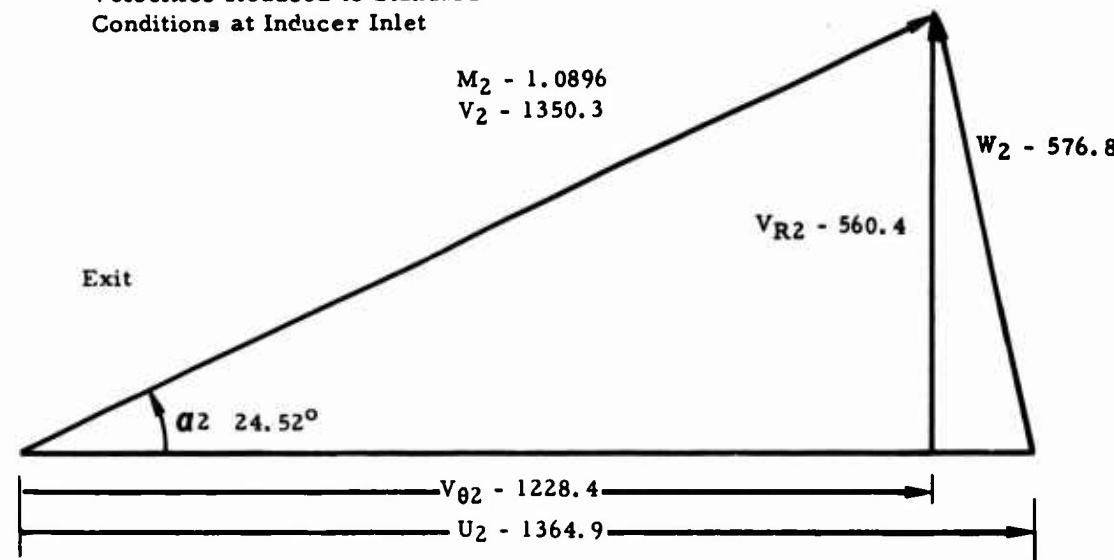


**Figure X-52.** TS120 Radial Compressor Rotor Inlet and Exit Velocity Triangles.

**Section X**

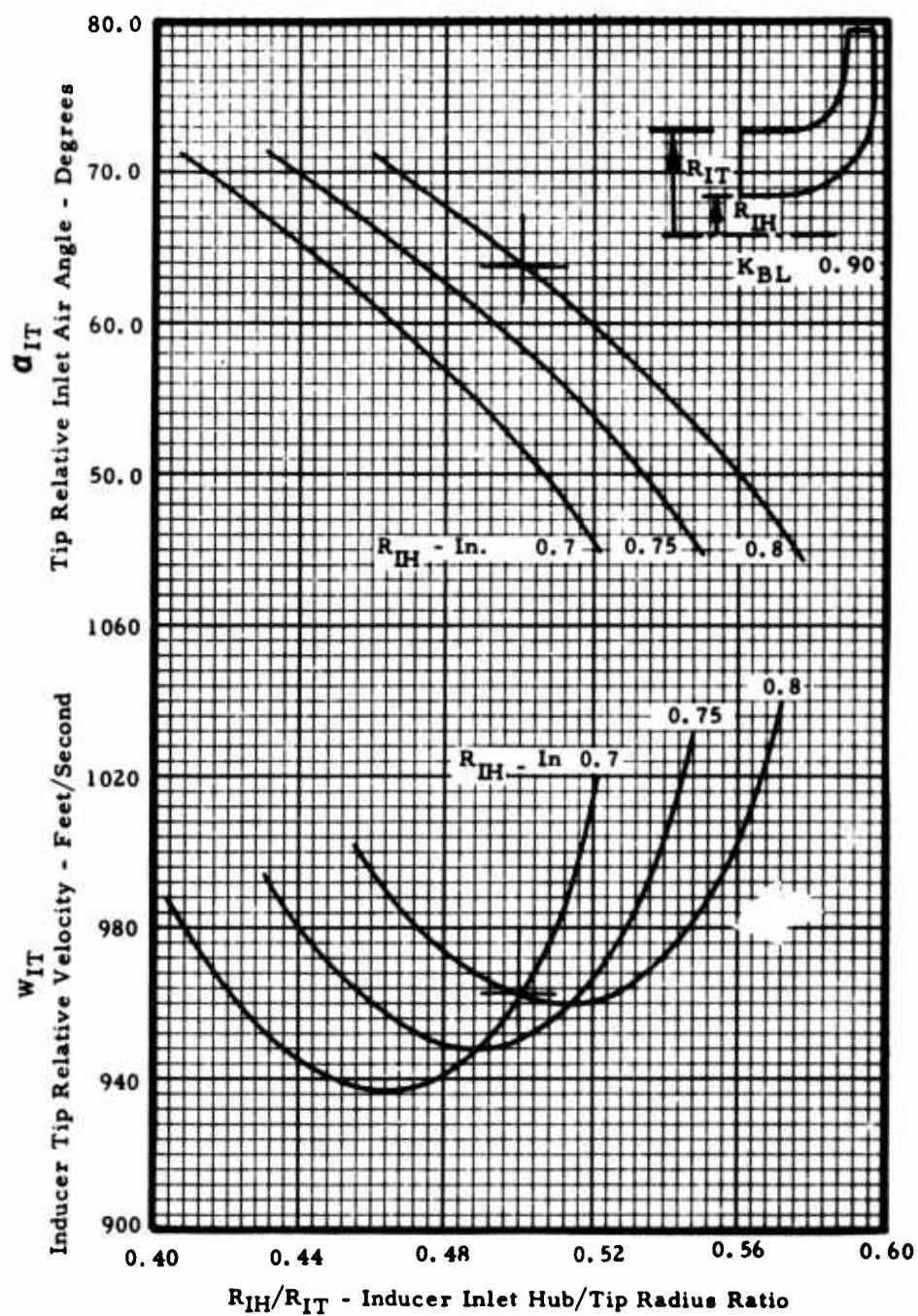


**Figure X-53. Variation of Inducer Inlet Flow Properties With Inducer Inlet Geometry Preliminary.**

Section X

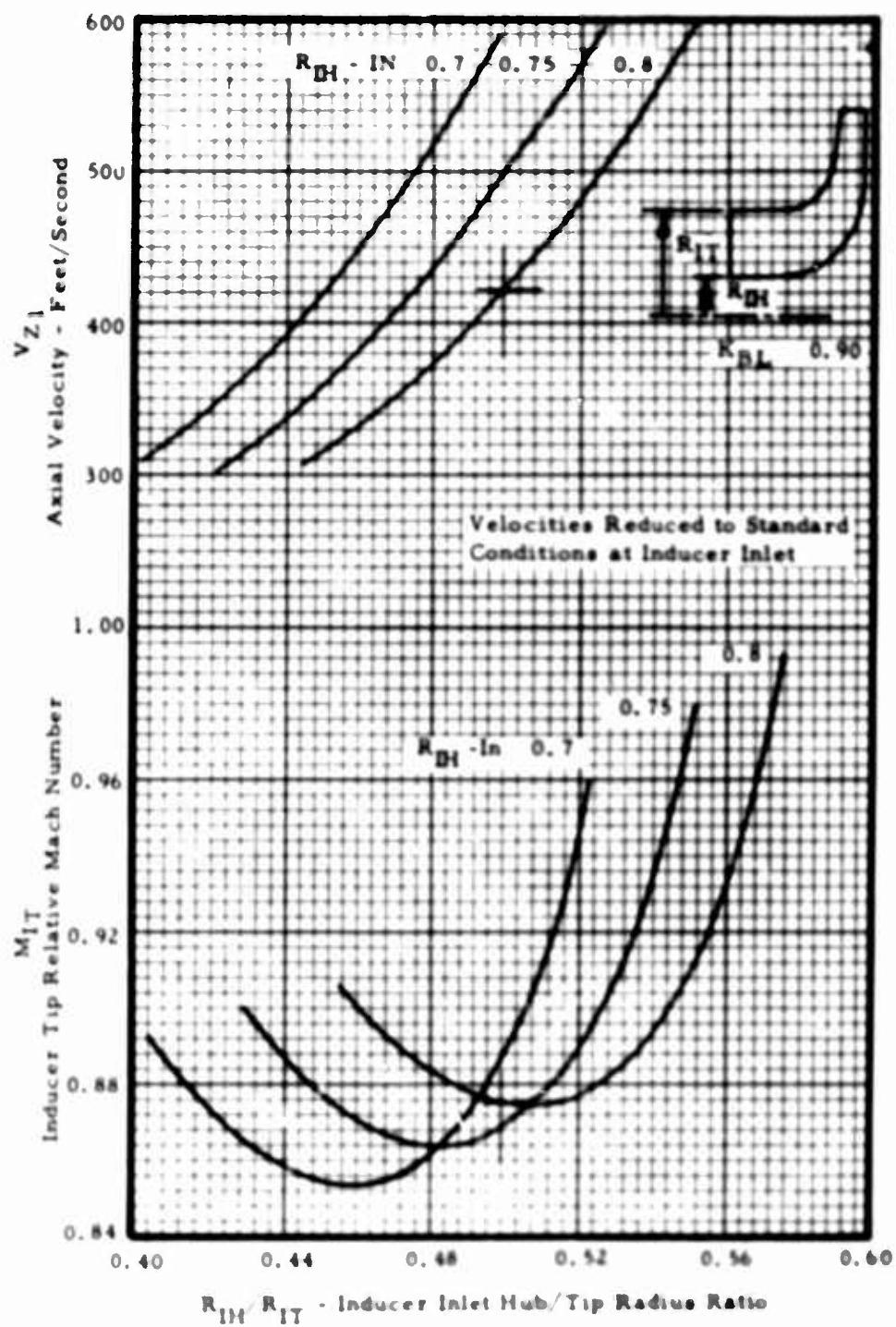


Figure X-54. Variation of Inducer Tip Flow Properties With Inducer Inlet Geometry Preliminary.

Section X

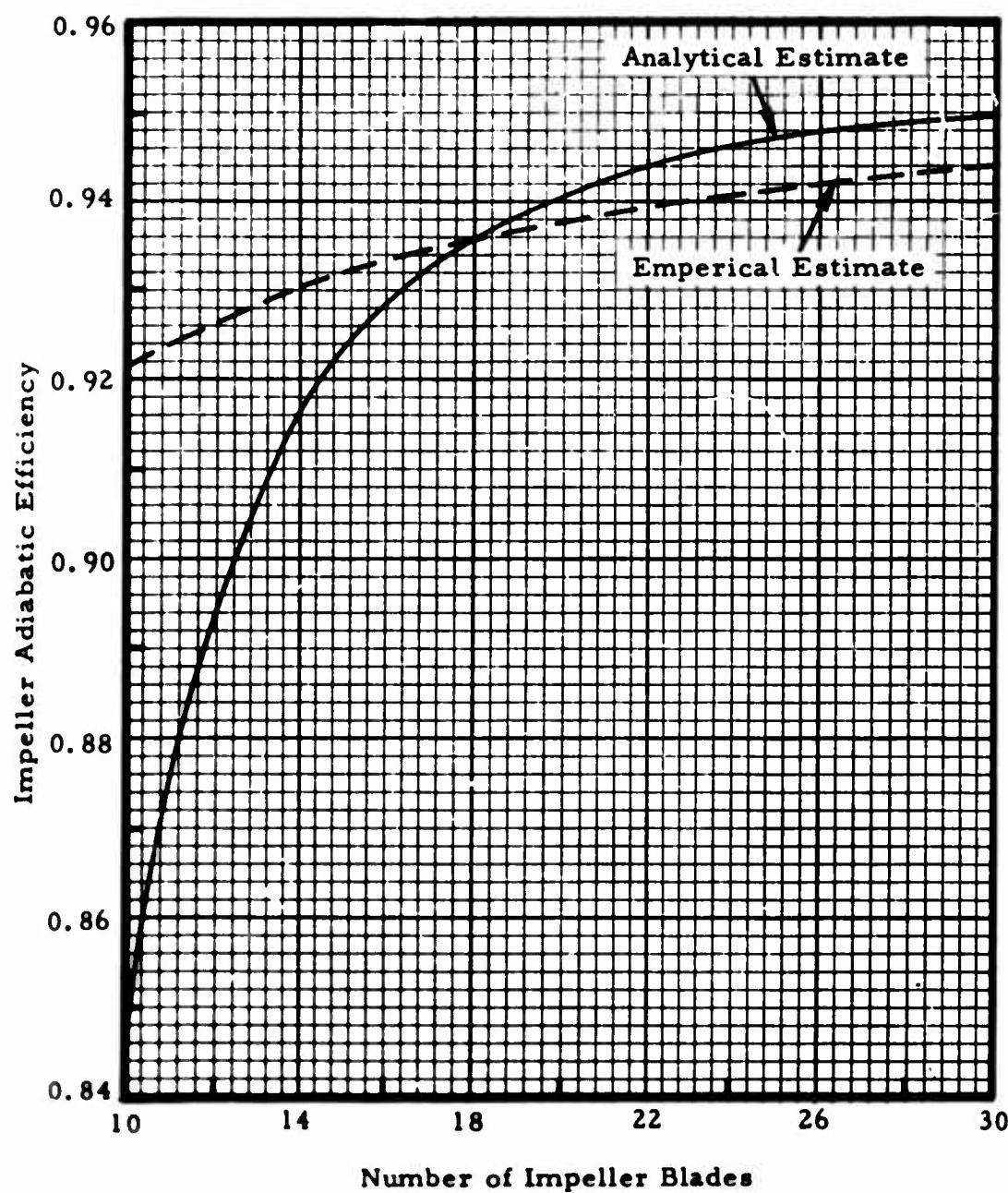


Figure X-55. TS120 Radial Impeller Losses.

## Section X

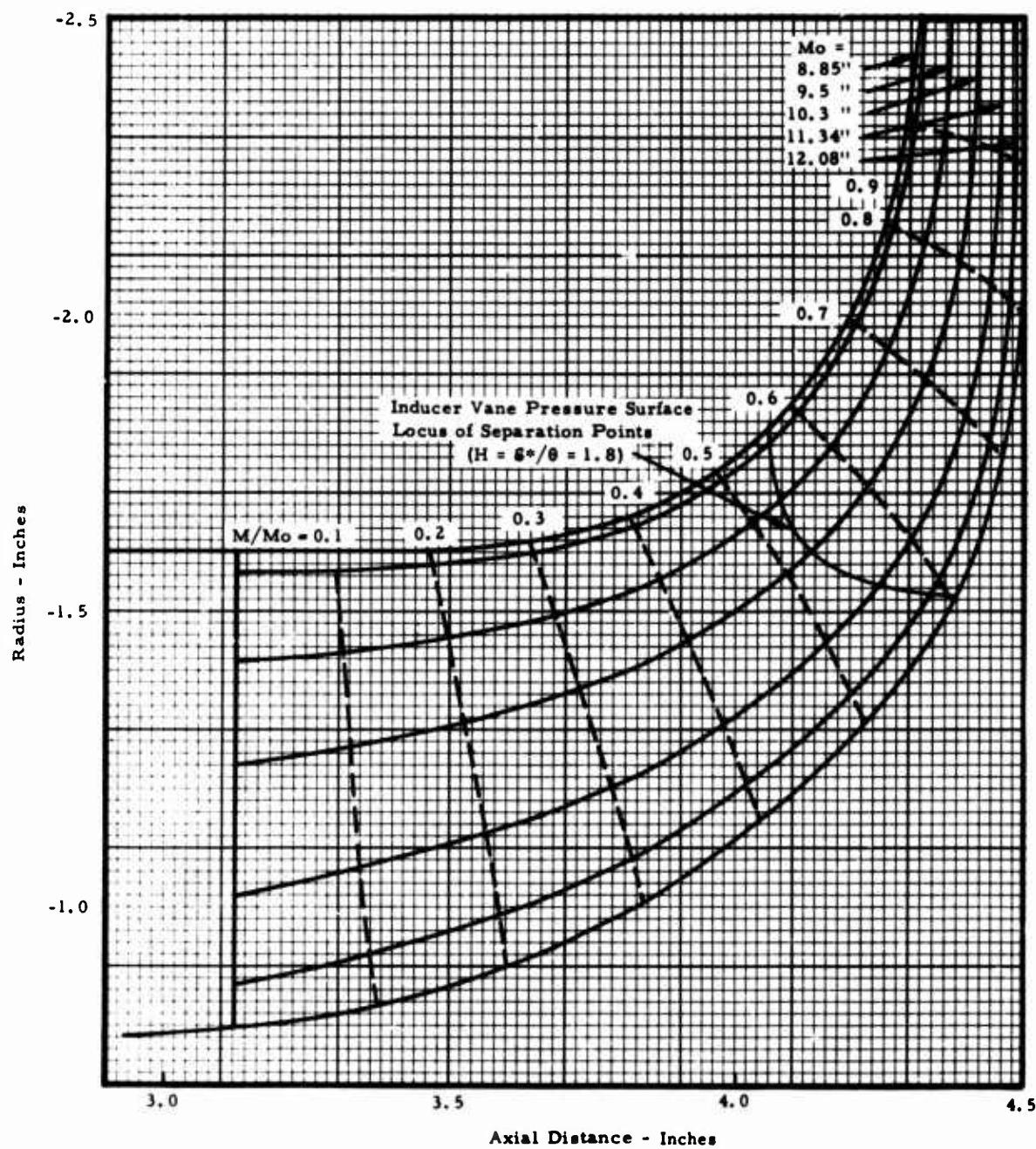
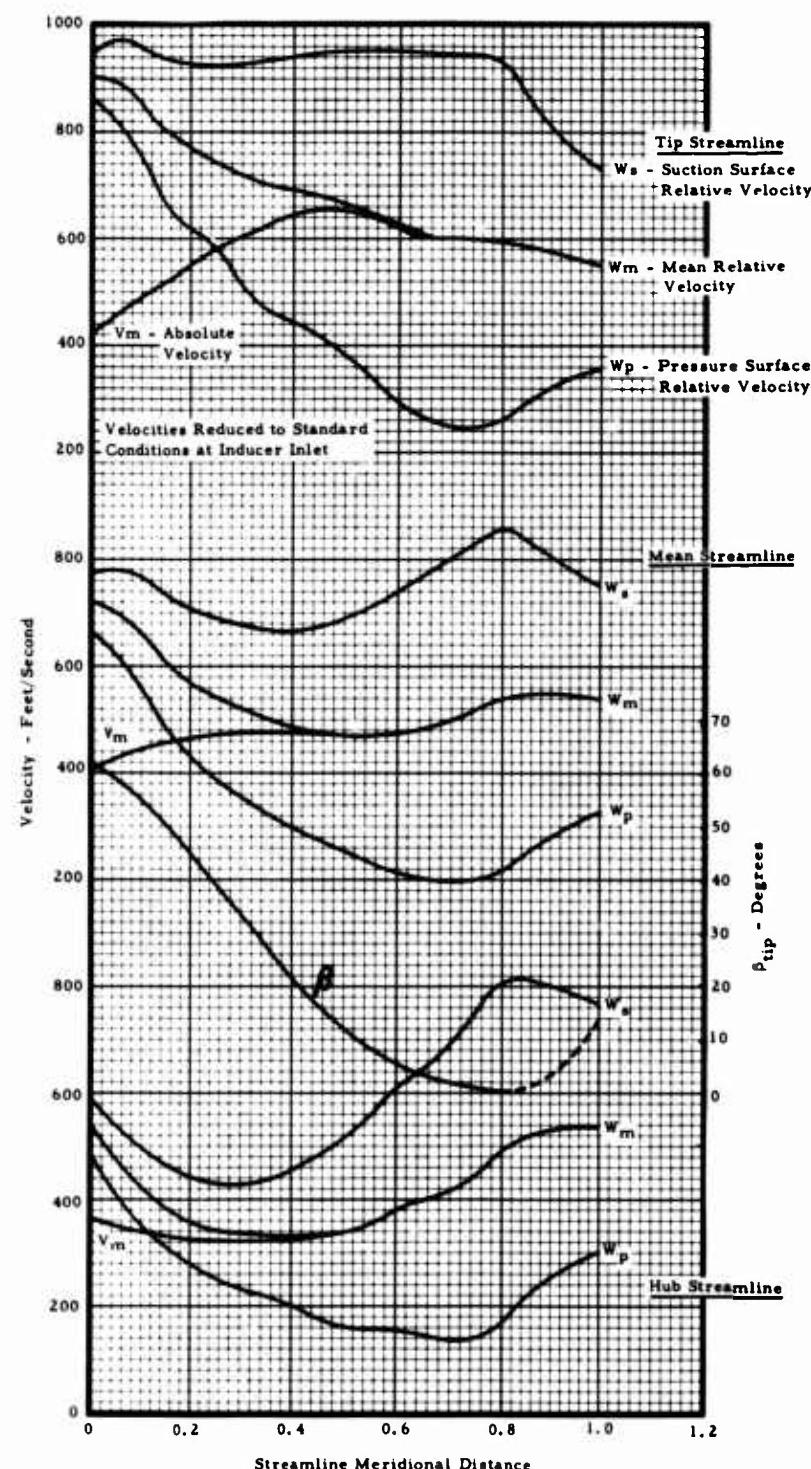


Figure X-56. TS120 Rotor Flow Path Locus of Separation Points on Rotor Pressure Surface.

**Section X**



**Figure X-57. TS120 Compressor Rotor Loading Distribution.**

Section X

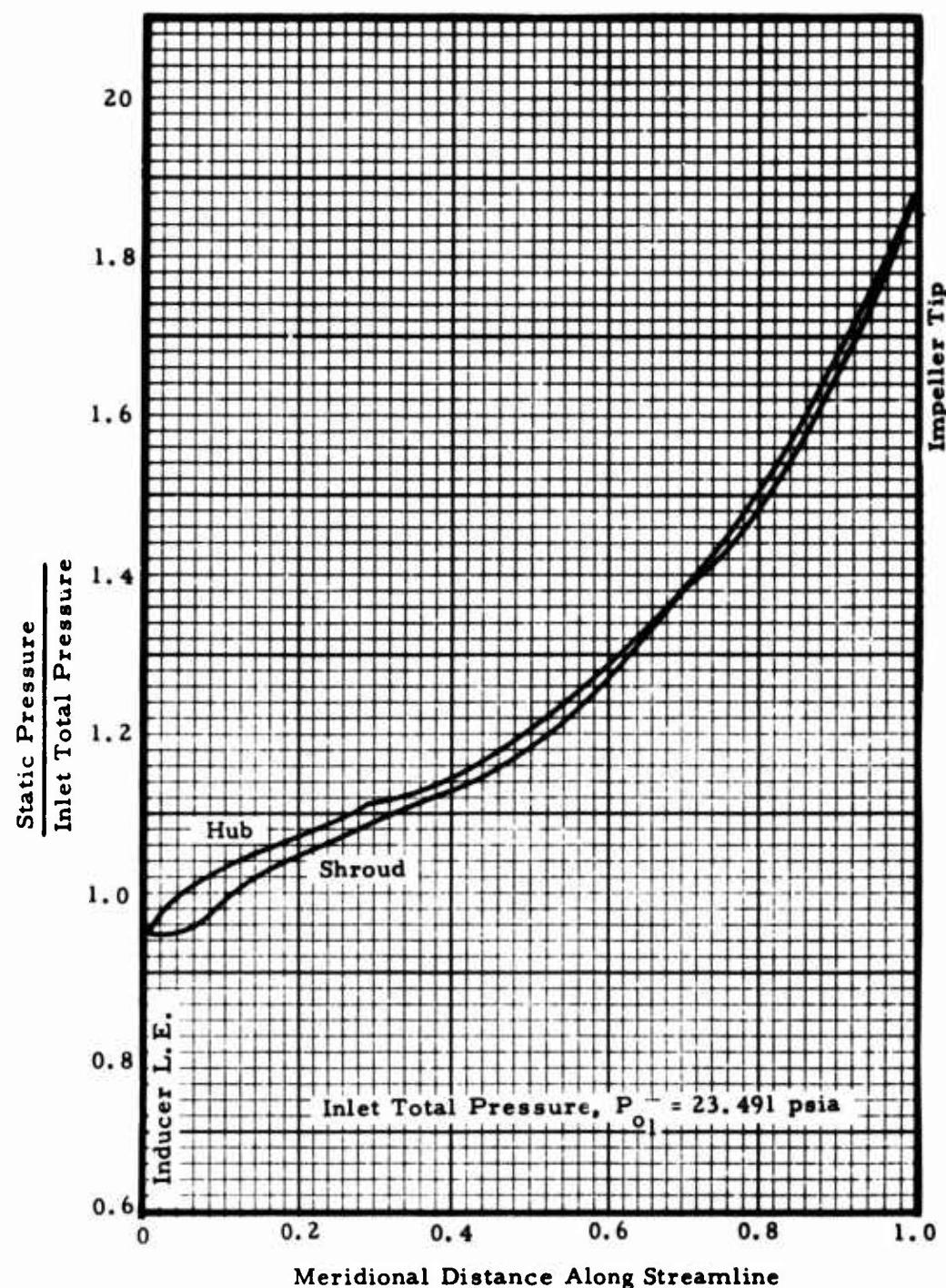


Figure X-58. TS120 Rotor - Static Pressure Distribution.

Section X

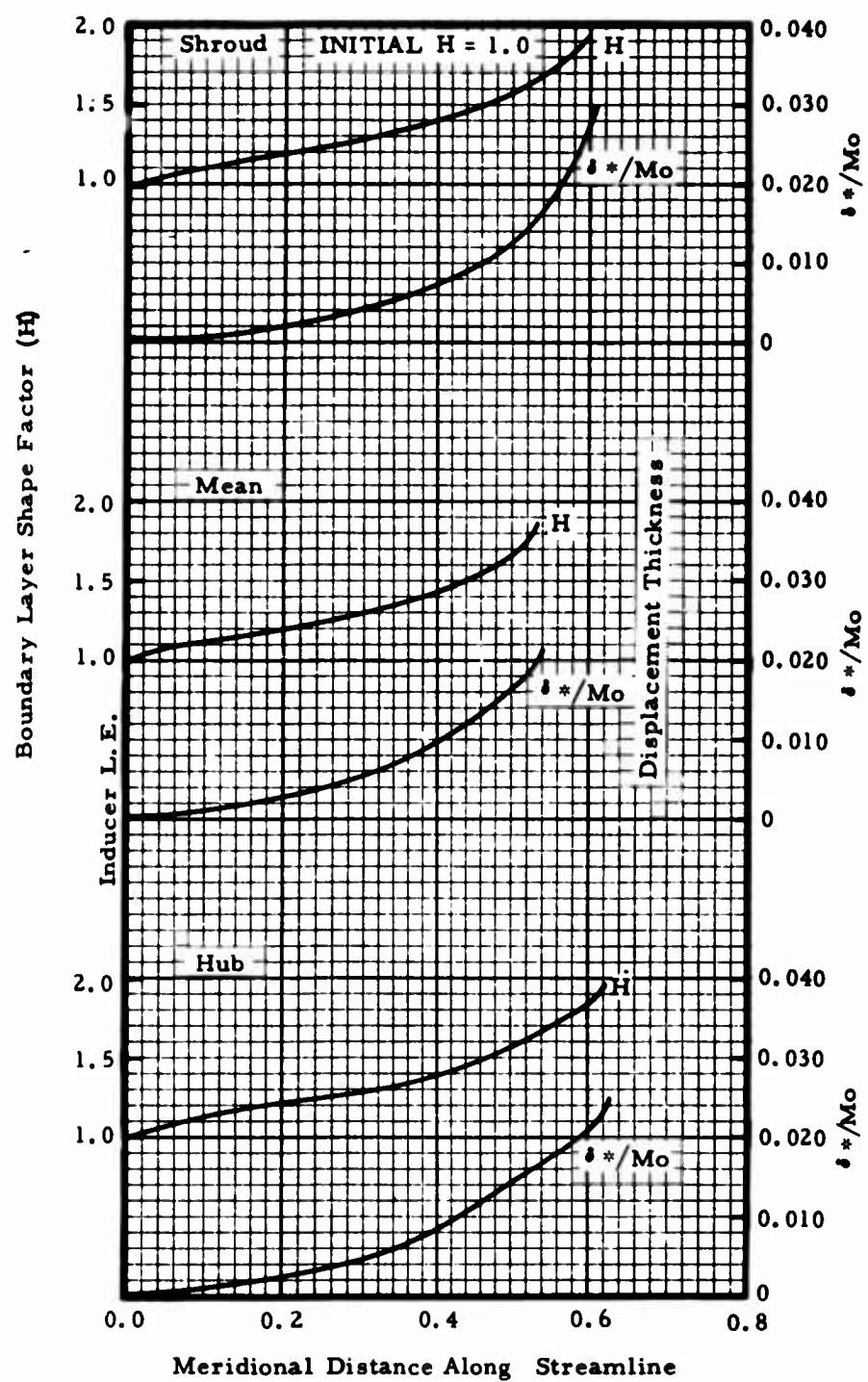
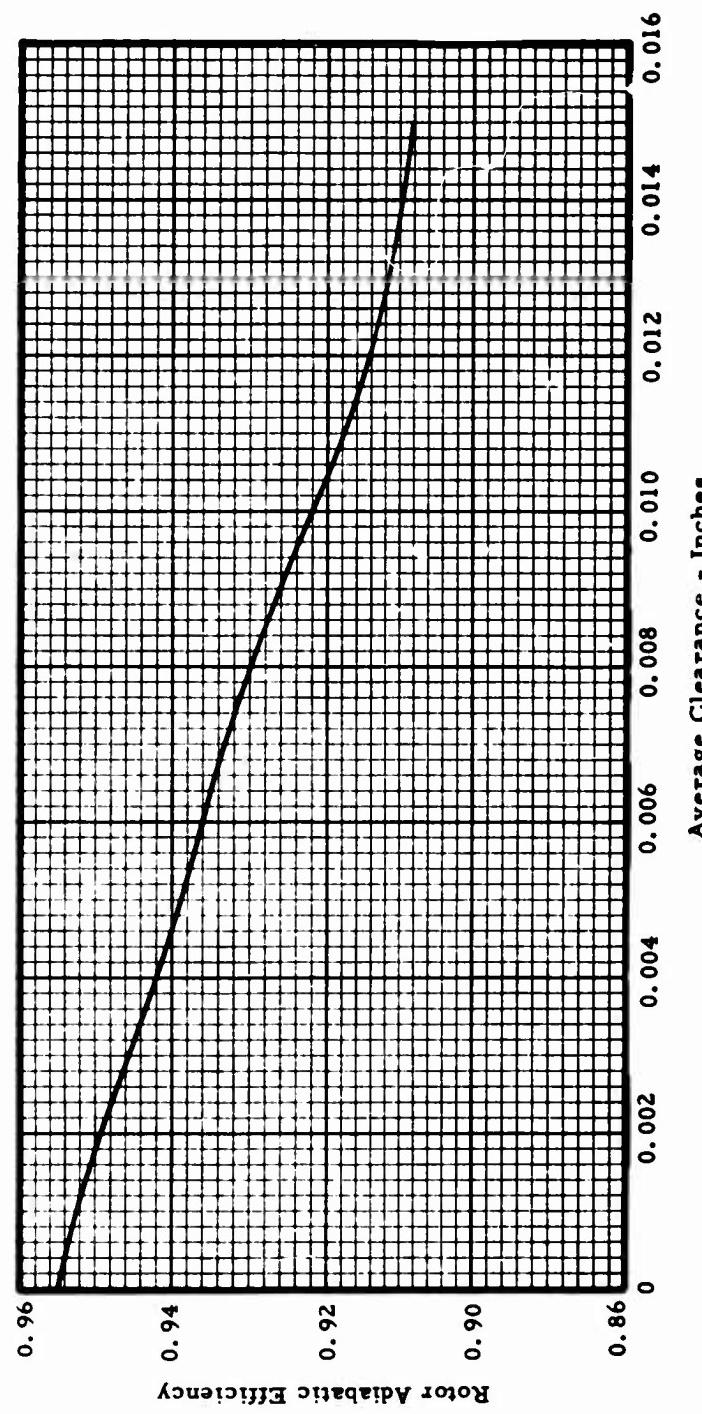


Figure X-59. TS120 Rotor Vane Pressure Surface - Turbulent Boundary Layer Parameters.

**Section X**



**Figure X-60. TS120 Radial Impeller Losses Effect of Rotor Tip Clearance.**

Section X

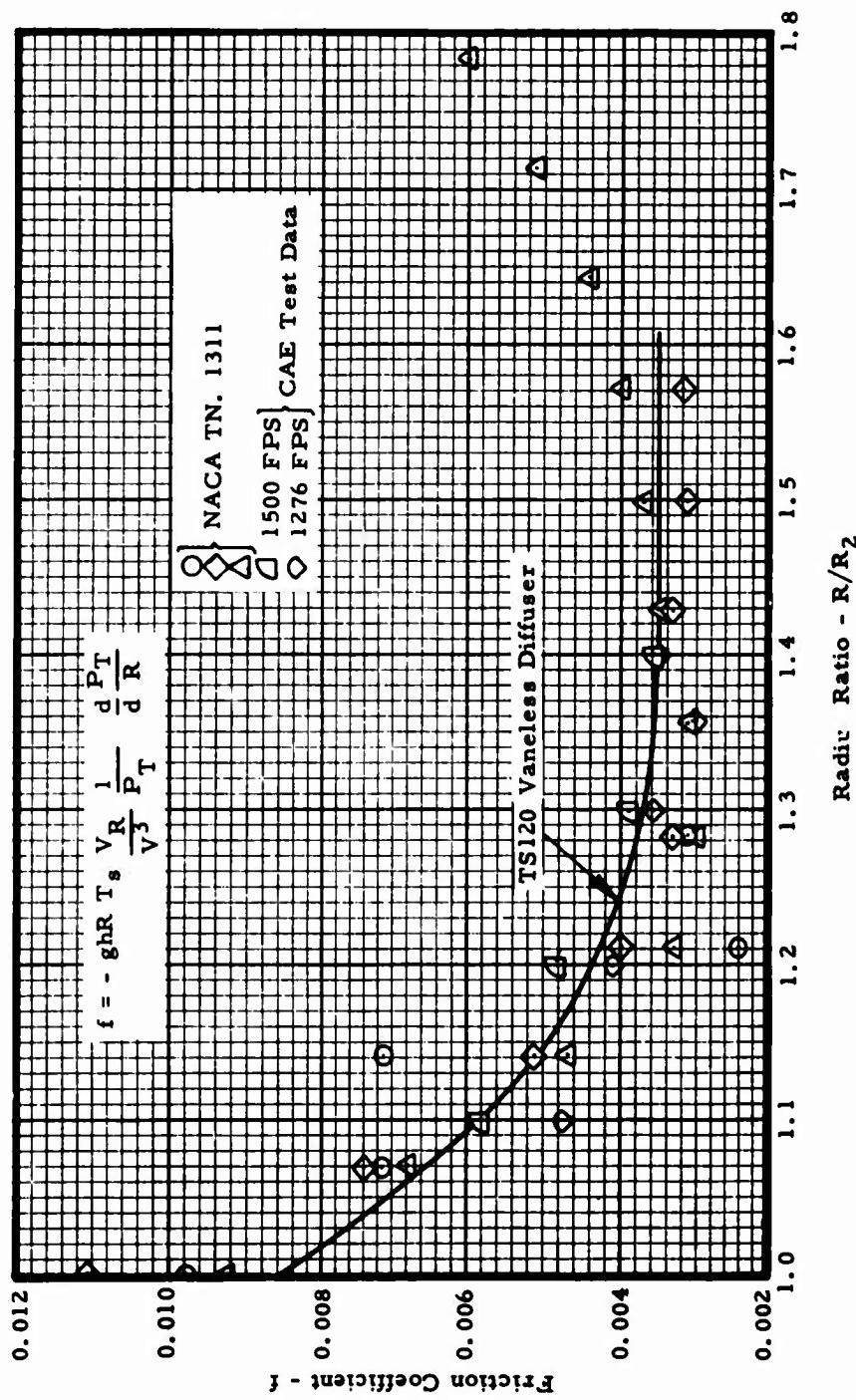


Figure X-61. Radial Variation of Friction Coefficient.

## Section X

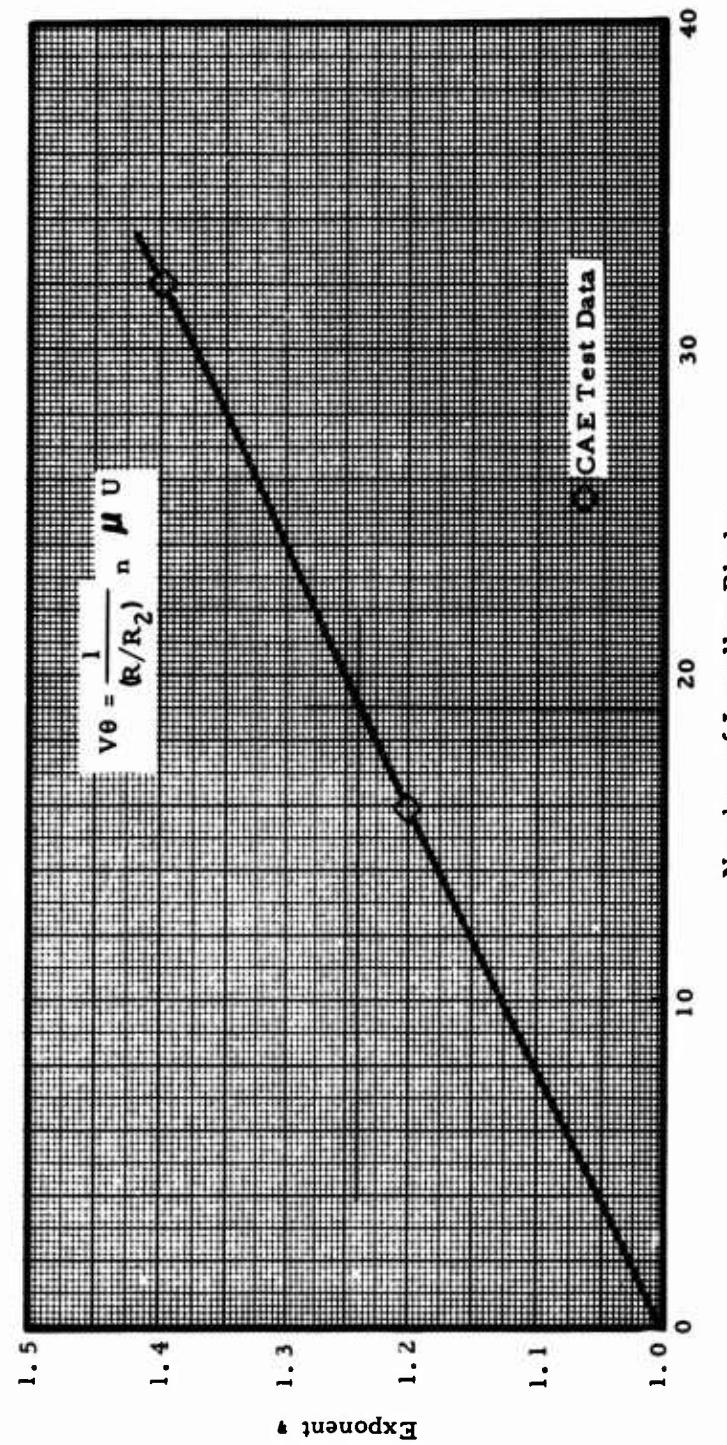


Figure X-62. Vaneless Space Located Behind a Radial Impeller, Effect of Blade Number on Tangential Velocity.

Section X

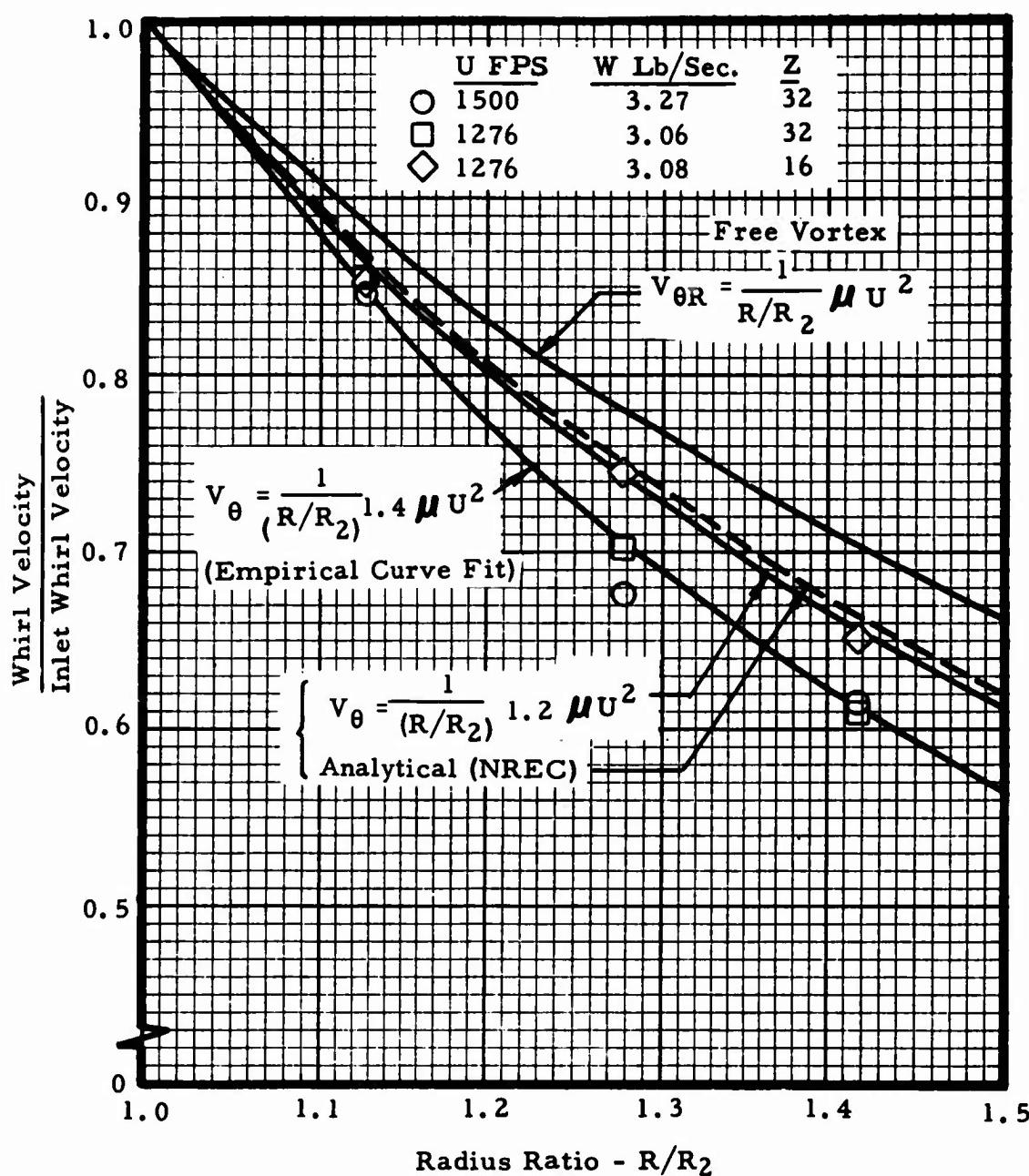


Figure X-63. Decoy In Whirl Velocity Due to Viscosity, CAE Vane-less Diffuser Data.

Section X

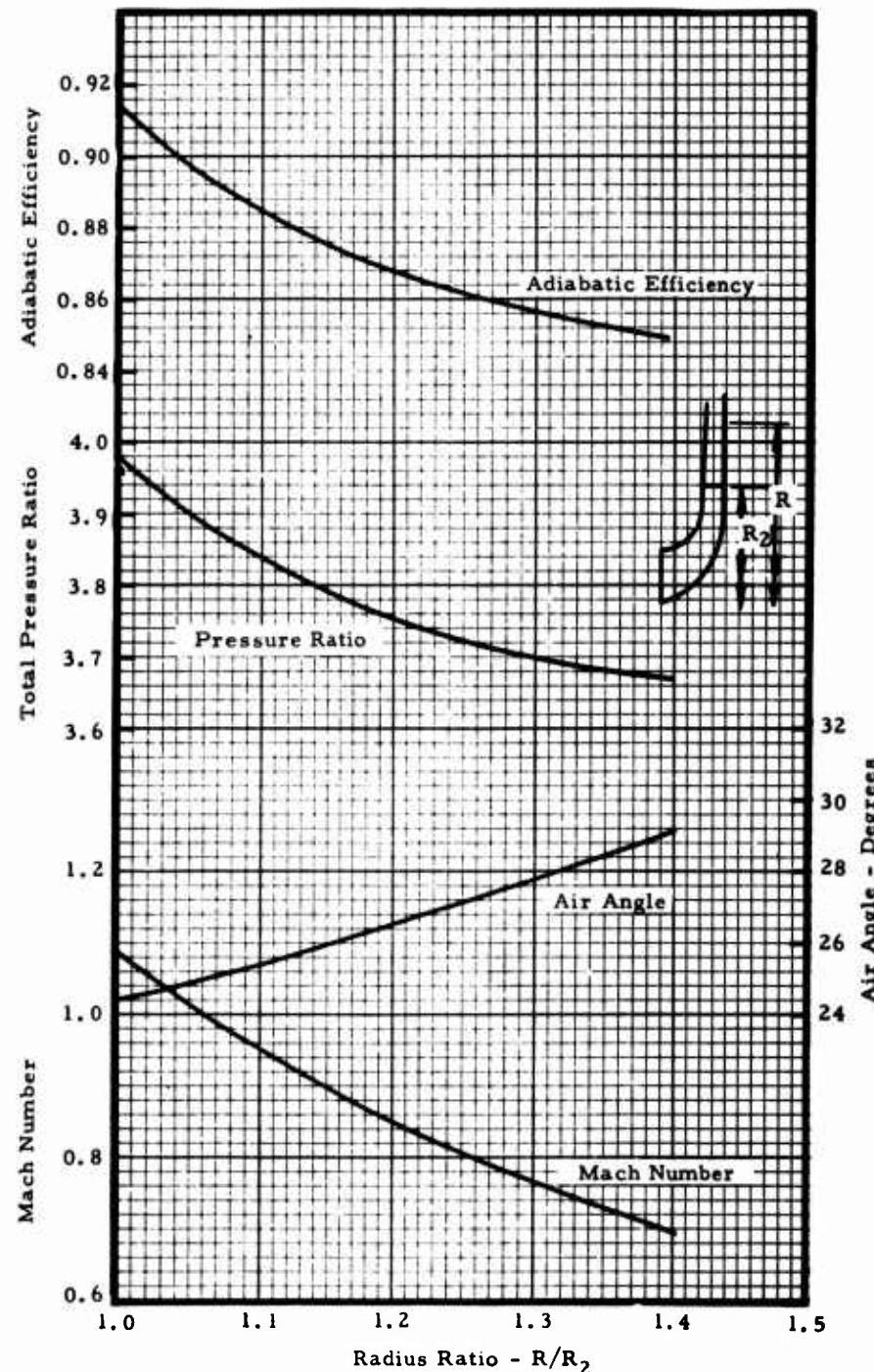


Figure X-64. TS120 Radial Compressor Vaneless Space Flow Properties.

Section X

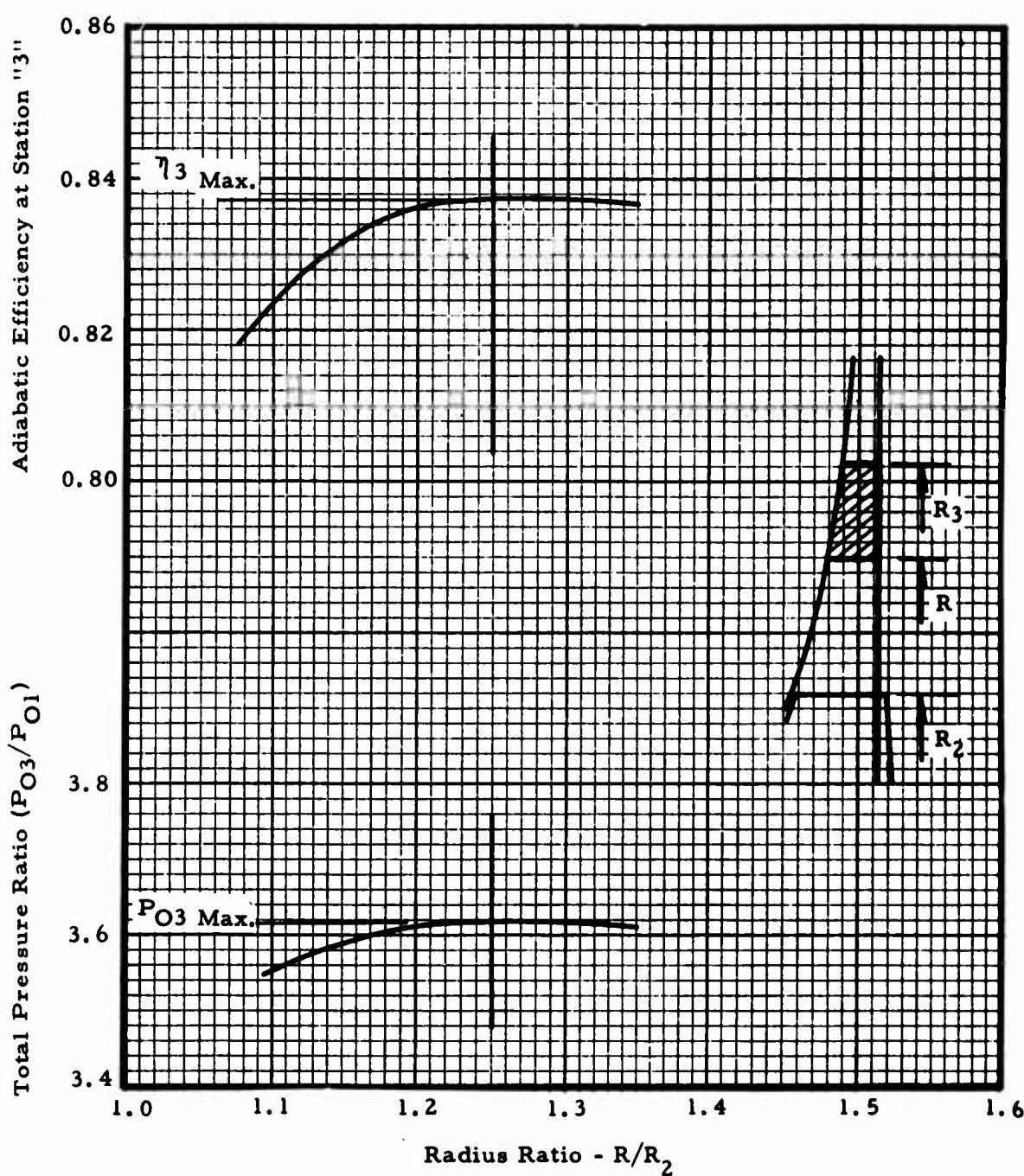


Figure X-65. TS120 Radial Diffuser Determination of First Row Leading Edge Location.

Section X

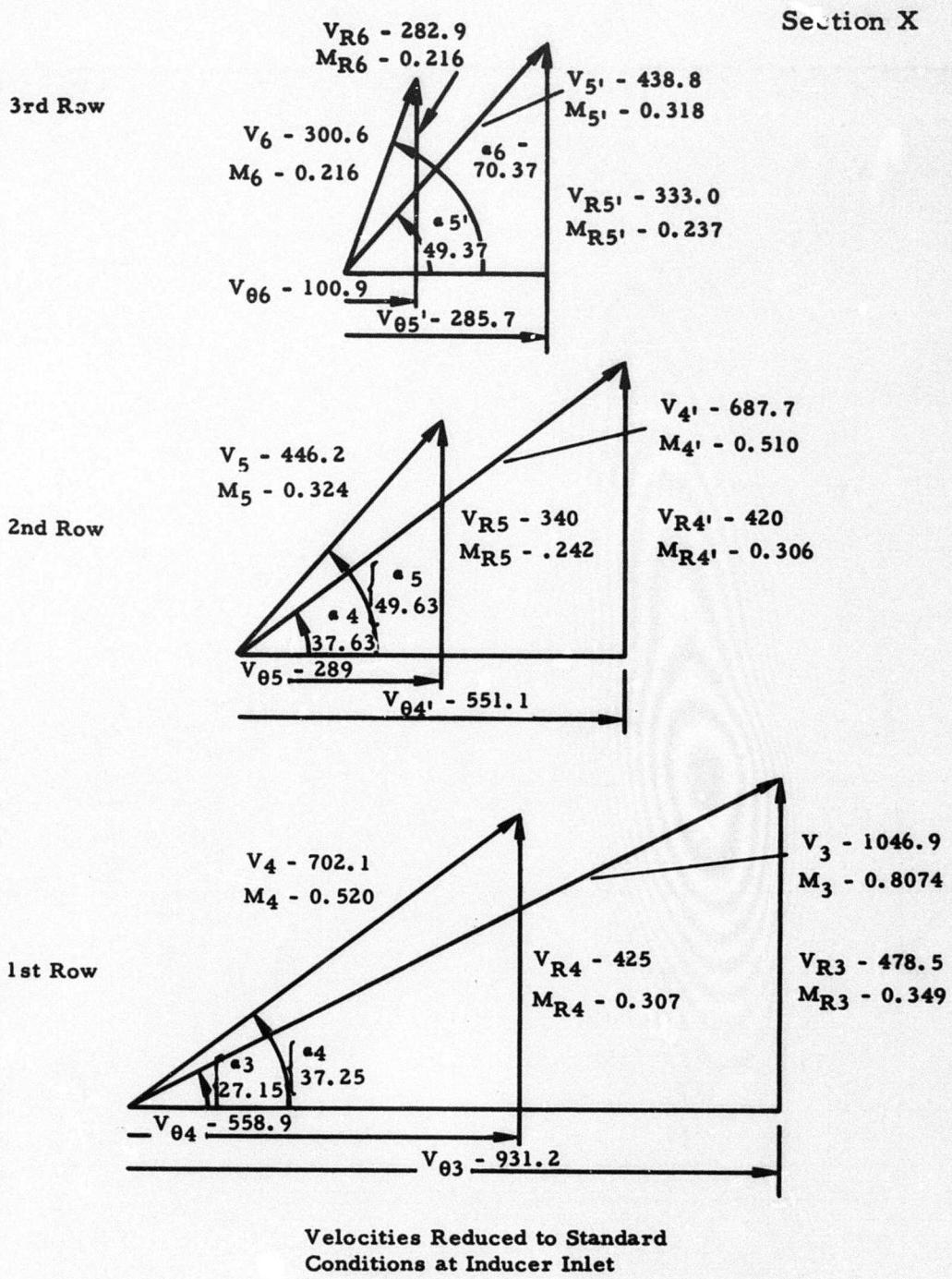


Figure X-66. TS120 Radial Compressor Three-Row Diffuser Vane Velocity Triangles.

## Section X

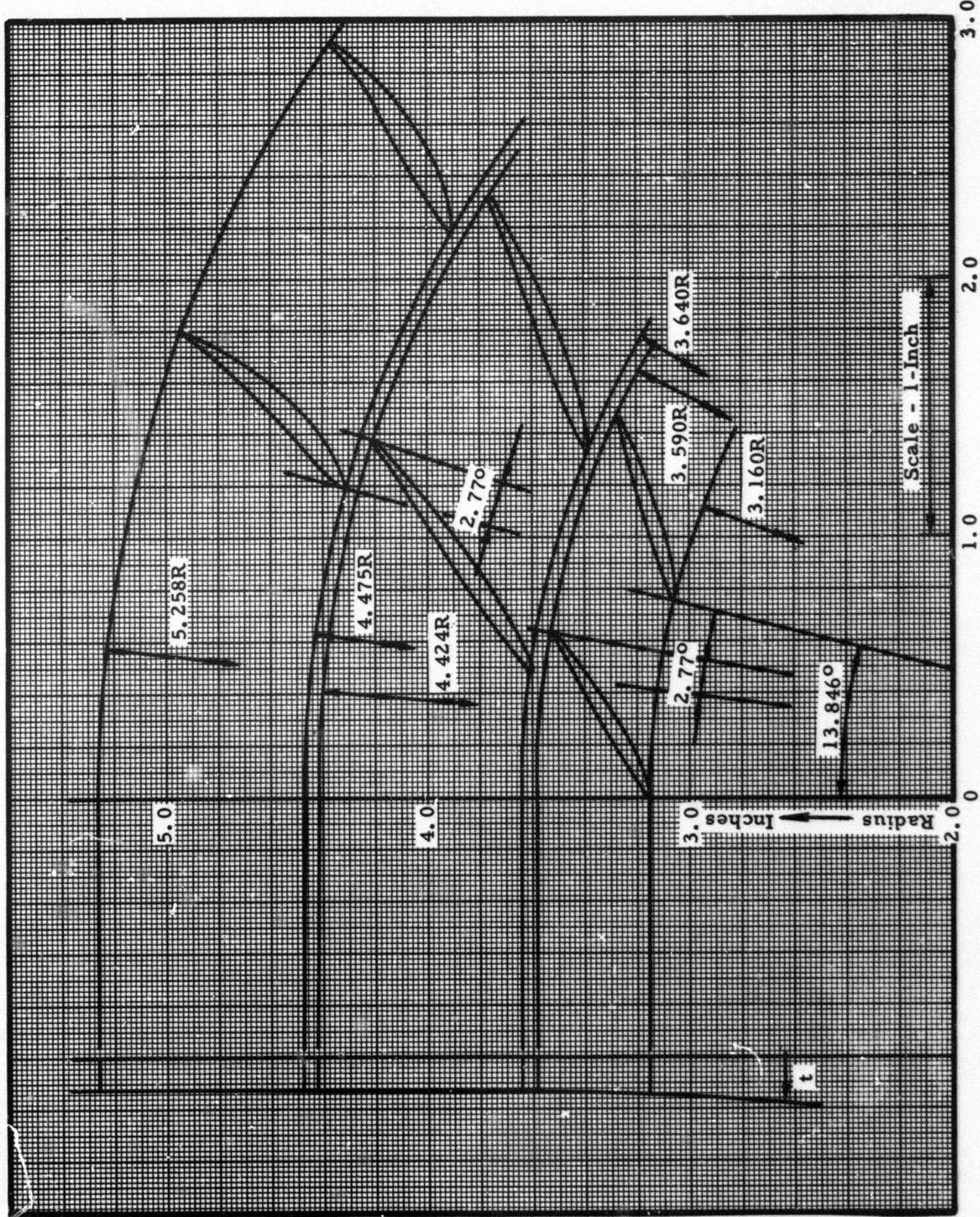


Figure X-67. TS120 Three-Row Radial Diffuser Nominal Setting Angles.

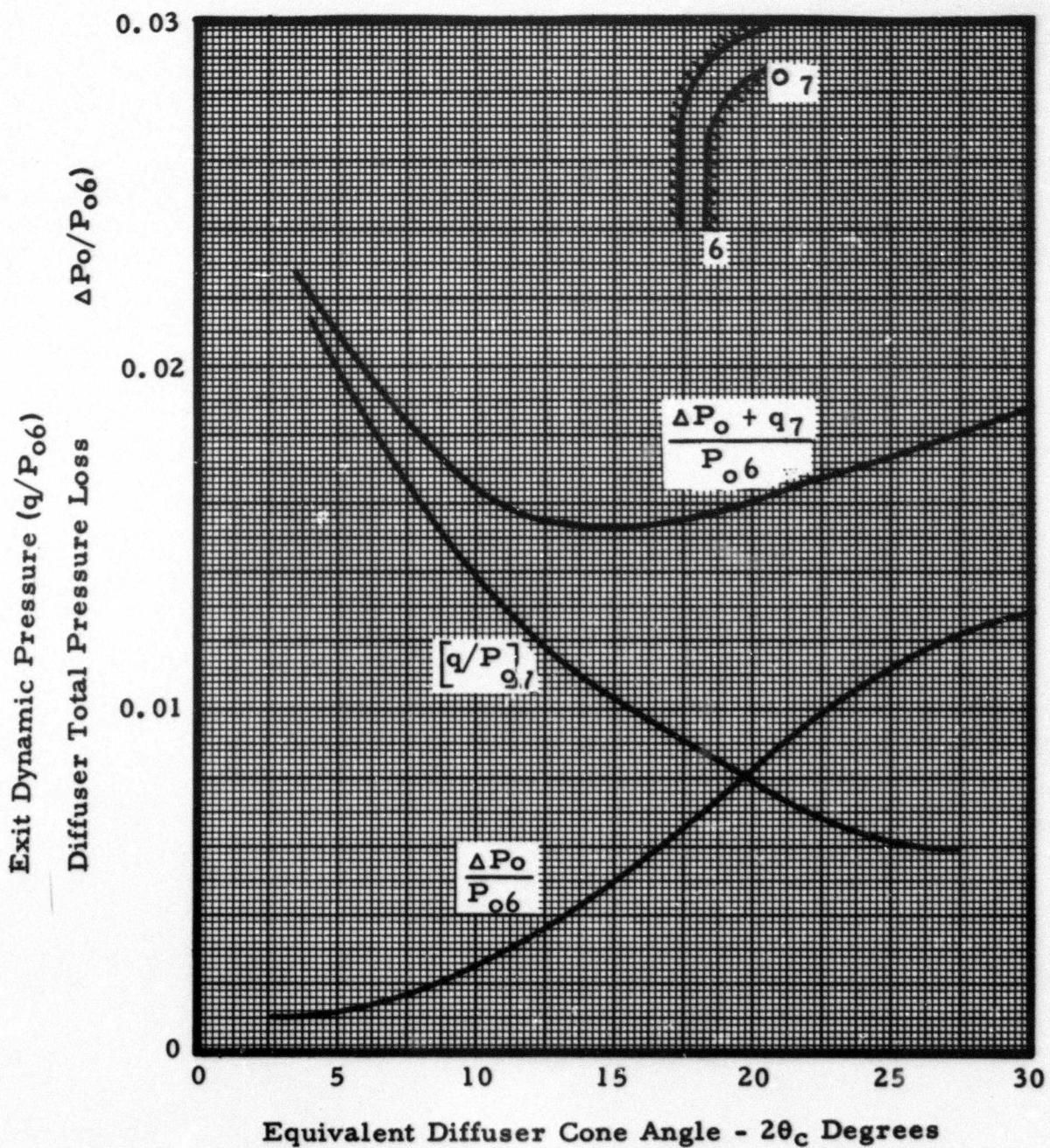


Figure X-68. Variation In Vaneless Diffuser Losses With Equivalent Cone Angle.

## Section X

### COMBUSTOR DESIGN

This section presents the design of the TS120-1 simple cycle gas turbine combustor. Specific objectives arise from purchase description requirements and engine operation and maintenance requirements. There are also requirements arising from integration into the engine mechanical configuration, and the power control system requirements.

The engine cycles parameters affecting combustor design are summarized in Appendix X-A along with relevant combustion design parameters.

The purchase description requirements are extracted from Reference 1 into Appendix X-A. The most difficult objective is the temperature spread requirement (100°F maximum to minimum), particularly in view of the limited combustor size and pressure drop.

The requirements arising from integrating the combustor into the engine design are concerned with keeping the combustor size small so as to reduce engine weight, improve engine structural efficiency as a pressure vessel, and keep the fuel system pressure down to minimize fuel pump horsepower. These are discussed in Appendix X-A in detail.

To make the most use of available time for combustion development, a simplified reverse flow combustor rig, Figure X-69, was initiated shortly after the design phase initiation. The size of the combustor for this rig was selected after a parametric study, Figure X-70, which resulted in adopting one percent pressure loss in the combustor. After detailed design, this combustor was 5.80 inches in diameter and 12.125 inches long. Later, with the engine design essentially frozen in the combustion area, a new smaller combustor design was initiated. The design of this smaller combustor is discussed in detail.

In summary, the initial rig testing indicated a fairly high level of performance for a first run. It was decided that flame tube size reduction was feasible within the development time available. Also, the

## Section X

Initial objective of maintaining common combustors for the simple cycle and regenerative engine was abandoned in favor of a substantial reduction in combustor diameter for the simple cycle engine. The engine design indicated that the combustor would have an offset inlet which would give reverse flow on the primary zone end only, and through-flow on the mixer section. The net effect of these three considerations was that the combustor diameter was reduced from 5.80 to 4.50 inches, and the length from 12.125 to 11.375 inches, Figure X-71.

### DISCUSSION

The combustor design selected is that shown in Figure X-72. It uses a free vortex swirler which gives excellent recirculation characteristics, a wasp waist to stabilize primary zone pressure fluctuations, deflector cooling strips to economize on air consumption for cooling and to ensure freedom from deposits, and a muff around the mixer section to provide means for controlling the approach of air to the combustor. The combustor is designed essentially by the sizing of the mixer section, and with the selection of the primary zone type.

There are two basic primary zone types: the Nerad and the Lubbock, Figure X-73, and numerous variations of these two basic types. The best performance is generally obtained with a primary zone incorporating features from both types; given these features, a 5/1 burning range can be relied on with well cooled primary zone walls and freedom from deposits. This primary zone requires a fuel/air ratio of 0.055 at design point conditions to place the operating point correctly in the burning range, and the balance (65 percent) of the air is introduced through the mixer section to dilute the primary zone efflux down to the required turbine inlet temperature. Thus, the mixer section must be sized to pass 65 percent of the air with one percent pressure loss.

## Section X

### MIXER SECTION

The design of the mixer section is an "iterative" process in which an initial design is selected and then modified until several requirements are met. The requirements are:

1. One percent pressure loss passing 65 percent of the air-flow.
2. Best length-diameter combination.
3. Mixer ports large enough to ensure penetration of dilution air.
4. Adequate flow area between mixer ports to ensure satisfactory ventilation of the primary zone.
5. Mixer section approach velocity head ( $1/2\rho V^2$ ) approximately one-half the mixer section pressure drop to ensure the most effective smoothing of inlet velocity distortions.

The data of Reference 2 are used to calculate the hot loss and mixer port coefficients of discharge under crossflow conditions. It can be seen that as the mixer section approach velocity head, Figure X-74, increases the mixer port coefficients of discharge reduce, and the mixer section length must increase to accommodate the increased port area. As the approach velocity head reduces, the length reduction reaches a condition of diminishing return, and the mixer section diameter begins to increase rapidly. It is found that if the approach velocity head is set at one-half of the mixture section pressure drop, the mixer section length and diameter are found to be reasonably well proportioned. Fortunately, this matches the fifth requirement, Reference 3.

Obtaining adequate penetration is achieved by making the mixer ports large enough to deliver dilution air to the center of the combustor. The data of References 4 and 5, and past experience in using this data led to the selection of the mixer ports shown in Figure X-75.

## Section X

Ensuring adequate ventilation of the combustion zone, Figure X-74, is achieved by providing sufficient area for the high temperature low density gases leaving the combustion zone to flow into the mixer section. It should be noted that the mixer port's air jets exert a blockage effect on the crossflow. Prior Continental experience shows that if the area of obstruction of a jet is taken as  $3/2 W^2$  where  $W$  is the port width, then the combustion zone exit velocity head can be made as large as 30 percent of the combustor pressure drop without excessive developmental difficulty. Reference to Figure X-76 shows that this velocity head is in series with the pressure drop across the primary zone and thus if the ratio " $1/2 \rho V^2 c_z / \text{combustor drop}$ " were allowed to get too high (even only 50 percent), then control of airflow into the primary zone by the primary zone ports is made impossible.

The net result of these considerations was the selection of the combustor mixer section indicated in Figure X-71.

### PRIMARY ZONE

The design of the primary zone involves fuel atomization, aerodynamics, fuel droplet trajectories, and droplet burning time.

Fuel atomization data are available from a number of sources and is generally similar to that shown in Figure X-77. As can be seen, accepting low fuel pressure imposes some serious problems on the combustion system in that droplet burning time increases rapidly.

First, for the atomizer selected, the atomization results in a droplet burning time of 8.0 milliseconds. Then the primary zone residence time must be eight milliseconds also, in order to approach 99 percent chemical combustion efficiency.

The fuel droplets follow a complex flight path dictated by inertia and aerodynamic drift effects, and Figure X-78 shows the type of path that the larger droplets probably follow; a simplified treatment calculates a flight time from atomizer to flame tube wall at fuel injection velocity and a drift time from the point of impingement on the flame tube wall to the primary zone exit at gas velocity. This simplified

## Section X

calculation gives droplet residence times accurate enough for most practical purposes. For the primary zone of Figure X-72, the length was selected to give the required eight millisecond residence time. Note that the relevant gas velocity in the primary zone is controlled by the combustor pressure drop and not by the primary zone diameter. Reducing the primary zone diameter has effects not immediately obvious; first, it reduces the quantity of gas recirculated, worsening the stability limit and increasing the combustor's tendency to form carbon deposits.

### ATOMIZER

As discussed above, the selection of the atomizer has a direct effect on the primary zone sizing. Improved atomization (to less than 165 microns indicated by Figure X-77) reduces the primary zone length, and possibly reduces the chance of fuel spray impinging on the flame tube wall due to reduced spray penetration.

Alternate atomizer systems investigated were air assist and spill atomizers. The air assist atomizer significantly reduced fuel pressure, but calls for a specialized air pump which, in the final analysis, does nothing to reduce over-all fuel system horsepower. The spill atomizer, like the air assist atomizer, requires an auxiliary pump (fuel instead of air) which adds to the complexity of the fuel atomizing system.

Therefore, the conventional dual orifice atomizer with internal pressure relief valve was adopted as the basic design for this program. In the development program, an effort will be made to reduce the fuel pressure required for satisfactory ignition so that the over-all system fuel pressure can be reduced, and testing will include specific tests to determine whether atomization is satisfactory under conditions where the pressure relief valve is just opening.

## Section X

## IGNITION

The choice of an ignition system involves the atomizer, the igniter, and the primary zone type. With the dual orifice atomizer and swirler primary zone selected, the problem is to choose a compatible ignition system. As indicated in Figure X-79, the flame pilots right next to the atomizer; the igniter to achieve an effective light must initiate a flame kernel which must then be carried into the piloting zone. The factors which affect the ability to initiate a flame kernel are (Reference 4):

- velocity at the igniter tip set by combustor pressure drop.
  - pressure and temperature set by light-up conditions.
  - fuel/air ratio set by the positioning of the igniter tip.
  - igniter energy level set by the selection of the ignition unit.

To obtain the best chance of the kernel reaching the piloting zone, the ignition zone should be as far upstream as possible, and logically the very best position should be at the atomizer tip. Therefore, we are proposing to use the shroud and atomizer to form a spark gap, Figure X-71, and if the performance is not substantially improved, then revert to the more conventional igniter in the side as indicated in Figure X-79. Apart from the igniter position, there are two avenues for improving ignition performance. First, the atomizer pressure drop may be increased at light-off conditions, Figure X-77; to light 12 centistoke fuel it is expected that the pressure drop should be 25 psi, and it can be seen that while increased pressure drop will permit lighting more viscous fuels, it will also result in increasing the maximum system fuel pressure. Second, the igniter energy level may be increased which normally increases the ignition system cost. The least expensive system is the induction coil unit, and it is proposed to start testing with such a unit. To obtain increased energy at the spark,

## Section X

the next logical step is to adapt a capacitor discharge system (of approximately one joule stored energy per spark). This will be investigated if the initial system proves inadequate. Glow plugs promise to be the least expensive and the most effective system, but it is not known how such a system would stand up to combat gasoline.

### FLAME TUBE COOLING

Since very high gas temperatures are encountered in combustors, it is necessary to cool them to metal temperatures which will ensure acceptable life.

The technique used for cooling is similar to that described in Reference 6. A blanket of cooling air is placed between the hot gases and the flame tube walls to insulate the walls from heat. Figure X-80 shows the expected variation of flame tube temperature with distance downstream of each cooling band for the combustor design shown in Figure X-72. With the deflector type cooling band the cooling air injection velocity can be controlled and adjusted to achieve satisfactory cooling with the minimum quantity of cooling air. Reference to Figure X-85 indicates adequate cooling may be achieved with 24 percent of the total airflow. Reference 1 indicates that metal temperatures of less than 1500°F are required, and Continental experience suggests that 1200°F, Figure X-81, would be desirable.

The factors controlling flame tube life seem to be thermal shock during engine acceleration and thermal stressing under steady-state operating conditions; rough combustion can cause vibrations which result in fatigue failure, and if the combustor has a high pressure loss, buckling stresses can be a factor. Other factors are damage caused by field handling conditions and corrosion from fuels such as combat gasoline.

In general, thermal shock is minimized by adopting relatively thick flame tubes, and thermal stressing is minimized by reducing temperature gradients, and by adopting combustor design features which allow the affected part to flex without being over-stressed.

## Section X

For example, the combustor is supported from the atomizer end, and the floating joint at the volute inlet (Figure X-71) is a spring seal arrangement which will accommodate axial and radial expansion.

Three choices could then be made. If metal temperatures can be kept below 1200°F, then except for field handling problems, the flame tube could be 0.003-inch thick. For the minimum combustor cost the flame tube should be 0.015-inch thick (0.010-inch,

01	84	02
\$6 — /ft. 2; 0.015-inch,	\$5 — /ft. 2; 0.020-inch,	\$7 — /ft. 2
100	100	100

for Hastelloy X). If the metal temperatures cannot be held below 1500°F, then up to 0.060-inch metal thickness might be required. It was decided to make the flame tube 0.045-inch thick, and if metal temperatures can be kept low enough, based on combustor testing and engine testing, the tube thickness could be reduced for a reduction in combustor cost and weight.

### COMBUSTOR CHAMBER DEPOSITS

The two fuels which will most likely result in combustion chamber deposits are the combat gasoline (lead-sulphur deposits) and the VVF 800 DF2 (carbon deposits). Continental's experience is that carbon deposits occur wherever partly reacted fuel-air mixtures are allowed to touch metal. Therefore, carbon deposits will be minimized if the film cooling of the combustor is effectively carried out. On the other hand, lead-sulphur deposits will probably accumulate (Reference 7) wherever combustion products touch metal walls. Therefore, while the air film cooling is expected to effectively prevent lead deposits in the primary zone, some deposits are to be expected in the mixer section and the turbine inlet volute. The test rig program will indicate the seriousness of this deposit problem.

## Section X

### SWIRLER DESIGN

The swirler performs dual functions; it shapes the recirculation zone, and so induces hot gases to flow back to the atomizer to ensure a good lean limit blowout, and it acts as a film cooling device for the flare. The swirler design chosen for this combustor is a free vortex type which provides a particularly good flow pattern around the atomizer tip. It is relatively inexpensive and of sturdy construction. The method of design is described as follows and in Figure X-82.

Because the total pressure at any radius in the throat is constant and the axial velocity on the shroud (hub) must be small but positive to avoid having a stagnation point on the shroud (which would result in carbon deposits there), the following equations apply:

$$V_{CO}^2 + V_{AO}^2 = V_{C1}^2 + V_{A1}^2$$

$$V_{CO} R_O = V_{C1} R_1$$

$$\text{then } R_O R_1 = \sqrt{t \tan^2 \theta + 1}$$

$$\text{when } \frac{V_C}{V_A} = t \tan \theta \quad \theta = 1/2 \text{ Cone Angle}$$

To get a resultant cone angle of 110°, relying on the Coanda effect to pull the air onto the 130° flare

$$R_O/R_1 = 1.50$$

$$Cd = 0.57$$

$$\text{with } R_O = 1.50\text{-inch}$$

$$R_1 = 1.00\text{-inch}$$

Calculated flow area, 0.57 inch<sup>2</sup>

## Section X

Tests on a swirler flow rig gave 0.61-square inch flow area indicating some small deviation from free vortex conditions, probably due to viscous effects. Using the calculated flow area, the effective air film thickness at the throat, and the distance from the throat to the first flame tube cooling band, the effective cooling length for the same reference conditions as Figure X-80 is 1.57 inches, which implies that the flare should be well cooled.

### PERFORMANCE

The performance characteristics which can be estimated for a combustor are the pressure loss and the efficiency. This combustor was designed to give the effective flow area characteristic, shown in Figure X-83, which will give one percent pressure loss at design point conditions. The combustor size was selected to give the target efficiency characteristic indicated in Figure X-84. This figure also shows the efficiency measured on the first build of the 5.80-inch diameter combustor.

The prediction of combustor temperature spread (or T. D. F.) requires advance knowledge of the air distribution entering the combustor. This knowledge is not available at this time.

The air distribution and zone air/fuel ratios calculated for this combustor are shown in Figure X-85.

## Section X

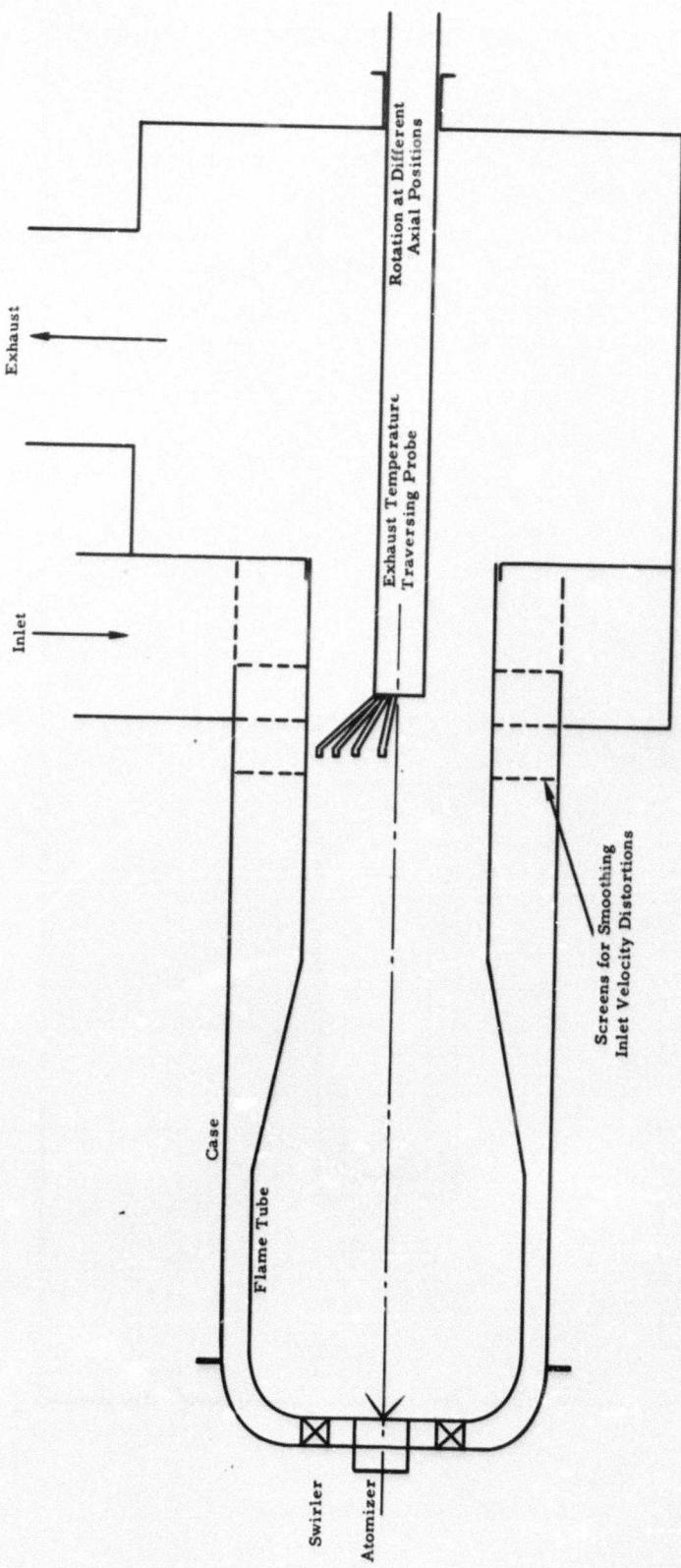


Figure X-69. Reverse Flow Combustor Rig Test Section.

## Section X

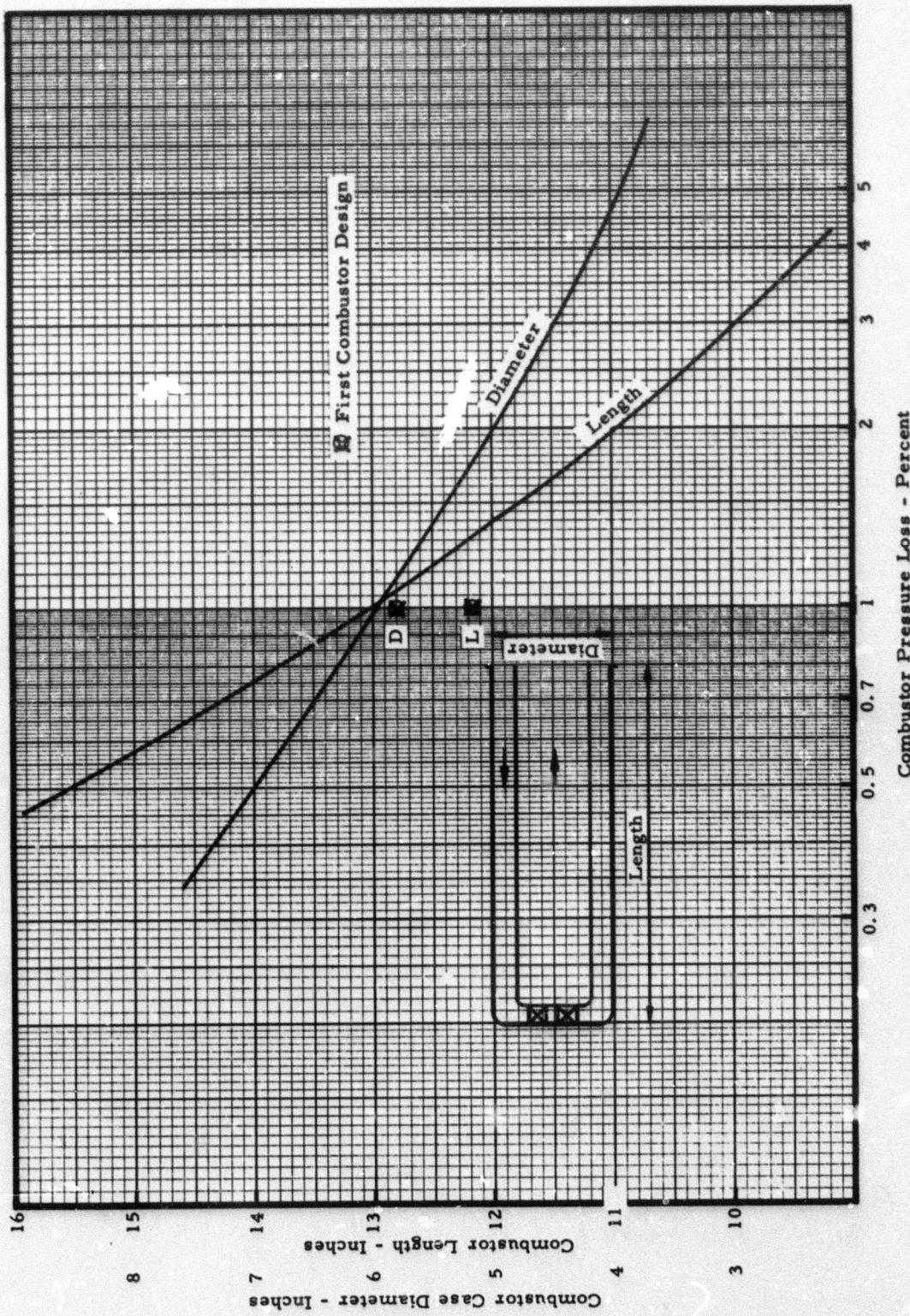


Figure X-70. Combustor Diameter and Length Versus Combustor Pressure Loss for 1500-Hour Life and 15 Months Development Program Prior to Engine Running.

104

## Section X

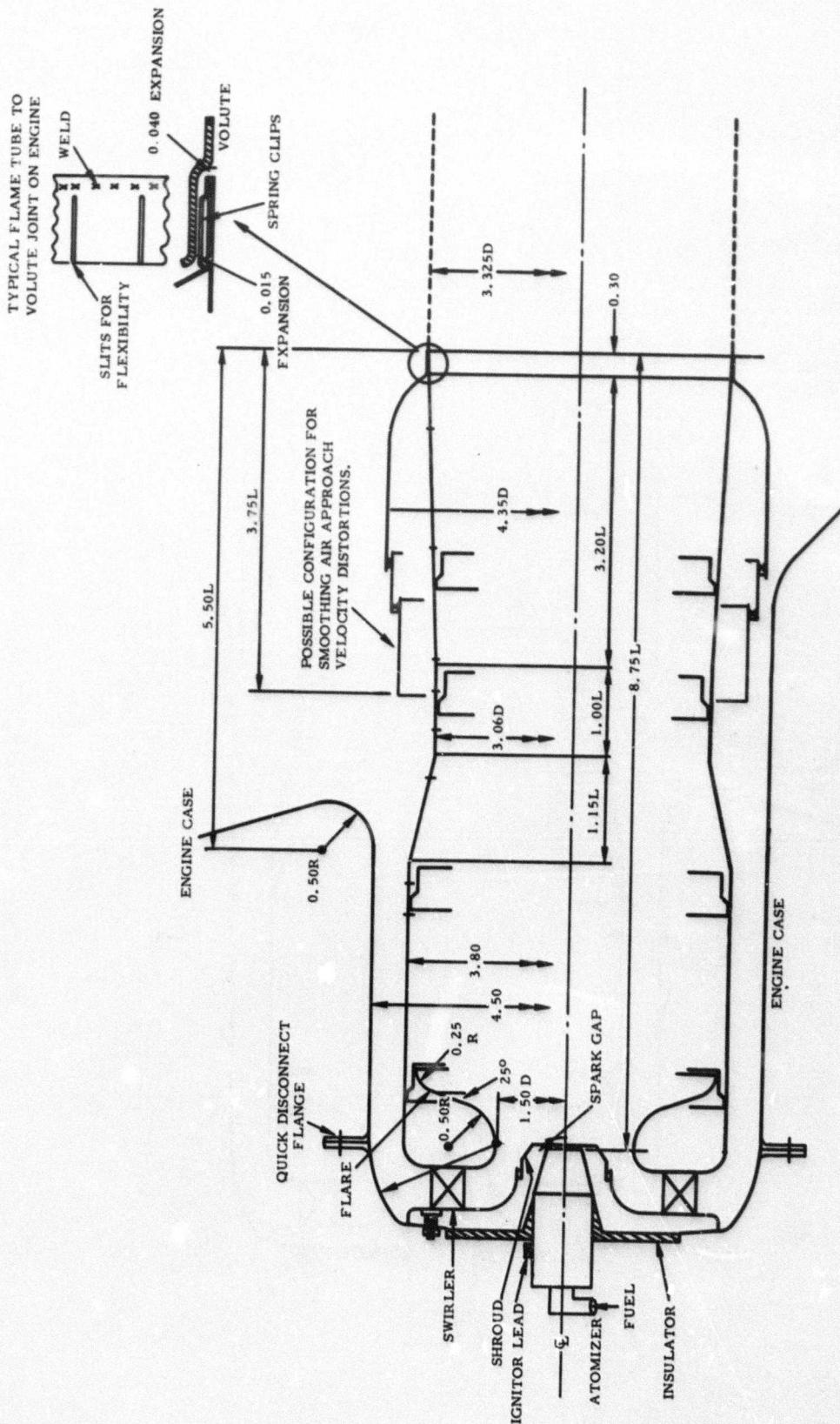


Figure X-71. TS120 Combustor Envelope Dimensions.

## Section X

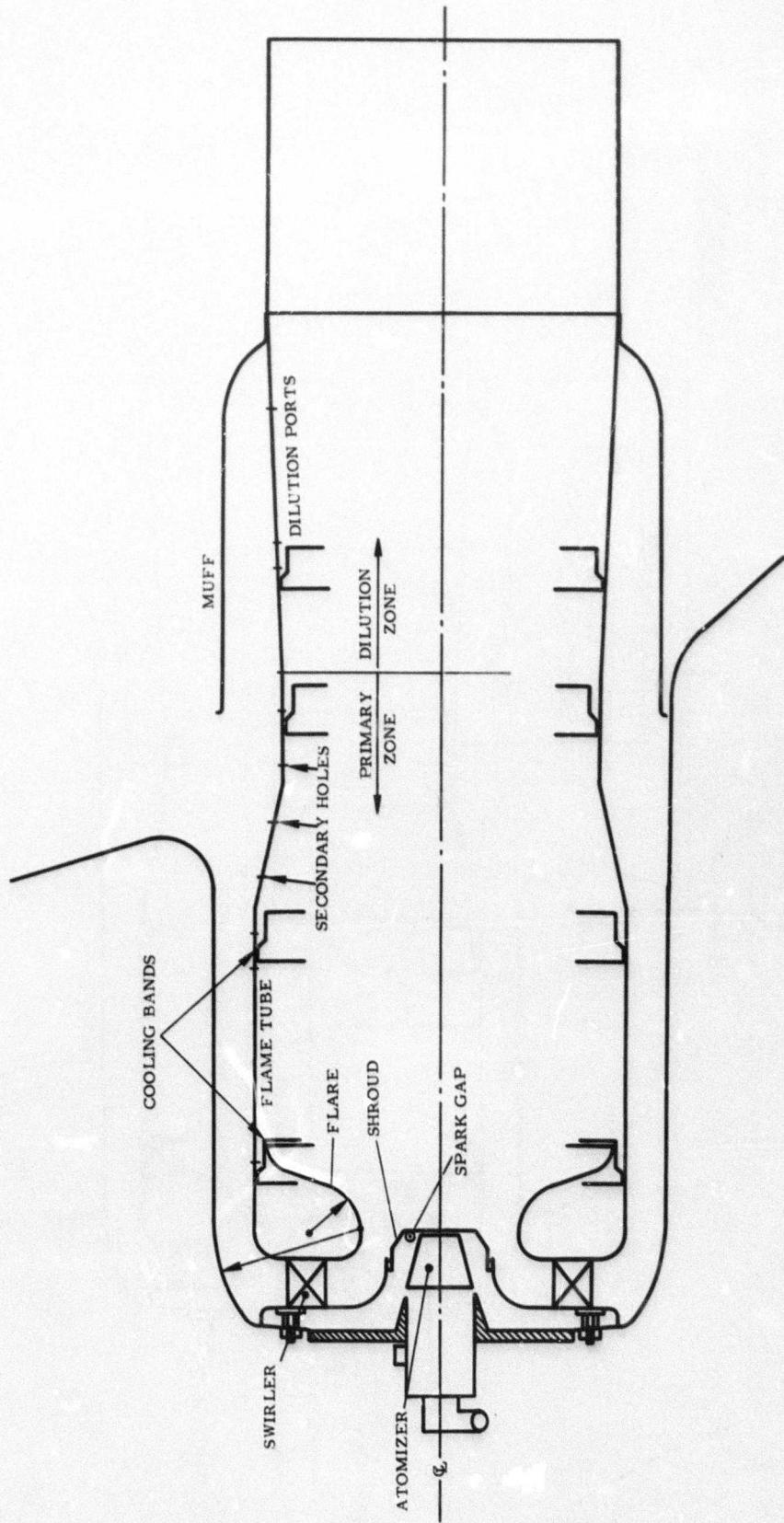
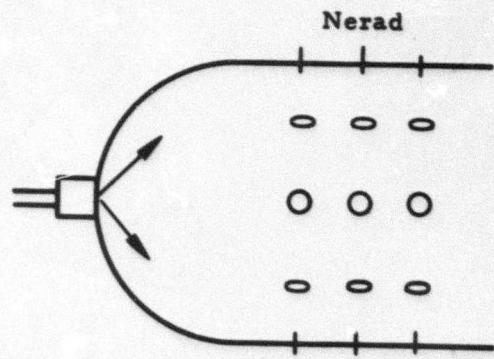
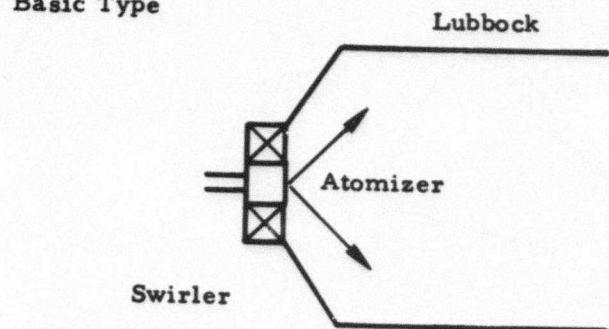


Figure X-72. TS120 Combustor.

## Section X

**Basic Type**



**Variations**

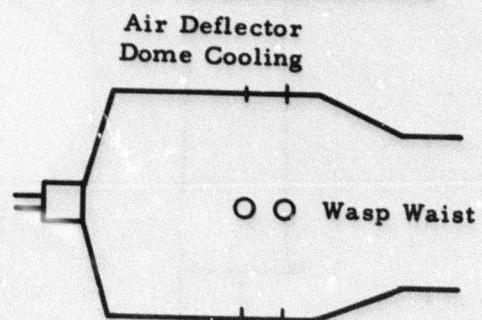
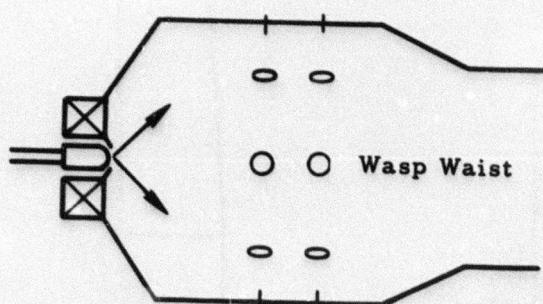
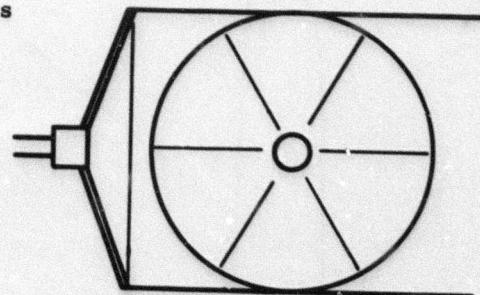
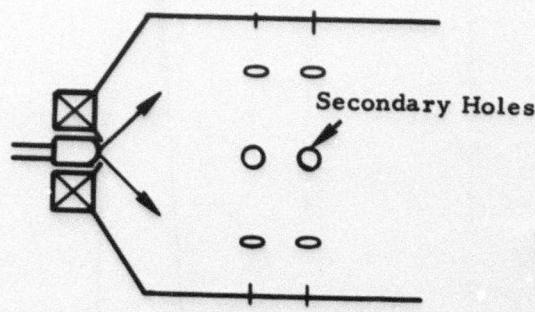
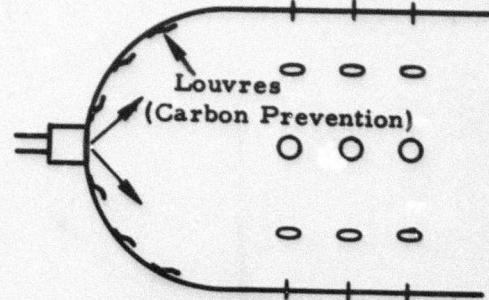
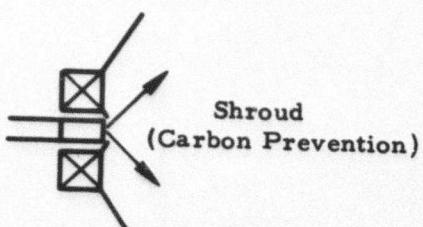


**Figure X-73. Atomizer Can Types.**

Section X

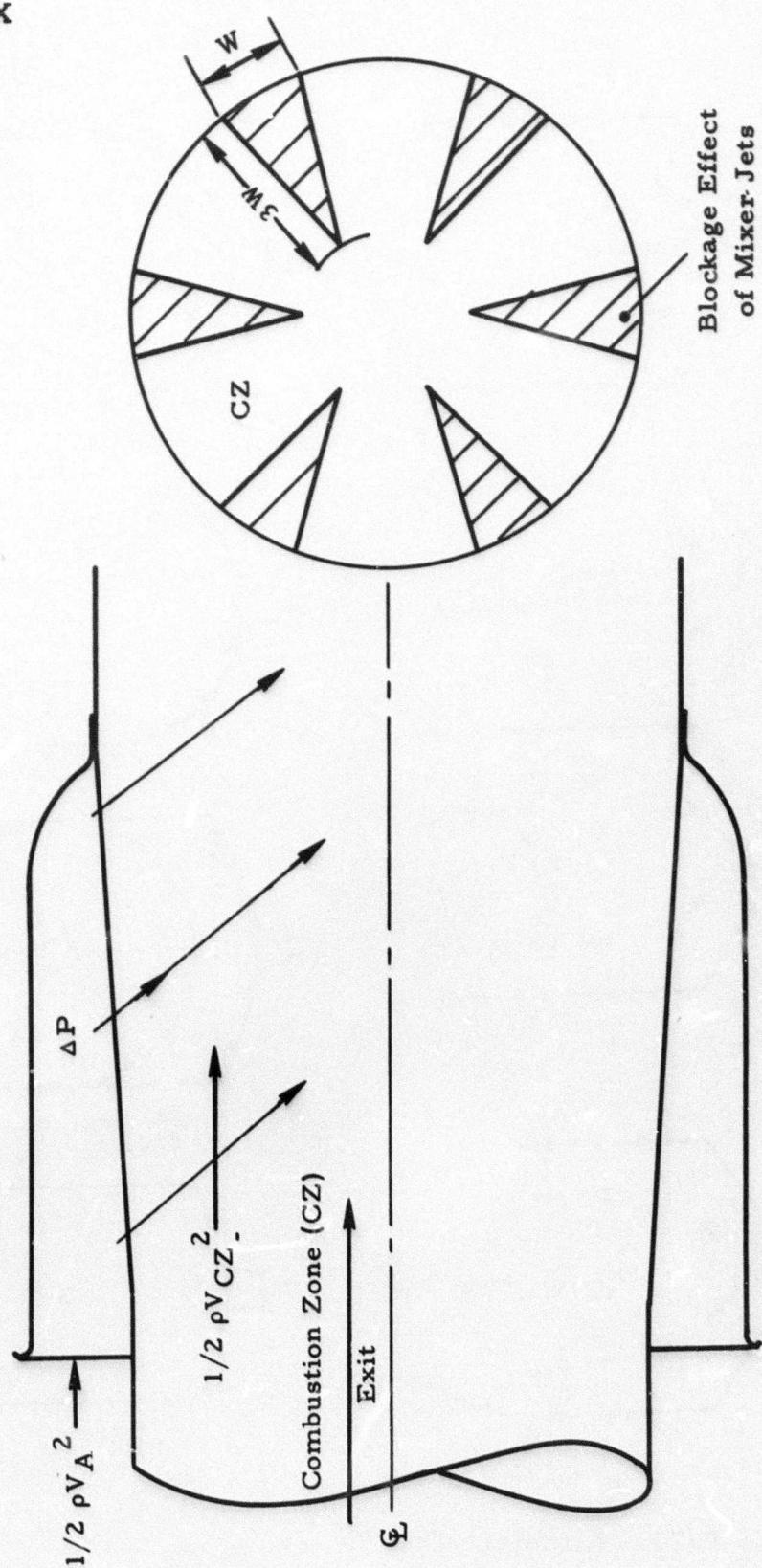


Figure X-74. Mixer Section Aerodynamics.

## Section X

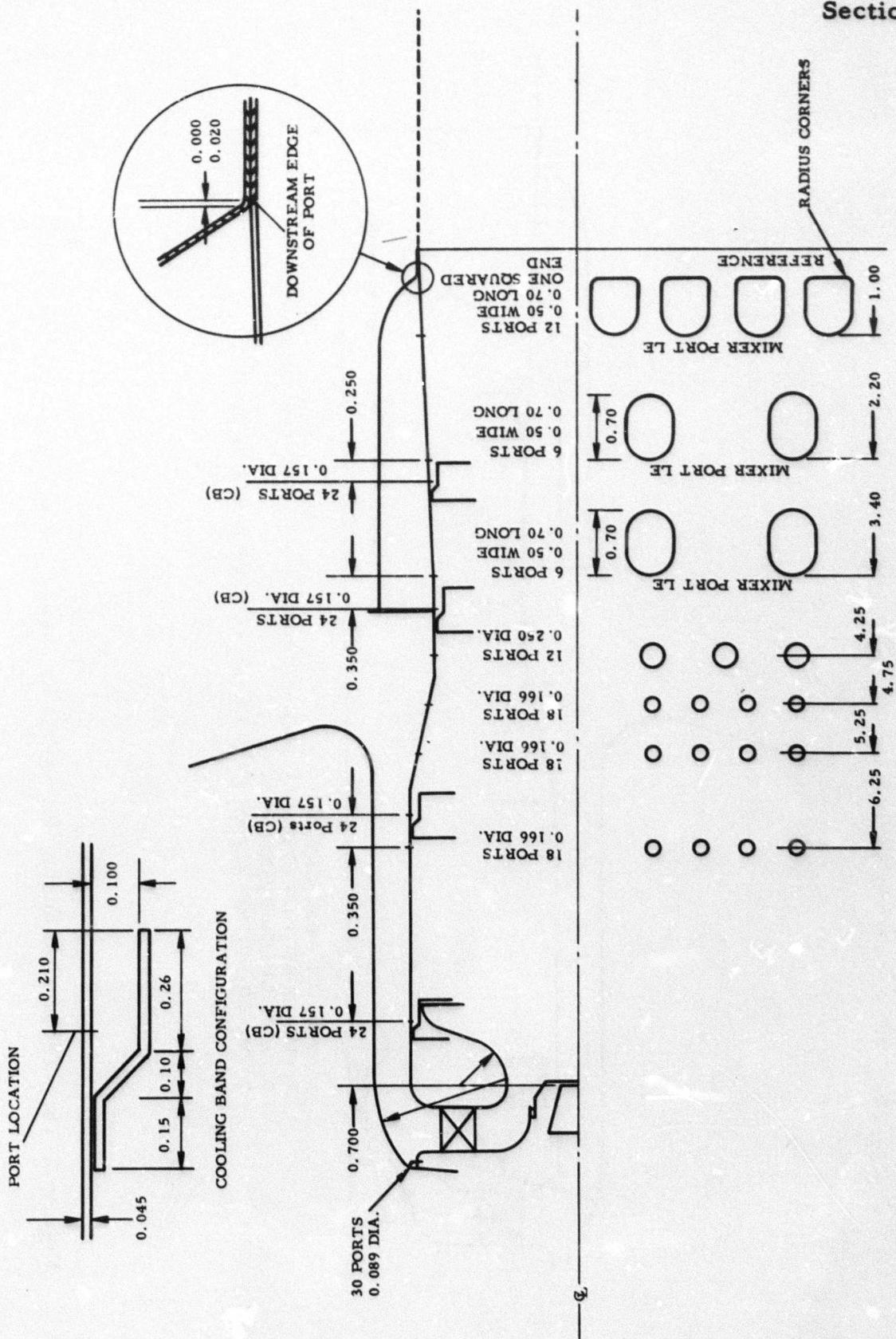


Figure X-75. TS120 Combustor Hole Pattern.

Section X

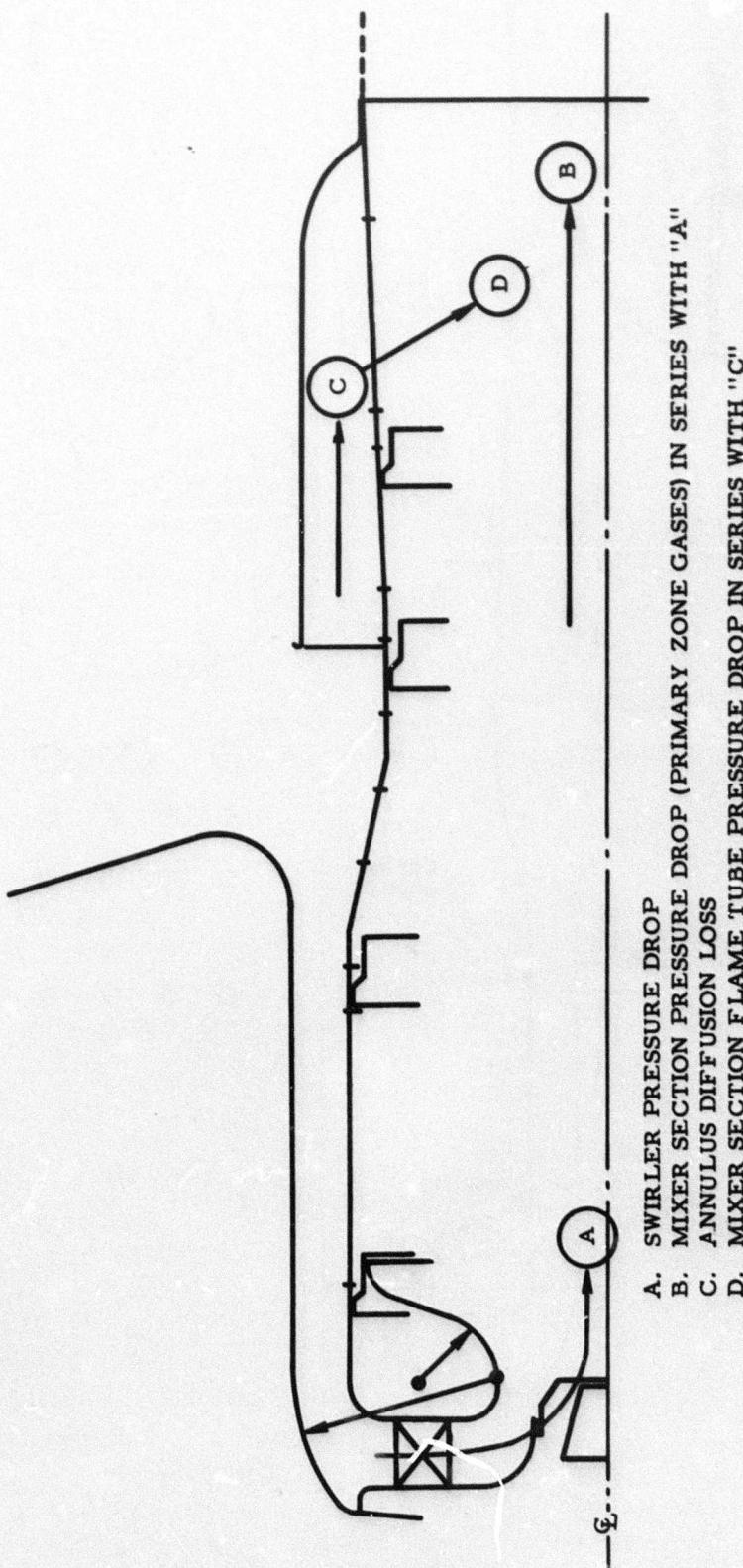


Figure X-76. TS120 Combustor Principal Pressure Losses and Flow Network.

Section X

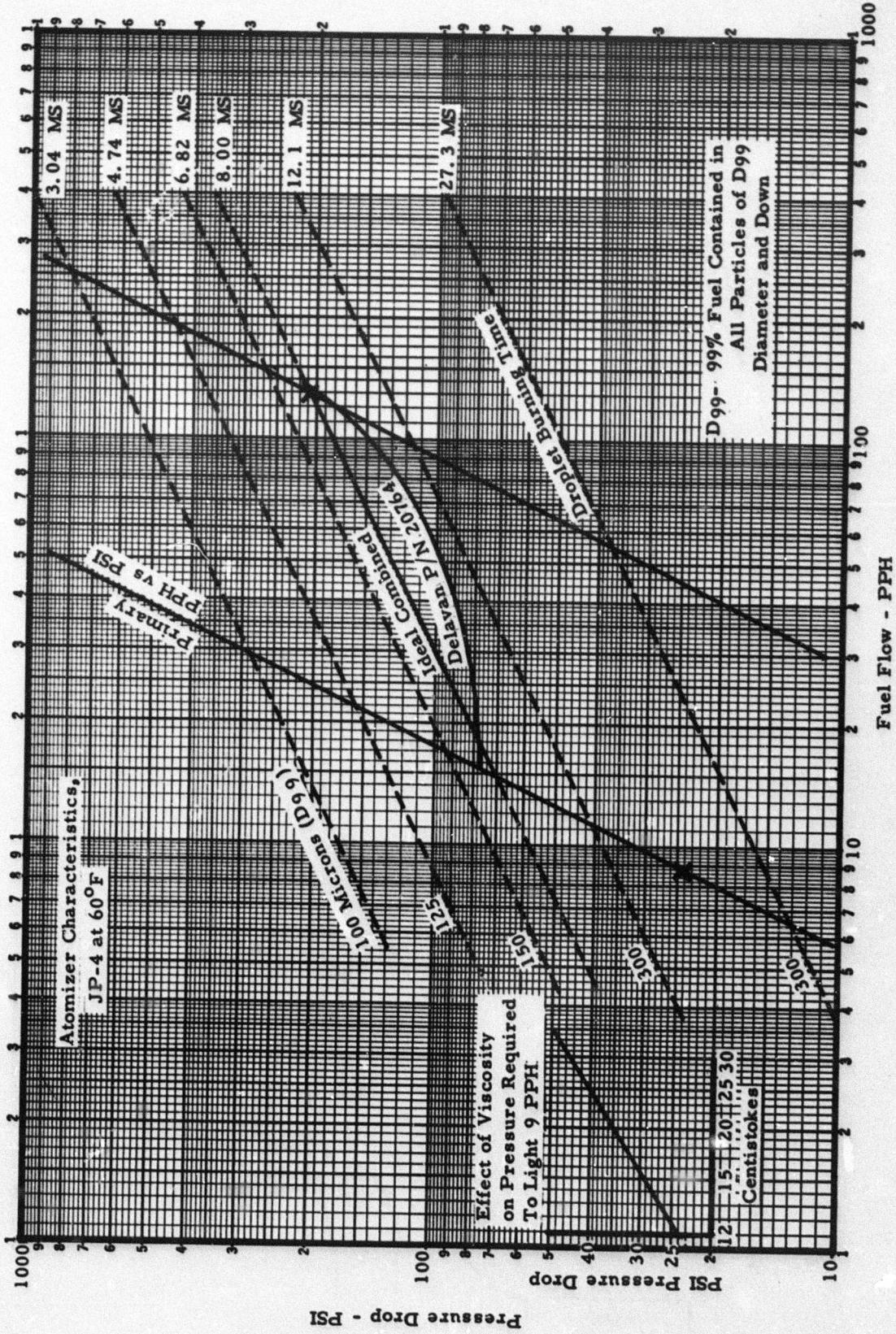


Figure X-77. Atomizer Characteristics JP4 at 60°F.

## Section X

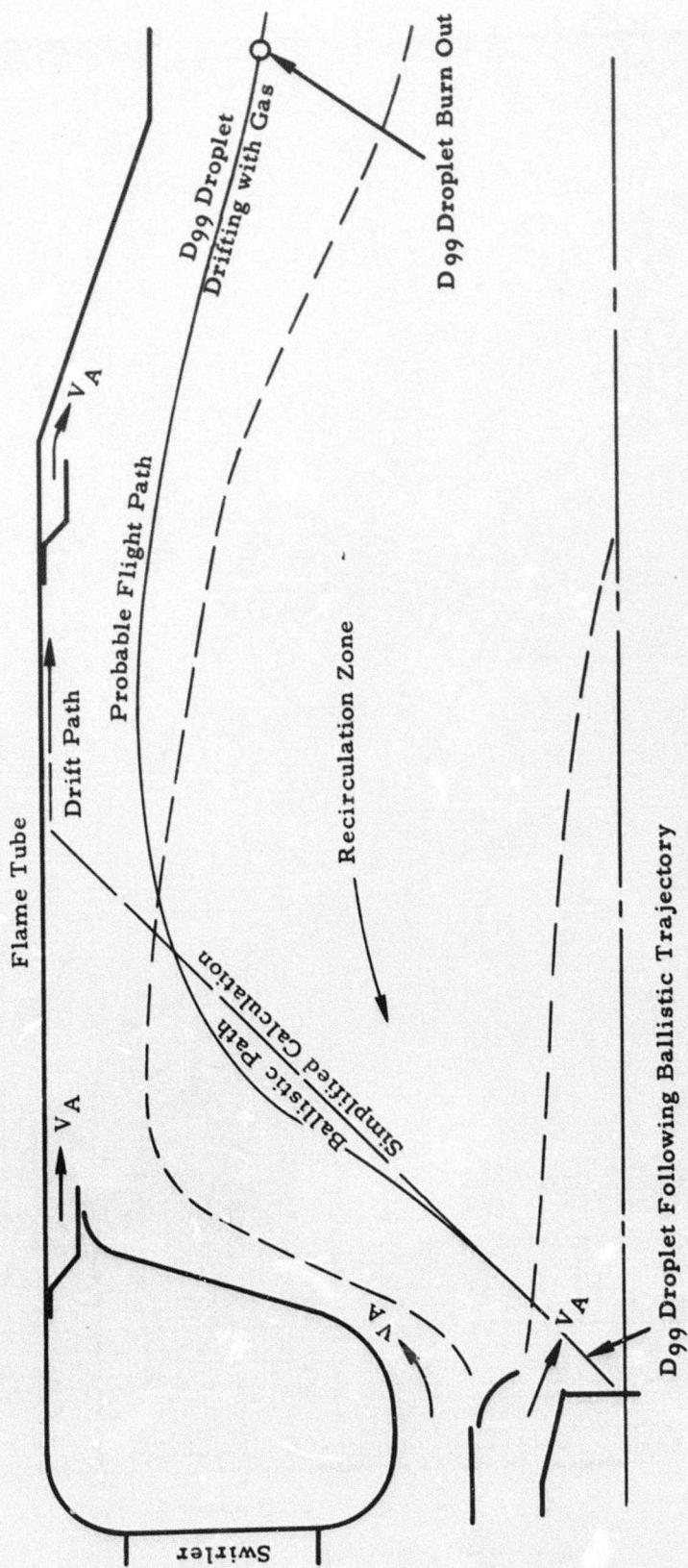


Figure X-78. Fuel Droplet Trajectory.

## Section X

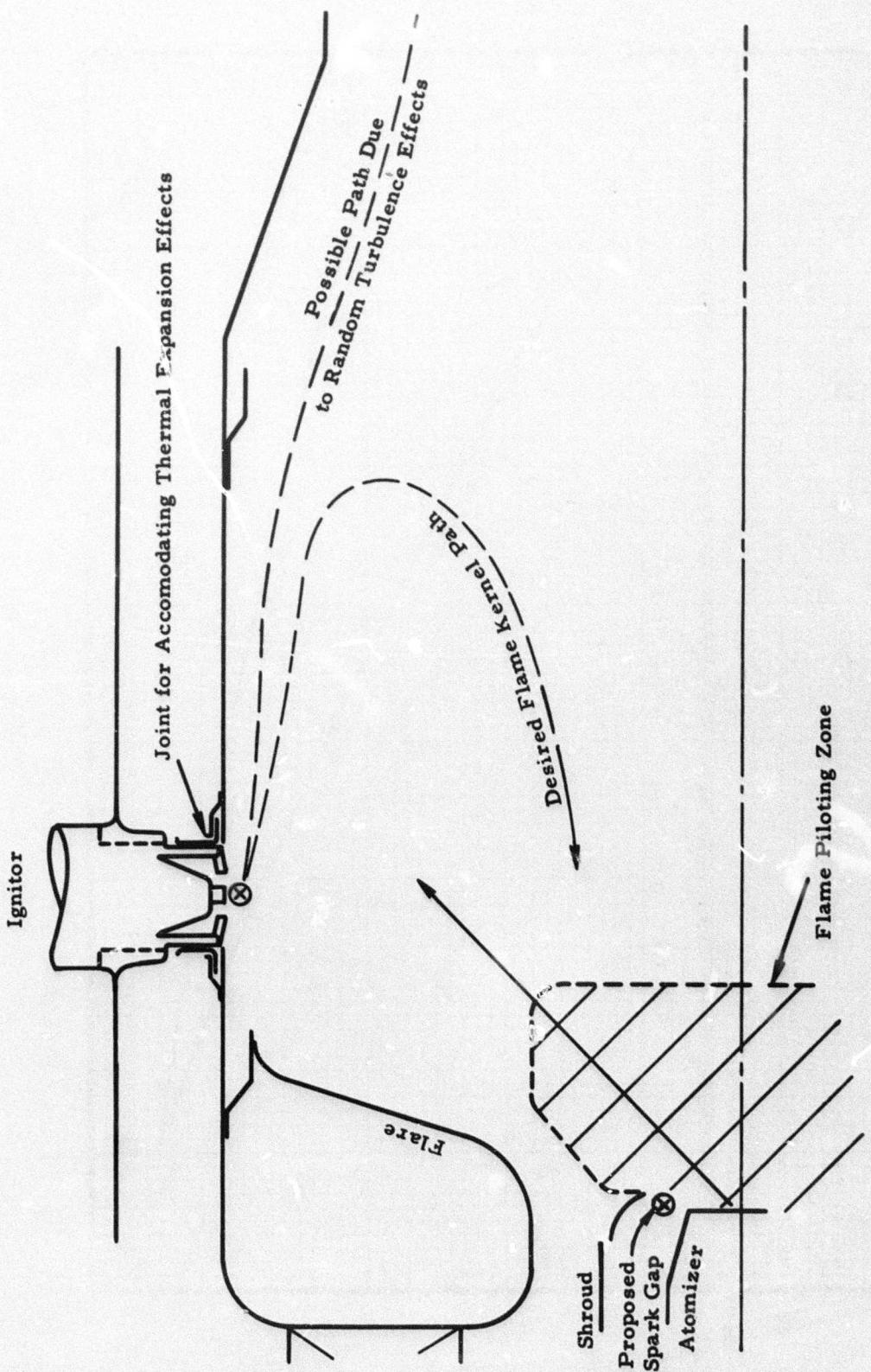


Figure X-79. Ignition Aerodynamic Characteristics.

Section X

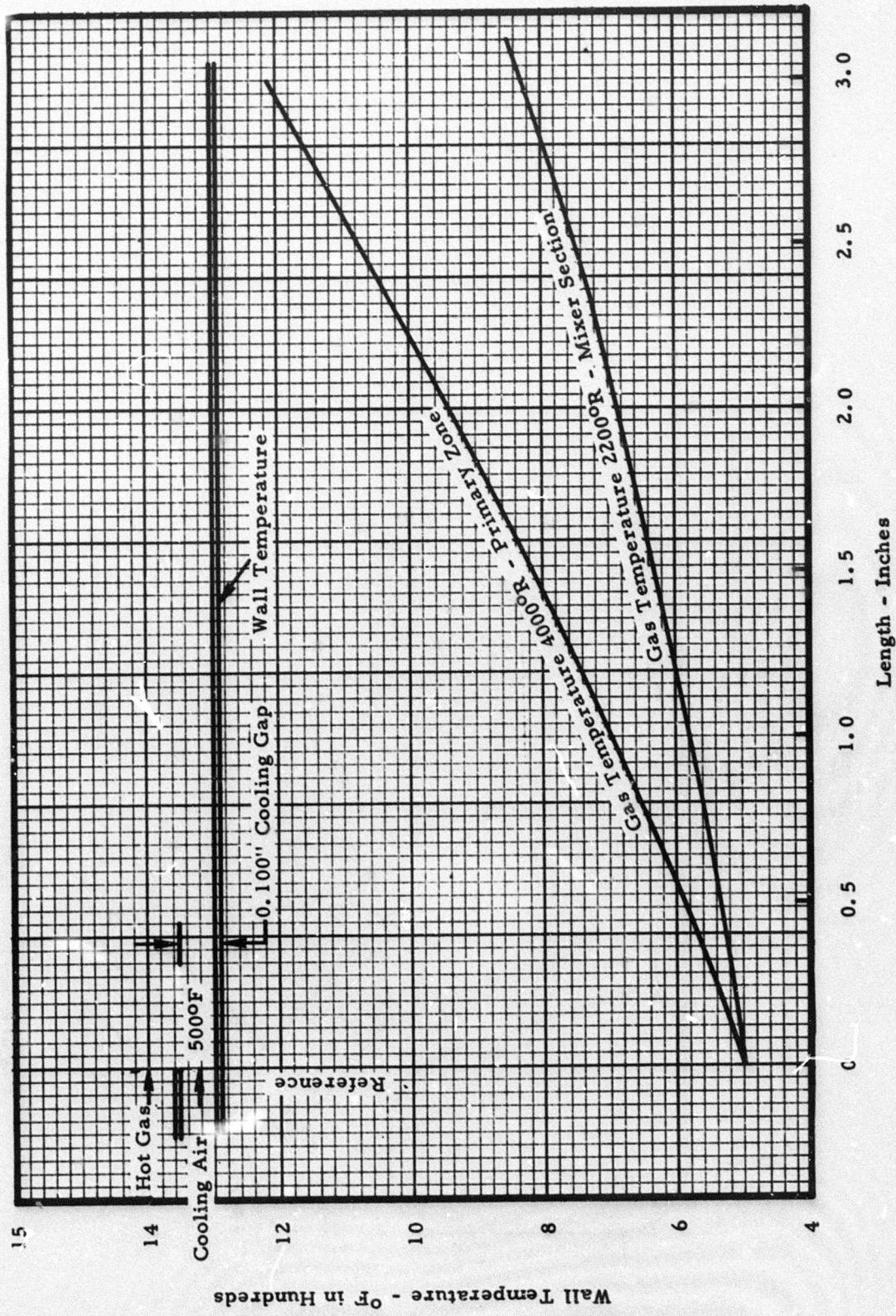


Figure X-80. Variation of Flame Tube Wall Temperature With Distance Downstream of B and No Radiation and No External Connection.

Section X

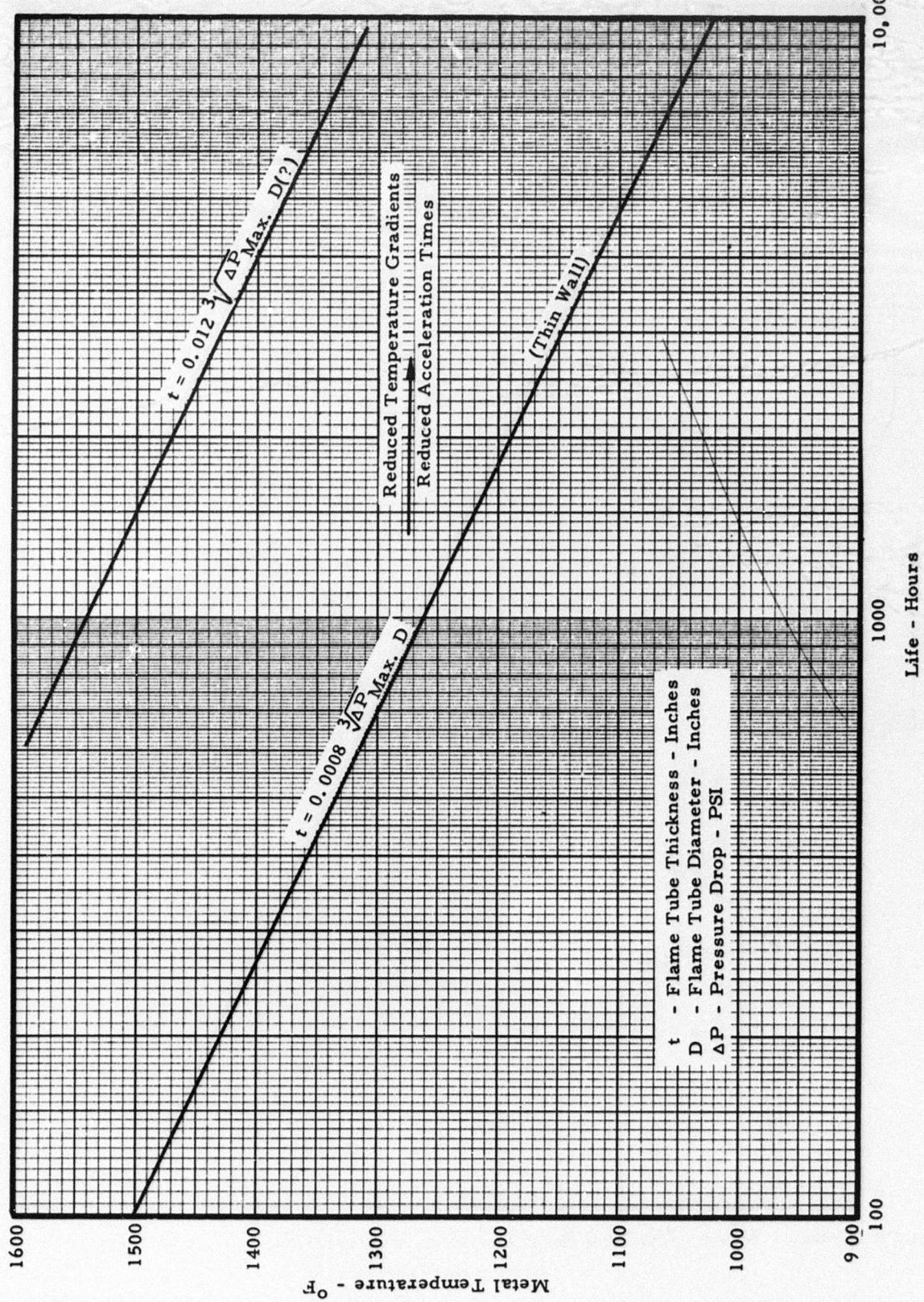
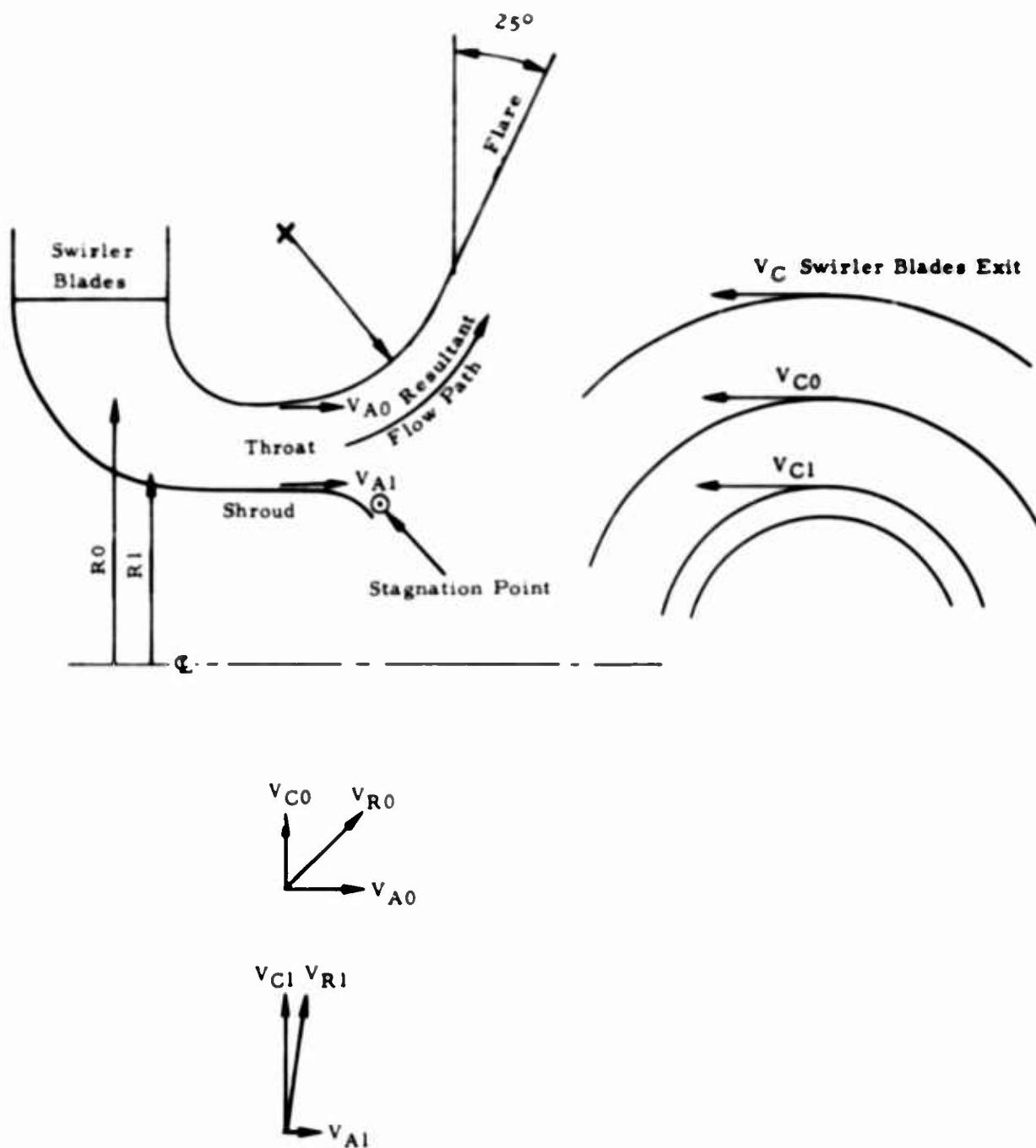


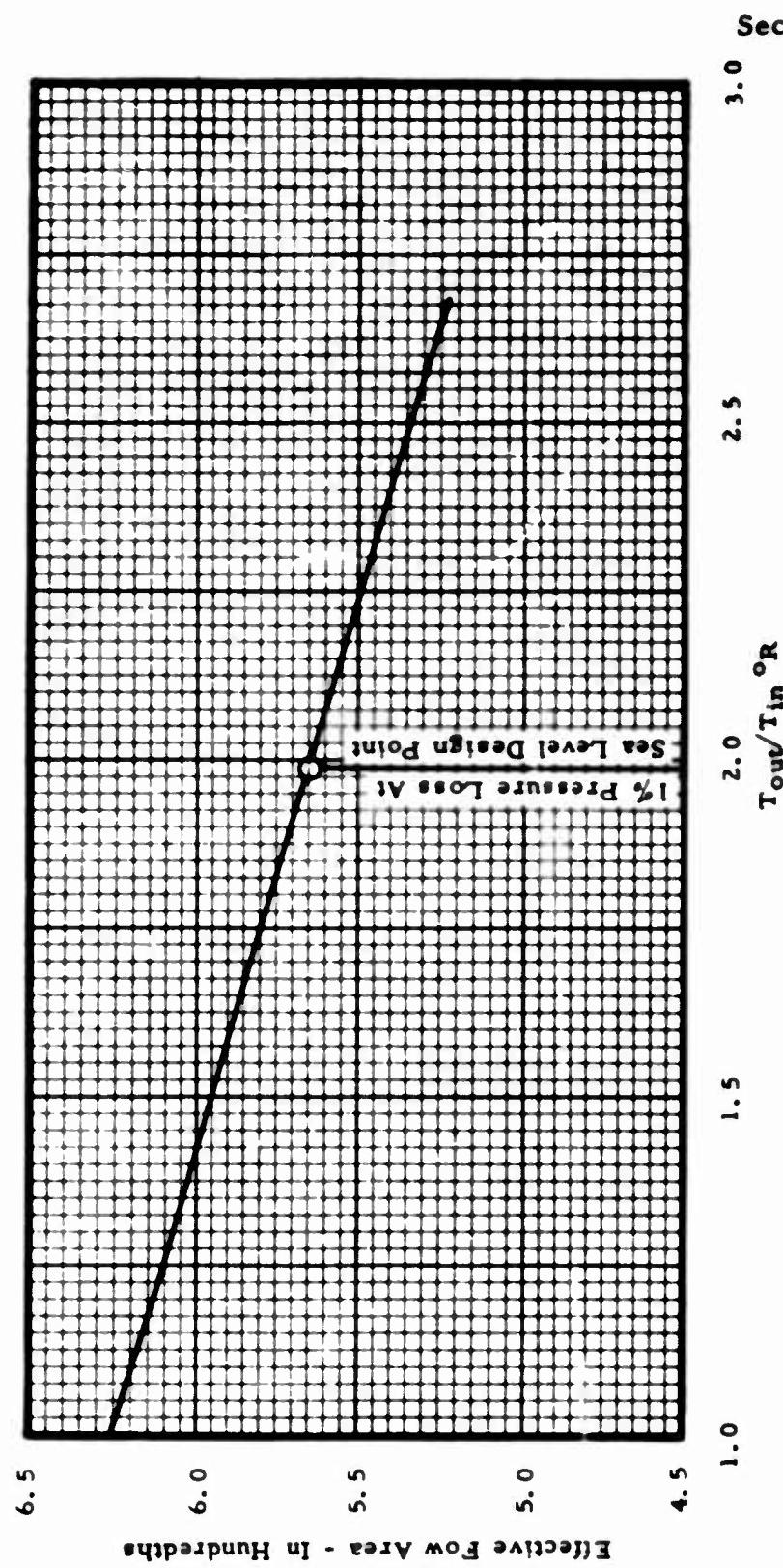
Figure X-81. Flame Tube Life Versus Metal Temperature (Hastelloy X) and Flame Tube Thickness for 5000°F Cooling Air.

**Section X**



**Figure X-82. Free Vortex Swirler Air Velocities.**

Figure X-83. Effective Flow Area Versus Combustor Temperature Ratio.



**Section X**

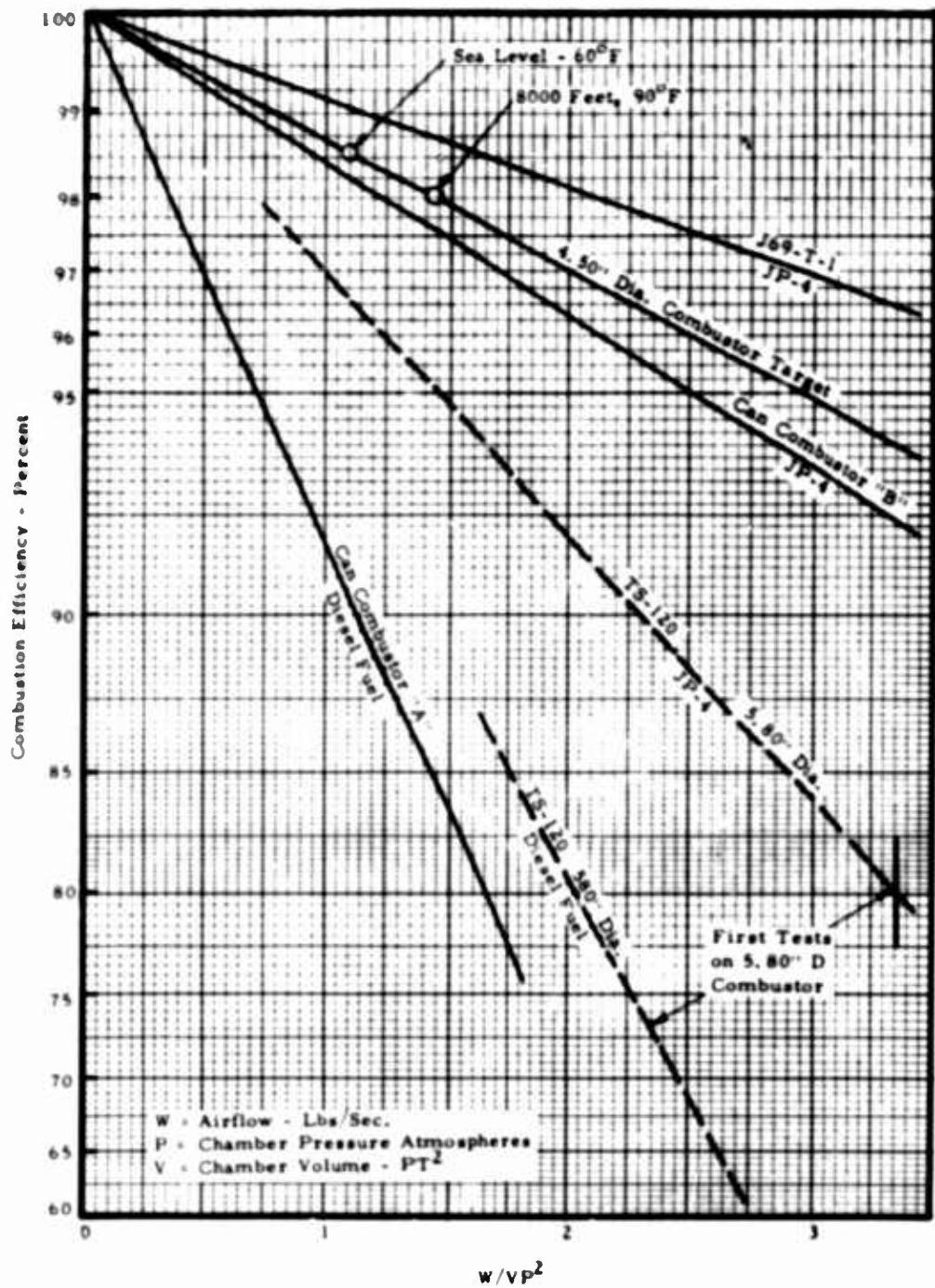


**Figure X-84. Aerodynamic Loading Versus Combustion Efficiency.**

**Section X**

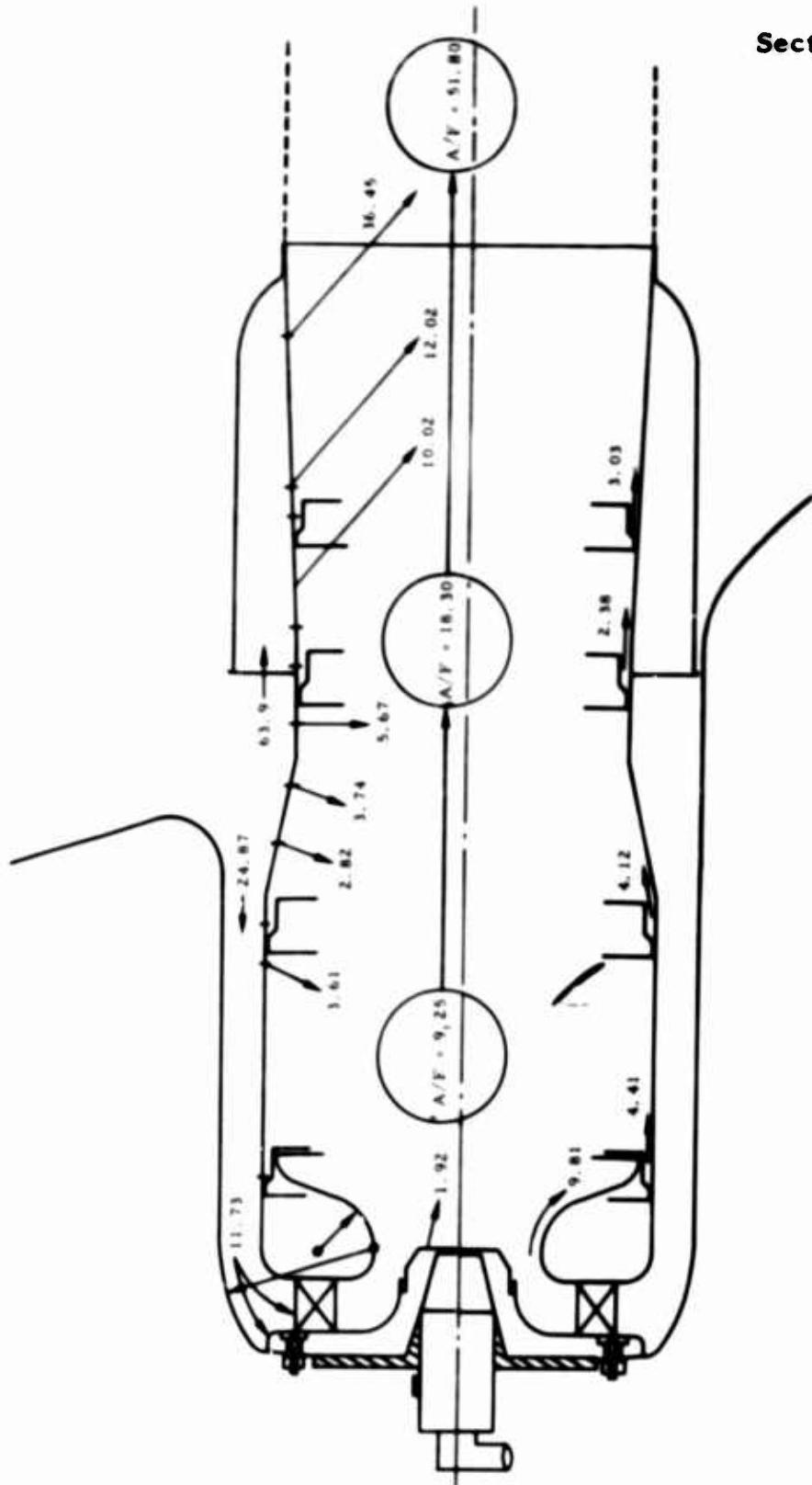


Figure X-85. TSI20 Combustor Air Distribution (Percent) and Air/Fuel Ratios.

APPENDIX X-A

## APPENDIX X-A - PURCHASE DESCRIPTION REQUIREMENTS

### CYCLE REQUIREMENTS

Table X-A-I lists the cycle parameters which have a bearing on the combustor design.

TABLE X-A-I

#### COMBUSTOR DESIGN CYCLE PARAMETERS

Altitude, Temperature	Sea Level 60°F	8000 Ft. 90°F
Combustor Inlet Airflow Lbs/Sec. (W)	1.671	1.110
Pressure psia	83.7	59.7
Temperature °R	924	959
Fuel Flow pph	76.6	81.5
Combustor Outlet Temperature	1834°R	2210°R
Fuel/Air Ratio	0.01355	0.01920 (1)
Combustor Effective Flow Area for One Percent Pressure Loss - In. <sup>2</sup>	5.64 (1)	5.34
Fuel Loading pph/Atmosphere	13.43	20.10 (1)
Aerodynamic Loading	$\frac{W}{PV^2}$ (2)	1.095
		1.430 (1)

(1) Control Values

(2) Combustor Volume 0.047 Ft.<sup>3</sup>, P Atmospheres, W Lbs/Sec.

From these figures it is possible to conclude that the combustor must give high efficiency at fuel/air ratios up to 0.020, with an effective flow area of not less than 5.64 square inches.

## Appendix X-A

From the compressor map, with a minimum fuel flow of nine pph, the lean limit blowout (LLBO) fuel/air ratio must be less than 0.0026 (for zero combustion efficiency). That is the combustor burning range must approach 5.5/1.

### CONTRACT REQUIREMENTS

From Reference 1, the following pertinent facts are extracted.

The combustor is to be a single offset can with one atomizer and one igniter. The arrangement is to be such that the combustor can be replaced in 15 minutes.

In conjunction with a 1500-hour life and metal temperatures less than 1500°F, the temperature pattern at the combustor outlet must be sufficiently uniform so there is less than 100°F between the maximum and minimum temperatures, and the combustor must be able to light 12 centistoke fuel.

The fuels to be burnt are:

MIL-G-3056	Combat Gasoline
MIL-J-5161	Jet, Referee
MIL-G-5572	80/87, 91/96, 100/130, and 115/145
MIL-J-5624	JP4 and JP5
MIL-F-45121	Compression Ignition and Turbine Referee
MIL-F-46005	Compression Ignition and Turbine
VVF-800	DF1, DF2, and DFA

## Appendix X-A

The most difficult objective here is the 100°F temperature spread, which is particularly difficult if the combustor size and/or pressure drop are restricted. The temperature spread usually arises from nonuniform air delivery and is minimized by increasing combustor pressure drop, (Reference 3), by using as many vortex mixing patterns inside the combustor as possible, and by increasing the mixing length between the combustor and the turbine inlet. Therefore, in a sense, the uniformity of air delivery, the combustor pressure drop and the required temperature spread have a direct control on the combustor size that must be adopted. The avenues left open are devices for improving the uniformity of air delivery (usually at the expense of pressure loss), and combustor designs which have improved mixing characteristics.

The next most difficult problem will be burning combat gasoline and VVF-800 DFA. These two fuels tend to leave deposits, and if this occurs in the flame tube, the sheet metal becomes thermally stressed and distorts until operation is impaired. The crucial point is to develop a deposit free combustor.

### ENGINE INTEGRATION REQUIREMENTS

From studies on the combustor and related parts of the engine, the following requirements became apparent.

First, because the combustor approach velocity head should be one half of the combustor pressure drop in order to obtain the most uniform air delivery (Reference 3), the compressor exit duct area should be more than eight square inches.

Second, in order to minimize the starter motor size, the combustor should light at the lowest possible gas generator speed. This implies lighting at low fuel flows to avoid over-temperaturering the hot end.

Third, in order to minimize fuel pump horsepower, the atomizer maximum fuel pressure should be as low as possible.

## Appendix X-A

Fourth, in order to light 12 centistoke fuel, with the least expensive igniter, the atomizer pressure drop at light off should be as high as possible.

The second, third and fourth requirements are conflicting and are added to the basic requirement of obtaining adequate atomization for combustion purposes. The result is that the atomizer selection becomes difficult, and a considerable part of the combustor development program will have to be devoted to selection of the atomizer.

Fifth, the combustor size affects engine weight directly and indirectly. Directly, the smaller the combustor, the lighter the combustor and case. Indirectly, the smaller the combustor, the more efficient the engine case becomes as a pressure vessel and the lighter the engine can be made.

Finally, the combustor size can have an effect on the turbine inlet volute pressure loss if the volute is made small to suit the combustor, rather than being made to a size to achieve a specific pressure loss.

## Section X

### TURBINE AND EXHAUST SYSTEM DESIGN

The turbine function is to drive the gas generator compressor and accessories, and to produce useful shaft horsepower with minimum fuel consumption. It must be efficient, light, compact, simple, rugged and inexpensive to manufacture. Serious consideration was given to axial, radial, and combinations, thereof, to best satisfy these requirements. Many of the objectives are obviously conflicting and, only as a result of a detailed study (Reference 8), was a single-stage radial flow turbine geometry derived. The aerothermodynamic design of this geometry and the associated ducting is detailed in the following sections.

#### Turbine

The design conditions at sea level static and 8000 feet are given in Figure X-3. These requirements were evolved by extensive matching calculations. Actual performance maps derived from test data on Continental's array of components were used for the over-all performance optimization. Details are given in the Aerodynamic Cycle Section.

The sea level information along with the geometry is translated into familiar turbine design parameters as:

Specific Work	$\frac{\Delta H}{\theta_{cr}}$	= 43.6	B Lb.
Referred Speed	$\frac{N}{\sqrt{\theta_{cr}}}$	= 35,910 rpm	
Flow Parameter	$\frac{WN}{S60}$	$\epsilon = 354.6$	Lb-Rev. Sec. <sup>2</sup>
Turbine Efficiency	$\eta_t$	= 88.1 percent	
Pressure Ratio	$\frac{P_{t1}}{P_{t4}}$	= 5.25	

## Section X

$$\text{Exit Critical Velocity Ratio } \frac{V_x}{V_{cr}} = 0.46$$

$$\text{Specific Speed } N_s = 70$$

$$\text{Specific Diameter } D_s = 1.44 \text{ feet}$$

$$\text{Tip to Eye Diameter Ratio } \epsilon = 1.58$$

$$\text{Isentropic Velocity Ratio } \frac{U_t}{C_o} = 0.656$$

Dimensional analysis and similarity relations have shown that

$N_s, \frac{U_t}{V_{cr}}, \frac{V_x}{V_{cr}}$  along with Reynolds number considerations

can uniquely define the attainable efficiency levels of turbomachinery components (References 9 and 10). Figure X-86 from Reference 9 gives the relationship between specific speed, specific diameter, spouting velocity ratio, and total to static adiabatic efficiency. The TS120 turbine design point is also superimposed and found to lie in the peak efficiency zone. Once the approximate similarity relationships are satisfied, the major portion of the turbine design consisted of:

- i. Establishing the turbine velocity triangles from work and flow conditions.
2. Fixing hub and shroud geometry.
3. Choosing the number of nozzle and rotor blades.
4. Specifying blade shapes and thickness distributions.
5. Minimizing, where possible, all the parasitic losses - evaluating relative effects especially with regard to over-all package, i. e., volute, nozzles, rotor and diffuser.

## Section X

6. Satisfying mechanical and thermal stress-life requirements simultaneously with the items above.

Velocity triangles were derived from the well known simplified axisymmetric equations of motion and energy, References 11 and 12. The principal equations are:

$$gJC_p \frac{\partial T}{\partial r} = gJ_t \frac{\partial s}{\partial r} + v_\theta \frac{\partial v_\theta}{\partial r} + \frac{v_\theta^2}{r} + v_x \frac{\partial v_x}{\partial r} - v_x \frac{\partial v_r}{\partial x}$$

(radial equilibrium equation) (1)

$$W = 2\pi g \int_{A_h}^{A_t} \rho V A dA = \text{const. (continuity equation)} \quad (2)$$

$$gJ\Delta H = \Delta UV_\theta = gJC_p\Delta T \quad (\text{energy equation long a steamtube}) \quad (3)$$

Minimizing exit diffuser and strut losses required near zero whirl and a low leaving velocity. The outlet average critical velocity ratio was

$\frac{V_x}{V_{cr}}$  set at  $= 0.46$  as a suitable compromise of loss and exducer

stresses. This resulted in an exducer stress parameter of  $A_4 N^2 = 3.54 \times 10^8$  which was deemed satisfactory for structural requirements. The hub, mean, and tip velocity diagrams for both the sea level static and 8000 feet altitude design conditions are given in Figures X-87 and X-88. The rotor flow path was then optimized to attain the best compromise of aerodynamic blade loading.

Once the design point is fixed, the principal methods of velocity variation are restricted to meridional flow path shape, blade angle distribution and number of blades. Systematic variation of all three parameters were conducted. Velocities were determined at the hub and shroud and also on the driving and trailing faces of the blading. Over 30 variations were generated before suitable blade loading was achieved. Figures X-89 and X-90 give the sea level and altitude design point rotor

## Section X

velocity distributions while the geometry is shown in Figures X-91 and X-92. The streamlines in the meridional plane are also superimposed on Figure X-91.

The number of blades was fixed at 17 from the above detailed aerodynamic study and stress requirements. An approximate verification is also given by Zweifel's coefficient of 0.8 for optimum aerodynamic loading, Reference 13. It is defined as

$$\Phi = 0.8 = \frac{4\pi}{Z_r} \frac{R_4 h_4}{S} \cos^2 \alpha_4 \left[ \tan \alpha_4 - \frac{R_3}{R_4} \frac{W_{3x}}{W_{4x}} \tan \alpha_3 + \frac{U_4}{W_{4x}} \left( \frac{R_3^2}{R_4^2} - 1 \right) \right] \text{(see list of symbols)}$$

Using the sea level velocity triangle values gives a  $Z_r \approx 17$ .

### Nozzle

Aerodynamic criteria similar to that used on the rotor was used on the nozzle. Test information on existing Continental hardware fulfilling the design requirements, was also utilized. Figure X-93 shows a conformal transformation of a 30-vane version of the nozzle, and Figure X-94 shows the agreement of theoretical to experimental mean velocities. Conformal mapping techniques were used to supplement the blade load analysis (see Reference 14 for equations of mapping). Subsequent analysis showed that 25 vanes could be used without separation.

Figure X-95 shows a comparison of blade loading diagrams for the two versions. As the number of blades is decreased, the blade loading increases and suction side velocities increase rapidly. The suction side, downstream of the throat, is a particularly troublesome region because the vanes must be unloaded at the trailing edge. If too few vanes are used, a severe diffusion zone develops resulting in separated flow and accompanying high losses. On the basis of loading considerations, the vane number was fixed at 25. Figure X-95 presents the nozzle geometry finalized for the TS120 turbine.

## Section X

A low drag, symmetrical, airfoil shape was used for the vanes. Thickness distribution is defined by the NACA 65 - series applied to a nine percent thickness to chord ratio.

To maximize efficiency, a far thinner trailing edge thickness than shown, is desirable. Ease of casting and requirements of ruggedness and resistance to foreign object damage are conflicting factors in favor of thick trailing edges. A review of the aerodynamics of this machine showed that significant penalties are paid, even for a 0.020-inch thickness. A loss comparison analysis of a "desired" 0.007-inch T. E. and a "more practical" 0.020-inch T. E. is as follows:

Pressure losses across a nozzle are expressed as

$$Y_{Tot} = \frac{P_1 - P_2}{P_2 - p_2}, \text{ where}$$

$P_1$  = Inlet total pressure

$P_2$  = Exit total pressure

$p_2$  = Exit static pressure

$T_{Tot} = 0.0558$  is the design value (based on experimental data) used for a 0.007-inch T. E. 25 vane cascade. Increasing the T. E. to 0.020 gives a  $\Delta Y_{Tot} = 0.008$ , or an increase in pressure loss of 14 percent. The loss increase is exponential and particularly sensitive because of the very low nozzle setting angle (see Reference 15 for T. E. loss evaluation effects). The associated loss penalty of a 0.020-inch T. E. thickness was found to be within the limits of performance acceptability.

Another factor which was emphasized in this design was dimensional adherence. Because of the small size and low setting angles, the flow capacity and performance is drastically affected by tolerances which are acceptable on most other machines. The total nominal throat area on the TS120 nozzle is less than two square inches.

## Section X

If the average setting angle is off by only one degree, this turbine will increase its flow capacity by nine percent. (This has been verified in rig testing of a similar, large version, radial turbine.) This means rigorous dimensional adherence and calibration of each nozzle and rotor assembly to specified limits.

In view of this aerodynamic sensitivity, the clearances, thermal, and mechanical growths were also evaluated for nozzle stagger change.

### Turbine Volute

The primary function of the volute is to uniformly feed the nozzles with minimum loss and pressure gradients. This must be done with a suitable compromise of size and loss. The usual treatment of scrolls is to use the compressible flow relations and to make the simplifying assumption of constant angular momentum with corrections for pressure loss and blockage factor, Reference 16. This procedure was followed in the design of the TS120 volute. Once the loss is specified, integration permits the area distribution to be evaluated as a function of angular displacement, Figure X-97.

Pressure loss data on turbine volutes are scarce. The usual treatment is, therefore, to apply conventional pipe loss data in incremental lengths and to sum up these losses either by calculus or by numerical integration. One of the classical solutions of a circular type cross-section is that given by Eckert (Reference 17). The simplified version of this method assumes incompressible flow and mathematically sums up the pressure losses via a combination of conservation of angular momentum and conventional straight pipe friction theory. Since the Mach numbers are generally low ( $M_u = 0.3$ ), this type of analysis is adequate for friction loss estimation.

If a near circular cross-section is assumed, the pipe friction loss is given by

$$h_f = K \lambda C_{r1} C_{lu}^2 \ln \left[ \frac{\sqrt{2r_1 C} + 3 \sqrt{\theta_1}}{\sqrt{2r_1 C} + 3 \sqrt{\theta_0}} \right] \quad \text{where} \quad (1)$$

## Section X

### English Units

$h_v$  = head loss ft.

$K$  = const.,  $0.904 \times 10^{-4}$

$\lambda$  = conventional pipe friction factor (see Ref. 18 or 19)

$$C = \frac{720 \pi (C_{l_u} r_1)}{V_1} = \text{ft.}^{-1}$$

$r_1$  = radius of nozzle leading edge ft.

$c_{l_u}$  = tangential velocity component at nozzle leading  
edge -  $\frac{\text{ft.}}{\text{sec.}}$

$\theta_0$  = start of volute degrees

$\theta_1$  = end of volute degrees

This loss equation has been applied to the TS120 volute and its results reconfirmed by station to station numerical integrations. The resulting pressure drop expressed as a percentage of the inlet head is 0.9 percent for dirty pipe and 0.7 percent for clean pipe. An additional loss factor has been provided to account for the component of turning the gas flow into turbine nozzle direction. A realistic analysis should consider this factor. Pipe turning loss data has therefore been incorporated in the theory. Appendix X-B gives this derivation. Summing the turning and pipe friction losses gives a  $\Delta P/p$  of 1.3 and 1.1 percent for dirty or clean, pipe, respectively.

Summarizing the parameters pertinent to the volute design,

## Section X

$w_g$  = 1.69 gas flow - lbs/sec.  
T = 1834 inlet temperature - °R  
P = 81.1 psia inlet pressure  
D = 3.3 in. inlet diameter to volute  
 $M_{in}$  = 0.12 inlet Mach No. to volute  
 $M_{exit}$  = 0.196 exit Mach No. from volute  
Nr  $\approx$  340,000 average Reynolds number  
 $\frac{E}{D}$  = 0.0036 to 0.007 relative roughness factor for smooth pipes.

### Exhaust System

In any turbine powerplant designed to drive a generator, considerable attention must be devoted to the performance of the exhaust diffuser system so that a maximum amount of energy is available for useful output. Figure X-98 shows the results of excess exhaust pressure loss on specific fuel consumption.

As stated in the Purchase Specification - "The turbine exhaust system shall incorporate provisions for axial and radial direction of exhaust gases for both the simple cycle and regenerative cycle engine configuration. The preferred design is an axial exhaust with a bolt-on or clamp-on collector to discharge the exhaust radially. The radial exhaust design shall be capable of directing the exhaust upward or to either side...".

## Section X

### AXIAL EXHAUST DIFFUSER

The diffuser inlet flow conditions dictated from cycle analysis and component optimization are as follows:

Inlet total pressure ( $P_5$ )	= 15.3 psia
Inlet total temperature ( $T_5$ )	= 1281°R
Gas flow ( $W_g$ )	= 1.694 Lb-M/Sec.

Turbine design and rear bearing size have predetermined the inlet geometry of the diffuser as well as the characteristic flow path. They are as follows:

Inlet outside diameter	= 4.276 inch
Inlet inside diameter	= 1.932 inch
Inlet critical velocity ratio, $\frac{V_x}{V_{cr}}$	= 0.46

Theoretical methods, either exact or approximate, do not exist that allow a direct solution to the design of a diffuser with completely predictable results. The design approach to the TS120 exhaust duct is therefore based on the application of the fundamental aerodynamics involved, the use of empirical data and a combination of Continental's previous diffuser experience.

Test data on annular diffuser losses of Continental and NACA configurations is shown in Figure X-99. Preliminary calculations revealed that an area ratio of 3.0 would best define a diffuser to meet the TS120 design requirements.

The centerbody shape was dictated by rear bearing compartment size. This compartment must be supported by hollow struts used for oil supply and scavenge. Three equally spaced, constant section, airfoil shape struts were used for this purpose, Figure X-100. The thickness - chord ratio of 17 percent has been used in previous Continental diffuser tests, Reference 20, with satisfactory performance. A trial and error procedure was then used to match area

## Section X

distribution and equivalent cone angle corresponding to a proven Continental diffuser. The inner and outer walls have been "bumped" to maintain a steady area variation through the strut section. Continental tests, Reference 20, showed improved performance when the flow area was relieved through this region.

With an initial assumption of unseparated flow, the velocity distributions were calculated on the hub and shroud, Figure X-101. Contour modifications were made to delay separation for a best compromise of over-all effectiveness. Figures X-102 and X-103 give the area distribution and equivalent cone angle as a function of axial distance.

Exhaust diffuser losses are expressed in various forms in the literature. Some of the more frequently used simplified parameters are:

a. Total-pressure-loss coefficient ( $\frac{\Delta P}{P}$ ).

$$\frac{\Delta P}{P} = \frac{P_5 - P_e}{P_5} . \text{ This coefficient is actually a combination of two separate losses, i.e., the total pressure loss in the diffuser plus the leaving loss in the diffuser.}$$

b. Diffuser effectiveness ( $\omega_e$ ).

$$\eta_e = \frac{P_e - P_5}{q_5 (1 - [A_5]^2)} . \text{ The diffuser effectiveness is defined as the actual gain in static pressure within the diffuser divided by the ideal gain in static pressure within the diffuser.}$$

## Section X

### c. Diffuser recovery ( $\eta_R$ ).

$$\eta_R = \frac{P_e - P_5}{q_5} . \text{ The diffuser recovery is defined as}$$

the actual gain in static pressure gain within the diffuser divided by the dynamic velocity head at the diffuser inlet. The three performance coefficients evaluation in this design are therefore estimated as:

$$\frac{\Delta P}{P} = \frac{P_5 - P_e}{P_5} = 0.0415$$

$$\eta_\epsilon = \frac{P_e - P_5}{q_5 \left( 1 \left[ \frac{A_5^2}{A_e} \right] \right)} = 0.765$$

$$\eta_R = \frac{P_e - P_5}{q_5} = 0.69$$

There are other factors that determine whether this performance can be met. Losses and distribution are affected by the inlet boundary layer, whirl, total pressure and temperature gradients, and straightening by the support struts. These unknowns can only be evaluated by actual test. During Component Development, a scale model of this diffuser will be flow tested. Inlet gradients will be simulated by a radial flow turbine preceding the model. Figure X-104 gives a layout of the test rig.

In conjunction with the above factors, a scheme of ribbed walls will also be studied and tested. The ribbed diffuser design techniques published in Soviet open source literature, References 21 and 22, will be investigated. This method of increasing the efficiency of diffusers

## Section X

with intensive flow separation has been applied primarily to wide angle diffusers ( $2\theta \geq 40^\circ$ ) (the Soviet report indicates that negative effects could be obtained with angles below  $2\theta = 20^\circ$ ). The prime interest in the case of the TSI20 exhaust duct is the possible use of fins to produce a more uniform velocity profile at the diffuser exit for lower over-all losses.

### RADIAL EXHAUST DIFFUSER

Since the flow conditions at the exit of the axial diffuser will not be known until test results are available, the approach to the radial exhaust design was simply to make preliminary estimates to indicate nominal size and length requirements.

Three radial exhausts were considered worthy of a preliminary analysis. They are (1) a two path volute collector, Figure X-105, (2) one path volute collector, Figure X-105, and (3) right angle turn, Figure X-107.

The three versions were all sized to produce the same design point engine power and fuel consumption. The two path volute collector version appears to be the smallest and lightest of the three. It is conceivable that an engine loading schedule could result in a unidirectional swirl from the turbine exit. If this would be the case, a one path volute collector would show much better part power fuel consumption. Geometries 1 and 3, on the other hand, will be better for a wide range of loading. Final selection of the geometry will be predicated on these factors and the results of component testing of the axial diffuser model. The loss estimate of the radial exhaust system is estimated as:

$$\frac{\Delta P}{P} = \frac{P_5 - P_e}{P_5} = 0.060$$

## Section X

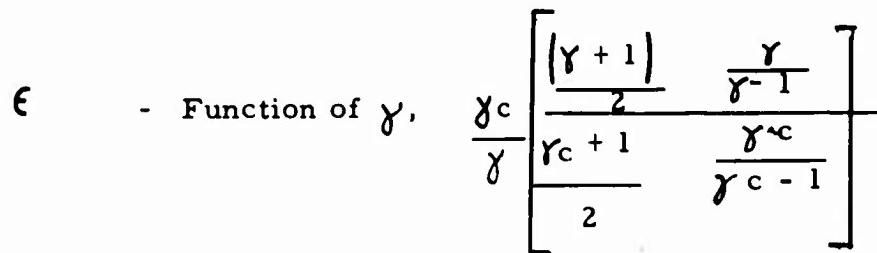
$$\eta_E = \frac{P_e - P_5}{q_5 \left[ 1 - \left( \frac{A_5}{A_e} \right)^2 \right]} = 0.61$$

$$r = \frac{P_e - P_5}{q_5} = 0.51$$

### LIST OF SYMBOLS

$\Delta H$  - Total to total enthalpy drop  $\frac{B}{Lb.}$

$\theta_{cr}$  - Squared ratio of critical velocity at turbine inlet to critical velocity at NACA standard sea level temperature.



$\gamma$  - Ratio of specific heats

$H_{ad}$  - Total to static adiabatic head

$C_o$  - Velocity head corresponding to  $H_{ad}$ , fps

$U_t$  - Impeller tip speed, fps

$N$  - Rotational speed, rpm

$Q$  - Volume flow from exit of turbine, cfs

## Section X

$$N_s = \frac{N \sqrt{Q}}{H_{ad}^{3/4}}$$

$$D_s = \frac{D_s H_{ad}^{1/4}}{\sqrt{Q}}$$

$Z_r$  - Number of rotor blades

$Z_n$  - Number of nozzle blades

$S$  - Meridional blade surface area  $\times R_s$ , In.<sup>3</sup>

$h$  - Blade height, in.

$R$  - Average radius, in.

### SUBSCRIPTS

1 - Nozzle Leading Edge

2 - Nozzle Trailing Edge

3 - Rotor Leading Edge

4 - Rotor Trailing Edge

5 - Diffuser Entrance

6 - End of Axial Diffuser

7 - End of Radial Diffuser

e - Exit

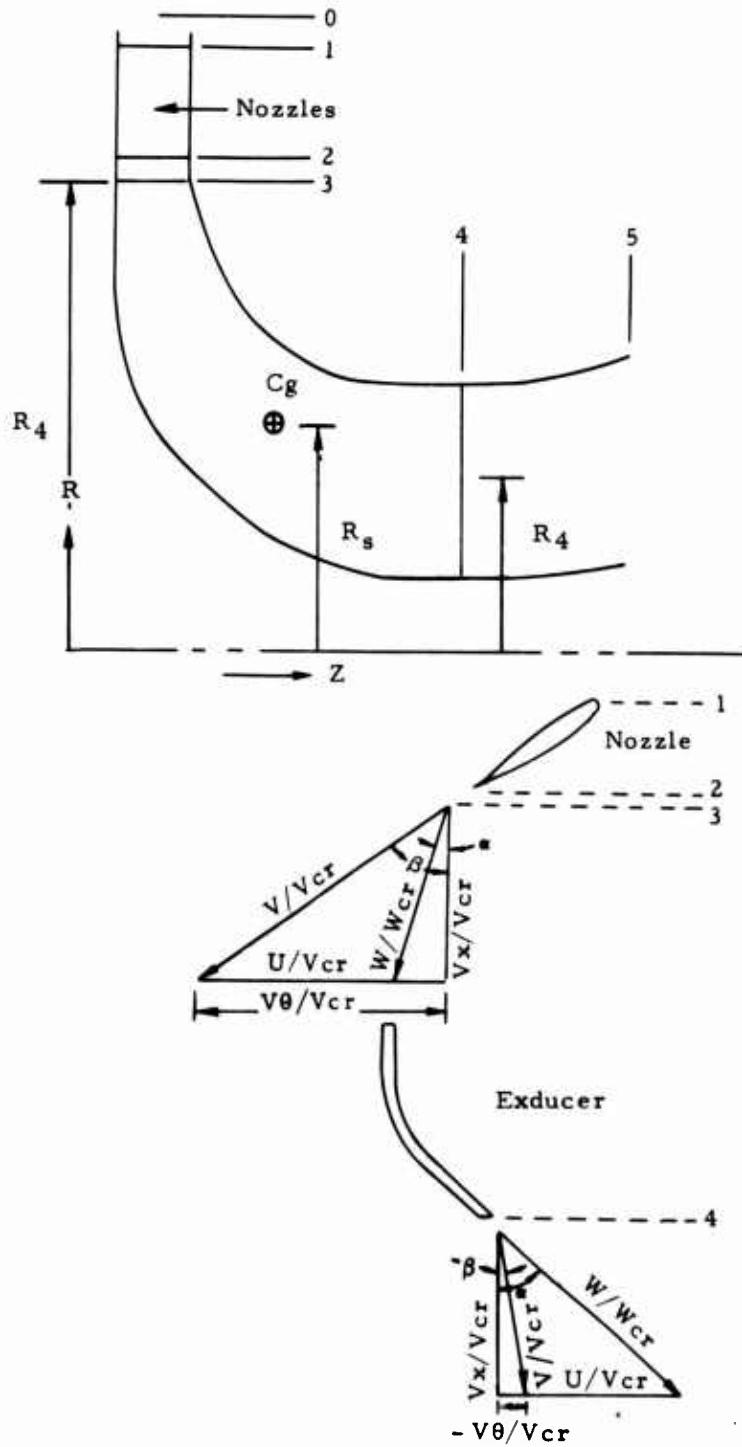
cr - Critical

## Section X

t	- Tip
h	- Hub
x	- Axial
$\theta$	- Tangential
V	- Absolute velocity, tps
W	- Relative velocity, tps
P	- total pressure, psia
p	- Static pressure, psia
T	- Stagnation temperature, °R
t	- Static temperature, °R

## **Section X**

## NOMENCLATURE



Section X

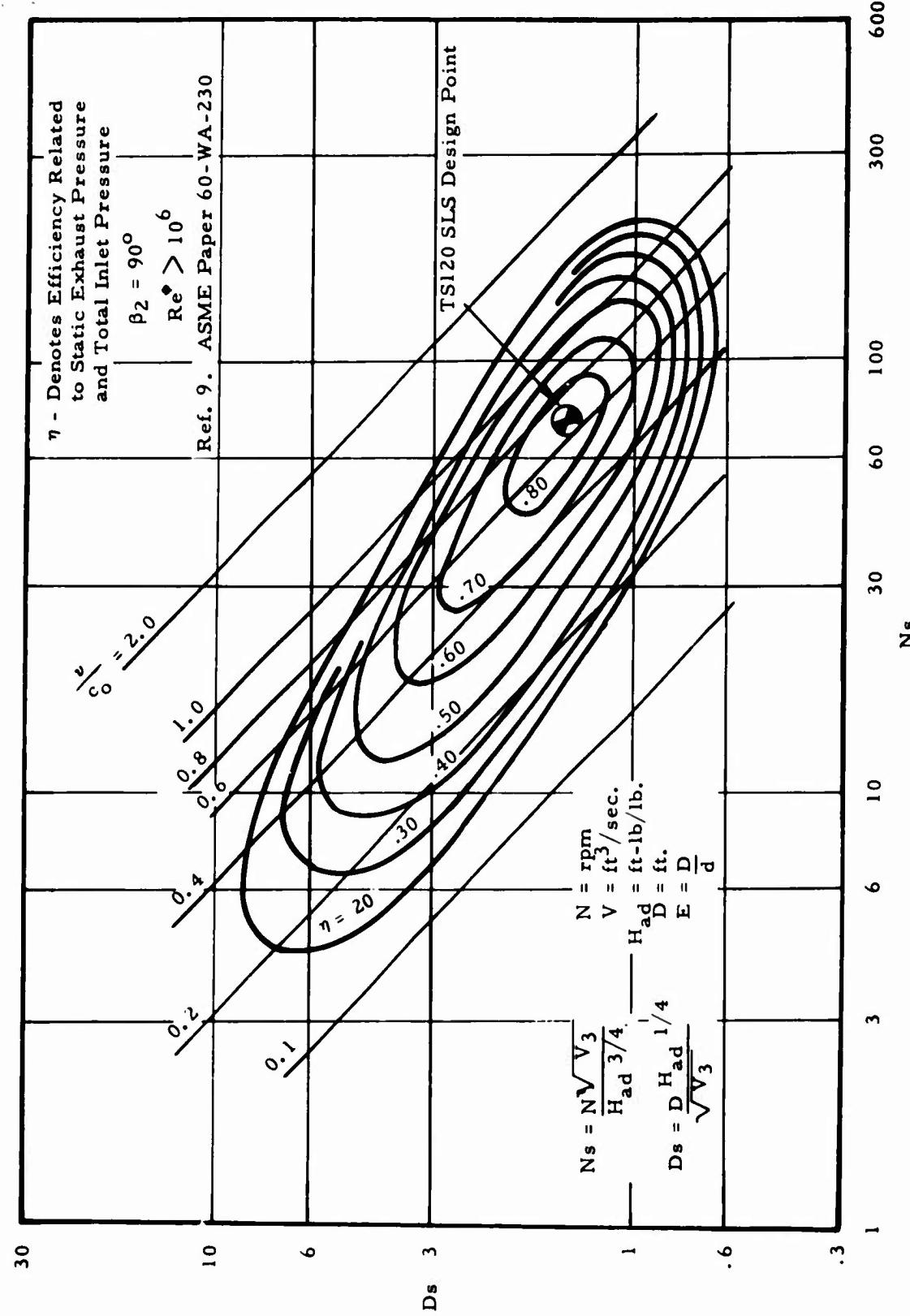


Figure X-86. Specific Speed Versus Specific Diameter Dimensionless Performance for Radial Turbines.

## Section X

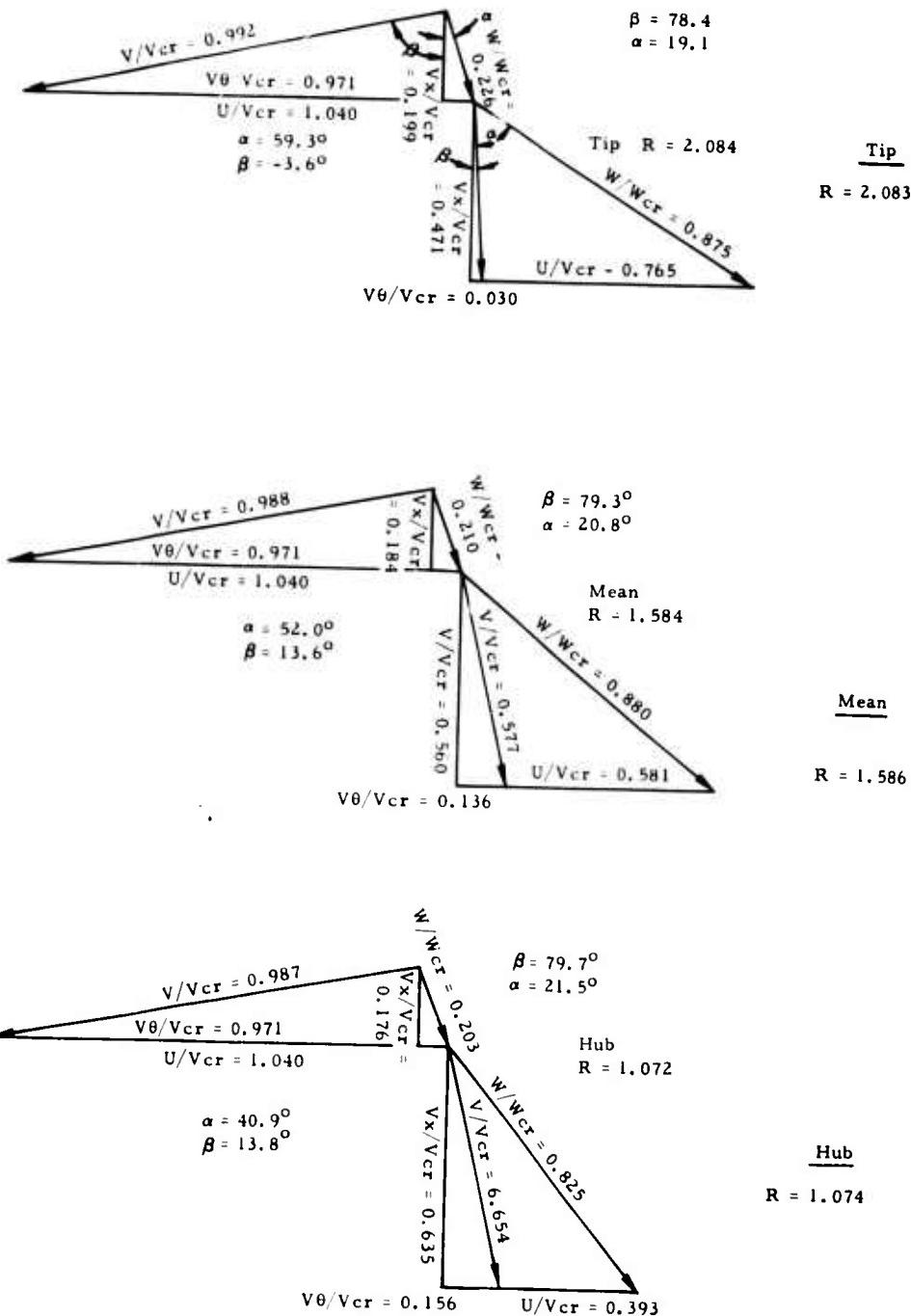


Figure X-87. TS120 Radial Turbine Velocity Diagrams Sea Level Design Point.

## Section X

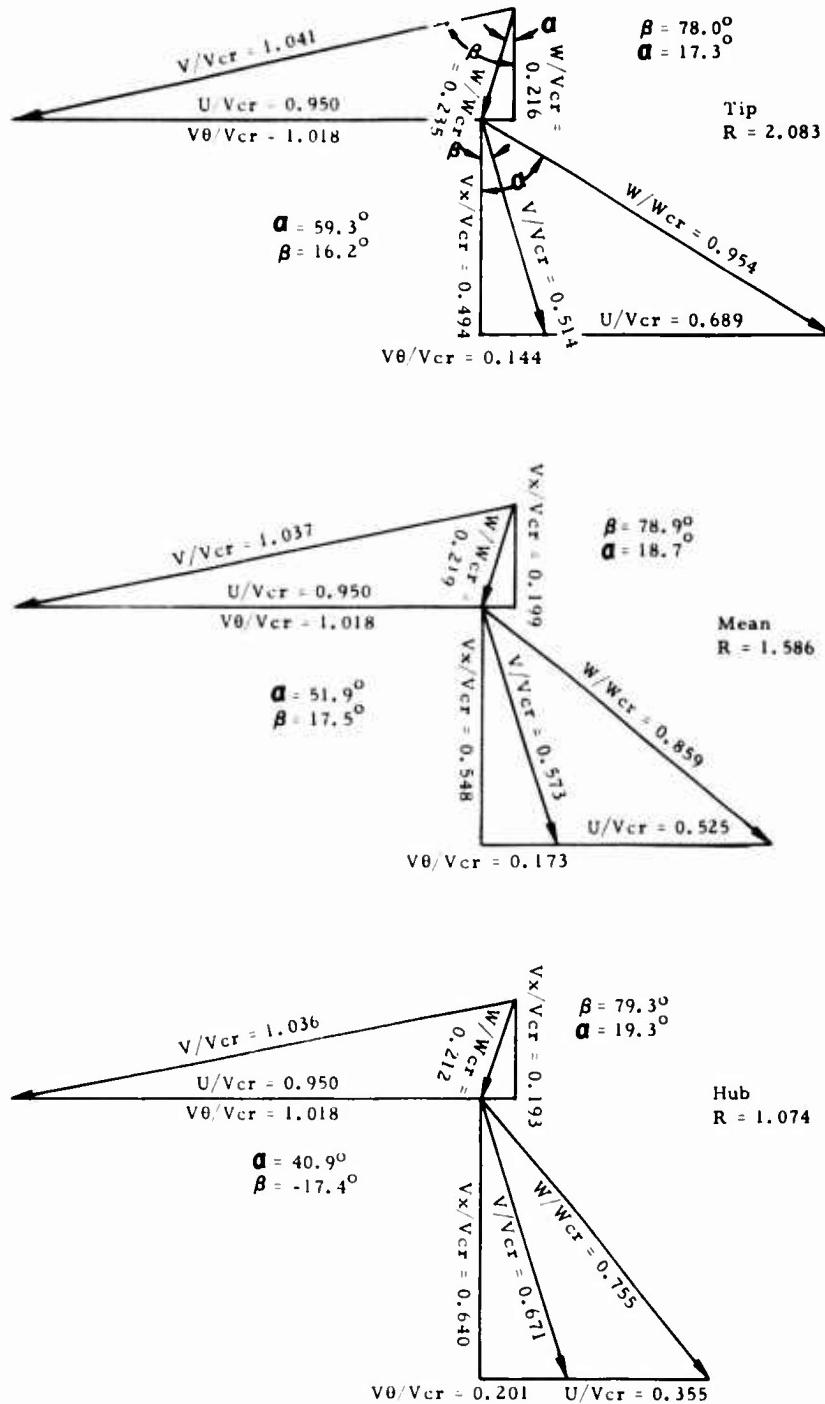
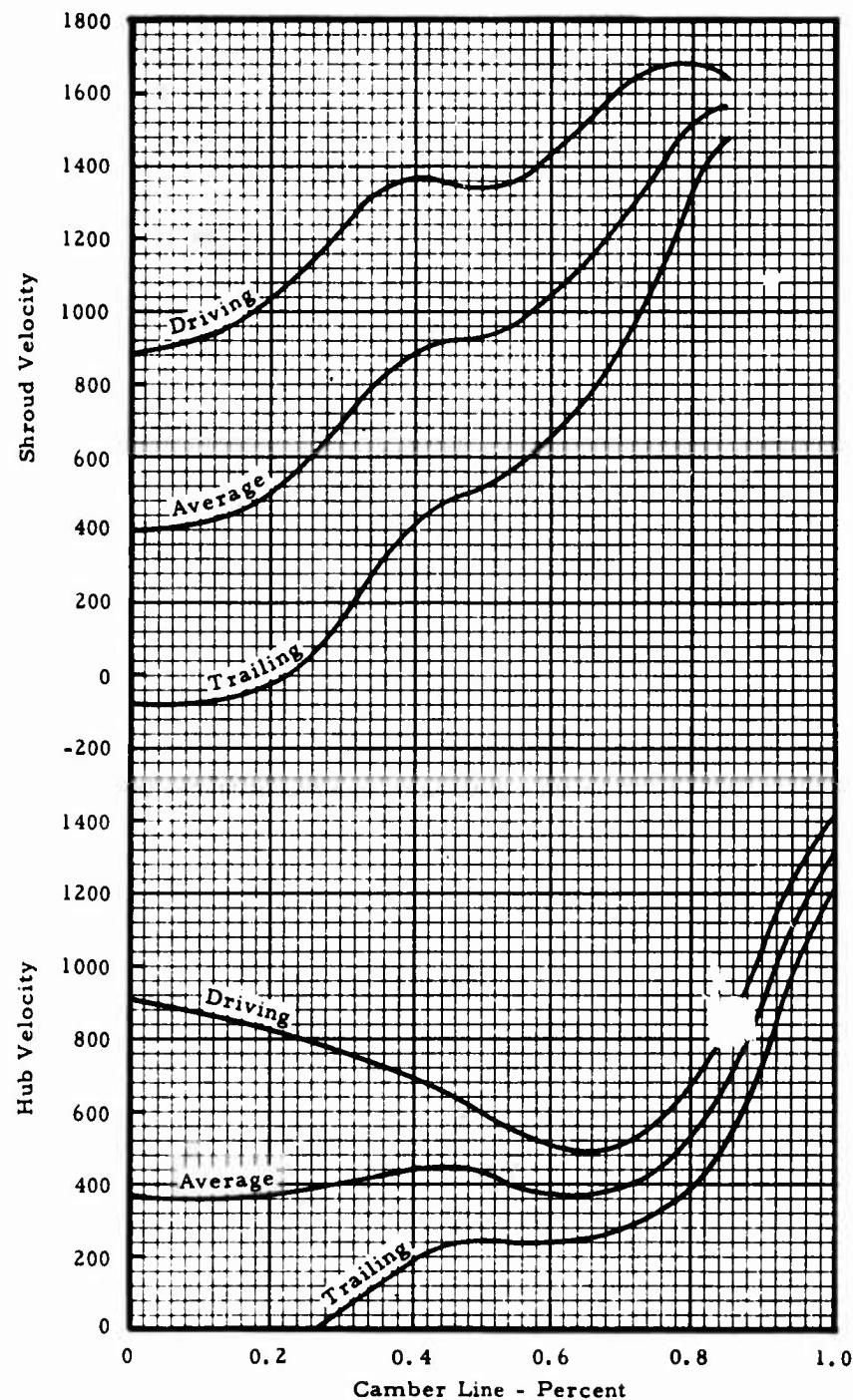


Figure X-88. TS120 Radial Turbine Velocity Diagrams Altitude Design Point.

**Section X**



**Figure X-89. TS120 Turbine Rotor Velocity Distribution Sea Level Design Point.**

**Section X**

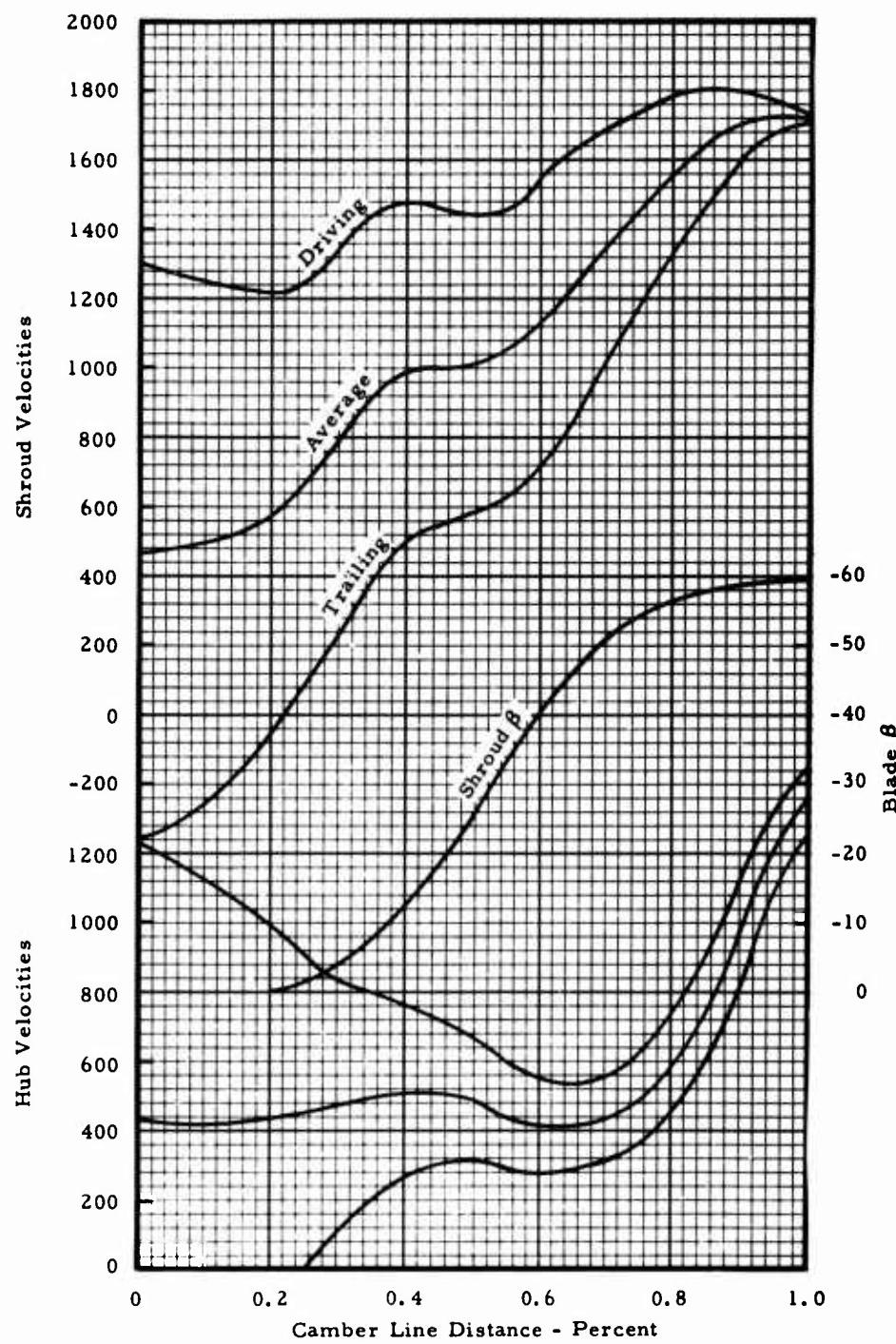


**Figure X-90. Radial Turbine Velocity Distribution Altitude Design Point.**

**Section X**

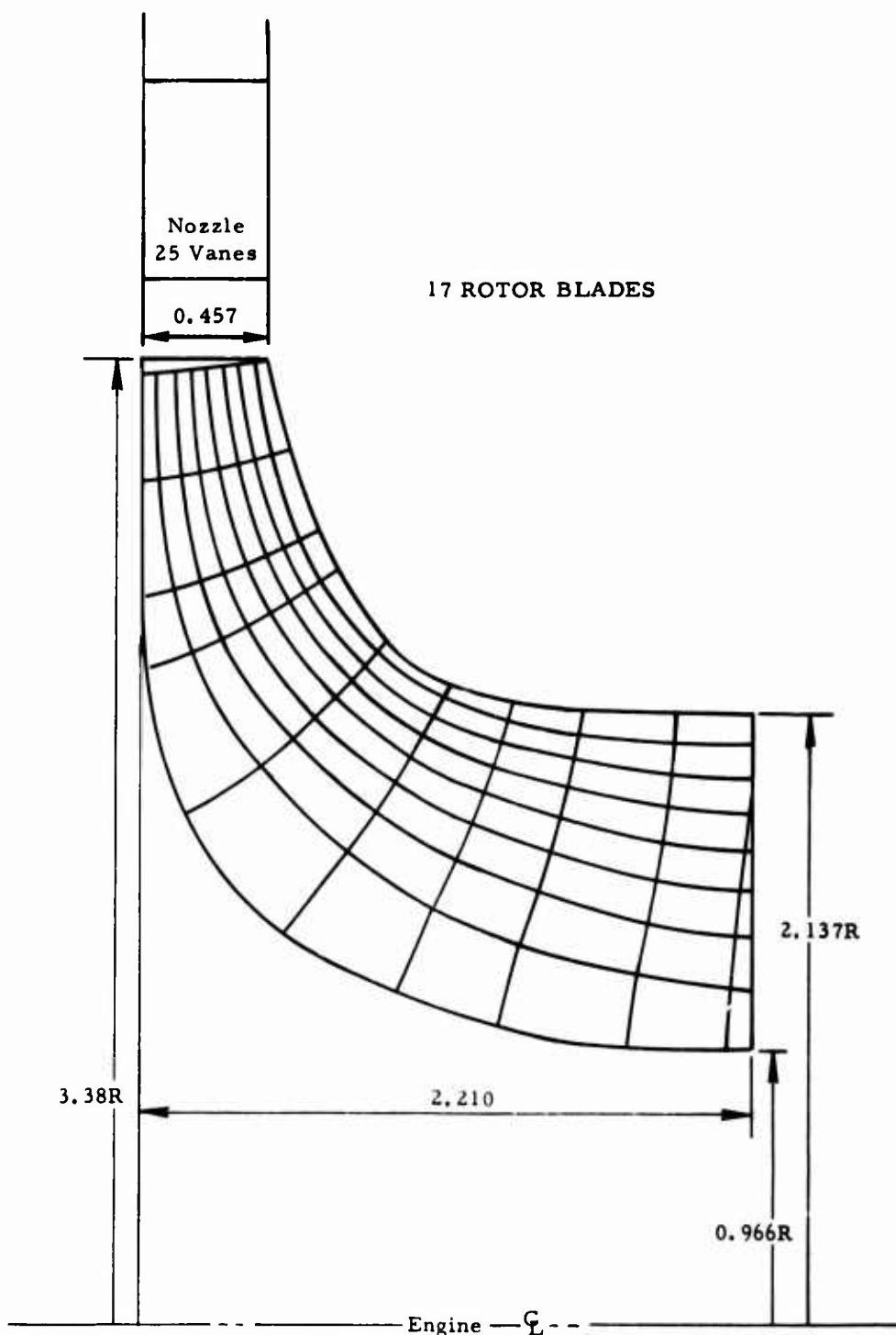


**Figure X-91. TS120 Radial Turbine Geometry and Streamline Location in Meridional Plane.**

**Section X**

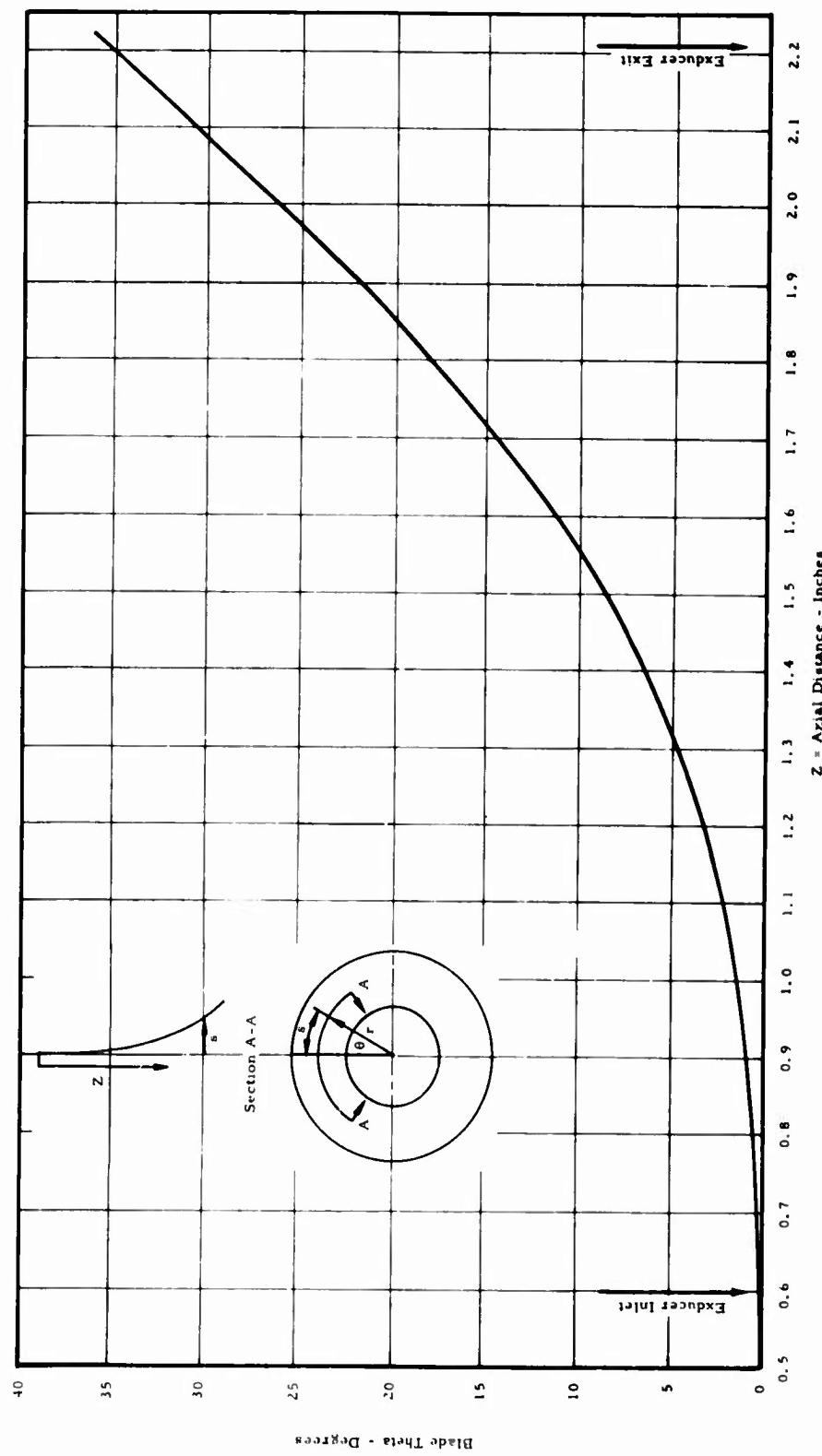


Figure X-92. TS120 Exducer Blade Angle Distribution at Meanline - 17 Blades.

## Section X

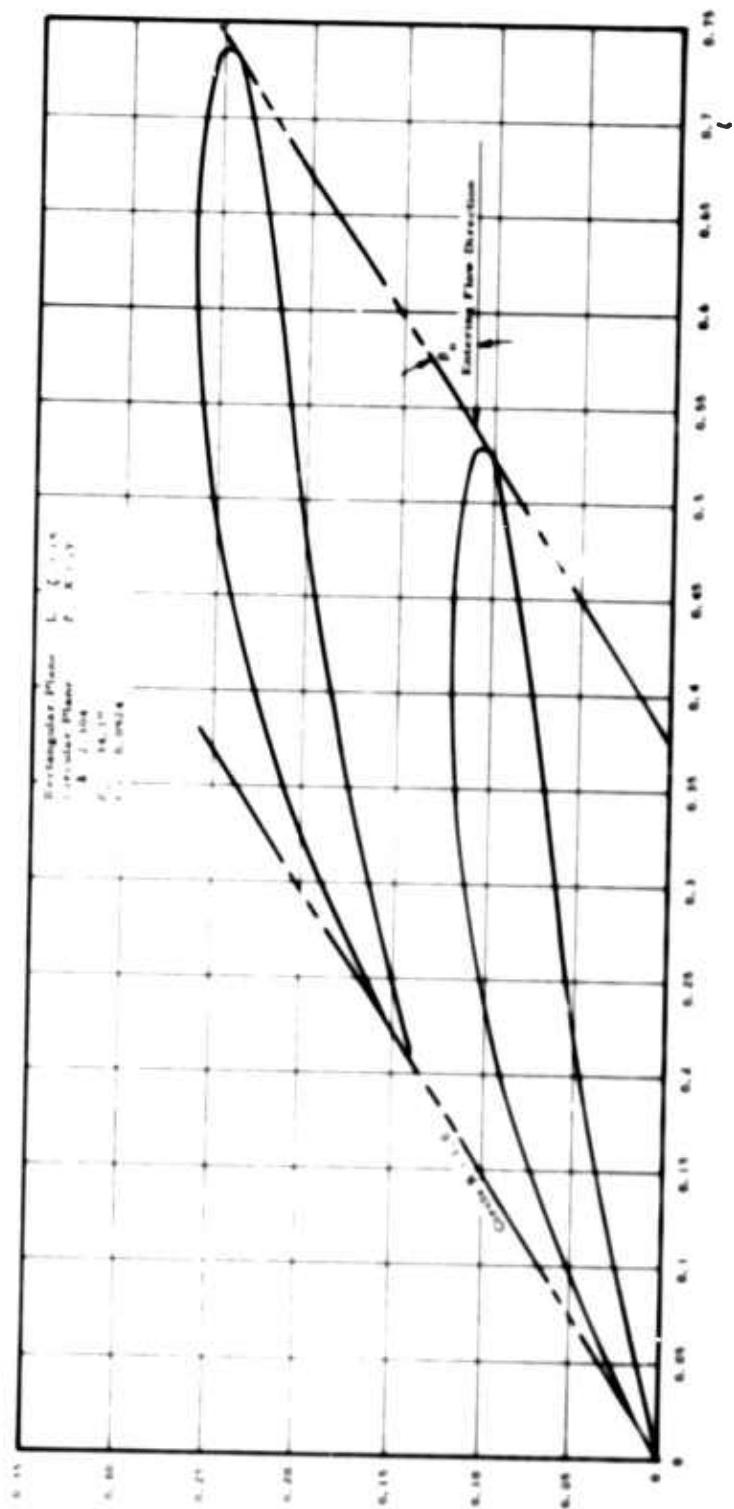


Figure X-93. TS120 Conformal Transformation of Turbine Nozzle - 30 Vanes.

Section X

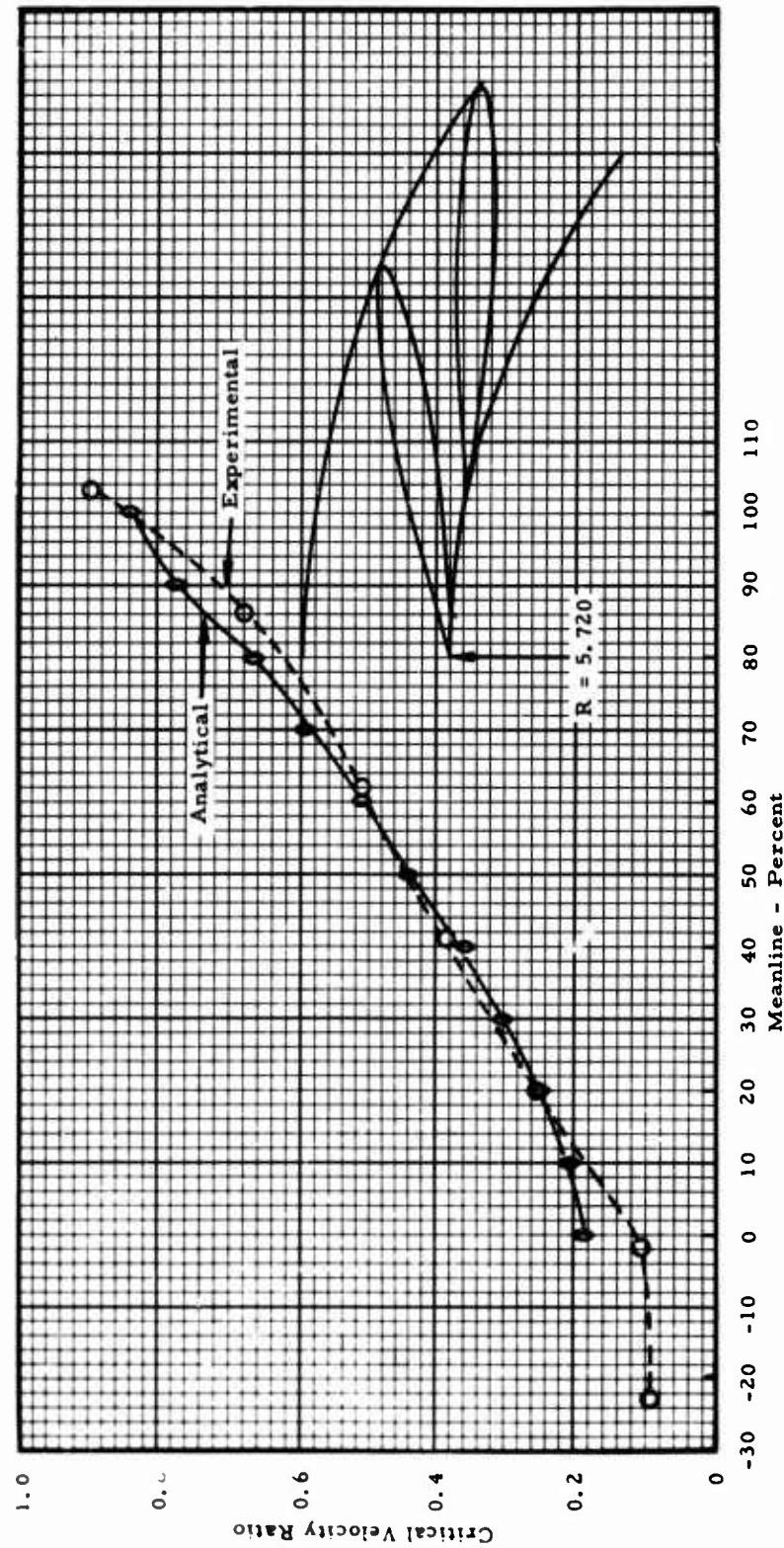
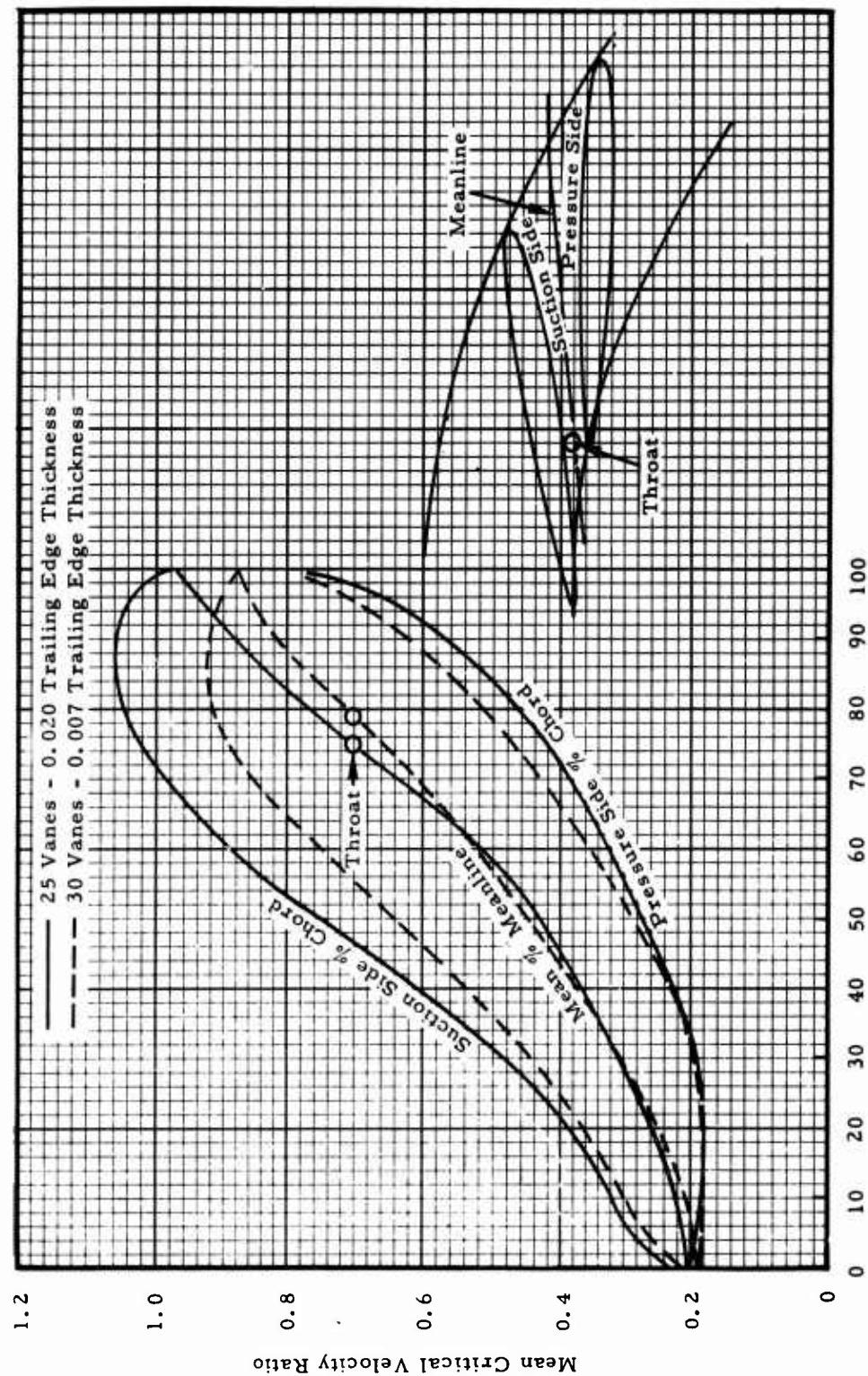
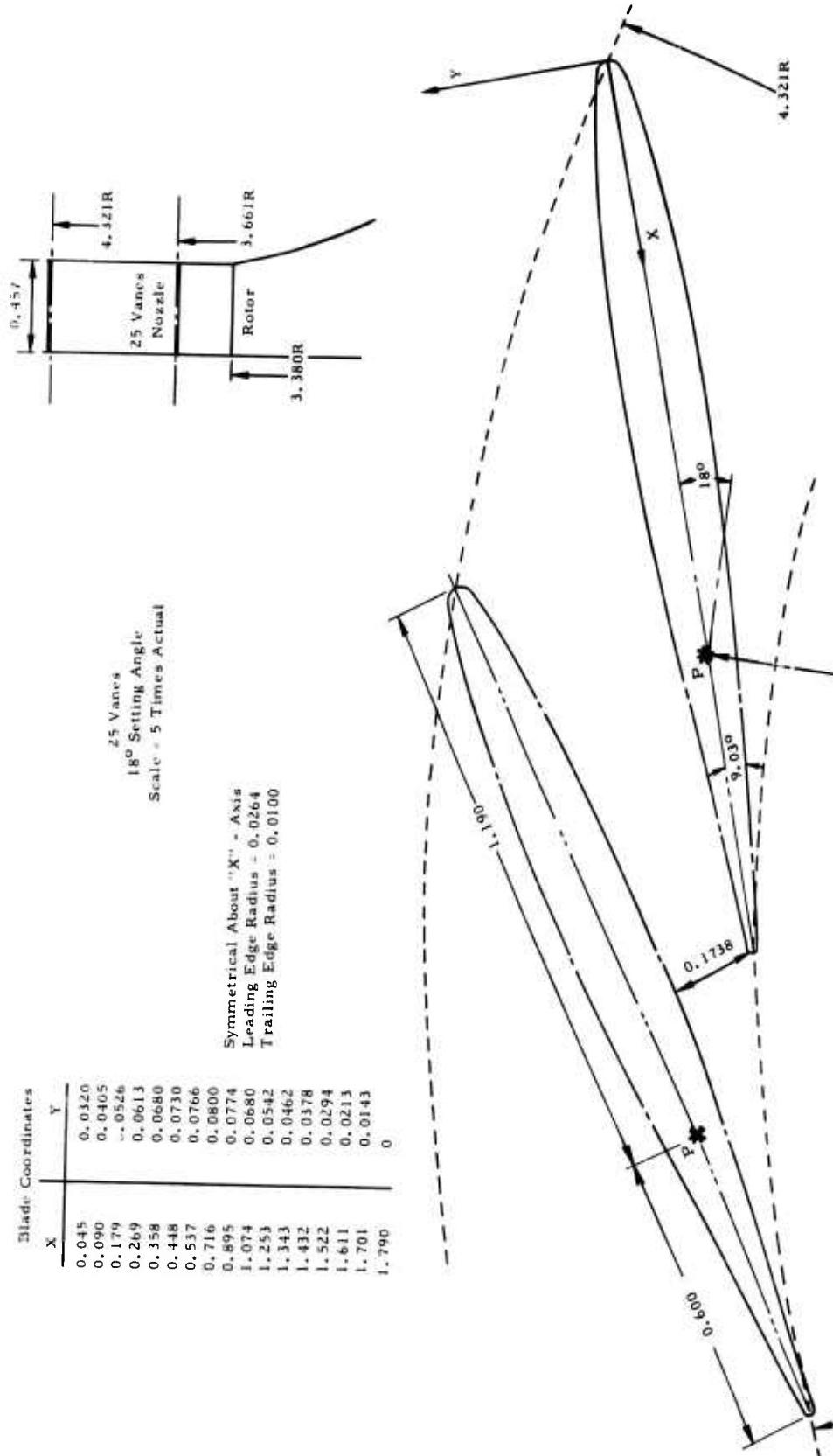


Figure X-94. Comparison of Analytical to Experimental Velocity Distribution in a Radial Turbine Nozzle.

**Section X**



**Figure X-95.** Velocity Distributions in the TS120 Nozzle.



**Figure X-96.** TS120 Radial Turbine Inlet Nozzle Geometry.

**Section X**

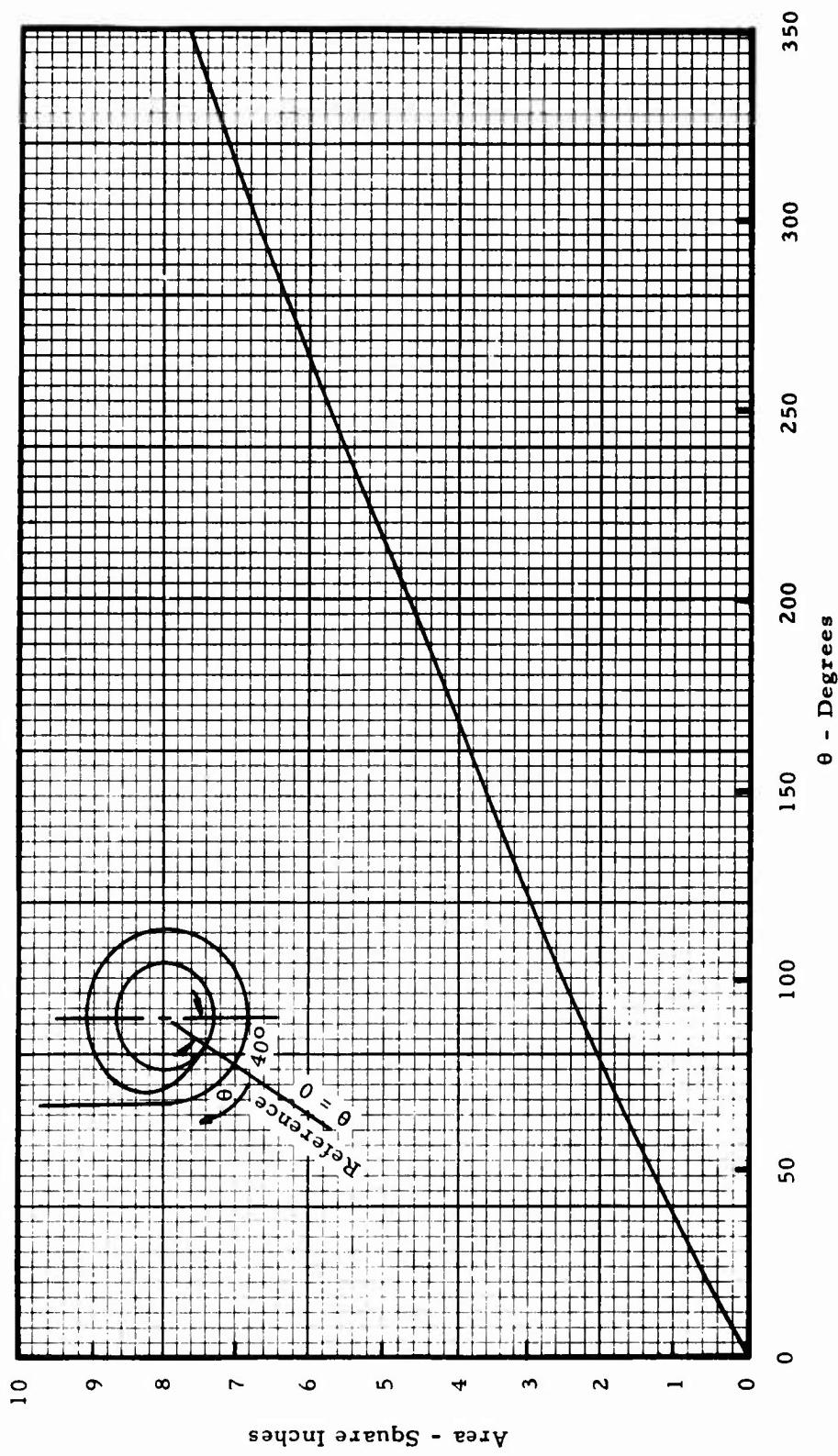


**Figure X-97.** TS120 Turbine Volute Area Distribution.

**Section X**

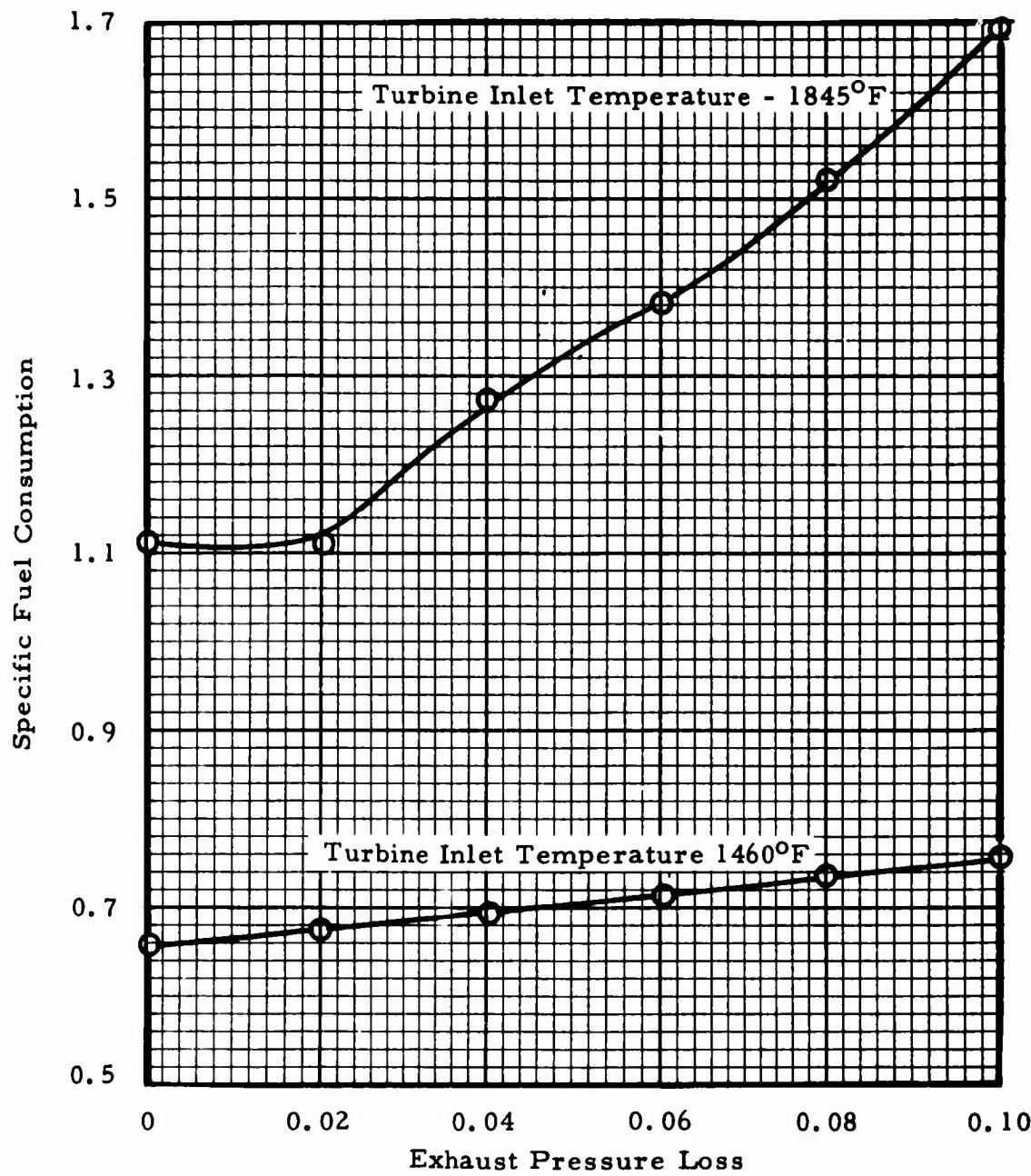


Figure X-98. SFC Versus Exhaust Pressure Loss.

## Section X

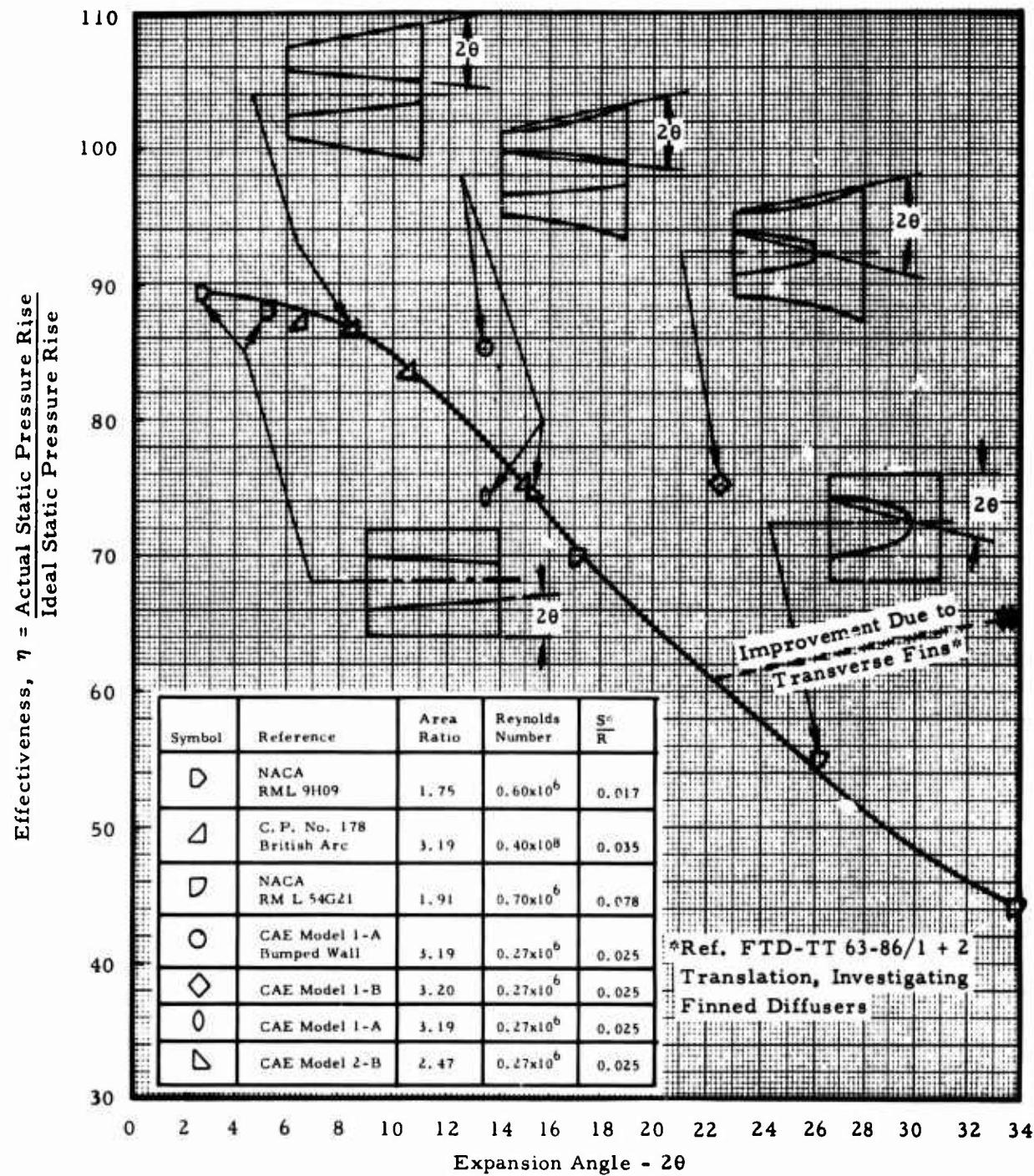


Figure X-99. Annular Diffuser Effectiveness at Inlet Mach Number 0.2.

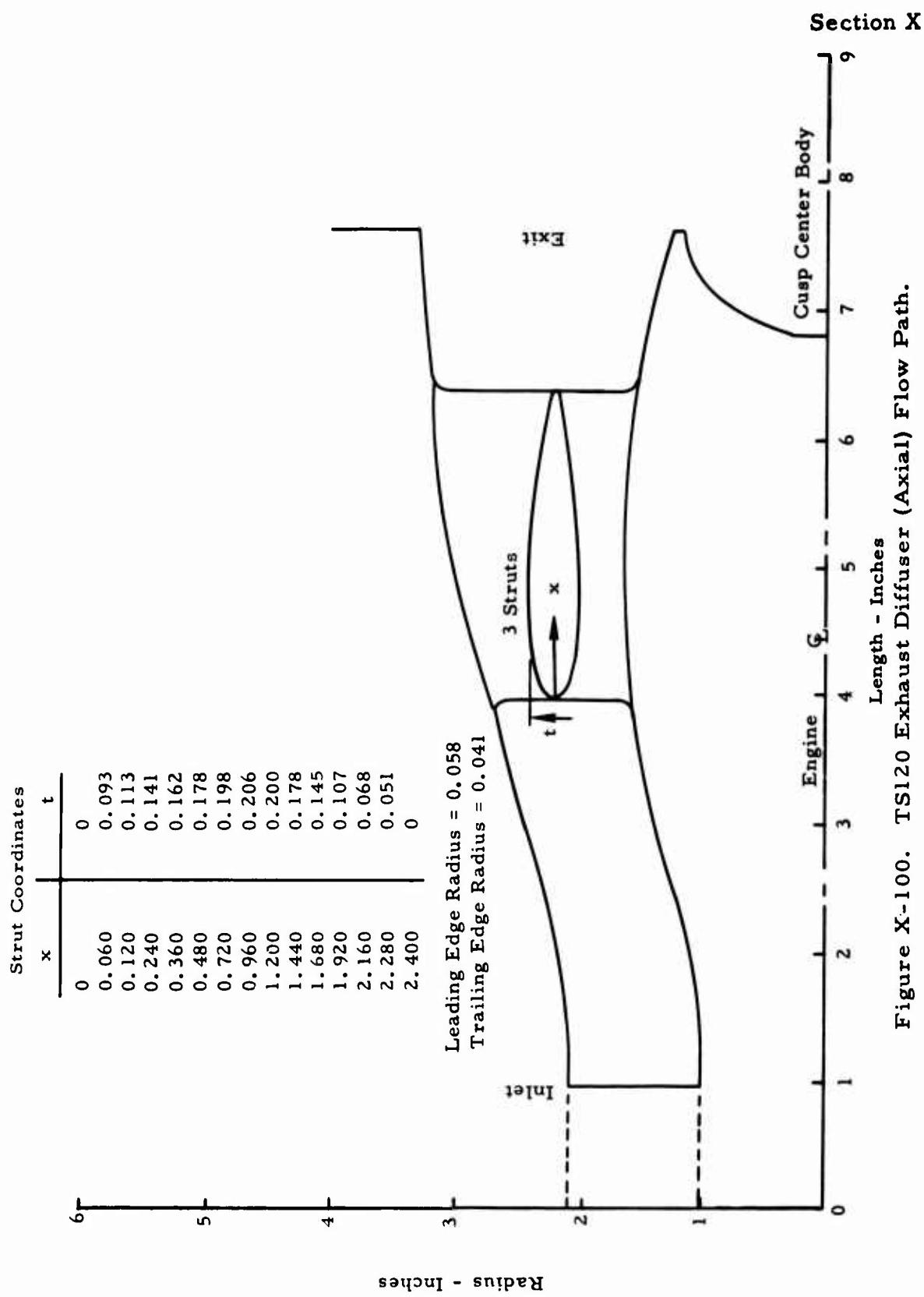
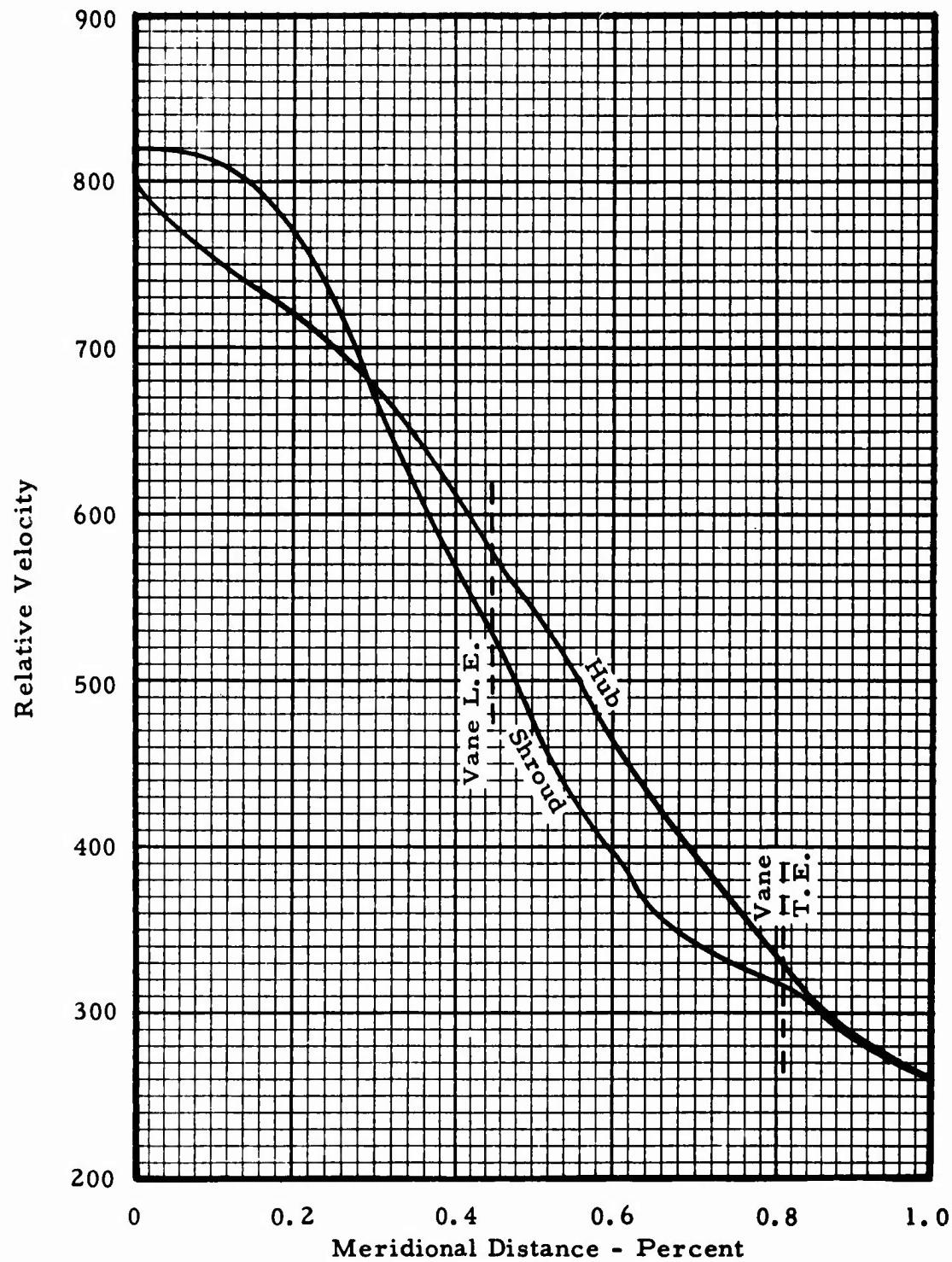


Figure X-100. TS120 Exhaust Diffuser (Axial) Flow Path.

**Section X**



**Figure X-101. TS120 Exhaust Diffuser Relative Velocity Distribution.**

Section X

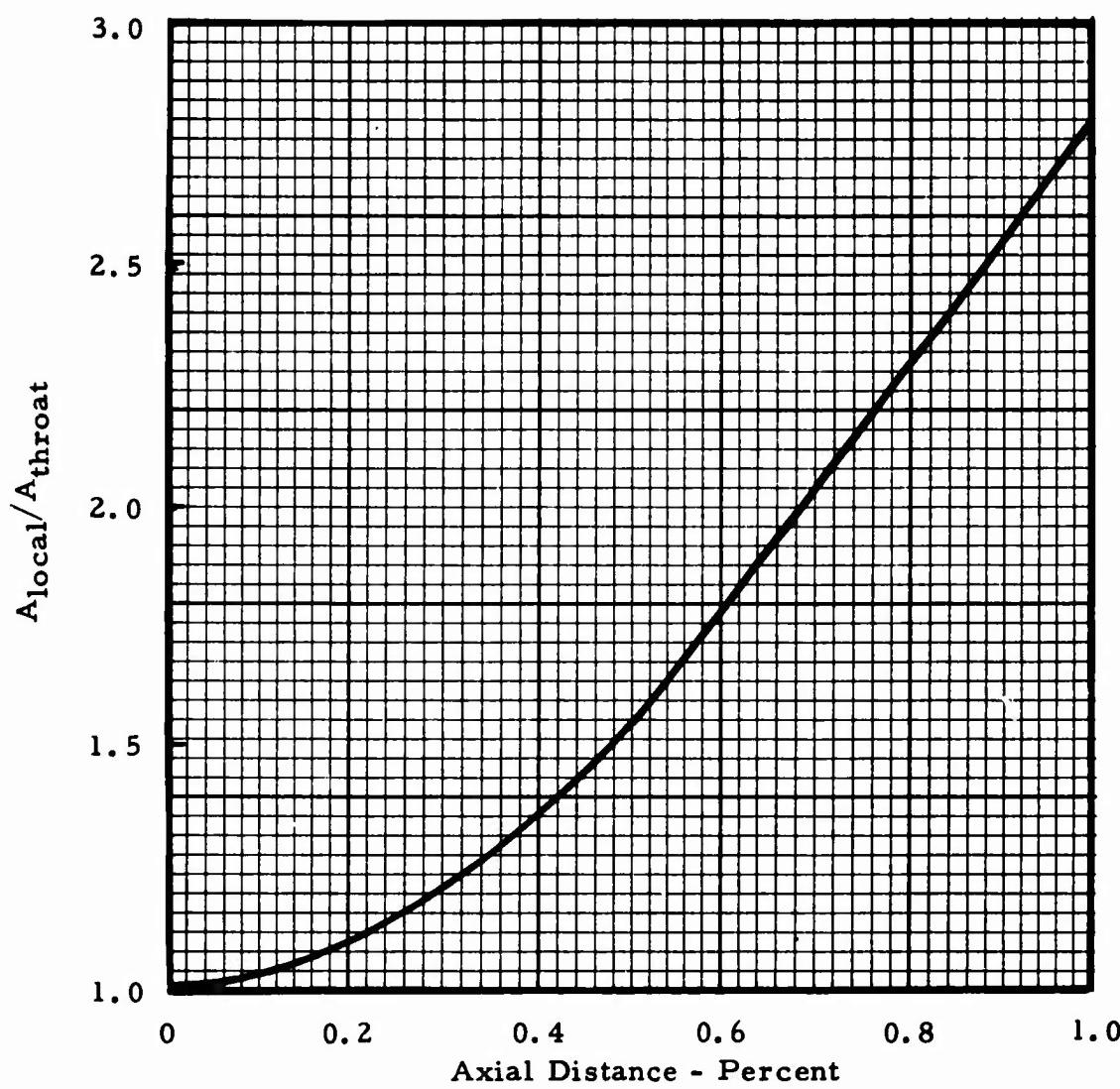


Figure X-102. Exhaust Diffuser Area Distribution as a Function of Distance.

**Section X**

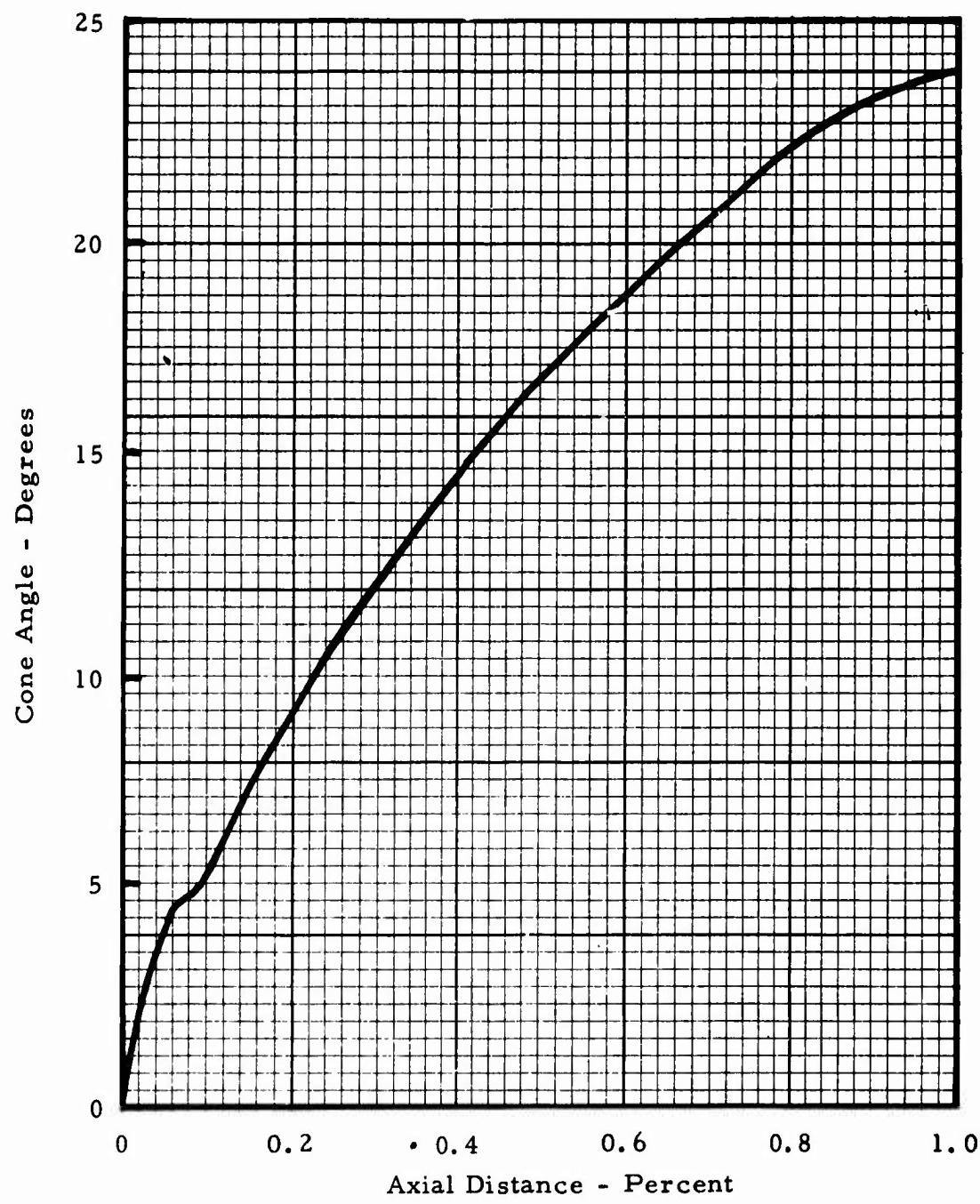
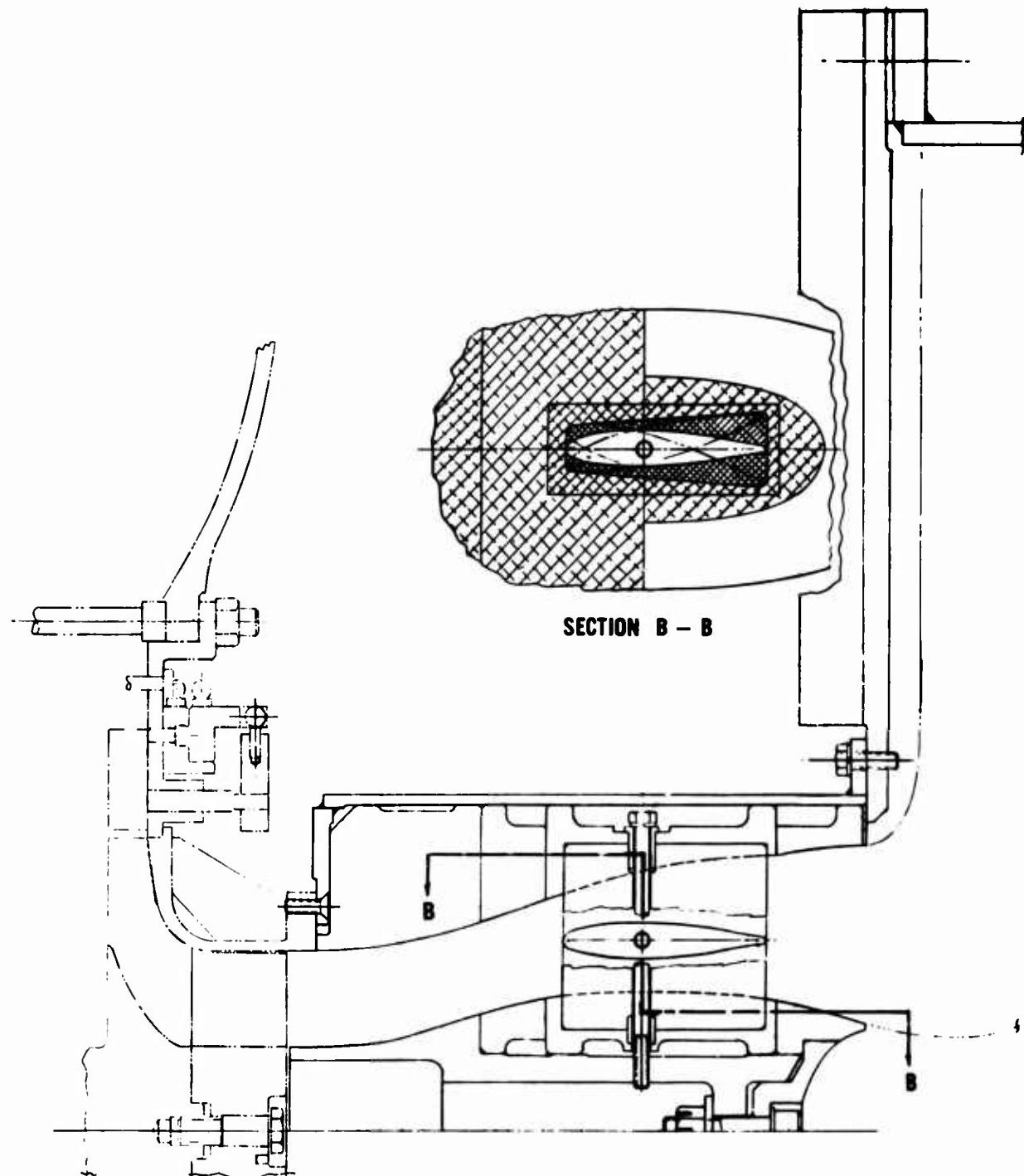


Figure X-103. Equivalent Cone Angle as a Function of Distance.

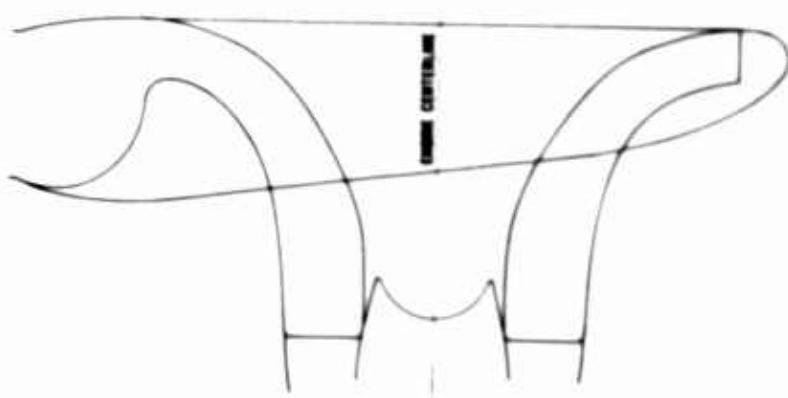
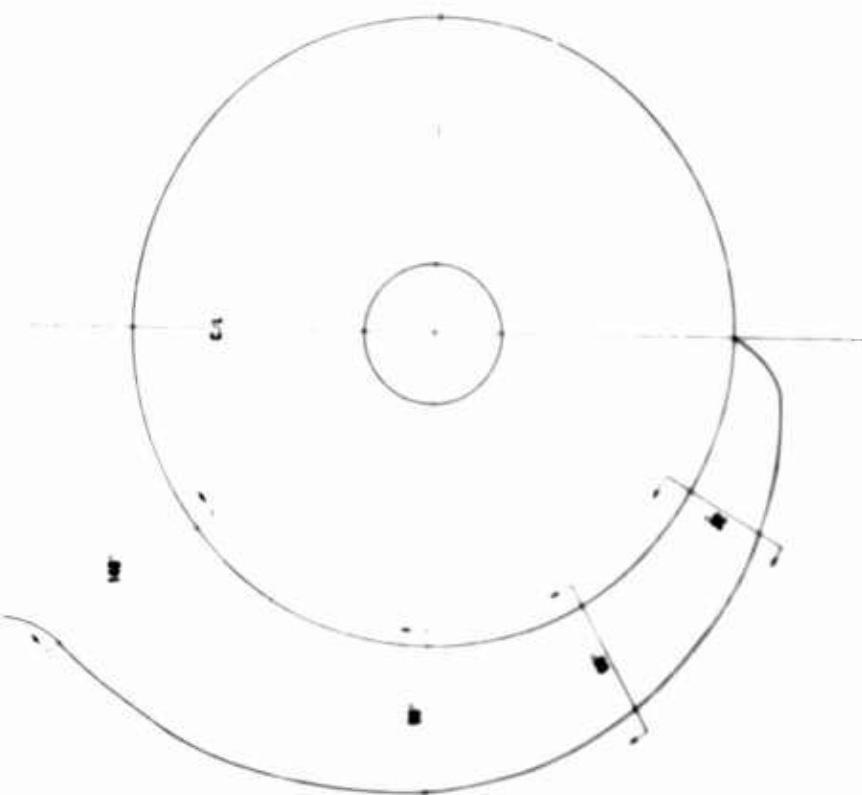
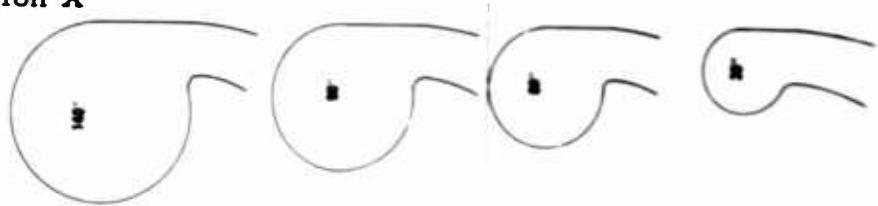
**Section X**



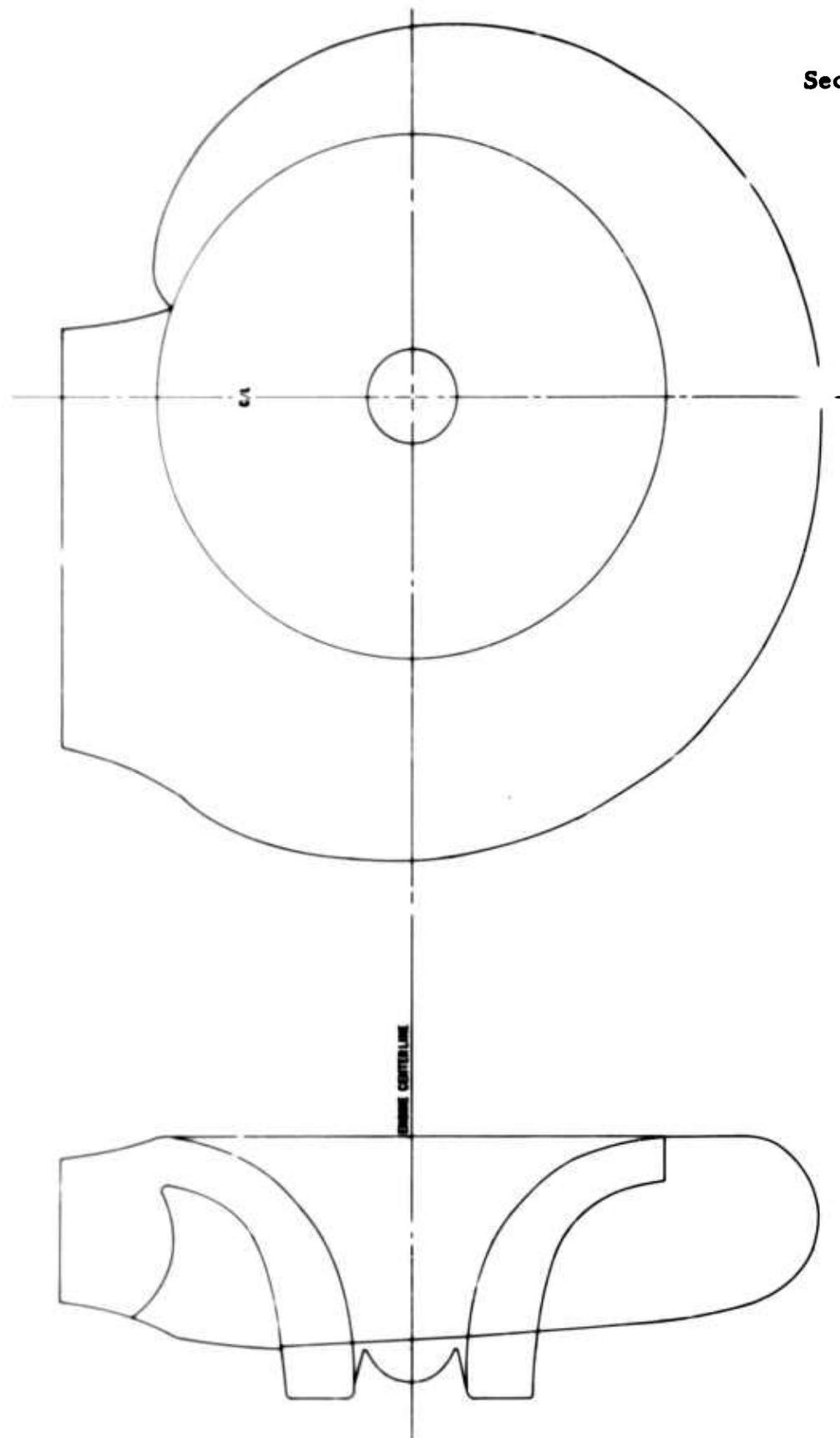
**Figure X-104. Axial Diffuser Test Rig Layout.**

Figure X-105. Preliminary Flow Path Radial Exhaust - Two Path Volute.

Section X



**Section X**



**Figure X-106. Preliminary Flow Path Radial Exhaust - One Path Volute.**

**Section X**

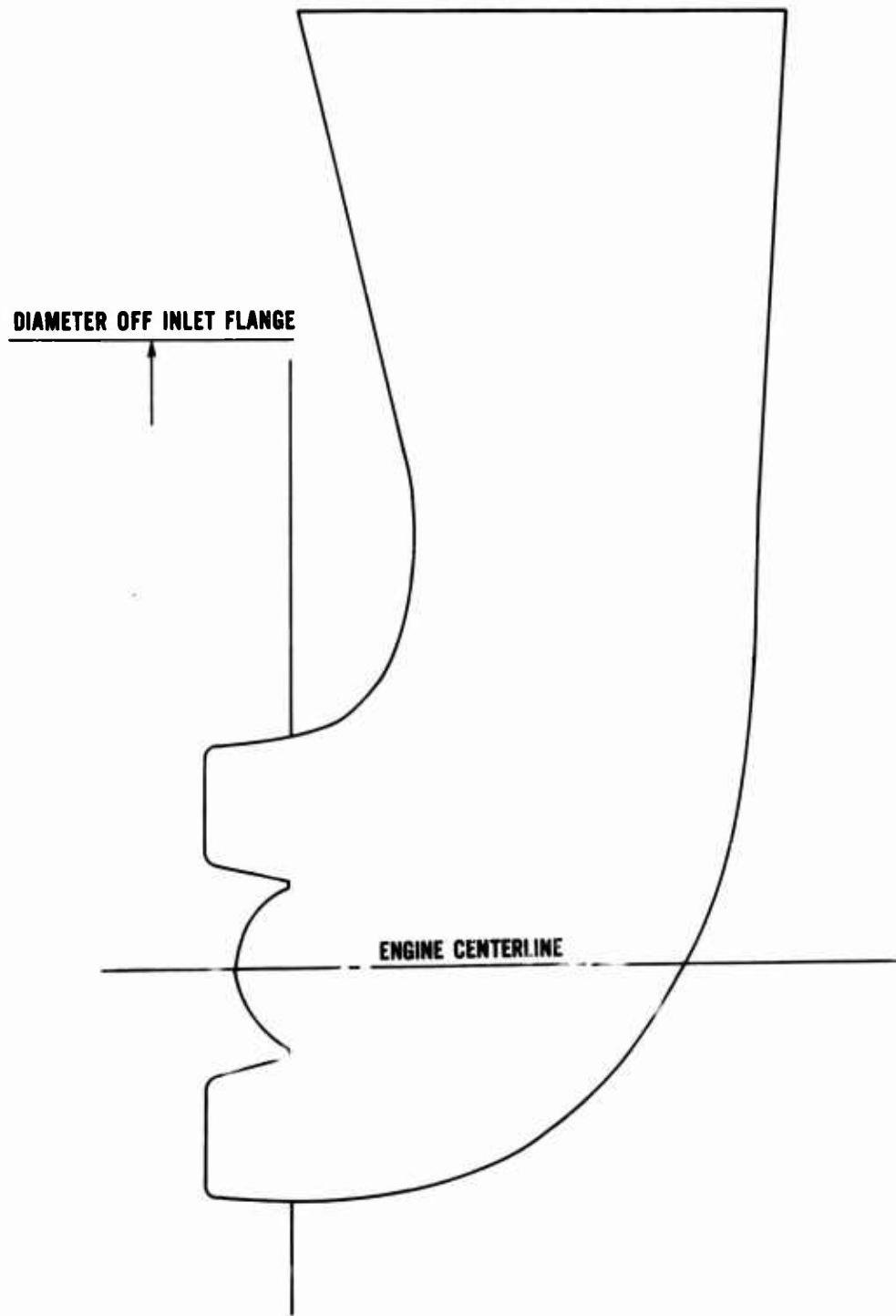


**Figure X-107. Preliminary Flow Path Radial Exhaust - 90° Elbow.**

APPENDIX X-B

## APPENDIX X-B - EXHAUST SYSTEM PIPE TURNING LOSS DATA

### TURNING LOSSES IN VOLUTE

Flow losses in turning pipes can be expressed in a general form,

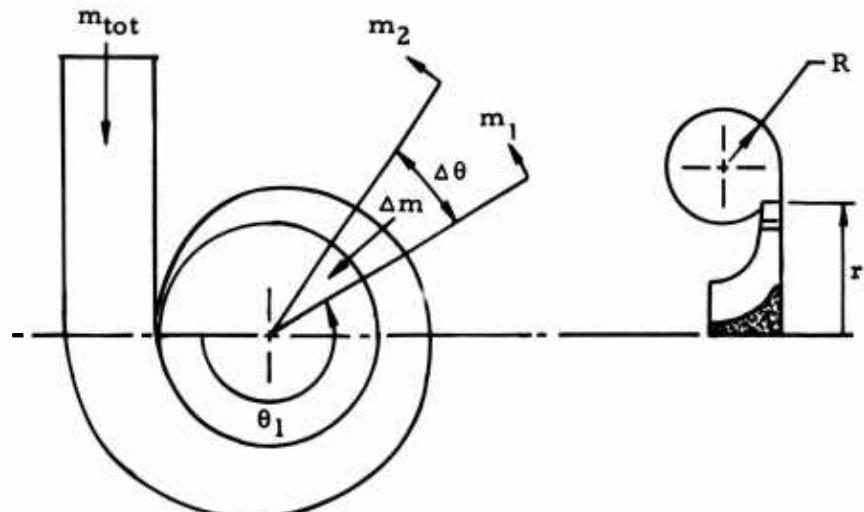
$$\frac{\Delta P}{q} = KC$$

where  $\frac{\Delta P}{q}$  = pressure loss expressed as a percentage of the dynamic head

K = bend radius factor

C = turning angle factor.

The empirical factors K and C are given in Ref. 23. The variable K is found to be nearly constant and minimum over a range of  $2 \frac{R}{D} \leq 6$ . This is typical of the ERDL volute and a volute of  $K = 0.2$  is assigned to this part of the loss. The factor C, however, is a function of turning angle  $\theta$ .



## Appendix X-B

A fairly good curve fit is given by the relation

$$C = \sqrt{\frac{2\theta}{\pi}}, \quad \theta \text{ in radians} \quad (3)$$

Referring to Figure A, and assuming incompressible flow, the flow in the volute at any station,  $\theta$  is given by

$$m = m_{\text{tot}} \left( 1 - \frac{\theta}{2} \right) \quad \text{where } m_{\text{tot}} \text{ is the total mass flow and } \theta \text{ is} \quad (4)$$

in radians. The flow entering the nozzles in any increment  $\Delta\theta$  is then given by,

$$\Delta m = (m_1 - m_2) = m_{\text{tot}} \left( 1 - \frac{\theta_1}{2\pi} \right) - m_{\text{tot}} \left( 1 - \frac{\theta_2}{2\pi} \right) = \left( \frac{\Delta\theta}{2\pi} \right) m_{\text{tot}} \quad (5)$$

The pressure loss can now be mass averaged over the turning angle  $2$  as

$$\left[ \frac{\Delta P}{q} \right]_{\text{MA}} = \frac{\sum_{\theta=0}^{\theta=2} K C \Delta m}{m_{\text{tot}}} \quad (6)$$

Substituting (3) and (5) gives,

$$\frac{\Delta P}{q}_{\text{MA}} = \sum_{\theta=0}^{\theta=2} \frac{(0.2)}{2\pi} \sqrt{\frac{2}{\pi}} \theta^{1/2} \Delta\theta \quad (7)$$

**Appendix X-B**

$$\left[ \frac{\Delta P}{q} \right]_{MA} = \int_0^{2\pi} \frac{0.2}{2\pi} \sqrt{\frac{2}{\pi}} \theta^{1/2} d\theta$$

$$\left[ \frac{\Delta P}{q} \right]_{MA} = 0.266$$

Based on an average dynamic head, the turning loss expressed as a percentage of the inlet total pressure becomes

$$\frac{\Delta P}{q} = 0.41\% \quad (9)$$

## SECTION X - REFERENCES

1. Contract No. DA-44-009-AMC-760(T); Engine Gas Turbine, 60, 90, and 120 Horsepower; 28 October 1963.
2. NASA Memo 11-26-58E; Comparison of Calculated and Experimental Total Pressure Loss and Airflow Distribution in Tubular Turbojet Combustors with Tapered Liners; J. S. Grobman; 1959.
3. ARC R and M No. 1867; The Effect of a Gauze on the Velocity Distribution in a Uniform Duct; A. R. Collar; February 1939.
4. NACA R1300; Basic Considerations in the Combustion of Hydrocarbon Fuels With Air; 1957.
5. NACA TN 2855; General Correlation of Temperature Profiles Downstream of a Heated Air Jet Directed at Various Angles to Air Stream; R. S. Ruggeri; December 1952.
6. NASA TN D-9; Experimental Investigation of Air Film Cooling Applied to an Adiabatic Wall by Means of an Axially Discharging Slot; S. S. Papell and A. M. Trout.
7. SAE 63-767D; Operation of Small Industrial Gas Turbines on Military Fuels; J. H. Horton, J. E. Montgomery, and W. F. McGovern.
8. CAE Proposal No. 64-019, "Design and Development of USAERDL 60, 90, and 120 Horsepower Gas Turbine Engine," Vol. IIA and IIB, 20 May 1964.
9. O. E. Balje, "A Study on Design Criteria and Matching of Turbomachines," Parts A and B, ASME Papers 60-WA-230, 60-WA-231.
10. H. J. Wood, "Current Technology of Radial-Inflow Turbines for Compressible Fluids," ASME Paper 62-GTP-9.

## Section X

11. Wu, "A General Theory of Three-Dimensional Flow in Subsonic and Supersonic Turbomachines of Axial-, Radial-, and Mixed-Flow Types," NACA TN 2604, January 1952.
12. Northern Research and Engineering Corporation, Cambridge, Massachusetts, "The Design and Performance Analysis of Radial-Inflow Turbines," Volumes I and II.
13. O. Zweifel, "The Spacing of Turbomachine Blading, Especially With Large Angular Deflection," The Brown Boveri Review, December 1945, Volume 32, pp. 436-444.
14. Faulders, C. R., "An Aerodynamic Investigation of Vaned Diffusers for Centrifugal Compressors," Gas Turbine Laboratory, M. I. T.; ASTIA No. AD 107717.
15. N. M. Markov, "Evaluation of the Aerodynamic Characteristics of Turbine Blading," Translated and Published by Associated Technical Services, Incorporated, Glen Ridge, New Jersey, USA, 1958.
16. W. B. Brown and G. R. Bradshaw, "Design and Performance of Family of Diffusing Scrolls with Mixed-Flow Impeller and Vaneless Diffuser," NACA Report 936, 1949.
17. Eckert, B., "Axial Kompressoren und Radial Kompressoren," Springer-Verlag, Berlin, Germany, 1953.
18. L. F. Moody, "Friction Factors for Pipe Flow," Trans. ASME, Volume 66, 1944, page 671.
19. R. P. Benedict and N. A. Carlucci, "Flow With Losses," ASME Paper No. 63-WA-105, 1963.
20. Textor, E., "Tests of Area Ratio Exhaust Diffuser Configuration 1-A With Five Struts and Without Struts," Data and Test Report No. 466, CAE Component and Environmental Laboratory, Toledo, Ohio, 1961.

Section X

21. Migay, V.K., "Increase of Diffuser Efficiency by Means of Transverse Fins," Teploenergetika, No. 4, 1961, 41-43.
22. Migay, V.K., "A Study of Finned Diffusers," Teploenergetika, No. 10, 1962, 55-59.
23. Committee A-9, "Aircraft Air Conditioning Equipment, Engineering Data Fluid Dynamics," SAE Aeronautical Information Report No. 23, 15 October 1951.

SECTION XI

**POWER CONTROL SYSTEM**

## SECTION XI - POWER CONTROL SYSTEM

The control system as initially proposed by Continental and as modified in the early part of the program is shown schematically in Figure XI-1. This system in essence centers about the closed loop acceleration scheduling control and a governor for the direct drive, simple-cycle engine. The characteristics of the closed loop control has inherent ability to handle the variety of fuels to be encountered without adjustment.

Estimated performance and scheduling parametric studies, sizing, and detailing of the closed loop control were completed.

The governor characteristics for the direct drive simple-cycle were examined and a preliminary computer study and analysis made. Other components of the system were also investigated with the approach that these would be secured from other vendors and be integrated into the system.

The requirements of the geared drive system, however, required a different governing system and Continental's governor would have been replaced by a system from an outside supplier.

In light of more detailed knowledge of the system technical and cost considerations as the program progressed, per mutual agreement with the program management of Continental and ERDL, a specification defining the control system requirements for the complete family of engines was prepared, coordinated, and proposals were requested from several vendors.

The evaluation of these proposals has resulted in the selection of the system proposed by Woodward Governor Company. Since this approach has been adopted, there has been a schedule delay introduced to the control system design phase. The control system design study will be started by Woodward Governor Company before the end of May and is expected to be completed by late in July 1965. This design study of the control system will be published as a supplement to this Design Report upon its completion. The results of the system transient analysis made by Continental to investigate the governor-engine dynamic characteristics based on the estimated engine performance are presented below. This study is applicable to the governing system for the direct drive engine.

## Section XI

### SYSTEM TRANSIENT ANALYSIS

The purpose of the transient analysis is twofold; first, to assure that the system is stable with reasonable margin, and second, to assure that the system responds to load fluctuations according to specifications. The response requirement was outlined in the ERDL Purchase Specification, and states that there be less than an eight percent transient variation for any sudden load application or removal, as measured from the speed at which the load change occurred, and that the system stabilize to its final value within three seconds with no more than one overshoot or undershoot of speed outside of  $\pm 1$  percent of the final speed value. In addition, the specification states that total steady-state speed regulation (droop) shall be no more than 2.5 percent from zero to rated load.

The block diagram used for the system transient analysis is shown in Figure XI-2. The values listed are predicted from the cycle analysis of the 120 horsepower non-regenerative engine, and considering a direct drive generator. It is assumed that the generator is equipped with a voltage regulator with negligible dynamics, which results in a constant horsepower operating line. A further assumption is that the shaft connecting the engine and generator is rigid, consequently engine and generator speed are identical at all times. The value of combustor lag shown, 0.05 second, is considered to be somewhat pessimistic.

Stability is studied by use of the Bode plot. Briefly, the Bode plot is an examination of the open loop system frequency response (that is, considering no feedback of the actual engine speed to the governor). The examination consists of plotting the amplitude (measured in decibels) and phase shift of the system against the frequency of a set speed exciting signal. At the frequency where the phase shift is  $180^\circ$  (because of the comparator the actual speed signal would be in phase with the exciting speed signal) the system gain must be less than unity (0 db), or instability will result. If the system is stable, the difference between  $180^\circ$  and the actual phase shift at the frequency where the gain curve crosses zero db is called phase margin and is an indication of the degree of stability. A phase margin of  $30^\circ$ , or greater, is considered acceptable.

## Section XI

The frequency response of the engine and generator show that the combined engine-generator time constant is very large so that considerable gain attenuation occurs at frequencies above one radian per second. This allows the use of a reasonably fast proportional governor with relatively high gain. The ERDL droop requirement of 2.5 percent and the predicted engine performance determined the governor gain listed in Figure XI-2. In addition, it is felt that a governor time constant of 0.05 seconds is reasonably attainable. Bode plots for the full-load and no-load conditions are shown in Figures XI-3 and XI-4, respectively. Note that the Bode plots for the two conditions are practically identical in the frequency range of gain crossover so that either condition can be used for applying stability criteria. Both plots show phase margin of about  $80^\circ$ .

Transient response of the system was examined by using a digital computer in the capacity of an analog computer. Figure XI-5 shows the results of a step in load from 0 torque to 100 percent rated torque (112 inch-pound) with the parameters as listed in Figure XI-2. The system is overdamped with an equivalent first-order time constant of about 0.27 seconds. Figure XI-6 shows the same system with torque stepped from full to zero rated value. Figure XI-7 illustrates the effect of reducing combustor dead time to zero. The equivalent first-order lag without dead time is about 0.30 seconds. The system is slightly faster with dead time because the corrective fuel flow is delayed. Ultimately the consequences of excessive dead time will result in instability, but there is sufficient margin for the system under consideration, as was shown in the Bode plots.

Figure XI-8 shows the response of the system if the governor gain was increased to give a droop of one percent than 2.5 percent. This alteration from the system of Figure XI-2 results in an 0.3 percent of design speed overshoot and 0.18 seconds to initial crossing of the steady-state value. A Bode plot evaluation may be made by increasing the gain of Figure XI-3 or XI-4 by 2.5 (add 8 db). The phase margin is then observed to be about  $60^\circ$ , which is satisfactory. Figure XI-9 demonstrates the response with an 0.10 governor time constant.

## Section XI

Figure XI-10 shows the system of Figure XI-1, but with engine performance figures calculated for an 8000 foot altitude and -65°F ambient temperature. The torque step is 112 inch-pound as for previous cases. System droop has decreased to less than two percent and there is a slight overshoot.

Thus the system with a proportional type of governor with 2.5 percent droop, and a 0.05 second governor time constant, easily meets the ERDL transient performance specification. In addition, reasonable system parameter variations do not cause the performance of the system to exceed the specification.

This data will be made available to the control vendor.

## Section XI

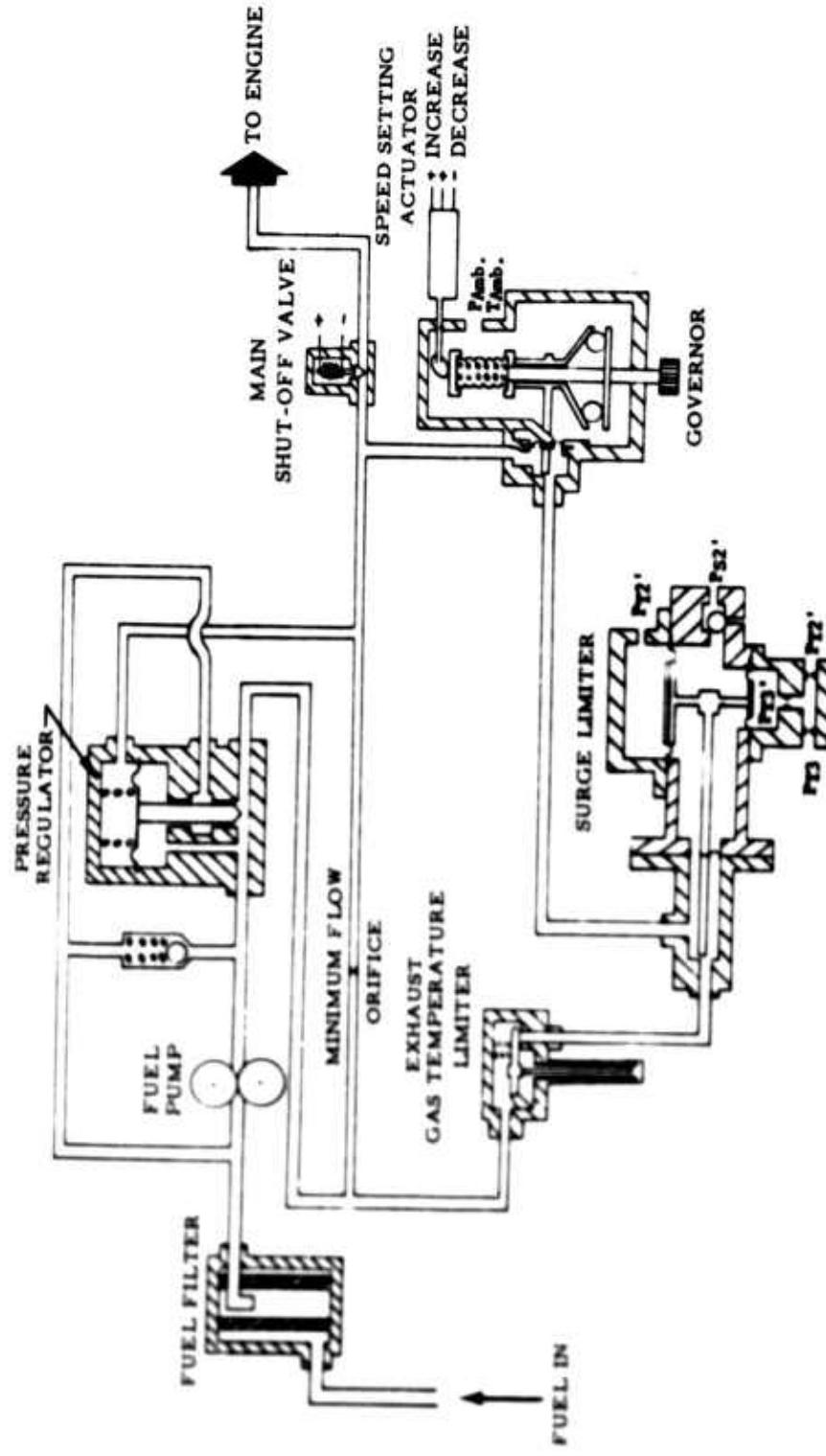
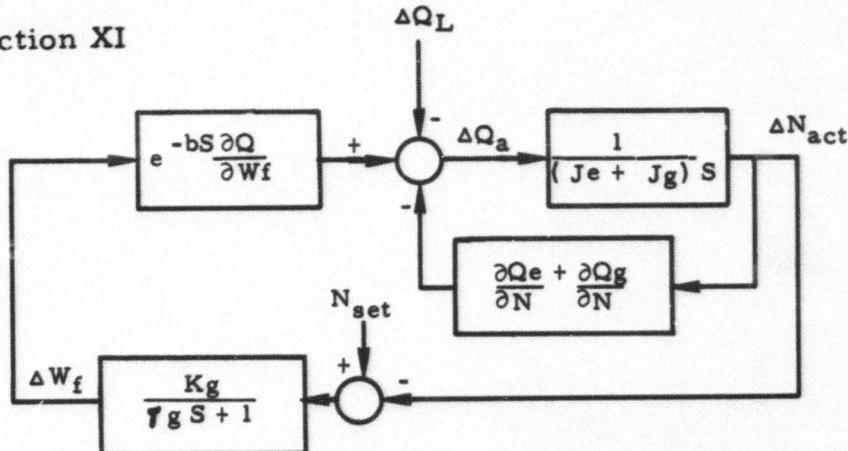


Figure XI-1. TS-120 Fuel System Schematic Diagram.

**Section XI**



<u>SYMBOL</u>	<u>DESCRIPTION</u>	<u>VALUE AT FULL LOAD</u>	<u>VALUE AT NO LOAD</u>
W <sub>f</sub>	Fuel Flow	83.5 pph	35.5 pph
Q <sub>a</sub>	Torque Available to Accelerate the Engine		
Q <sub>L</sub>	Load Torque on Generator	112 In-Lb.	0 In-Lb.
N <sub>set</sub>	Desired Engine and Generator Speed	100%	100%
N <sub>act</sub>	Actual Engine and Generator Speed	100%	102.5%
b	Combustor Lag	.05 sec.	.05 sec.
∂Q/∂W <sub>f</sub>	Partial Derivative, Torque to Fuel Flow	2.15 In-Lb. pph	2.15 In-Lb. pph
Je	Engine Inertia	.0298 In-Lb. Sec <sup>2</sup>	.0298 In-Lb. Sec <sup>2</sup>
Jg	Generator Inertia	.2235 In-Lb. Sec <sup>2</sup>	.2235 In-Lb. Sec <sup>2</sup>
∂Qe ∂N	Partial Derivative, Torque to Engine Speed	2.085 In-Lb./%	2.085 In-Lb./%
∂Qg ∂N	Partial Derivative, Torque to Generator Speed	-1.12 In-Lb./%	0 In-Lb./%
K <sub>g</sub>	Governor Gain	19.9 pph/%	19.9 pph/%
T <sub>g</sub>	Governor Time Constant	.05 Sec.	.05 Sec.
S	La Place Operator		

Figure XI-2. TS-120 Engine Block Diagram.

## Section XI

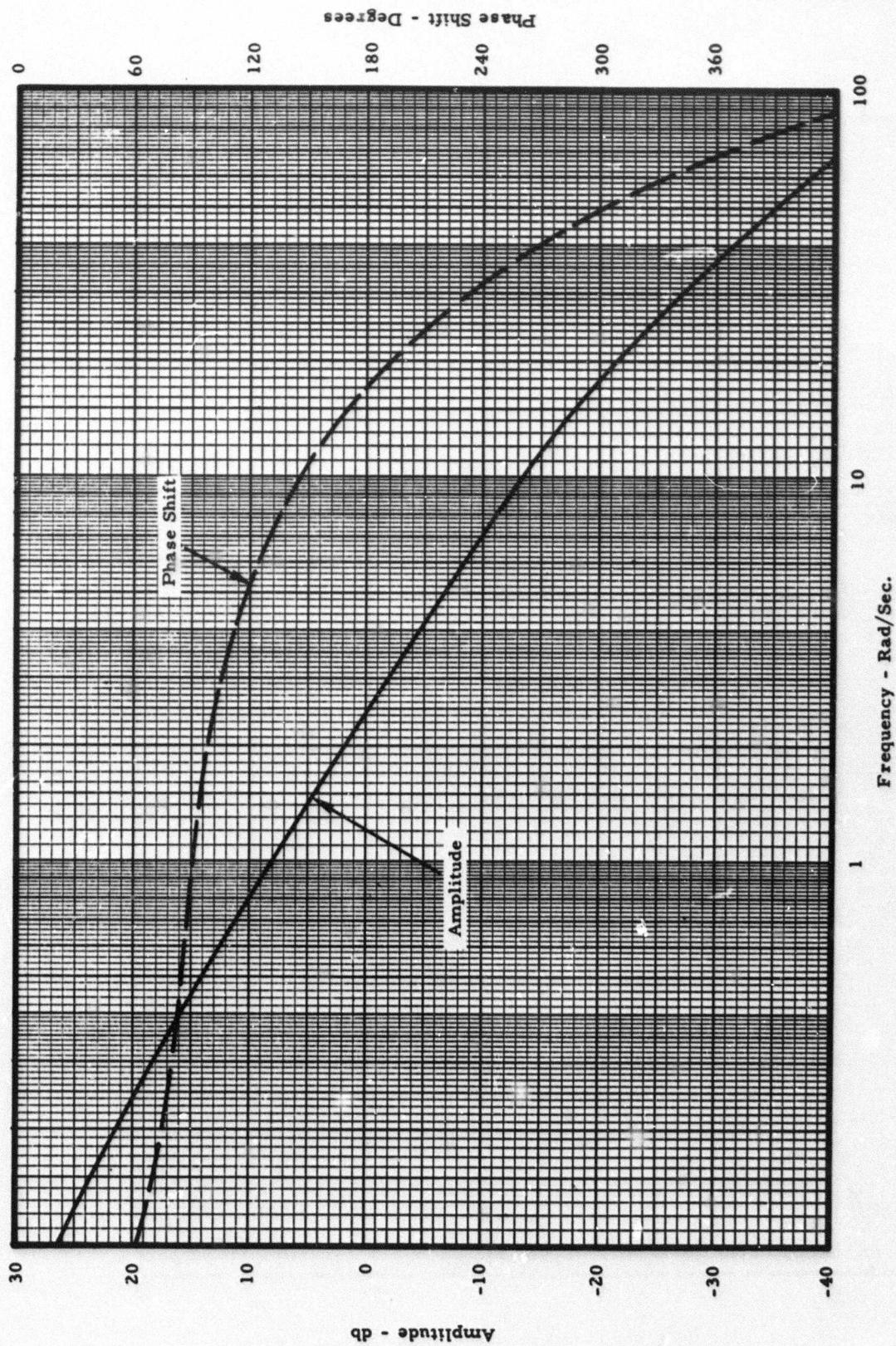


Figure XI-3. Bode Plot - Full-Load Condition.

## Section XI

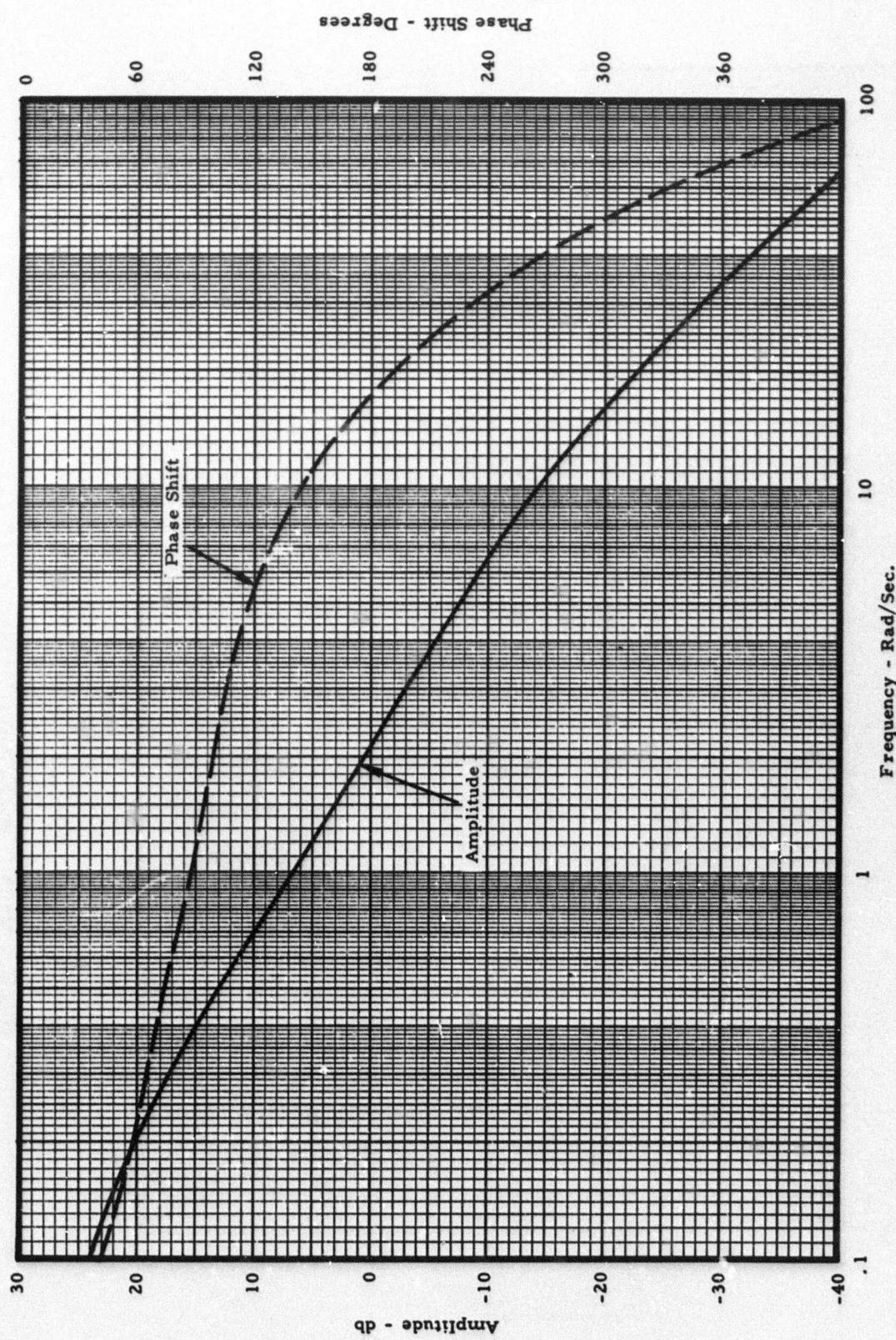


Figure XI-4. Bode Plot - No-Load Condition.

## Section XI

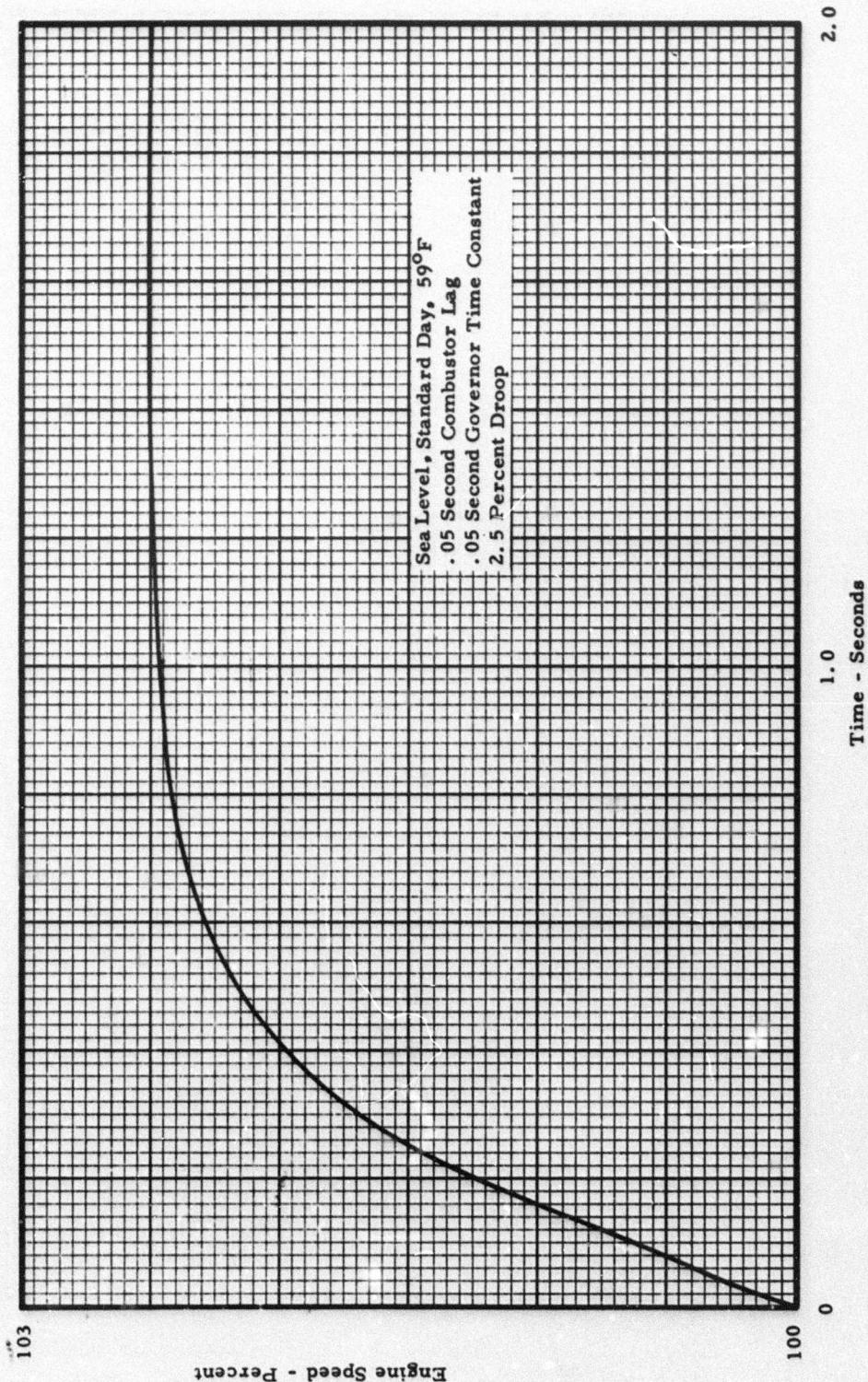


Figure XI-5. Transient Response - Full-Load to No-Load Step.

## Section XI

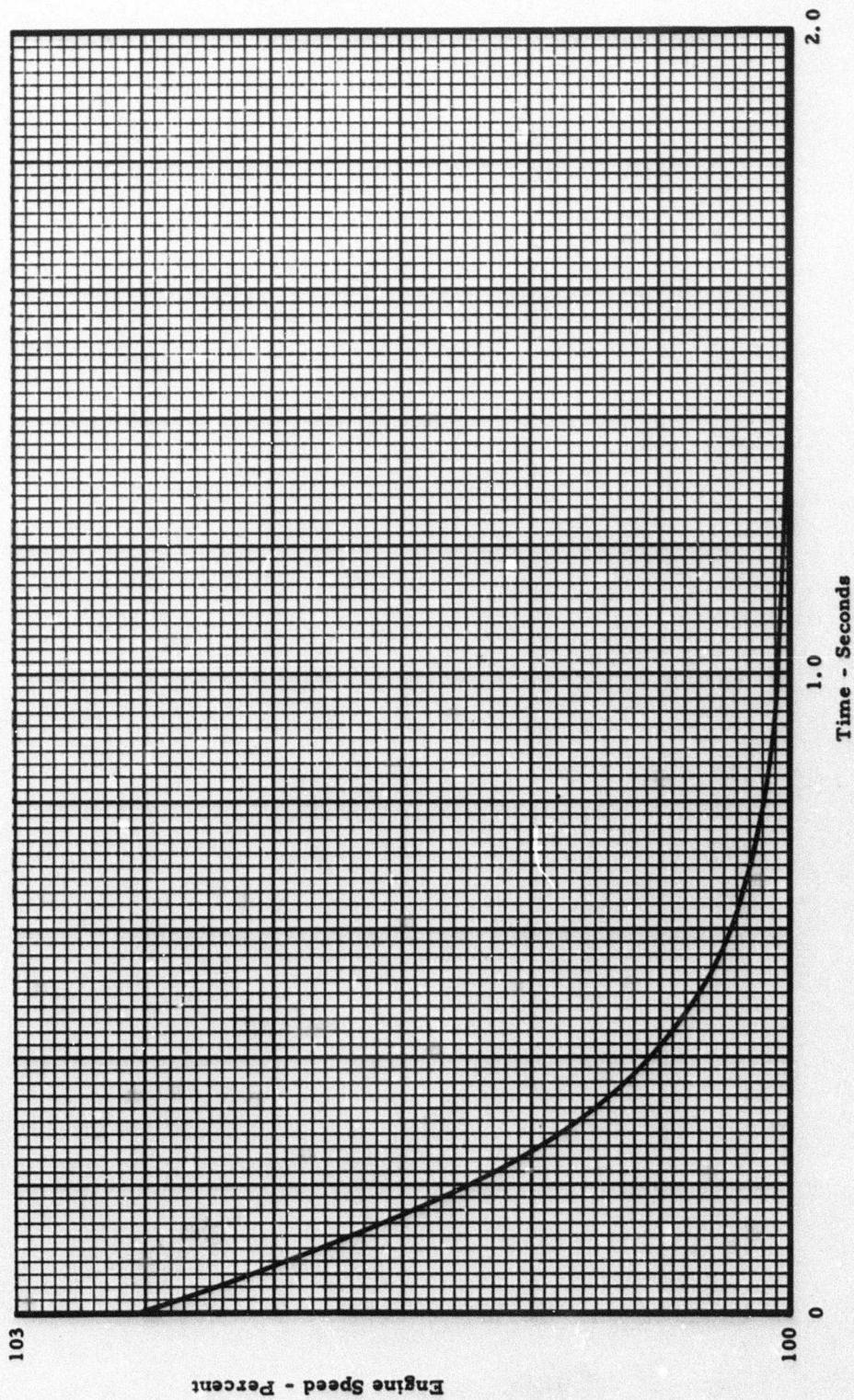


Figure XI-6. Transient Response - No-Load to Full-Load Step.

## Section XI

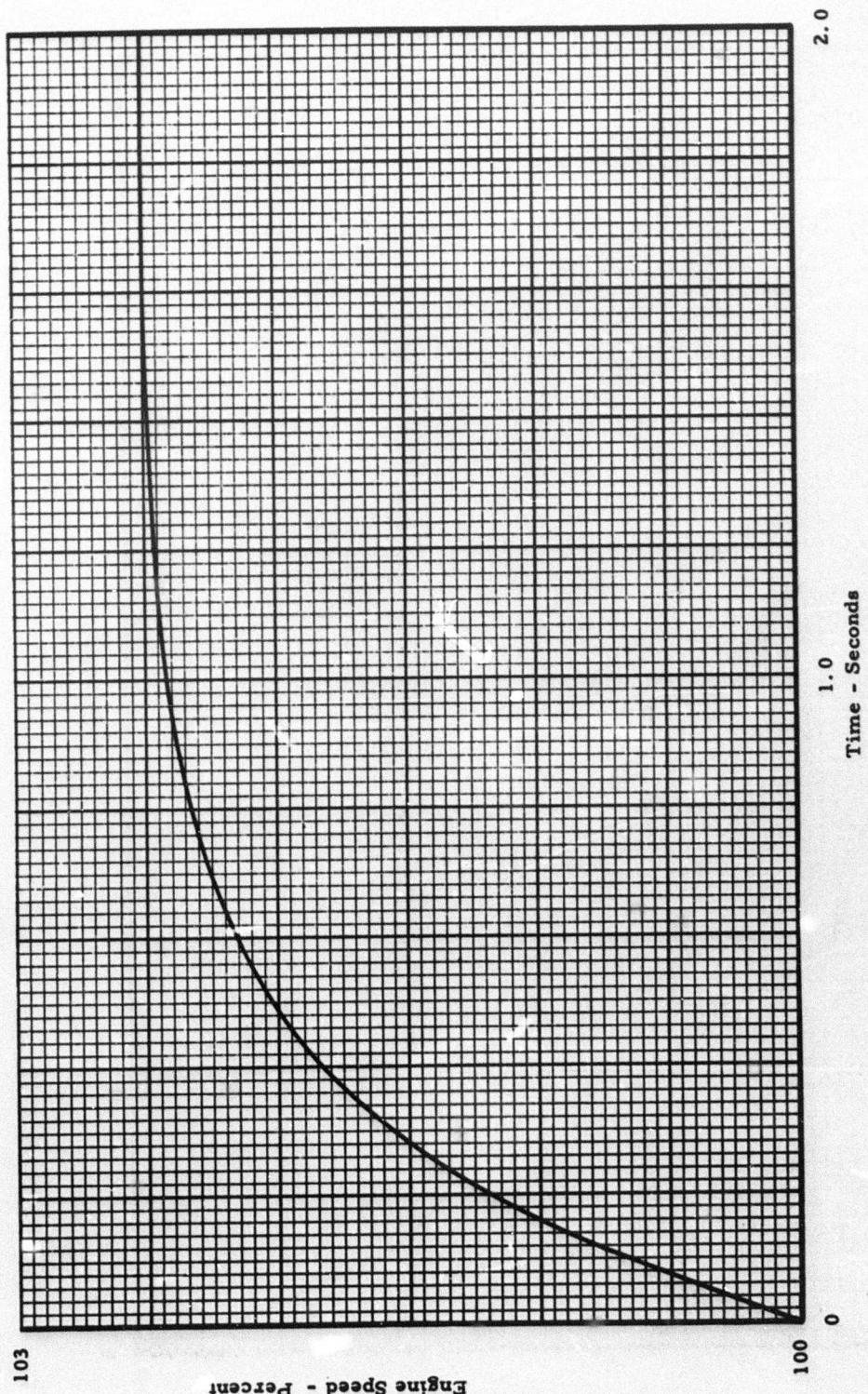
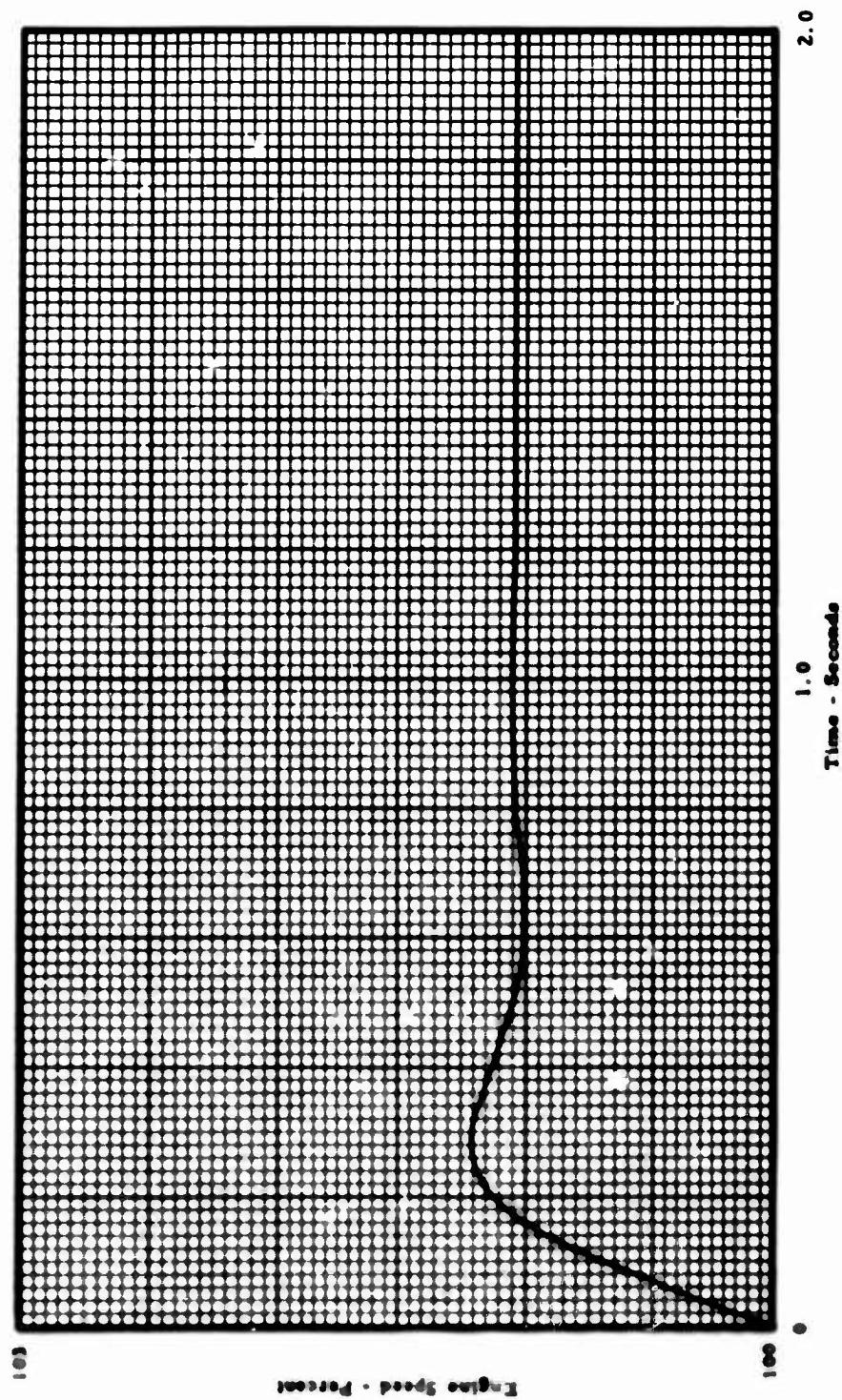


Figure XI-7. Transient Response - No Combustor Lag.

**Section XI**



**Figure XI-8. Transient Response - One Percent Droop.**

**Section XI**

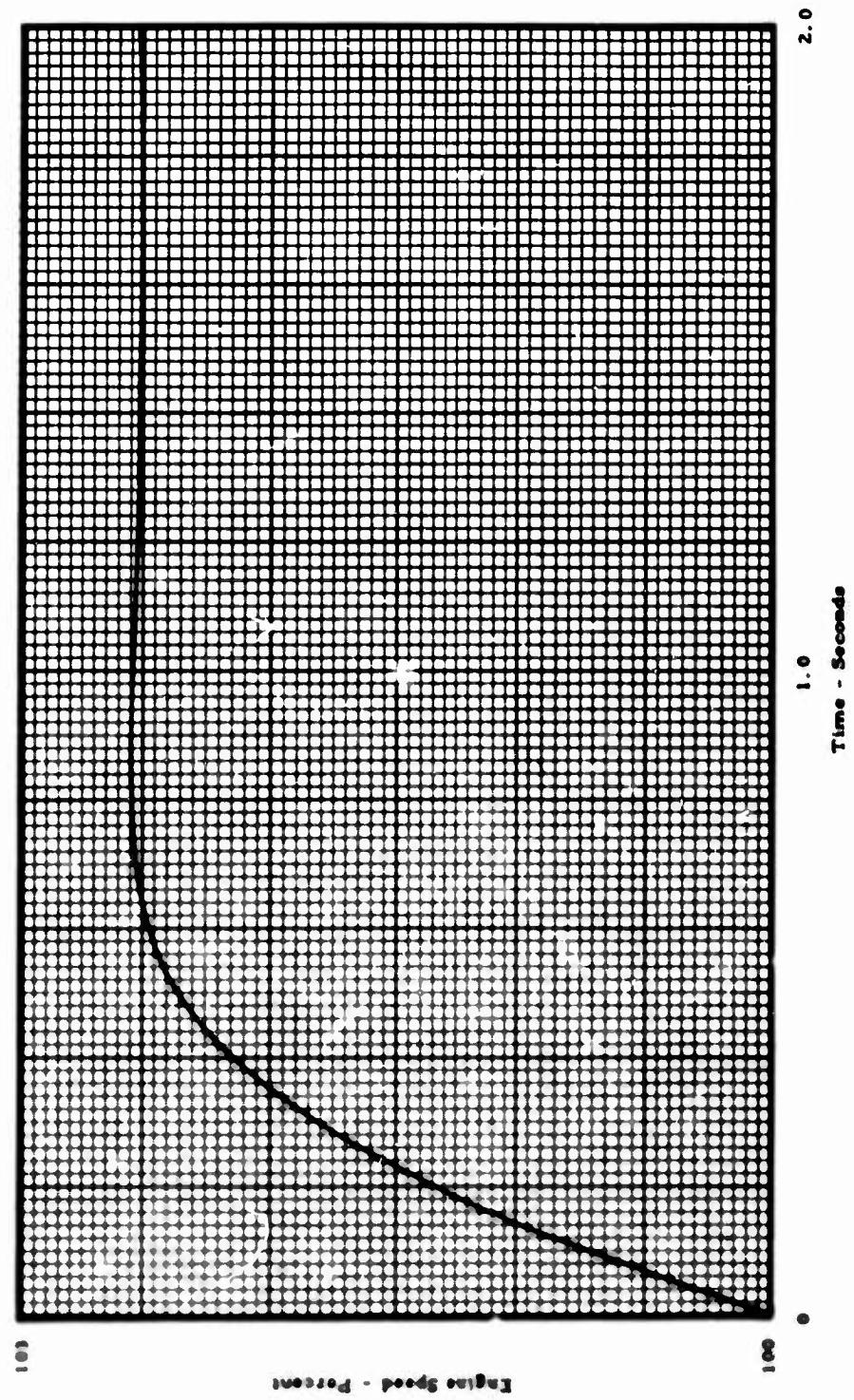


**Figure XI-9. Transient Response - 0.10 Second Governor Time Constant.**

Section XI

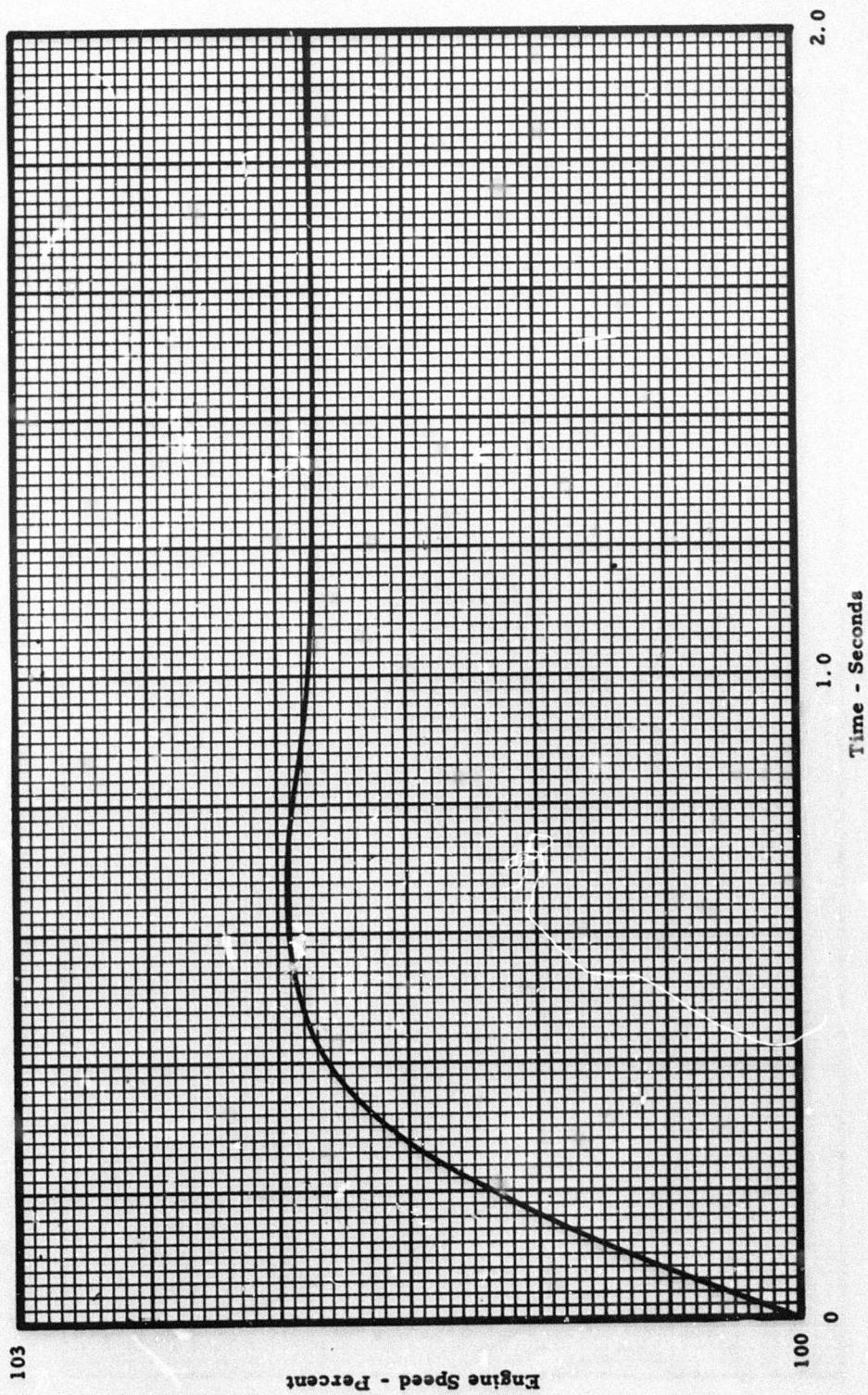


Figure XI-10. Transient Response - 8000 Feet Altitude, -65° F.

**SECTION XII**

**MAINTENANCE**

## SECTION XII - MAINTENANCE

The Model TS120 features accessibility and versatility. The accessories, Figure XII-1, are mounted at right angles to the engine axis. The starter (No. 1, Figure XII-1) alternator (2), and fuel control (3) are accessible from the side and placed to provide room for changes during development. A free drive (4) is provided. The engine sequence control unit (5), combination oil filter and dipstick (6), are located at the top of the accessory case. An oil drain plug (7), is located at the bottom of the oil sump and the oil filter (8), at the side of the accessory case. The location of the oil cooler fan and the oil cooler has been discussed in the lubrication section. The ignition coil (9), and fuel nozzle (10), excess fuel drain (11), and the exhaust gas temperature limiter (12), are all located exterior to the engine. The position of the engine mounts and lifting provisions are shown.

Referring to Figure XII-2, the combustor (13), and combustor cover is removed by detaching a quick-disconnect clamp. The combustor housing (15), and exhaust duct and rear bearing support (16), are removed after disassembly of the fastener row (17). The volute (18), is removed by disassembly of six bolts (19). The turbine inlet nozzle (20), is removed by disassembly of six bolts (21). The disassembly to this point allows for complete replacement of the hot end static parts and inspection of the turbine wheel.

Disassembly of the front end of the engine is accomplished by removing the accessory covers (22), the accessory drive gears (23), the accessory drive shafts (24), and the power take-off adaptor (25). The main rotor thrust bearing (26) is disassembled by removing the nut and the drive coupling (27), and then pulling the bearing cage (28). The combination oil pump and cover assembly (29), and overrunning clutch (30), may be removed at any time. The accessory case (31), and the conical diaphragm (32), may then be removed. The axial compressor (33), is removed by disassembling the nut (34). The axial stators (35), the interstage duct (36), the radial diffuser (37), and the split interstage diaphragm (38), may be removed in sequence. The balance of the rotor may be disassembled by removing the nut (39), the front shaft (40), the nut (41), and separating the radial compressor (42) from the turbine (43).

**Section XII**

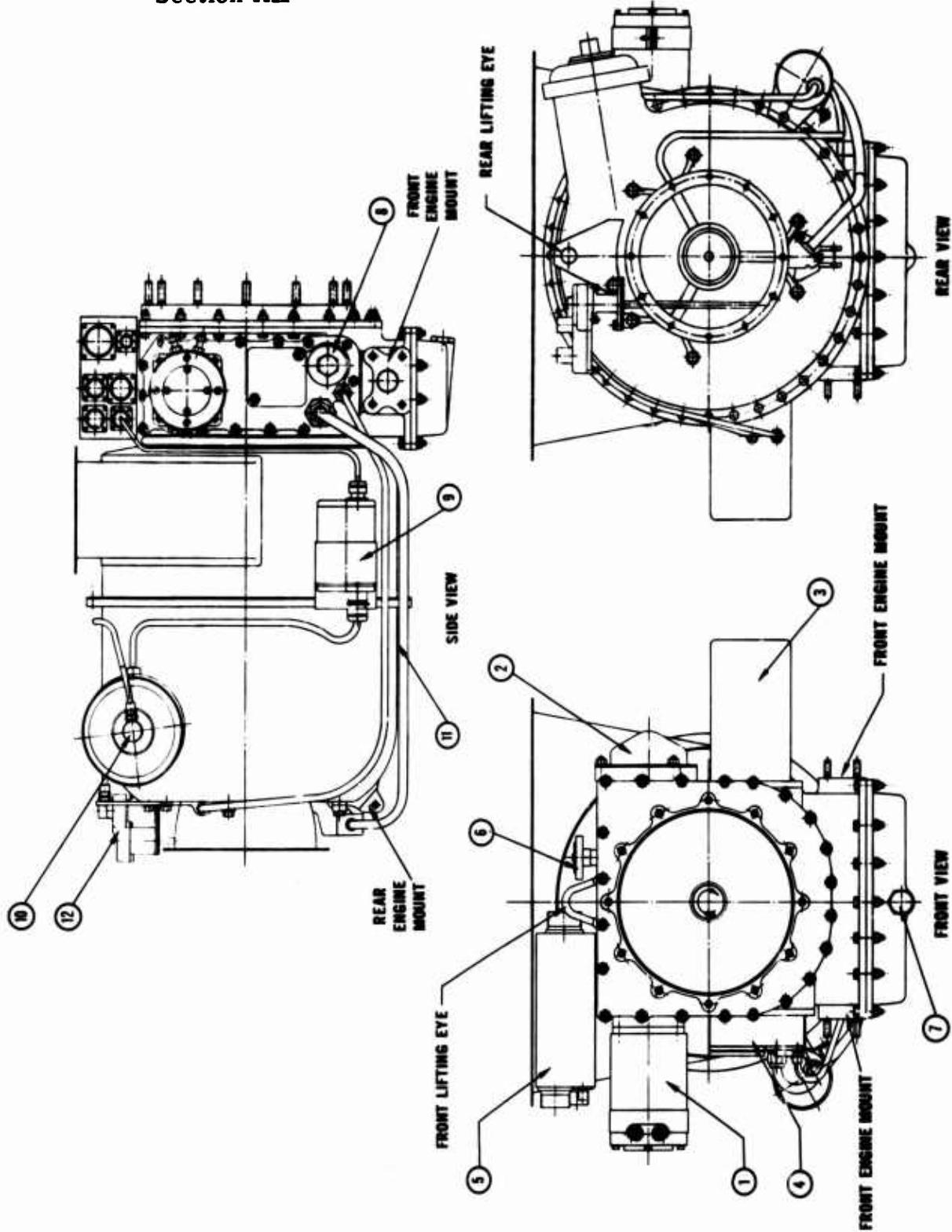


Figure XII-1. Model TS120 Engine Installation.

**Section XII**

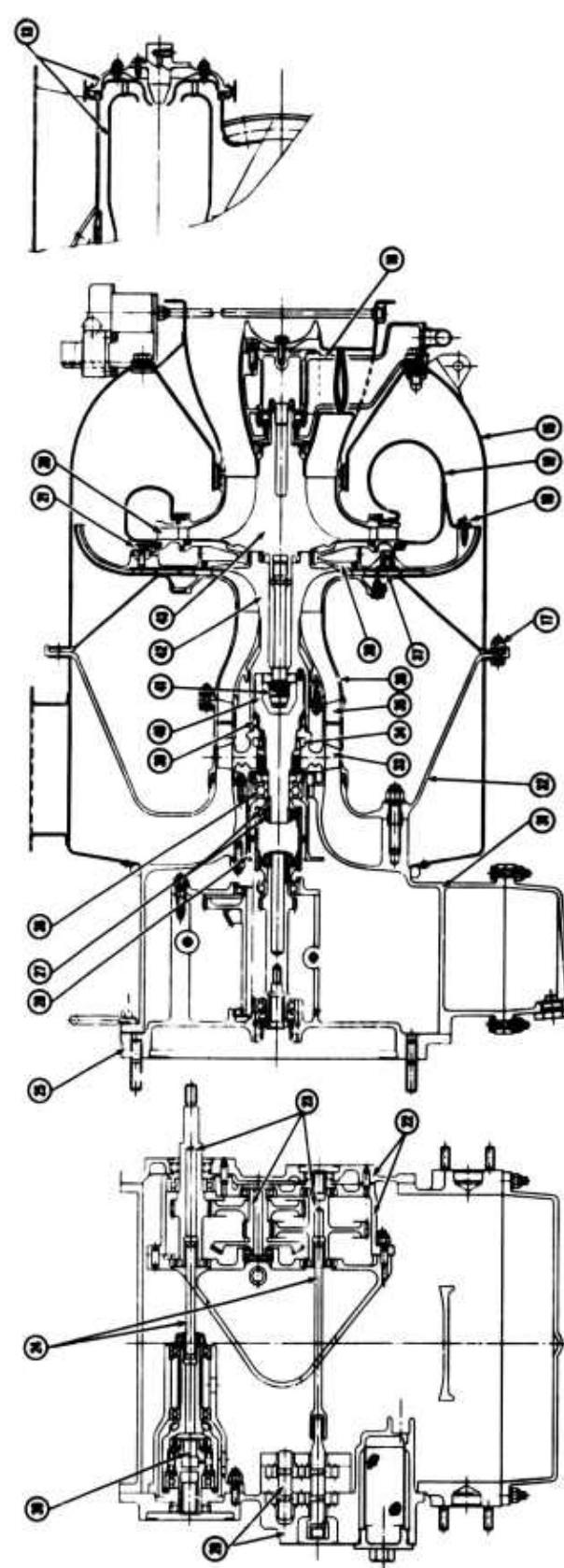


Figure XII-2. Model TS120 Basic Engine Cross Section.

SECTION XIII

**MANUFACTURING**

### SECTION XIII - MANUFACTURING

During the initial design stage and throughout the detail release of engine drawings, liaison has been and will continue to be maintained with the production division of the company so that their advice and experience may be fully utilized. Maximum effort is being maintained to provide for low production costs consistent with basic engine performance objectives.

The basic two-bearing rotor suspension results in a simplification from the standpoint of structural components, bearings, couplings, main shaft seals, and lubrication system complexity. The axial rotor, subsequent to initial development, can be a precision cast part. The use of ECM machining, combined with a finish skin cut, offers possibilities for low-cost radial compressor and turbine rotors machining.

The radial diffuser is a brazed sheet and strip-stock construction consistent with present production techniques. Flanges on sheet metal housing are designed to utilize stamped flanges. The inter-stage seal diaphragm, turbine inlet nozzle, and rear bearing support are steel castings.

The axial stators are a precision aluminum casting but can be die cast in two pieces when production rates warrant tooling costs. All the magnesium casting in the cool end of the engine are designed to permit die-casting when production rates warrant tooling costs.

SECTION XIV

**NOISE CONTROL**

## SECTION XIV - NOISE CONTROL

### INTRODUCTION

The services of the firm of Dilworth, Secord, Meagher and Associates Limited, with consultation by Dr. H. S. Ribner of the Institute for Aerospace Studies of the University of Toronto has been acquired to assist in the study of noise control for the TS-120 engine. The scope of their work has been to advise on design aspect to produce minimum noise, and propose modifications to the basic engine that would be necessary to reduce the sound pressure level of the engine below the values required by the engine specification. The material presented herein is largely the results of their efforts to date.

The study commenced with a survey of the current state-of-the-art in gas turbine silencing. A recent review (Ref. 1) by Dr. Ribner provided an appropriate starting point. Later, analytical and experimental studies were initiated and are continuing. The recommendations of the present report may later be refined as studies proceed.

### LITERATURE SURVEY

#### Spinning Modes of Turbo Machinery

Tyler and Sofrin (Ref. 2) recently have put forward their spinning mode theory, from which it is possible, knowing the r.p.m. and the number of rotor and stator vanes, to predict which type of spiral sound wave will propagate. This must always be a harmonic of the blade passage frequency, but the theory so far does not predict the amplitude of this pure tone, hence in an actual engine it is possible that it is at a lower amplitude than the general aerodynamic noise, and its nuisance value is difficult to estimate.

A simplified theory of spinning modes is put forward by Bragg and Bridge (Ref. 3) which dispenses with the complex mathematics in Ref. 2. From this theory it is easy to see that for typical small gas turbines, the first harmonic of the blade passage fre-

## Section XIV

quency tends to be out of the normal hearing range, and the second harmonic is definitely inaudible.

On looking at a plot of the sound pressure level (SPL) versus frequency for a gas turbine it is very apparent that there are many peaks, extending over an appreciable frequency span, that are not pure tones as such. Griffiths (Ref. 4) has put forward reasons, but no mathematical equations, for these peaks. They are likely to be at shaft frequency and its harmonics, and at blade passage frequency and its harmonics and sub harmonics. They are caused by turbulence and imperfection in the wheel symmetry, and are likely to be completely random in their distribution. Griffiths does not think that it will be possible to predict their distribution analytically.

### Exhaust Silencing

In Ref. 5 is described a system of Exhaust Silencing using aspirated air to cool the exhaust pipe. This system is claimed to be very efficient at pumping secondary air, and at the same time acts as an effective noise attenuator. The system depends on setting up a radial temperature and velocity gradient across the exhaust pipe, and thereby bending the effective acoustical path from the turbine outlet so that the sound waves impinge on the exhaust duct walls. If the exhaust duct is lined with sound absorbing material, attenuation of the noise results.

Also in the above reference the exhaust jet noise is calculated for a 250 horsepower turbine, and it is shown that for the low gas speeds and temperatures involved this noise is small compared to the measured noise of turbine and exhaust combined, and it is shown not to be a problem at present.

### Sound Absorbing Materials

It is a well known fact that porous materials act as sound absorbers with varying degrees of effectiveness. By calculating the flow resistance of the material, and its acoustic compliance, a series of analogies can be drawn between acoustic, electrical and mechanical networks. A complete analysis is given in Refs. 6 and 7. An attempt to calculate actual absorption coefficients and cor-

## Section XIV

relate them with experimental data was made in Ref. 4. The theory only deals with the absorption of sound waves normal to the absorbing material, and it was only this type of wave that was dealt with by the experiment. Randomly incident waves were not dealt with at all.

In order to use sound absorbing materials in a turbine as close as possible to the source of noise, a whole new series of absorbing materials has been developed, but so far it is difficult to say how effective they are in practice. The main problem is that because of their inherent porosity, they introduce leakage and hence unacceptable performance losses in turbo machinery. From the tests reported in Ref. 5, it would appear that in actual practice acoustical absorbing materials are not as effective as the theory might predict, since most of the noise in the voice frequency range appears to radiate from the turbine casing. This means it is transmitted by mechanical vibrations from the blades and bearings etc. direct to the outer casing, and short circuits, as it were the absorbing material.

### ANALYSIS OF THE NOISE SPECTRUM OF THE T72 ENGINE

#### General Noise Spectrum

Before any concrete recommendations could be made for acoustical treatment of the TS-120 Engine, it was essential to know approximately the noise spectrum to be expected. It was apparent from the literature survey that this could not be done with any degree of accuracy by analytical means, and hence the spectrum of a geometrically similar, but larger, engine has been taken as the most probable noise spectrum for the TS-120 engine.

The data used were photographed Cathode Ray Oscillograph (CRO) traces of the sound spectrum taken during the development of the T72 engine. These were taken during combustor trials, and were not intended at the time for a noise analysis as such. Hence the measurements must be assumed to be approximate only. But, having this information available, it was not worth running another test series in order to repeat the noise analysis more accurately.

## Section XIV

The data consisted of the five sets of continuous noise spectra, taken at different shaft speeds. A typical spectrum is shown in Figure XIV-1. The pure tones are shown by the single vertical lines. In order to compare the data with the engine performance specifications of the TS120 engine, which is given for a full octave band spectrum, it was converted to this form and it is shown in Figure XIV-2. The small vertical lines indicate the presence of pure tones. The ERDL specification is superimposed on the plot for comparison.

The T72 engine has an identical blade and vane count on the transonic axial stage as the TS120 engine but has one more blade on the centrifugal stage rotor, hence both engines can be expected to have fairly similar noise spectra. The maximum attenuation appears to be required in the mid-range of the vocal frequencies, and if pure tones are present, this would require a maximum attenuation of nearly 30 db. If pure tones are not present 20 db would be sufficient. This is a large attenuation, but fortunately it is only over a limited frequency range, so that it may be possible to tune all the attenuating material to have maximum absorption in this region.

### Comparison with Spinning Mode Theory

During the analysis of the data of the T72 engine, the locations of all probable pure tones were taken. If the frequency of the pure tone is divided by the rotational speed in revolutions per second, the probable cause of the tone can be found as shown in Table XIV-I.

From this table it can be seen that even if the blade passage frequency tone does propagate, it will be in the very high frequency range, and nearly out of the hearing range. The axial stage first harmonic did not propagate with one exception. The first harmonic of the centrifugal stage propagated strongly in all cases. It is predicted theoretically that both pure tones would propagate along a duct, as shown below.

## Section XIV

TABLE XIV-I  
ANALYSES OF THE T72 ENGINE SOUND SPECTRUM

TEST RPM	38,000	39,000	39,800	40,000	41,100	
N REV/S SEC	633	650	664	667	685	
PURE TONE FREQUENCY	F	F	F	F	F	
	N/F	N/F	N/F	N/F	N/F	Probable Harmonic
720	1.14	730	1.12	730	1.1	.285
870	1.37	900	1.38	870	1.31	285
1130	1.79	1200	1.85	990	1.49	720
1400	2.21	1500	2.31	1460	2.20	1.17
1620	2.56	1750	3.00	1450	2.18	N
1820	2.87	1950		1480	2.16	
4150				2480	3.72	3N
					2900	4.24
7200						4N
10900	17.2	11800	18.2	11600	17.5	6N
						BN ax.al
						BN centrifugal

## Section XIV

From Ref. 3, any wave due to blade interaction will propagate if there is a solution to the equation

$$\cos d = \frac{a}{u} \left( \frac{KS - 1}{nB} \right)$$

For the T72 engine axial stage

$$B = 11$$

$$S = 23$$

K is an integer such that  $\left| \frac{KS - 1}{nB} \right|$  is minimized and n is the harmonic number. Hence it can be seen for the first harmonic the minimum value of the bracket in the quation is -1. Since U, the blade speed is greater than a, the acoustical velocity, there is a solution to the equation, and the wave should propagate. It could, however, be detected at only one shaft speed in the data available. Possibly this exception from the theory is due to the interstage shock, preventing the upstream passage of the pressure fluctuations. For the centrifugal stage

$$B = 18$$

$$S = 23$$

Then for n = 1

$$\left| \frac{KS - 1}{nB} \right|_{\text{Min.}} = 5/18$$

The mode will propagate, and it could be detected in all cases. For a centrifugal compressor the tip speed is normally close to the acoustical velocity and there will be a shock wave around the vaneless space. Hence it is unlikely that the pure tone of the blade passage frequency will propagate up stream to the inlet. It is more probable that the sound is transmitted via the diffuser guide vanes, to the casing. Since the frequency of this pure tone is very high (12,000 cps/sec.) it is not a great annoyance, and it can be fairly

## Section XIV

easily attenuated, so that it should not be any great problem in the TS-120 engine.

These deviations from the theory make it difficult to derive analytically a probable spectrum for the TS-120 engine, and the spectrum for the T72 engine is assumed to be the best indication available of the noise levels to be expected.

### NOISE CONTROL

In the TS-120 engine, the main sources of noise may be classified as follows:

1. Axial Compressor
2. Centrifugal Compressor Diffuser
3. Combustion Can
4. Turbine and Exhaust Noise
5. Casing Vibrations
6. Accessory Noise

In this section the probable method of controlling these sources of noise will be put forward. These recommendations can only be considered tentative, because the optimum arrangement of noise attenuating modifications can only be found after extensive testing, but they will indicate how the problem will be attacked.

#### Axial Compressor and Inlet

It is proposed to line the inlet duct as heavily as possible with acoustical absorbing material, as shown in Figure XIV-3, item 1. The optimum thickness of the material has not yet been decided, but it will most probably be in the region of 3/4-inch as shown. It does not appear likely that an additional external inlet silencer will be of any value, since sufficient attenuation of the inlet noise should be obtained within the casing itself, and other engine noises would then be predominant.

Provisions have been made to adjust the width of the engine air inlet to allow for sound absorbing material thickness. It requires the addition of a spacer to the struts in the flow path, an increased length bearing support and drive coupling.

## Section XIV

### Centrifugal Compressor Diffuser

Because of the inefficiencies of any vaned diffuser, it is probable that there is in this region a large amount of turbulence. This will be a broad band noise source that will probably be one of the most predominant in the engine. Because of the leakage losses incurred, it would be impossible to line the diffuser or the shroud with acoustical material, even if there was room.

It would be desirable to introduce damping material, such as silicone rubber, within the engine structure, as close as possible to the vanes, but because of the stiffness requirement of the engine in this region, and also the temperatures involved, this does not appear practical. It is possible to line the inlet duct of the centrifugal compressor with acoustic material, as shown in item 2, Figure XIV-3, but because of the high gas velocities in this region, the performance penalty is likely to be severe.

The vibrations to the casing can be damped by using a silicone rubber damper on the central flange of the engine, as shown in item 3. This material would support an outer shell, covering the whole rear section of the engine, which would be isolated from the diffuser, and hence minimize the structure transmitted noise from this region.

### Combustor Can and Turbine Inlet

This section of the engine can be expected to be a significant source of broad band noise, and it will be necessary to line the outside with absorbing material, as shown in item 5, Figure XIV-3. Because of the high temperatures in this region, cooling air will probably be required to protect the acoustic material, so use can be made of the secondary air, pumped by an exhaust silencer, to do this. The size and weight penalty of this arrangement is large, but since the effectiveness of any acoustical material rapidly decreases with increase in temperature, some compromise will have to be reached.

## Section XIV

### Exhaust Silencing

It is proposed that a refractive exhaust silencer similar to that in Ref. 4 should be used in the TS-120 engine. The arrangement will be as shown in Figure XIV-3. Again, the exact dimensions of this modification are not yet known, but it is shown in the next section how it is hoped to derive an optimum design by experimental means. From approximate calculations it appears that the exhaust duct should be lengthened by about six inches in order to take full advantage of the bending of the sound waves. The performance penalty of this type of modification should not be too severe according to Ref. 4, but that study did not use a silencer that was integral with the turbine outlet.

### Accessory Noise

The noise from the engine accessories are not expected to be a major problem as regards noise generation, with the possible exception of the oil cooler fan.

The gears have been made wide faced, with a large helix angle, so that, providing they are accurately machined, they should be quiet running. From the literature survey, very little information would be found of gear noise and it is felt that a policy of 'wait and see' would be most appropriate for this part of the engine. If a significant amount of noise is generated by the gears, then narrow band analysis of this noise will give a fairly clear indication of where the trouble lies, and appropriate redesign should be sufficient to cure it.

In the work carried out in Ref. 5, it was found that the predominant noise source in the accessories was the oil cooling fan. It is suggested that this be designed so that the blade passage fundamental frequency is above 10 kc, so that it will be inaudible to the normal adult, and then the noise generated should only be a broad band type due to air turbulence. In Ref. 5 it was suggested that spiral type silencers be used that combine the function of stator blade and silencer, but the size penalty of this unit is severe, and its effectiveness not known.

## Section XIV

### EXPERIMENTAL WORK

There does not appear to be at present any theory that can accurately predict the acoustic effect of lining a small annular passage with sound absorbing material. If an attempt is made to apply the theory used for calculating the sound attenuation in a regular enclosure resembling a room, to a compressor inlet for example, inconsistent results are obtained, depending on the assumed boundaries of the 'room'.

Also in the results reported in Ref. 5, there appear to be a lack of agreement between the effectiveness of materials tested by a standing wave tube method, and those found in practice. Hence, it was felt that any experimental work done on sound absorbing materials should be more closely related to actual field conditions.

The sound rig being developed for the sound study of the TS 120 turbine engine is shown in Figure XIV-4. The aim is to simulate an annular noise source, and then to study the effects of various types and thicknesses of sound absorbing materials placed around the surfaces of an annular passage.

#### Material Testing

Using the rig shown in Figure XIV-4, tests are at present being carried out to investigate suitable acoustical materials which can be used in a gas turbine. The types of materials used in Ref. 5 will be the main guide as to the choice of materials to be tested, but it is hoped that some more readily available and cheaper substitutes may be found.

All tests are carried out in the open to eliminate reverberation. The method of testing is to produce at the speaker a pure frequency tone, and then to measure the SPL of the noise three feet from the speaker, along the axis of the duct on a narrow band sound recorder. The band width used is 1/10 octave, and in this way the effects of background noise are minimized. Two annular ducts have been made; one with sound absorbing material on the inside surfaces and one without. They were designed so that the free area of the annulus in either case were the same.

## Section XIV

Repeatability tests have been carried out, and over the full range of frequencies, results are repeatable to within 1 db. The insertion loss, or attenuation produced by the sound absorbing material is found by comparing the spectrum produced by the two ducts.

### Inlet Investigations

When suitable materials for a turbine have been compared in the rig as it now stands, and the most suitable type found, it is proposed to further modify the rig to simulate more precisely the TS 120 inlet flow path. An approximate full-size mockup of the inlet will be made so that the sound pressure level of an acoustically treated inlet can be compared to an untreated one. In this way an accurate estimation of the effectiveness of any particular arrangement can be deduced before the full-scale testing of the gas turbine. The type of rig proposed is shown in Figure XIV-5.

### Exhaust Investigation

Before any firm recommendations are made for modifying the exhaust, so as to fit a silencer integral with the engine, it is proposed to investigate the effectiveness of this arrangement in the laboratory, using a modified version of the sound rig as shown in Figure XIV-6. This rig will be a full-scale model of the exhaust duct, and it will be possible to produce a radial temperature profile across the annular space by heating the inner cylinder and therefore the acoustic velocity will change with radius. The effect of varying this temperature profile on the SPL along the axis will be measured using similar methods as before. In this way an optimum design for the silencer can be derived.

### CONCLUSION

The proposed modifications required for silencing the TS 120 horsepower gas turbine engine so that the noise spectrum lies below the engine specifications, are at present only tentative. A comparison of the size of the modified engine with the standard engine is shown in Figure XIV-7. The modifications indicate the type of design that may be required, but the final design cannot be decided upon until the engine has been tested in its normal form.

## Section XIV

This is because it will not be precisely known until then which section of the engine will produce the most noise, and it is possible that some of the changes proposed will not be required.

The present untreated design should in theory produce a relatively quiet engine because of the double casing around the compressors, and the indirect inlet path. In view of this, the further noise attenuation requirements should not be difficult to obtain, using the methods outlined in this report.

REFERENCES

Section XIV

1. H. S. Ribner; The Noise of Aircraft; General Lecture; Fourth Congress of the International Council of Aeronautical Sciences; August 1964.
2. J. M. Tyler & T.G. Sofrin; Axial Flow Compressor Noise Studies; Society of Automotive Engineering; SAE Paper 345-D, 1961.
3. S. L. Bragg & R. Bridge; Noise From Turbojet Compressors; J. Roy, Aero Soc., Vol. 68 No. 637; January 1964.
4. J. W. R. Griffiths; The Spectrum of Compressor Noise of a Jet Engine; J. Sound and Vibration, Vol. 1 (2); 1964.
5. Gas Turbine Sound Attenuation, Final Report; U. S. Army, ERDL Contract Number DA-44-009-Eng-5183, July 1963.
6. S. N. Rchekin; Theory of Sound; Pergaman Press; 1963.
7. P. M. Morse; Vibration and Sound; McGraw Hill, 1948.

Section XIV

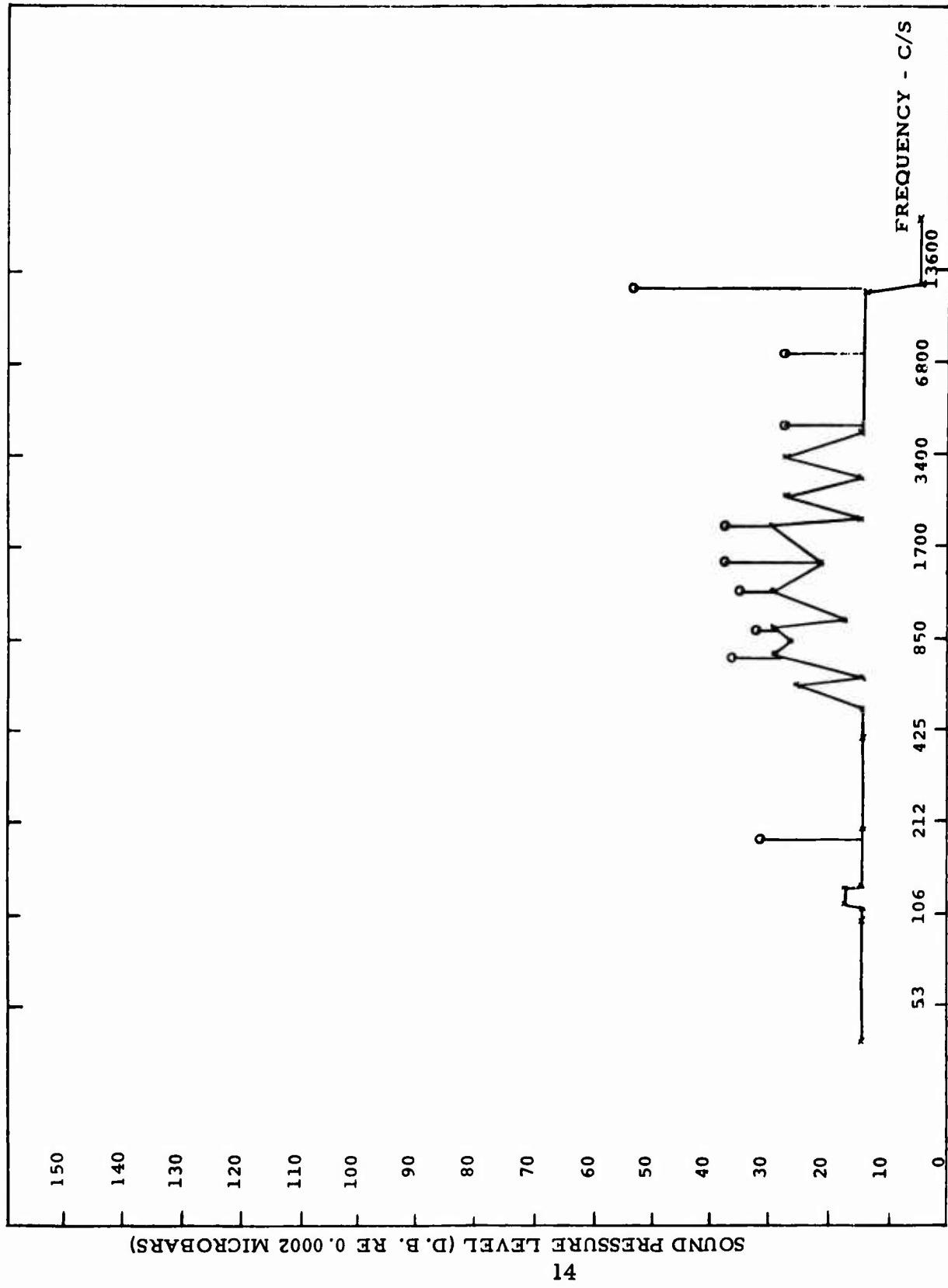


Fig. XIV-1. Narrow Band Pass Noise Spectrum of T72 Engine at 38,300 R.P.M.

## Section XIV

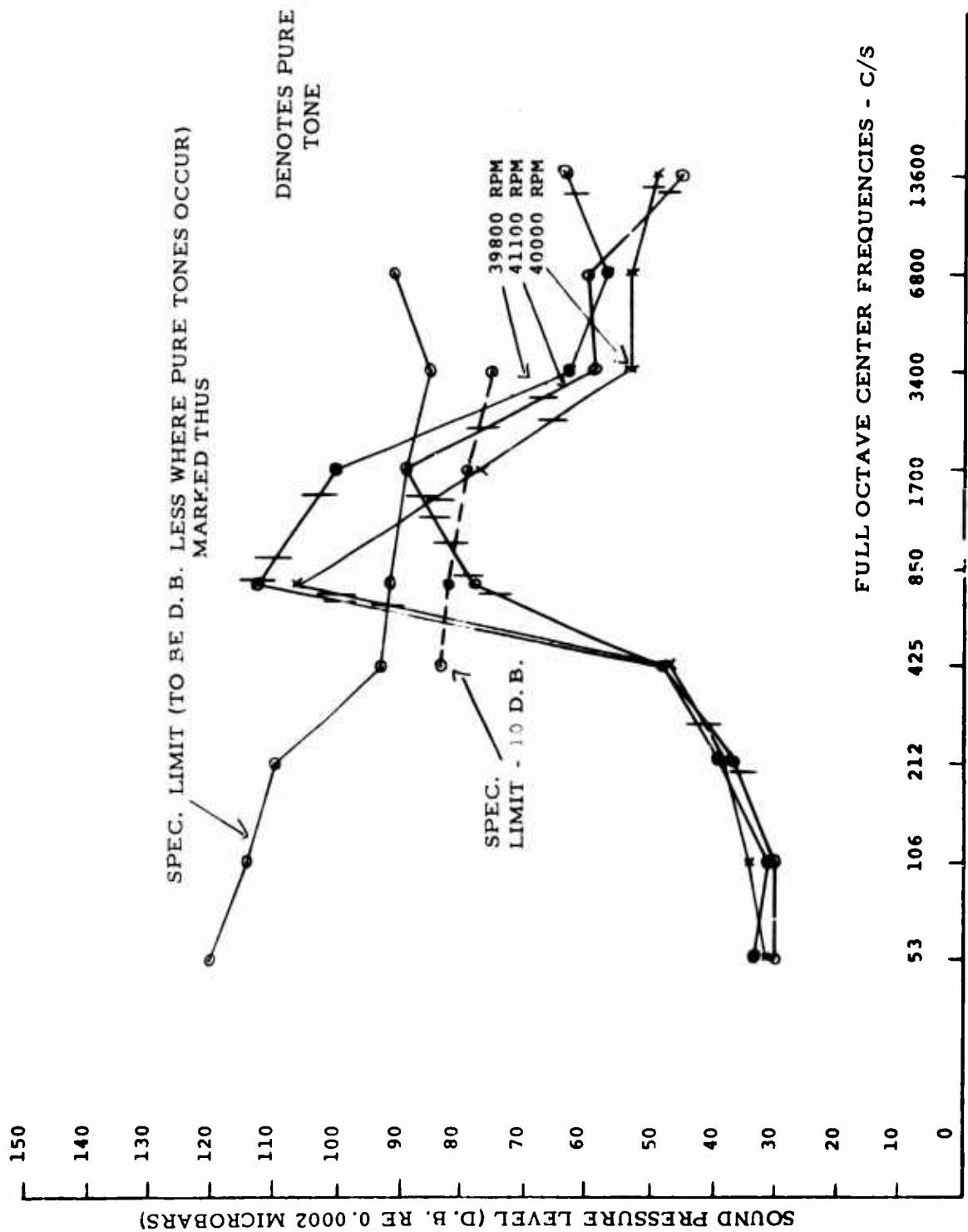


Fig. XIV-2. Full Octave Band Pass Spectrum of T72 Engine at 3800 R. P. M.

**Section XIV**

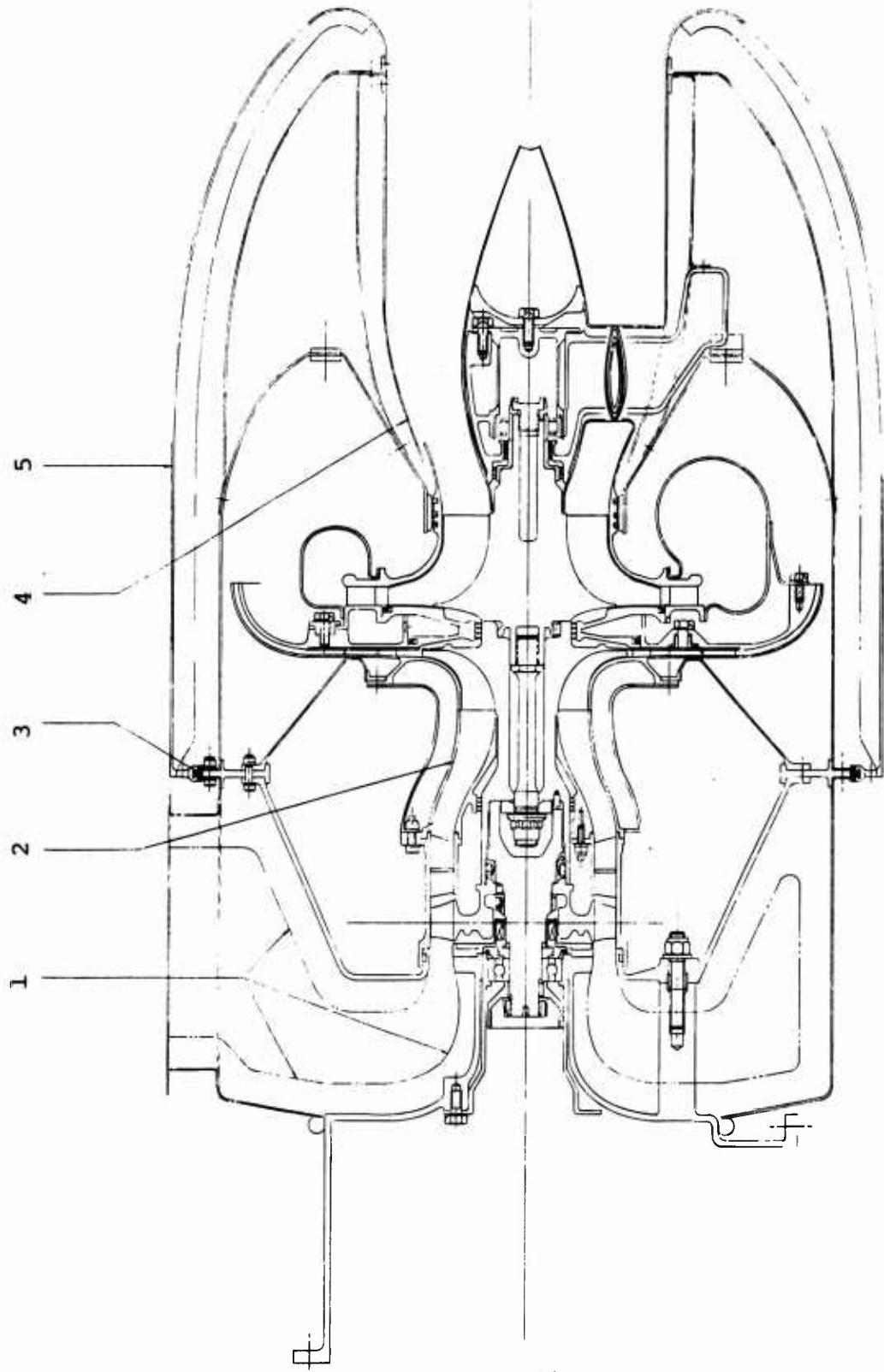


Fig. XIV-3. Proposed Modifications for Sound Attenuation of Model TS-120 Engine.

## Section XIV

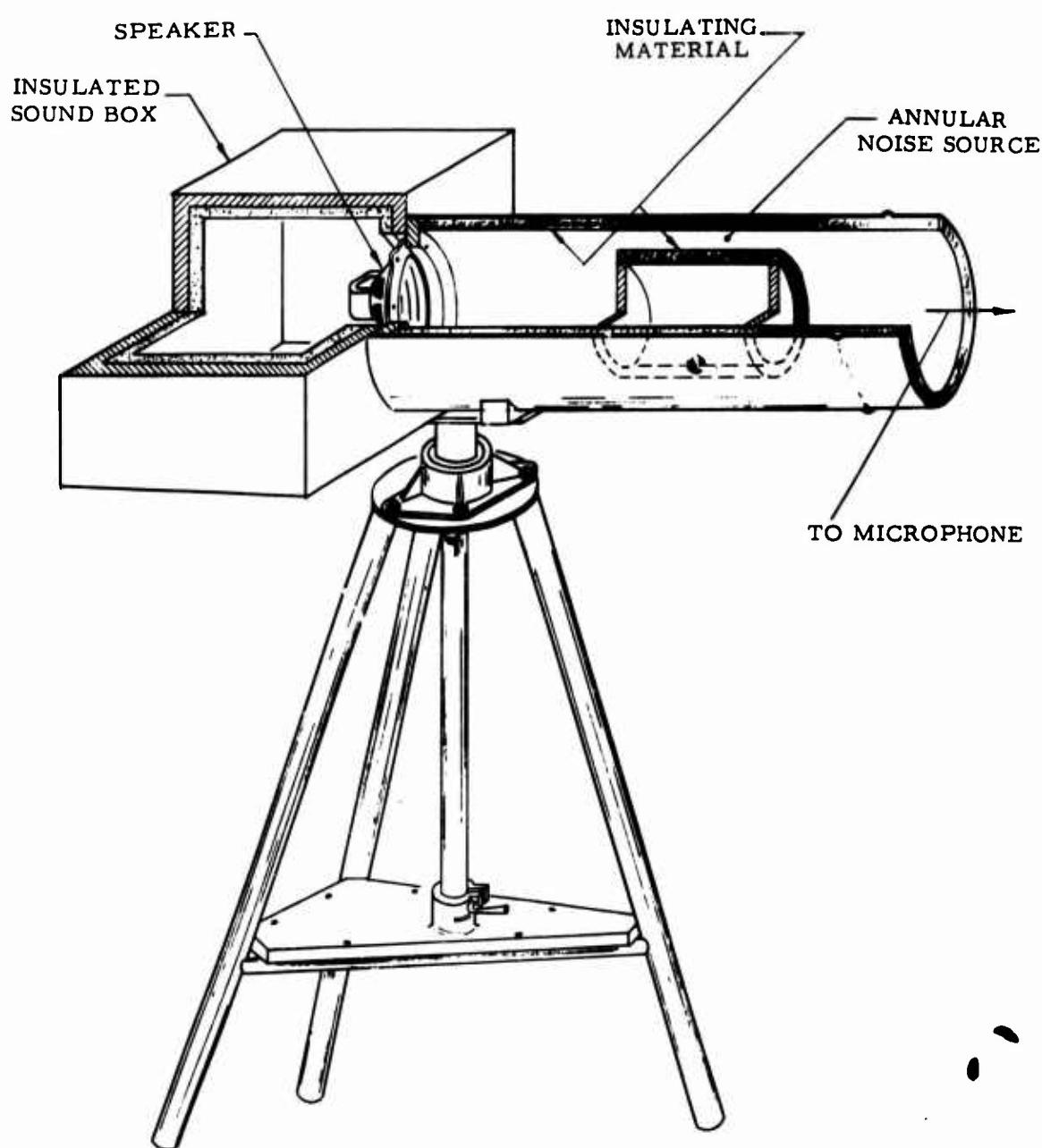
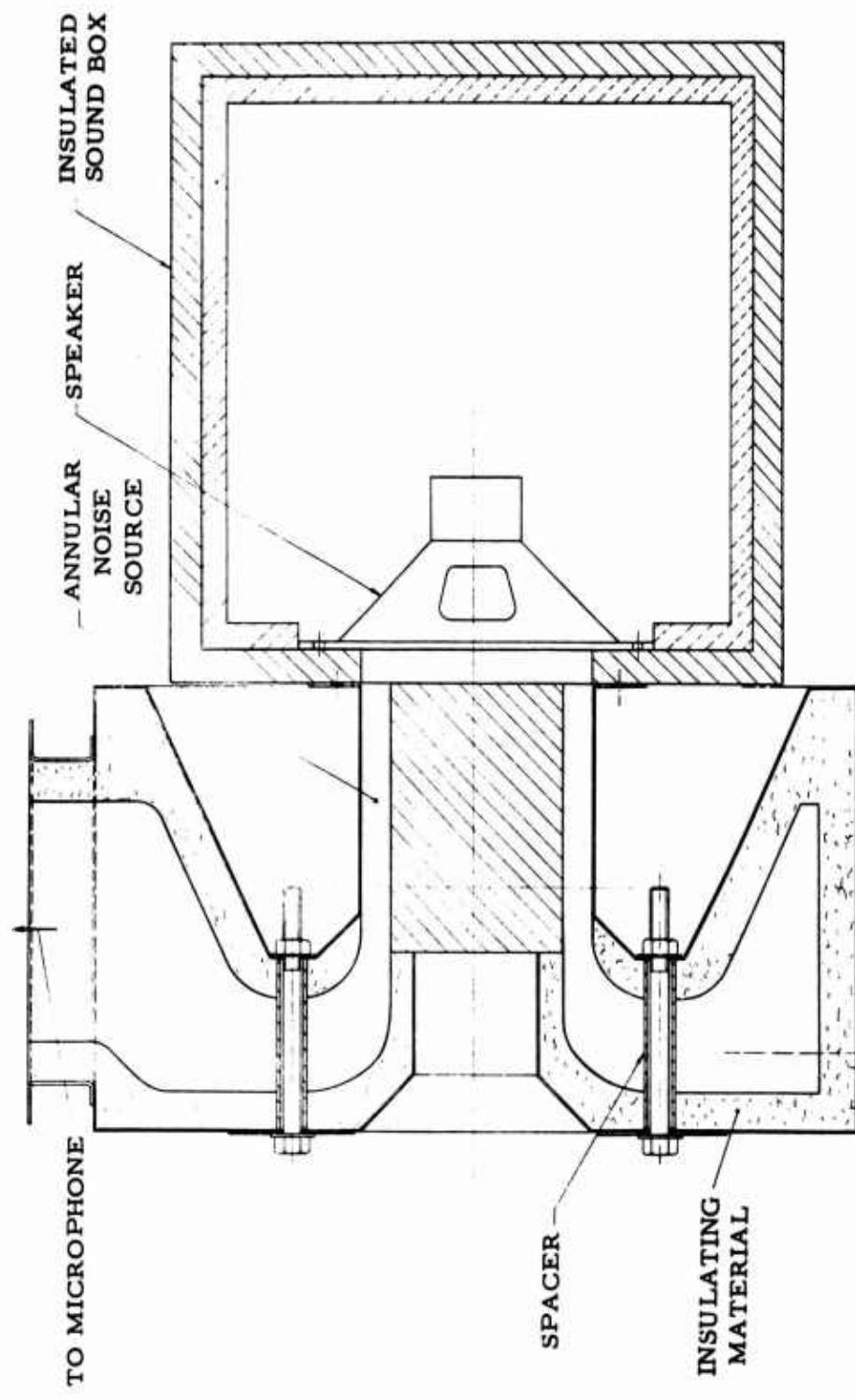


Fig. XIV-4. Sound Rig for Testing Acoustic Material.

**Section XIV**



**Fig. XIV-5. Proposed Rig to Investigate Inlet Attenuation.**

**Section XIV**

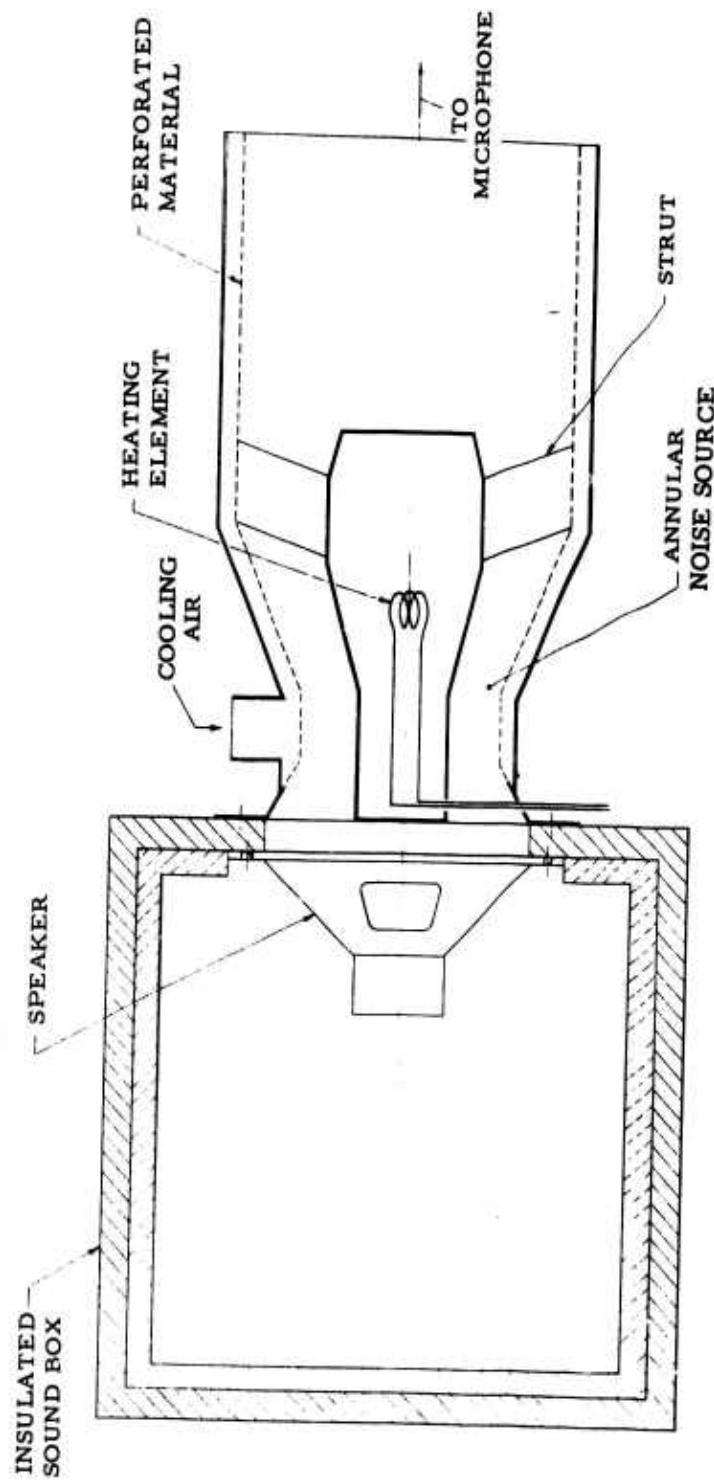


**Fig. XIV-6. Proposed Rig to Investigate Exhaust Silencer Effectiveness.**

Section XIV

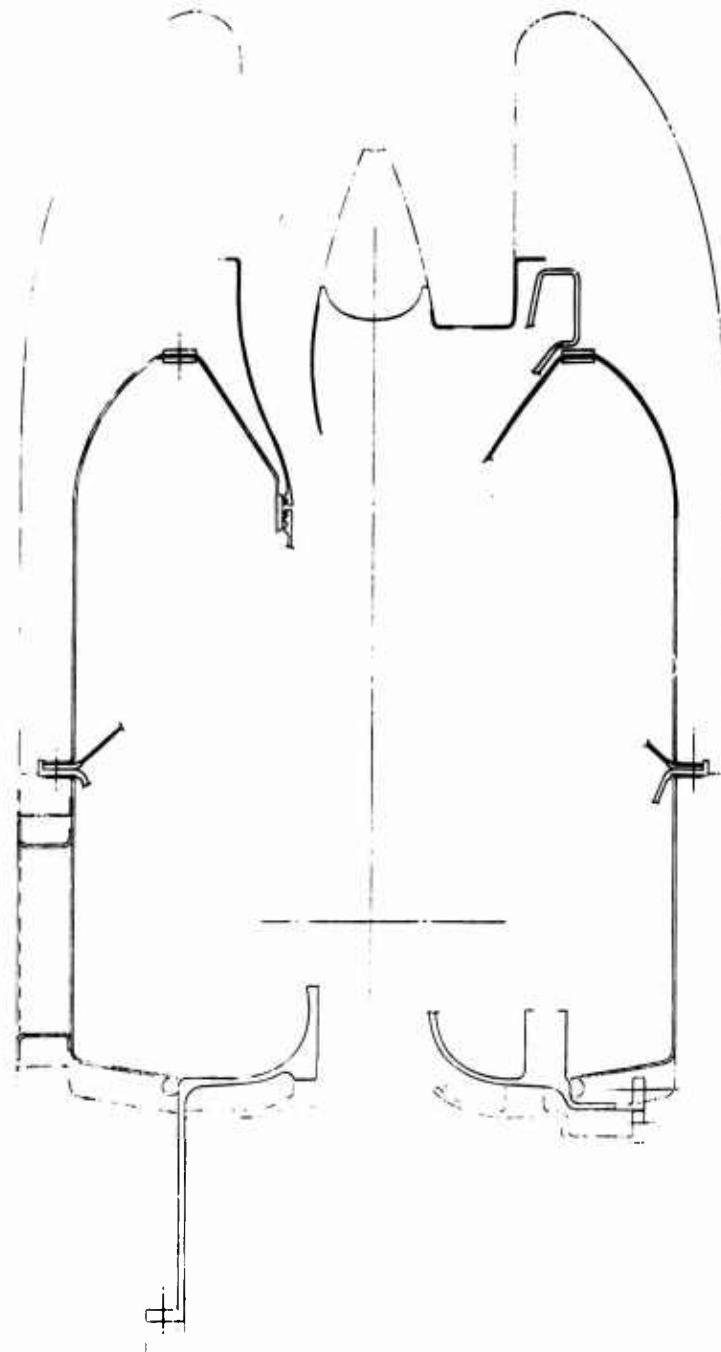


Fig. XIV-7. Size Comparison of Modified and Standard TS-120 Engines.

SECTION XV

**HUMAN FACTORS**

## SECTION XV - HUMAN FACTORS

Engine features related to human factors are discussed in detail throughout the design report. These features are summarized as follows:

1. The side mounting of accessories providing wide angle open access for service and replacement.
2. The external mounting of control and electrical components for maximum access.
3. The installation flexibility provided in the ability to rotate the air inlet, the combustor, and the optional axial and rotatable right angle exhaust.
4. The potential low noise level being investigated under noise control.
5. The potential of low skin temperatures resulting from the proposed silencing method in the combustor and exhaust area.

SECTION XVI

**REGENERATIVE ENGINES**

## SECTION XVI - REGENERATIVE ENGINES

This section describes the design of regenerative engine versions of the 120, 90, and 60 horsepower turboshaft engines. A number of preliminary recuperator designs were evaluated as a basis for a purchase specification from which proposals were solicited from nine vendors to design a recuperator for the range of regenerative engines.

Four vendors submitted recuperator design proposals which were evaluated on the basis of performance, mechanical reliability, proposed development program, and recuperator background. On the basis of this evaluation, Harrison Division of General Motors Corporation was awarded the recuperator Component Design Study. The results of the recuperator Component Design Study are presented in Appendix XVI-A. The Model TS120R regenerative engine shown in Figure XVI-1, minimizes over-all length and features a maximum interchangeability of parts with both regenerative and non-regenerative engine versions. The regenerative engine is 38.62 inches long, 35.62 inches wide and 30.40 inches high.

The basic regenerative engine component arrangement and the parts common to the non-regenerative engine versions is shown in Figure XVI-2. The recuperator comprises four-pass air through tubes and exhaust gas moves over the tubes. The close coupling of the recuperator will result in minimum pressure drop and will minimize flow distribution and leakage problems. Only the basic 120 horsepower direct drive engine version is shown in detail. The design is equally applicable to all engine versions. The design point performance of the regenerative engines is shown in Table XVI-I and Figure XVI-3.

### AERODYNAMIC CYCLES

A design point study was conducted for the basic 120 horsepower engine with a nominal regenerator to examine the feasibility of adding on a regenerator and meeting the specification requirement. Figures XVI-4 and XVI-5 show a range of performance at sea level 60°F and 8000 feet 90°F. The data show that at the TS120R compressor pressure ratio, no difficulty will be encountered in meeting the specification requirements.

## Section XVI

TABLE XVI-I  
DESIGN POINT PERFORMANCE OF RECUPERATIVE ENGINES

Performance Item	Nominal Regenerative Engine Rating					
	120 HP		90 HP		60 HP	
Design	Spec.	Design	Spec.	Design	Spec.	
Altitude HP	118	120	90	90	60	60
Sea Level BSFC	0.513	0.500	0.520	0.520	0.550	0.55
Design Speed - RPM	68,000	68,000 (Max.)	66,600	68,000 (Max.)	59,130	68,000 (Max.)
Max. Turb. Inlet Temp. °R	2260	2260 (Max.)	2238	2260 (Max.)	2260	2260 (Max.)
Weight Increase		125		100		95
Recuperator Efficiency	79.1	-	79.5	-	80.1	-
Recuperator Press. Loss	5.55	-	4.07	-	4.62	-

### Engine Matching

The regenerator characteristics based on Harrison's data that were used in the matching calculation are shown on Figures XVI-6 through XVI-8.

A parametric approach was used in optimizing the engine-regenerator combination. The variables involved were:

1. Turbine nozzle setting - i.e., airflow.
2. Engine speed.
3. Regenerator design.

## Section XVI

### 4. Turbine inlet temperature.

The engine rating points established by the matching study for sea level 60°F and 8000 feet, 90°F, are shown in Figure XVI-9, for the 120, 90, and 60 horsepower regenerative engines respectively. The performance of various components and the losses in the flow path are also indicated. Figures XVI-10 through XVI-15 show the no-load, part-load, and full-load performance characteristics for sea level 60°F and 8000 feet, 90°F, for the three regenerative engines. Figure XVI-16 shows the sea level and altitude operating points on an unscaled TS120 R compressor map for all regenerative engines. Appropriate flow scale factors are indicated.

#### Variable Inlet Guide Vane Study

A study was made to discover the effect of variable inlet guide vanes on both the simple cycle and regenerative engines. The simple cycle was examined with the hope of reducing altitude turbine inlet temperature. It was found that the 8000 feet, 90°F turbine inlet temperature could be decreased by only 30 degrees.

This temperature decrease is limited by the sea level turbine work which was considered maximum. Since axial compressor stage redesign with its higher design risk and cost would also be required, it was felt that a 30 degree increase in turbine inlet temperature was not justifiable by this approach. This method was therefore dropped from further consideration.

The study also shows that variable inlet guide vane will improve regenerative engine performance. Closing the I. G. V. from 15 to 30 percent will decrease sea level 60°F BSFC from 4 to 9.5 percent. However, the I. G. V. must be open 10 percent to obtain 120 horsepower at 8000 feet, 90°F.

## Section XVI

### PRELIMINARY DESIGN

One recuperator was selected as an initial design. This is a cross-headered counterflow (Z-flow) plate-fin recuperator as described in Figures XVI-17, XVI-18, and XVI-19 and with geometry as follows:

Air side plate spacing	0.030-inch
Gas side plate spacing	0.060-inch
Airflow length	0.225-foot
Gas flow length	0.225-foot
No flow length	4.44 feet
Volume	0.61 cubic feet
Weight	50 pounds

The performance characteristics of this heat exchanger were used to determine the preliminary design points at 60°F sea level and at 90°F 8000 foot altitude for use in the purchase specification. These design points are shown in Table XVI-II.

The engine requirements for regeneration were determined simultaneously; i. e., BSFC as a function of regenerator effectiveness and pressure drop and power as a function of air loss and pressure drop, which are independent of regenerator design. These data are presented in Figures XVI-20 and XVI-21.

To determine the effects of recuperator core configuration on engine recuperator packaging, seven additional recuperators of varying configuration were sized to meet the engine requirements. These recuperators, described in Appendix XVI-B, were selected to cover a wide range of performance level, size, weight, and ratio of gas side face area to flow length.

### RECUPERATOR DESIGN

A preliminary recuperator, shown in Figure XVI-22 as proposed, satisfied the engine requirements with following properties:

## Section XVI

**TABLE XVI-II**  
**TS120R ENGINE PERFORMANCE WITH VARIOUS  
 DESIGN RECUPERATORS**

Z Flow	Design No. 1		Design No. 2		Design No. 3		Design No. 2		Design No. 3		Non-Regen.	
	Sea Level	Altitude	Sea Level	Altitude								
W <sub>a</sub> /θ <sub>c</sub>	1.725	1.173	1.725	1.176	1.723	1.176	1.723	1.176	1.723	1.176	1.670	1.112
PR	1.735	1.633	1.735	1.638	1.734	1.638	1.733	1.638	1.733	1.638	1.640	1.549
RPM	5.77	5.70	5.77	5.68	5.80	5.68	5.82	5.68	5.82	5.68	5.73	5.50
KWNT	68.000	68.000	68.000	68.000	68.000	68.000	68.000	68.000	68.000	68.000	68.000	68.000
T.I.T.	186.66	186.66	186.66	186.66	186.66	186.66	186.66	186.66	186.66	186.66	186.66	186.66
T <sub>a</sub>	935	970	925	935	970	925	970	935	970	925	959	959
T <sub>g</sub>	1328	1622	1367	1641	1364	1638	1385	1645	1385	1645	-	-
SFC	81.1	87.8	78.9	81.1	79.1	81.1	79.1	81.0	81.0	81.0	-	-
AP/P <sub>a</sub>	1.58	1.44	3.65	3.44	2.64	2.76	3.60	3.76	3.60	3.76	-	-
AP/P <sub>b</sub>	2.12	2.22	4.06	2.88	2.91	2.88	4.02	3.96	2.91	4.02	-	-
EP/P <sub>a</sub>	3.70	3.66	7.71	6.32	5.55	5.64	7.62	7.72	5.55	7.62	120	120
HP	120	120	117	120	118	120	115	120	118	120	100	100
SFC %NR SFC	72.1	60.6	74.2	65.7	73.9	65.0	74.4	66.7	73.9	66.7	71.5	71.5
W <sub>a</sub>	1.413	.911	1.418	.911	1.411	.911	1.410	.911	1.425	.926	1.407	.911
W <sub>a</sub> /θ <sub>c</sub>	1.336	1.281	1.281	1.434	1.281	1.433	1.281	1.448	1.281	1.448	1.430	1.281
PR	5.26	4.97	5.22	4.97	5.27	4.97	5.28	4.97	5.34	5.05	5.30	5.30
RPM	66.250	66.250	66.250	66.250	66.250	66.250	66.250	66.250	66.250	66.250	66.250	66.250
KWNT	589.96	589.96	589.96	589.96	589.96	589.96	589.96	589.96	589.96	589.96	589.96	589.96
T.I.T.	1794	2248	1833	2260	1822	2260	1841	2260	1819	2238	1773	2260
T <sub>a</sub>	902	936	901	936	903	936	903	936	907	940	903	936
T <sub>g</sub>	1324	1644	1318	1698	1304	1670	1324	1676	1299	1648	-	-
AP/P <sub>a</sub>	3.87	6.0	1.83	2.48	2.18	2.95	3.10	79.5	82.5	82.7	-	-
AP/P <sub>b</sub>	4.85	1.30	2.56	1.92	2.10	2.62	2.83	2.11	2.11	2.24	-	-
EP/P <sub>a</sub>	4.52	1.90	4.39	4.40	4.08	4.36	5.57	5.93	4.07	4.35	-	-
HP	90	90	90	90	90	90	88	90	90	90	90	90
SFC	.996	.386	.519	.433	.420	.517	.428	.520	.423	.520	.729	.52/.73
%NR SFC	68.3	55.1	71.4	61.7	70.9	60.0	71.1	61.0	71.3	60.4	100	71.3
W <sub>a</sub>	1.341	.885	1.332	.885	1.333	.885	1.219	.800	1.230	.800	1.174	.755
W <sub>a</sub> /θ <sub>c</sub>	1.368	1.245	1.354	1.245	1.355	1.245	1.238	1.250	1.193	1.052	1.063	.885
PR	4.74	4.55	4.74	4.55	4.77	4.55	4.16	3.96	4.13	1.125	1.246	1.246
RPM	64.000	64.000	64.000	64.000	64.000	64.000	64.000	64.000	64.000	64.000	64.000	64.000
KWNT	628.60	628.60	61934	61934	63008	63008	63008	63008	63008	63008	63008	63008
T.I.T.	1666	1989	1660	1986	1675	1987	1750	2170	1757	2200	1778	2260
T <sub>a</sub>	873	906	874	906	874	906	874	906	874	906	906	906
T <sub>g</sub>	1217	1491	1209	1466	1226	1488	1328	1693	1337	1725	1365	1795
AP/P <sub>a</sub>	2.29	3.48	2.53	2.72	3.48	3.72	4.18	3.20	3.20	4.18	3.75	4.55
AP/P <sub>b</sub>	2.37	2.92	1.54	1.72	2.14	2.30	2.06	1.75	2.10	2.35	1.19	4.39
EP/P <sub>a</sub>	4.66	6.40	4.07	4.44	5.62	6.02	6.24	4.95	4.95	5.62	2.04	2.04
HP	60	60	60	60	60	60	60	60	60	60	60	60
SFC	.624	.506	.614	.492	.619	.499	.573	.469	.578	.465	.845	.845
%NR SFC	73.9	65.0	72.6	63.1	73.1	63.9	67.8	60.5	67.8	60.5	100	100

## Section XVI

$\epsilon$	= 82.3%	Matrix OD	- 28 In.
$\epsilon \Delta P/P$	= 4.45%	Matrix ID	- 15 In.
Tube Weight	= 53 Lb.	Matrix Length	- 14 In.

Figures XVI-23 and XVI-24 show the estimated change in engine performance as a function of recuperator heat transfer surface weight. It is seen that a change of 38 percent in tube weight to 32 pounds results in a minor compromise in TS120R engine performance resulting in 117 horsepower at altitude, and 0.515 SFC and 120 horsepower at sea level. The estimated performance of this modified recuperator is shown as the No. 1 design in Table XVI-II. Basic engine design progress necessitated that a 17-inch ID matrix be used. Two additional recuperators, design No. 2, Figure XVI-25, and design No. 3, Figure XVI-26, were evaluated and are described in Table XVI-III.

**TABLE XVI-III**  
**RECUPERATOR DESIGN COMPARISON**

<u>Parameter</u>	<u>No. 2 Design</u>	<u>No. 3 Design</u>
Effectiveness - Percent	79.1	79.1
Pressure Drop - Percent	5.55	7.62
Outside Diameter - Inches	27.5	26.5
Inside Diameter - Inches	17.0	17.0
Length - Inch	13.35	12.88
Tube Weight - Pound	40.5	35

The low pressure drop, No. 2 design recuperator, was selected for the least performance compromise over the range of regenerative engines. The details of component performance and component structural design, as completed by Harrison Radiator Division of General Motors Corporation, are presented in the recuperator design study, included in this section as Appendix XVI-A.

The effects on recuperator effectiveness, pressure drop, tube number and core weight versus No. 2 design recuperator outer diameter is shown in Figure XVI-A-3, Appendix XVI-A.

## Section XVI

### REGENERATIVE ENGINE DESIGN

In order to meet the specified turbine inlet temperature distribution and to meet pressure drop requirements, the higher burner temperature levels of the regenerative cycle dictate an increase in burner tube size to 4.3-inch diameter by 13.25 inches long. Changes in the engine outer shell, burner cap, and turbine inlet volute necessarily follow. One series of such changes is necessary for all regenerative engines.

The transient response of the regenerative cycle, as influenced by the heat capacity of the regenerator material and contained gases, requires a modified control system to assure precise, safe control, within the specification limits. For starting and acceleration, recuperator air outlet temperature is sensed to adjust fuel flow rates for safe maximum temperature limits. For deceleration and speed modulation, the heat stored in the recuperator section must be dissipated from the burner inlet through a blow-off valve. One set of modified controls is required for all regenerative engines.

Engine structural and ducting components must be altered to support the recuperator assembly and to provide a regenerative flow path. The extent of these modifications is minimized only by careful component arrangement.

In order to assure the maximum commonality of components among all engine versions, it was decided to allow engine design point changes only by variations of the following items:

1. Recuperator design.
2. Turbine inlet nozzle area.
3. Rotor speed.
4. Turbine inlet temperature.

## Section XVI

The performance of 13 regenerative engines, incorporating the No. 2 and No. 3 design recuperators, was investigated to define recuperator performance limits and regenerative engine design points.

Table XVI-II shows the relative performance of the two recuperator designs operating at the original design points. Note that performance at the 120 horsepower level suffers the expected two percent loss; the 90 horsepower requirements are satisfied with the low pressure drop No. 2 design recuperator, and the 60 horsepower design does not satisfy the requirements.

The first effort to improve regenerative engine performance was to change the matched design point by changing engine speed in the No. 2 design. Table XVI-II shows the revised performance. It will be noted that the 120 horsepower requirements can be met at 68,700 rpm (one percent overspeed); the 90 horsepower requirements are met, and the 60 horsepower performance is improved.

It is concluded that the low pressure drop No. 2 design recuperator is a minimum heat exchanger at the 120 horsepower level to meet target performance and that the high pressure drop No. 3 design is a minimum heat exchanger at the 90 horsepower level to meet target sea level SFC.

The second effort to improve 60 horsepower regenerative engine performance was a change to a lower matched design point by changing speed in the "D" design. Table XVI-II shows the revised performance. It will be noted that the 60 horsepower requirements are met by the No. 2 design recuperator.

It is concluded that the low pressure drop No. 2 design recuperator is a minimum heat exchanger at the 60 horsepower level.

Therefore, the low pressure drop No. 2 design recuperator is selected for application to all regenerative engines. This selection offers maximum commonality.

The design points selected are summarized in Table XVI-IV and Figure XVI-16.

## Section XVI

TABLE XVI-IV  
REGENERATIVE ENGINE - DESIGN POINT COMPARISON

Parameter	TS120R		TS90R		TS60R	
	Sea Level	Altitude	Sea Level	Altitude	Sea Level	Altitude
Airflow - Lb/Sec.	1.725	1.176	1.425	0.926	1.174	0.748
Airflow-Corrected - Lb/Sec.	1.735	1.638	1.448	1.302	1.193	1.052
Pressure Ratio	5.77	5.68	5.34	5.05	3.96	3.76
Rotor Speed-r.p.m.	68,000	68,000	66,600	66,600	59,130	59,130
Turbine Inlet Temp. °R	1923	2260	1819	2238	1746	2245
Regenerator Descrp.		No. 2		No. 2C		No. 2D
Air Inlet Temp. °R	935	970	907	940	824	859
Gas Inlet Temp. °R	1364	1638	1299	1648	1330	1769
Effectiveness - %	79.1	81.7	79.5	82.7	80.1	84.1
Air Pressure Drop-%	2.64	2.76	2.15	2.24	3.19	3.16
Gas Pressure Drop-%	2.91	2.88	1.92	2.11	1.43	1.65
Pressure Drop Sum-%	5.55	5.64	4.07	4.35	4.62	4.81
Horsepower	120	118	90	90	60	60
BSFC	0.513	0.429	0.520	0.423	0.550	0.451
Scale Factors						
Compressor Flow	0.406		0.367		0.367	
Compressor Speed	52.18		53.6		53.6	
Compressor Efficiency	0.997		0.986		0.986	
Turbine Flow	0.688		0.6011		0.662	
Turbine Speed	1.587		1.587		1.587	
Turbine Efficiency	1.0		1.0		1.0	

## **Section XVI**

### **ENGINE WEIGHT**

The TS120R estimated engine weight is shown in Table XVI-V. The identification of strategic national defense materials is shown in Table XVI-VI.

## Section XVI

**TABLE XVI-V**  
**MODEL TS120R TURBOSHAFT ENGINE WITH INTEGRATED  
 HEAT EXCHANGER WEIGHT SUMMARY**

<u>Part Name</u>	<u>Weight</u>	<u>Part Name</u>	<u>Weight</u>
<b><u>ROTOR ASSEMBLY</u></b>			
Rotor-Radial Compressor		Case Accessory	9.15
Rotor-Turbine		Power Take-Off Cover	3.20
Shaft, Front-Turbine		Power Take-Off Shaft	.84
Rotor-Axial Compressor		Cover-Accessory Gears	3.50
Miscellaneous		Clutch Assembly-Starter Overrunning	2.10
Total	<u>16.90</u>	Cover Assembly-Oil Pump	3.50
<b><u>COMPRESSOR ASSEMBLY</u></b>			
Stator-Axial Compressor	.80	Oil Pump	3.50
Housing-Compressor	4.86	Sump-Oil	2.00
Diffuser-Radial Compressor	4.00	Alternator	2.00
Housing - Air Intake	2.45	Power Control	11.00
Duct - Air Intake	1.70	Starter-Assembly	8.75
Miscellaneous	<u>1.00</u>	Filler-Oil	.50
Total	<u>14.81</u>	Gears and Shafts	4.30
		Bearing	.62
		Miscellaneous	<u>4.00</u>
		Total	<u>58.96</u>
<b><u>COMBUSTOR ASSEMBLY</u></b>			
Interstage Diaphragm	2.12	Indicator - Exhaust Gas Temperature	2.00
Nozzle - Turbine Inlet	5.50	Switch - Oil Pressure	.32
Volute-Combustor	13.73	Control Assembly - Sequence	4.00
Cover - Radial Diffuser	6.20	Thermocouple	.20
Cover-Combustor	10.00	Cooler Assembly - Oil	4.50
Combustor	2.50	Fan - Cooling	3.50
Miscellaneous	3.20	Miscellaneous	<u>2.00</u>
Total	<u>1.87</u>	Total	<u>16.52</u>
<b><u>EXHAUST DUCT AND REAR BEARING SUPPORT</u></b>			
Duct-Exhaust	Miscellaneous	Lines/Fitting/Ignition Total	8.05
	Total		
<b><u>HEAT EXCHANGER ASSEMBLY</u></b>			
16.00		Heat Exchanger	111.00
6.00		Exhaust Plenum	21.00
22.00		Exhaust Elbow	13.50
		Blow Off Valve	5.00
		Miscellaneous	<u>7.50</u>
		Total	<u>158.00</u>
<b><u>TOTAL ENGINE WEIGHT</u></b>			
			<u>340.36</u>

Section XVI

TABLE XVI-VI  
MODEL TS120R TURBOSHAFT ENGINE WITH INTEGRATED HEAT EXCHANGER  
STRATEGIC NATIONAL DEFENSE MATERIALS

Piece	Wt.	Material	Tungsten						Tungsten					
			Cobalt	Nickel	Chromium	Columbium	Molybdenum	Tungsten	Cobalt	Nickel	Chromium	Columbium	Molybdenum	Tungsten
Rotor-Radial Compressor	4.00	AMS 5662	1.0	.04	52.5	2.10	19.0	.76	4.8	.19	3.0	.12		
Rotor-Turbine	6.90	Udimet 700	17.0	1.17	55.0	3.80	15.0	1.04			5.0	.34		
Rotor-Axial Compressor	1.60	AMS 5398		3.0		.05	15.5	.25	.45	.01				
Intake-Diaphragm	2.10	AMS 5391	1.0	.02	70.0	1.47	12.0	.25	1.8	.04	3.8	.08		
Nozzle-Turbine Inlet	5.50	AMS 5391	1.0	.06	70.0	3.85	12.0	.66	1.8	.10	3.8	.21		
Volute-Combustor	13.73	AMS 5532	19.0	2.22	20.0	2.34	21.0	2.46	.8	.09	3.0	.35	2.5	.29
Housing-Combustor	10.00	AMS 5512		10.0		1.36	18.0	2.45	1.1	.15	.5	.07		
Cover-Combustor	2.50	AMS 5512		10.0		.25	18.0	.45	1.1	.28	.5	.13		
Combustor	3.20	AMS 5532	19.0	.61	20.0	.64	21.0	.67	.8	.03	3.0	.10	2.5	.08
Duct - Exhaust	16.00	AMS 5512		10.0	1.60	18.0	2.88	1.1	.18	.5	.08			
Heat Exchanger	111.00	AMS 5512		10.0	11.10	18.0	19.98	1.1	1.22	.5	.56			
Plenum Exhaust	21.00	AMS 5512		10.0	2.10	18.0	3.78	1.1	.23	.5	.11			
Elbow Exhaust	13.50	AMS 5512		10.0	1.35	18.0	2.43	1.1	.15	.5	.07			
Weight Totals	<u>211.03</u>			<u>4.12</u>		<u>32.01</u>		<u>38.06</u>		<u>2.67</u>		<u>2.22</u>		<u>.37</u>

**Section XVI**

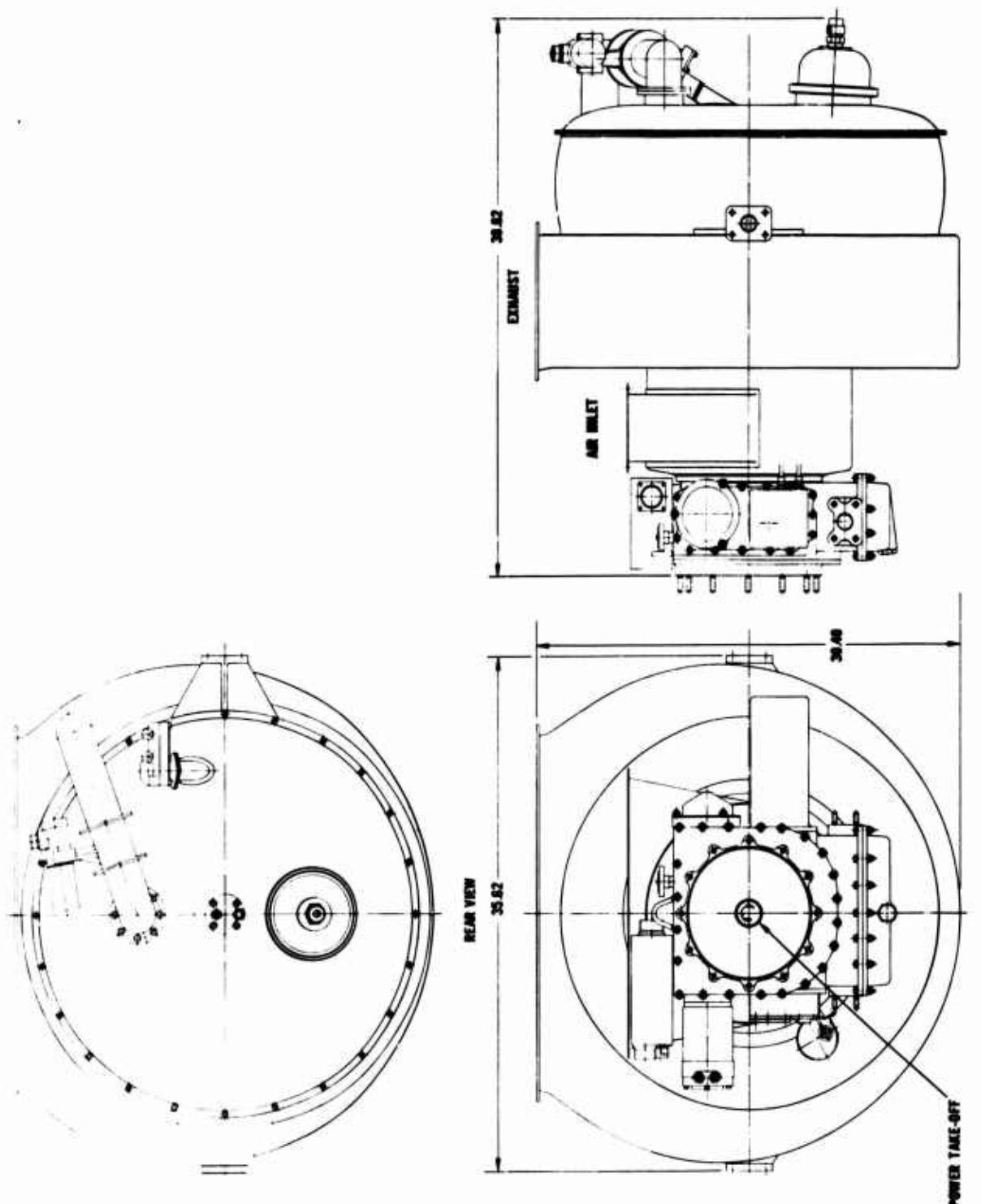
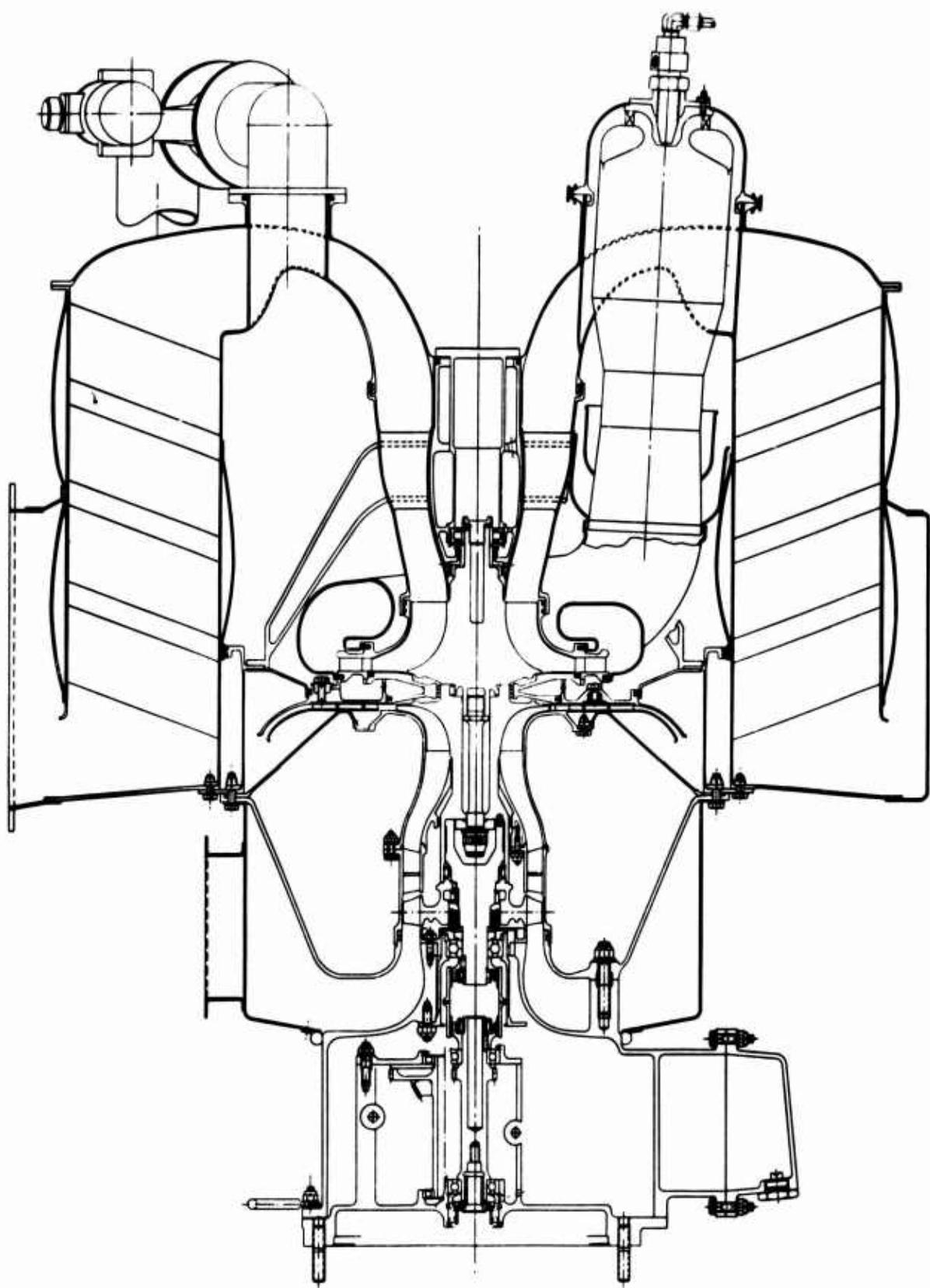


Figure XVI-1. Continental Model TS120R Regenerative Engine Installation Drawing.

**Section XVI**



**Figure XVI-2. TS120R Engine Assembly.**

**Section XVI**

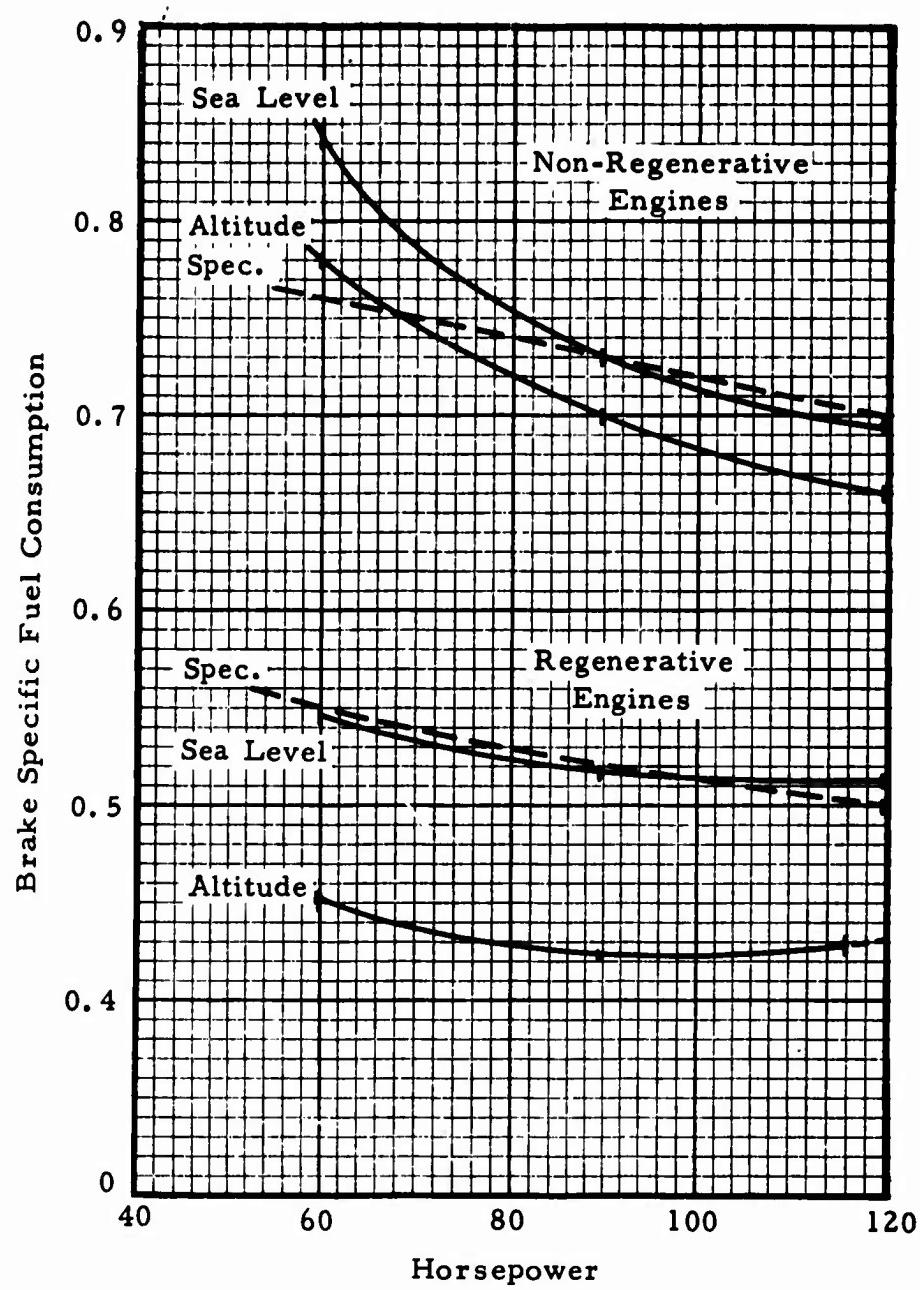


**Figure XVI-3. Regenerative Engine Design Point Performance.**

## Section XVI

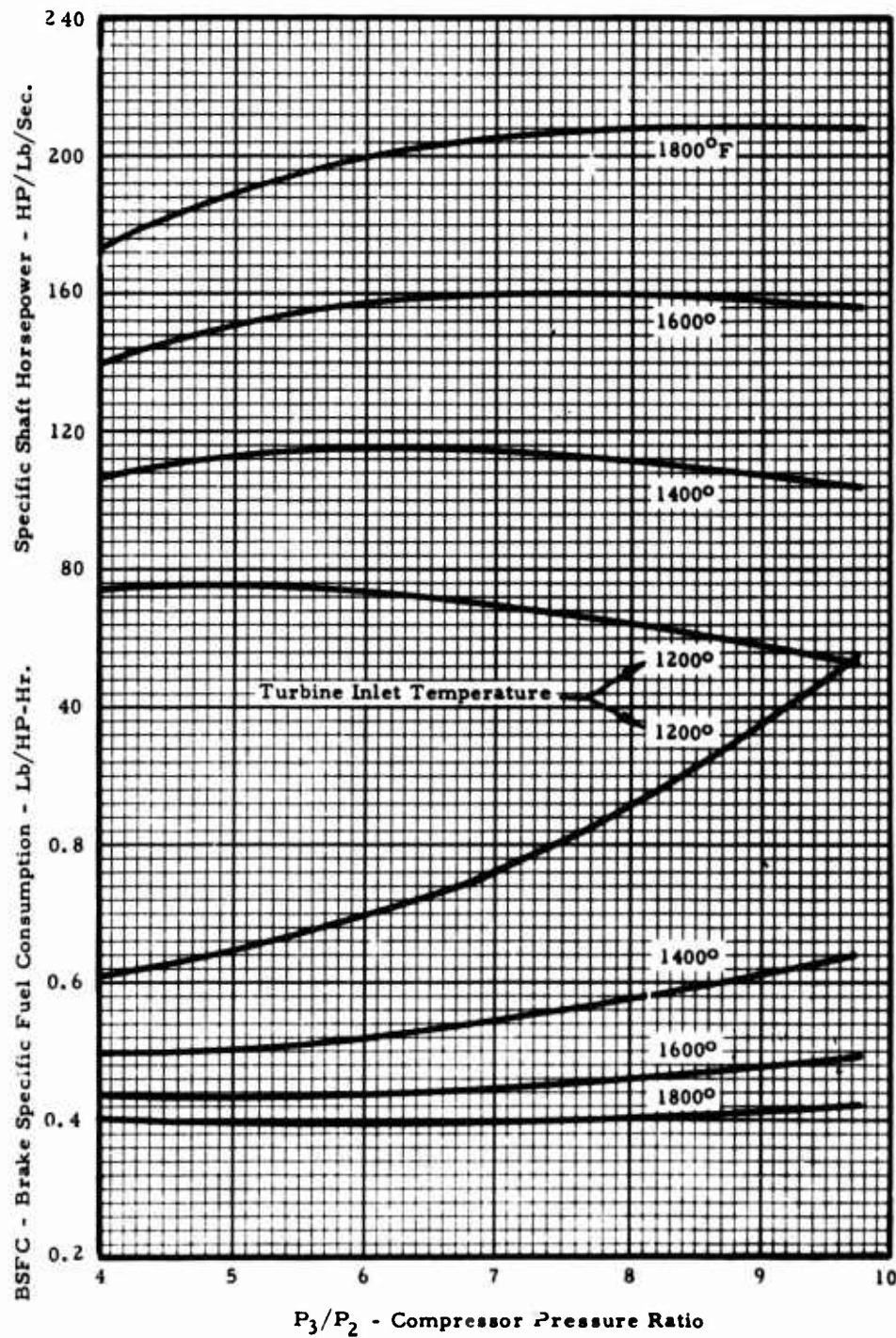


Figure XVI-4. TS120R Design Point Study 120 Horsepower Regenerative Engine Sea Level, 60°F.

Section XVI

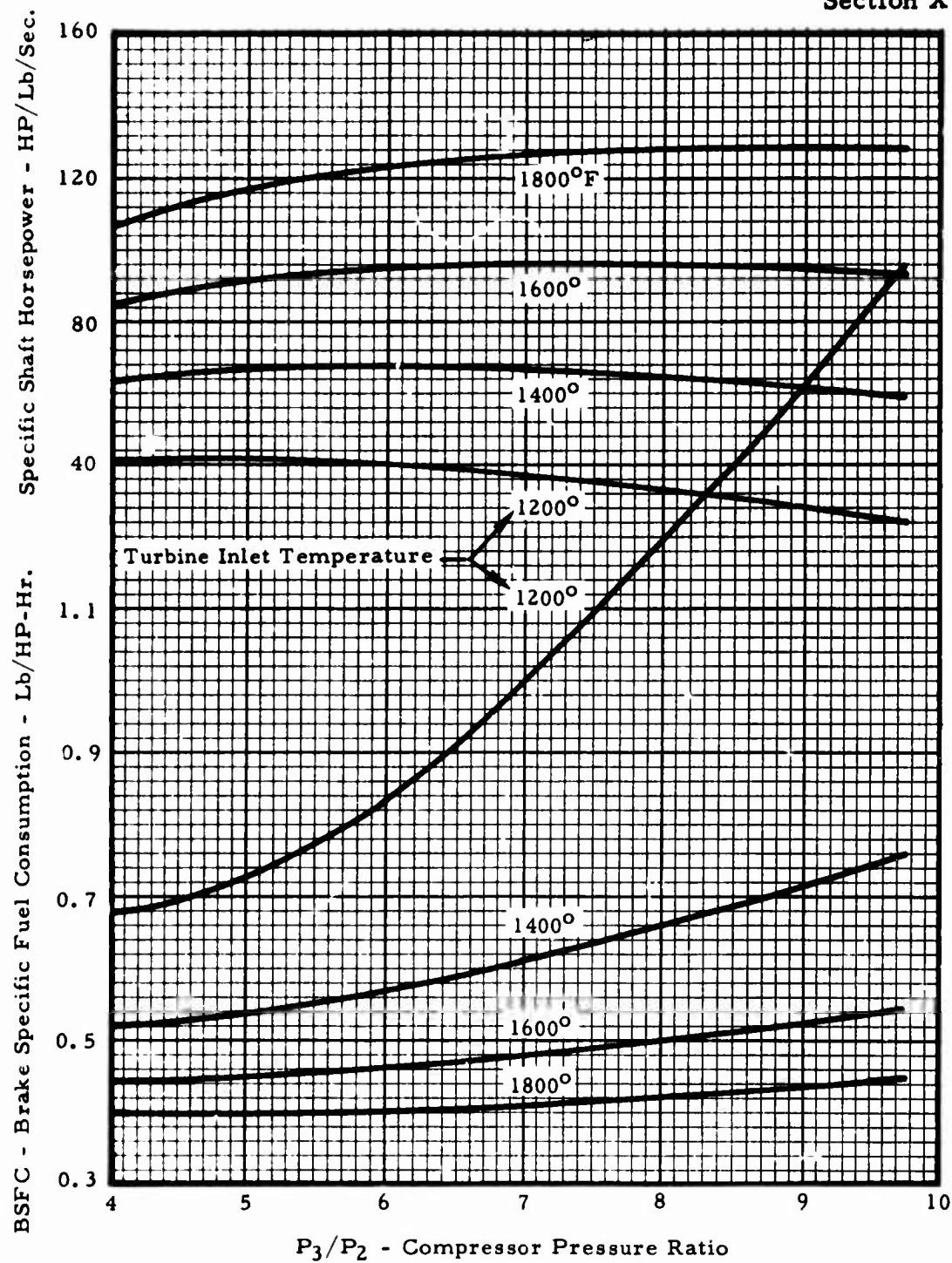


Figure XVI-5. TS120R Design Point Study 120 Horsepower Regenerative Engine 8000 Feet, 90°F.

Section XVI

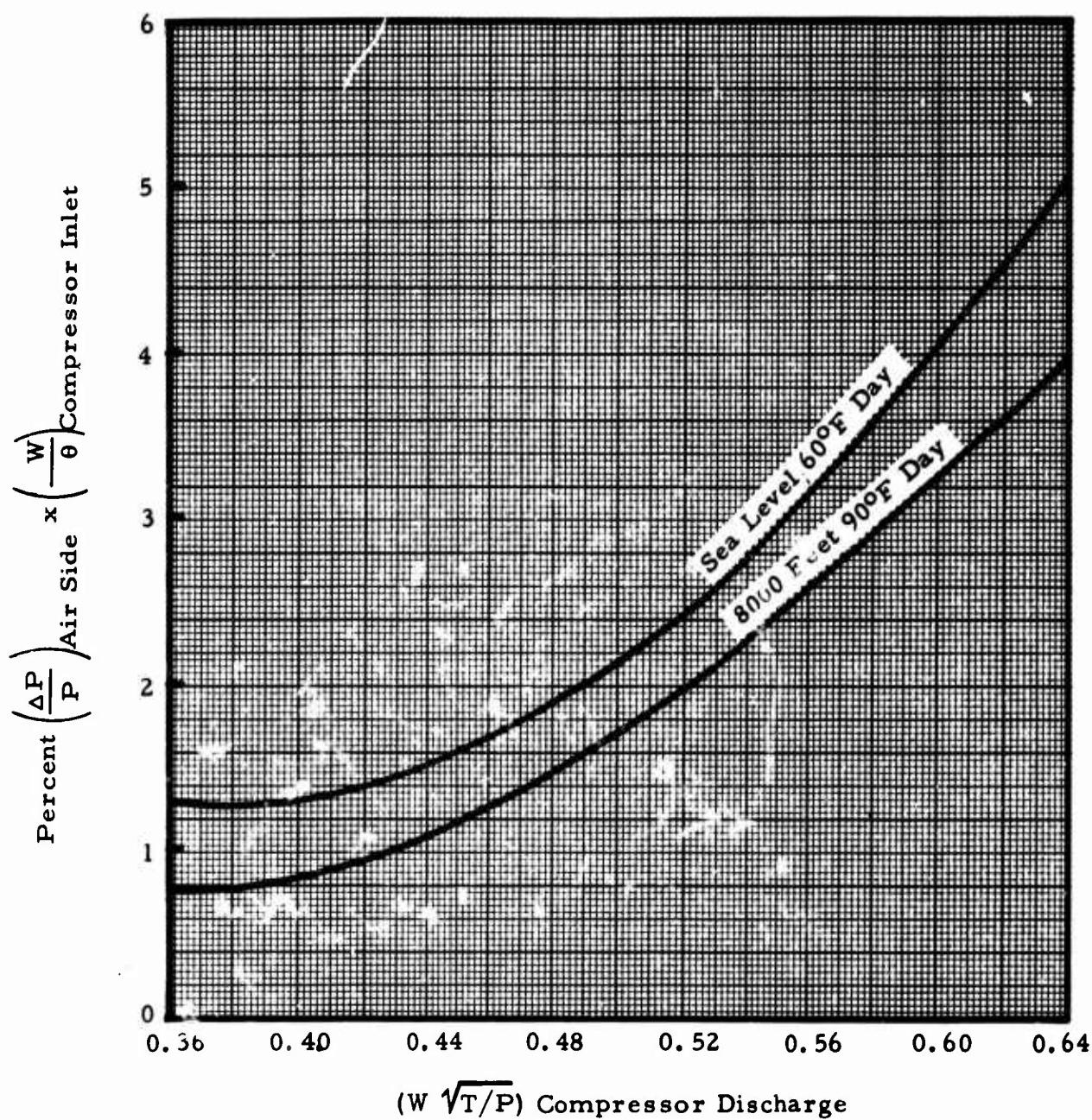


Figure XVI-6. TS120R Regenerative Engine Air Side Pressure Drop Characteristics.

## Section XVI

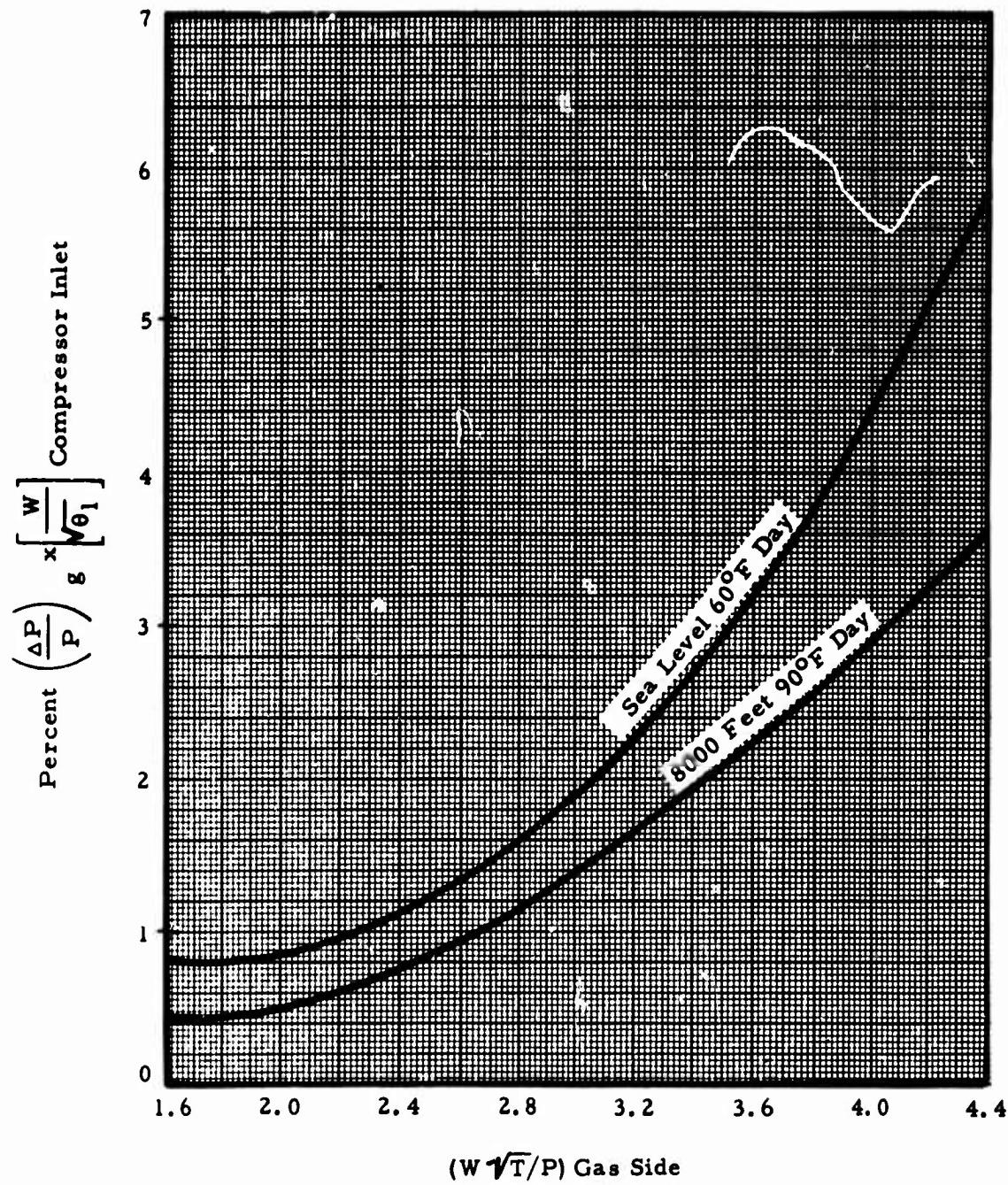


Figure XVI-7. TS120R Regenerative Engine Gas Side Pressure Loss Characteristics.

## Section XVI

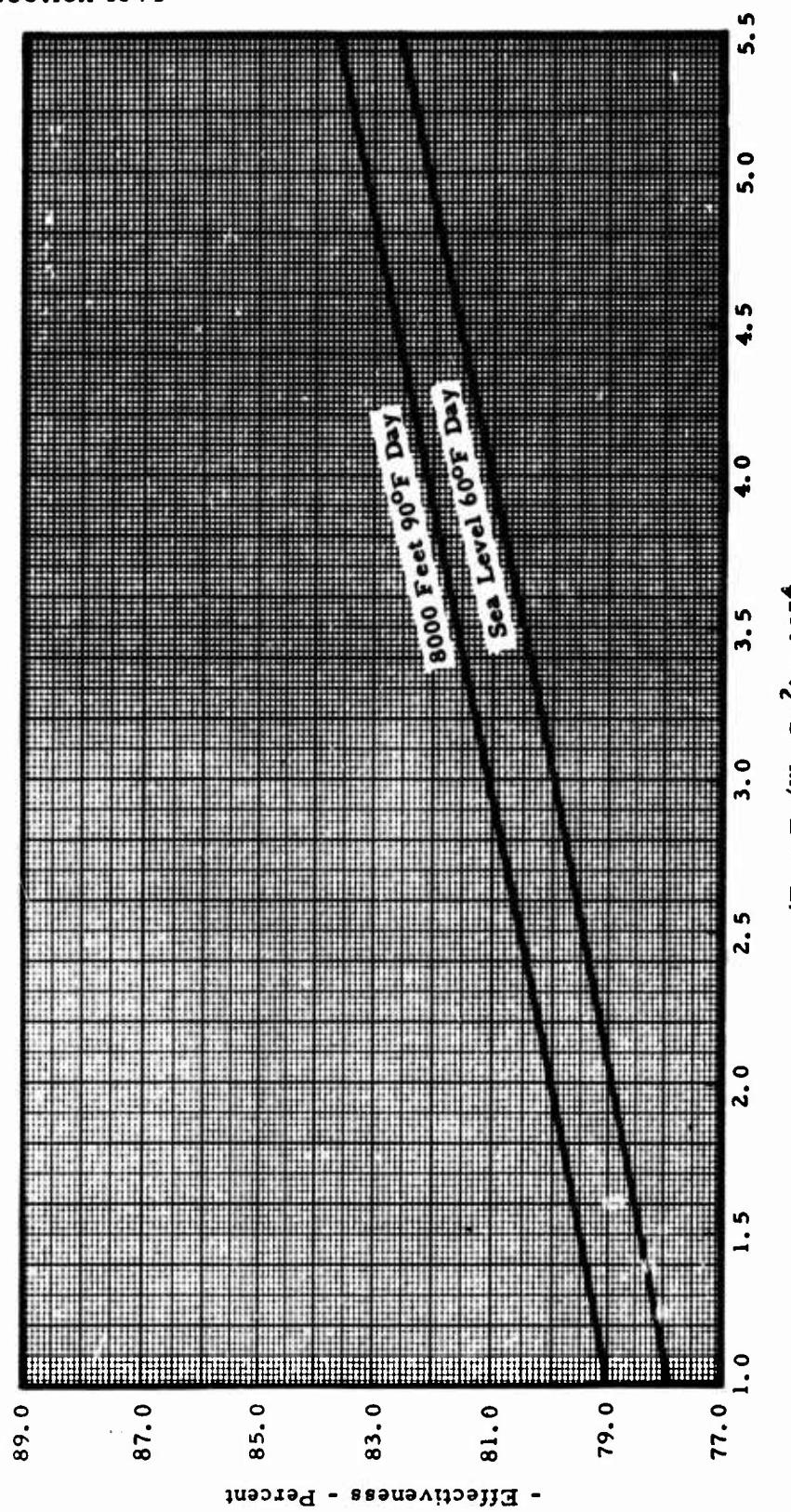


Figure XVI-8. TS120R Regenerative Engine Effectiveness Characteristics.

ERDL REGENERATIVE CYCLE  
ENGINE RATING DATA  
SEA LEVEL 60°F AND 8000 FEET, 90°F

	Sea Level - 60°F			8000 Feet 90°F		
	120 HP	90 HP	60 HP	120 HP	90 HP	60 HP
Shaft Output Power	120.0	90	60	118.3	90	60
BSFC - Lb/HP-Hr.	.513	.520	.550	.428	.423	.451
Engine Speed - RPM	68,000	66,600	59,130	68,000	66,600	59,130
Airflow - Lb/Sec.	1.72	1.43	1.17	1.18	.926	.748
Corrected Airflow - Lb/Sec.	1.73	1.45	1.19	1.64	1.30	1.05
Comp. Press. Ratio	5.81	5.34	3.96	5.68	5.05	3.76
Comp. Efficiency - %	80.3	81.3	81.6	82.5	81.5	80.9
Comp. Discharge Temp. - °F	475.7	447.2	364.4	510.1	480.6	399.2
Combustor Efficiency - %	.985	.985	.985	.985	.985	.985
Fue LHV - Btu/Lb.	18,400	18,400	18,400	18,400	18,400	18,400
Turbine Inlet Temp. - °F	1461.3	1359.3	1286.3	1800	1778	1785.3
Turbine Exit Temp. - °F	904.8	839.2	870.4	1178.2	1187.9	1308.9
Turbine Efficiency - %	88.3	88.5	88.1	87.4	87.3	85.2
Inlet Total Press. Loss - %	0.5	1.5	1.5	0.5	1.5	1.5
Comb. Sect. Total. Press. Loss - %	4.12	3.21	4.05	4.33	3.43	4.36
Exh. Diff. Total Press. Loss - %	3.33	2.16	1.28	3.398	2.095	
Exh. Flange Total Press. Loss - %	1.5	1.5	1.5	1.5	1.5	1.5
Access. Extracted Horsepower	3.5	3.5	3.5	3.5	3.5	3.5
Regenerator Effectiveness - %	79.1	79.5	80.1	81.7	82.7	84.1
Total Regenerator Cold Side-ΔP/p - %	4.13	3.12	3.83	4.28	3.17	3.79
Total Regenerator Hot Side - ΔP/p - %	4.40	2.89	2.07	4.41	3.04	3.27

NOTE: All Efficiencies are total to total values.

Figure XVI-9. TSI120R Regenerative Engine Rating Data Sea Level 60°F and  
8000 Feet 90°F.

## Section XVI

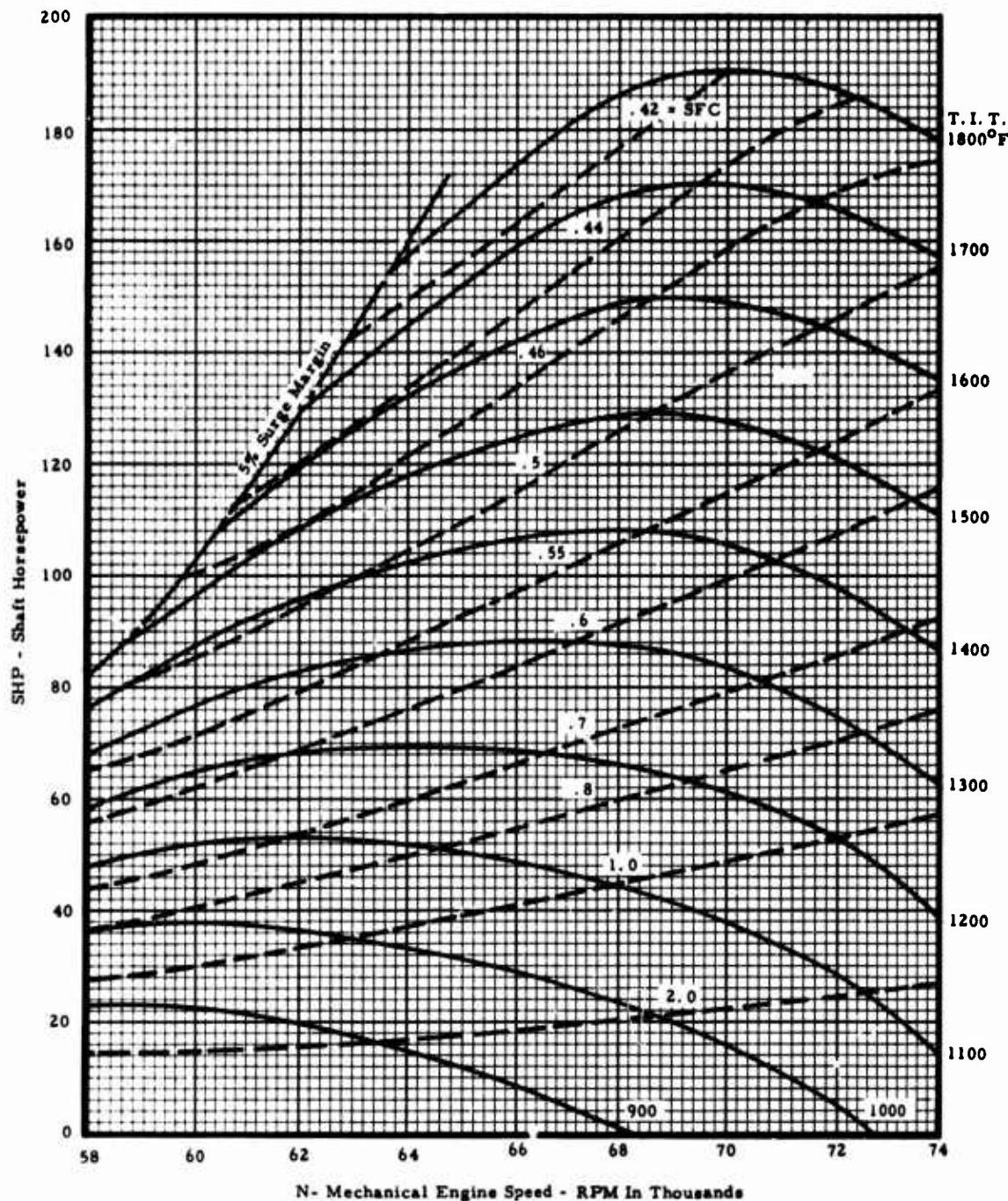


Figure XVI-10. TS120R Regenerative Engine Estimated Performance Characteristics Sea Level, 60°F.

## Section XVI

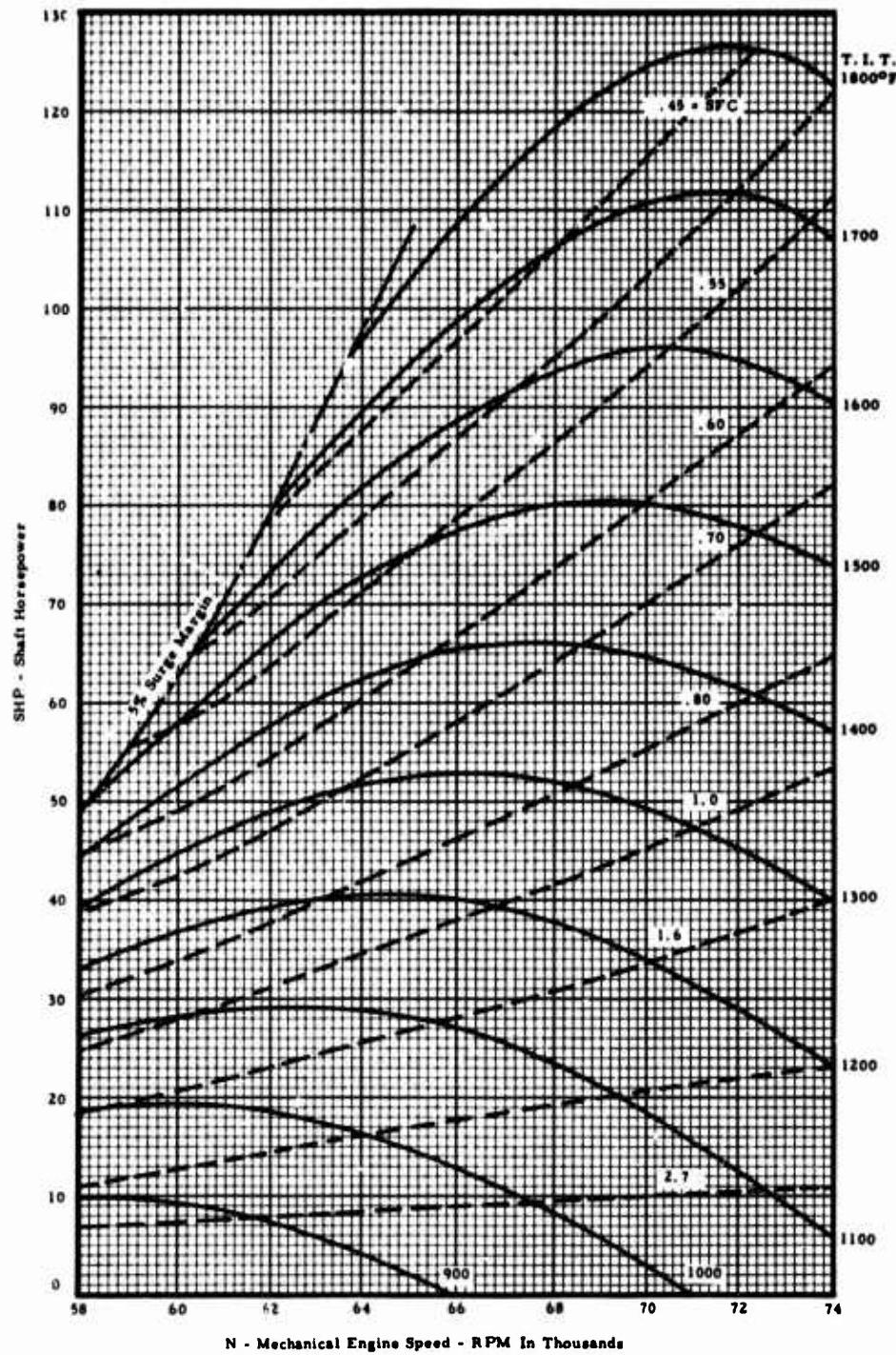
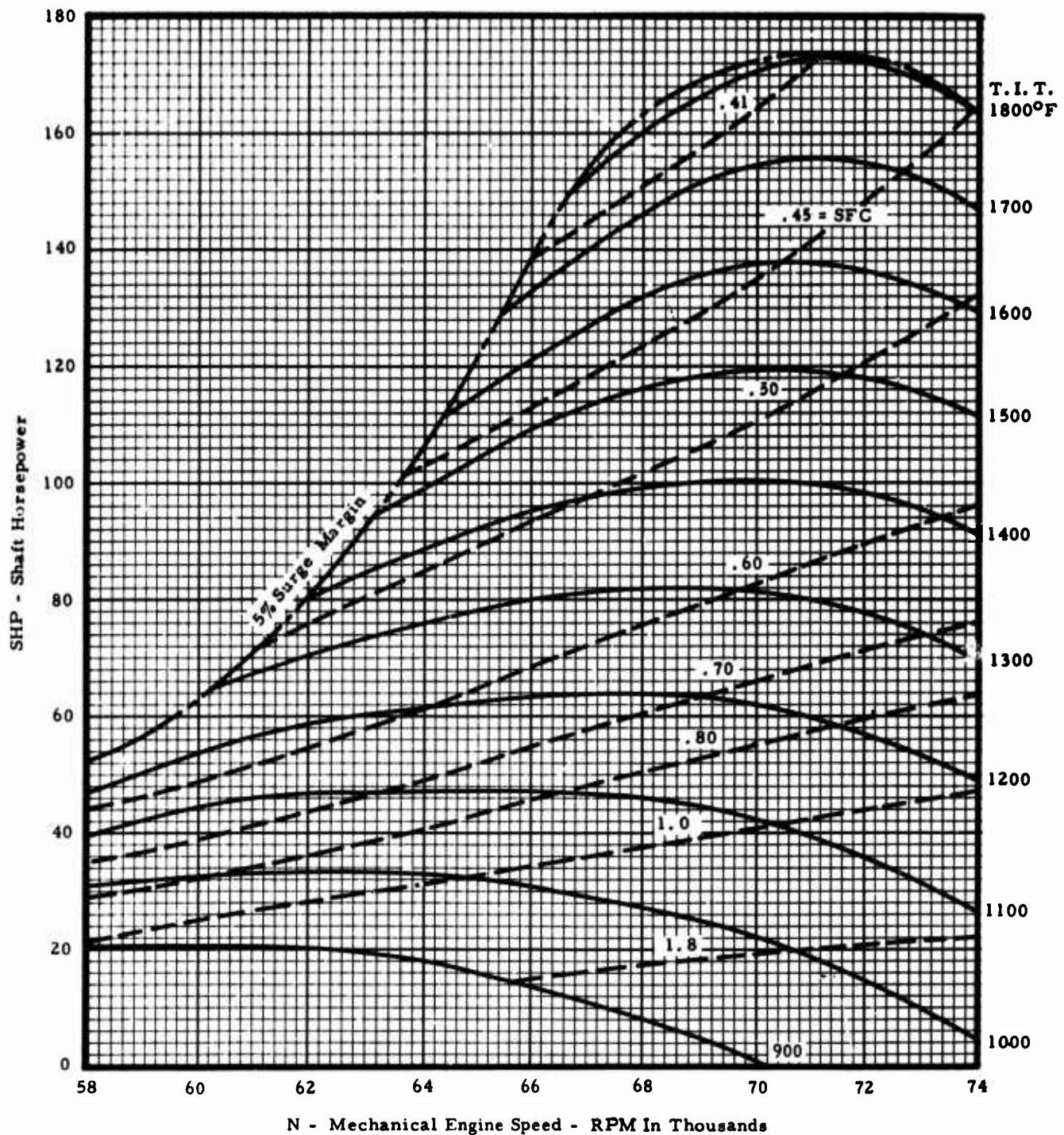


Figure XVI-11. TS120R Regenerative Engine Estimated Performance Characteristics 8000 Feet, 90°F.

**Section XVI**



**Figure XVI-12. TS90R Horsepower Regenerative Engine Estimated Performance Characteristics Sea Level, 60 $^{\circ}\text{F}$ .**

## Section XVI

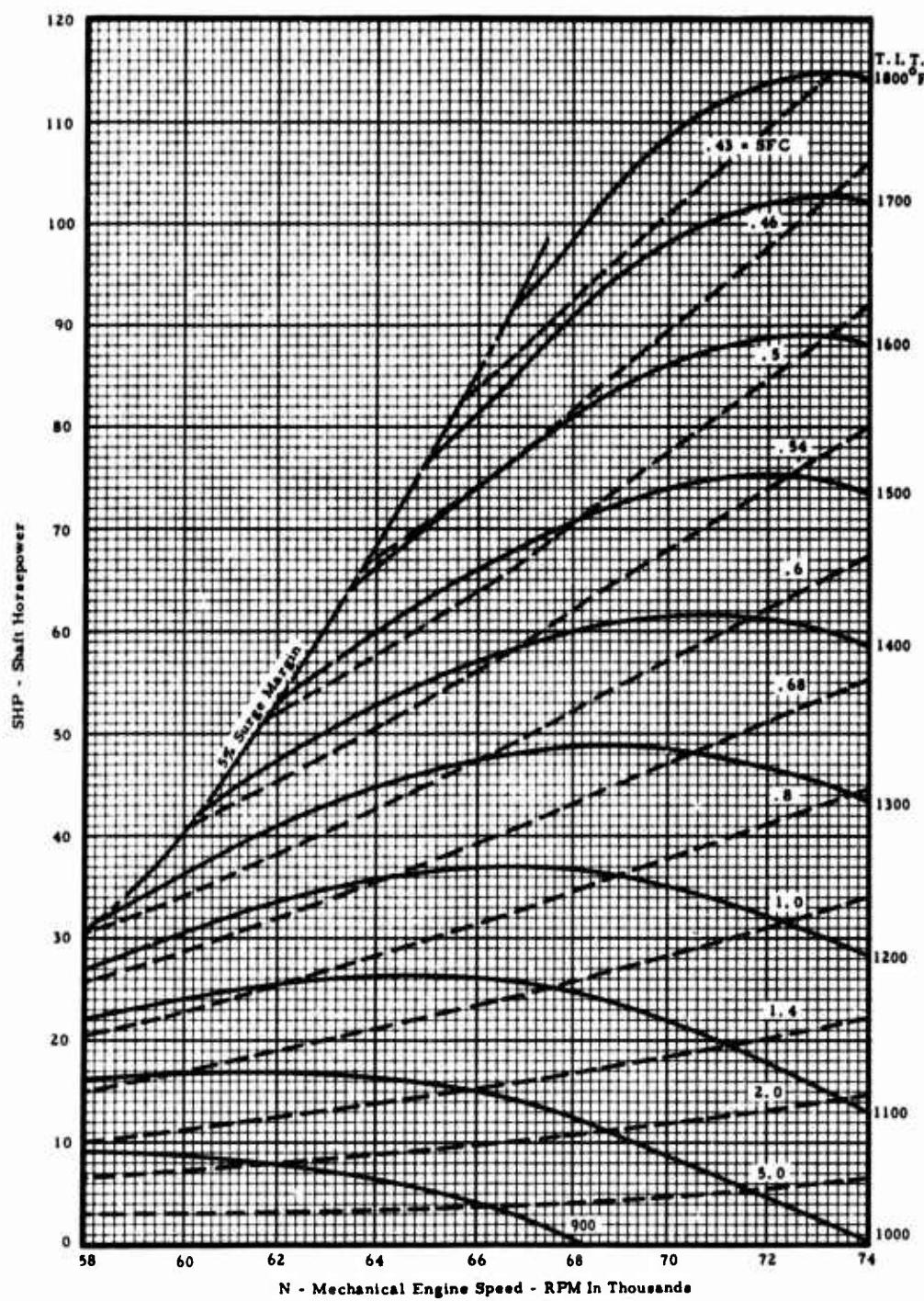


Figure XVI-13. TS90R Horsepower Regenerative Engine Estimated Performance Characteristics 8000 Feet, 90°F.

## Section XVI

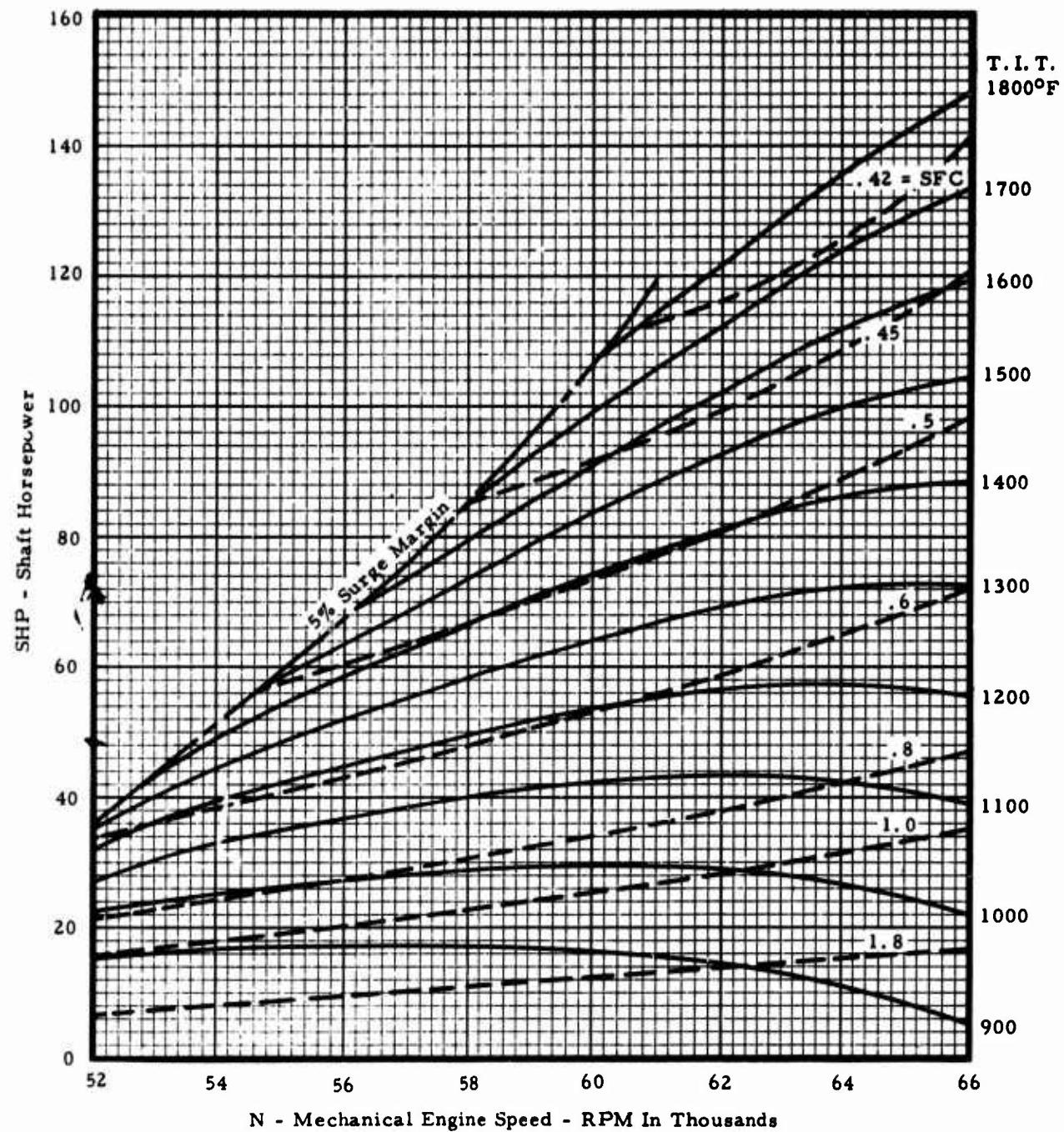


Figure XVI-14. TS60R Horsepower Regenerative Engine Estimated Performance Characteristics Sea Level, 60°F.

## Section XVI

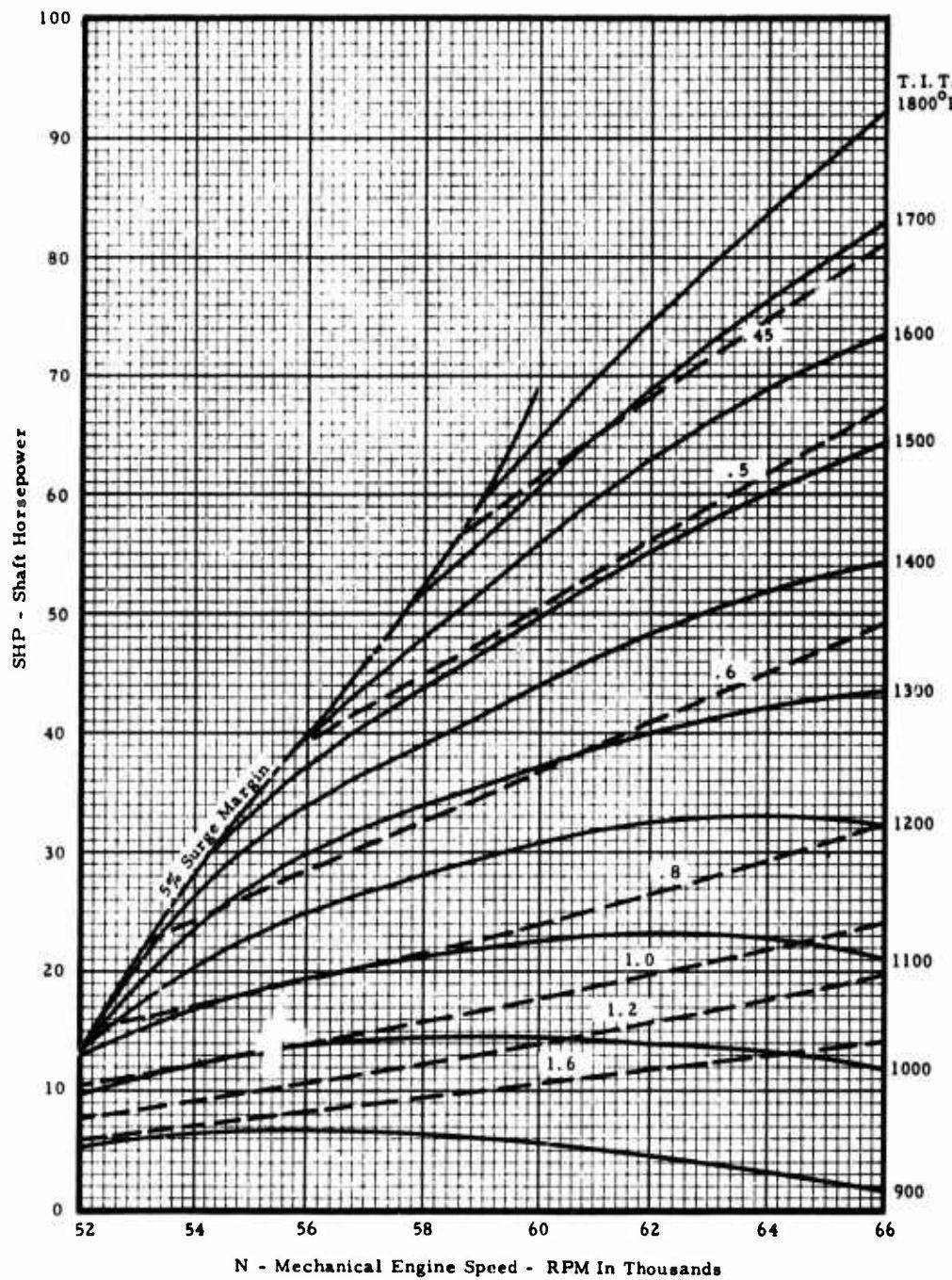


Figure XVI-15. TS60R Regenerative Engine Estimated Performance Characteristics 8000 Feet, 90°F.

## Section XVI

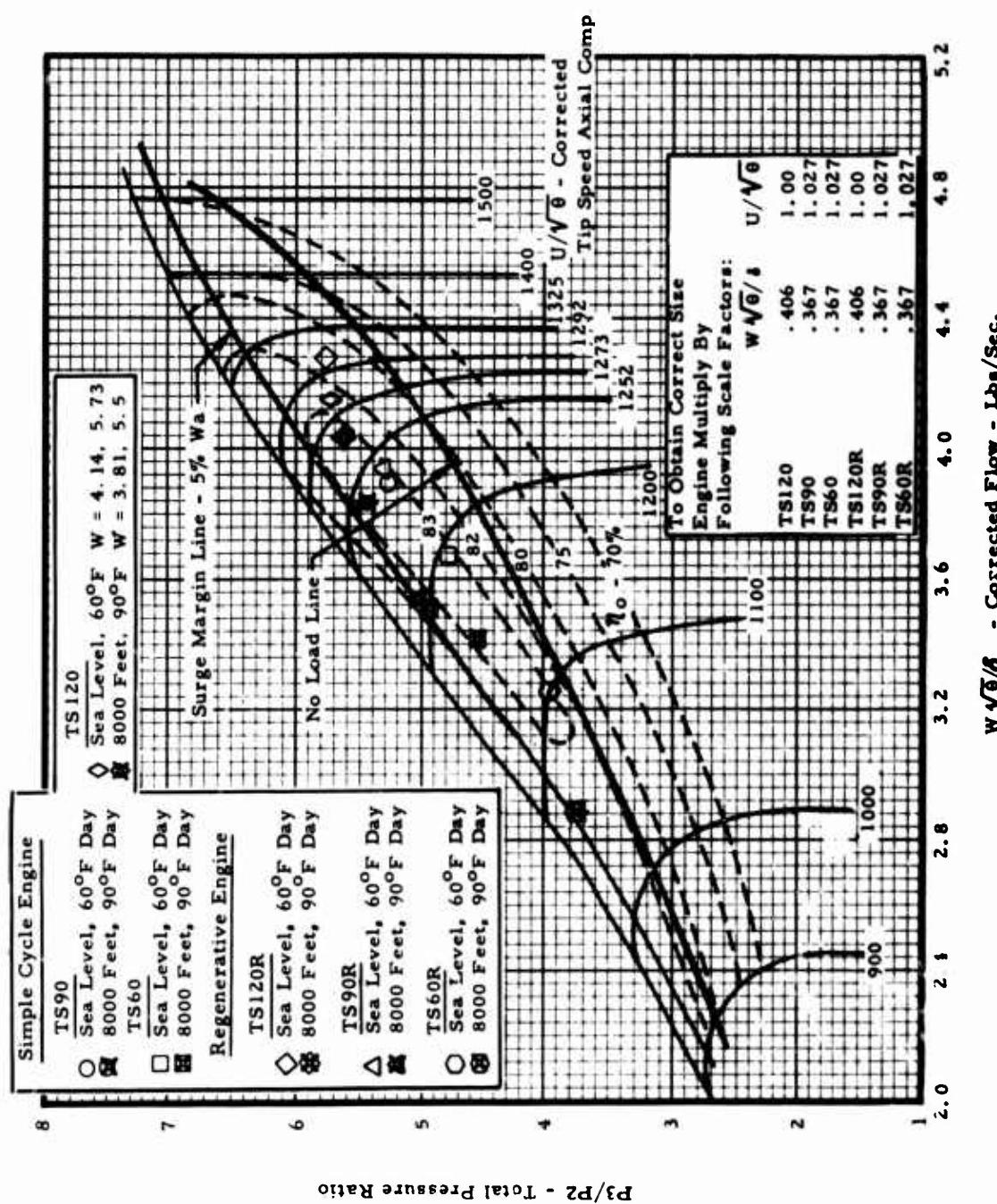
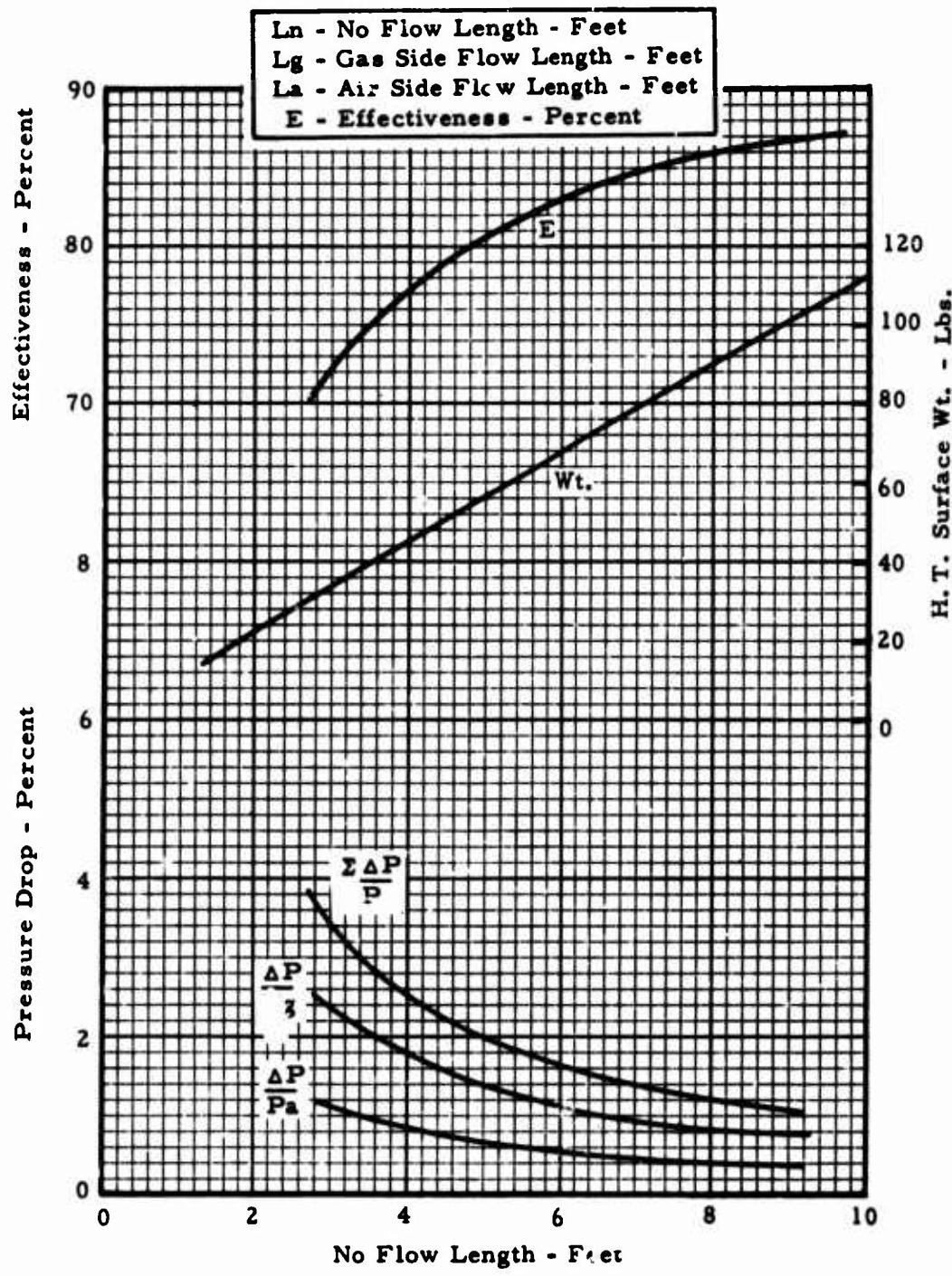


Figure XVI-16. Compressor Map Showing Design Points.

**Section XVI**



**Figure XVI-17. Z-Flow Recuperator - Sea Level Performance.**

Section XVI

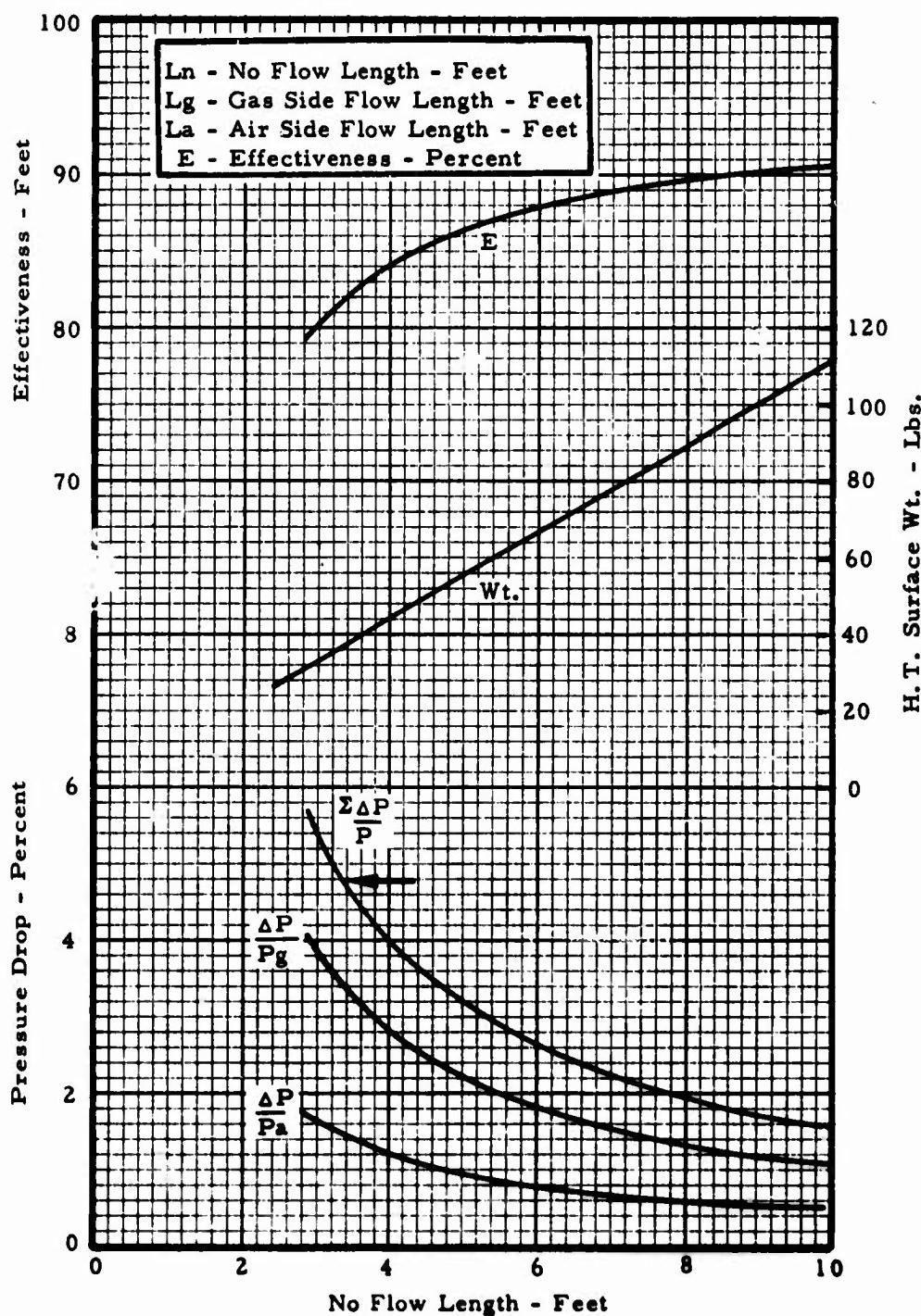
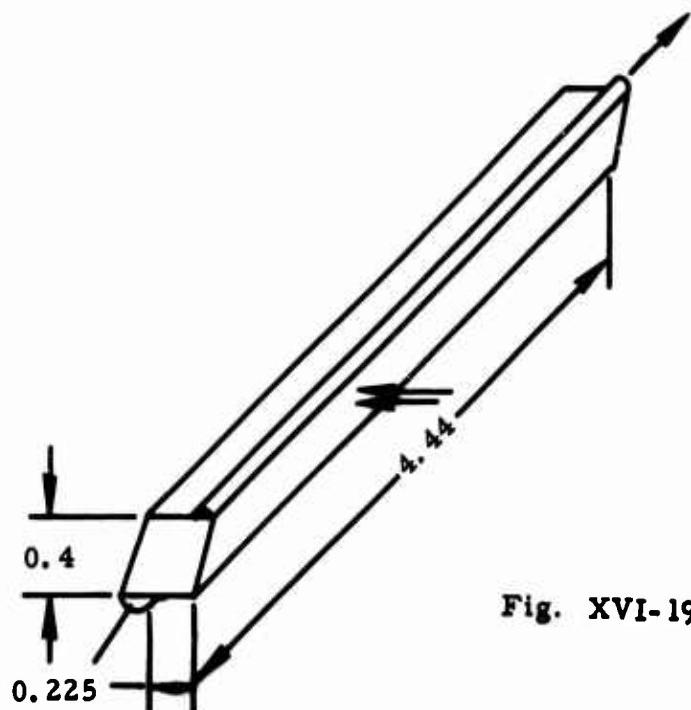
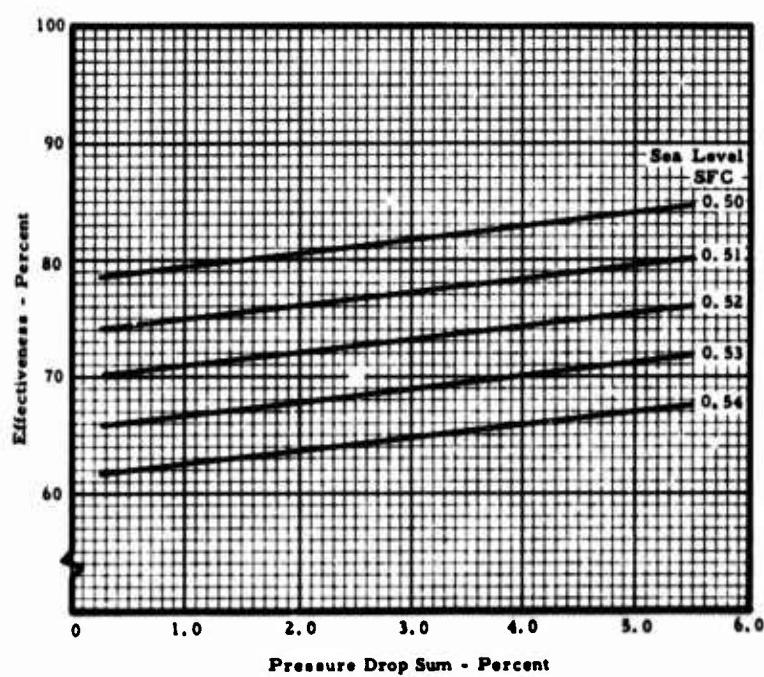


Figure XVI-18. Z-Flow Recuperator - Altitude Performance.

**Section XVI**



**Fig. XVI-19. Z Flow Recuperator Sketch.**



**Fig. XVI-20. Regenerative Engine Characteristics At Sea Level.**

**Section XVI**

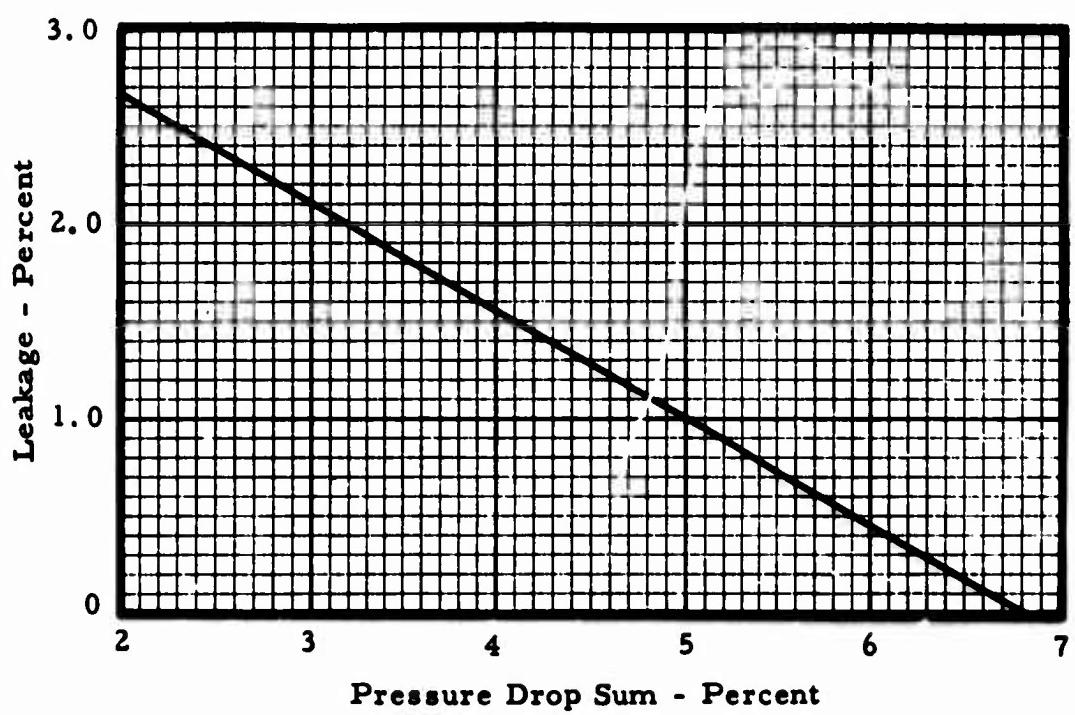


**Figure XVI-21. Regenerative Engine Characteristics at Altitude.**

**Section XVI**

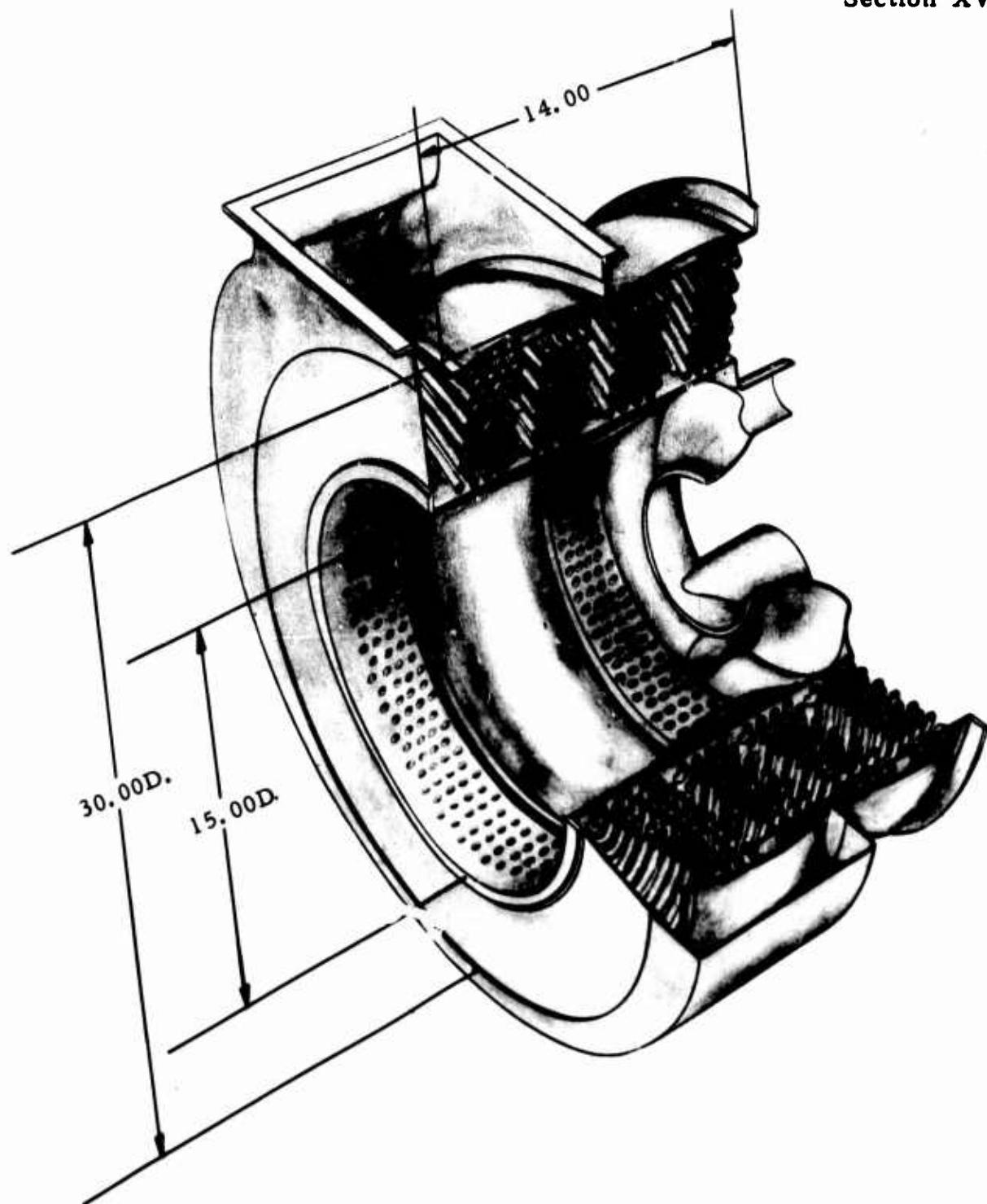


**Figure XVI-22. Sketch - Harrison Proposed Recuperator.**

## Section XVI

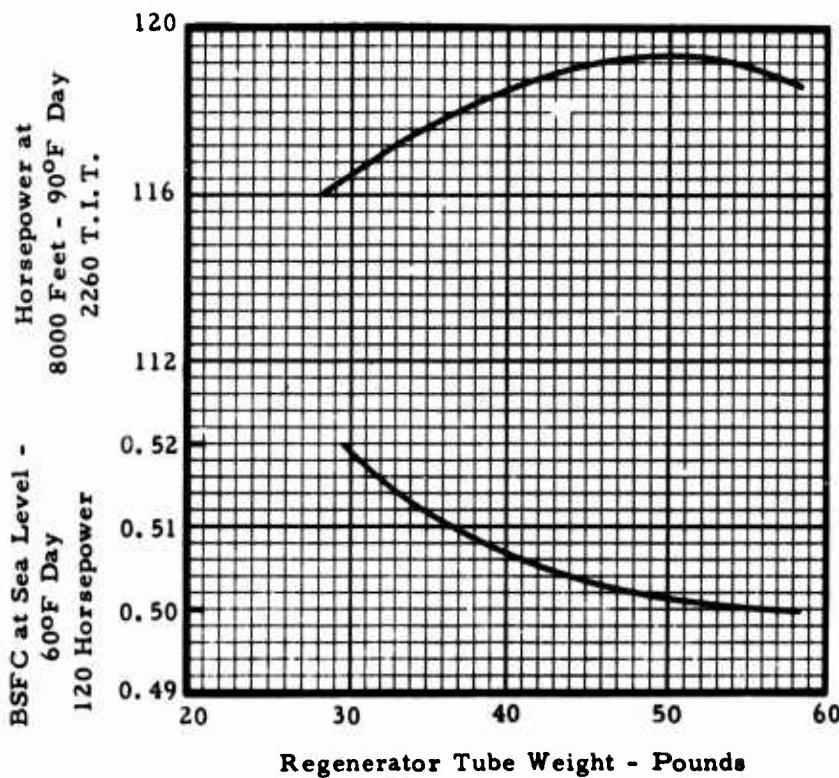


Fig. XVI-23. Performance of 120 Horsepower Engine Version With Harrison Proposed Recuperator.

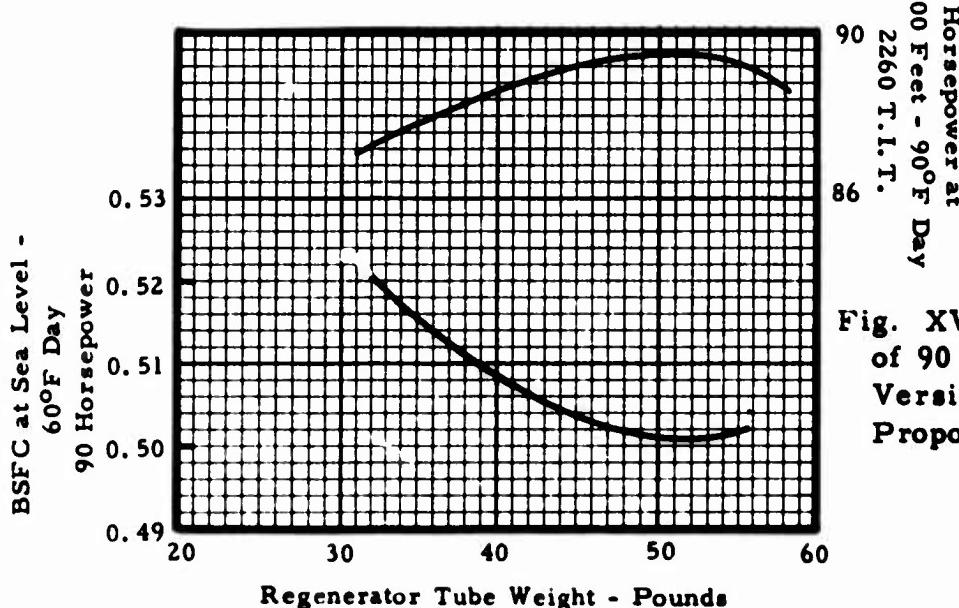


Fig. XVI-24. Performance of 90 Horsepower Engine Version With Harrison Proposed Recuperator.

Section XVI

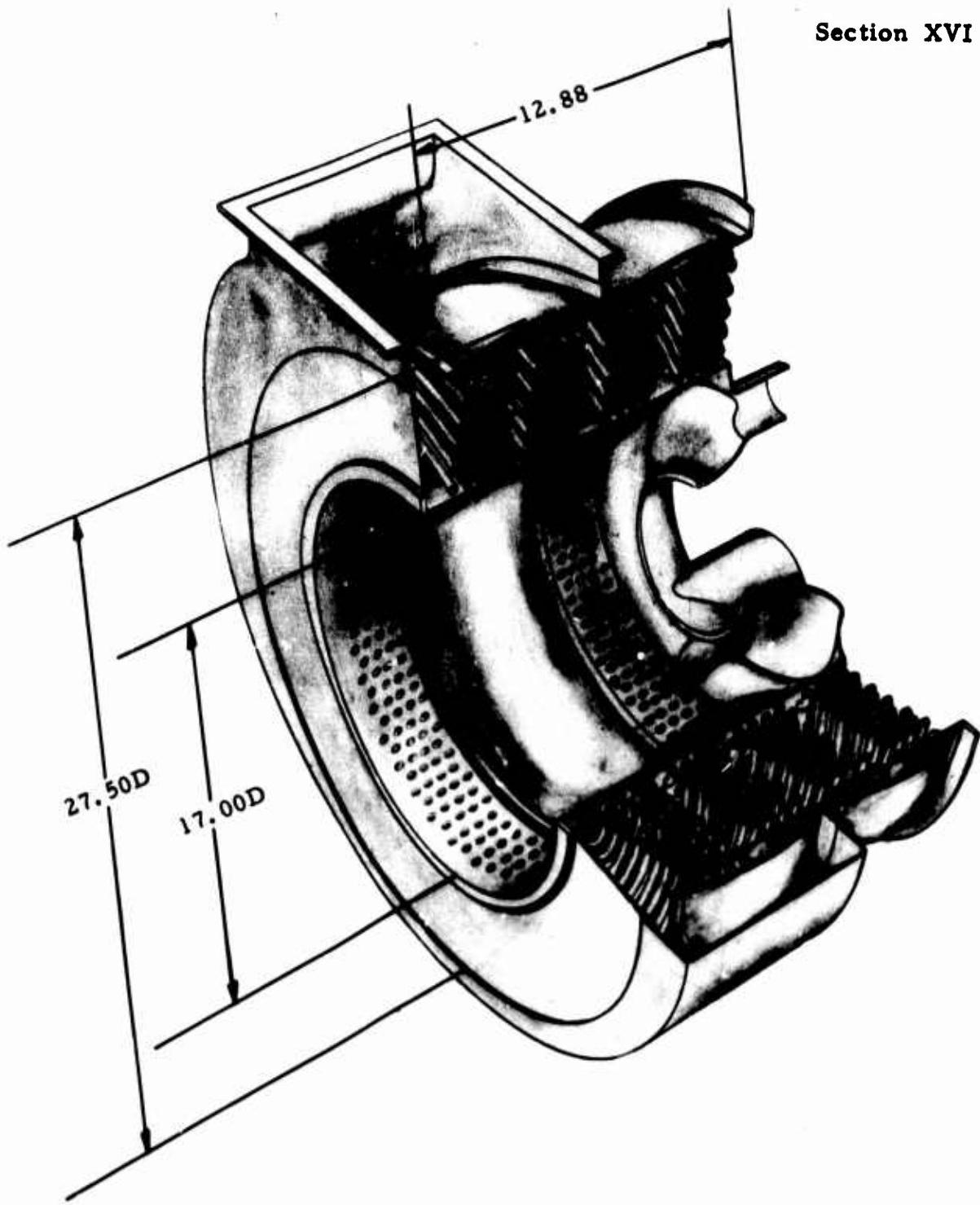
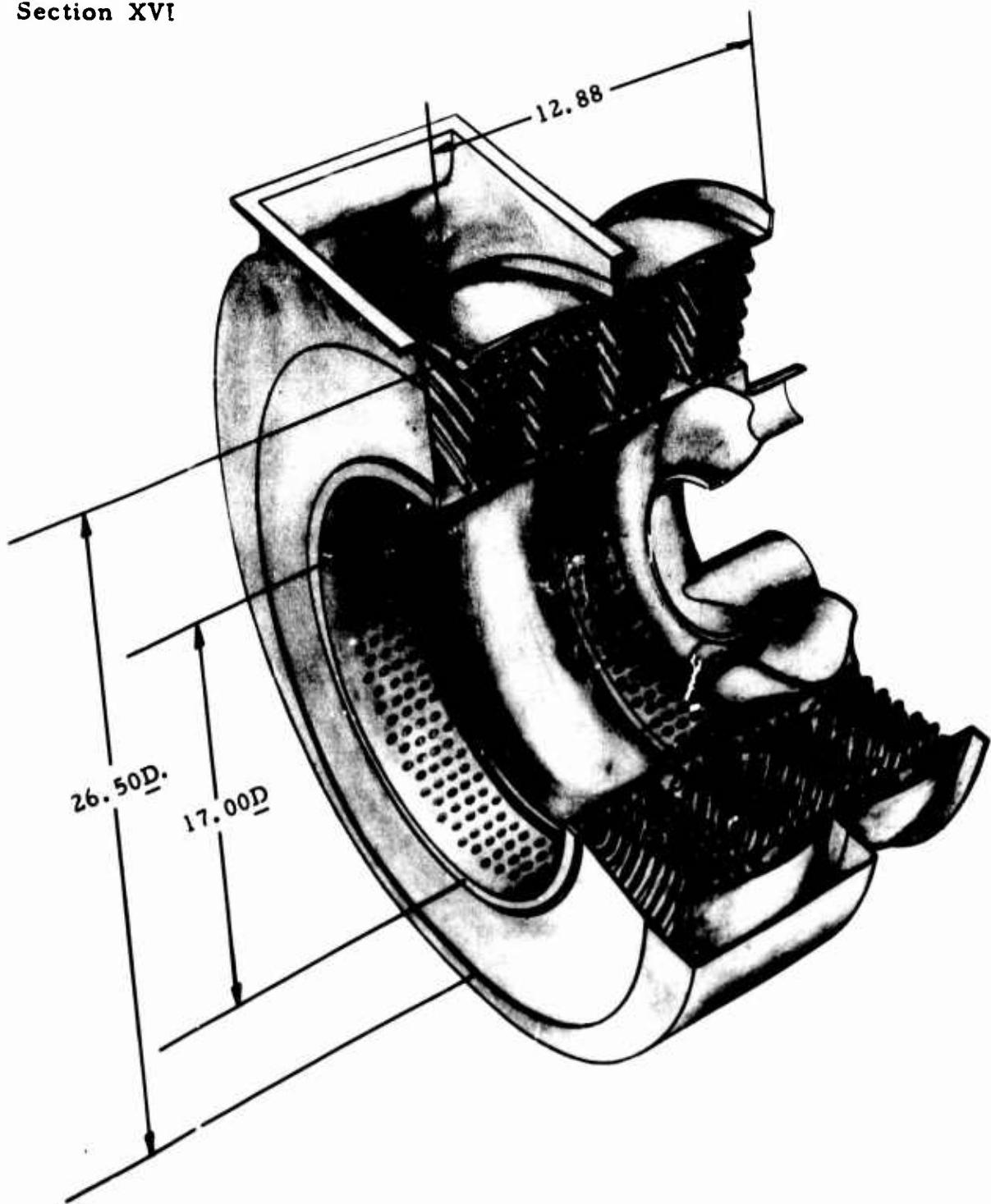


Figure XVI-25. Sketch - Harrison No. 2 Design Recuperator.

**Section XVI**



**Figure XVI-26. Sketch - Harrison No. 3 Design Recuperator.**

APPENDIX XVI-A

Appendix XVI-A

NER-52

Final Report

Exhaust Gas  
Heat Exchanger Design Study  
for  
C. A. E. Model TS-120-1 Turboshaft Engine

June 4, 1965

Submitted to

Continental Aviation and Engineering Corporation  
Research Division  
Detroit 15, Michigan  
(Order No. RD-98098)

Prepared by S. S. Tramuta  
S. S. Tramuta

Approved by C. C. Eckles  
C. C. Eckles

Harrison Radiator Division  
General Motors Corporation  
Lockport, New York

Appendix XVI-A

Table of Contents

	<u>Page</u>
Introduction	1
Summary	2
Discussion	3
Recuperator Description	3
Performance	4
Mechanical Design & Stress Analysis	4
Weight Analysis	6
Leakage	6
Recommendations	7
Tables	
I - Design Point Recuperator	9
II - #1 Alternate	10
III - #2 Alternate	11
IV - #3 Alternate	12
Figures	
1 - Recuperator Perspective NE-1590-R)	13
2 - Assembly Drawing (NE-1590-R)	14
3 - Performance Data	15
4 - Tubular Recuperator Photo	16
Appendix (Stress Analysis)	17

**Appendix XVI-A**

**INTRODUCTION**

This report was prepared by the Harrison Radiator Division of General Motors Corporation, Lockport, New York, under subcontract to Continental Aviation and Engineering Corporation, Research Division, Detroit, Michigan, on contract No. DA 44-009-AMC-760(T). It presents a summary of the work done, during the period April 12, 1965 through June 4, 1965, toward the design of a recuperator for Continental Aviation and Engineering Corporation's TS-120-1 Turboshaft Engine. Information presented will be recuperator description, performance, mechanical design and stress analysis, weight analysis, leakage, and recommendations.

## Appendix XVI-A

### SUMMARY

The design and performance analysis of this study resulted in the following:

1. A recuperator design, NE-1590-R, Fig. 2 , (p. 15 ), for C.A.E's. TS-120-1 Turboshaft Engine.
2. A number of alternate designs as presented in Tables II through IV, and Fig. 3 , (p. 16 ).
3. The conclusion that it appears to be practicable for the fabrication of recuperator NE-1590-R within the present state of the art. In the past H.R.D. has fabricated an annular recuperator with a plate-type involuted tube, and has designed and is presently fabricating an annular recuperator employing a .125" O.D. involuted round tube.

DISCUSSION

During the period of April 12, 1965 through June 4, 1965, Harrison Radiator Division of General Motors Corporation, Lockport, New York, conducted a recuperator design study for Continental Aviation and Engineering Corporation, Research Division, Detroit, Michigan. Discussion of this study follows.

Recuperator Description

The recuperator, Fig. 1 (p. 14), provides a surface for the exchange of heat between hot exhaust gas and cool compressor discharged air. This transfer is accomplished while maintaining a hermetic barrier between the hot exhaust gas and air. The recuperator assembly consists of one major assembly, the core. The core, consisting primarily of plain round tubes, tube sheets and baffles, serves as the transport and heat transfer mechanism for the low pressure exhaust gas from the turbine outlet and the high pressure air from the compressor outlet.

As shown in Fig. 1, (p. 14), the recuperator is an annular round tube and shell heat exchanger. The design is such that the core is free to move in the axial and radial directions to compensate for the thermal growth. Flexibility in the tubes is also provided to minimize thermal stresses due to differential expansion of various component parts such as tubes and tube sheets.

High pressure air enters the recuperator from the compressor, makes four passes through the inside of the tubes, leaves the recuperator and enters the burner. From the burner the exhaust gas goes on to the turbine and then on to the shell side of the recuperator. The low pressure exhaust gas from the turbine makes one pass through the core (outside the tubes), and then exhausts to the atmosphere.

## Appendix XVI-A

### Performance

The design point recuperator is described in Table I and Fig. 2, (p. 15), (Dwg. NE-1590-R). This design was attained after a parametric study was completed on the thermal and mechanical design in which the trade-offs in performance, weight, and packaging were evaluated. Tables II through IV are alternate recuperators, and Fig. 3 , (p. 16 ), is a plot of the thermal and mechanical features of the design point and alternate recuperators. The tube diameter, wall, effective length, and pitch are kept constant in all recuperators. This characteristic was decided upon when the parametric study revealed that this combination appeared more profitable in system trade-offs of performance, weight, and packaging.

### Mechanical Design

The fabrication of the recuperator appears to be practicable within the present state of the art. Material will be type 347 stainless steel throughout.

As shown in Fig. 2 , (p.15 ), the recuperator is a four-pass cross-counter flow type. For fabrication the core will be made of four annular sections, each section composed of three 120° segments. A segment will contain 406 tubes, a 120° segment of the inner tube sheet, a 120° segment of the outer tube sheet, and the necessary tube spacer bars. The tubes, tube sheets, and spacer bars will be assembled in a braze fixture. The tube to tube sheet joints will be sealed by vacuum brazing with GE8100 brazing alloy. Thin sheet baffles, shaped to block the open areas on the gas side at the tube end radii adjacent to the tube sheets, will be inserted and tacked to the tube sheets.

Three core segments will be assembled to form a core section. Baffles composed of dummy tubes and spacer bars will be placed between segments. T.I.G. welding will join the tube sheets to complete the annular section. Each section will be leak tested and repaired if necessary.

## Appendix XVI-A

Four sections will be assembled by T.I.G. welding the tube sheets to complete the core. Each core assembly will be leak tested and repaired if necessary.

The inner header assembly will be assembled to the core by T.I.G. welding. The outer header assemblies will be assembled to the core by T.I.G. and seam welding. All welds will be pressure tested.

The ducts, gas inlet and outlet, will be assembled and T.I.G. welded to the inner tube sheet. All welds will be pressure tested.

Final machining and drilling will complete the recuperator.

### Detail Parts:

Tubes - .150" O.D. x .004" thk. wall.

4992 tubes will be mandrel bent to the involute shape with a .375" radius at each end. One hundred and twenty of these tubes will have .125" cut from each end and will be used as the dummy tubes for baffles. The remaining 4872 tubes will be deburred and the ends sized.

Inner tube sheet - .038" thk.

Roll formed to proper radius.

Tube holes drilled and reamed for braze fit to tubes.

Outer tube sheet - .063" thk.

Same as inner tube sheet.

Tube spacer bars - .038" thk.

Sheared from 2.625" wide strip perforated with properly spaced elongated holes.

Baffle, tube to tube sheet - .003" thk.

Formed as required.

Baffle, between segments.

Ten dummy tubes mounted in a special spacer bar.

## **Appendix XVI-A**

**Filler strips - .063" thk.**

**Strips at end of inner header and the center joint  
of the outer headers.**

**Inner header assembly.**

**.025" thk. spin formed header T.I.G. welded to a  
machined ring.**

**Outer header assembly.**

**.038 thk. spin formed header T.I.G. welded to a  
machined ring.**

A preliminary stress analysis was conducted by Dr. Herbert D. Becker of Allied Research Associates, Inc., Concord, Mass. Results of this study are reported in the Appendix. It should be recognized that the recuperator was analyzed for effects of pressure and temperature only. The effects of attachments to the turbine structure were not considered since these details were not established at the time of the analysis.

### **Recuperator Weight Analysis (lbs.)**

**(Per Dwg. NE-1590-R)**

Recuperator	O.D. Ins.	Inner		Outer		Spacers & Baffle Wt.	H. E. Wt.	Duct & Flange Wt.	Total Wt.	
		Total Tube Tube Wt.	Tube Sht. Wt.	Tube Sht. Wt.	Inner Hdr. Wt.	Outer Hdr. Wt.				
Design	27.50	43.00	6.53	18.75	3.65	12.98	3.32	88.23	11.75	99.98
#1 Alt.	27.00	38.00	6.66	18.54	3.65	12.77	2.93	82.55	11.23	94.78
#2 Alt.	26.12	34.00	6.75	18.38	3.65	12.42	2.52	77.72	10.76	88.48
#3 Alt.	25.62	29.75	6.93	18.15	3.65	12.19	2.26	72.93	10.45	83.38

### **Leakage**

A goal of Harrison Radiator Division in this program will be to fabricate a heat exchanger approaching zero leakage. H.R.D. has accomplished this in the past and feels that the design of this recuperator (NE-1590-R) is such that this can be attained.

## Appendix XVI-A

Fig. 4 , (p. 17 ) is an H. R. D. built recuperator for exhaust gas turbine application with zero leakage when pressure tested at operating stress levels. This is a .210'O.D., .004" wall round tube unit. Like NE-1590-R, it is a four-pass (air) tubular recuperator and has been in service for over 300 hours of turbine operation and continues to function as designed.

H. R. D. has also designed, fabricated, and tested liquid metal (Sodium-Potassium)heat exchangers for high temperature (1500°F and 75 PSIA) application with zero leakage. A helium mass spectrometer test is conducted on each liquid metal unit before it is put into service. Because of the behavior of alkali metals at high temperatures when exposed to air, all liquid metal heat exchangers must be designed and fabricated for zero leakage service. H. R. D. has accomplished this many times.

As previously stated, one of our goals will be to design and fabricate an exhaust gas recuperator having zero leakage. If an allowable leakage rate is permissible, H. R. D. feels that the degree of leakage allowed should be determined and agreed upon by both H. R. D. and C. A. E.

### Recommendations

The efficiency of the gas turbine can be greatly improved by the use of a recuperator, but at the expense of added weight and bulk. These penalties can be minimized by use of compact heat exchangers having small flow passages. However, with small flow passages the reduction of flow area with small amounts of fouling is significant so that cleanliness is demanded. Optimization of heat exchanger design for minimum weight compatible with reasonable tolerance to fouling of flow passages requires detailed knowledge of the rate of fouling under various operating conditions, and the effects of such fouling on both pressure drop and heat transfer rate.

One source of fouling is deposition of soot when combustion is

## Appendix XVI-A

poor. Soot buildup can be rapid, but it may be reversible with change of conditions. A second source of fouling is deposition of fuel ash resulting from small quantities of metallic additives used to improve fuel properties. Such deposits may accumulate slowly, but may eventually prove troublesome to remove.

Harrison Radiator Division recognizes this fouling problem and would recommend that a fouling and cleaning program be conducted early in Phase II of this development program. This program can be conducted on small recuperators (NE-1590-R) sections, or on a full size recuperator (NE-1590-R). We also recommend that these tests be conducted at Continental Aviation and Engineering Corporation, and that H.R.D. support these tests by providing C.A.E. with test cores and a liaison engineer.

TABLE I

Appendix XVI-A

Design Point Recuperator  
 (per Dwg. NE-1590-R)  
 O.D. 27.5 inches  
 I.D. 15.88 inches  
 Length = 13.375 inches

HP	120		90		60	
<u>Condition</u>	<u>S.L.</u>	<u>Alt.</u>	<u>S.L.</u>	<u>Alt.</u>	<u>S.L.</u>	<u>Alt.</u>
Air Flow - #/sec	1.725	1.176	1.425	.926	1.176	.751
Gas Flow - #/sec	1.742	1.1895	1.4417	.9395	1.1927	.7645
Air Temp. In - °R	935	970	907	940	831	868
Gas Temp. In - °R	1364	1638	1299	1648	1347	1777
Air P. in - PSIA	87.50	63.62	80.13	56.28	61.57	43.09
Gas P. in - PSIA	15.15	11.25	15.00	11.13	14.92	11.06
Effectiveness - %	79.00	81.00	79.50	81.50	80.50	83.75
Core Air $\frac{\Delta P}{P}$ - %	2.56	2.69	2.03	2.18	2.36	2.59
Core Gas $\frac{\Delta P}{P}$ - %	3.00	3.13	2.05	2.04	1.45	1.43

Design

Type	plain round tube and shell (annular design)
Air passes	4
Gas passes	1
Tube O.D. - in.	.150
Tube wall - in.	.004
Tube eff. length - in.	16
Tube pitch - in.	X <sub>T</sub> = .250; X <sub>L</sub> = .156
Tube shape	involute
No. Tubes	4872
Tubes/pass	1218
Material	347 S.S.
H. T. Tube wt. - lbs.	40.8
Total H. E. wt. - lbs.	99.98

## Appendix XVI-A

TABLE II

#1 Alternate Recuperator  
 O.D. 27 inches  
 I.D. 15.88 inches  
 Length = 13.375 inches

HP	120		90		60	
<u>Condition</u>	<u>S.L.</u>	<u>Alt.</u>	<u>S.L.</u>	<u>Alt.</u>	<u>S.L.</u>	<u>Alt.</u>
Air Flow - #/sec	1.725	1.176	1.425	.926	1.176	.751
Gas Flow - #/sec	1.742	1.1895	1.4417	.9395	1.1927	.7645
Air Temp. In - °R	935	970	907	940	831	868
Gas Temp. In - °R	1364	1638	1299	1648	1347	1777
Air P. in - PSIA	88.18	64.14	80.63	56.65	62.01	43.42
Gas P. in - PSIA	15.32	11.38	15.12	11.21	15.00	11.12
Effectiveness - %	78.50	80.50	79.00	81.00	80.00	83.00
Core Air $\frac{\Delta P}{F}$ - %	3.32	3.47	2.64	2.82	3.05	3.34
Core Gas $\frac{\Delta P}{P}$ - %	4.07	4.25	2.79	2.79	1.99	1.98

Design

Type	plain round tube and shell (annular design)
Air Passes	4
Gas passes	1
Tube O.D. - in.	.150
Tube Wall - in.	.004
Tube eff. length - in.	16
Tube pitch - in.	X <sub>T</sub> = .250; X <sub>L</sub> = .156
Tube shape	involute
No. tubes	4160
Tubes/pass	1040
Material	347 S.S.
H. T. Tube wt. - lbs.	35
Total H. E. wt. - lbs.	94.78

TABLE III

Appendix XVI-A

#2 Alternate Recuperator  
 O.D. 26.12 inches  
 I.D. 15.88 inches  
 Length = 13.375 inches

HP	120		90		60	
<u>Condition</u>	<u>S.L.</u>	<u>Alt.</u>	<u>S.L.</u>	<u>Alt.</u>	<u>S.L.</u>	<u>Alt.</u>
Air Flow - #/sec	1.725	1.176	1.425	.926	1.176	.751
Gas Flow - #/sec	1.742	1.1895	1.4417	.9395	1.1927	.7645
Air Temp. In - °R	935	970	907	940	831	868
Gas Temp. In - °R	1364	1638	1299	1648	1347	1777
Air P. in - PSIA	88.98	64.75	81.22	57.09	62.54	43.81
Gas P. in - PSIA	15.44	11.47	15.20	11.27	15.05	11.16
Effectiveness - %	77.50	79.50	78.00	80.00	79.50	82.00
Core Air $\frac{\Delta P}{P}$ - %	4.19	4.39	3.35	3.56	3.88	4.21
Core Gas $\frac{\Delta P}{P}$ - %	4.77	4.95	3.26	3.27	2.33	2.34

Design

Type	plain round tube and shell (annular design)
Air passes	4
Gas passes	1
Tube O.D. - in.	.150
Tube wall - in.	.004
Tube eff. length - in.	16
Tube pitch - in.	X <sub>T</sub> = .250; X <sub>L</sub> = .156
Tube shape	involute
No. tubes	3648
Tubes/pass	912
Material	347 S.S.
H. T. Tube wt. - lbs.	30.7
Total H. E. wt. - lbs.	88.48

## Appendix XVI-A

TABLE IV

#3 Alternate Recuperator  
 O.D. 25.62 inches  
 I.D. 15.88 inches  
 Length = 13.375 inches

<u>HP</u>	120		90		60	
<u>Condition</u>	<u>S.L.</u>	<u>Alt.</u>	<u>S.L.</u>	<u>Alt.</u>	<u>S.L.</u>	<u>Alt.</u>
Air Flow - #/sec	1.725	1.176	1.425	.926	1.176	.751
Gas Flow - #/sec	1.742	1.1895	1.4417	.9395	1.927	.7645
Air Temp. In - °R	935	970	907	940	831	868
Gas Temp. In - °R	1364	1638	1299	1648	1347	1777
Air P. in - PSIA	89.99	65.54	81.96	57.63	63.21	44.31
Gas P. in - PSIA	15.63	11.61	15.32	11.36	15.14	11.23
Effectiveness - %	77.00	79.00	77.50	79.50	79.00	81.50
Core Air $\frac{\Delta P}{P}$ - %	5.26	5.54	4.22	4.48	4.89	5.28
Core Gas $\frac{\Delta P}{P}$ - %	5.96	6.11	4.07	4.07	2.90	2.92

Design

Type	plain round tube and shell (annular design)
Air passes	4
Gas passes	1
Tube O. D. - in.	.150
Tube wall - in.	.004
Tube eff. length - in.	16
Tube pitch - in.	$X_T = .250; X_L = .156$
Tube shape	involute
No. tubes	3200
Tubes/pass	800
Material	347 S.S.
H. T. Tube wt. - lbs.	26.9
Total H. E. wt. - lbs.	83.38

Appendix XVI-A

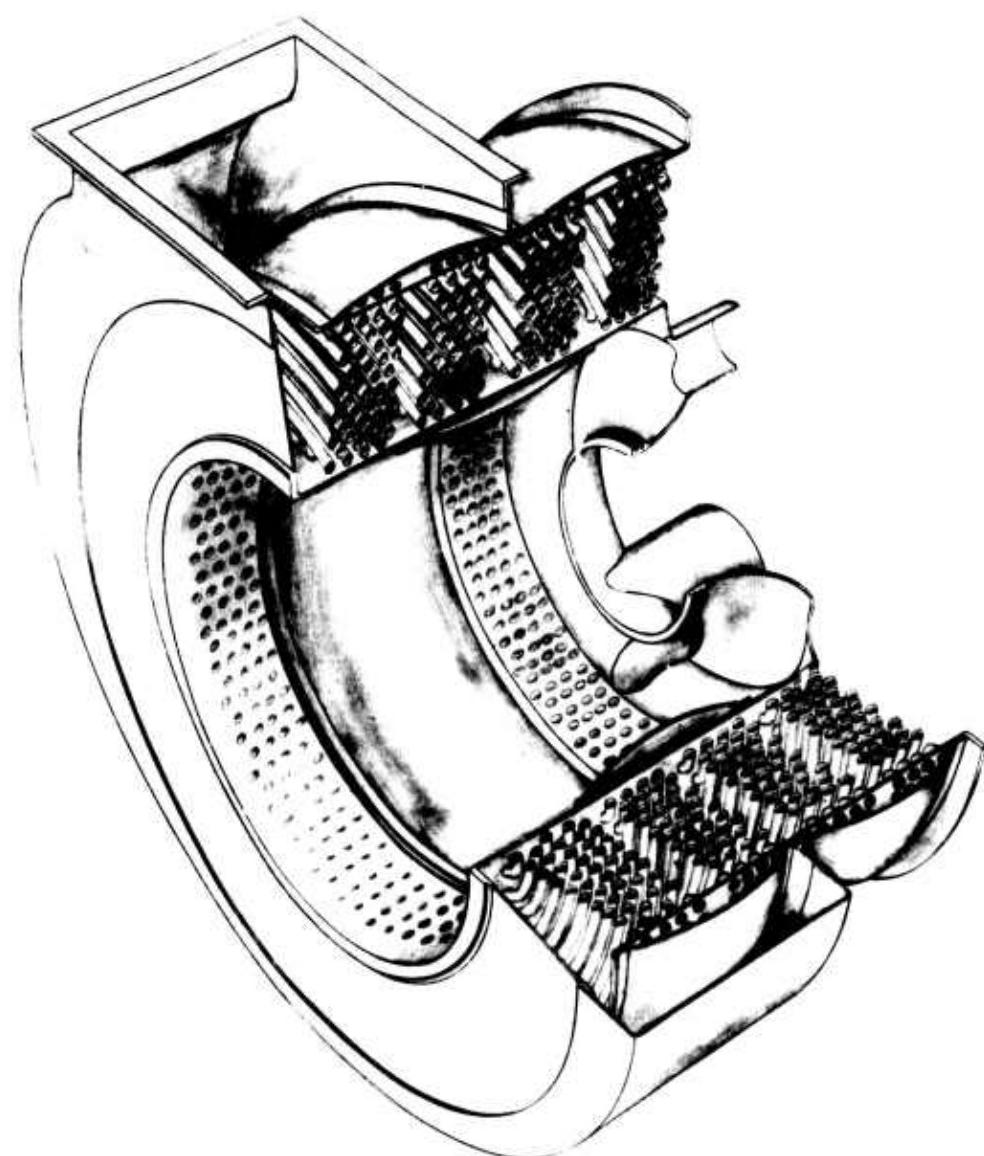


Fig. 1. Continental TS120-1 Recuperator, NE-1590-R

Appendix XVI-A

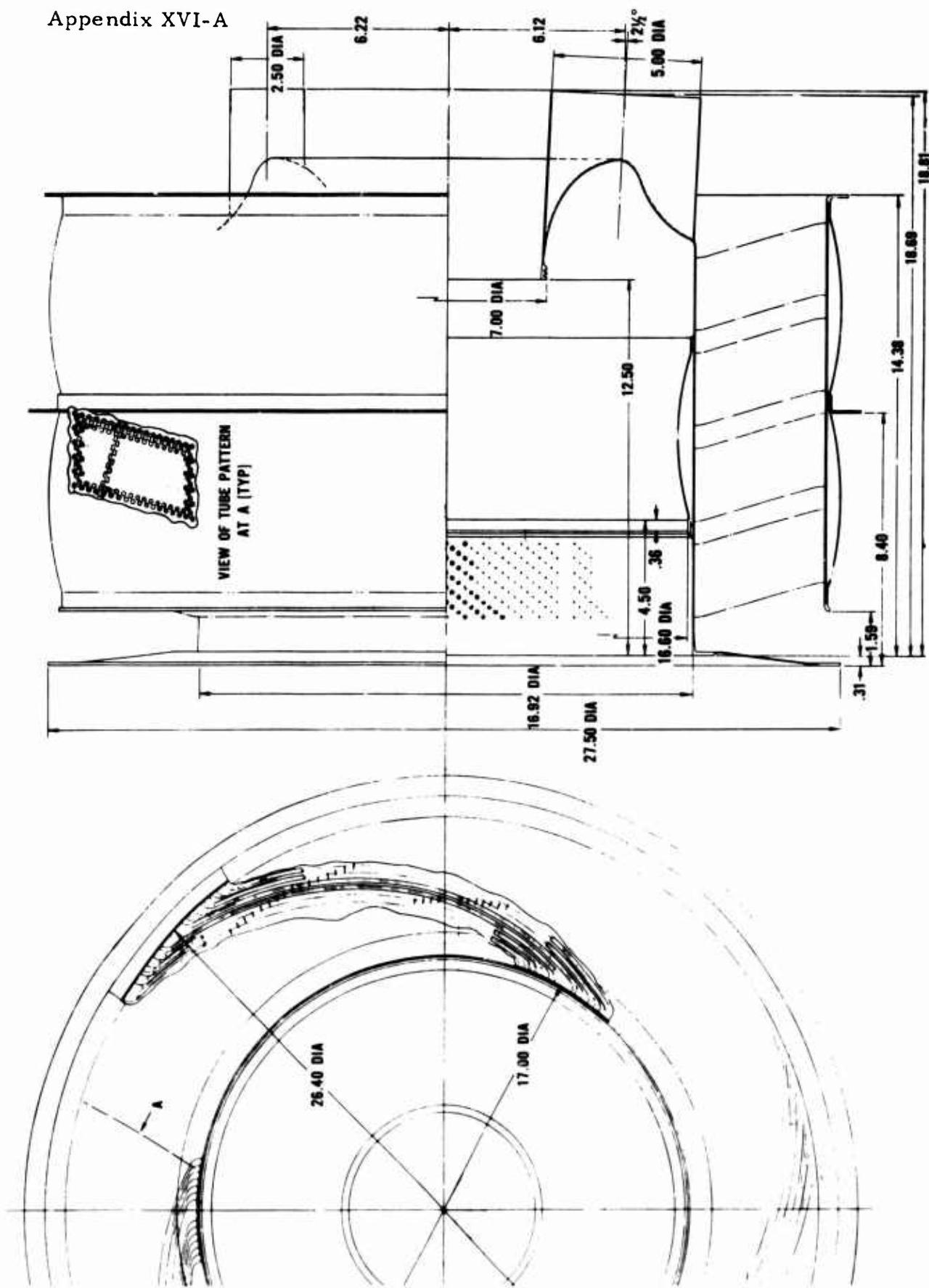


Fig. 2. Harrison Radiator Division Recuperator Drawing No. NE - 1590 - R.

Appendix XVI-A

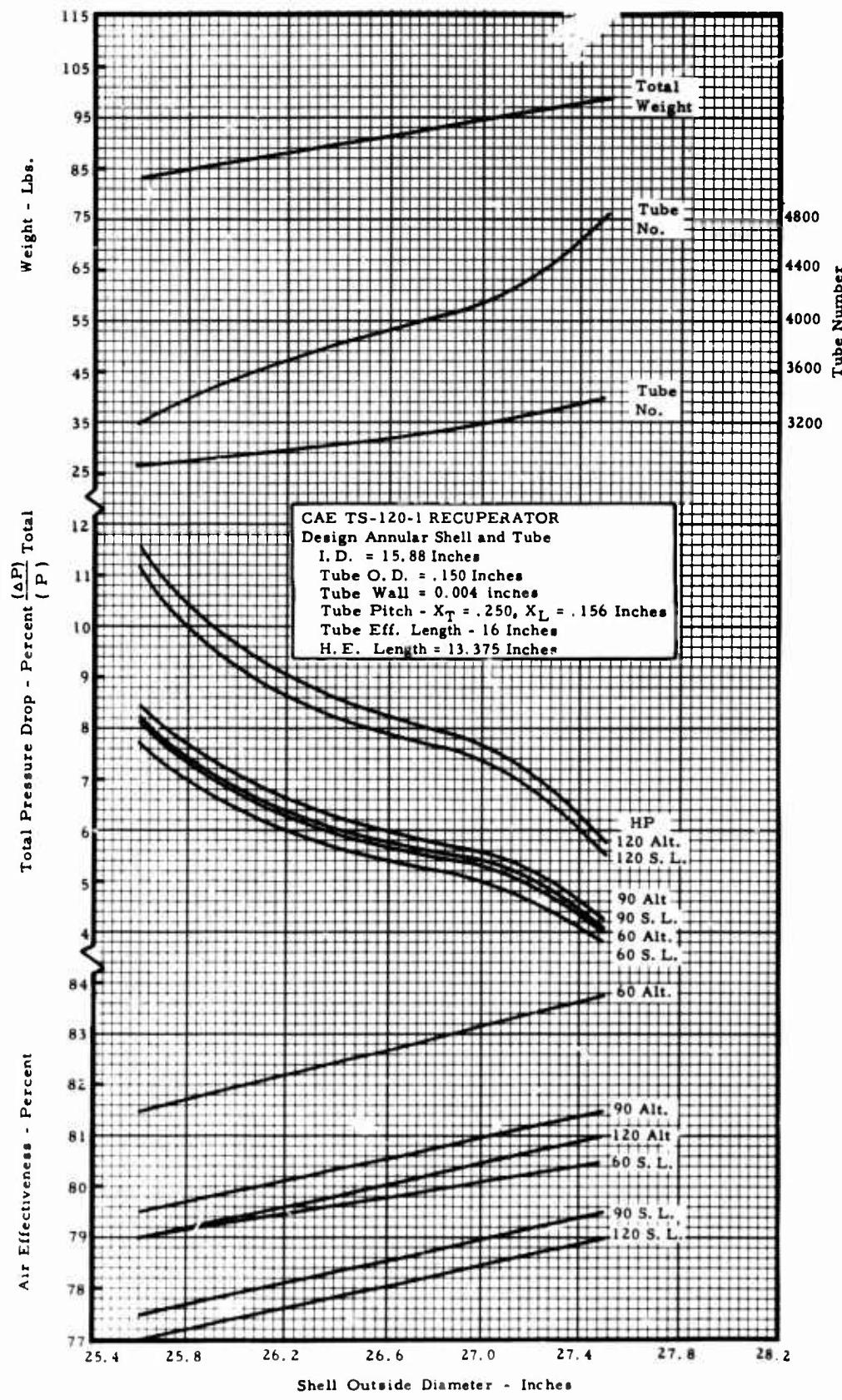


Fig. 3

Appendix XVI-A

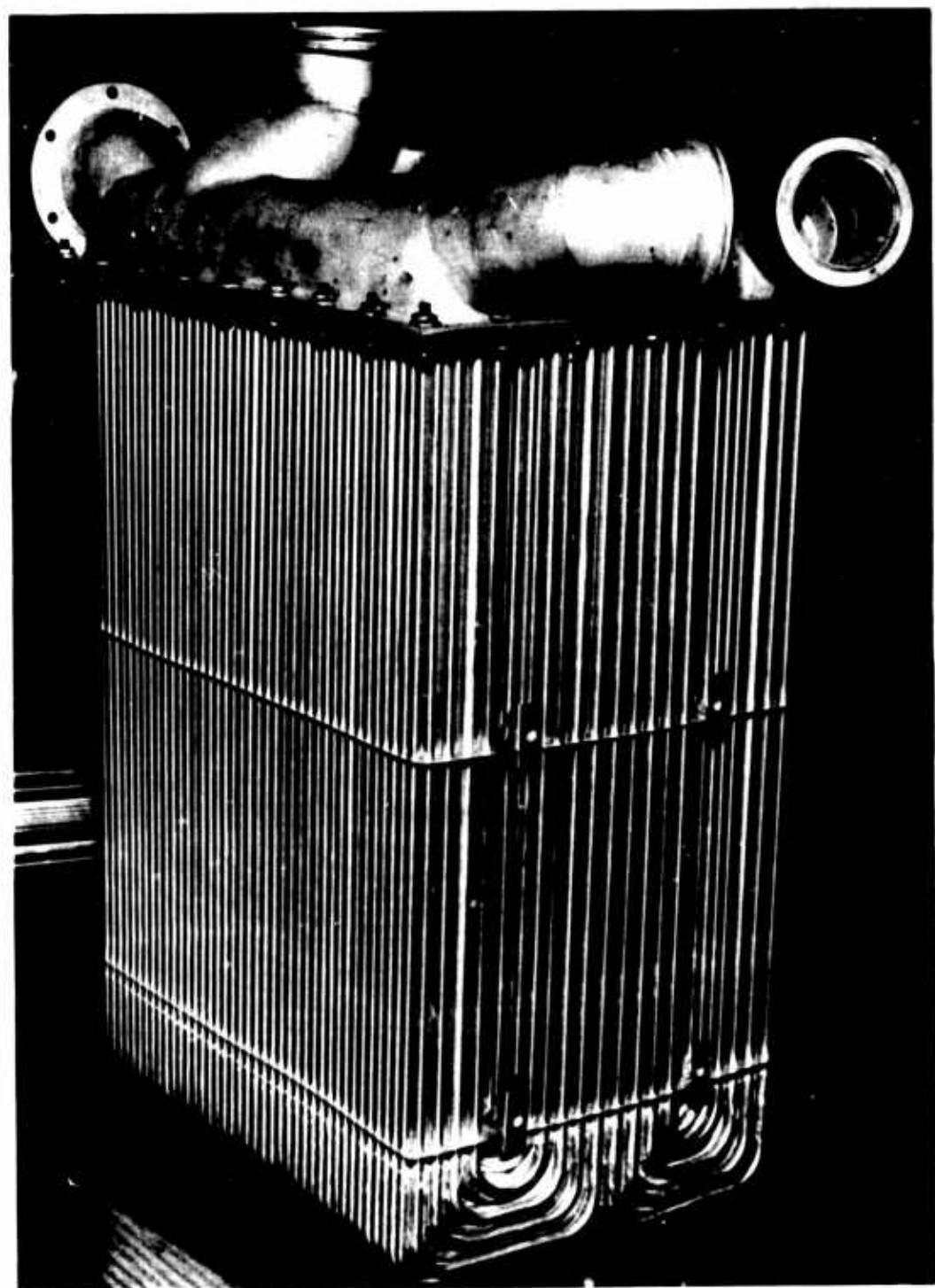


Fig. 4. Tubular Recuperator.

**Appendix XVI-A**

**APPENDIX**  
**(Stress Analysis)**

Appendix XVI-A



ANALYSIS OF RECUPERATOR DESIGN

Herbert Becker

Document No. ARA-F-8295-1

26 May 1965

Prepared for

P. O. 43426  
Harrison Radiator Division  
General Motors Corporation  
Lockport, N. Y.

EDWARD J. ARCH ASSOCIATES

ANALYSIS OF RECUPERATOR DESIGN

Summary

The recuperator which was designed by the Harrison Radiator Division of the General Motors Corporation (Dwg. NE1590R, Revision 1) was analyzed for stresses due to design pressure and to anticipated temperature gradients determined by Harrison. The design was found satisfactory according to published data on properties of type 347 stainless steel at design temperatures.

## Appendix XVI-A

### Problems Investigated

The following problems were analyzed to determine how stresses compared to published data on allowable values of type 347 stainless steel.

1. Bending and shear thermal stresses in the outer and inner shells due to the longitudinal temperature changes.
2. Buckling of the outer cylindrical shell under the design net pressure of 68.83 psi.
3. Pressure stresses in the inner and outer shells.
4. Pressure stresses in the tubes.
5. Tube forces and stresses due to restrained expansion relative to the inner and outer shells.
6. Combined tube stresses due to pressure and restrained expansion.

In addition to these calculations, estimates were made of the natural frequency of a tube with restrained ends.

Geometric data were obtained from HR Dwg. NE1590R, Revision 1. Performance information was furnished by Harrison on separate data sheets.

### Discussion of Results

The peak stress was found to occur in the inner cylindrical shell at a value of 15,500 psi. This is essentially equal to 60 percent of the minimum value of yield strength ( $0.6\sigma_y$ ) for 347 steel at temperatures as high as 850F.

Thermal stresses were found to be a small fraction of  $0.6\sigma_y$  in all locations investigated. Furthermore, calculations were based conservatively upon shaft temperature discontinuities instead of gradual transitions.

The tubes were found to be lightly loaded both by pressure and restrained expansion. The natural frequency for pinned ends, with the tube assumed straight, was found to be 25 cycles/sec., while for fixed ends the

**Appendix XVI-A**

**calculated frequency was twice that value. Further use of this information would require a vibration spectrum for the machinery system in which the recuperator would function.**

APPENDIX XVI-B

## APPENDIX XVI-B

This appendix contains a description of seven additional recuperators designed in the Preliminary Design Phase. These recuperator designs were selected to cover a wide range of size, weight, performance and ratio of gas side face area to gas side flow length.

The objects of this effort are to define reasonable maximum limits of regenerative engine envelope to be included as a part of Preliminary Purchase Specification 7-27; and to indicate the trends of regenerative engine bulk and weight with recuperator characteristic dimensions.

As a result of this effort, layout L-7109 was included as a part of Preliminary Purchase Specification 7-27, and the annular recuperator design was indicated considering the characteristic dimensions of the proposed Harrison recuperator.

The characteristic dimensions of the seven recuperators are shown in Table XVI-B-I. Each recuperator was sized for minimum pressure drop with respect to effectiveness and for 0.5 BSFC at 120 horsepower, sea level -60°F engine conditions. Figures XVI-B-1 through XVI-B-25 are estimated performance characteristics used to define the optimum recuperator sizes.

Quarter scale wood models of the base engine and of five recuperators were fabricated. These models were used to construct a variety of engine arrangements shown in Figures XVI-B-26 through XVI-B-44. This study resulted in layout L-7109 as a definition of reasonable maximum limits of regenerative engine envelope for Preliminary Purchase Specification 7-27.

Appendix XVI-B

TABLE XVI-B-1  
DESCRIPTION - PRELIMINARY RECUPERATOR DESIGNS

Geometric Description	Reference - Figure	XVI-B-4			XVI-B-8			XVI-B-11			XVI-B-14			XVI-B-18			XVI-B-21		
		4-Pass Plate-Fin	Crossflow	4-Pass Plate-Fin	Crossflow	5-Pass Air Over Tubes - Crossflow	4-Pass Air Over Tubes - Crossflow	5-Pass Air Over Tubes - Crossflow	4-Pass Air Over Tubes - Crossflow	5-Pass Air Over Tubes - Crossflow	5-Pass Air Over Tubes - Crossflow	4-Pass Air Over Tubes - Crossflow	5-Pass Air Over Tubes - Crossflow						
Plate Spacing - ba/ba-In.		.03/.06	.06/.06	.03/.06	.06/.06	-	-	-	0.125	0.125	0.125	-	-	-	-	-	-	-	
Tube Diameter - Do-In.	-	-	-	-	-	-	-	-	1.0 x 1.25	1.0 x 1.25	1.0 x 1.25	1.0 x 2.0							
Tube Spacing - X <sub>6</sub> x X <sub>6</sub>	-	-	-	-	-	-	-	-	-	-	-	-	-	-	-	-	-	-	
Airflow Length - La-Ft.	0.2	0.5	0.25	0.5	0.25	0.5	0.25	0.5	0.25	0.25	0.25	0.25	0.25	0.25	0.25	0.25	0.25	0.25	
Gas Flow Length - Lo-Ft.	0.1	0.08	0.1	0.08	0.1	0.08	0.1	0.08	0.4	0.4	0.4	0.4	0.4	0.4	0.4	0.4	0.4	0.4	
No-Flow Length - La-Ft.	8.1	6.3	9.8	7.95	4.5	4.5	4.5	4.5	5.65	5.65	5.65	5.65	5.65	5.65	5.65	5.65	5.65	5.65	
Volume - Ft. <sup>3</sup>	0.65	1.01	0.59	0.95	2.25	2.25	2.25	2.25	2.26	2.26	2.26	2.26	2.26	2.26	2.26	2.26	2.26	2.26	
Weight - Lb.	61	72	55	69	66	66	66	66	67	67	67	67	67	67	67	67	67	67	
Length/Area Ratio - 1/Ft.	0.25	0.09	0.15	0.06	1.78	1.78	1.78	1.78	1.13	1.13	1.13	1.13	1.13	1.13	1.13	1.13	1.13	1.13	

## APPENDIX XVI-B

This appendix contains a description of seven additional recuperators designed in the Preliminary Design Phase. These recuperator designs were selected to cover a wide range of size, weight, performance and ratio of gas side face area to gas side flow length.

The objects of this effort are to define reasonable maximum limits of regenerative engine envelope to be included as a part of Preliminary Purchase Specification 7-27; and to indicate the trends of regenerative engine bulk and weight with recuperator characteristic dimensions.

As a result of this effort, layout L-7109 was included as a part of Preliminary Purchase Specification 7-27, and the annular recuperator design was indicated considering the characteristic dimensions of the proposed Harrison recuperator.

The characteristic dimensions of the seven recuperators are shown in Table XVI-B-1. Each recuperator was sized for minimum pressure drop with respect to effectiveness and for 0.5 BSFC at 120 horsepower, sea level -60°F engine conditions. Figures XVI-B-1 through XVI-B-25 are estimated performance characteristics used to define the optimum recuperator sizes.

Quarter scale wood models of the base engine and of five recuperators were fabricated. These models were used to construct a variety of engine arrangements shown in Figures XVI-B-26 through XVI-B-44. This study resulted in layout L-7109 as a definition of reasonable maximum limits of regenerative engine envelope for Preliminary Purchase Specification 7-27.

Appendix XVI-B

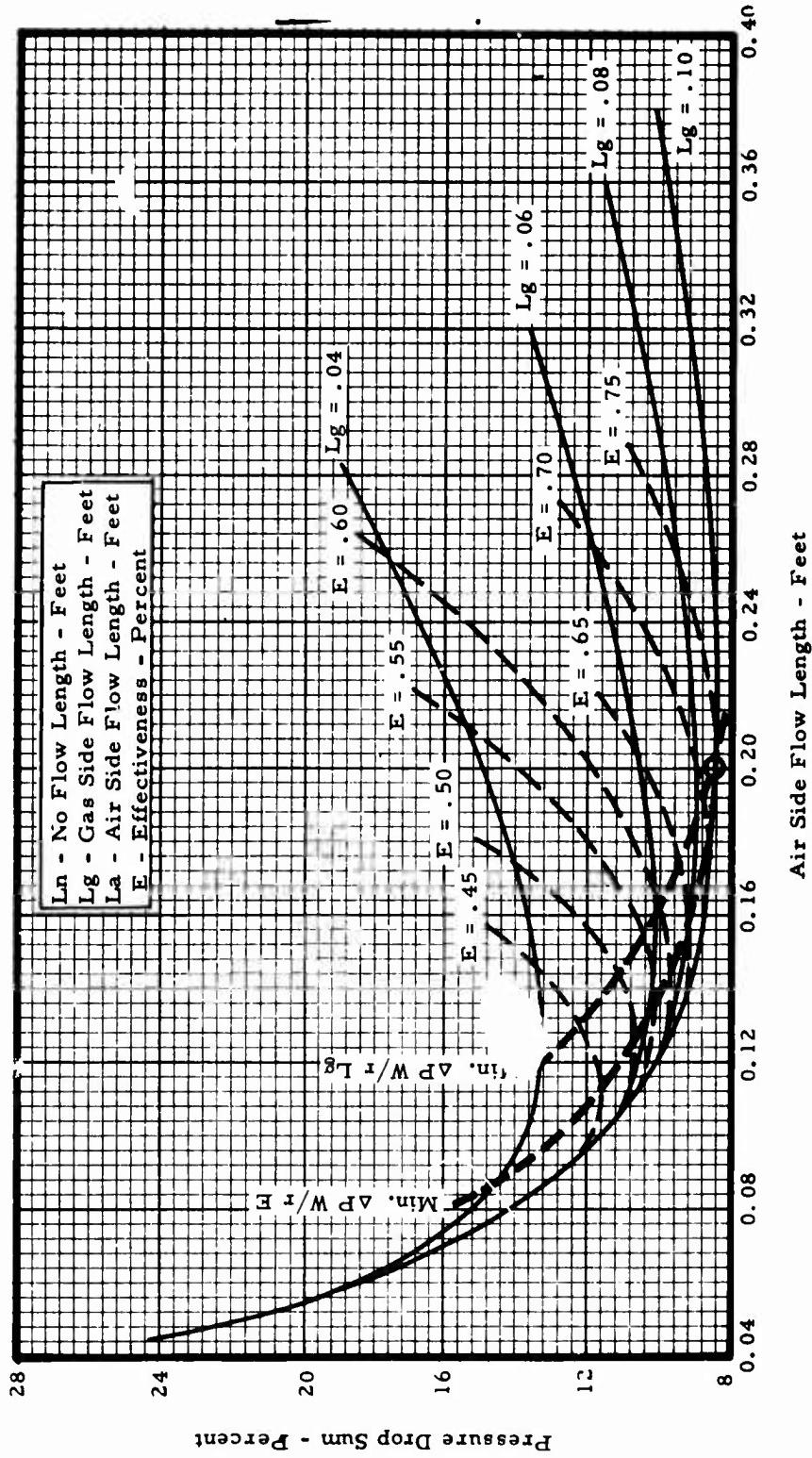


Figure XVI-B-1. Four-Pass Plate Fin Cross Flow Recuperator  $ba/b_g = .03/.06$  - Optimization.

Appendix XVI-B

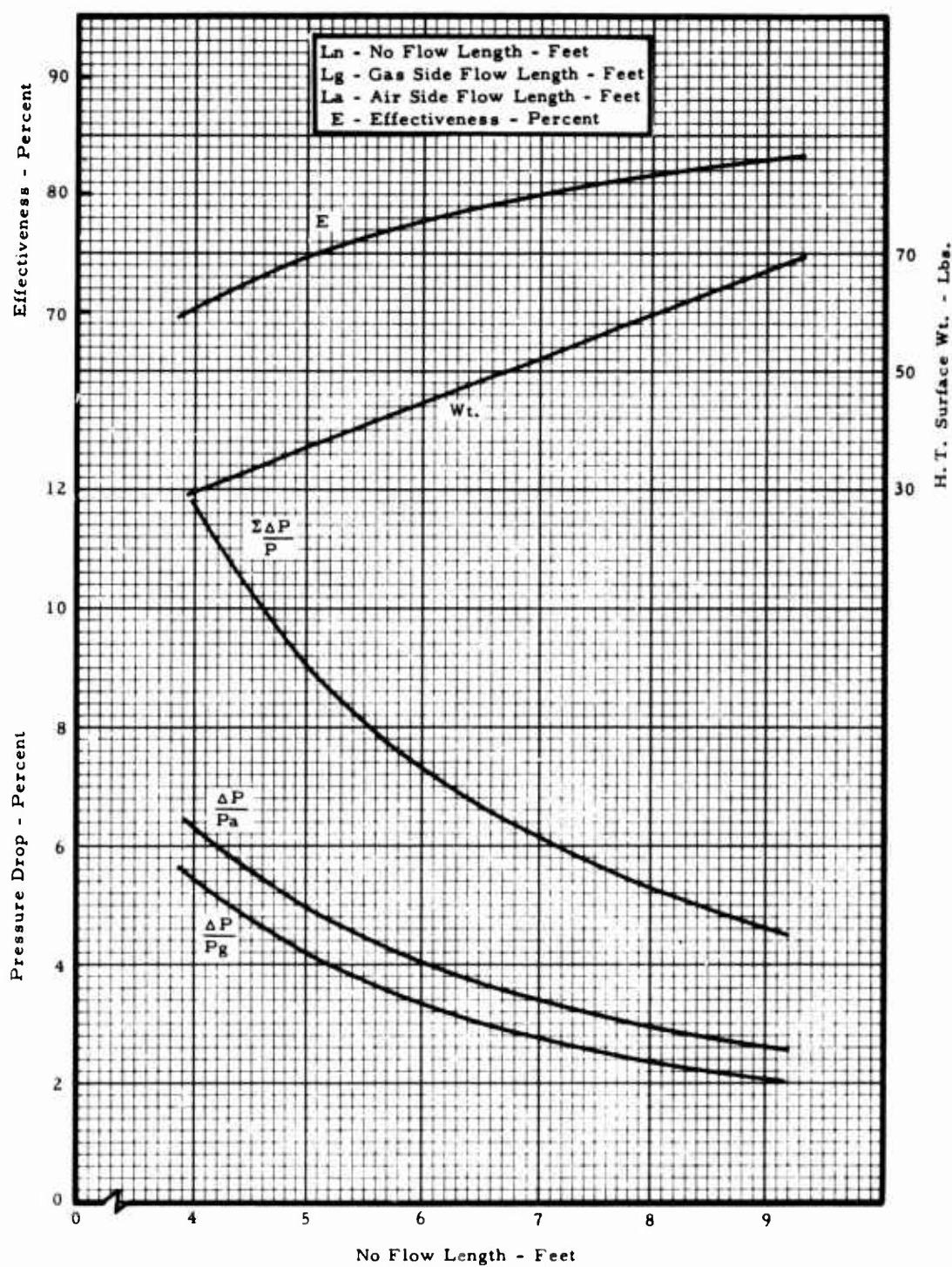


Figure XVI-B-2. Four-Pass Plate Fin Crossflow Recuperator  
 $b_a/b_g = .03/.06$  - Sea Level Performance.

## Appendix XVI-B

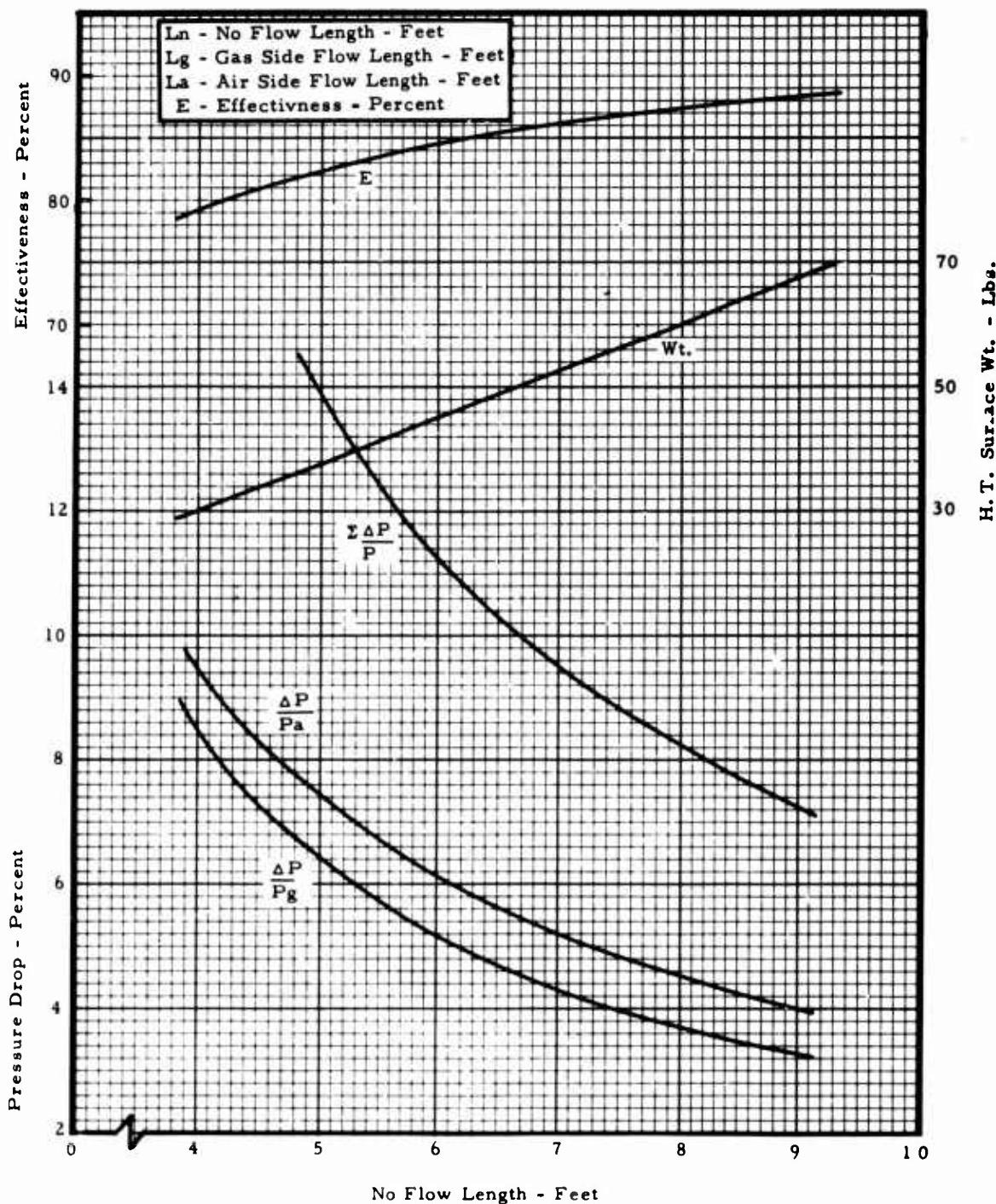


Figure XVI-B-3. Four-Pass Plate Fin Crossflow Recuperator  
 $b_a/b_g = .03/.06$  - Altitude Performance.

Appendix XVI-B

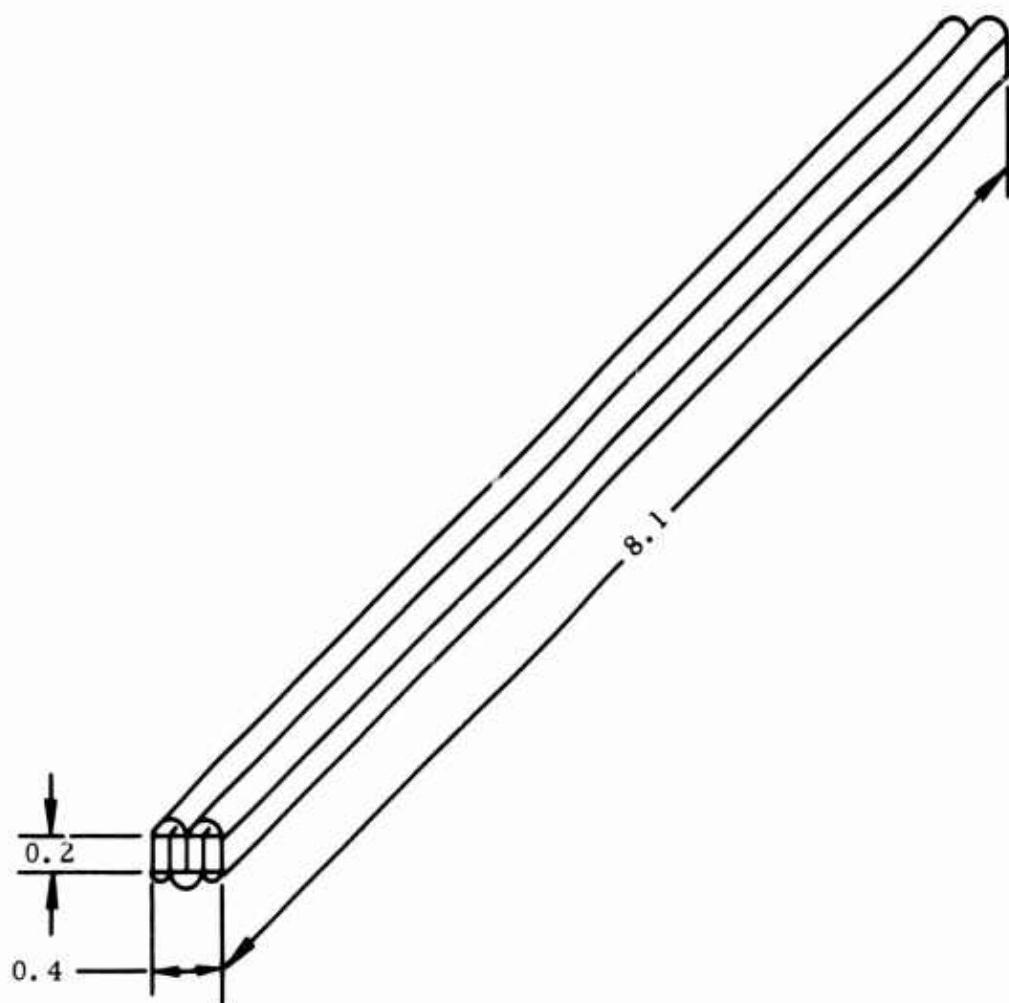


Figure XVI-B-4. Four-Pass Plate Fin Crossflow Recuperator -  
 $ba/bg = .03/.06$  - Sketch.

Appendix XVI-B

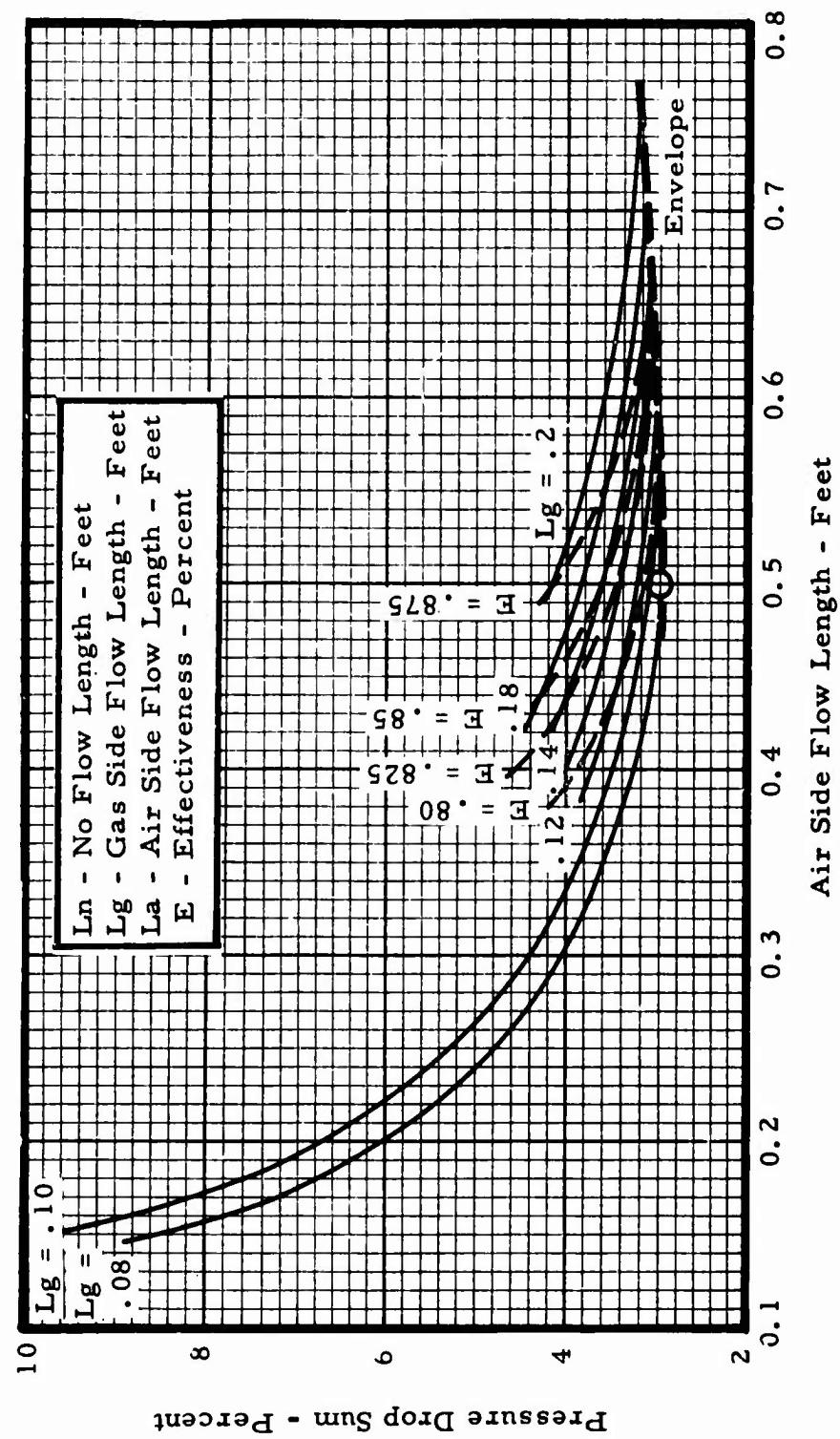


Figure XVI-B-5. Four-Pass Plate Fine Crossflow Recuperator  $ba/bg = .06/.06$  - Optimization.

Appendix XVI-B

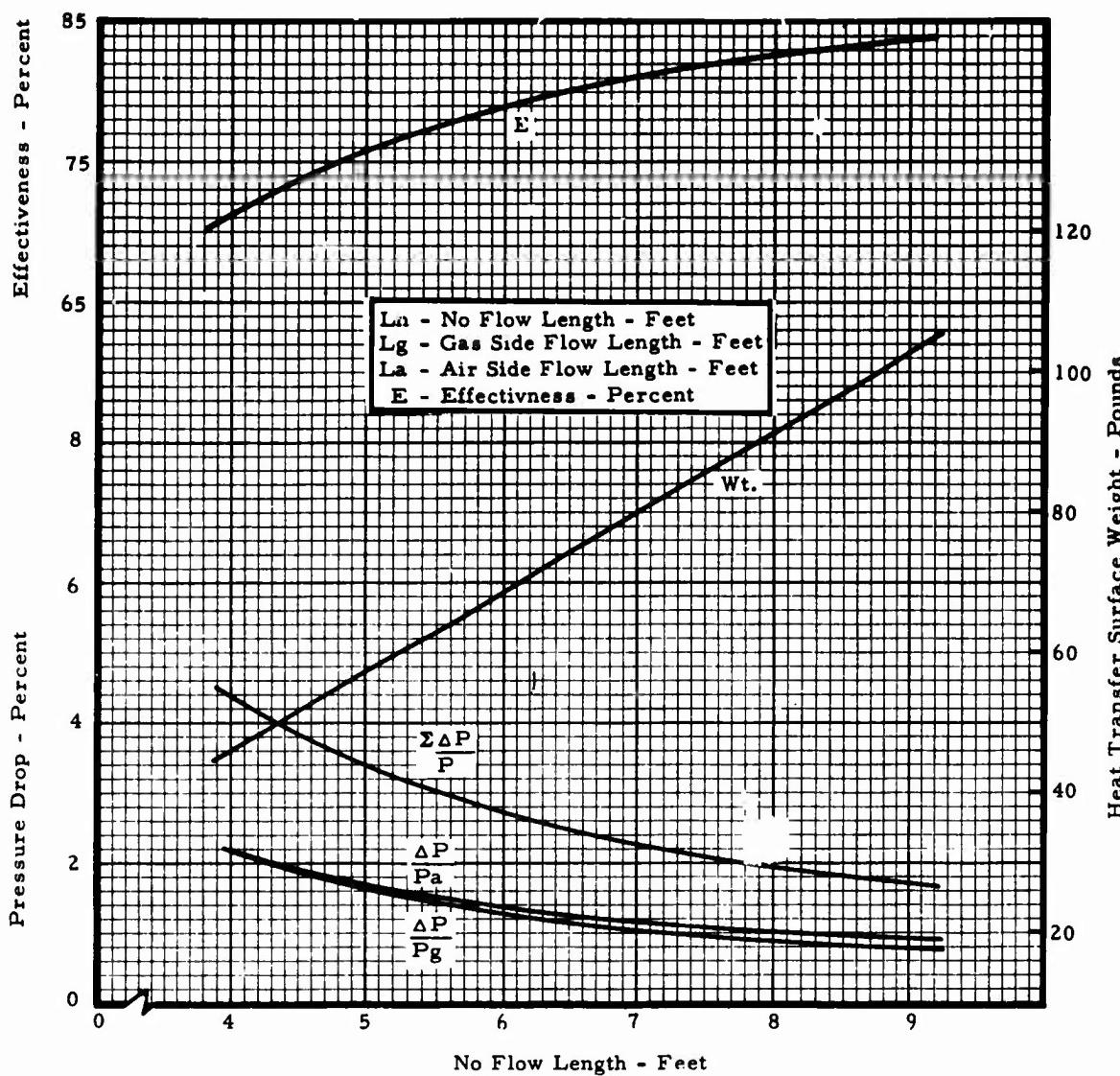
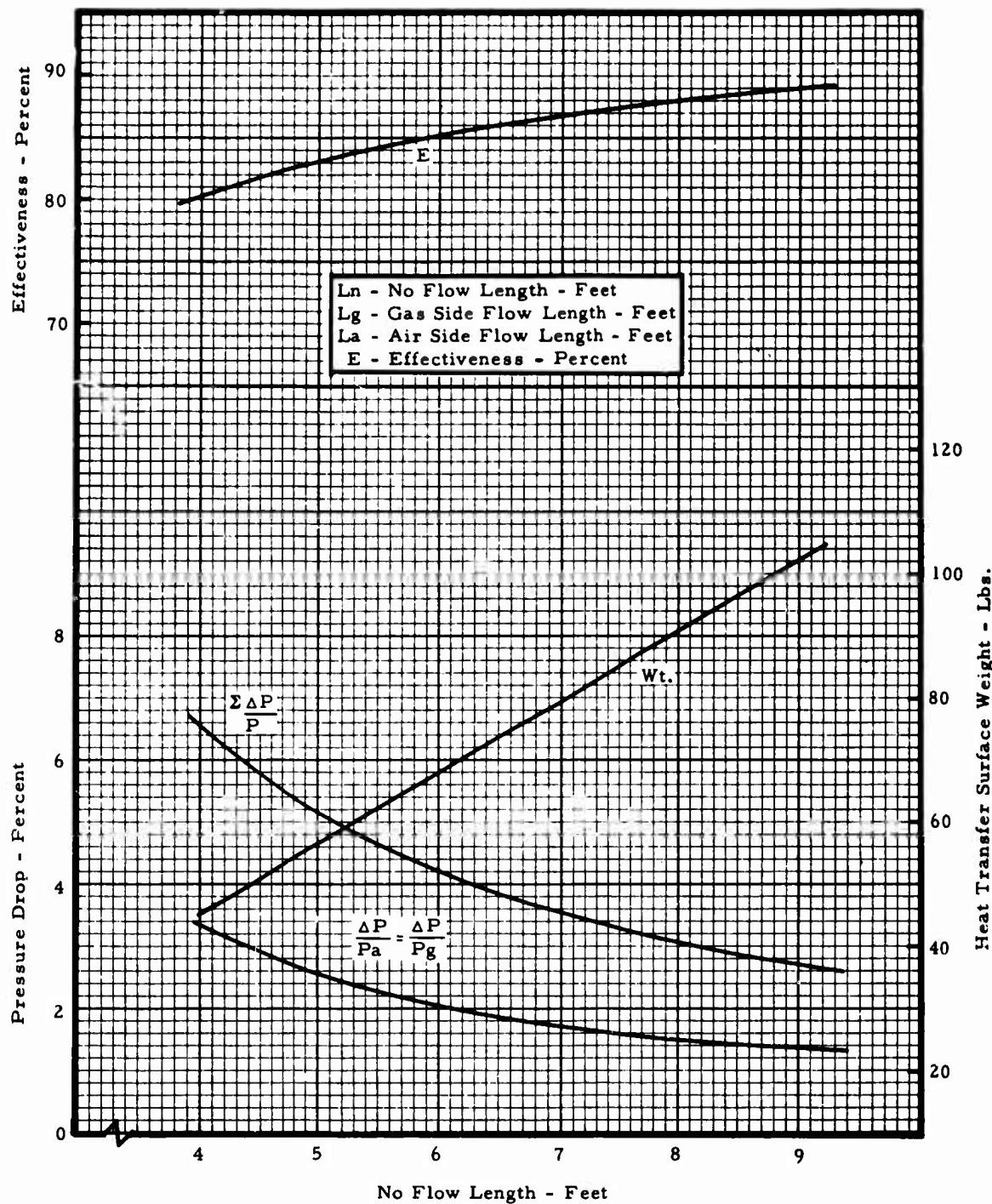


Figure XVI-B-6. Four-Pass Plate Fin Crossflow Recuperator -  
ba/bg - .06/.06 - Sea Level Performance.

**Appendix XVI-B**



**Figure XVI-B-7. Four-Pass Plate Fin Crossflow Recuperator -  
 $ba/bg = .06/.06$  - Altitude Performance.**

Appendix XVI-B

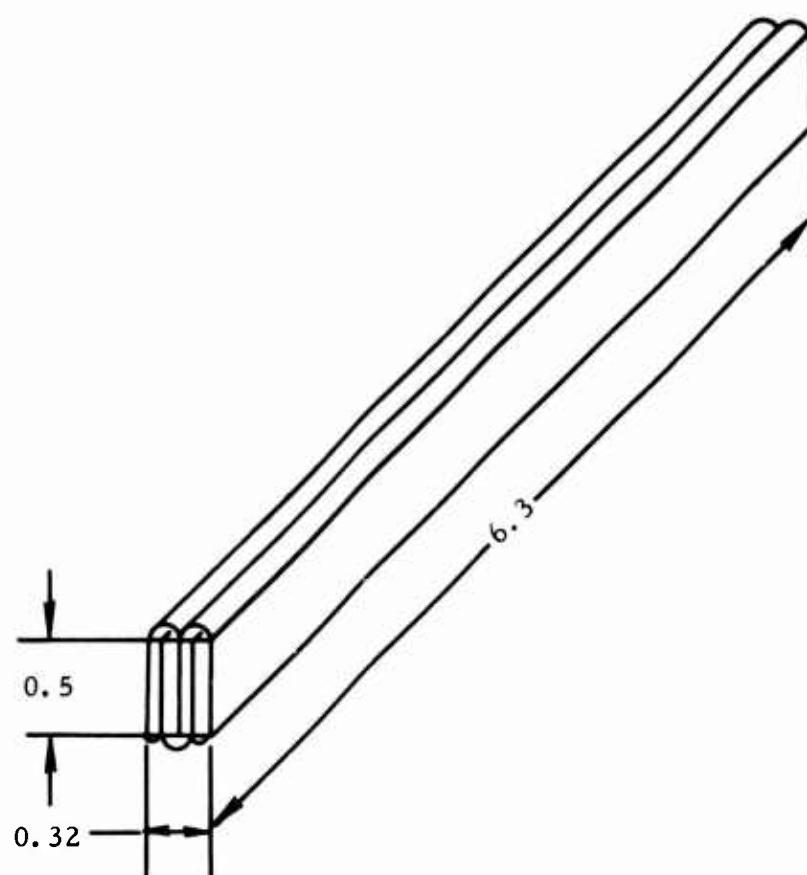


Figure XVI-B-8. Four-Pass Plate Fin Crossflow Recuperator -  
 $ba/bg = .06/.06$  - Sketch.

Appendix XVI-B

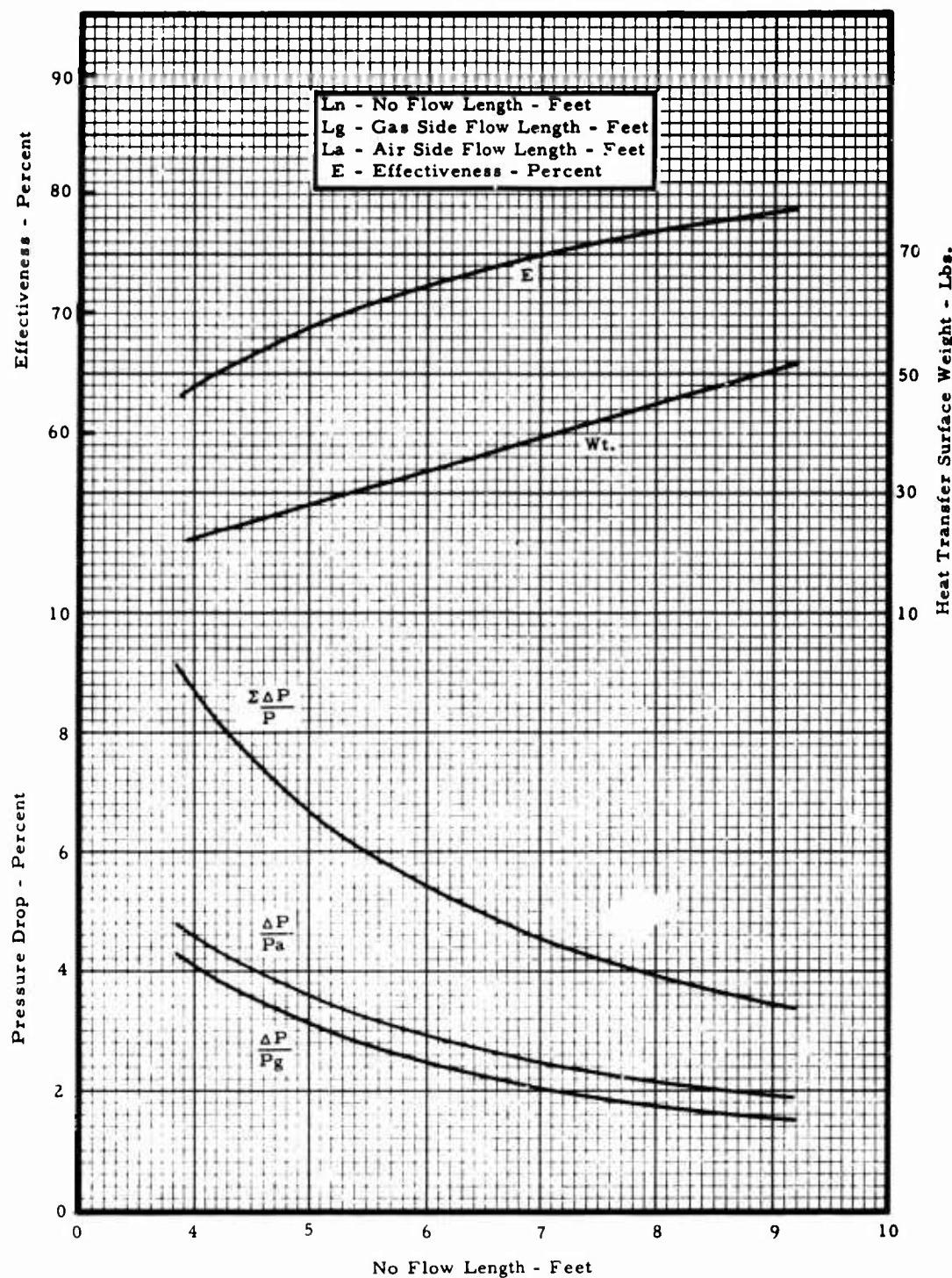


Figure XVI-B-9. Three-Pass Plate Fin Crossflow Recuperator -  
 $ba/bg = .05/.06$  - Sea Level Performance.

Appendix XVI-B

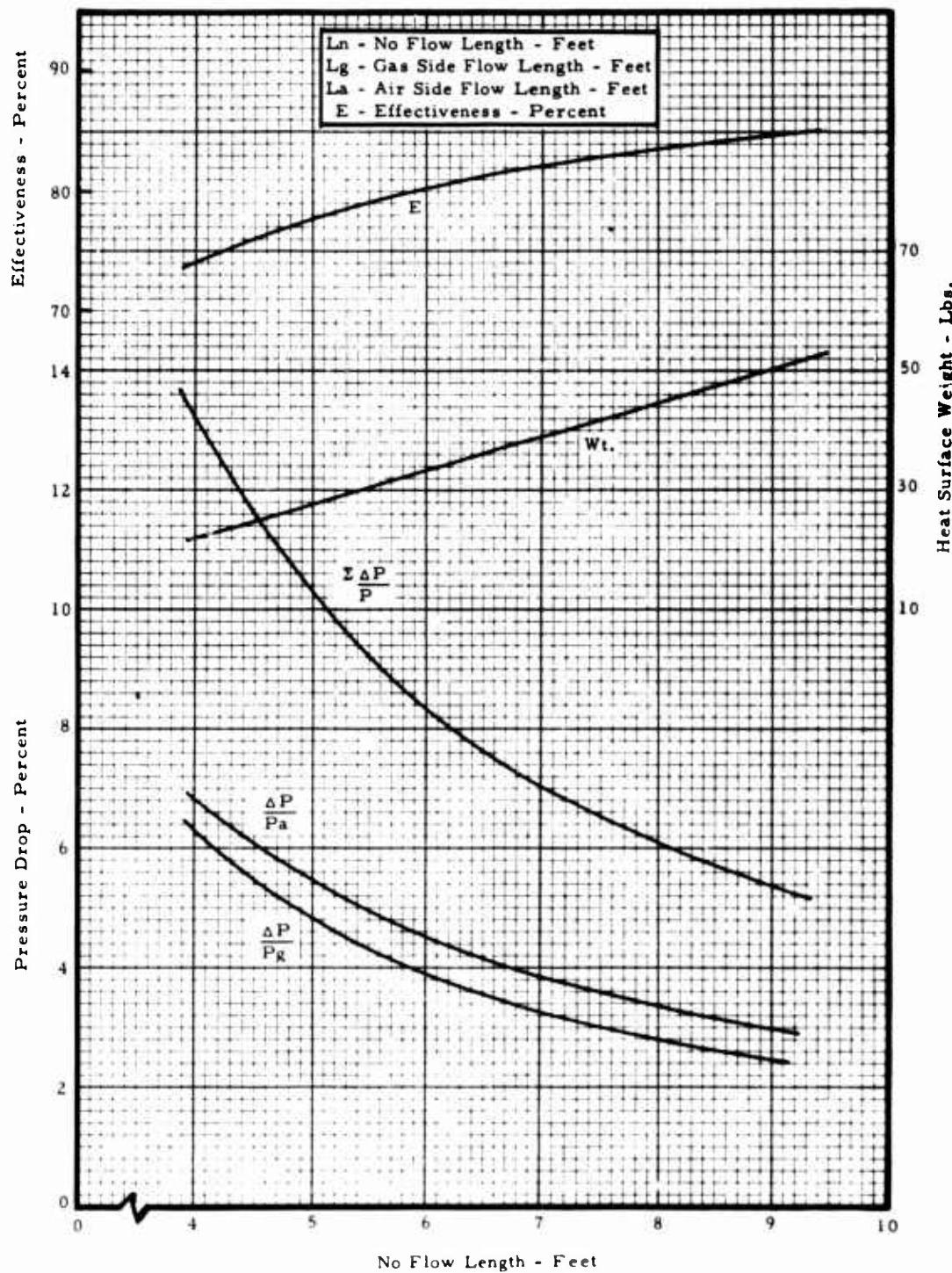
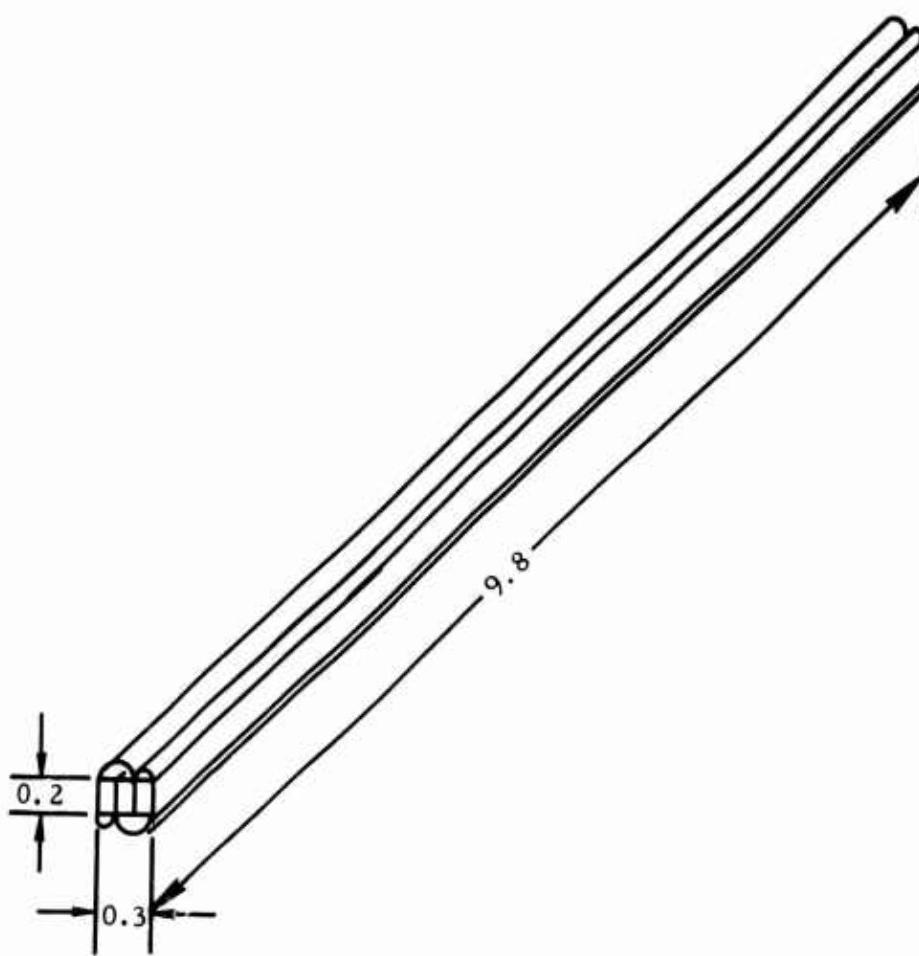


Figure XVI-B-10. Three-Pass Plate Fin Crossflow Recuperator -  
 $b_a/b_g = .05/.06$  - Altitude Performance.

**Appendix XVI-B**



**Figure XVI-B-11. Three-Pass Plate Fin Crossflow Recuperator -  
ba/bg = .05/.06 - Sketch.**

Appendix XVI-B

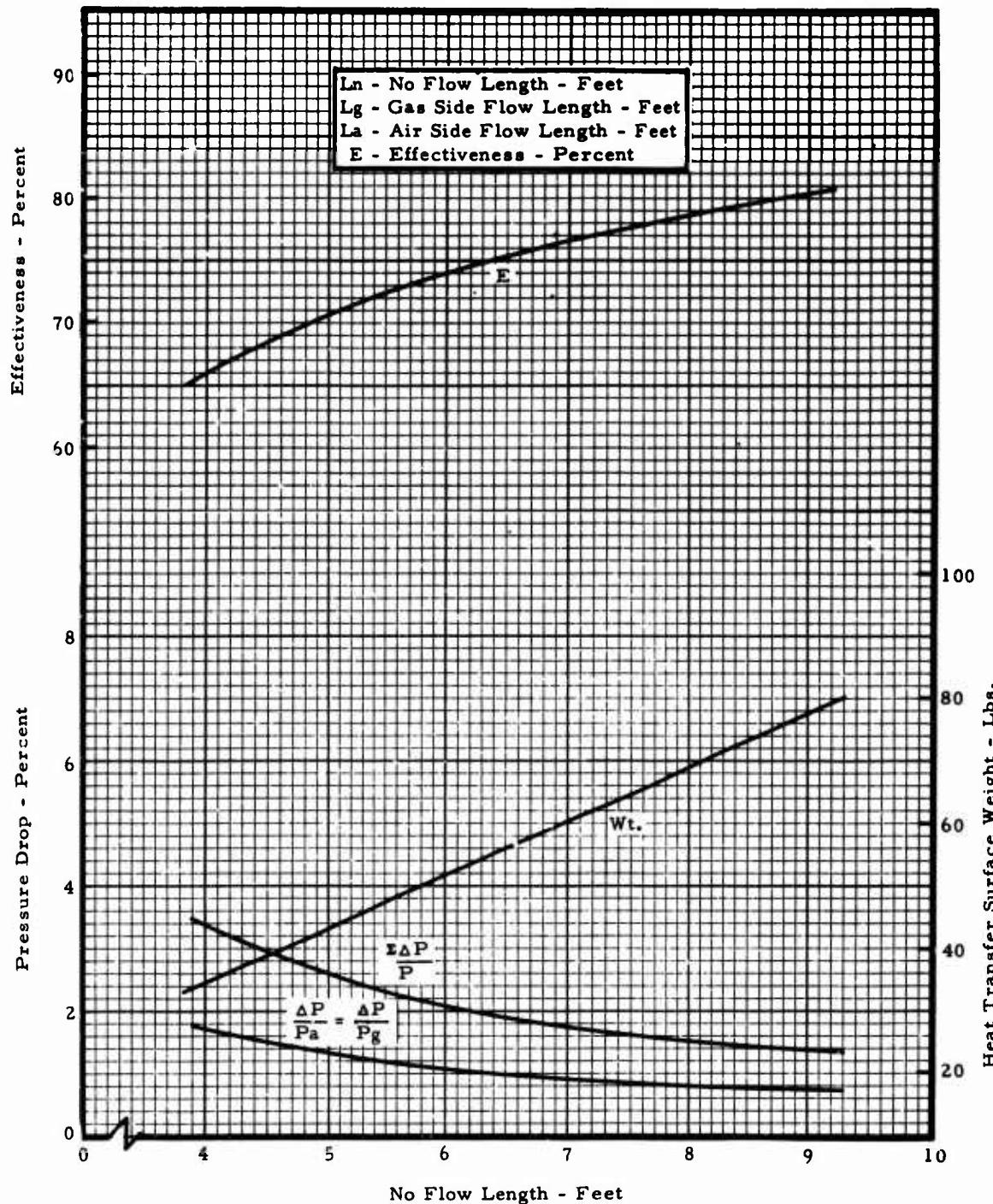
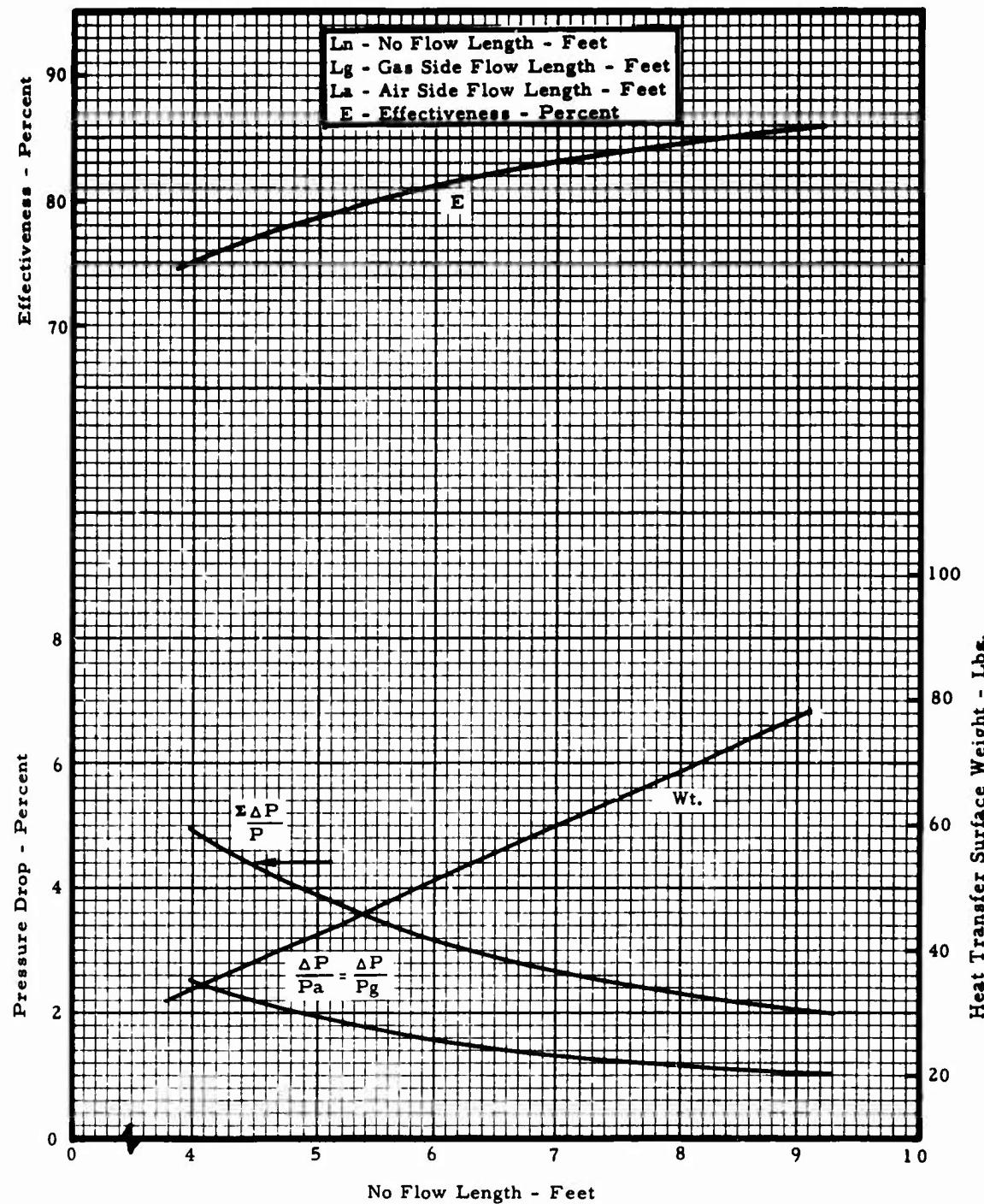


Figure XVI-B-12. Three-Pass Plate Fin Crossflow Recuperator -  
 $b_a/b_g = .06/.06$  - Sea Level Performance.

**Appendix XVI-B**



**Figure XVI-B-13. Three-Pass Plate Fin Crossflow Recuperator -**  
 $ba/bg = .06/.06$  - Altitude Performance.

**Appendix XVI-B**

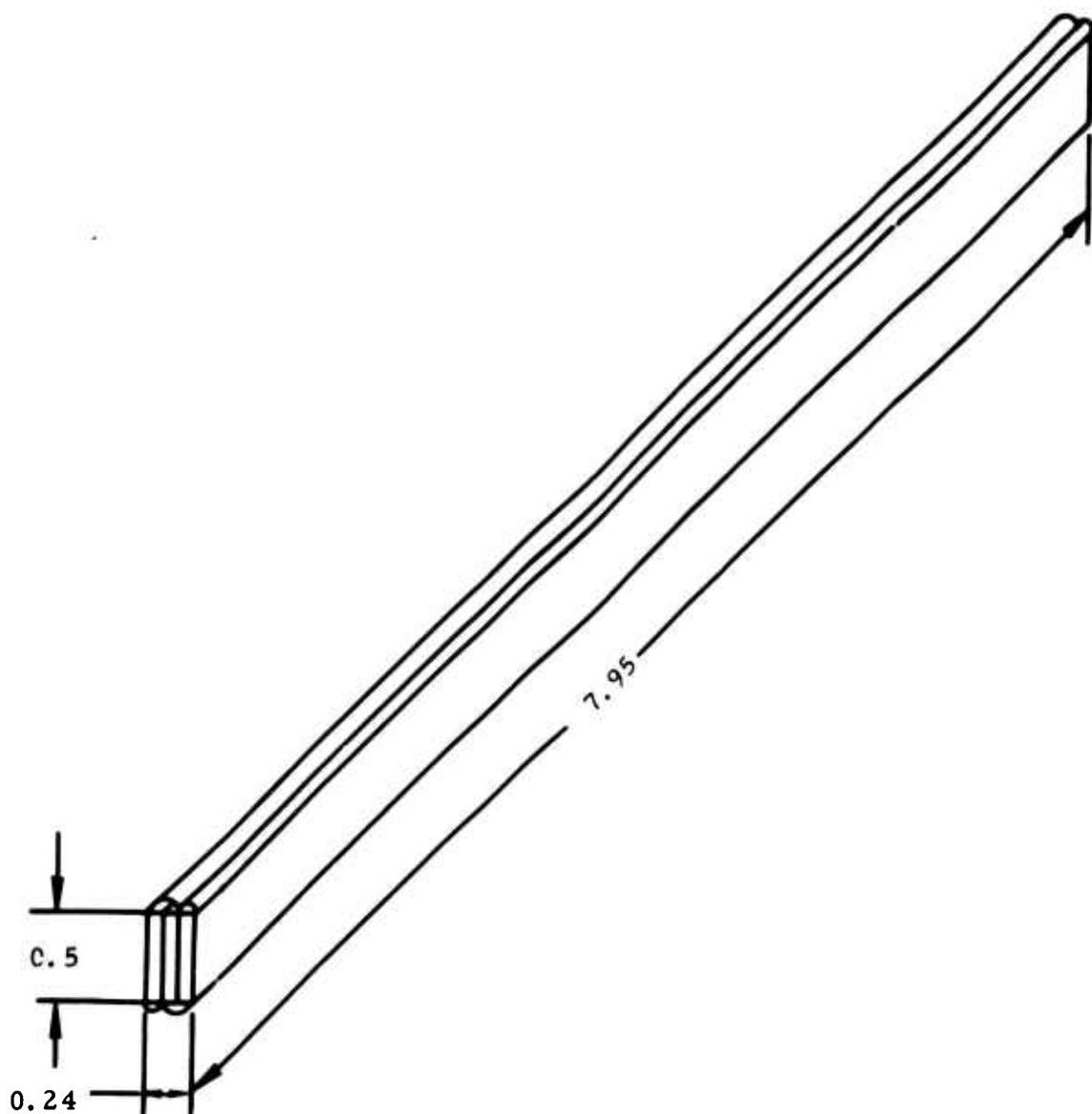


**Figure XVI-B-14. Three-Pass Plate Fin Crossflow Recuperator -  
ba/bg = .06/.06 - Sketch.**

## Appendix XVI-B

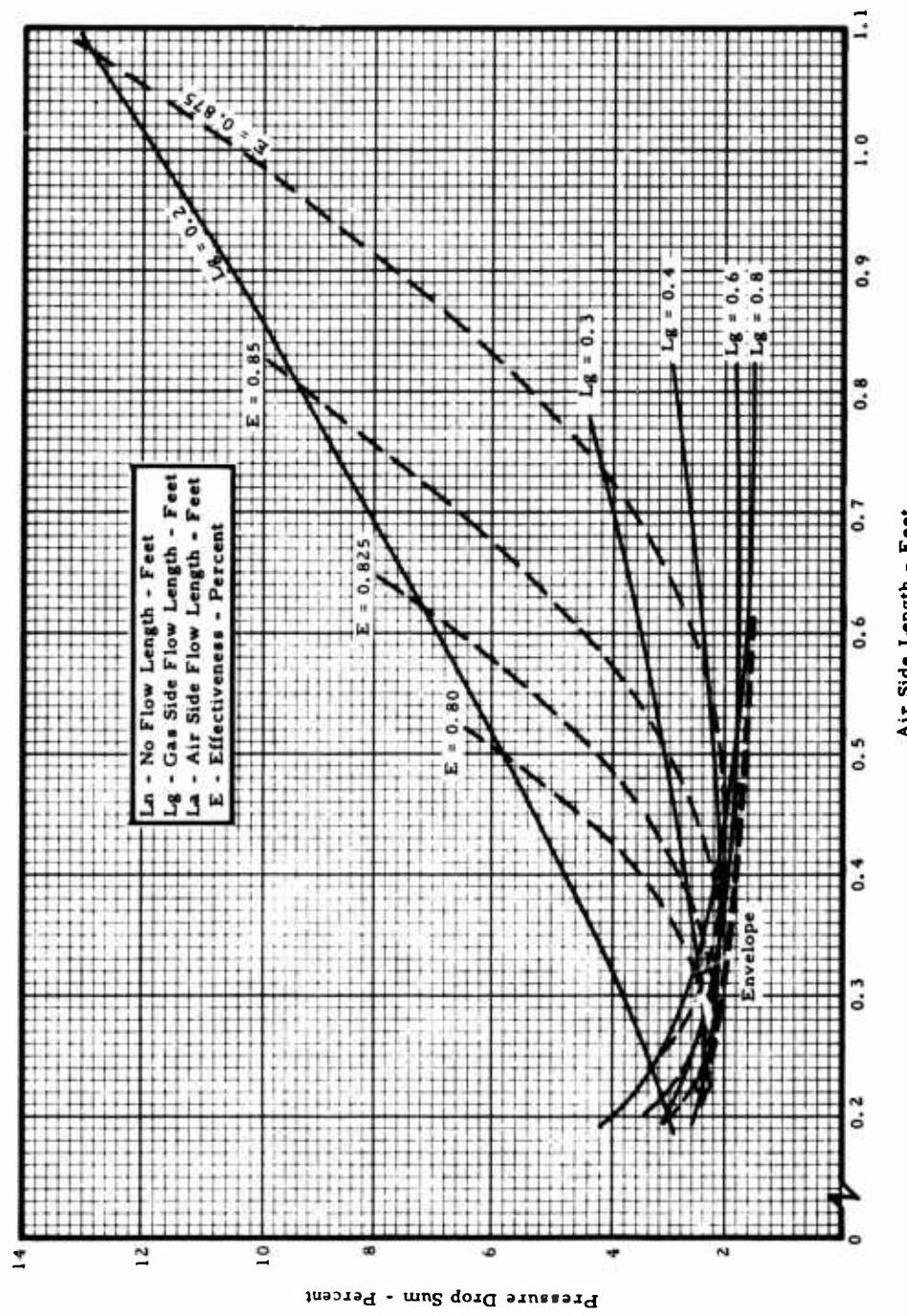


Figure XVI-B-15. Five-Pass Air Over Tube Crossflow Recuperator - Optimization.

Appendix XVI-B

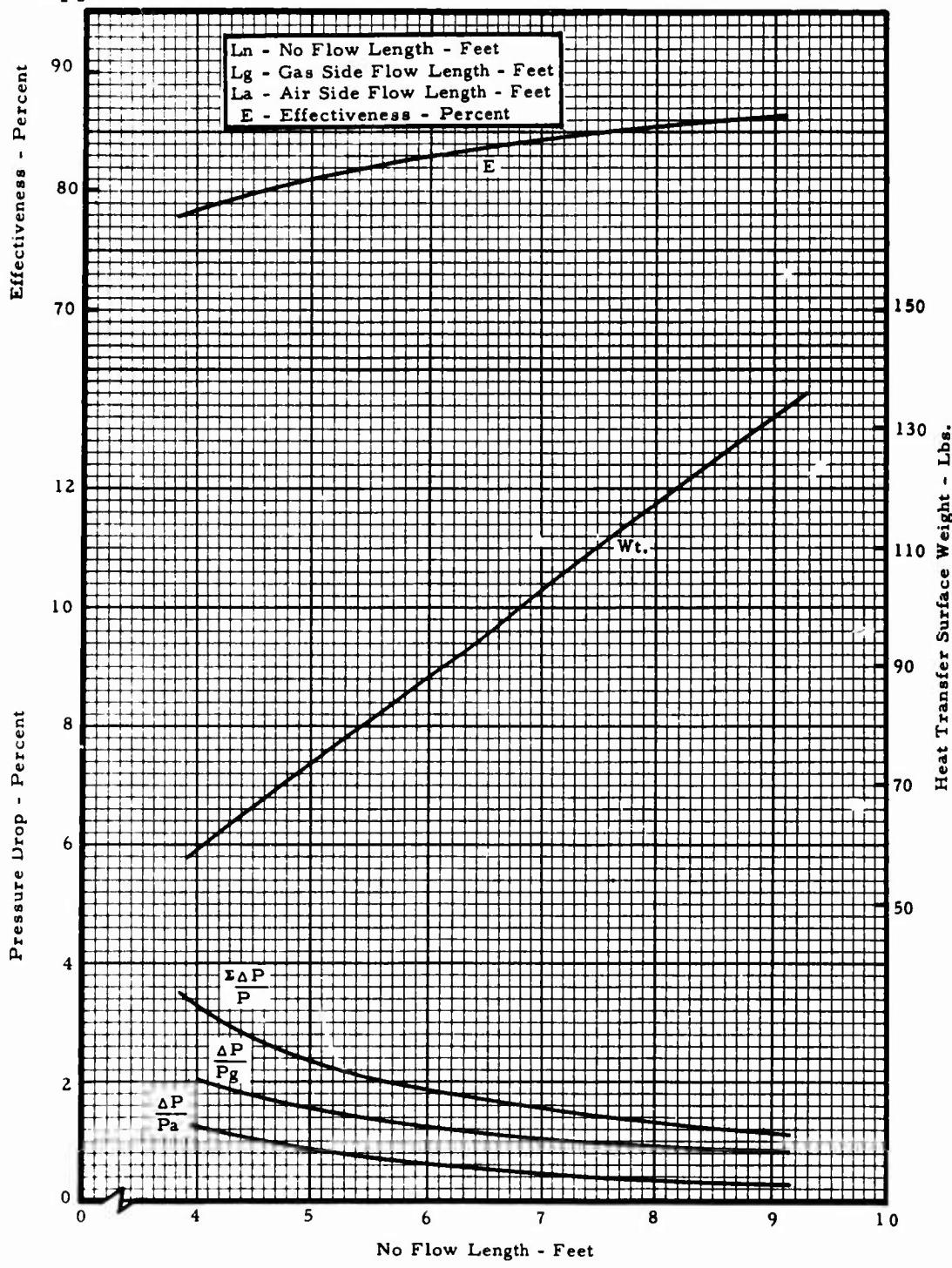
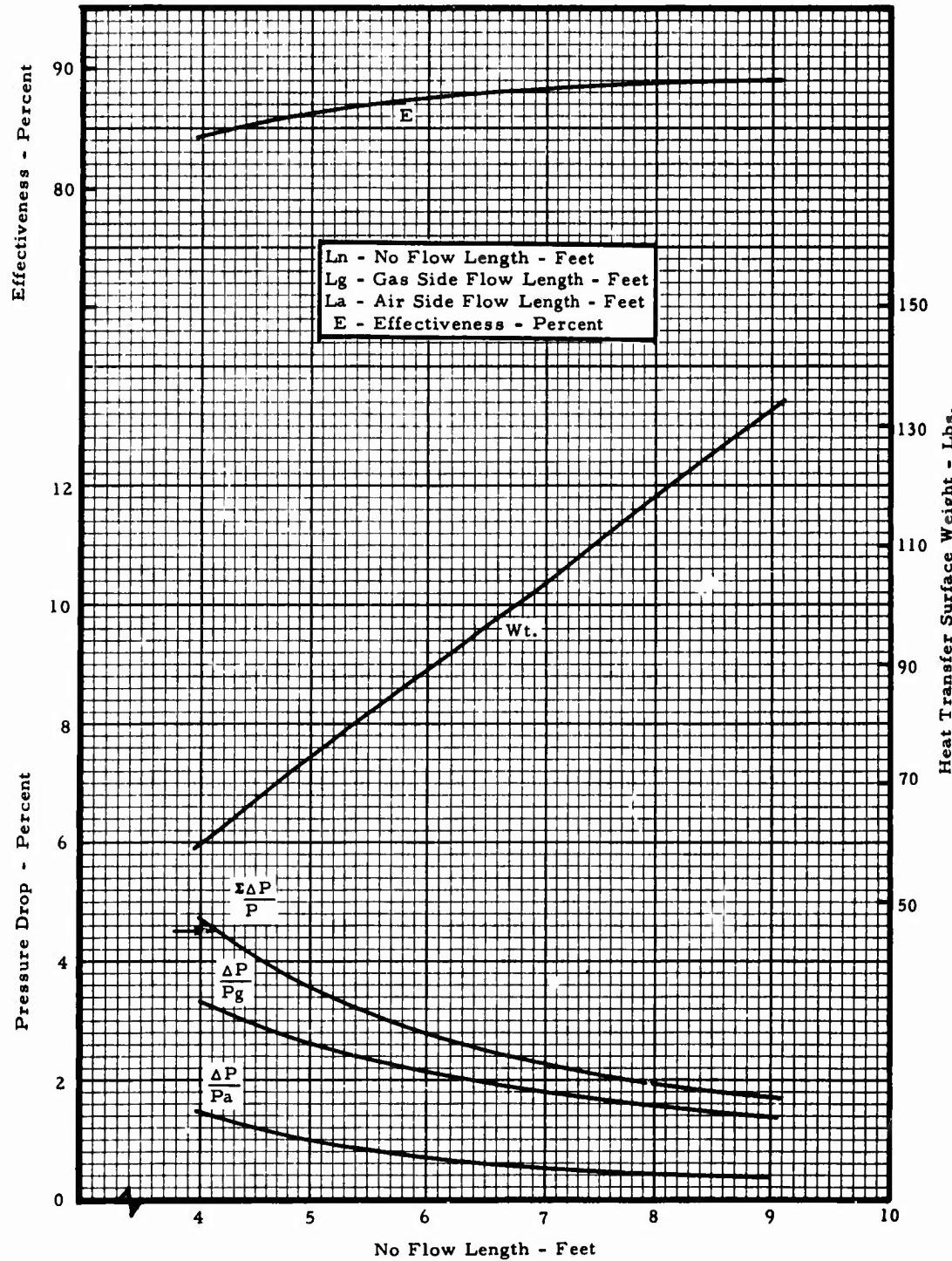


Figure XVI-B-16. Five-Pass Air Over Tube Crossflow Recuperator - Sea Level Performance.

**Appendix XVI-B**



**Figure XVI-B-17. Five-Pass Air Over Tube Crossflow Recuperator - Altitude.**

**Appendix XVI-B**

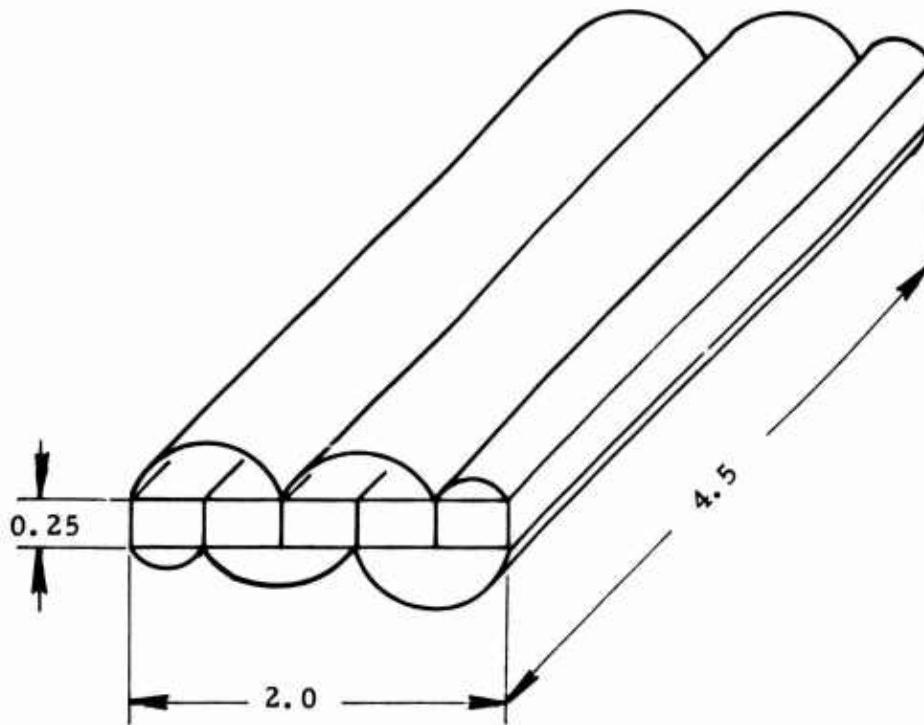


**Figure XVI-B-18. Five-Pass Air Over Tube Crossflow Recuperator - Sketch.**

**Appendix XVI-B**

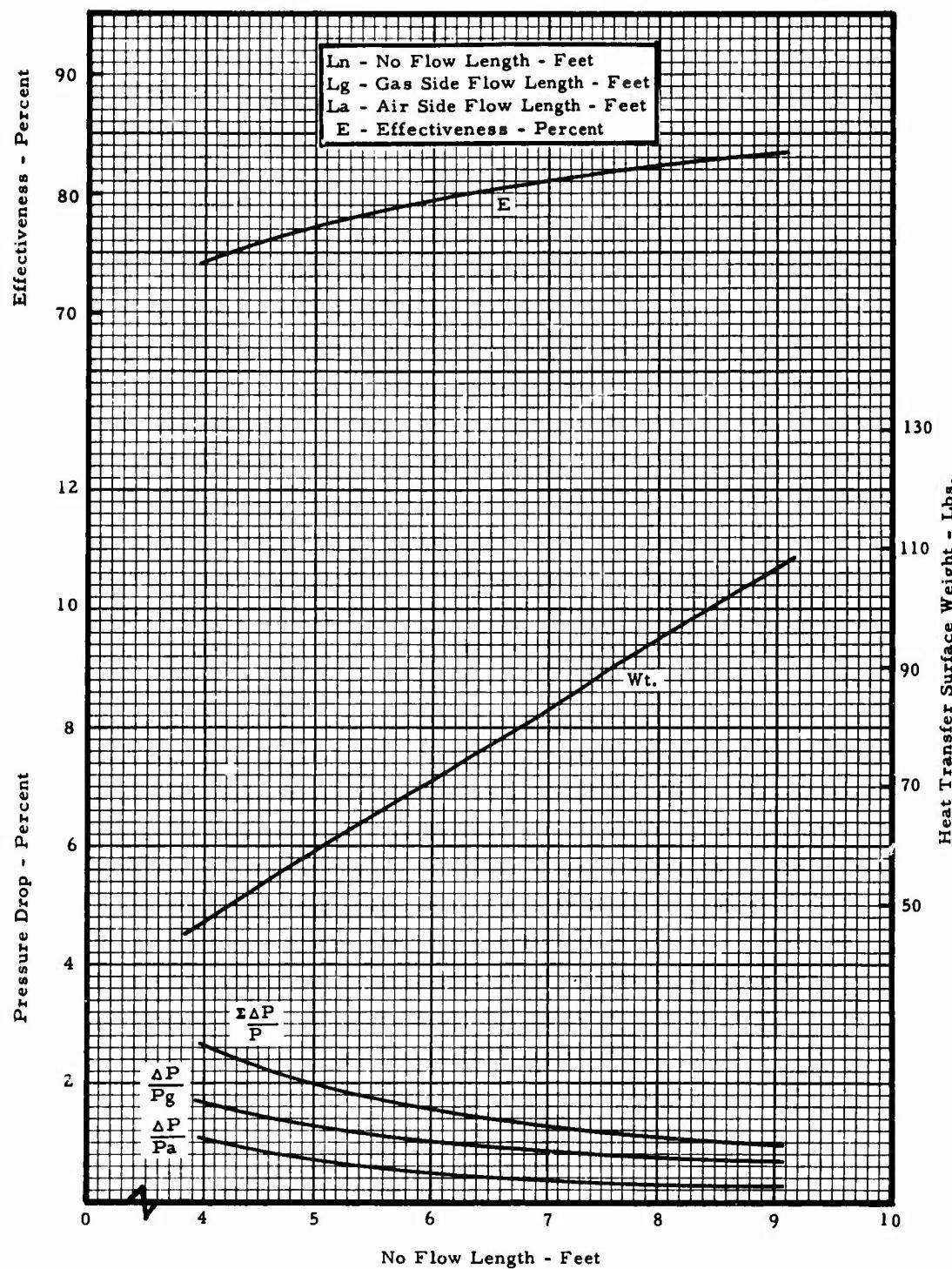


**Figure XVI-B-19. Four-Pass Air Over Tube Crossflow Recuperator - Sea Level Performance.**

Appendix XVI-B

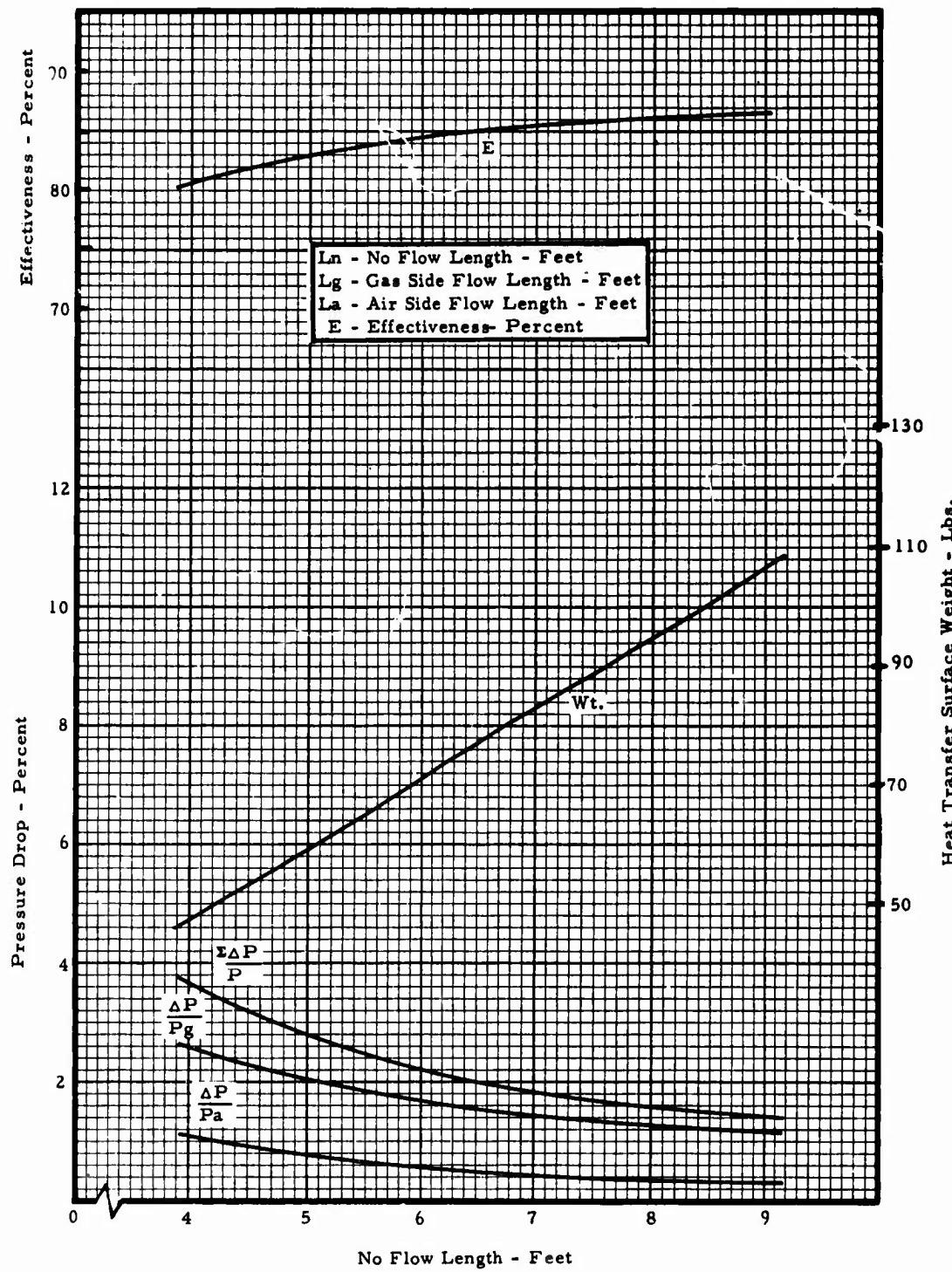
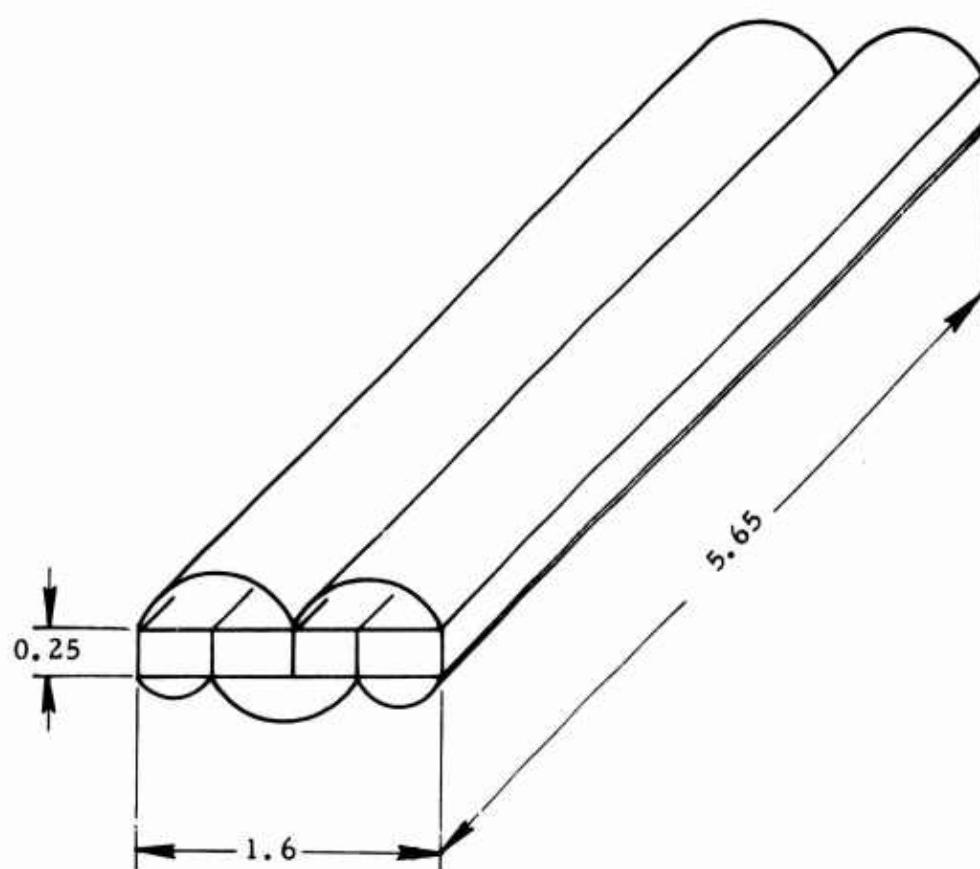


Figure XVI-B-20. Four-Pass Air Over Tube Crossflow Recuperator - Altitude Performance.

**Appendix XVI-B**



**Figure XVI-B-21. Four-Pass Air Over Tube Crossflow Recuperator - Sketch.**

Appendix XVI-B

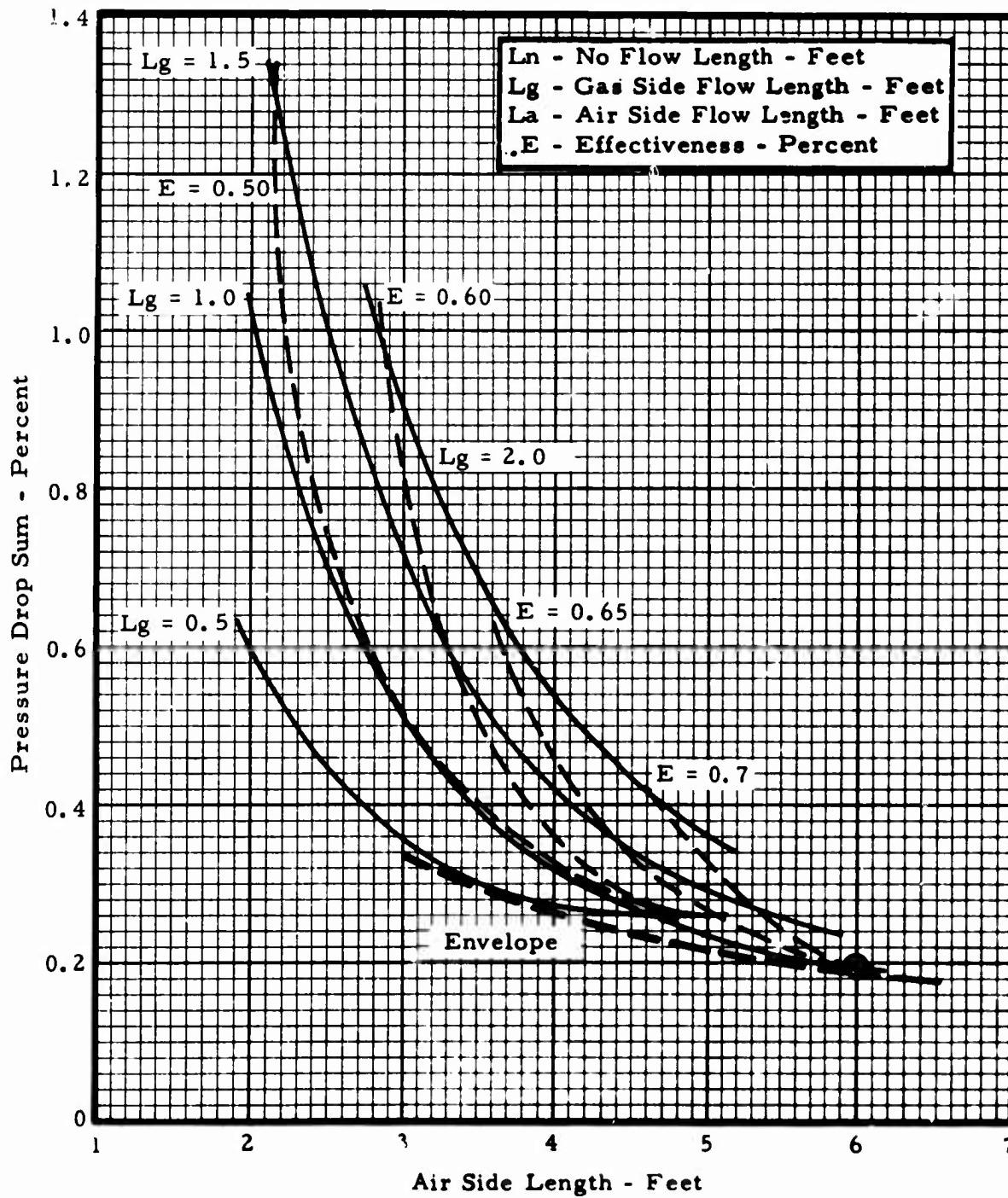


Figure XVI-B-22. Five-Pass Air Through Tube Crossflow Recuperator - Optimization.

**Appendix XVI-B**

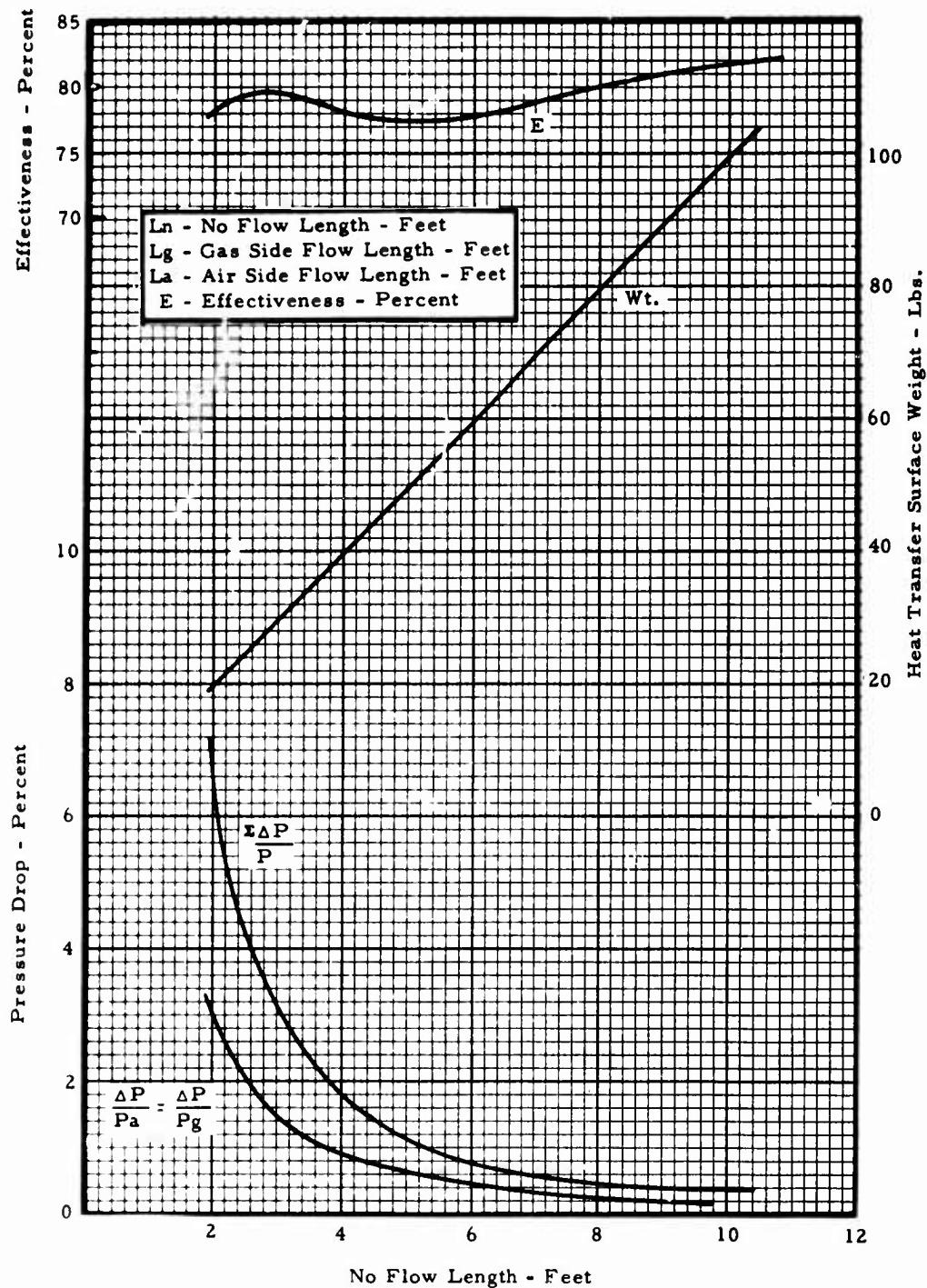
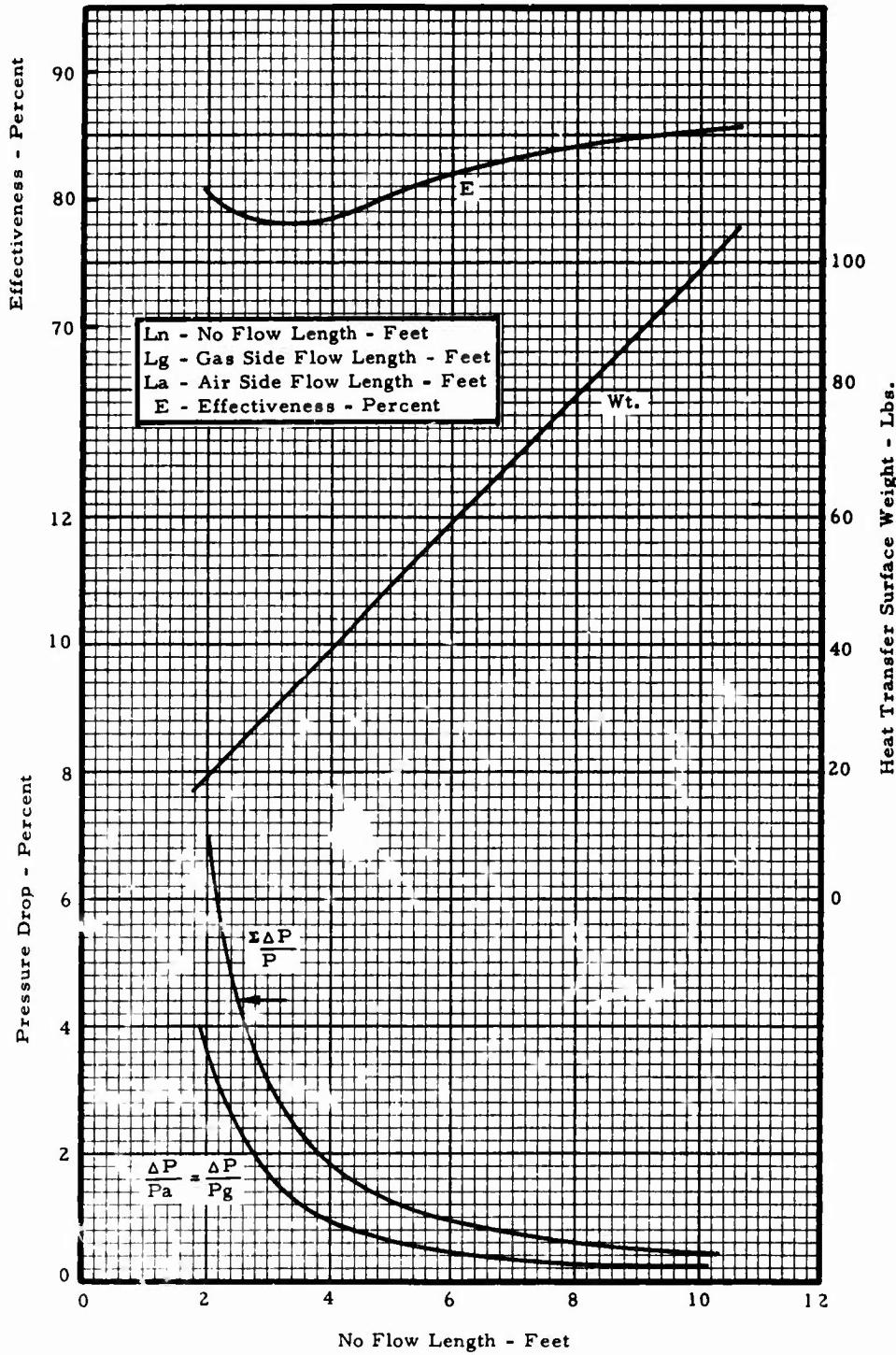


Figure XVI-B-23. Five-Pass Air Through Tube Crossflow Recuperator - Sea Level Performance.

**Appendix XVI-B**



**Figure XVI-B-24. Five-Pass Air Through Tube Crossflow Recuperator - Altitude Performance.**

**Appendix XVI-B**

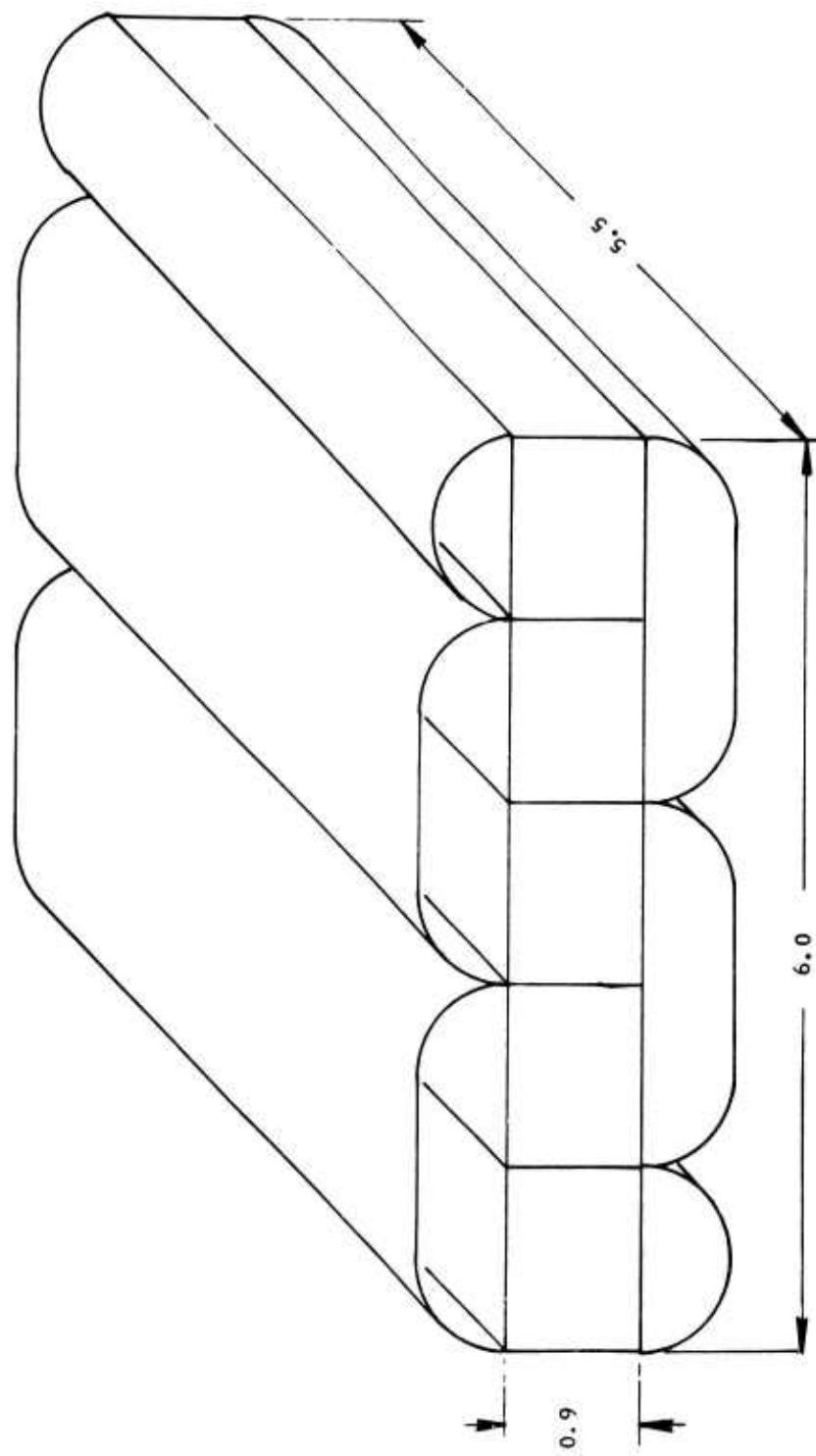


**Figure XVI-B-25.** Five-Pass Air Through Tube Crossflow Recuperator - Sketch.

**Appendix XVI-B**

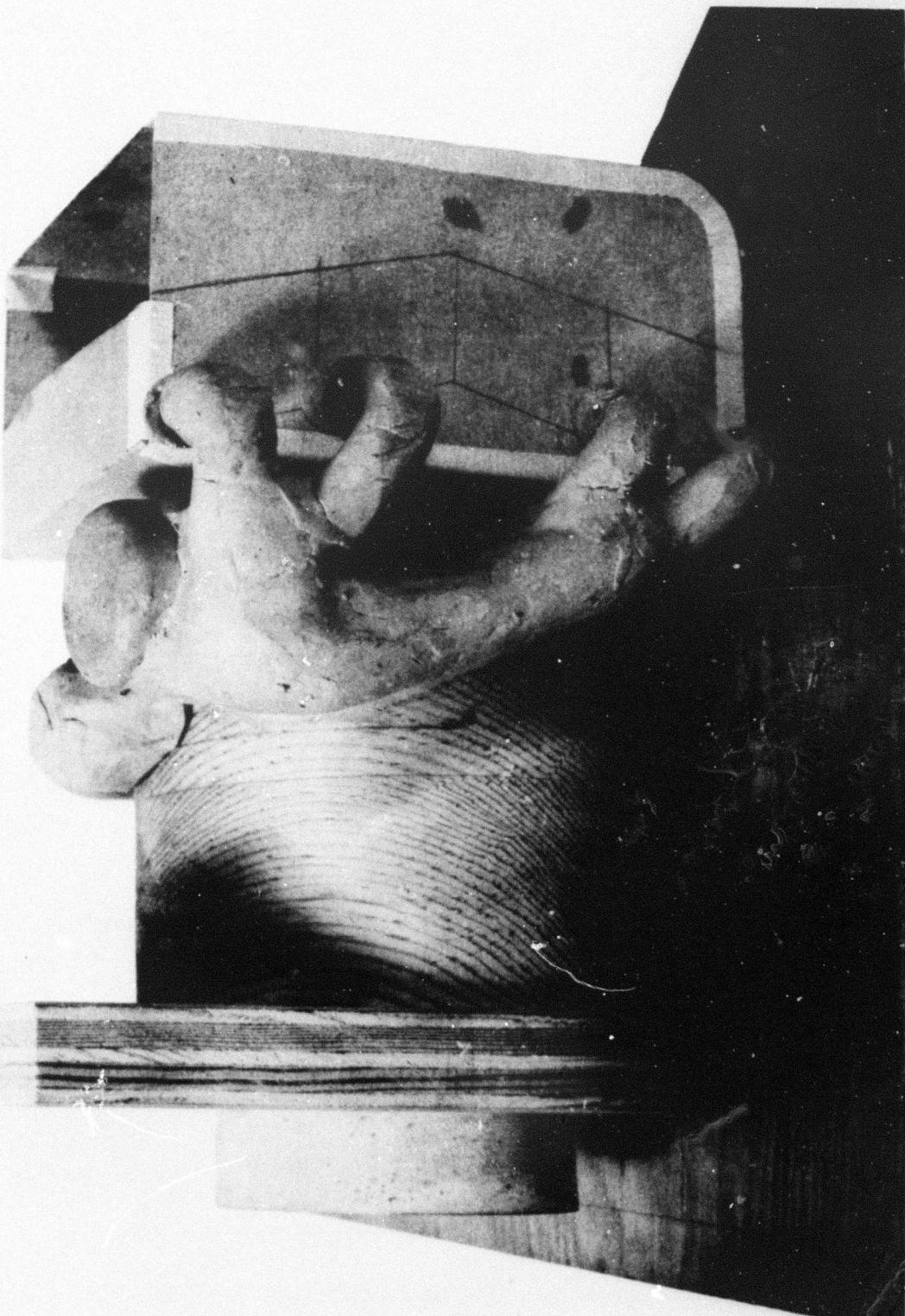


**Figure XVI-B-26. Recuperator Mock-Up - Z Flow Aft Mounting - Side View.**

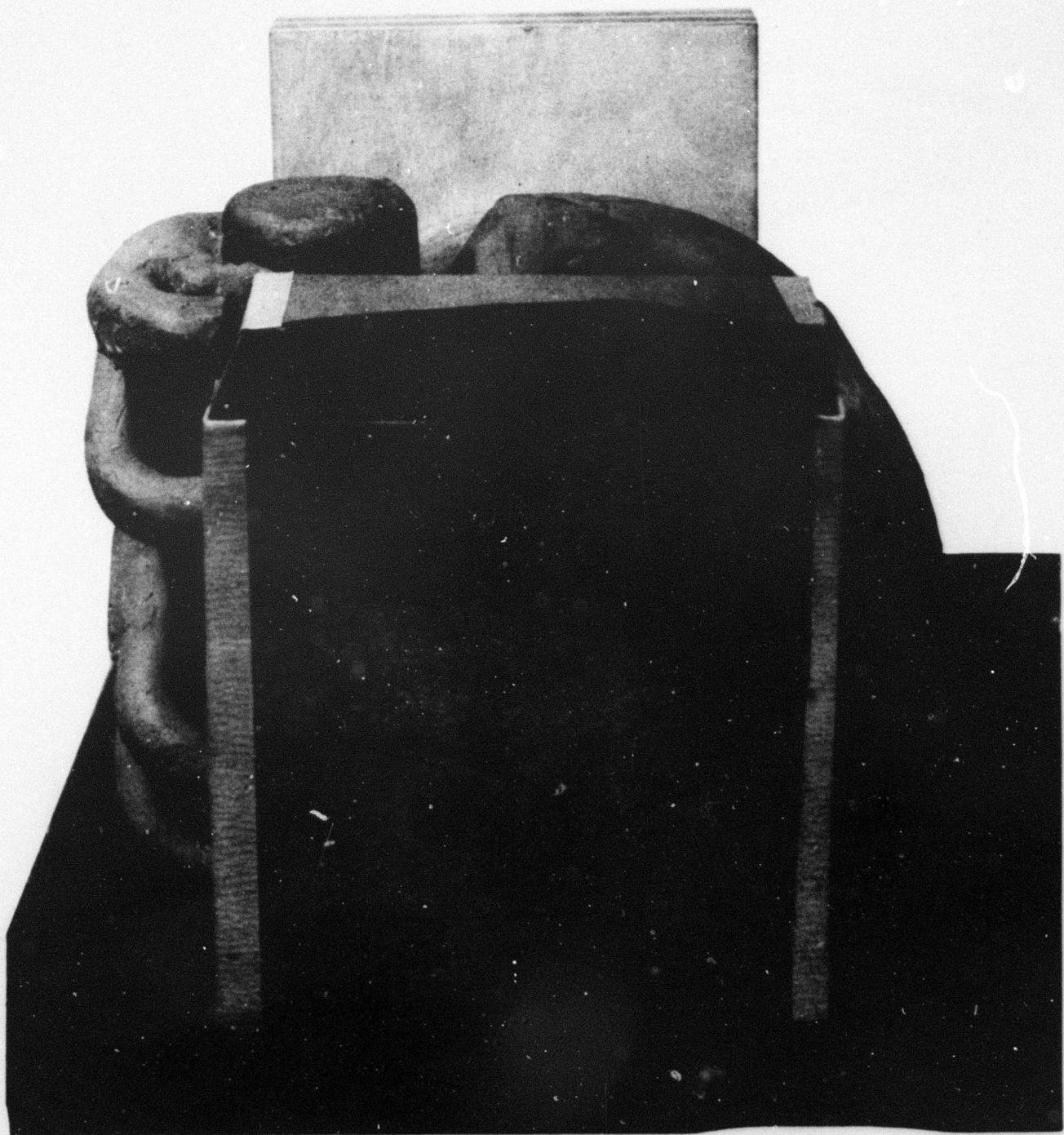


**Figure XVI-B-27. Recuperator Mock-Up - Z Flow Aft Mounting - Rear View.**

**Appendix XVI-B**

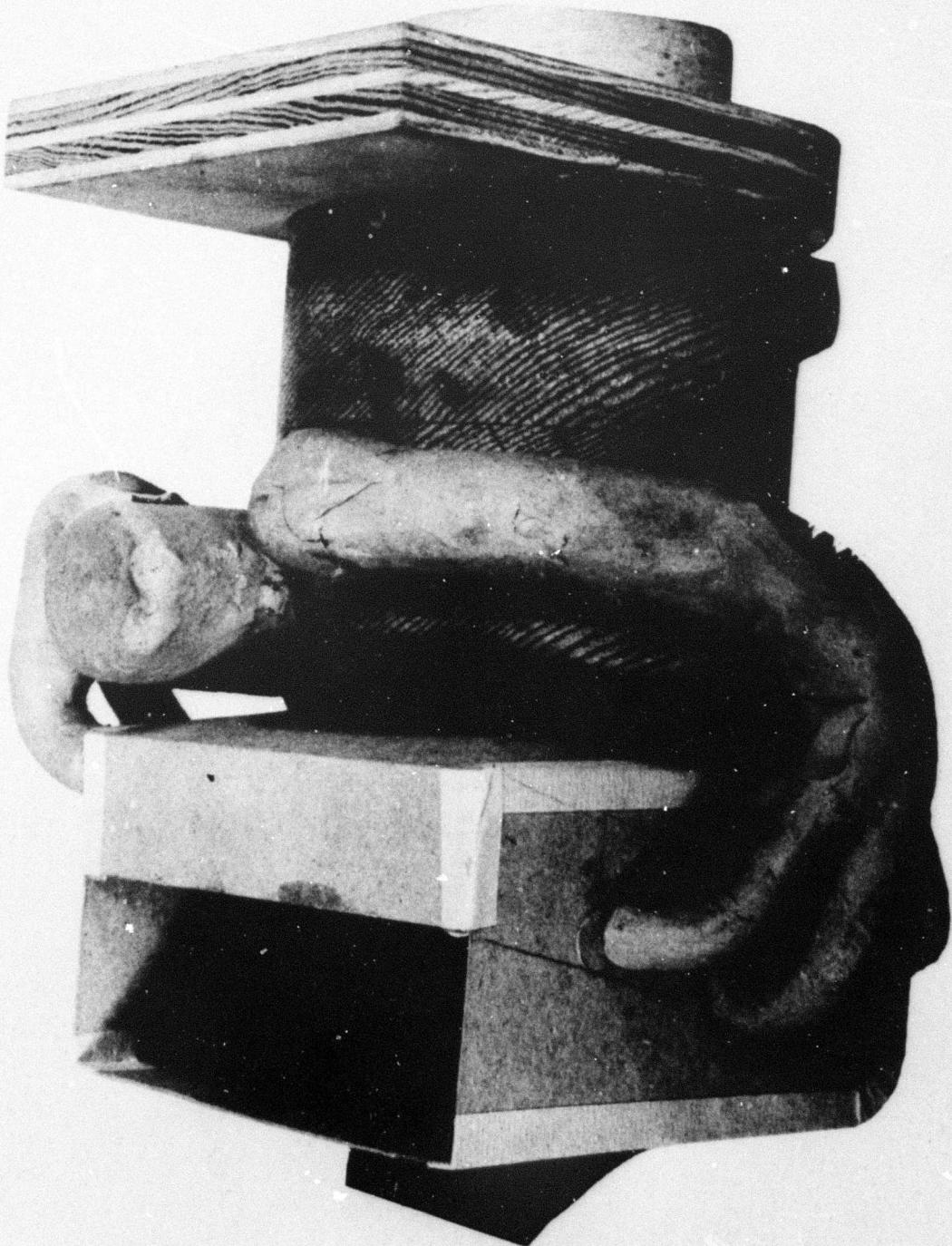


**Figure XVI-B-28. Recuperator Mock-Up - Z Flow Aft Mounting - Top View.**

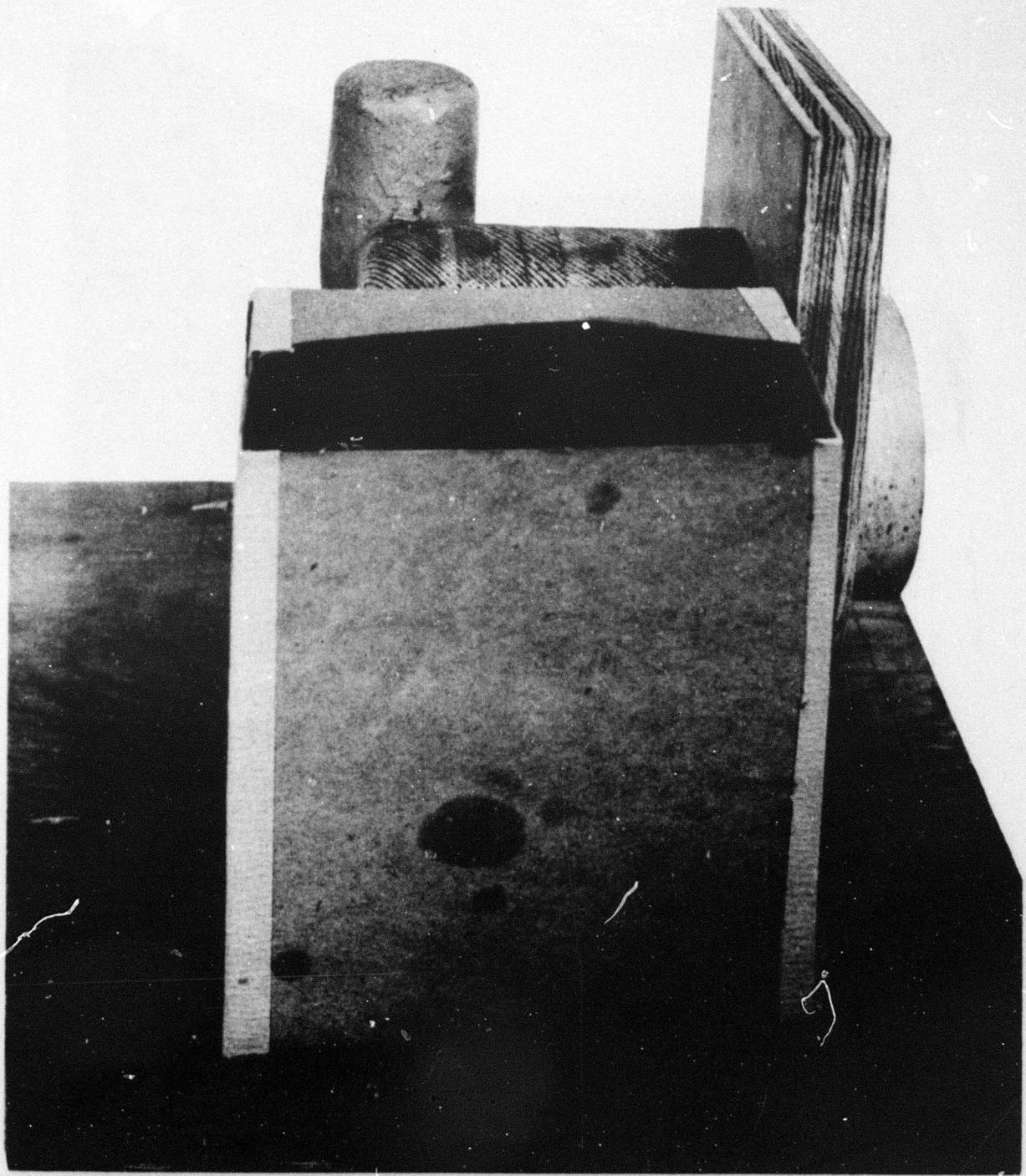


**Figure XVI-B-29. Recuperator Mock-Up - Z Flow Side Mounting - Side View.**

**Appendix XVI-B**

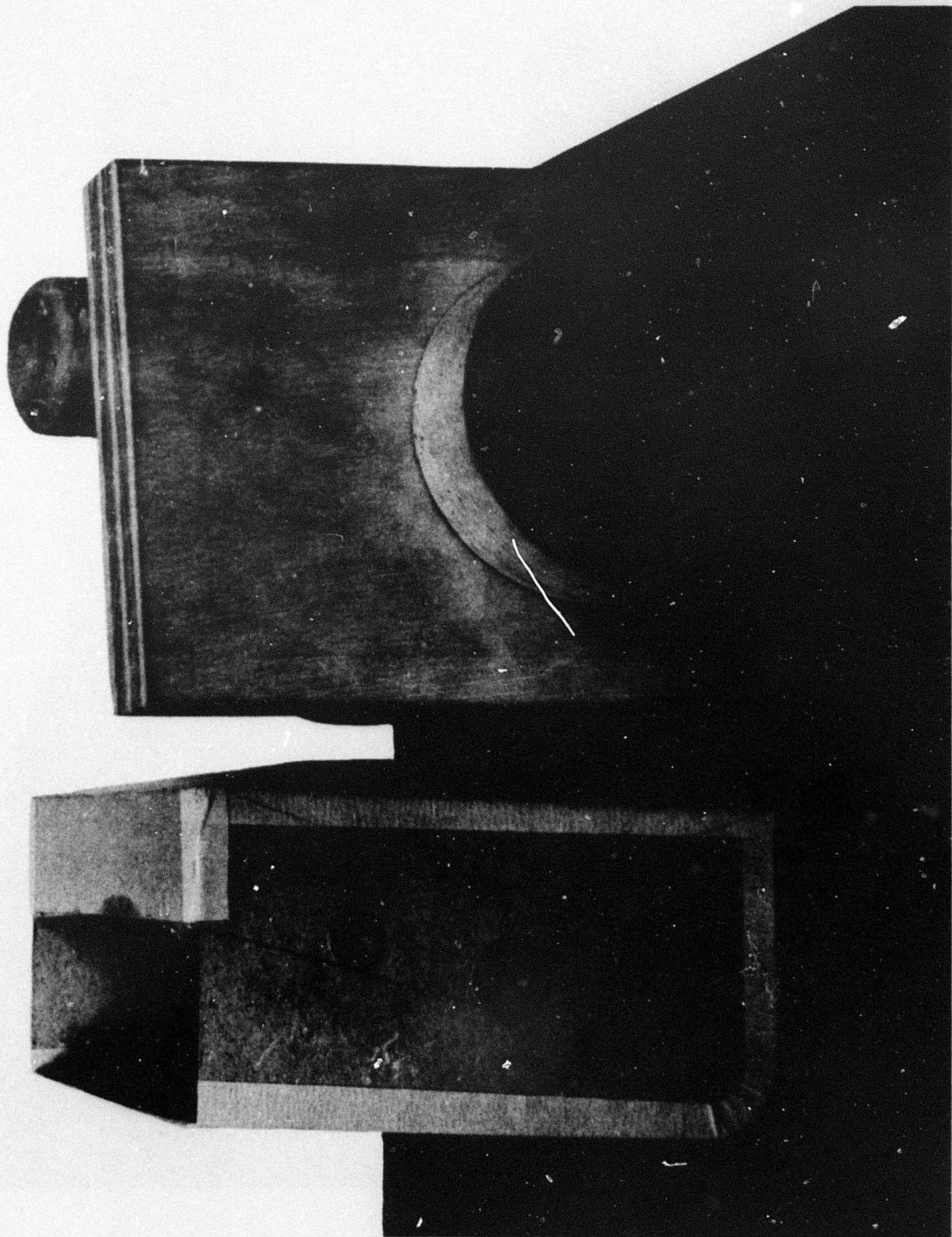


**Figure XVI-B-30. Recuperator Mock-Up - Z Flow Side Mounting - Front View.**

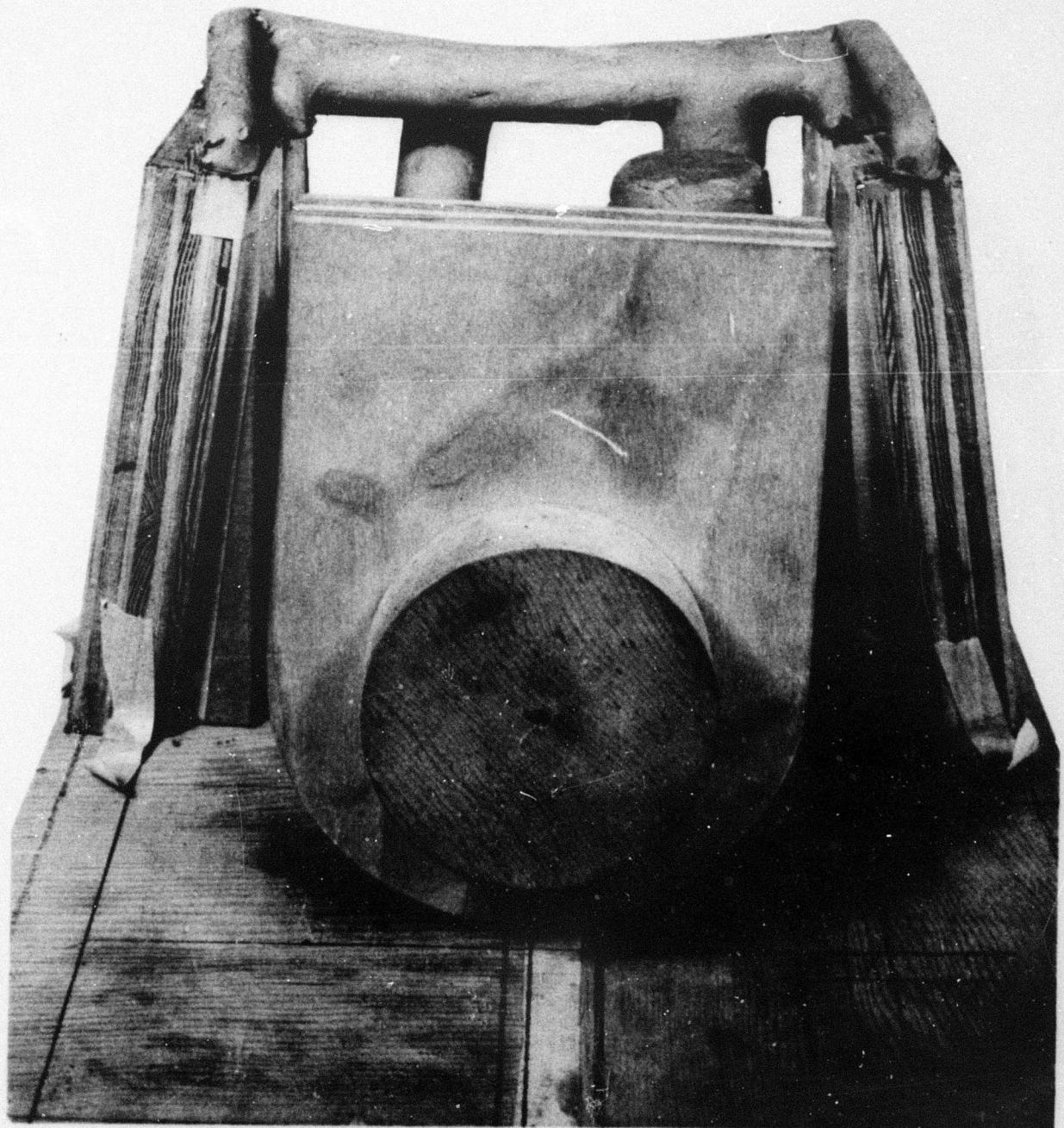


**Figure XVI-B-31. Recuperator Mock-Up - Four-Pass Plate Fin Side Mounting - Front View.**

**Appendix XVI-B**

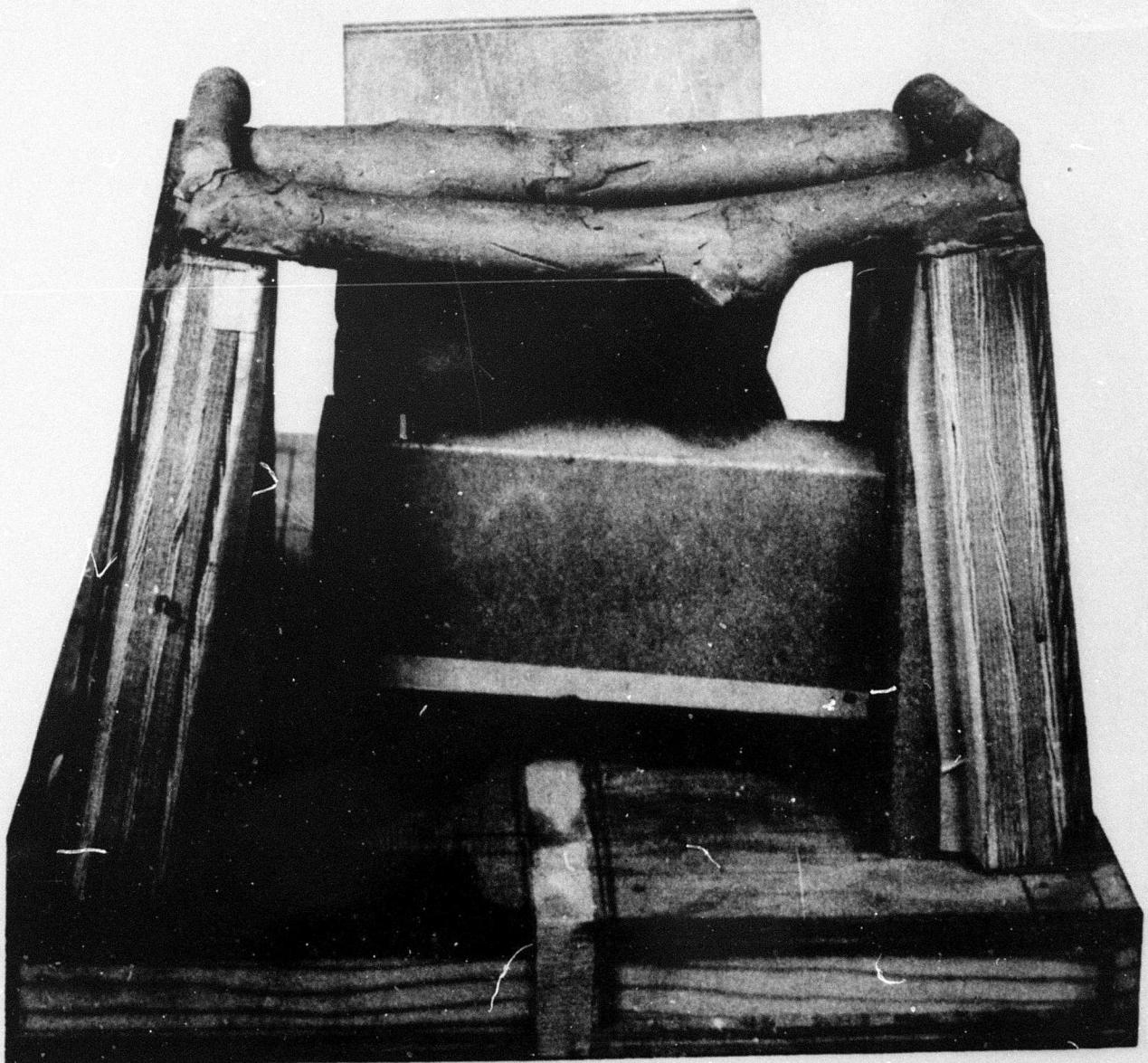


**Figure XVI-B-32. Recuperator Mock-Up - Four-Pass Plate Fin Side Mounting - Rear View.**

## Appendix XVI-B

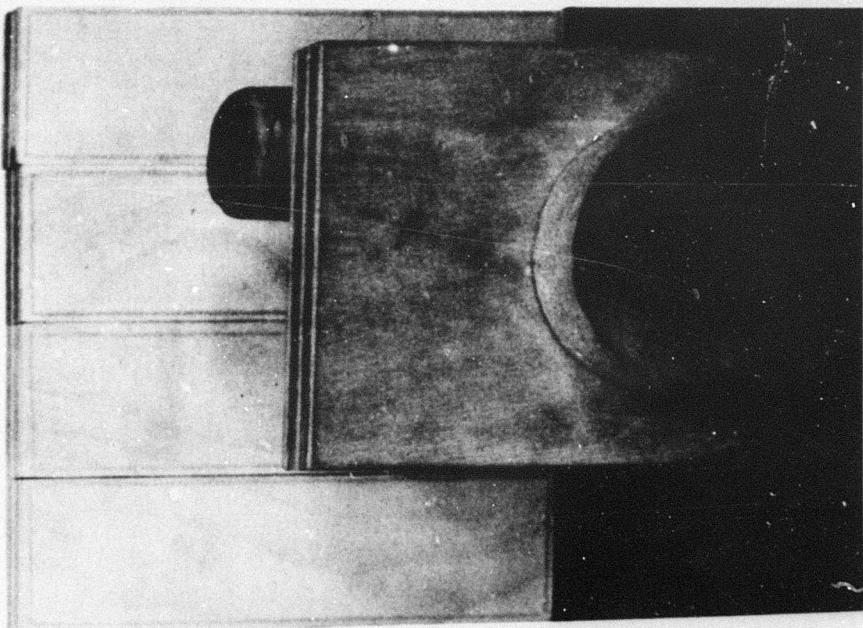


Figure XVI-B-34. Recuperator Mock-Up - Three Pass Plate Fin Aft Mounting - Front View.

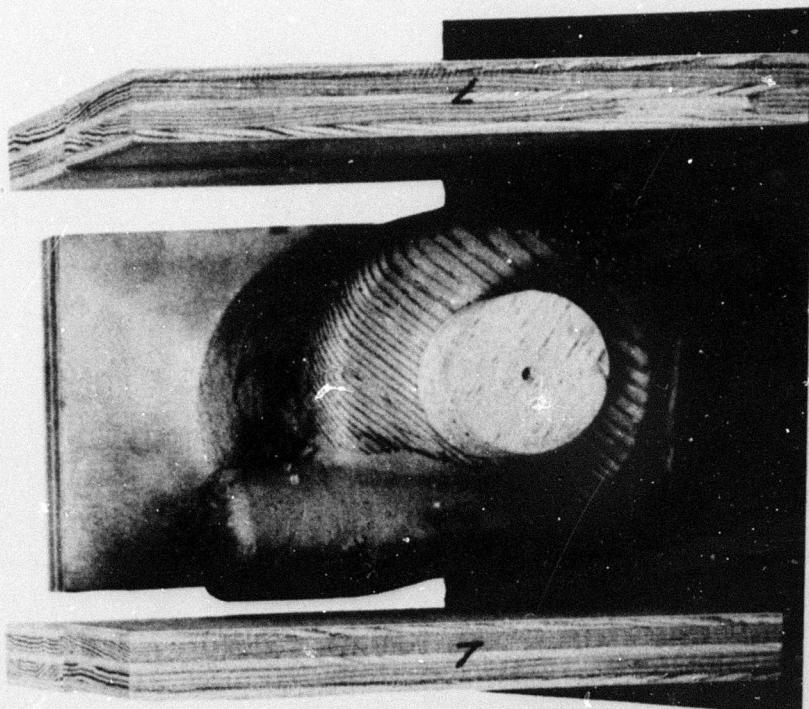


Figure XVI-B-33. Recuperator Mock-Up - Three Pass Plate Fin Side Mounting - Front View.

## Appendix XVI-B

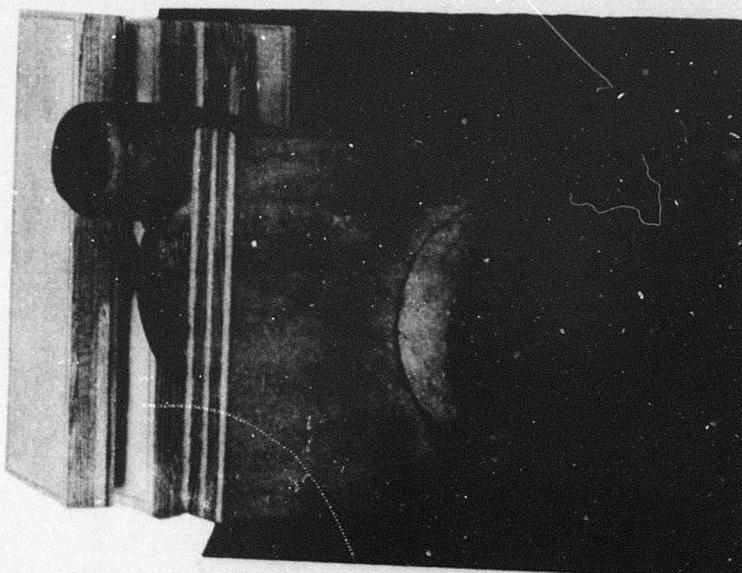


Figure XVI-B-36. Recuperator Mock-Up - Three Pass Plate Fin Folded Mounting - Front View.

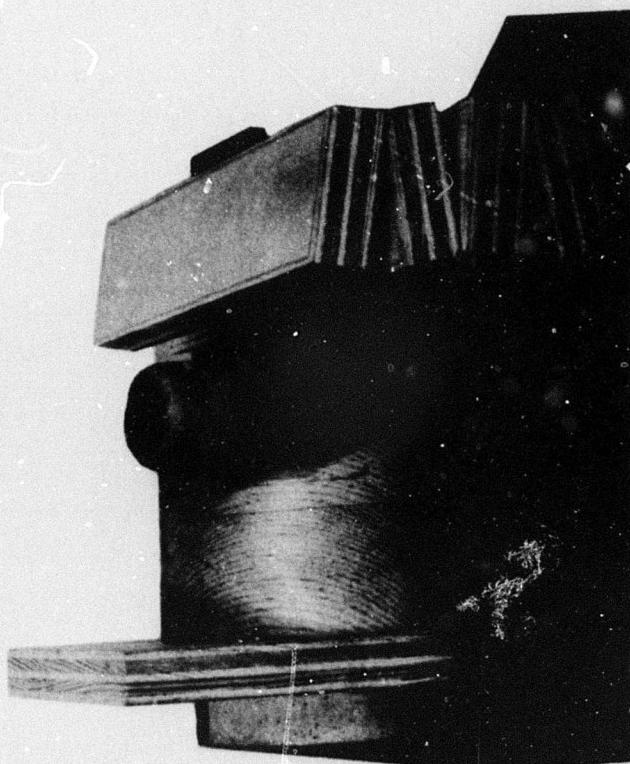
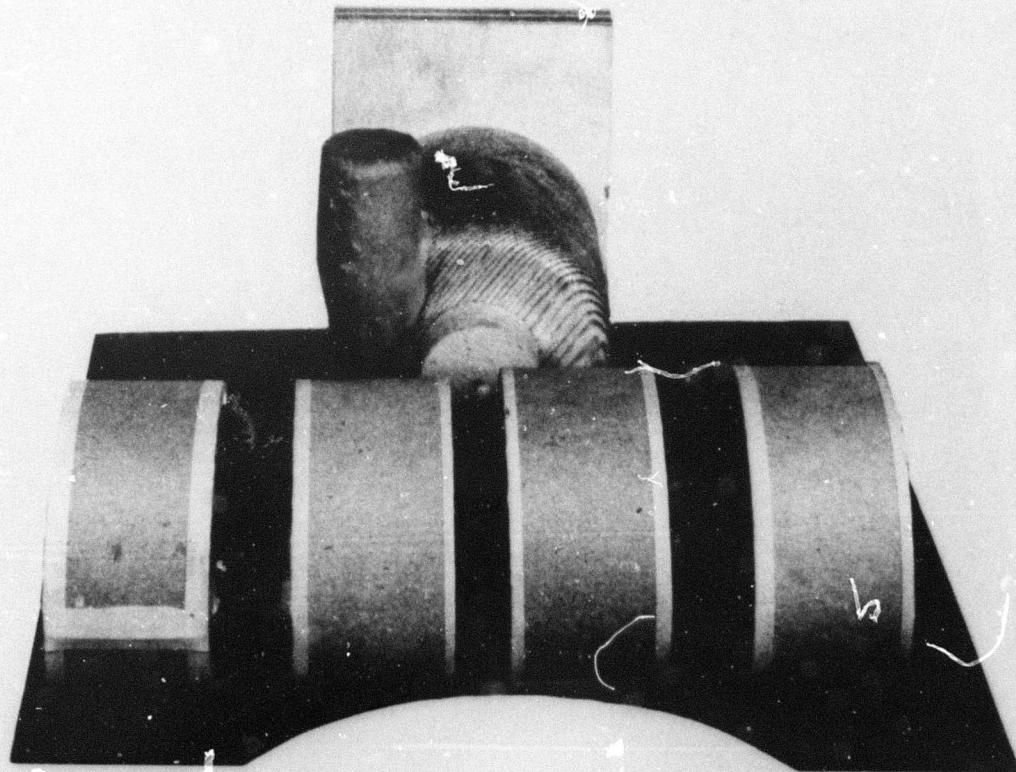
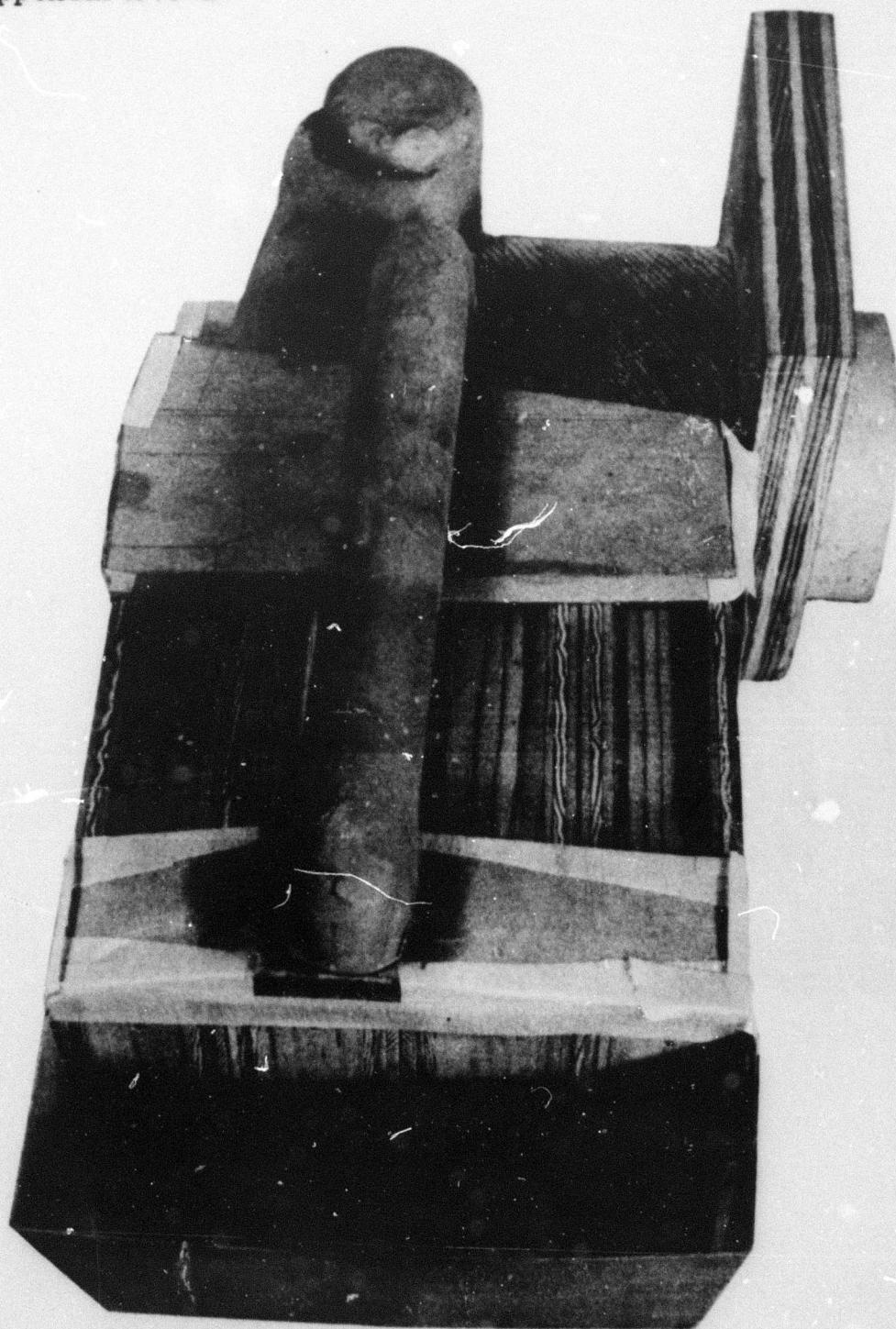


Figure XVI-B-35. Recuperator Mock-Up - Three Pass Plate Fin Folded Mounting - Side View.



**Figure XVI-B-37. Recuperator Mock-Up - Three-Pass Plate Fin - Rolled Mounting - Rear View.**

**Appendix XVI-B**



**Figure XVI-B-38. Recuperator Mock-Up - Four-Pass Air Over Tubes - Side Mounting - Top View.**

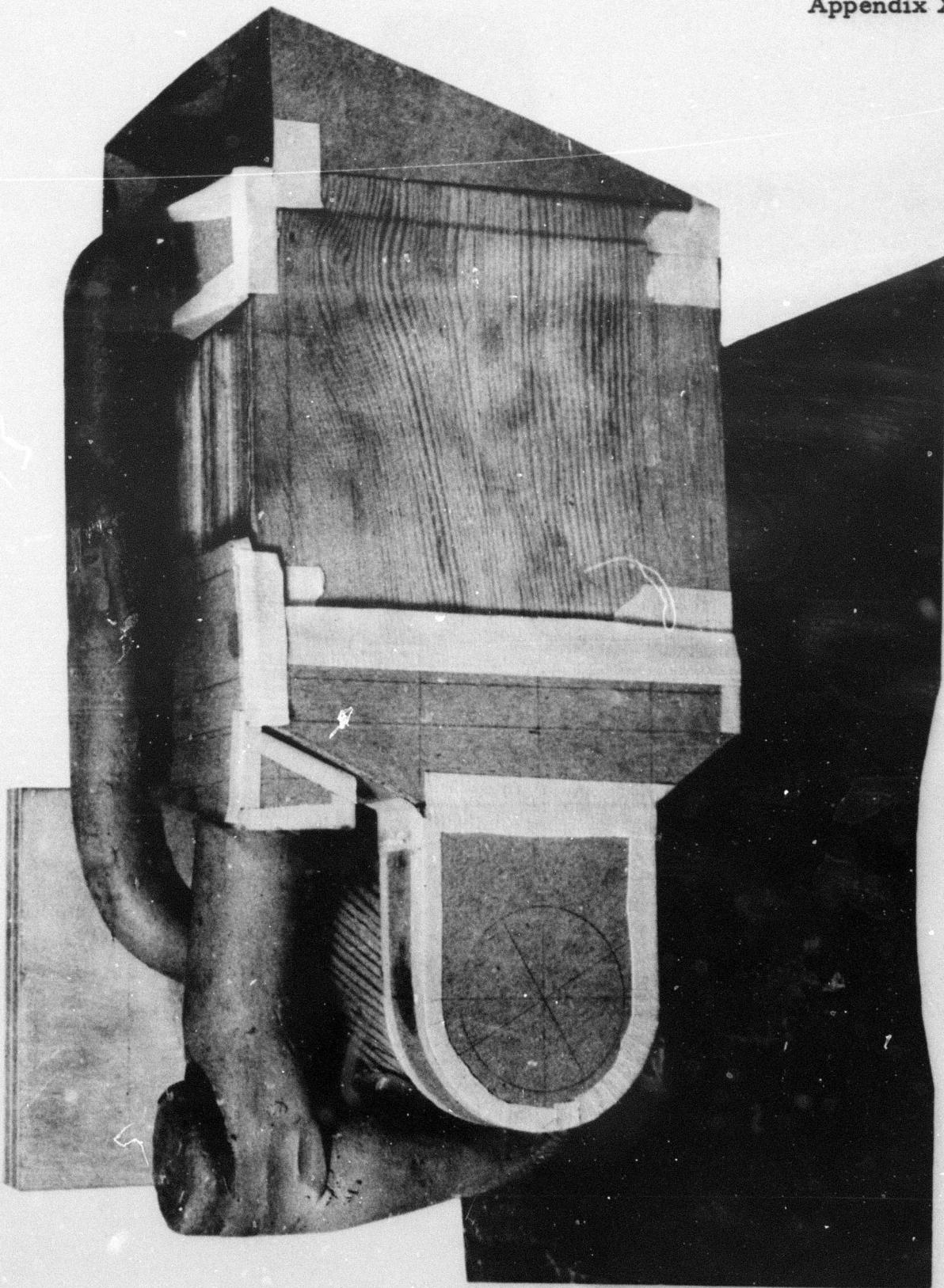
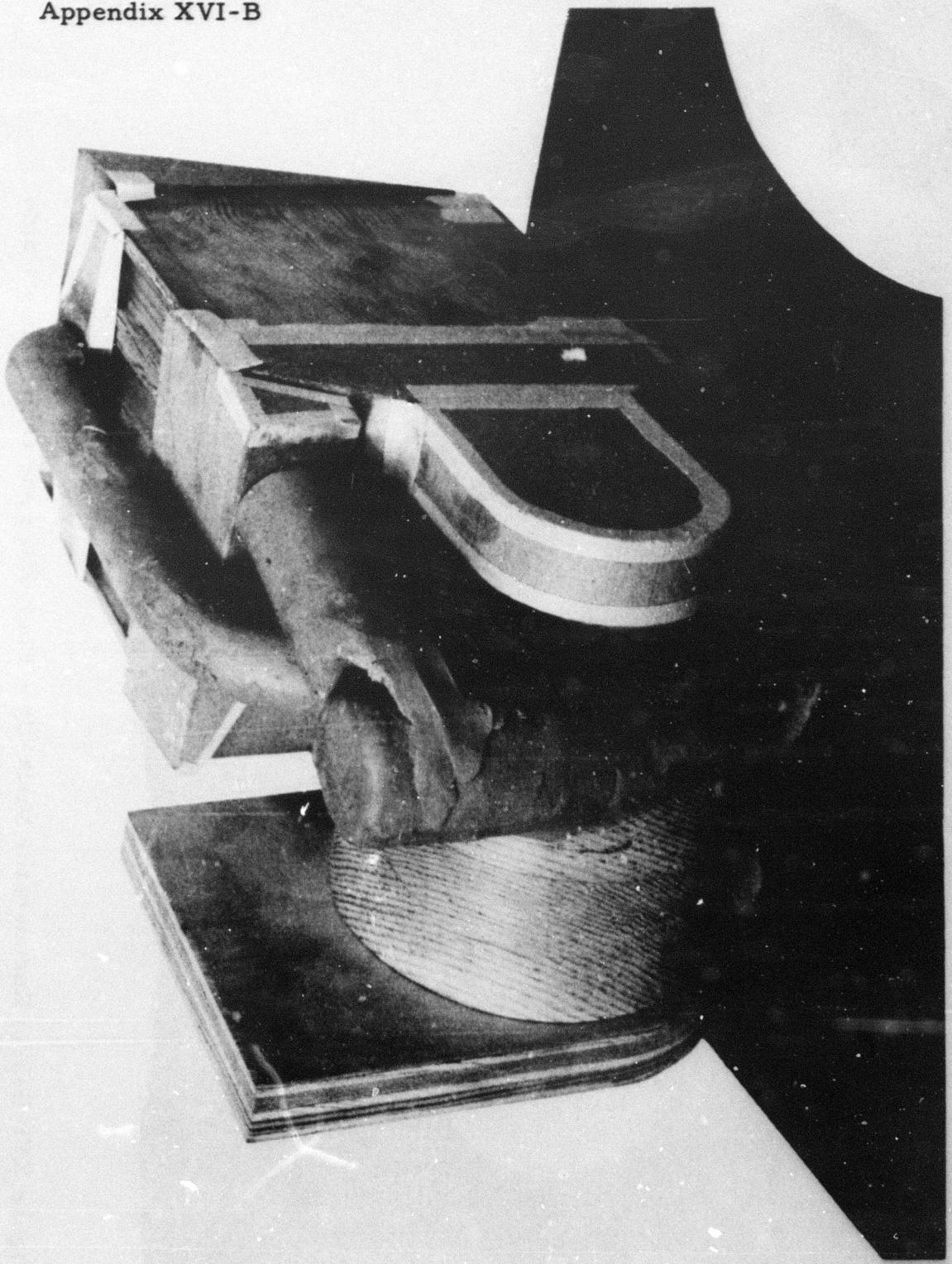
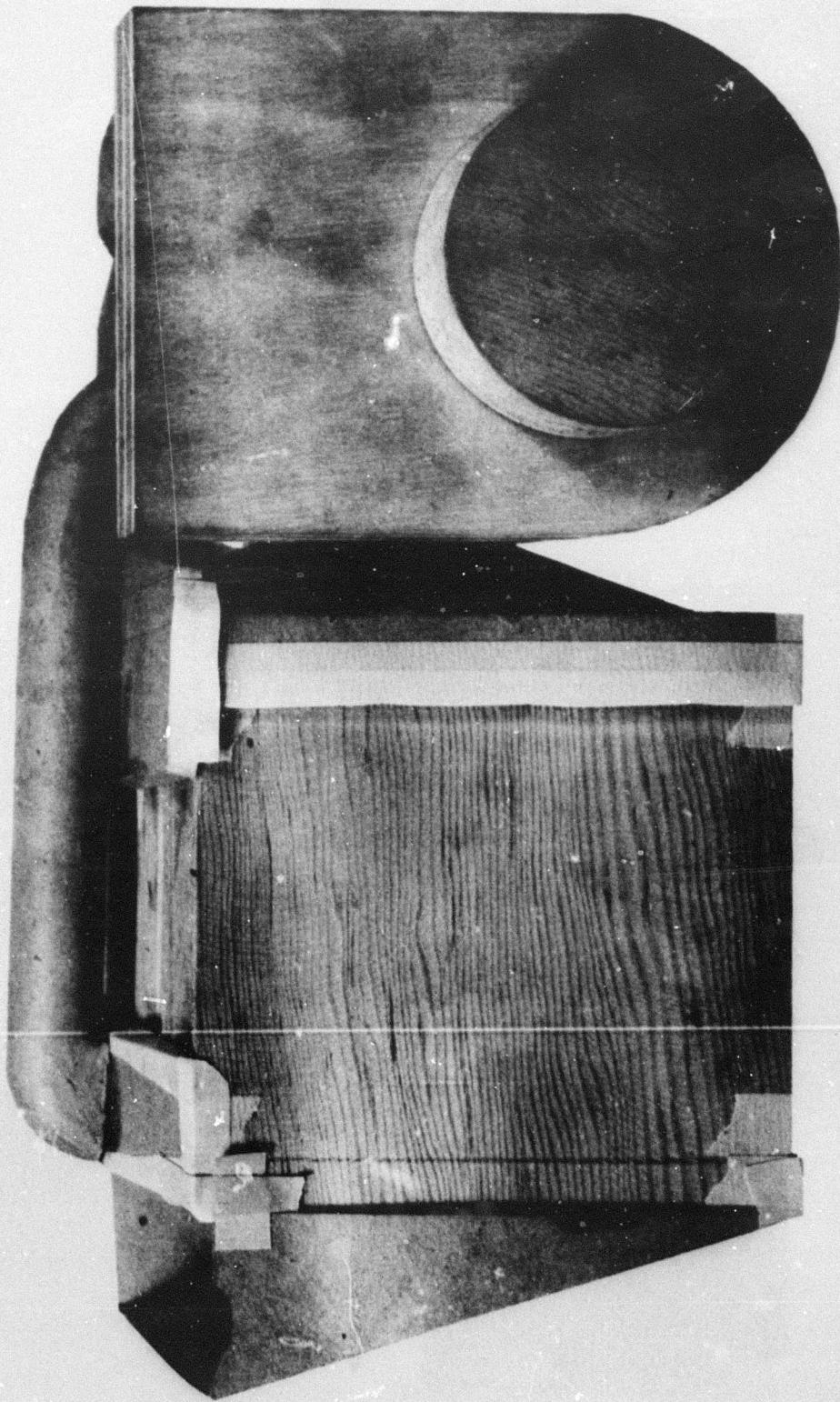


Figure XVI-B-39. Recuperator Mock-Up - Four-Pass Air Over Tubes - Side Mounting - Rear View.

**Appendix XVI-B**



**Figure XVI-B-40.** Recuperator Mock-Up - Four-Pass Air Over Tubes - Side Mounting - Side View.



**Figure XVI-B-41.** Recuperator Mock-Up - Four-Pass Air Over Tubes - Side Mounting - Front View.

Appendix XVI-B

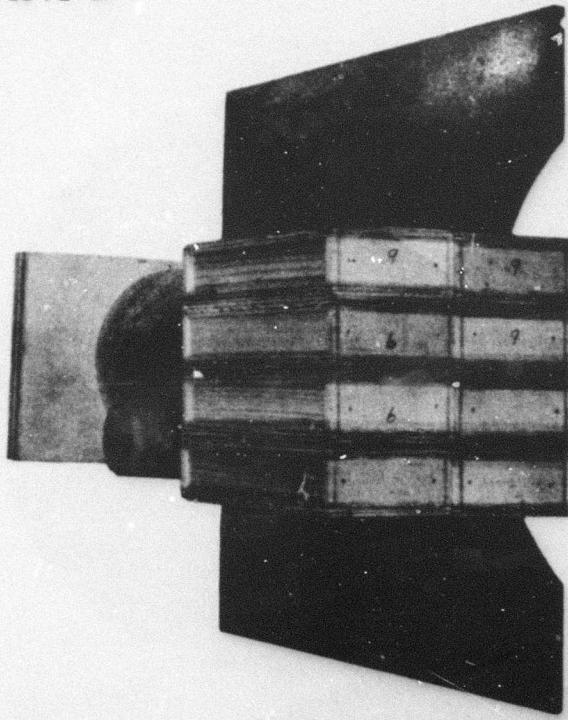


Figure XVI-B-43. Recuperator Mock-Up - Four Pass Air Over Tubes Aft Mounting - Side View.

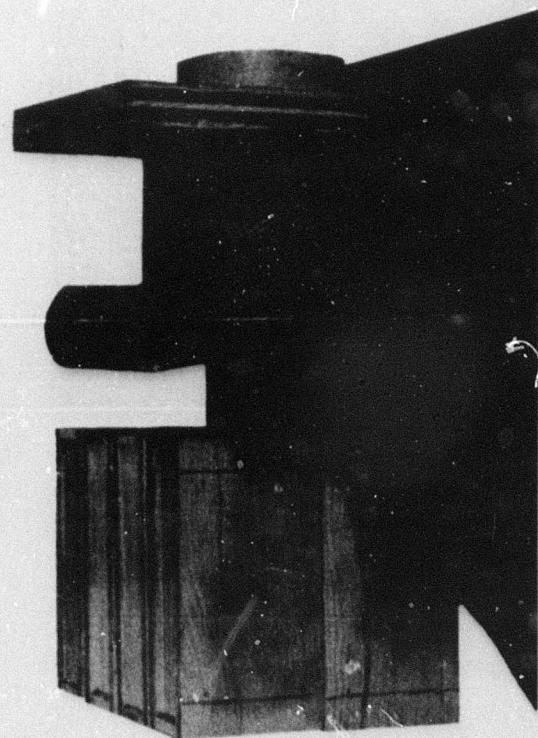
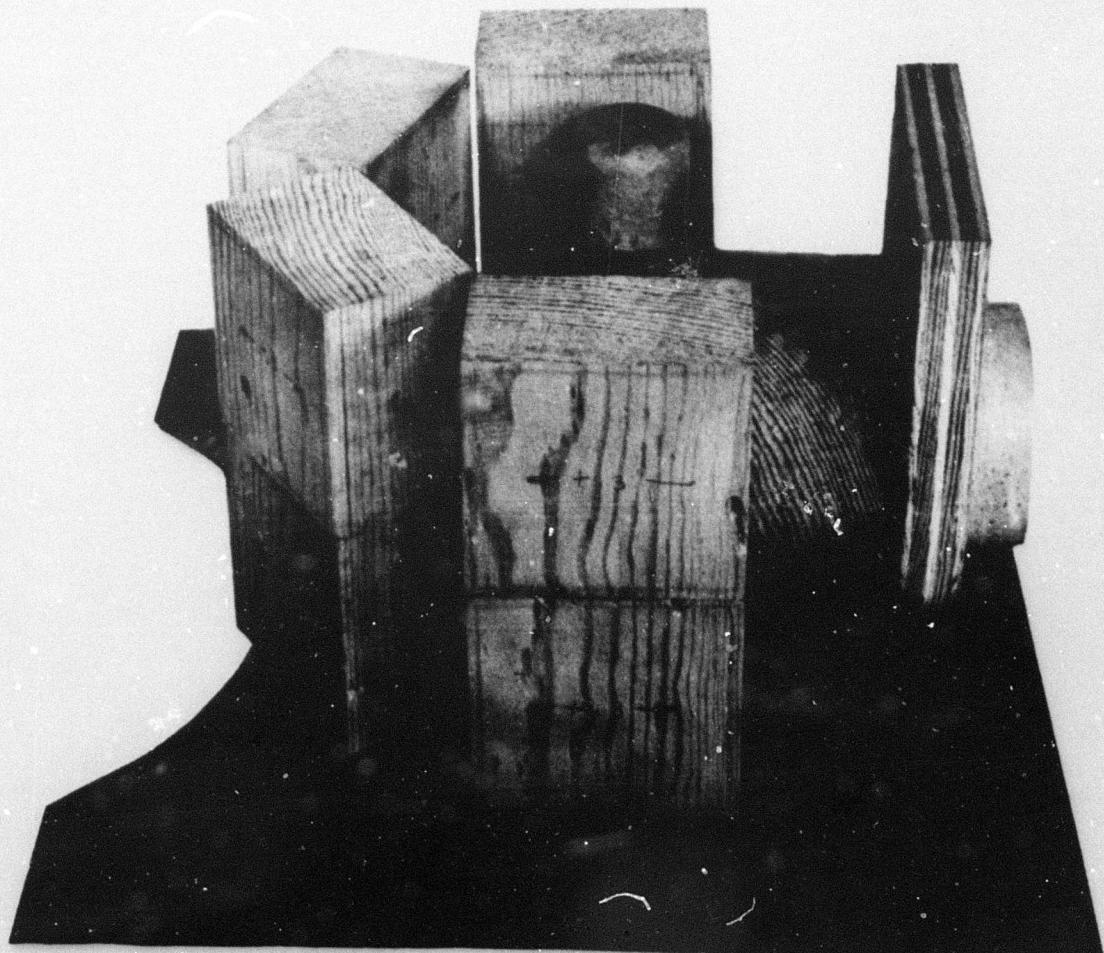


Figure XVI-B-42. Recuperator Mock-Up - Four Pass Air Over Tubes Aft Mounting - Rear View.



**Figure XVI-B-44. Recuperator Mock-Up - Five-Pass Air Through Tubes - Aft Mounting - Side View.**



